IMMUNE CELL INTERACTIONS WITH TARGET CELLS IN PHYSIOLOGICAL AND PATHOLOGICAL CONDITIONS OF THE NERVOUS SYSTEM

EDITED BY: Antje Kroner, Sven G. Meuth and Craig Stephen Moore
PUBLISHED IN: Frontiers in Immunology, Frontiers in Neurology and Frontiers in Molecular Neuroscience

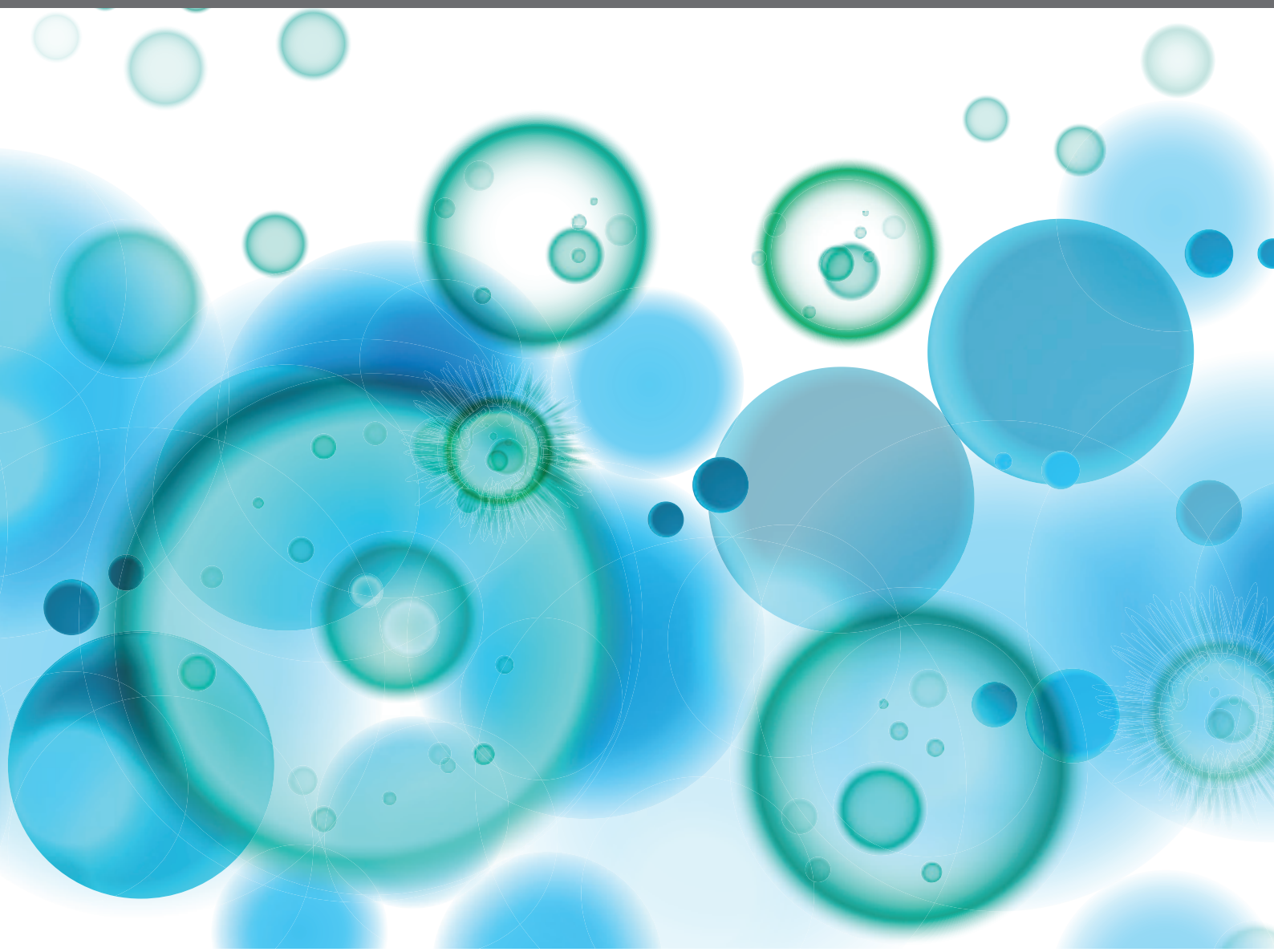

frontiers Research Topics

frontiers

ISSN 1664-8714
ISBN 978-2-88963-969-4
DOI 10.3389/978-2-88963-969-4

About Frontiers

Frontiers is more than just an open-access publisher of scholarly articles: it is a pioneering approach to the world of academia, radically improving the way scholarly research is managed. The grand vision of Frontiers is a world where all people have an equal opportunity to seek, share and generate knowledge. Frontiers provides immediate and permanent online open access to all its publications, but this alone is not enough to realize our grand goals.

Frontiers Journal Series

The Frontiers Journal Series is a multi-tier and interdisciplinary set of open-access, online journals, promising a paradigm shift from the current review, selection and dissemination processes in academic publishing. All Frontiers journals are driven by researchers for researchers; therefore, they constitute a service to the scholarly community. At the same time, the Frontiers Journal Series operates on a revolutionary invention, the tiered publishing system, initially addressing specific communities of scholars, and gradually climbing up to broader public understanding, thus serving the interests of the lay society, too.

Dedication to Quality

Each Frontiers article is a landmark of the highest quality, thanks to genuinely collaborative interactions between authors and review editors, who include some of the world's best academicians. Research must be certified by peers before entering a stream of knowledge that may eventually reach the public - and shape society; therefore, Frontiers only applies the most rigorous and unbiased reviews.
Frontiers revolutionizes research publishing by freely delivering the most outstanding research, evaluated with no bias from both the academic and social point of view. By applying the most advanced information technologies, Frontiers is catapulting scholarly publishing into a new generation.

What are Frontiers Research Topics?

Frontiers Research Topics are very popular trademarks of the Frontiers Journals Series: they are collections of at least ten articles, all centered on a particular subject. With their unique mix of varied contributions from Original Research to Review Articles, Frontiers Research Topics unify the most influential researchers, the latest key findings and historical advances in a hot research area! Find out more on how to host your own Frontiers Research Topic or contribute to one as an author by contacting the Frontiers Editorial Office: researchtopics@frontiersin.org

IMMUNE CELL INTERACTIONS WITH TARGET CELLS IN PHYSIOLOGICAL AND PATHOLOGICAL CONDITIONS OF THE NERVOUS SYSTEM

Topic Editors:
Antje Kroner, Medical College of Wisconsin, United States
Sven G. Meuth, University Hospital Münster, Germany
Craig Stephen Moore, Memorial University of Newfoundland, Canada

Citation: Kroner, A., Meuth, S. G., Moore, C. S., eds. (2020). Immune Cell Interactions With Target Cells in Physiological and Pathological Conditions of the Nervous System. Lausanne: Frontiers Media SA. doi: 10.3389/978-2-88963-969-4

Table of Contents

frontiers in Immunology

ORIGINAL RESEARCH
published: 04 April 2019
doi: 10.3389/fimmu.2019.00710

The iNOS Activity During an Immune Response Controls the CNS Pathology in Experimental Autoimmune Encephalomyelitis

*Sandip Ashok Sonar and Girdhari Lal**

National Center for Cell Science, Pune, India

Inducible nitric oxide synthase (iNOS) plays a critical role in the regulation of multiple sclerosis (MS) and experimental autoimmune encephalomyelitis (EAE). Previous studies have shown that iNOS plays pathogenic as well as regulatory roles in MS and EAE. However, how does iNOS alters the pathophysiology of the central nervous system (CNS) in neuronal autoimmunity is not clearly understood. In the present work, we show that treatment of mice with L-NAME, an iNOS inhibitor, during the antigen-priming phase primarily alters brain pathology, while in the subsequent effector phase of the immune response, the spinal cord is involved. Inhibition of iNOS during the priming phase of the immune response promotes the infiltration of pathogenic $CD11b^{+}F4/80^{-}Gr\text{-}1^{+}$ cells, but there is low recruitment of regulatory $CD11b^{+}F4/80^{+}$ cells in the brain. Inhibition of iNOS during the effector phase shows similar pathogenic alterations in the spinal cord, instead of in the brain. Treatment of wild-type mice with L-NAME or mice having genetic deficiency of iNOS show lower MHC-II expression on the dendritic cells, but not on macrophages. Our data suggest that iNOS has a critical regulatory role during antigen-priming as well as in the effector phase of EAE, and inhibition iNOS at different stages of the immune response can differentially alter either the brain or spinal cord pathology. Understanding the cellular and molecular mechanisms through which iNOS functions could help to design a better strategies for the clinical management of neuroinflammation and neuronal autoimmunity.

Keywords: experimental autoimmune encephalomyelitis, inducible nitric oxide synthase, $NOS2^{-/-}$ neuroinflammation, central nervous system, autoimmunity

OPEN ACCESS

Edited by:
Antje Kroner,
Medical College of Wisconsin,
United States

Reviewed by:
Stefan Bittner,
Johannes Gutenberg University
Mainz, Germany
Stella Tsirka,
Stony Brook University, United States

****Correspondence:***
Girdhari Lal
glal@nccs.res.in

Specialty section:
This article was submitted to Multiple Sclerosis and Neuroimmunology, a section of the journal Frontiers in Immunology

Received: *16 January 2019*
Accepted: *15 March 2019*
Published: *04 April 2019*

Citation:
Sonar SA and Lal G (2019) The iNOS Activity During an Immune Response Controls the CNS Pathology in Experimental Autoimmune Encephalomyelitis. Front. Immunol. 10:710. doi: 10.3389/fimmu.2019.00710

INTRODUCTION

Nitric oxide (NO) is a small bioactive lipophilic molecule that diffuse across the cell membrane and controls many physiological functions of the body (1). NO production requires nitric oxide synthase (NOS), which catalyze the oxidation of L-arginine to L-citrulline (2, 3). In mammals, there are three different isoforms of NOS - endothelial NOS (eNOS), neuronal NOS (nNOS) and inducible NOS (iNOS) (4). Constitutive expression of eNOS and nNOS controls the vasodilation of vessels and neuronal functions, respectively (5). Several inflammatory stimuli can induce the expression of iNOS in various cell types such as macrophages, dendritic cells, neutrophils, epithelial cells in the gut and lung mucosa, smooth muscle cells, and stromal cells of secondary

lymphoid organs (6–9). iNOS is also expressed in microglial cells, astrocytes, neurons in the central nervous system (CNS), and endothelial cells at the blood-brain barrier (BBB) (7, 10, 11). A clinical association between iNOS and pathogenesis has been reported in many organ-specific autoimmune inflammatory diseases, including multiple sclerosis (MS) and experimental autoimmune encephalomyelitis (EAE) (12–15).

Proper neuronal function requires the presence of the minimal physiological concentrations of NO in the CNS, with sustained high NO levels leading to detrimental effects (16). The active MS patients show high NO levels in the cerebrospinal fluid (CSF), and high concentrations of NO, peroxynitrite, and other reactive nitrogen species have been found to correlate with greater severity and chances of relapse of clinical symptoms (15, 17). The expression of iNOS in the CNS is very tightly regulated, and several intrinsic and extrinsic stimuli can induce its expression in immune cells (14, 18). The T cell-derived cytokine, IFN-γ induces the expression of iNOS in macrophages and microglial cells which leads to the generation of higher NO and peroxynitrite productions, and cause tissue destruction in the CNS (13, 19, 20). However, iNOS$^{-/-}$ mice are hypersusceptible to EAE, suggesting that iNOS may have a regulatory function during CNS inflammation and autoimmunity (21, 22). Several studies have shown that iNOS can regulate the function of regulatory dendritic cells (regulatory DCs) which in turn can induce apoptosis of inflammatory CD4$^+$ T cells and help in controlling the development of EAE (23–25). Furthermore, iNOS expression in macrophages is linked with the suppression of inflammasome activation-induced IL-1β production (26), as well as a reduction in the frequency of M1 macrophages (27). Myeloid cell-derived iNOS is also known to control the CD4$^+$ T cell response (28, 29). High levels of APCs-derived NO suppresses CD4$^+$ T cell response, while low levels favor the generation of a Th1 response (30). Th17-intrinsic iNOS has been shown to suppress Th17 response through nitration of the tyrosine residues of RORγt, and limiting its promoter binding capacity (31). While it is known that Th17 cells in the CNS express iNOS during EAE, the functional importance of iNOS production by Th17 cells in the inflamed CNS is not clearly understood. During chronic demyelination, a pathogenic phenotype of microglial cells has been found to be associated with iNOS expression (32, 33). Since both lesion-associated and non-associated astrocytes express iNOS, the contribution of astrocyte-derived iNOS is still unclear. Some *in vitro* experiments suggest that inflammatory cytokine-induced iNOS reduces the expression of myelin proteins and causes oligodendrocyte death in the mixed glial cultures (34). All these observations indicate that iNOS plays a dual role during neuronal autoimmunity. Anti-IFN-γ treatment and IFN-γR$^{-/-}$ mice show hypersusceptibility to the development of EAE, with preferential involvement of the brain stem and cerebellum, resulting in the atypical EAE symptoms with the critical participation of neutrophil effector function (35–37). Given that IFN-γ regulates the iNOS expression in several immune cells, how does iNOS controls the inflammation in the brain and the spinal cord, and whether iNOS performs different functions during the antigen-priming and effector phases of EAE is not known.

In the present study, we assessed the role of iNOS using L-NAME-mediated inhibition of its activity during various stages of the immune response in EAE, including the antigen-priming phase and the effector phases, accompanied by monitoring of cellular pathology in the CNS. Our results showed that inhibition of iNOS during the antigen-priming as well as effector phases of EAE worsened the disease, and histology indicated differential regulation of infiltration of CD11b$^+$F4/80$^-$GR-1$^+$ and CD11b$^+$F4/80$^+$ cells in the brain and spinal cord. iNOS inhibition during the antigen-priming phase selectively promoted the infiltration of inflammatory CD11b$^+$F4/80$^-$GR-1$^+$ cells, while lowering the frequency of infiltration of CD11b$^+$F4/80$^+$ cells into the brain. Conversely, inhibiting iNOS during the effector phase led to mostly CD11b$^+$F4/80$^-$GR-1$^+$ cells migrating into the spinal cord. A similar phenotype with higher infiltration of CD11b$^+$F4/80$^-$GR-1$^+$ cells and reduced infiltration of CD11b$^+$F4/80$^+$ cells in the CNS was observed in iNOS$^{-/-}$ mice or wild-type mice in which IFN-γ, a known inducer of iNOS, was blocked. We show that iNOS plays a regulatory role in promoting the infiltration of CD11b$^+$F4/80$^+$ suppressor cells, while at the same time inhibiting the mobilization of pathogenic CD11b$^+$F4/80$^-$GR-1$^+$ cells into the CNS.

RESULTS

Inhibition of NO Production in the Priming Phase Promotes Granulocytic Myeloid Cells Infiltration Specifically in the Brain

Active EAE was induced in C57BL/6 mice and given an intraperitoneal injection of NOS inhibitor L-NAME (100 mg/kg/every day) in the antigen-priming phase (one injection/day for seven days). The inhibition of NO production by L-NAME at the antigen-priming phase significantly increased the severity of EAE mice, compared to control mice (**Figure 1A**). Interestingly, the severity of the clinical symptoms of EAE increased with time in mice that received L-NAME (**Figure 1A**). Analysis of the brain and spinal cord tissues showed enhanced infiltration of CD45$^+$ leukocytes, including CD4$^+$ T cells, in the brain but not in the spinal cord (**Figure 1B**). CD11b$^+$F4/80$^+$ cells include mainly macrophages and monocytic myeloid-derived suppressor cells (Mo-MDSCs). The F4/80-expressing MDSCs are known to have a suppressive function in EAE (38), whereas CD11b$^+$GR-1$^+$ cells show a pathogenic phenotype (39). L-NAME-treated mice showed a significant reduction in the infiltration of CD11b$^+$F4/80$^+$GR-1$^-$ cells selectively in the brain, but not

Abbreviations: APCs, Antigen-presenting cells; BMDCs, Bone marrow-derived DCs; CNPase, 2',3'-cyclic nucleotide 3'-phosphodiesterase; CNS, Central nervous system; CFA, Complete Freund's adjuvant; DCs, Dendritic cells; EAE, Experimental autoimmune encephalomyelitis; eNOS, Endothelial NOS; GFAP, Glial fibrillary acidic protein; iNOS, inducible NOS; L-NAME, *N*-ω-nitro-l-arginine methyl ester; MDSCs, Myeloid-derived suppressor cells; MOG, Myelin oligodendrocyte glycoprotein 35-55 peptide; Mo-MDSCs, Monocytic myeloid-derived suppressor cells; MS, Multiple sclerosis; NO, Nitric oxide; NOS, Nitric oxide synthase; nNOS, neuronal NOS.

in the spinal cord (**Figure 1C**). However, L-NAME treatment significantly increased infiltration of $CD11b^+F4/80^-GR\text{-}1^+$ cells (mainly neutrophils) in the brain but not in the spinal cord (**Figure 1C**). Together, our results showed that inhibition of NOS in the priming phase of EAE mostly affected the infiltration of inflammatory $CD4^+$ T cells and GR-1^+ neutrophils in the brain, and reduced the frequency of $CD11b^+F4/80^+$ cells, which might account for the severity of EAE in the later phase of the disease.

Inhibition or Deficiency of iNOS in the Antigen-Priming Phase Does Not Alter the Differentiation of Effector $CD4^+$ T Cells

Since L-NAME injections at day 0-7 coincided with the antigen-specific priming, activation, and differentiation of effector $CD4^+$ T cells, we measured the frequency of Th1 cytokine (IFN-γ) and Th17 cytokine (IL-17A) producing cells, and $Foxp3^+$ regulatory $CD4^+$ T cells in the spleen and lymph nodes. Our results showed no significant alteration in the intracellular expression of IL-17A and IFN-γ in $CD4^+$ T cells (**Figures 2A,B**) or γδ T cells (**Figure S1A**). To further confirm the role of iNOS in the priming-phase of EAE, we immunized wild-type and $iNOS^{-/-}$ mice with MOG in complete Freund's adjuvant (CFA). On day 8, we compared the differentiation of effector immune cells in their spleen and lymph nodes with those of L-NAME (d0-7)-treated and untreated wild-type C57BL/6 mice. $iNOS^{-/-}$ mice also did not show any significant change in the expression of the Th lineage-specific transcription factors, T-bet, RORγt, Foxp3, and Eomes in $CD4^+$ T cells, as compared to the control group (**Figures 2C,D** and **Figures S1B,C**). However, L-NAME treated mice showed a lower frequency of T-bet expressing $CD4^+$ T cells in the draining lymph nodes, as compared to the control group (**Figures 2C,D**). We did not observe any significant changes in the expression of intracellular IL-17A, IFN-γ, and GM-CSF in the $CD4^+$ T cells or γδ T cells (data not shown). On day 28, L-NAME treated mice showed severe EAE symptoms but did not show a significant change in the percentages of Th1, Th17, and Tregs or IL-$17A^+$ and IFN-γ^+ or IL-$17A^+$IFN-γ^+ γδ T cells in the secondary lymphoid organs (**Figures 2A,B** and **Figure S1A**). Together, these results suggest that inhibition of iNOS during the priming phase of EAE does not affect the differentiation of Th1, Th17, and Treg cells in the secondary lymphoid tissues.

Inhibition of iNOS in the Effector Phase Shows Increase Cellular Infiltration in the Spinal Cord

To understand how inhibition of NO production during the effector phase of EAE changes the pathophysiological phenotype and transmigration of effector immune cells in the CNS, L-NAME was administered (100 mg/kg/day; i.p.; day 8–15 of MOG injection) in C57BL/6 mice. Inhibition of NO production during the effector phase resulted in exacerbated EAE in these mice, as compared to control mice (**Figure 3A**). Interestingly, while increased infiltration of $CD45^+$ leukocytes and $CD4^+$ T cells was observed in the spinal cord in mice treated with L-NAME in the effector phase, infiltration of these cells in the brain was similar in L-NAME-treated and control mice (**Figure 3B**). This suggested that inhibition of NO production during the effector phase of EAE differentially diverts the inflammatory cells to the spinal cord and worsens the disease. Both meningeal and parenchymal regions showed higher infiltration in L-NAME-treated mice, as compared to control group (data not shown). Surprisingly, immunohistological analysis showed higher expression of iNOS in the brain-infiltrating $CD45^+$ leukocytes in the priming phase, as compared to that observed upon treatment with L-NAME in the effector phase (**Figure 3C**). However, inhibition of NO production during the effector phase showed a higher frequency of iNOS-expressing $CD45^+$ leukocytes in the spinal cord as compared to control group, or the mice that received iNOS inhibitor in the priming phase (**Figure 3D**). Analysis of iNOS expression in the brain and spinal cord astrocytes further revealed that the frequency of iNOS-expressing $GFAP^+$ astrocytes was significantly lower in the brains of mice treated with L-NAME during the antigen-priming phase as compared to control, whereas the spinal cord resident astrocytes did not show alteration in the number of iNOS-expressing cells (**Figures 3C,D**). These results indicate that L-NAME-mediated transient inhibition of NOS during the antigen-priming and effector phase of EAE leads to the reappearance of iNOS expression selectively in the infiltrated $CD45^+$ leukocytes and possibly in the $CD45^{int}$ CNS-resident microglial cells, in the brain and spinal cord, respectively. Consistent with the previous reports (21, 22), our results also showed that the a genetic deficiency of iNOS in mice leads to the development of more severe EAE than that observed in wild-type animals (**Figure 3E**). Immunohistological analysis of the brain and spinal cord in $iNOS^{-/-}$ mice showed significantly increased infiltration of $CD45^+$ leukocytes and $CD4^+$ T cells in the brain but not in the spinal cord (**Figure 3F**). These observations were consistent with those we obtained with the L-NAME injections in the early priming phase of the EAE, suggesting that lack of NO production in the initial stage of EAE directs pathological mechanisms specifically to the brain but not the spinal cord.

Furthermore, inhibition of NO production during the effector phase showed significantly reduced infiltration of $CD11b^+F4/80^+GR1^-$ cells in the brain and spinal cord as compared to control animals (**Figure S2A**). Interestingly, substantially higher infiltration of $CD11b^+F4/80^-GR\text{-}1^+$ cells was observed in the spinal cord but not in the brain tissue during effector phase iNOS inhibition as compared to control mice (**Figure S2A**).

To further confirm the role of iNOS in the infiltration of the $CD11b^+F4/80^+GR\text{-}1^-$ cells and $CD11b^+F4/80^-GR\text{-}1^+$ cells in the CNS, we induced active EAE in $iNOS^{-/-}$ mice and analyzed myeloid cell infiltration in the brain and spinal cord. Consistent with our observations with L-NAME treatment during the priming or effector phase, our results showed that deficiency of iNOS leads to reduced infiltration of $CD11b^+F4/80^+GR\text{-}1^-$ cells and increased infiltration of $CD11b^+F4/80^-GR\text{-}1^+$ cells in the brain and spinal cord, as compared to wild-type mice (**Figure S2B**). These results suggest that inhibition of NOS or a genetic deficiency of iNOS selectively promotes the neutrophilic infiltration and inhibits the infiltration of $CD11b^+F4/80^+GR\text{-}1^-$ cells in the CNS.

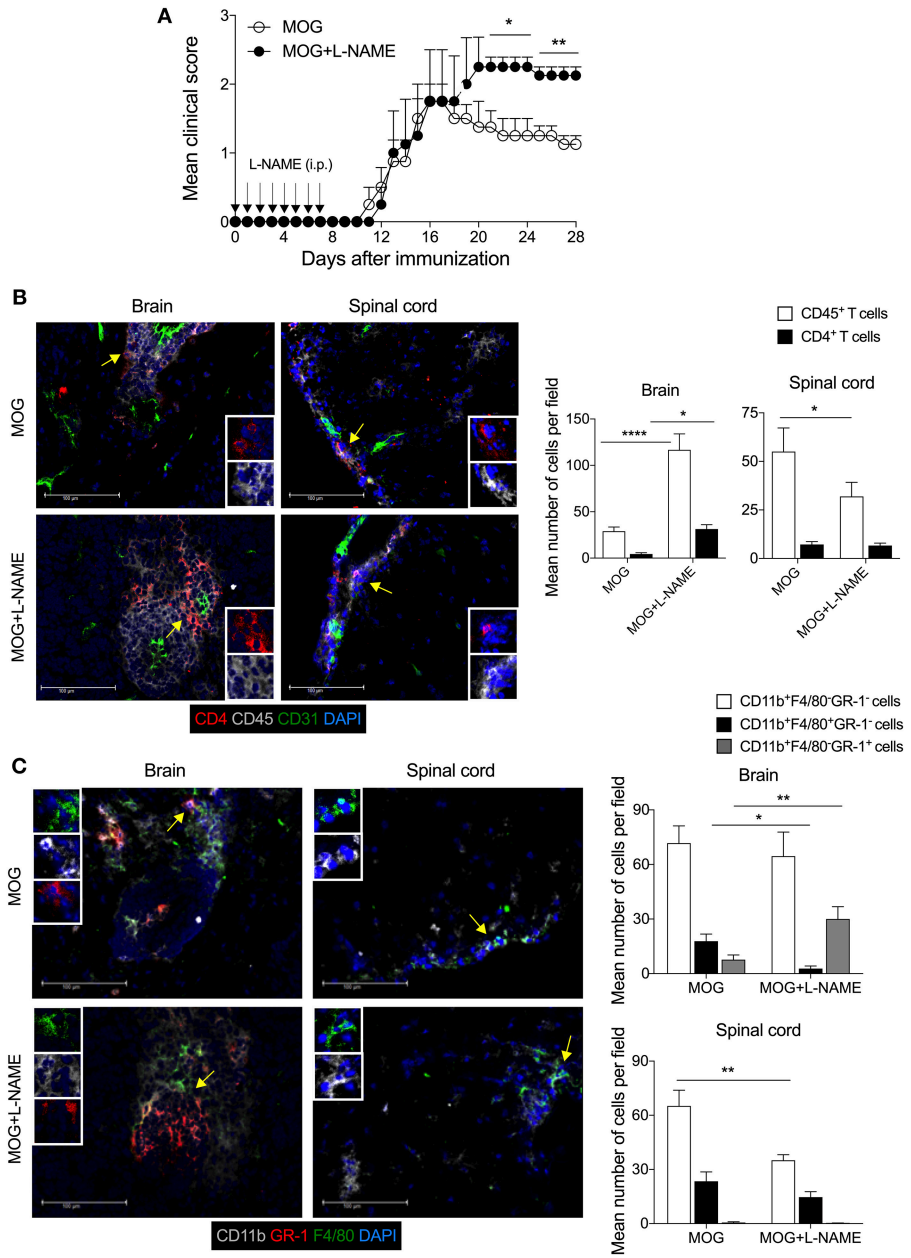

FIGURE 1 | Inhibition of iNOS during the antigen-priming phase of EAE lead to increased infiltration of myeloid cells in the brain. C57BL/6 mice were *s.c.* injected with 200 μg MOG_{35-55} (MOG) in CFA emulsion, and two doses of *i.v.* pertussis toxin (PTx, 200 ng/mouse) at day 0 and 2. Mice were administered *i.p.* with L-NAME (100 mg/kg) from day 0 to 7 daily. Control groups were given i.p. PBS. **(A)** EAE clinical score was monitored and plotted. Arrow shows the day of L-NAME injection. Error bars represent ± standard error of mean (SEM). **(B)** Mice were sacrificed on day 28, and the brain and spinal cord were analyzed by immunofluorescence staining. Representative images of CD4 (red), CD45 (gray), CD31 (green), and nuclear stain DAPI (blue) stained brain and spinal cord tissues are shown (left). The mean number of infiltrated $CD4^+$ T cells and $CD45^+$ leukocytes were quantified from at least 25–30 sections of the brain and spinal cord and plotted (right). **(C)** Representative images of the brain and spinal cord tissues stained with CD11b (gray), GR-1 (red). F4/80 (green), and nuclear stain DAPI (blue) are shown (left). The mean number of infiltrated $CD11b^+F4/80^-GR\text{-}1^-$, $CD11b^+F4/80^+GR\text{-}1^-$ and $CD11b^+F4/80^-GR\text{-}1^+$ cells from at least 25–30 sections of the brain and spinal cord are plotted (right). Error bars represent ± standard error of mean (SEM) **(A–C)**. Original magnification 400x **(B,C)**. Scale bar 100 μm **(B,C)**. $^*p < 0.05$, $^{**}p < 0.01$, $^{****}p < 0.0001$; two way ANOVA followed by Tukey's test **(B)**, Student *t*-test **(A,C)**. $n = 5$ mice/group.

Together, our results show that lack of iNOS during EAE development facilitates inflammation in both the brain and spinal cord, with enhanced inflammatory cell infiltrations specifically in the brain but not the spinal cord as compared to wild-type mice. However, differential preference observed with L-NAME-mediated inhibition of NOS during the priming versus effector phase of EAE. These results suggest that inhibition of NOS in the different stages of EAE differentially regulates the infiltration of

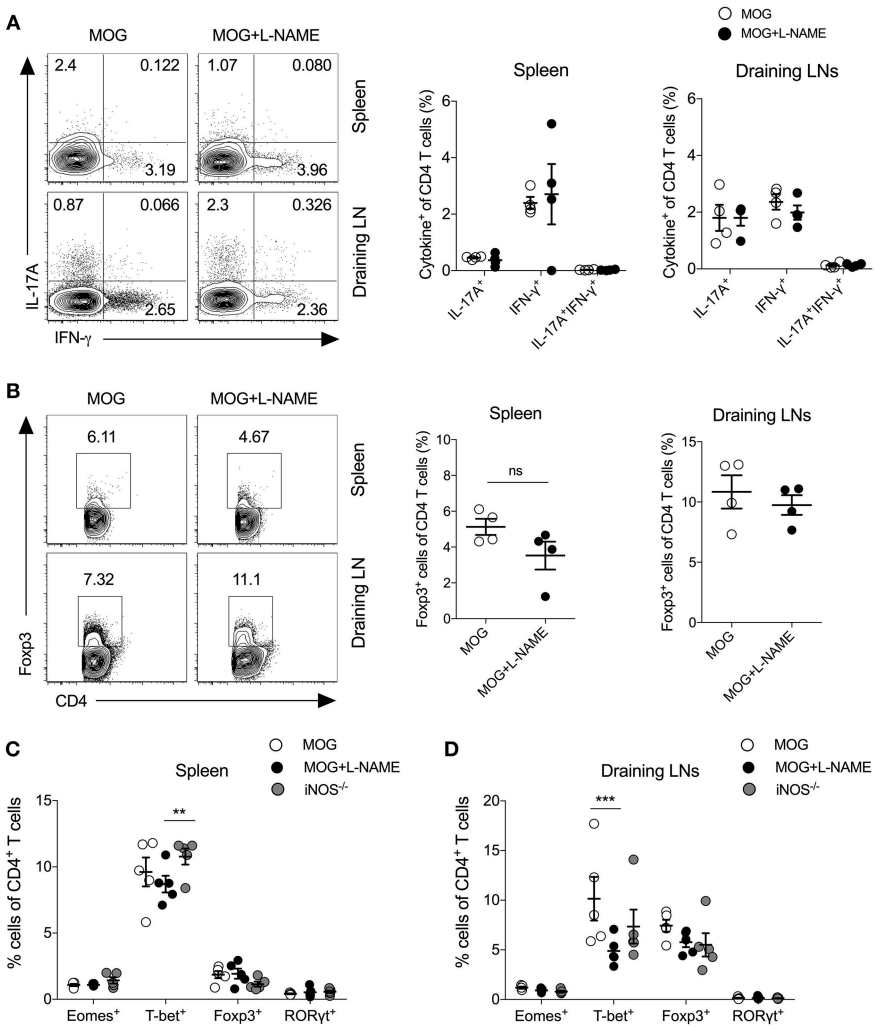

FIGURE 2 | Inhibition of iNOS during the antigen-priming phase of EAE does not affect Th1, Th17, and Tregs in the secondary lymphoid organs. Active EAE was induced as given in **Figure 1**. **(A,B)** On day 28, single cell suspensions were prepared from the spleen and draining lymph nodes. Intracellular IL-17A and IFN-γ were analyzed in the $CD4^+$ T cells using flow cytometry and plotted. **(A)** FACS plots show the intracellular expression of IL-17A and IFN-γ in the $CD4^+$ T cells (left). Quantifications of the percentage of intracellular cytokines in the $CD4^+$ T cells are shown (right). **(B)** Foxp3 expression in the $CD4^+$ T cells (left). Quantifications of $Foxp3^+CD4^+$ T cells (right). **(C,D)** C57BL/6 and $iNOS^{-/-}$ mice were *s.c.* injected with 200 μg MOG_{35-55} (MOG) in CFA emulsion, and two doses of *i.v.* pertussis toxin (PTx, 200 ng/mouse) at day 0 and 2. Mice were administered *i.p.* L-NAME (100 mg/kg) from day 0 to 7 daily. Control groups were given *i.p.* PBS. On day 8, single cell suspensions were prepared, and expression of Eomes, T-bet, Foxp3, and RORγt were analyzed in $CD4^+$ T cells. **(C)** Spleen and **(D)** draining lymph nodes were analyzed using flow cytometry and plotted. Numbers in the dot plots show the percentages of $CD4^+$ T cells **(A,B)**. Each dot represents an individual mouse, and the horizontal line denotes mean and error bars represent ± SEM **(A–D). (A–D)**. Student's *t*-test **(A,B)**, $^{**}p < 0.01$, $^{***}p < 0.001$; ANOVA followed by Tukey's test **(C,D)**. $n = 4$–5 mice/group.

effector $CD45^+$ leukocytes, $CD4^+$ T cells, $CD11b^+F4/80^-GR\text{-}1^+$ cells, and $CD11b^+F4/80^+GR1^-$ cells in the CNS, and this may, in turn, account for the severity of the disease.

Inhibition of iNOS During the Priming-Phase Reduces MHC Class II Expression on DCs and Reduces the Frequency of Monocytic-MDSCs in Secondary Lymphoid Tissues.

Myeloid cells like macrophages and dendritic cells serve as antigen presenting cells (APCs) and significant producers of iNOS, and play a crucial role in the pathogenesis of EAE (23, 24). Our result showed that EAE induced in $iNOS^{-/-}$ mice, as well as L-NAME-treated mice (day 0–7), had significantly reduced frequency of $CD11c^+I\text{-}A^{b+}$ DCs (**Figure 4A**), and significantly lower median fluorescence intensity (MFI) of the class II MHC molecule ($I\text{-}A^b$) on the DCs, as compared to control mice (**Figure 4B**). Further analysis showed that among the various subsets of DCs, the $CD11b^+CD11c^+$ and $CD11b^-CD11c^+$ subsets showed reduced expression of class II MHC in L-NAME-treated mice and $iNOS^{-/-}$ mice, as compared to control EAE mice (**Figure 4C**). L-NAME-treated and $iNOS^{-/-}$ mice also showed a reduced percentage of $CD11b^+F4/80^+$ macrophages

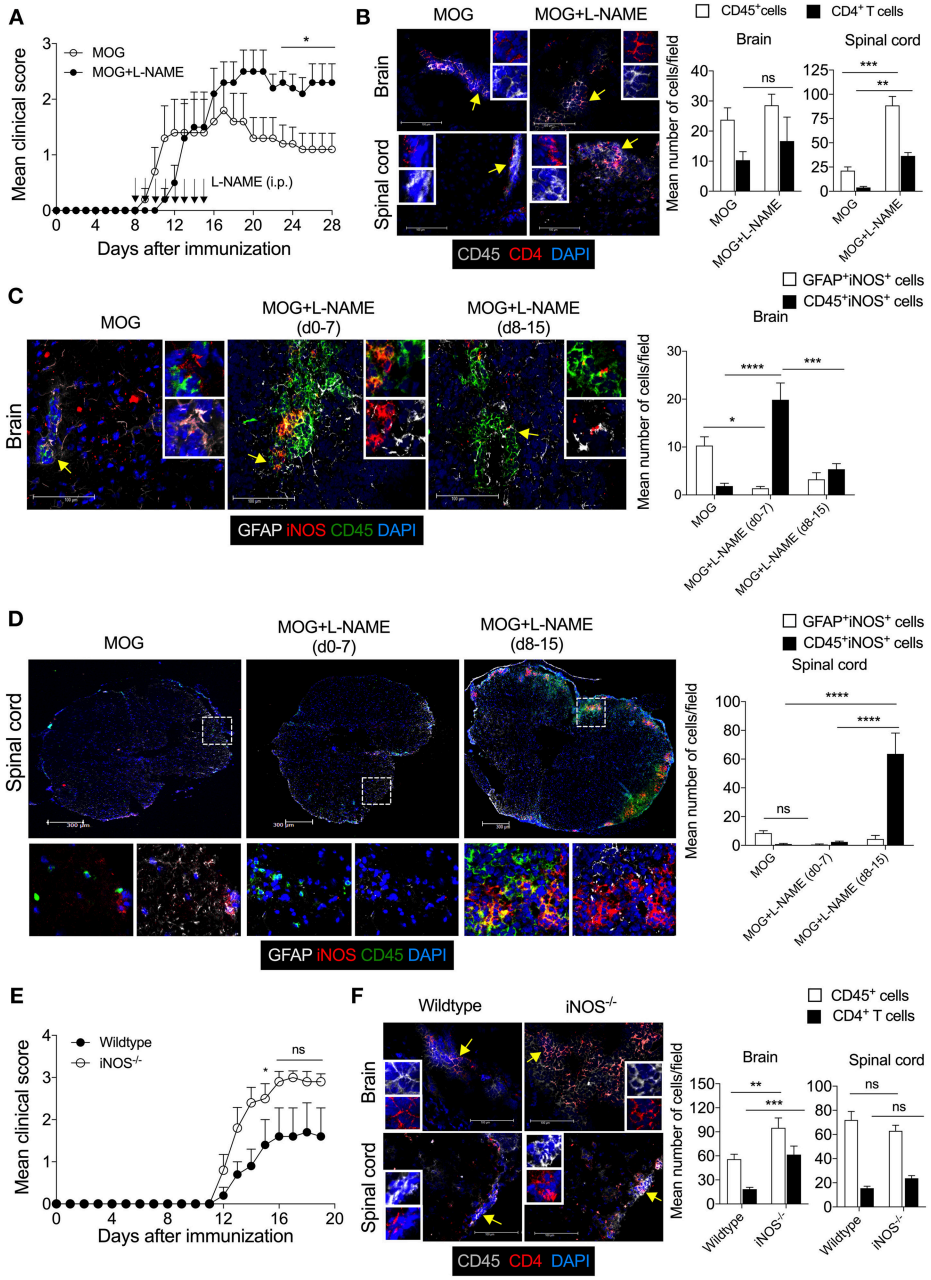

FIGURE 3 | The Inhibition of iNOS during the effector phase exacerbates inflammation in the spinal cord, leading to the development of severe EAE. Active EAE was induced as in **Figure 1**. Mice were administered *i.p.* L-NAME from day 8 to 15 daily. Control groups were given *i.p.* PBS. **(A)** EAE clinical scores were monitored and plotted. **(B)** On day 28, brain and spinal cord cryo-sections were analyzed by immunofluorescence staining. Representative images of the brain and spinal cord tissue sections stained with CD45 (gray), CD4 (red), and nuclear stain DAPI (dark blue) are shown (left). Mean numbers of infiltrating $CD45^+$ and $CD4^+$ cells from 16 to 25 images of the brain and spinal cord were quantitated and plotted (right). **(C,D)** Representative images of the **(C)** brain and **(D)** spinal cord sections stained with GFAP (gray), iNOS (red), CD45 (green), and nuclear stain DAPI (dark blue) are shown (left). Magnified images of the regions marked with the dotted square and are shown at the bottom **(D)**. Mean numbers of $GFAP^+iNOS^+$ and $CD45^+iNOS^+$ cells from 15 to 35 images of the brain and spinal cord were quantitated and plotted (right). **(E)** C57BL/6 and $iNOS^{-/-}$ mice were *s.c.* injected with 200 μg MOG_{35-55} (MOG) in CFA emulsion, and two doses of *i.v.* pertussis toxin (PTx, 200 ng/mouse) at day 0 and 2. Mice were monitored for the development of clinical symptoms of EAE and the mean clinical scores were plotted (5 mice/group). **(F)** Mice in **(E)** were sacrificed on day 20, and brain and spinal cord cryo-sections were analyzed by immunofluorescence staining. Representative images of the brain and spinal cord tissue sections stained with CD45 (gray), CD4 (red), and nuclear stain DAPI (dark blue) and analyzed are shown (left). Mean numbers of infiltrating $CD45^+$ and $CD4^+$ cells from 25 to 35 images of the brain and spinal cord were quantitated and plotted (right). Error bars represent ± SEM **(A–F)**. Original magnification 400x (Brain; **B,C,F**); 200x (spinal cord; **B,D,F**). Scale bar, 100 μm (Brain; **B,C,F**), 300 μm (spinal cord; **B,D,F**). $^*p < 0.05$, $^{**}p < 0.01$, $^{***}p < 0.001$, $^{****}p < 0.0001$; Student's *t*-test **(A,B,F)**, two way ANOVA followed by Tukey's test **(C,D)**. $n = 5$ mice/group.

in the spleen (**Figure 4D**), which may correspond to the lower infiltration of $CD11b^+F4/80^+$ cells observed in the brain of L-NAME-treated mice, as compared to untreated mice (**Figure 1C** and **Figure S2B**). L-NAME treatment did not have any effect on the MFI of $I\text{-}A^b$ on non-DCs, whereas a lack of iNOS in $iNOS^{-/-}$ mice showed a significant decrease in the MFI of $I\text{-}A^b$ on non-DCs, as compared to control mice (**Figure 4E**). The $F4/80^+CD11b^+Ly6C^{hi}Ly6G^-$ cells mainly represent Mo-MDSCs, and are potent suppressors of effector $CD4^+$ and $CD8^+$ T cells, and known to express their suppressive effect via an iNOS-dependent mechanism (38). Our results showed a significantly reduced frequency of F4/80-expressing Mo-MDSCs in the $iNOS^{-/-}$ mice spleen, and to some extent in the L-NAME-treated mice, as compared to control mice (**Figure 4F**). These results suggest that inhibition or lack of iNOS can alter the generation of $CD11b^+F4/80^+$ cells, including suppressive $F4/80^+$Mo-MDSCs and mature antigen-presenting DCs in the spleen, leading to reduced infiltration of $CD11b^+F4/80^+GR\text{-}1^-$ cells and increased infiltration of $CD11b^+F4/80^-GR\text{-}1^+$ cells in the brain.

Neutralization of IFN-γ Shows iNOS Expression and Apoptosis of $CNPase^+$ Oligodendrocytes in the CNS

IFN-γ is a potent inducer of class II MHC molecules on APCs. It can render either inflammatory or tolerogenic function to DCs, depending on the presence or absence of a Toll-like receptor (TLR) and CD40L signaling, and is essential for the development of allograft tolerance. IFN-γ is also a known inducer of iNOS in a variety of cell types, including neutrophils, monocytes, macrophages, dendritic cells, microglial cells, and astrocytes (28). The IFN-$\gamma^{-/-}$ or IFN-$\gamma R^{-/-}$ mice or antibody-mediated neutralization of IFN-γ signaling, confers hyper-susceptibility to the EAE. Similarly, our findings revealed that L-NAME-mediated inhibition of NOS in the early and effector phase of EAE causes severe EAE in wild-type mice.

Since our results showed that lack of iNOS reduced the expression of class II MHC molecule on DCs, we further investigated the link between IFN-γ and iNOS during EAE. We analyzed the influence of IFN-γ on iNOS-expression in astrocytes and CNS-infiltrated immune cells, and on apoptosis of the myelin-synthesizing cells, oligodendrocytes. For this purpose, we neutralized the IFN-γ with the anti-IFN-γ (100 μg/mouse; *i.v.*) mAb during MOG-induced active EAE. Consistent with several published reports (35, 36), our results showed exacerbation of the clinical symptoms of EAE with the neutralization of IFN-γ (**Figure 5A**). We also observed an increased infiltration of $CD45^+$ leukocytes and $CD4^+$ T cells in the brain as well as spinal cord (**Figure 5B**). Both the meninges and parenchyma showed increased infiltration of immune cells in the anti-IFN-γ-treated group, as compared to the isotype control IgG-treated mice (data not shown). While anti-IFN-γ-treated mice showed significantly low infiltration of $CD11b^+F4/80^+GR\text{-}1^-$ cells, however, the numbers of $CD11b^+F4/80^-GR\text{-}1^+$ cells were dramatically increased in the brain and spinal cord, as compared to control group (**Figure 5C**). The neutralization of IFN-γ using mAb did not induce iNOS expression in the astrocytes (**Figure 5D**). However, with anti-IFN-γ-treatment, iNOS expression was significantly induced in $CD45^+$ leukocytes in both brain and spinal cord, as compared to isotype IgG-treated control mice (**Figure 5D**), suggesting that neutralization of IFN-γ leads to the reappearance of iNOS-expression on $CD45^+$ leukocytes and possibly in microglia, similar to the effects observed with L-NAME treatment.

We then asked whether increased infiltration of $CD11b^+F4/80^-GR\text{-}1^+$ cells could have an effect on the survival of oligodendrocytes during EAE. Our results showed that during EAE, the cleaved-caspase 3 signal co-localizes with $CNPase^+$ oligodendrocytes, suggesting that they are undergoing apoptosis (**Figure 5E**). The anti-IFN-γ-treated mice showed significantly higher co-localization of cleaved-caspase 3 with $CNPase^+$ oligodendrocytes in the brain, as compared to the isotype control group (**Figure 5E**), suggesting that the neutralization of IFN-γ signaling lead to increased apoptosis of oligodendrocytes during EAE. Furthermore, treatment with anti-IFN-γ mAb increased the infiltration of effector $CD4^+$ T cells, $CD11b^+F4/80^-GR\text{-}1^+$ cells, and iNOS-expressing inflammatory immune cells, and reduced infiltration of suppressive $CD11b^+F4/80^+$ cells (includes F4/80-expressing suppressive Mo-MDSCs) in the CNS. These could have contributed to increased oligodendrocyte and neuronal damage, consequently exacerbating the EAE pathology.

DISCUSSION

In the present study, we show that iNOS critically regulates neuroinflammation at different phases of EAE by controlling the infiltration of immune cells in the brain and spinal cord. Inhibition of iNOS in the antigen-priming phase or effector phase of EAE exacerbates the symptoms of the disease via selectively increasing the infiltration of inflammatory $CD11b^+F4/80^-GR\text{-}1^+$ cells, while at the same time reducing the infiltration of $CD11b^+F4/80^+GR\text{-}1^-$ cells in the brain and spinal cord, respectively. Similarly, with anti-IFN-γ mAb treatment, we showed differential infiltration of $CD11b^+F4/80^+GR\text{-}1^-$ and $CD11b^+F4/80^-GR\text{-}1^+$ cells in the CNS during EAE. Furthermore, lack of iNOS or neutralization of IFN-γ promoted the infiltration of $CD11b^+F4/80^-GR\text{-}1^+$ cells in the brain or spinal cord and enhanced the inflammation and apoptosis of $CNPase^+$ oligodendrocytes.

Compelling evidence has suggested that various types of myeloid cells do infiltrate into inflamed CNS along with myelin-reactive Th1 and Th17 cells (40). These cells contribute to the various inflammatory pathways leading to demyelination and axonal damage in the CNS. iNOS controls the function of a variety of myeloid and lymphoid cell populations in both a cell-intrinsic and extrinsic manner (41). iNOS is also critically involved in the pathogenesis of EAE and MS (17). However, how it affects neuroinflammation in the various phases of EAE was not clear. In the present work, we showed that inhibition of iNOS during the antigen-priming phase leads to a selectively increased infiltration of $CD45^+$ leukocytes and $CD4^+$ T cells selectively in the brain but not in the spinal cord. Together with

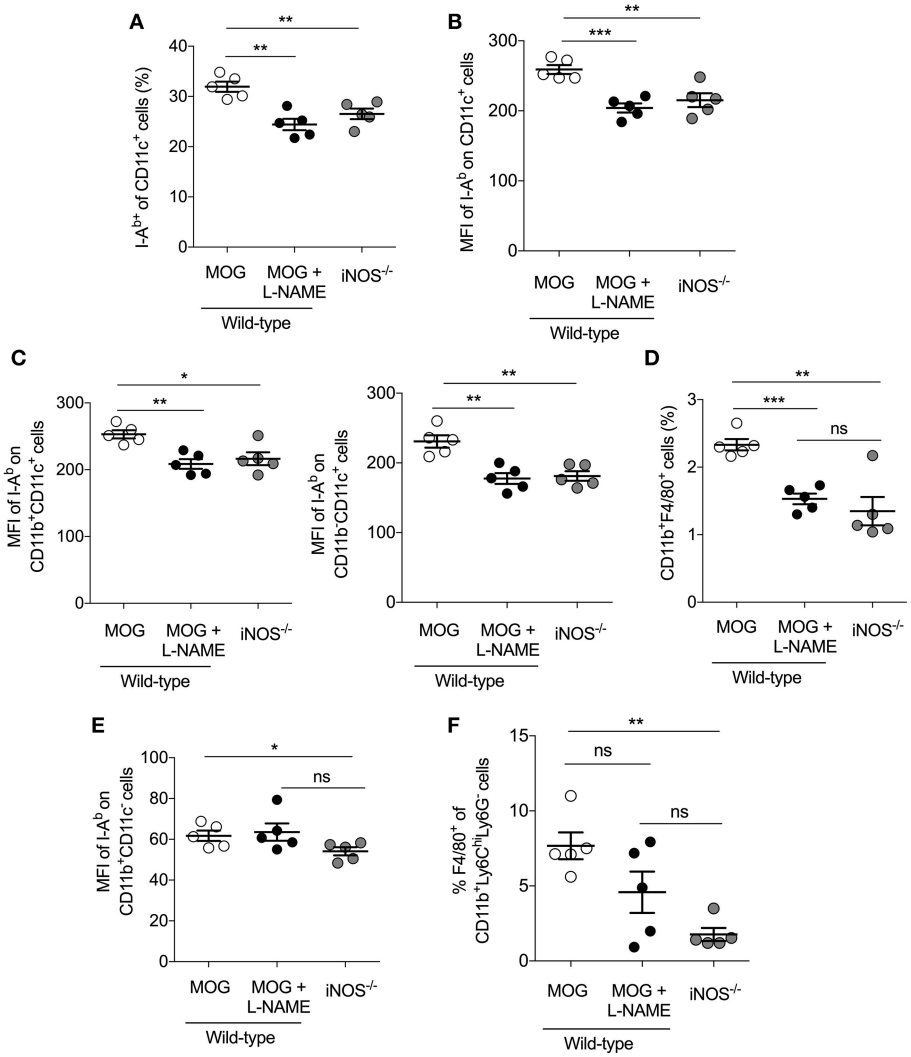

FIGURE 4 | Inhibition of iNOS in the priming phase inhibits MHC class II expression on DCs and reduces the frequency of monocytic-MDSCs in the secondary lymphoid tissues. C57BL/6 and iNOS$^{-/-}$mice were *s.c.* injected with 200 μg MOG_{35-55} (MOG) in CFA emulsion, and two doses of *i.v.* pertussis toxin (PTx, 200 ng/mouse) at day 0 and 2. Mice were administered *i.p.* with L-NAME (100 mg/kg) from day 0 to 7 daily. Control groups were given *i.p.* PBS. On day 8, single cell suspensions were prepared, and myeloid cell populations in the secondary lymphoid organs were analyzed using flow cytometry. **(A)** The percentages of I-A^{b+}CD11c^{+} cells and **(B)** mean fluorescence intensity (MFI) of I-A^{b} expression on CD11c^{+} cells are shown **(C)** The MFI of I-A^{b} on CD11b^{+}CD11c^{+}, CD11b^{-}CD11c^{+} and CD11b^{-}CD11c^{+} myeloid cells were quantitated and plotted. **(D)** Data show the percentage of CD11b^{+}F4/80^{+} cells in the spleen. **(E)** The MFI of I-A^{b} on CD11b^{+}CD11c^{-} cells were analyzed and plotted. **(F)** The percentage of F4/80^{+} of CD11b^{+}Ly6C^{hi}Ly6G^{-} cells in the spleen were analyzed and plotted. Each dot represents an individual mouse, and the horizontal line denotes mean and error bars represent ± SEM. **(A–F)**. Student's *t*-test **(A–F)**. $^{*}p < 0.05$, $^{**}p < 0.01$, $^{***}p < 0.001$; $n = 5$ mice/group.

data from iNOS$^{-/-}$ mice, our results suggest that a lack of iNOS in the priming phase induces inflammation in the secondary lymphoid organs in a manner that causes pathogenic cells to be mobilized into the brain. The molecular details of trafficking of these cells across the blood-brain barrier to CNS and the effect of iNOS and possibly other isoform of NOS, such as eNOS in their transmigration need further investigation. Previous studies have shown that while iNOS does not affect the differentiation of Th1, Th2 and Tregs, it does influence Th17 differentiation (31). However, studies on the mechanism through which iNOS and NO influence Th17 differentiation have yielded mixed results. Studies in mice have revealed that this inhibitory function of endogenous iNOS is via the nitration of tyrosine residues in RORγt, and the inhibition of aryl hydrocarbon receptor (Ahr)-signaling (31, 42). However, others have reported that iNOS and NO support human Th17 differentiation via the cyclic guanosine monophosphate (cGMP)-dependent protein kinase pathway, and endogenous iNOS play an essential role in the stability of human Th17 cells when differentiated in the presence of IL-1β, IL-6, and IL-23 (43). Our data show that inhibition of NOS or genetic deficiency of iNOS neither affect the generation of pathogenic Th1, Th17 cells, and Foxp3^{+} regulatory CD4^{+} T

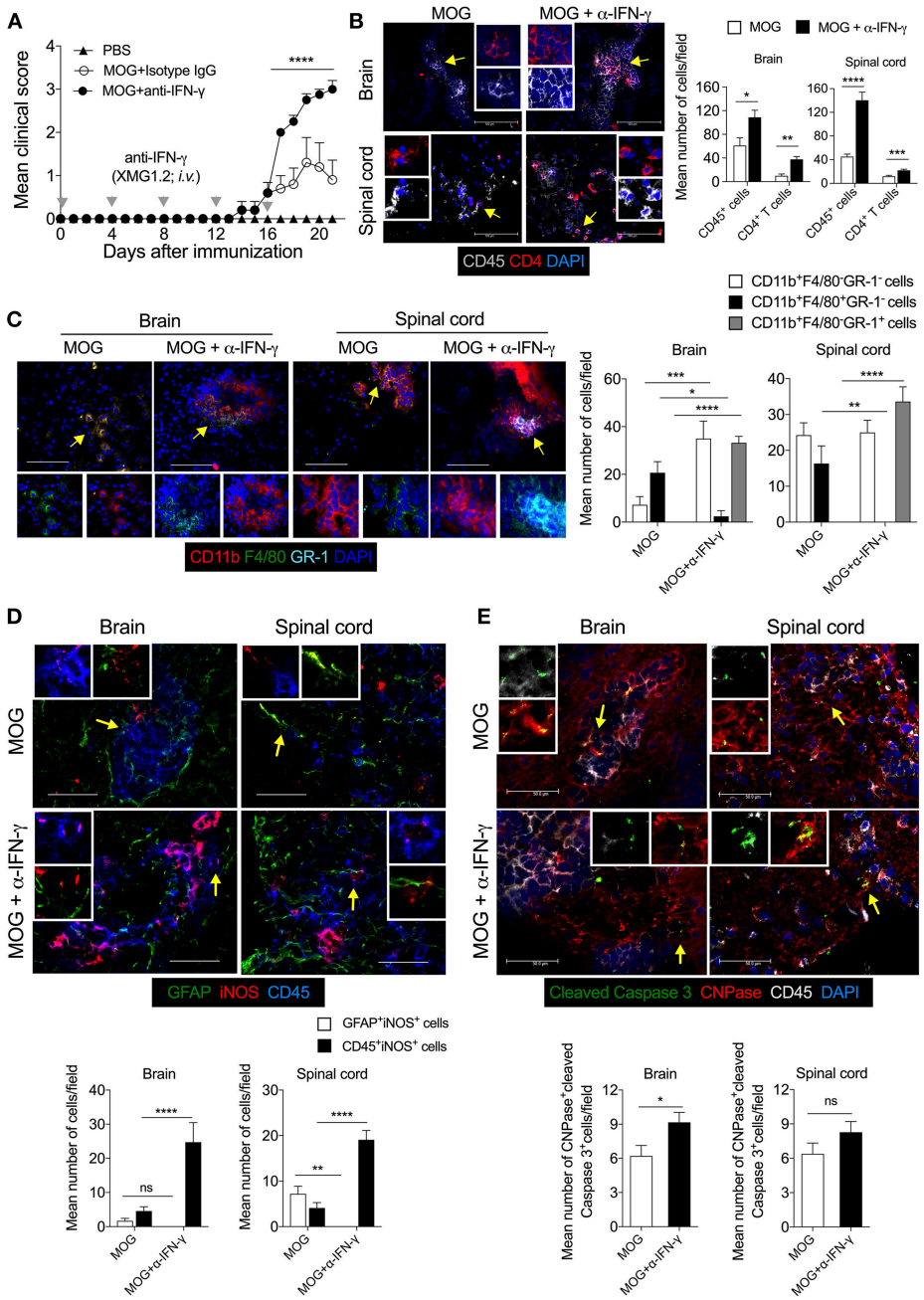

FIGURE 5 | Neutralization of IFN-γ induces the expression of iNOS in the effector immune cells and results in apoptosis of CNPase$^+$ oligodendrocytes in EAE. Active EAE was induced in C57BL/6 mice. Anti-IFN-γ monoclonal antibody (XMG1.2, 100 μg/mouse) monoclonal antibody was *i.v.* injected at days 0, 4, 8, 12, 16 after MOG-immunization. **(A)** The clinical symptoms of EAE were recorded and mean clinical scores are plotted (5 mice/group). **(B)** On day 21, the brain and spinal cord cryo-sections were analyzed by immunofluorescence staining. Representative images of the brain and spinal cord tissue sections stained with CD45 (gray), CD4 (red), and nuclear stain DAPI (dark blue) are shown (left). Mean numbers of infiltrating CD45$^+$ and CD4$^+$ cells from 25 to 35 images of the brain and spinal cord were quantitated and plotted (right). **(C)** Representative images of the brain and spinal cord stained with CD11b (red), F4/80 (green), GR-1 (light blue), and nuclear stain DAPI (dark blue) are shown (left). Infiltration by indicated cell populations was quantified and plotted (right). **(D)** Representative images stained with GFAP (green), iNOS (red) and CD45 (blue) are shown (left). iNOS-expressing GFAF$^+$ cells and CD45$^+$ cells were quantified from 20 to 30 images of the brain and spinal cord and plotted as mean number of cells/field (right). **(E)** Representative images stained for cleaved caspase 3 (green), CNPase (red), CD45 (gray), and DAPI (blue) are shown (left). Cleaved-caspase 3 expressing CNPase$^+$ cells oligodendrocytes were quantified from 20 to 30 images of the brain and spinal cord and plotted as mean number of cells/field (right). Regions marked with white dotted square **(D,E)** are shown as magnified images at the right. Error bars represent ± SEM **(A–E)**. Original magnification 200x (**B**, spinal cord), 400x (**B**, brain**)** and **(C)**, 630x **(D,E)**. Scale bar 50 μm **(D,E)**, 100 μm (**B**, brain) and **(C)** and 300 μm (**B**, spinal cord). *$p < 0.05$, **$p < 0.01$, ***$p < 0.001$, ****$p < 0.0001$, ANOVA followed by Tukey's test **(A)**, ANOVA followed by Sidak's test **(C)**, Student's *t*-test **(B,D,E)**. $n = 5$ mice/group.

cells nor IFN-γ and IL-17A-expressing γδ T cells in the secondary lymphoid organs.

iNOS regulates the generation and function of regulatory DCs that control the effector function of $CD4^+$ and $CD8^+$ T cells, and helps in amelioration of EAE (23–25). $CD11b^+F4/80^+$ cells and F4/80-expressing Mo-MDSCs are known to have a regulatory role in EAE (38). We show that a lack of iNOS function in the priming-phase results in a significant reduction in the frequency of $CD11b^+F4/80^+$ cells as well as F4/80-expressing Mo-MDSCs in the spleen. L-NAME-treatment or lack of iNOS in mice yielded significantly lower infiltration of these cells in the inflamed CNS. In contrast, lack of iNOS significantly increased the previously reported pathogenic $CD11b^+F4/80^-GR\text{-}1^+$ cells in the brain (39). In contrast, inhibition of iNOS in the effector phase of EAE, when ongoing inflammation in the CNS causes demyelination and axonal damage, resulted in higher infiltration of $CD4^+$ T cells and $CD11b^+F4/80^-GR\text{-}1^+$ cells preferentially in the spinal cord, but not in the brain. These results suggest that temporal inhibition of iNOS during EAE modulates differential clinical pathology in the brain and spinal cord. iNOS inhibition during the antigen-priming phase of EAE showed a high frequency of iNOS-expressing $CD45^+$ leukocytes selectively in the brain, but not in the spinal cord. Since CNS-resident microglia express iNOS under inflammation and microglia are also characterized by $CD45^{int}$ expression, our study cannot exclude the potential role of iNOS-expressing microglia in exacerbation of EAE symptoms. Instead, this further opens the avenue to investigate the relative functions of iNOS-expressing microglia and circulation-derived macrophages in the early and late phases of neuroinflammation during EAE. The $GFAP^+$ astrocytes are also an important source of iNOS-expression during neuroinflammation (16). We also observed higher iNOS-expressing astrocytes in the brain and spinal cord in EAE mice. However, inhibition of iNOS in the priming phase selectively reduced the frequency of iNOS-expressing $GFAP^+$ astrocytes in the brain, whereas it was mostly unaffected upon inhibition of iNOS during the effector phase.

IFN-γ is the upstream regulator of iNOS expression in a variety of myeloid and lymphoid cells, and cells of non-hematopoietic lineages (9, 12). The neutralization of IFN-γ using anti-IFN-γ mAb during EAE in mice have been observed to result in more severe symptoms and pathology (44). IFN-γ is a known suppressor of Groα/KC (CXCL1) (45) and MIP-2 (CXCL2) (46), both being neutrophil chemoattractants that recruit neutrophils to the site of inflammation (47). In the absence of IFN-γ signaling, Th17 cells predominate infiltrate into the CNS, and predominantly recruit neutrophils in the CNS (48, 49), possibly via CXCL1- and CXCL2-mediated neutrophil chemoattraction. Neutralization of IFN-γ therefore promotes neutrophil trafficking to the inflamed CNS. Consequently, we reasoned that a lack of iNOS function during anti-IFN-γ treatment (12) may contribute for bias differentiation of $CD11b^+F4/80^+$ cells and F4/80-expressing Mo-MDSCs in the lymphoid organs, and infiltration of these cells in CNS may cause severe EAE. However, we also observed an increase in the expression of iNOS in the CNS-infiltrating immune cells and possibly $CD45^{int}$ microglia in anti-IFN-γ-treated mice, suggesting that in the absence of IFN-γ, some other factors can also induce the expression of iNOS in the inflamed CNS (50). Furthermore, the enhanced expression of iNOS in the CNS infiltrating immune cells was associated with increased apoptosis of myelin-synthesizing oligodendrocytes in anti-IFN-γ-treated mice, suggesting that high level of iNOS produced by inflammatory CNS infiltrates can affect the remyelination process and contribute to severity of the disease. A study with cuprizone-induced demyelination model reported that infiltration and the inflammatory function of $CXCR2^+$ neutrophils are required to induce oligodendrocyte damage and demyelination in addition to the toxic effect of cuprizone on mitochondrial function (51). The increased apoptosis of $CNPase^+$ oligodendrocytes in anti-IFN-γ treated mice, might be in part due to increased neutrophilic infiltration in the CNS. A similar pathological mechanism may exist in iNOS-deficient, or L-NAME treated wild-type mice and warrants further investigation. We showed that MOG-induced inflammation caused the induction of iNOS-expression in the astrocytes, and that anti-IFN-γ treatment completely inhibits the iNOS expression in astrocytes. The numbers of iNOS-expressing astrocytes and the iNOS produced by them have different consequences. While low levels of iNOS or NO are beneficial, and their sustained high levels are detrimental to the CNS homeostasis (52). Therefore, the high levels of iNOS produced in the anti-IFN-γ recipients in our studies might have caused apoptosis of oligodendrocytes in the brain, and thus contributed to increased the clinical severity of the EAE. In conclusion, we have shown here that immunoregulatory role of iNOS safeguards the brain and spinal cord from inflammatory granulocytic infiltration during the antigen-priming and effector phase of EAE, respectively.

MATERIALS AND METHODS

Mice

Wild-type C57BL/6 and $iNOS^{-/-}$ (B6.129P2-*Nos2*^{tm1Lau}/J) mice were obtained from The Jackson Laboratory (Bar Harbor, ME). Mice were maintained and bred in the Experimental Animal Facility of the National Centre for Cell Science (NCCS), Pune, India. All mice experiments were performed with the protocols approved by the Institutional Animal Ethics Committee. (Project Id: EAF/2016/B-257).

Antibodies and Reagents

Alexa Fluor 488-CD4 (GK1.5), APC-eFluor 780-CD4 (GK1.5), FITC-γδTCR (GL3), APC-γδTCR (GL3), APC-CD45 (30F-11), FITC-F4/80 (BM8), APC-Cy7-F4/80 (BM8), FITC-Ly6G (1A8), Alexa Fluor 647-Ly6C (HK1.4), biotin-CD11b (M1/70), APC-GR-1 (RB6-8C5), PE-GM-CSF (MP1-22E9), Brilliant violet 421-IL-17A (TC11-18H10.1), and purified anti-mouse GFAP (MCA-5C10) were purchased from BioLegend (San Diego, CA). Biotin-CD11c (N418), PE/Cy7-IFN-γ (XMG1.2), Pacific blue-Foxp3 (FJK-16s), PE-Foxp3 (MF-14), PE-Eomes (Dan11mag), eFluor 450-IA^b (AF6-1201) were obtained from eBioscience (San Diego, CA). Purified anti-IFN-γ (XMG1.2), and rat IgG2b, k isotype control (LTF-2) were purchased from BioXcell (West Lebanon, NH). PE-Cy7-CD11b (M1/70) antibody was from BD Biosciences (San Diego, CA). Purified anti-iNOS antibody (EPR16635) was purchased from Abcam (Cambridge,

MA). Purified cleaved caspase 3 (5A1E) and purified anti-CNPase (D83E10) was obtained from Cell Signaling Technology (Danvers, MA). *N*-ω-nitro-l-arginine methyl ester (L-NAME) was purchased from MP Biomedicals (Santa Ana, CA).

Induction of Active EAE

Wild-type C57BL/6 or iNOS$^{-/-}$ mice were given subcutaneous (*s.c.*) injections of an emulsion of MOG_{35-55} (MOG) (200 μg/mouse) in complete Freund's adjuvant (CFA) containing *Mycobacterium tuberculosis H37Ra* (5 mg/ml), and also given intravenous injections (*i.v.*) of pertussis toxin (PTx, 200 ng/mouse) at day 0 and 2. L-NAME was administered intraperitoneally (i.p. 100 mg/kg) daily from day 0 to 7 (priming phase) or day 8 to 15 (effector phase). Control animals received *i.p.* injections of PBS. For the neutralization of IFN-γ, animals were given anti-mouse IFN-γ mAb (clone XMG1.2; 100 μg/mouse) *i.v.* on days 0, 4, 8, 12, and 16. The animals that received isotype control IgG were used as a controls. Mice were followed for the development of clinical signs of EAE. Scoring of clinical symptoms was performed as follows; score 0, no symptoms; 1, limp tail or hind limb weakness but not both; 2, limp tail and hind limb weakness; 3, partial hind limb paralysis; 4, complete hind limb paralysis; and 5, death by EAE.

Immunofluorescence Staining of the Brain and Spinal Cord

Mice were sacrificed, ice-cold PBS was transcardially perfused, and the brain and spinal cord were harvested. The tissues were immediately snap-frozen in OCT compound (Sakura Finetek, Torrance, CA). Seven-micrometer-thick cryosections were prepared using a cryomicrotome. Sections were fixed with chilled acetone for 5 min, air dried, followed by washing with PBS. The tissue sections were blocked with 10% horse serum (Jackson ImmunoResearch, West Grove, PA) in PBS at room temperature (RT) for 30 min, followed by washing thrice with ice-cold PBS. The sections were incubated with primary antibodies overnight (12–14 h) at 4°C, washed, further incubated with secondary antibodies at RT for 60 min, and then washed five times with PBS. The sections were stained with nuclear stain DAPI at RT for 5 min and washed twice with ice-cold PBS. Sections were mounted in mounting medium (Electron Microscopy Sciences, Hatfield, PA). Images were acquired on a Leica DMI6000 inverted fluorescent microscope (Leica Microsystems, Germany) at 100, 400, and 630x magnifications. Images were analyzed using Leica MMAF (Leica) or Image J software (National Institute of Health, Bethesda, MD).

The quantification of cells from microscopic images was performed using the MMAF software (Leica Microsystems, Germany). The single channel and multi-channel overlay images of sufficient magnification (original magnification, 400x) were used for quantification of the number of cells. At least 10 different microscopic fields per organ and more than three mice/group were analyzed. Each cell was analyzed for its cellular morphology, nuclear staining with DAPI, and specific markers. For evaluating cellular infiltration into the CNS, complete brain tissues sections were used.

Flow Cytometry

Cells were harvested from spleen and draining lymph nodes of the mice. RBCs were lysed using ACK lysis buffer, and single cell suspensions were prepared. Cells were surface-stained with PE/Cy7-anti-mouse CD11b, PE/Cy5-anti-mouse CD11c, Alexa fluor 647-anti-mouse Ly6C, FITC-anti-mouse Ly6G, APC/Cy7-anti-mouse F4/80 and pacific blue-anti-mouse I-Ab (MHC class II) antibodies. Cells were incubated on ice in the dark for 30 min, washed with ice-cold PBS, and fixed with 1% paraformaldehyde. Cells were acquired on FACS Canto-II (BD Biosciences), and data were analyzed using the FlowJo software.

Intracellular Cytokine Staining

Single cell suspensions were prepared from spleen and draining lymph nodes of mice. For transcription factor analysis, 1×10^6 cells were stained for the surface molecules CD4 and γδ TCR on ice for 30 min and washed with ice-cold PBS. Cells were subjected to fixation, and permeabilization with the Foxp3 fixation/permeabilization buffer kit (Biolegend), and intracellular staining for Foxp3, T-bet, RORγt, and Eomes was performed as per the manufacturer's instructions. For intracellular cytokine analysis, cells (6×10^6 cells/well) were stimulated with phorbol myristate acetate (PMA; 50 ng/ml) and ionomycin (850 ng/ml) in the presence of brefeldin-A (5 μg/ml) and monensin (2 μM) in 500 μl/well complete RPMI 1,640 medium in 24-well plates at 37°C in a humidified 5% CO_2 incubator for 6 hours. Cells were collected, washed with PBS, and stained for the surface molecules CD4 and γδ TCR on ice for 30 min, and washed with ice-cold PBS. Cells were subjected to fixation and permeabilization using the Foxp3 fixation/permeabilization buffer kit (Biolegend) and intracellular staining for IL-17A, Foxp3, Eomes, and IFN-γ was performed as per the manufacturer's instructions. Cells were acquired on FACS Canto II (BD Bioscience), and data were analyzed using the FlowJo software.

Statistical Analysis

Statistical comparisons were performed using the GraphPad Prism 6 software (GraphPad, San Diego, CA). Unpaired two-tailed Student's *t*-test was used to compare two variables. The ANOVA test was used to compare the means of more than two groups followed by appropriate multiple comparison tests. The other statistical methods used are described in the figure legends. A $p < 0.05$ was considered statistically significant.

ETHICS STATEMENT

All mice experiments were performed with the approved protocols from the NCCS Institutional Animal Ethics Committee (Project Id: EAF/2016/B-257).

AUTHOR CONTRIBUTIONS

SAS and GL designed the experiments, analyzed the data, and wrote the manuscript. SAS performed all the experiments.

ACKNOWLEDGMENTS

We thank Dr. Ramanamurthy Boppana and Dr. Rahul Bankar for help with animal experiments. We also thank Dr. Jyoti Rao for critical suggestions and edits. SAS received senior research fellowship from the Council of Scientific and Industrial Research, Government of India. GL received NCCS intramural funding and grants from the Department of Biotechnology, (Grants numbers, BT/PR4610/MED/30/720/2012, BT/PR15533/MED/30/1616/2015; BT/PR14156/BRB/10/1515/2016), Science and Engineering Research Board (EMR/2016/007108), Ministry of Science and Technology, Government of India.

SUPPLEMENTARY MATERIAL

The Supplementary Material for this article can be found online at: https://www.frontiersin.org/articles/10.3389/fimmu.2019.00710/full#supplementary-material

Figure S1 | Inhibition of iNOS or lack of iNOS does not affect the generation of Th1, Th17, and Tregs in the secondary lymphoid organs. **(A)** EAE was induced in C57/BL/6 mice as shown in **Figure 1A**. The intracellular expression of IL-17A and IFN-γ in the γδ T cells of the spleen and draining lymph nodes of the mice was monitored and plotted (left). The dot plot shown is gated on γδ T cells. Quantifications of the percentage of intracellular cytokines in the γδ T cells are shown (right). **(B,C)** C57BL/6 and iNOS$^{-/-}$mice were *s.c.* injected with 200 μg MOG_{35-55} (MOG) in CFA emulsion, and two doses of *i.v.* pertussis toxin (PTx, 200 ng/mouse) at day 0 and 2. Mice were administered *i.p.* L-NAME from day 0 to 7 daily. Control groups were given PBS. On the day 8, single cell suspensions were prepared from spleen and draining lymph nodes, and expression of the transcription factors, Eomes, Foxp3, RORγt, and T-bet in CD4$^+$ T cells from the **(B)** spleen and **(C)** draining lymph nodes were analyzed using flow cytometry. Dot plots show the expression of the indicated transcription factors in CD4$^+$ T cells. Numbers in the dot plots show percentage of indicated molecules in γδ T cells **(A)** and CD4$^+$ T cells **(B,C)**. The horizontal line denotes mean and error bars represents ± SEM **(A)**. Student's *t*-test **(A)**. $n = 4$ mice/group **(A)** and 5 mice/group **(B)**.

Figure S2 | Inhibition of iNOS or its deficiency differentially regulates the infiltration of myeloid cells in the CNS. The brain and spinal cord tissue sections of mice from **Figures 3A,E** were stained with CD11b (red), F4/80 (green), GR-1 (light blue) and nuclear stain DAPI (dark blue). **(A)** Representative images of the brain and spinal cord of mice either untreated or treated with L-NAME in the effector phase of EAE are shown (upper). Magnified views of the areas marked with the dotted squares are shown next to the images. The mean number of infiltrated CD11b$^+$F4/80$^-$GR-1$^-$, CD11b$^+$F4/80$^+$GR-1$^-$ and CD11b$^+$F4/80$^-$GR-1$^+$ cells from at least 11–14 fields of the brain and spinal cord sections were quantitated and shown (lower). **(B)** Representative images of the brain and spinal cord sections of wild-type and iNOS$^{-/-}$ mice with EAE at day 20 are shown (upper). Magnified views of the areas marked with the dotted squares are shown next to the images. The mean numbers of infiltrated CD11b$^+$F4/80$^-$GR-1$^-$, CD11b$^+$F4/80$^+$GR-1$^-$ and CD11b$^+$F4/80$^-$GR-1$^+$ cells from at least 19–29 fields of the brain and spinal cord were quantitated and shown (lower). Original magnification, 400x **(A,B)**. Scale bar, 100 μm **(A,B)**. $^*p < 0.05$, $^{**}p < 0.01$, $^{***}p < 0.001$, $^{****}p < 0.0001$. Student's *t*-test **(A,B)**. Error bars represents ± SEM **(A,B)**. $n = 5$ mice/group.

REFERENCES

1. Moncada S, Higgs EA. Molecular mechanisms and therapeutic strategies related to nitric oxide. *FASEB J.* (1995) 9:1319–30. doi: 10.1096/fasebj.9.13.7557022
2. Knowles RG, Moncada S. Nitric oxide synthases in mammals. *Biochem J.* (1994) 298 (Pt 2):249–58. doi: 10.1042/bj2980249
3. Nathan C, Xie QW. Nitric oxide synthases: roles, tolls, and controls. *Cell.* (1994) 78:915–8. doi: 10.1016/0092-8674(94)90266-6
4. Fukuto JM, Chaudhuri G. Inhibition of constitutive and inducible nitric oxide synthase: potential selective inhibition. *Ann Rev Pharmacol Toxicol.* (1995) 35:165–94. doi: 10.1146/annurev.pa.35.040195.001121
5. Niu X, Zhao L, Li X, Xue Y, Wang B, Lv Z, et al. beta3-Adrenoreceptor stimulation protects against myocardial infarction injury via eNOS and nNOS activation. *PLoS ONE.* (2014) 9:e98713. doi: 10.1371/journal.pone.0098713
6. Saini R, Patel S, Saluja R, Sahasrabuddhe AA, Singh MP, Habib S, et al. Nitric oxide synthase localization in the rat neutrophils: immunocytochemical, molecular, and biochemical studies. *J Leukoc Biol.* (2006) 79:519–28. doi: 10.1189/jlb.0605320
7. Sheng W, Zong Y, Mohammad A, Ajit D, Cui J, Han D, et al. Pro-inflammatory cytokines and lipopolysaccharide induce changes in cell morphology, and upregulation of ERK1/2, iNOS and sPLA(2)-IIA expression in astrocytes and microglia. *J Neuroinf.* (2011) 8:121. doi: 10.1186/1742-2094-8-121
8. Eberhardt W, Pluss C, Hummel R, Pfeilschifter J. Molecular mechanisms of inducible nitric oxide synthase gene expression by IL-1beta and cAMP in rat mesangial cells. *J Immunol.* (1998) 160:4961–9.
9. Jaramillo M, Gowda DC, Radzioch D, Olivier M. Hemozoin increases IFN-gamma-inducible macrophage nitric oxide generation through extracellular signal-regulated kinase- and NF-kappa B-dependent pathways. *J Immunol.* (2003) 171:4243–53. doi: 10.4049/jimmunol.171.8.4243
10. Li W, Xia J, Sun GY. Cytokine induction of iNOS and sPLA2 in immortalized astrocytes (DITNC): response to genistein and pyrrolidine dithiocarbamate. *J Interferon Cytokine Res.* (1999) 19:121–7. doi: 10.1089/107999099314261
11. Heneka MT, Feinstein DL. Expression and function of inducible nitric oxide synthase in neurons. *J Neuroimmunol.* (2001) 114:8–18. doi: 10.1016/S0165-5728(01)00246-6
12. Willenborg DO, Staykova M, Fordham S, O'Brien N, Linares D. The contribution of nitric oxide and interferon gamma to the regulation of the neuro-inflammation in experimental autoimmune encephalomyelitis. *J Neuroimmunol.* (2007) 191:16–25. doi: 10.1016/j.jneuroim.2007.09.007
13. Danilov AI, Andersson M, Bavand N, Wiklund NP, Olsson T, Brundin L. Nitric oxide metabolite determinations reveal continuous inflammation in multiple sclerosis. *J Neuroimmunol.* (2003) 136:112–8. doi: 10.1016/S0165-5728(02)00464-2
14. Smith KJ, Lassmann H. The role of nitric oxide in multiple sclerosis. *Lancet Neurol.* (2002) 1:232–41. doi: 10.1016/S1474-4422(02)00102-3
15. Calabrese V, Scapagnini G, Ravagna A, Bella R, Foresti R, Bates TE, et al. Nitric oxide synthase is present in the cerebrospinal fluid of patients with active multiple sclerosis and is associated with increases in cerebrospinal fluid protein nitrotyrosine and S-nitrosothiols and with changes in glutathione levels. *J Neurosci Res.* (2002) 70:580–7. doi: 10.1002/jnr.10408
16. Ghasemi M, Fatemi A. Pathologic role of glial nitric oxide in adult and pediatric neuroinflammatory diseases. *Neurosci Biobehav Rev.* (2014) 45:168–82. doi: 10.1016/j.neubiorev.2014.06.002
17. Okuda Y, Nakatsuji Y, Fujimura H, Esumi H, Ogura T, Yanagihara T, et al. Expression of the inducible isoform of nitric oxide synthase in the central nervous system of mice correlates with the severity of actively induced experimental allergic encephalomyelitis. *J Neuroimmunol.* (1995) 62:103–12. doi: 10.1016/0165-5728(95)00114-H
18. Tran EH, Hardin-Pouzet H, Verge G, Owens T. Astrocytes and microglia express inducible nitric oxide synthase in mice with experimental allergic encephalomyelitis. *J Neuroimmunol.* (1997) 74:121–9. doi: 10.1016/S0165-5728(96)00215-9
19. Cross AH, Manning PT, Stern MK, Misko TP. Evidence for the production of peroxynitrite in inflammatory CNS demyelination. *J Neuroimmunol.* (1997) 80:121–30. doi: 10.1016/S0165-5728(97)00145-8
20. Cross AH, San M, Stern MK, Keeling RM, Salvemini D, Misko TP. A catalyst of peroxynitrite decomposition inhibits murine experimental autoimmune encephalomyelitis. *J Neuroimmunol.* (2000) 107:21–8. doi: 10.1016/S0165-5728(00)00242-3

21. Fenyk-Melody JE, Garrison AE, Brunnert SR, Weidner JR, Shen F, Shelton BA, et al. Experimental autoimmune encephalomyelitis is exacerbated in mice lacking the NOS2 gene. *J Immunol.* (1998) 160:2940–6.
22. Kahl KG, Schmidt HH, Jung S, Sherman P, Toyka KV, Zielasek J. Experimental autoimmune encephalomyelitis in mice with a targeted deletion of the inducible nitric oxide synthase gene: increased T-helper 1 response. *Neurosci Lett.* (2004) 358:58–62. doi: 10.1016/j.neulet.2003.12.095
23. Xu X, Yi H, Guo Z, Qian C, Xia S, Yao Y, et al. Splenic stroma-educated regulatory dendritic cells induce apoptosis of activated CD4 T cells via Fas ligand-enhanced IFN-gamma and nitric oxide. *J Immunol.* (2012) 188:1168–77. doi: 10.4049/jimmunol.1101696
24. Verinaud L, Issayama LK, Zanucoli F, de Carvalho AC, da Costa TA, Di Gangi R, et al. Nitric oxide plays a key role in the suppressive activity of tolerogenic dendritic cells. *Cell Mol Immunol.* (2015) 12:384–6. doi: 10.1038/cmi.2014.94
25. Bhatt S, Qin J, Bennett C, Qian S, Fung JJ, Hamilton TA, et al. All-trans retinoic acid induces arginase-1 and inducible nitric oxide synthase-producing dendritic cells with T cell inhibitory function. *J Immunol.* (2014) 192:5098–108. doi: 10.4049/jimmunol.1303073
26. Gao Q, Zhang Y, Han C, Hu X, Zhang H, Xu X, et al. Blockade of CD47 ameliorates autoimmune inflammation in CNS by suppressing IL-1-triggered infiltration of pathogenic Th17 cells. *J Autoimmun.* (2016) 69:74–85. doi: 10.1016/j.jaut.2016.03.002
27. Lu G, Zhang R, Geng S, Peng L, Jayaraman P, Chen C, et al. Myeloid cell-derived inducible nitric oxide synthase suppresses M1 macrophage polarization. *Nat Commun.* (2015) 6:6676. doi: 10.1038/ncomms7676
28. Dalton DK, Wittmer S. Nitric-oxide-dependent and independent mechanisms of protection from CNS inflammation during Th1-mediated autoimmunity: evidence from EAE in iNOS KO mice. *J Neuroimmunol.* (2005) 160:110–21. doi: 10.1016/j.jneuroim.2004.11.004
29. Huang FP, Niedbala W, Wei XQ, Xu D, Feng GJ, Robinson JH, et al. Nitric oxide regulates Th1 cell development through the inhibition of IL-12 synthesis by macrophages. *Eur J Immunol.* (1998) 28:4062–70. doi: 10.1002/(SICI)1521-4141(199812)28:12<4062::AID-IMMU4062>3.0.CO;2-K
30. Xiong H, Zhu C, Li F, Hegazi R, He K, Babyatsky M, et al. Inhibition of interleukin-12 p40 transcription and NF-kappaB activation by nitric oxide in murine macrophages and dendritic cells. *J Biol Chem.* (2004) 279:10776–83. doi: 10.1074/jbc.M313416200
31. Jianjun Y, Zhang R, Lu G, Shen Y, Peng L, Zhu C, et al. T cell-derived inducible nitric oxide synthase switches off Th17 cell differentiation. *J Exp Med.* (2013) 210:1447–62. doi: 10.1084/jem.20122494
32. Lu F, Selak M, O'Connor J, Croul S, Lorenzana C, Butunoi C, et al. Oxidative damage to mitochondrial DNA and activity of mitochondrial enzymes in chronic active lesions of multiple sclerosis. *J Neurol Sci.* (2000) 177:95–103. doi: 10.1016/S0022-510X(00)00343-9
33. Cheret C, Gervais A, Lelli A, Colin C, Amar L, Ravassard P, et al. Neurotoxic activation of microglia is promoted by a nox1-dependent NADPH oxidase. *J Neurosci.* (2008) 28:12039–51. doi: 10.1523/JNEUROSCI.3568-08.2008
34. Jana M, Pahan K. Down-regulation of myelin gene expression in human oligodendrocytes by nitric oxide: implications for demyelination in multiple sclerosis. *J Clin Cell Immunol.* (2013) 4:157. doi: 10.4172/2155-9899.1000157
35. Ferber IA, Brocke S, Taylor-Edwards C, Ridgway W, Dinisco C, Steinman L, et al. Mice with a disrupted IFN-gamma gene are susceptible to the induction of experimental autoimmune encephalomyelitis (EAE). *J Immunol.* (1996) 156:5–7.
36. Willenborg DO, Fordham S, Bernard CC, Cowden WB, Ramshaw IA. IFN-gamma plays a critical down-regulatory role in the induction and effector phase of myelin oligodendrocyte glycoprotein-induced autoimmune encephalomyelitis. *J Immunol.* (1996) 157:3223–7.
37. Miller NM, Wang J, Tan Y, Dittel BN. Anti-inflammatory mechanisms of IFN-gamma studied in experimental autoimmune encephalomyelitis reveal neutrophils as a potential target in multiple sclerosis. *Front Neurosci.* (2015) 9:287. doi: 10.3389/fnins.2015.00287
38. Zhu B, Bando Y, Xiao S, Yang K, Anderson AC, Kuchroo VK, et al. CD11b+Ly-6C(hi) suppressive monocytes in experimental autoimmune encephalomyelitis. *J Immunol.* (2007) 179:5228–37. doi: 10.4049/jimmunol.179.8.5228
39. Yi H, Guo C, Yu X, Zuo D, Wang XY. Mouse CD11b+Gr-1+ myeloid cells can promote Th17 cell differentiation and experimental autoimmune encephalomyelitis. *J Immunol.* (2012) 189:4295–304. doi: 10.4049/jimmunol.1200086
40. Sonar SA, Lal G. Differentiation and transmigration of CD4 T cells in neuroinflammation and autoimmunity. *Front Immunol.* (2017) 8:1695. doi: 10.3389/fimmu.2017.01695
41. Wei XQ, Charles IG, Smith A, Ure J, Feng GJ, Huang FP, et al. Altered immune responses in mice lacking inducible nitric oxide synthase. *Nature.* (1995) 375:408–11. doi: 10.1038/375408a0
42. Niedbala W, Alves-Filho JC, Fukada SY, Vieira SM, Mitani A, Sonego F, et al. Regulation of type 17 helper T-cell function by nitric oxide during inflammation. *Proc Natl Acad Sci USA.* (2011) 108:9220–5. doi: 10.1073/pnas.1100667108
43. Obermajer N, Wong JL, Edwards RP, Chen K, Scott M, Khader S, et al. Induction and stability of human Th17 cells require endogenous NOS2 and cGMP-dependent NO signaling. *J Exp Med.* (2013) 210:1433–445. doi: 10.1084/jem.20121277
44. Lublin FD, Knobler RL, Kalman B, Goldhaber M, Marini J, Perrault M, et al. Monoclonal anti-gamma interferon antibodies enhance experimental allergic encephalomyelitis. *Autoimmunity.* (1993) 16:267–74. doi: 10.3109/08916939309014645
45. Ohmori Y, Hamilton TA. IFN-gamma selectively inhibits lipopolysaccharide-inducible JE/monocyte chemoattractant protein-1 and KC/GRO/melanoma growth-stimulating activity gene expression in mouse peritoneal macrophages. *J Immunol.* (1994) 153:2204–12.
46. Hayashi T, Ishida Y, Kimura A, Iwakura Y, Mukaida N, Kondo T. IFN-gamma protects cerulein-induced acute pancreatitis by repressing NF-kappa B activation. *J Immunol.* (2007) 178:7385–94. doi: 10.4049/jimmunol.178.11.7385
47. De Filippo K, Dudeck A, Hasenberg M, Nye E, van Rooijen N, Hartmann K, et al. Mast cell and macrophage chemokines CXCL1/CXCL2 control the early stage of neutrophil recruitment during tissue inflammation. *Blood.* (2013) 121:4930–7. doi: 10.1182/blood-2013-02-486217
48. Stromnes IM, Cerretti LM, Liggitt D, Harris RA, Goverman JM. Differential regulation of central nervous system autoimmunity by T(H)1 and T(H)17 cells. *Nat Med.* (2008) 14:337–42. doi: 10.1038/nm1715
49. Kroenke MA, Carlson TJ, Andjelkovic AV, Segal BM. IL-12- and IL-23-modulated T cells induce distinct types of EAE based on histology, CNS chemokine profile, and response to cytokine inhibition. *J Exp Med.* (2008) 205:1535–41. doi: 10.1084/jem.20080159
50. Hua LL, Kim MO, Brosnan CF, Lee SC. Modulation of astrocyte inducible nitric oxide synthase and cytokine expression by interferon beta is associated with induction and inhibition of interferon gamma-activated sequence binding activity. *J Neurochem.* (2002) 83:1120–8. doi: 10.1046/j.1471-4159.2002.01226.x
51. Liu L, Belkadi A, Darnall L, Hu T, Drescher C, Cotleur AC, et al. CXCR2-positive neutrophils are essential for cuprizone-induced demyelination: relevance to multiple sclerosis. *Nat Neurosci.* (2010) 13:319–26. doi: 10.1038/nn.2491
52. Calabrese V, Mancuso C, Calvani M, Rizzarelli E, Butterfield DA, Stella AM. Nitric oxide in the central nervous system: neuroprotection versus neurotoxicity. *Nat Rev Neurosci.* (2007) 8:766–75. doi: 10.1038/nrn2214

Conflict of Interest Statement: The authors declare that the research was conducted in the absence of any commercial or financial relationships that could be construed as a potential conflict of interest.

frontiers in Immunology

ORIGINAL RESEARCH
published: 10 May 2019
doi: 10.3389/fimmu.2019.01041

A T Cell Suppressive Circuitry Mediated by CD39 and Regulated by ShcC/Rai Is Induced in Astrocytes by Encephalitogenic T Cells

Cristina Ulivieri[1], Domiziana De Tommaso[1], Francesca Finetti[1], Barbara Ortensi[2,3], Giuliana Pelicci[2,3], Mario Milco D'Elios[4], Clara Ballerini[4] and Cosima T. Baldari[1]**

[1] Department of Life Sciences, University of Siena, Siena, Italy, [2] Department of Experimental Oncology, European Institute of Oncology, Milan, Italy, [3] Department of Translational Medicine, Piemonte Orientale University "Amedeo Avogadro", Novara, Italy, [4] Department of Experimental and Clinical Medicine, University of Florence, Florence, Italy

OPEN ACCESS

Edited by:
Craig Stephen Moore, Memorial University of Newfoundland, Canada

Reviewed by:
Igal Ifergan, Northwestern University, United States
Kingston H. Mills, Trinity College Dublin, Ireland

***Correspondence:**
Cristina Ulivieri
cristina.ulivieri@unisi.it
Cosima T. Baldari
cosima.baldari@unisi.it

Specialty section:
This article was submitted to Multiple Sclerosis and Neuroimmunology, a section of the journal Frontiers in Immunology

Received: 21 December 2018
Accepted: 23 April 2019
Published: 10 May 2019

Citation:
Ulivieri C, De Tommaso D, Finetti F, Ortensi B, Pelicci G, D'Elios MM, Ballerini C and Baldari CT (2019) A T Cell Suppressive Circuitry Mediated by CD39 and Regulated by ShcC/Rai Is Induced in Astrocytes by Encephalitogenic T Cells. Front. Immunol. 10:1041. doi: 10.3389/fimmu.2019.01041

Multiple sclerosis is an autoimmune disease caused by autoreactive immune cell infiltration into the central nervous system leading to inflammation, demyelination, and neuronal loss. While myelin-reactive Th1 and Th17 are centrally implicated in multiple sclerosis pathogenesis, the local CNS microenvironment, which is shaped by both infiltrated immune cells and central nervous system resident cells, has emerged a key player in disease onset and progression. We have recently demonstrated that ShcC/Rai is as a novel astrocytic adaptor whose loss in mice protects from experimental autoimmune encephalomyelitis. Here, we have explored the mechanisms that underlie the ability of $Rai^{-/-}$ astrocytes to antagonize T cell-dependent neuroinflammation. We show that Rai deficiency enhances the ability of astrocytes to upregulate the expression and activity of the ectonucleotidase CD39, which catalyzes the conversion of extracellular ATP to the immunosuppressive metabolite adenosine, through both contact-dependent and–independent mechanisms. As a result, Rai-deficient astrocytes acquire an enhanced ability to suppress T-cell proliferation, which involves suppression of T cell receptor signaling and upregulation of the inhibitory receptor CTLA-4. Additionally, Rai-deficient astrocytes preferentially polarize to the neuroprotective A2 phenotype. These results identify a new mechanism, to which Rai contributes to a major extent, by which astrocytes modulate the pathogenic potential of autoreactive T cells.

Keywords: astrocyte, EAE, neuroinflammation, molecular adaptor, T cell signaling, ATP-degrading enzyme

INTRODUCTION

Astrocytes are the first CNS resident cells encountered by infiltrating autoreactive T cells in multiple sclerosis (1, 2). Astrocytes contribute to neuroinflammation in multiple sclerosis and in the mouse experimental autoimmune encephalomyelitis (EAE) model by promoting encephalitogenic T-cell activation through their ability to act as antigen presenting cells (APC) and to upregulate the T-cell costimulatory molecules B7-1 and B7-2 (3–6). Intriguingly, T-cell suppression by astrocytes has also been documented, resulting from their ability to promote antigen-independent surface upregulation of inhibitory molecules on T cells, including the inhibitory receptor CTLA-4 and the

ectonucleotidases CD39 and CD73 (7, 8). Additionally, astrocytes actively influence the generation and maintenance of effector T cells both by modulating $CD4^+$ T-cell polarization to Th1 cells and by supporting IL-2-dependent Treg cell survival (9, 10). The finding that different subsets of reactive astrocytes are induced following CNS injury, of which the A1 is neurotoxic and the A2 neuroprotective (11), adds further complexity to the role of astrocytes in CNS diseases.

Astrocytes are themselves targets of infiltrating autoreactive T cells. Antigen-independent, contact-dependent upregulation of the integrin ligands VCAM-1 and ICAM-1 on astrocytes cocultured with activated T cells has been reported (8). Additionally, infiltrating Th1 and Th17 cells modulate astrocyte function via contact-independent mechanisms involving the release of inflammatory mediators that promote astrocytic secretion of pro-inflammatory cytokines and chemokines while repressing expression of anti-inflammatory cytokines (12–15). Interestingly, while both microglia and astrocytes are targets of Th1-derived soluble factors, Th17-derived soluble factors preferentially act on astrocytes (13, 15), highlighting astrocytes as central mediators of T cell-mediated neuroinflammation.

The concentration of ATP and its metabolite, adenosine, in the CNS microenvironment has emerged as a central factor in the modulation of neuroinflammation in multiple sclerosis/EAE (16). Elevated extracellular ATP (eATP) is sensed as a danger signal, promoting inflammation, while adenosine exhibits strong anti-inflammatory and immunosuppressive activities (17). The ectonucleotidases CD39 and CD73 are responsible for the conversion of ATP to adenosine. Altered expression and/or function of these enzymes have been associated to multiple sclerosis (18). Additionally, activation of the adenosine receptor A_2AR has been shown to attenuate CNS inflammation and EAE severity (19, 20), and conversely genetic ablation of A_2AR to exacerbate the disease (21), underscoring a key role for adenosine in controlling disease development. In support of this notion, treatment of multiple sclerosis patients or EAE mice with inosine, which similar to adenosine binds to the A_1A, A_2A, and A_3A receptors, ameliorates disease onset and severity by inhibiting inflammatory cell entry into the CNS, astroglial activation and demyelination (22).

We have recently reported that deficiency of ShcC/Rai, a member of the Shc family of protein adaptors, protects mice from demyelination and prevents reactive astrogliosis during EAE notwithstanding enhanced CNS infiltration by encephalitogenic Th17 cells, due to reduced astrocytic production of pro-inflammatory molecules in response to T cell-derived factors (23). Here we have addressed the outcome of Rai deficiency on the ability of astrocytes to generate a T cell suppressive microenvironment through eATP degradation. We show that Rai-deficient astrocytes have an enhanced ectonucleotidase activity and that they upregulate CD39 expression when exposed to conditioned media from encephalitogenic T cells, which results in their enhanced ability to suppress T cells through inhibition of TCR signaling and upregulation of CTLA-4.

MATERIALS AND METHODS

Mice

$Rai^{-/-}$ mice in the C57BL/6J background (24, 25) and C57BL/6J controls were used. Animals were housed in a pathogen-free and climate-controlled ($20 \pm 2°C$, relative humidity $55 \pm 10\%$) animal facility at the University of Siena. Mice were provided with water and pelleted diet *ad libitum*. All cages are provided with environmental enrichment in the form of nesting material and mouse houses. Procedures and experimentation were carried out in accordance with the 2010/63/EU Directive and approved by the Italian Ministry of Health.

Induction of EAE, Isolation of Glial Cells, and Generation of MOG-Specific T Cell Lines

EAE was induced in 8- to 10-week-old female mice (three $Rai^{-/-}$ and three wild-type C57BL/6J mice) by subcutaneous injection of 200 μg MOG_{35-55} peptide emulsified in an equal volume of complete Freund's adjuvant (CFA) containing 6 mg/ml *M. tuberculosis* H37Ra (Difco Laboratories, Detroit, MI). Mice, selected by sex, age and strain, were randomly allocated to experimental groups and randomly treated. The experimental unit was single animal. We observed similar variance between the groups that were compared. On day 0 and 2 mice were injected i.p. with 300 ng *B. pertussis* toxin (Calbiochem, Darmstadt, Germany). Mice were monitored daily by two independent researchers and clinical scores were assigned according to the standard 0 to 5 scale (23, 26). Brain and spinal cords were isolated from EAE mice (15 days post-immunization) and total glial cells were obtained as described (23).

To generate MOG_{35-55} specific T cells, splenocytes and lymph nodes were harvested at day 7 after immunization with MOG_{35-55} peptide (three wild-type C57BL/6J mice) and expanded with 50 μg/ml MOG_{35-55} and 20 U/ml IL-2 in RPMI1640 with 10% BCS. After 7 days cells were re-stimulated with autologous bone marrow-derived dendritic cells, MOG_{35-55} peptide and IL-2, for 7 days. Cells underwent 2 rounds of stimulation before being used. The frequency of GM-CSF-, TNFα-, IFNγ-, or IL-17a- producing cells among MOG-T cells have been assessed by flow cytometry (% $GM\text{-}CSF^+ = 4.5 \pm 1$, % $IL\text{-}17^+ = 19 \pm 4$, % $IFN\gamma^+ = 55 \pm 3$, and % $TNF\alpha^+ = 27 \pm 0.5$).

Primary Astrocyte Culture and Treatments

Astrocyte cultures were prepared from newborn mice (15 $Rai^{+/+}$ and 15 $Rai^{-/-}$) as described (27). Cerebral cortices were dissociated using the Neural Tissue Dissociation kit (T) (Miltenyi Biotec, Bergisch Gladbach, Germany) and the cells were cultured in flasks. For astrocytes monoculture, supernatants containing microglia were eliminated and adherent cells were trypsinized and replated. The purity of astrocytes was ≥95% as assessed by GFAP staining.

Treatment with IFNγ (10 ng/ml) or IL-17 (50 ng/ml) was performed in serum-free medium for ATP, adenosine and phosphate measurements or in complete medium for flow cytometric analysis and qRT-PCR analysis of CD39 and

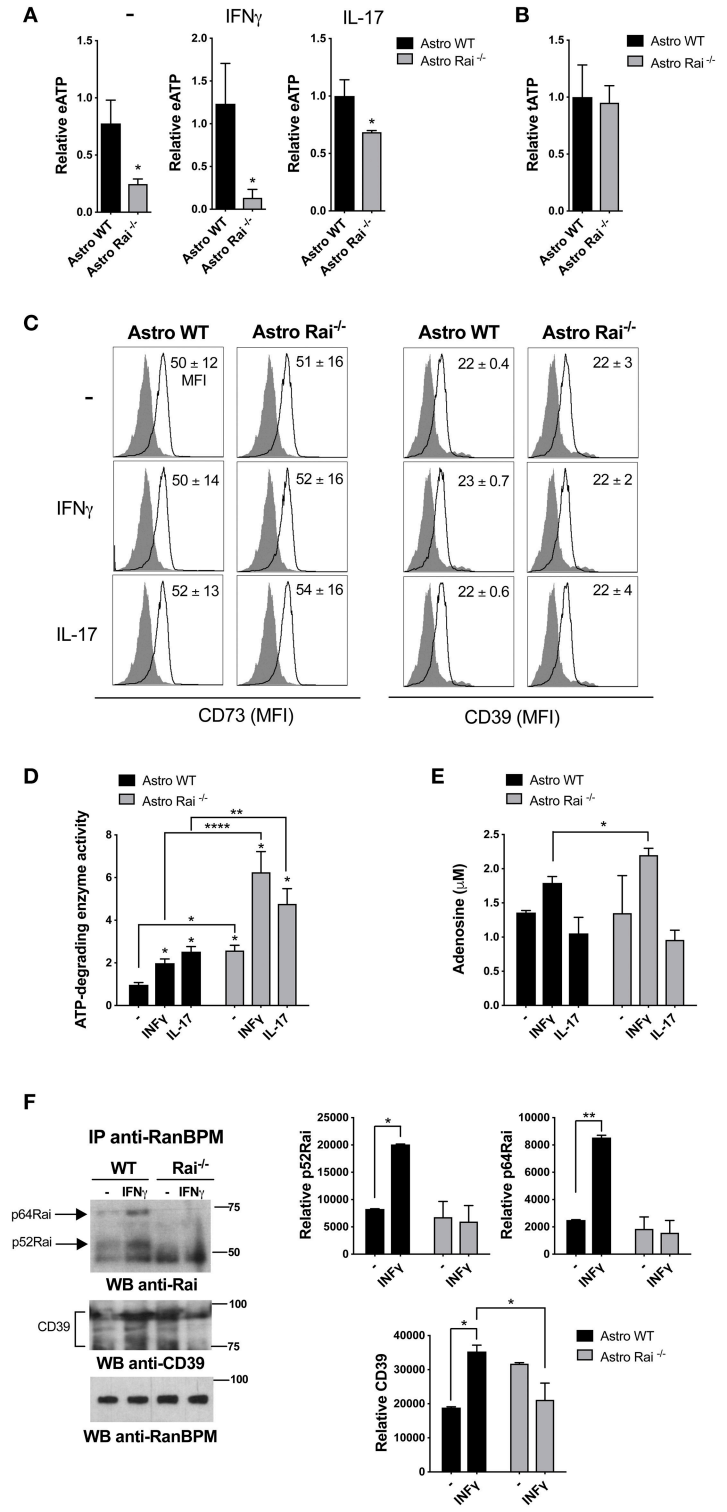

FIGURE 1 | Rai dampens extracellular ATP-degrading enzyme activity in astrocytes. **(A)** ATP (eATP) quantification in culture supernatants from Rai$^{+/+}$ (Astro WT) and Rai$^{-/-}$ (Astro Rai$^{-/-}$) astrocytes stimulated for 5 h with IFNγ (10 ng/ml) or IL-17 (50 ng/ml) or left untreated (-). Data are presented as mean ± SD of relative luciferase units (RLU) in supernatants from Rai$^{-/-}$ astrocytes vs. Rai$^{+/+}$ astrocytes. Data have been normalized to the mean RLU value of Rai$^{+/+}$ astrocytes ($n = 5$). **(B)** Total ATP (tATP) content in unstimulated Rai$^{+/+}$ (Astro WT) and Rai$^{-/-}$ (Astro Rai$^{-/-}$) astrocytes. **(C)** Flow cytometric analysis of surface CD73 and CD39 in Rai$^{+/+}$ (Astro WT) and Rai$^{-/-}$ (Astro Rai$^{-/-}$) astrocytes stimulated for 5 h with IFNγ (10 ng/ml), IL-17 (50 ng/ml) or left untreated (-). Data are presented as mean ± SD of mean fluorescence intensity (MFI) ($n = 4$). **(D)** Quantification of enzymatic activities of extracellular ATP-degrading enzymes in Rai$^{+/+}$ (Astro WT) and Rai$^{-/-}$ (Astro

(Continued)

FIGURE 1 | Rai$^{-/-}$) astrocytes stimulated with IL-17 or IFNγ for 5 h or left untreated (-), then depleted of their culture supernatant and incubated with 1 mM ATP. Data are presented as mean fold change ± SD of specific enzymatic activities (nmol free phosphate/mg protein/min) in Rai$^{+/+}$ astrocytes and Rai$^{-/-}$ astrocytes, with unstimulated Rai$^{+/+}$ astrocytes taken as 1 ($n = 3$). **(E)** Quantification of adenosine in culture supernatants of astrocytes treated as in D. Data are presented as mean ± SD of adenosine concentration (μM) ($n = 3$). **(F)** Immunoblot analysis with anti-Rai or anti-CD39 antibodies of RanBPM-specific immunoprecipitates from total cell lysates of Rai$^{+/+}$ and Rai$^{-/-}$ astrocytes treated with IFNγ (10 ng/ml) for 15 min ($n = 2$). The quantification by laser densitometry of the levels of each of the proteins normalized to the level of RanBPM in each sample is shown ($n = 2$). 2-Way ANOVA and Mann–Whitney test ****$p < 0.0001$, **$p < 0.01$, *$p < 0.05$.

CD73 expression and immunoprecipitation assays. Surface upregulation of CD39 and CD73 was analyzed in astrocytes stimulated for 120 h (peak of expression of CD39, as assessed in a preliminary time course analysis; **Supplementary Figure 2**) with pro-inflammatory cytokines. No surface upregulation of CD73 was found at any time point (data not shown). For the treatment with conditioned media from MOG-T cells, the culture medium was replaced with the culture supernatants from IL-2-stimulated MOG T cells in the presence or absence of a neutralizing anti-IFNγ mAb (e Bioscence). Alternatively, MOG T cells were added to astrocytes as such or previously pulsed with MOG_{35-55} peptide.

Splenocytes, CD4$^+$ T Cell Purification and Treatments

Mouse splenic mononuclear cells were separated by Mouse lympholyte gradient centrifugation (Cedarlane Laboratories, Netherlands) and resuspended in RPMI 10% BCS (two wild-type C57BL/6J mice).

Alternatively, CD4$^+$ T cells were enriched from spleen using Dynabeads^{TM} Untouched^{TM} Mouse CD4 Cells Kit (Invitrogen).

Cells were treated with immobilized anti-CD3 (2 mg/ml; eBiosciences) and anti-CD28 (2 mg/ml; eBiosciences) mAb for 72 h, alone or in combination with either the non-hydrolyzable adenosine analog NECA (10 μM) (Sigma-Aldrich) or supernatants from IFNγ-treated Rai$^{-/-}$ or Rai$^{+/+}$ astrocytes, in presence or absence of the ectonucleotidase inhibitor ARL67156 (100 μM) (Sigma-Aldrich). Alternatively, cells were pre-treated with supernatants from IFNγ-treated Rai$^{-/-}$ or Rai$^{+/+}$ astrocytes (diluted 1:2 with culture medium) in the presence or absence of ARL67156 (100 μM) for 1 h at 37°C and activated with soluble anti-CD3 and anti-CD28 mAbs in presence or absence of 10 μM NECA.

eATP, Adenosine, and Ectonucleotidase Activity Measurements

ATP levels in the astrocyte supernatants and cells were measured using a luciferin/luciferase assay (ATP Determination Kit A22066; Invitrogen) and a luminometer (Berthold Lumat LB 9501) according to the manufacturer's instructions. Adenosine levels were measured on astrocytes supernatants using a fluorometric assay (Adenosine Assay Kit; Cell Biolabs, INC.) and a Fluorometer (TECAN) according to the manufacturer's instructions.

For determination of nucleotide hydrolysis free phosphate was measured using the Malachite Green Phosphate Assay Kit (POMG-25H) (BioAssay Systems) at 620 nm on a microplate reader, according to the manufacturer's protocol. Specific activity was calculated using a calibration curve and expressed as nmol Pi released/mg protein/min.

Each sample was run in triplicate. Remaining cells were lysed in 0.02% SDS in phosphate-buffered saline (PBS) and protein content determined by the Pierce BCA protein assay kit (Thermo Fisher Scientific).

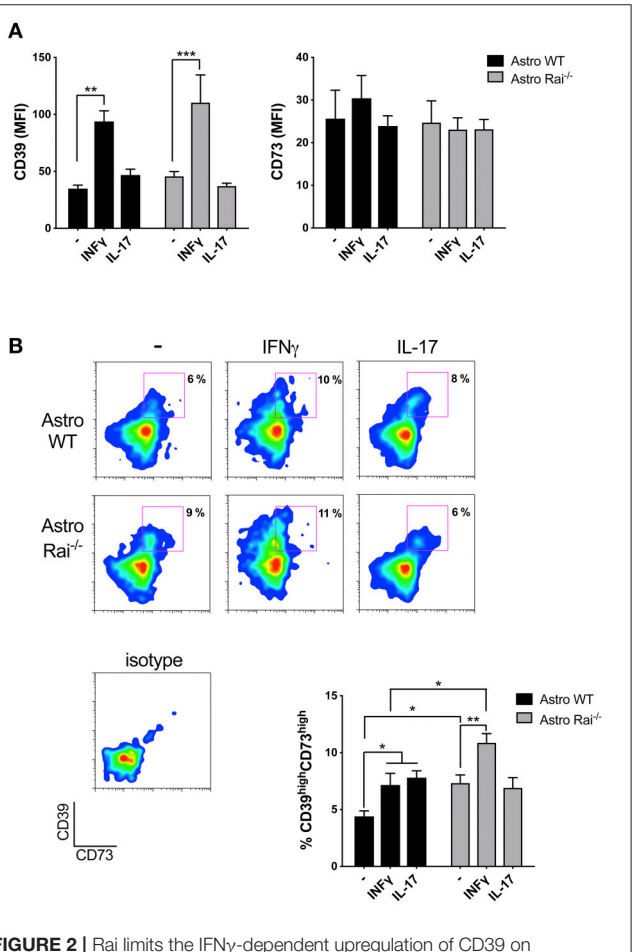

FIGURE 2 | Rai limits the IFNγ-dependent upregulation of CD39 on astrocytes. Flow cytometric analysis of surface CD73 and CD39 in Rai$^{+/+}$ (Astro WT) and Rai$^{-/-}$ (Astro Rai$^{-/-}$) astrocytes untreated (-) or stimulated for 120 h with IFNγ (10 ng/ml) or IL-17 (50 ng/ml). Data are presented as mean ± SD of mean fluorescence intensity (MFI) **(A)** or frequency of CD39^{high}CD73^{high} astrocytes **(B)**. Representative dot plots of CD39 and CD73 are shown ($n > 3$). Two-Way ANOVA, ***$p < 0.001$, **$p < 0.01$, *$p < 0.05$.

Cell Lysis, Immunoprecipitations, and Immunoblots

Cells were lysed in 1% (v/v) Triton X-100 in 20 mM Tris-HCl (pH 8), 150 mM NaCl in the presence of Protease

Inhibitor Cocktail Set III (Calbiochem) and 0.2 mg Na orthovanadate/ml. Postnuclear supernatants were resolved by SDS-PAGE and transferred to nitrocellulose. Alternatively, postnuclear supernatants were immunoprecipitated using RanBPM polyclonal antibody (Proteintech) and protein A Sepharose (GE Healthcare). Immunoblots were carried out using peroxidase-labeled secondary antibodies (GE Healthcare) and a chemiluminescence detection kit (Bio-rad Laboratories Inc., Milan, Italy). Immunoblots were scanned and quantitated using ImageJ software.

Flow Cytometry and Proliferation Assays

Flow cytometric analysis of astrocytes, MOG-T cells and splenocytes was performed using AlexaFluor488-, PE-, PerCP-conjugated anti-mouse antibodies to: GFAP (clone GA5; eBioscence), CD39 (clone 24DMS1; eBioscence), CD73 (clone TY11.8; Biolegend), CTLA-4 (clone UC10-4B9; Biolegend), IL-17A (clone TC11-18H10; Becton Dickinson), IFN-γ (clone XMG1.2; Becton Dickinson), GM-CSF (clone MPI-22E9; Biolegend), TNFα (Clone MP6-XT-22; Biolegend), and isotype control antibodies. Samples were acquired on Guava Easy Cyte cytometer (Millipore) and analyzed with FlowJo software (TreeStar Inc., Ashland, OR, USA).

Proliferation was measured on CFSE loaded cells (Molecular Probes, Thermo Fisher Scientific) by flow cytometry.

RNA Purification and RT-qPCR

Total RNA was isolated and purified from brain, astrocytes and splenocytes using the RNeasy Plus Mini Kit (Quiagen) according to the manufacturer's instructions. First-strand cDNAs were generated using the iScript^{TM} cDNA Synthesis Kit (Bio-Rad). RT-qPCR was performed using the SsoFast^{TM} EvaGreen® supermix kit (BIO-RAD) and specific pairs of primers listed in **Supplementary Table 1**.

Statistical Analyses

One-way ANOVA with *post-hoc* Tukey or 2-way ANOVA with *post-hoc* Sidak test were used for experiments where multiple groups were compared. Mann–Whitney rank-sum tests were also performed to determine the significance of the differences between two groups. Statistical analyses were performed using GraphPad Prism Software (Version 8). A $P < 0.05$ was considered as statistically significant.

RESULTS

Rai Dampens CD39 Enzyme Activity in Astrocytes in Response to IFNγ Treatment

To address the impact of Rai deficiency on the eATP-degrading activity of astrocytes, ATP was quantified in culture supernatants from Rai$^{+/+}$ and Rai$^{-/-}$ astrocytes generated from newborn mice brain, stimulated or not with IL-17 or IFNγ. Lower levels of eATP were found in culture supernatants of Rai$^{-/-}$ astrocytes compared to Rai$^{+/+}$ astrocytes, despite the fact that the total levels of ATP were comparable (**Figures 1A,B**). No differences in surface CD39/CD73 expression were observed under these conditions (**Figure 1C**, **Supplementary Figure 1**), suggesting that Rai might modulate the eATP-degrading activity of astrocytes.

To test this possibility we compared the ATP-degrading activity of control and Rai$^{-/-}$ astrocytes stimulated or not with IL-17 or IFNγ by incubating cells depleted of their culture supernatant with 1 mM ATP and measuring free phosphate production. Both cytokines promoted ATP-degradation, with Rai$^{-/-}$ astrocytes hydrolyzing ATP more efficiently, both under basal conditions and following IFNγ or IL-17 treatment (**Figure 1D**). Quantification of adenosine in culture supernatants from astrocytes added with exogenous ATP showed that IFNγ, but not IL-17, enhanced adenosine production, which was further enhanced by Rai deficiency (**Figure 1E**). These data indicate that IFNγ modulates adenosine generation by astrocytes and that Rai dampens the activity of ATP-degrading enzymes in these cells.

To translate these results to the context of EAE we measured the ATP-degrading activity of astrocytes isolated from the spinal cord of Rai$^{-/-}$ and control EAE mice. Similar to the results obtained on astrocytes derived from the brain of newborn mice, Rai$^{-/-}$ astrocytes obtained from the CNS of EAE mice degraded ATP more efficiently compared to their wild-type counterparts (**Supplementary Figure 3**). These data suggest that the protective role of Rai deficiency in astrocytes toward neuroinflammation in EAE could be dependent at least in part on the ability of Rai to negatively control eATP degradation and adenosine generation.

Rai Couples CD39 to its Negative Regulator RanBPM

To address the mechanism responsible for the ability of Rai to negatively control eATP degradation we focused on the rate-limiting enzyme of the cascade which converts ATP/ADP to adenosine, namely CD39. Since the scaffolding protein RanBPM binds to the cytosolic tail of CD39 and downregulates its ectonucleotidase activity (28), we hypothesized that Rai may participate in this molecular complex to restrain CD39 function. Rai$^{+/+}$ and Rai$^{-/-}$ astrocytes were left untreated or were treated with IFNγ and post-nuclear supernatants were immunoprecipitated with anti-RanBPM antibodies. RanBPM-specific immunoprecipitates were analyzed by immunoblotting with anti-Rai and anti-CD39 Abs. Rai was found to associate with RanBPM in response to IFNγ (**Figure 1F**). Interestingly, the IFNγ-dependent association of RanBPM with CD39 was reduced in Rai$^{-/-}$ astrocytes compared to control astrocytes (**Figure 1F**), indicating that IFNγR signaling promotes CD39 activation and suggesting that Rai limits CD39 activity by promoting RanBPM recruitment to CD39.

Rai Negatively Controls the Contact-Dependent and -Independent Upregulation of CD39 and CD73 Elicited by Encephalitogenic T Cells

Astrocytes have been demonstrated to suppress recently activated CD4^{+} T cells by inducing the upregulation of CD39/CD73 on their surface, which correlates with the acquisition of an immunosuppressive Th17 phenotype (8). Whether inflammatory

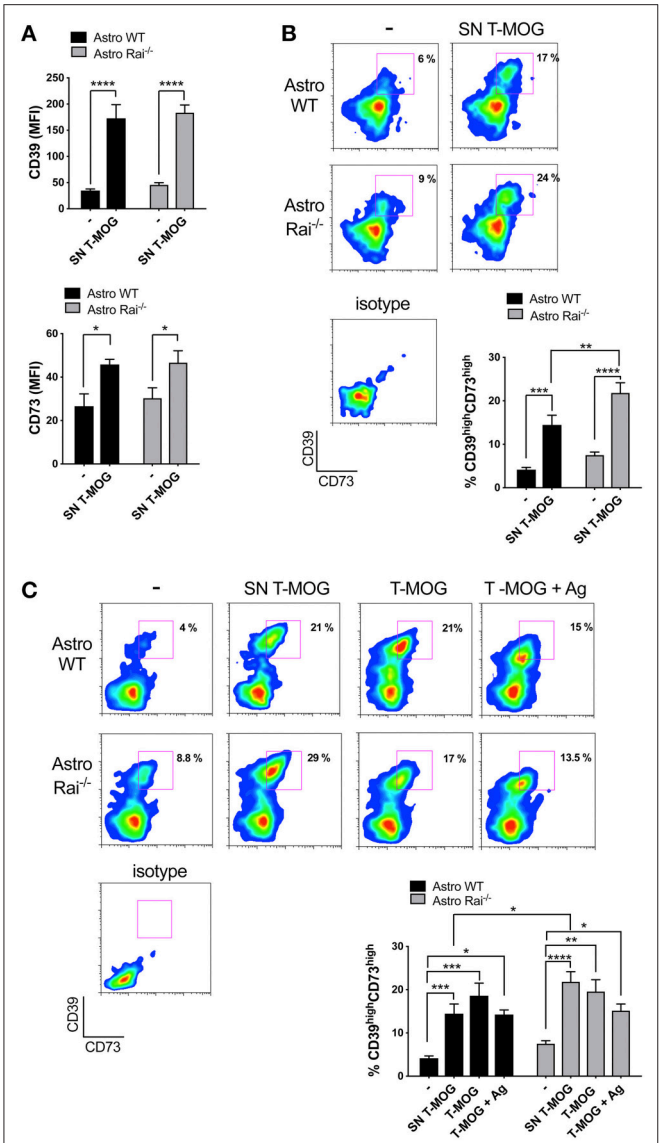

FIGURE 3 | Rai negatively controls the contact-dependent and -independent upregulation of CD39 and CD73 elicited by encephalitogenic T cells. **(A,B)** Flow cytometric analysis of surface CD73 and CD39 in $Rai^{+/+}$ (Astro WT) and $Rai^{-/-}$ (Astro $Rai^{-/-}$) astrocytes untreated (-) or stimulated for 120 h with culture supernatants from MOG-specific T cells generated from WT mice (SN T-MOG). Data are presented as mean ± SD of mean fluorescence intensity (MFI) **(A)** or frequency of $CD39^{high}CD73^{high}$ astrocytes ($n > 3$) **(B)**. **(C)** Flow cytometric analysis of surface CD73 and CD39 expression in $Rai^{+/+}$ (Astro WT) and $Rai^{-/-}$ (Astro $Rai^{-/-}$) astrocytes treated for 120 h with either culture supernatants from MOG-specific T cells generated from WT mice (SN T-MOG) or MOG-specific T cells depleted of their culture supernatants (T-MOG) in the presence (+Ag) or absence of MOG antigen. Representative dot plots are shown. The histograms show the frequency of the $CD39^{high}CD73^{high}$ population. Data are presented as mean ± SD of the percentage of $CD39^{high}CD73^{high}$ cells ($n > 3$). Representative dot plots are shown. Two-Way ANOVA, $^{****}p < 0.0001$, $^{***}p < 0.001$, $^{**}p < 0.01$, $^{*}p < 0.05$.

T cells can in turn affect the expression of these ATP-degrading enzymes in astrocytes, and the role of Rai in this process, have as yet not been explored. At present no published data are available on surface expression of CD39 and CD73 in mouse primary astrocytes either in the basal state or in response to cytokines. Surface CD39 and CD73 was measured by flow cytometric analysis of control and $Rai^{-/-}$ astrocytes following prolonged (120 h) treatment with IL-17 or IFNγ. IL-17 had no effect on either CD39 or CD73 surface expression (**Figure 2A**). At variance, IFNγ was found to promote CD39 upregulation with, a slight, yet not significant, further increase in $Rai^{-/-}$ astrocytes compared to control astrocytes (**Figure 2A**). The increase in surface CD39 correlated with an increase in the levels of CD39 mRNA, as assessed by RT-qPCR. An increase in the levels of CD73 mRNA was also observed in $Rai^{-/-}$ astrocytes compared to control astrocytes, however this was not paralleled by an global concomitant increase in surface CD73 (**Supplementary Figure 4**). Interestingly, co-upregulation of surface CD39 and CD73 was observed in response to both IFNγ and IL-17 in a small subpopulation of astrocytes (**Figure 2B**). This $CD39^{high}CD73^{high}$ subpopulation was larger in $Rai^{-/-}$ astrocytes compared to wild-type controls under steady-state conditions and was further expanded following IFNγ, but not IL-17, treatment (**Figure 2B**).

To mimic the CNS microenvironment shaped by infiltrating T cells during EAE, surface CD73 and CD39 were measured by flow cytometry on wild-type and $Rai^{-/-}$ astrocytes treated with conditioned media from MOG-specific T cells for 120 h. Under these conditions both CD39 and, to a lesser extent, CD73, were upregulated in both wild-type and $Rai^{-/-}$ astrocytes (**Figure 3A**). Additionally, a substantial increase in the abundance of the $CD39^{high}CD73^{high}$ wild-type astrocyte subpopulation was observed, with a further significant increase in $Rai^{-/-}$ astrocytes (**Figure 3B**). No significant effect on the frequency of $CD39^{high}CD73^{high}$ astrocytes was observed when an anti-IFNγ antibody was added to the conditioned media (data not shown), suggesting that other T cell-derived factors are responsible for the robust co-upregulation of CD39 and CD73 on this astrocyte subpopulation. These results indicate that encephalitogenic T cells promote co-upregulation of CD39 and CD73 on astrocytes in a contact-independent manner and that Rai deficiency results in an enhanced ability of astrocytes to respond to T cell-derived factors.

To understand whether surface ectonucleotidase expression on astrocytes can be further modulated by their physical contact with T cells, surface CD39 and CD73 were measured on wild-type and $Rai^{-/-}$ astrocytes co-cultured for 120 h in the presence or absence of MOG with encephalitogenic T cells previously depleted of their culture supernatant. Under these conditions an increase in the abundance of the $CD39^{high}CD73^{high}$ astrocyte subpopulation was observed, independently of the presence of antigen (**Figure 3C**). However, Rai deficiency did not affect the contact-dependent upregulation of CD39 or CD73, as opposed to the enhancement observed in the presence of conditioned media from MOG-specific T cells (**Figure 3C**). Hence, encephalitogenic T cells elicit a co-upregulation of CD39 and CD73 on astrocytes in both a contact-independent and a contact-dependent but antigen-independent manner, and the contact-independent response is enhanced in astrocytes lacking Rai.

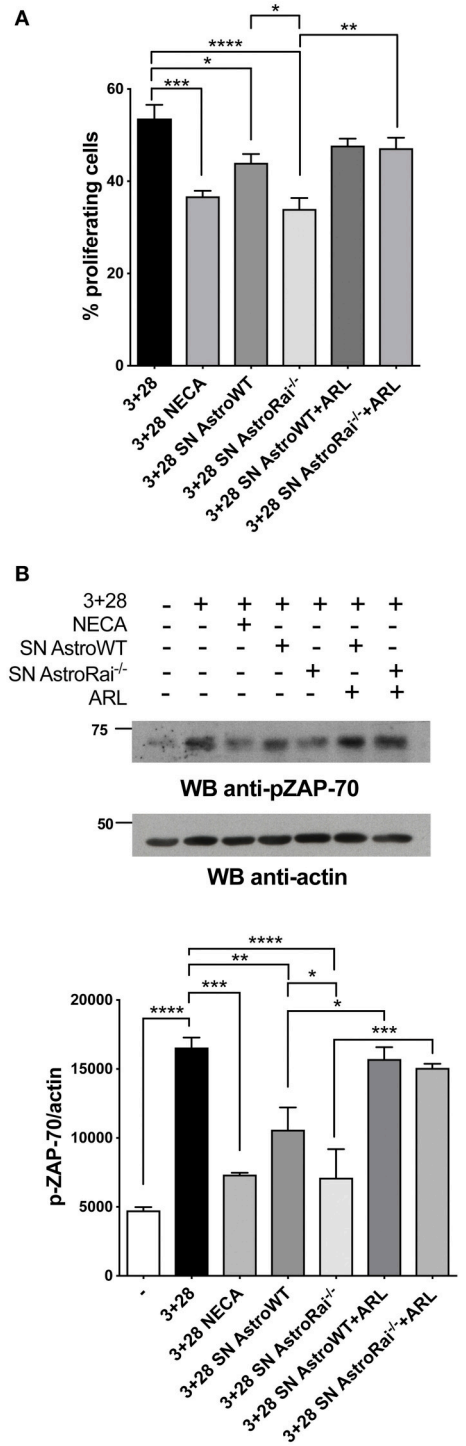

FIGURE 4 | Rai$^{-/-}$ astrocytes inhibit T-cell proliferation and TCR signaling through cell-cell contact-independent mechanisms. **(A)** Flow cytometric analysis of CFSE-labeled splenic mouse cells from wild-type mice stimulated for 72 h with anti-CD3/CD28 antibodies (3+28) in combination with either NECA or supernatants from IFNγ-treated Rai$^{-/-}$ (SN AstroRai$^{-/-}$) or Rai$^{+/+}$ (SN AstroWT) astrocytes in presence or absence of ARL67156 (100 μM) (ARL). The graph shows the mean value ± SD of the percentage of CFSE^{low} cells (proliferating cells) ($n = 5$). **(B)** Immunoblot analysis of ZAP-70 phosphorylation *(Continued)*

FIGURE 4 | in postnuclear supernatants of splenocytes from wild-type mice stimulated for 5 min with anti-CD3/CD28 antibodies (3+28) in combination with either NECA or supernatants from IFNγ-treated Rai$^{-/-}$ (SN AstroRai$^{-/-}$) or Rai$^{+/+}$ (SN AstroWT) astrocytes in presence or absence of ARL67156 (100 μM) (ARL). A control blot of the same filter is shown. The histogram shows the quantification by densitometric analysis of the levels of phosphorylated ZAP-70 relative to actin ($n = 3$). One-way ANOVA; $^{****}p < 0.0001$, $^{***}p < 0.001$, $^{**}p < 0.01$, $^{*}p < 0.05$.

Rai$^{-/-}$ Astrocytes Inhibit T Cell Proliferation by Suppressing TCR Signaling and Promoting Adenosine-Dependent CTLA-4 Upregulation

The enhanced ability of Rai$^{-/-}$ astrocytes to co-upregulate surface CD39/CD73 and hydrolyze eATP in the presence of the pro-inflammatory cytokines or factors released by encephalitogenic T cells suggests that Rai$^{-/-}$ astrocytes may suppress the activity of infiltrated T cells in an adenosine-dependent manner. To test this hypothesis we measured the proliferation of splenic T cells activated by CD3/CD28 costimulation in the presence of conditioned media from IFNγ-treated Rai$^{-/-}$ or Rai$^{+/+}$ astrocytes, using a non-hydrolysable adenosine analog as control. Flow cytometric analysis of CFSE-labeled splenocytes showed that culture supernatants from both IFNγ-treated wild-type and Rai$^{-/-}$ astrocytes, but not from untreated astrocytes, inhibited T cell proliferation (**Figure 4A**, **Supplementary Figure 5**). These effects were neutralized by treatment with the CD39/CD73 inhibitor ARL67156 (**Figure 4A**), indicating that they were mediated by adenosine. ARL67156 alone had no effect on CD3/CD28-dependent proliferation (**Supplementary Figure 5**). Suppression of T cell proliferation was more profound in the presence of conditioned media from Rai$^{-/-}$ astrocytes (**Figure 4A**), consistent with their higher adenosine content (**Figure 1**).

Adenosine binding to A_2AR results in an elevation in intracellular cAMP, which effectively inhibits TCR signaling through the PKA-dependent activation of the kinase Csk, a negative regulator of the initiating kinase Lck (29). Lck is required for the phosphorylation-dependent recruitment of the kinase ZAP-70 to the TCR, a key step for signal propagation (30). To explore the ability of astrocytes to modulate TCR signaling through their ATP-hydrolysing activity, splenic T cells were activated by CD3/CD28 costimulation in the presence of conditioned media from wild-type or Rai$^{-/-}$ astrocytes in the presence or absence of ARL67156, and the activation of ZAP-70 was measured by immunoblot using a phosphospecific antibody. Consistent with their inhibitory effect on T cell proliferation, supernatants from IFNγ-treated, but not from untreated, astrocytes suppressed ZAP-70 activation, with a higher efficiency for supernatants from Rai$^{-/-}$ astrocytes (**Figure 4B**, **Supplementary Figure 5**). Inhibition was fully relieved by the ectonucleotidase inhibitor (**Figure 4B**), supporting the notion that suppression of TCR signaling by astrocyte-derived factors is mediated by CD39/CD73-dependent adenosine production.

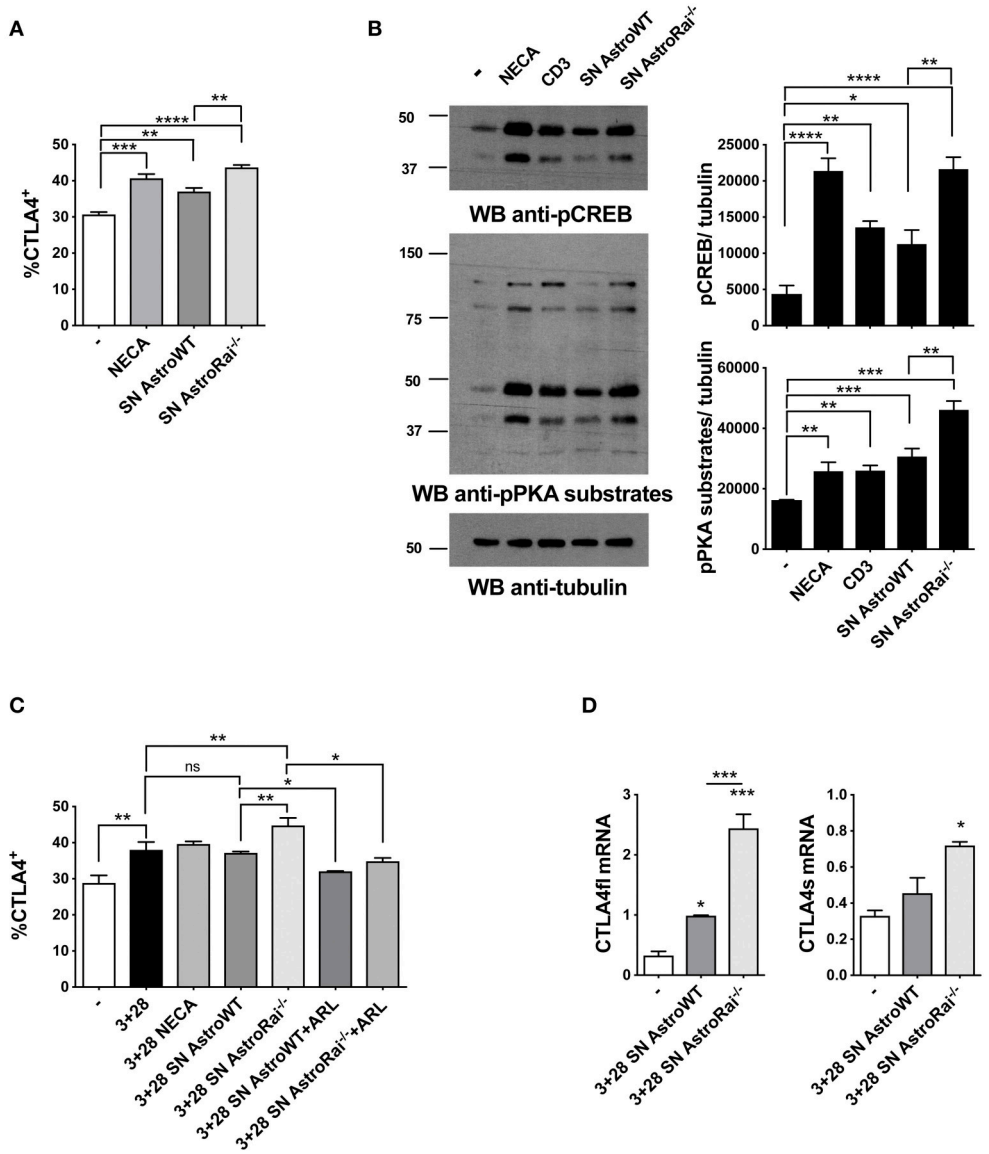

FIGURE 5 | Rai$^{-/-}$ astrocytes promote CTLA-4 expression on T cells through cell-cell contact-independent mechanisms. **(A)** Flow cytometric analysis of the frequency of CTLA-4 positive cells among splenic mouse T cells treated with culture supernatants from IFNγ-treated Rai$^{+/+}$ (SN AstroWT) or Rai$^{-/-}$ (SN AstroRai$^{-/-}$) astrocytes or NECA for 72 h. Data are presented as mean value ± SD of the percentage of CTLA-4 positive cells ($n = 3$). **(B)** Immunoblot analysis of phosphorylated PKA substrates and phospho-CREB in lysates of CD4^{+} T cells from wild-type mice stimulated with anti-CD3 antibodies, culture supernatants from IFNγ-treated Rai$^{+/+}$ (SN AstroWT) or Rai$^{-/-}$ (SN AstroRai$^{-/-}$) astrocytes or NECA for 5 min. β-Tubulin was used as loading control. The histogram shows the quantification by densitometric analysis of the levels of phosphorylated PKA substrates and CREB relative to tubulin ($n = 3$). **(C)** Flow cytometric analysis of the frequency of CTLA-4 positive cells among splenic mouse T cells stimulated with anti-CD3/CD28 antibodies (3+28) in combination with either NECA or supernatants from IFNγ-treated Rai$^{+/+}$ (SN AstroWT) or Rai$^{-/-}$ (SN AstroRai$^{-/-}$) astrocytes in presence or absence of ARL67156 (100 μM) (ARL). Data are presented as mean value ± SD of the percentage of CTLA-4 positive cells ($n = 5$). **(D)** Real-Time PCR analysis of full length and soluble CTLA-4 mRNA expression in splenic mouse cells stimulated for 24 h with anti-CD3/CD28 antibodies (3+28) in the presence of supernatants from IFNγ-treated Rai$^{+/+}$ (SN AstroWT) or Rai$^{-/-}$ (SN AstroRai$^{-/-}$) astrocytes. The levels of the different transcripts were normalized to GAPDH, used as housekeeping gene. Data are presented as mean value ± SD ($n = 3$). One-way ANOVA; $^{****}p < 0.0001$, $^{***}p < 0.001$, $^{**}p < 0.01$, $^{*}p < 0.05$.

In addition to directly inhibiting TCR signaling, adenosine suppresses T cell responses by inducing the cAMP/PKA-dependent expression of the inhibitory receptor CTLA-4, which blocks CD28-mediated costimulation (31, 32). Additionally, an upregulation of CTLA-4 expression has been reported in T cells exposed to astrocytes or to their conditioned media (7), suggesting a mechanistic link between these observations and our finding that astrocytes effectively degrade eATP. To address this issue, surface CTLA-4 was measured by flow cytometry on T cells exposed to conditioned media

from IFNγ-treated wild-type or Rai$^{-/-}$ astrocytes. The levels of T cell surface CTLA-4 were higher in the presence of IFNγ-treated astrocyte culture supernatants, similar to adenosine-treated T cells. Significantly higher levels of CTLA-4 were observed in the presence of supernatants from Rai$^{-/-}$ astrocytes compared to wild-type astrocytes (**Figure 5A**). The enhanced ability of conditioned media from IFNγ-treated Rai$^{-/-}$ astrocytes to induce A_2AR signaling compared with wild-type astrocytes was further supported by an enhancement of PKA activity and CREB phosphorylation (**Figure 5B**). Culture supernatants from untreated astrocytes had no effect on surface CTLA4 (**Supplementary Figure 5**). Supernatants from IFNγ-treated Rai$^{-/-}$ astrocytes, but not from IFNγ-treated WT astrocytes, induce significant CTLA4 upregulation also on CD3/CD28 activated T cells when comparing with activated T cells without addition of astrocytes supernatant (**Figure 5C**). This effect was completely neutralized by the ectonucleotidase inhibitor (**Figure 5C**), indicating that CTLA-4 upregulation by astrocytes is dependent on their ectonucleotidase activity. ARL67156 alone had no effect on CD3/CD28-dependent CTLA4 upregulation (**Supplementary Figure 5**).

While CTLA-4 can be rapidly expressed at the T-cell surface through the release of an intracellular pool stored in lysosomes (33), adenosine-dependent CTLA-4 upregulation involves *de novo* gene expression triggered by cAMP-dependent activation of the transcription factor CREB (34). To understand whether the increase in surface CTLA-4 observed in the presence of astrocyte culture supernatants was the result of transcriptional activation, we measured CTLA-4 mRNA levels on splenic T cells activated by CD3/CD28 costimulation in the presence of conditioned media from IFNγ-treated wild-type or Rai$^{-/-}$ astrocytes. Real-time RT-PCR analysis revealed an increase in the levels of the transcript for both the full length and the soluble form of CTLA-4, which results from alternative splicing and inhibits T-cell responses by binding B7 on APCs (35, 36) (**Figure 5D**). Collectively, these results indicate that astrocytes inhibit T cell activation and proliferation by suppressing TCR signaling and enhancing CTLA-4 expression through CD39/CD73-mediated adenosine production and cAMP/PKA signaling, which are enhanced in the absence of Rai.

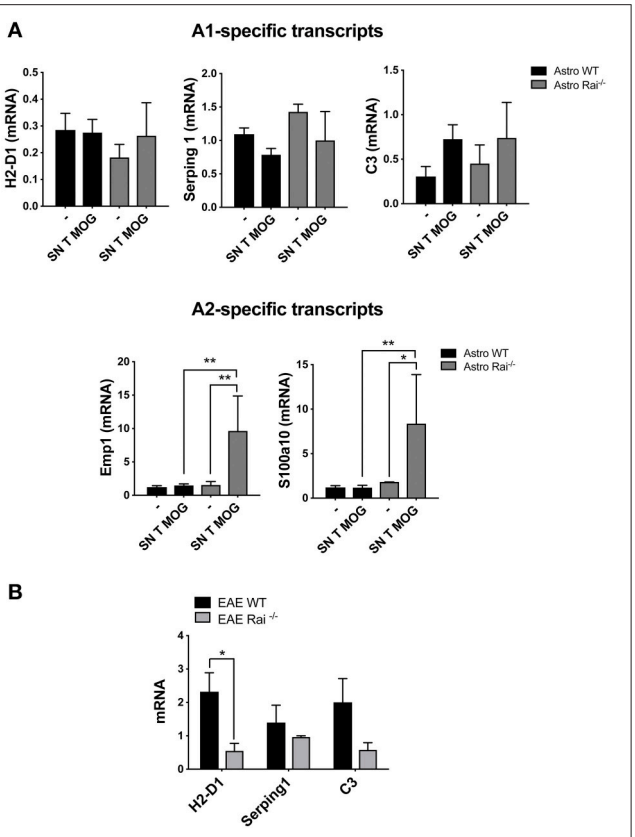

FIGURE 6 | Rai negatively controls the conversion of astrocytes toward a neuroprotective phenotype. **(A)** Real-Time PCR analysis of A1-specific (H2-D1, Serping and C3; upper panels) or A2-specific (Emp1 and S100a10; lower panels) transcripts in WT (Astro WT) and Rai$^{-/-}$ (Astro Rai$^{-/-}$) astrocytes either untreated or treated for 24 h with culture supernatants from MOG-specific T cells generated from WT mice. Data from 3 independent experiments, each carried out on the pooled astrocytes from at least 5 Rai$^{+/+}$ or 5 Rai$^{-/-}$ mice, are presented as mean value ± SD. The levels of the different transcripts were normalized to GAPDH, used as housekeeping gene. **(B)** Real-Time PCR analysis of the A1-specific transcripts H2-D1, Serping and C3 in the brain of Rai$^{+/+}$ EAE mice (EAE WT) and Rai$^{-/-}$ EAE mice (EAE Rai$^{-/-}$) 15 days post immunization. Data are presented as mean value ± SD obtained on three Rai$^{+/+}$ and three Rai$^{-/-}$ EAE mice. 2-way ANOVA; $^{**}p < 0.01$, $^{*}p < 0.05$.

A2 Reactive Astrocytes Are Induced by Encephalitogenic T Cells in the Absence of Rai

Astrocytes can polarize toward a neurotoxic A1 phenotype or a neuroprotective A2 anti-inflammatory phenotype depending on the disease. To date the signaling mechanisms responsible for the shift elicited by inflammatory cues remains largely unknown (11), and whether encephalitogenic T cells drive astrocyte polarization has as yet not been explored.

To investigate whether soluble factors released by encephalitogenic T cells induce astrocyte polarization, A1 or A2-specific transcripts were measured in astrocytes cultured for 24 h in conditioned media from encephalitogenic T cells. While no effect was detected in control astrocytes, under these conditions a strong induction of the A2-specific transcripts Emp1 and S100a10 was detected in Rai$^{-/-}$ astrocytes. At variance, Rai deficiency did not affect the levels of the A1-specific transcript H2-D1 and Serping1 (**Figure 6A**). Consistent with the protective role played by Rai deficiency in the EAE mouse model, lower levels of the A1-specific transcript H2-D1, Serping1 and C3 were found in the brain of Rai$^{-/-}$ EAE mice compared with control EAE mice (**Figure 6B**). These data identify Rai as a signaling molecule that restrains the polarization of astrocytes to the neuroprotective A2 phenotype.

DISCUSSION

The cross-talk of astrocytes with encephalitogenic T cells is centrally implicated in multiple sclerosis pathogenesis (13, 37).

Astrocytes respond to Th1 and Th17 cell-derived cytokines by producing factors that attract inflammatory cells. Additionally, they act as APC to promote effector T cell activation and expansion (38). However, activated astrocytes also deploy a variety of strategies to counteract inflammation and limit neuronal damage, including induction of Fas-mediated apoptosis of infiltrated T cells, skewing of T-cell polarization to a protective Th2 phenotype and Treg-dependent suppression of encephalitogenic T-cells (10, 39, 40). Here we document a new protective mechanism exploited by astrocytes to suppress T-cell activation and proliferation, which involves the upregulation of the astrocytic expression and activity of the ectonucleotidases CD39 and CD73 in response to pro-inflammatory factors released by encephalitogenic T cells. Additionally, we identify Rai as a negative regulator of this inhibitory circuitry.

The balance between eATP and adenosine has emerged as an important factor in the control of neuroinflammation to which both infiltrating T cells and astrocytes contribute. eATP boosts T-cell activation and promotes Th17 cell differentiation while inhibiting Treg cell differentiation and stability (41). Additionally eATP triggers microglia activation (42). On the other hand, ATP degradation to adenosine is a potent mechanism of T-cell suppression, and in fact CD39 has been established as a Treg cell marker that contributes to their inhibitory function (18, 43, 44). The function of $CD39^+$ Treg cells in MS is still unclear. Indeed in relapsing-remitting multiple sclerosis enhanced frequency of $CD39^+$ Treg cells has been reported both during relapse (45, 46) and during the remission phase (47). Adenosine suppresses TCR signaling by interacting with the adenosine receptor A_2AR (48), which activates a cAMP/PKA axis that inhibits TCR signaling at multiple steps (29). We found that conditioned media from IFNγ-activated astrocytes were able to inhibit T-cell proliferation and that this effect was abrogated by an ectonucleotidase inhibitor, indicating a contact-independent, adenosine-mediated mechanism of T-cell suppression. Accordingly, proximal TCR signaling, which requires activation of the kinase Lck that is inhibited by cAMP (49), was impaired when T cells were activated in the presence of conditioned media from astrocytes. The ability of the ectonucleotidase inhibitor to reverse this effect highlights a major role for the ATP-degrading, adenosine-elevating activity of CD39 in T-cell suppression by astrocytes.

Interestingly, we found that the ATP-degrading activity of astrocytes contributes to the suppression of T-cell proliferation through an additional, cAMP-dependent mechanism involving upregulation of the inhibitory receptor CTLA-4. Astrocytes have been shown to induce the contact-independent CTLA-4 upregulation on activated T cells, suggesting the presence of soluble inhibitory factors (7). The fact that the enhancing effect of culture supernatants from IFNγ-activated astrocytes on T cell expression of CTLA-4 can be reversed by an ectonucleotidase inhibitor supports the notion that a major one among these factors is adenosine. Of note, we found that surface CTLA-4 upregulation was paralleled by an increase in the levels of specific transcripts, consistent with the fact that A_2AR triggering on T cells promotes CTLA-4 transcription through its cAMP-elevating activity and the resulting activation of the transcription factor CREB (34). Indeed, we found that conditioned media from IFNγ-treated astrocytes were able to trigger CREB activation in an ectonucleotidase-dependent manner.

Interestingly, the levels of surface CD39 expression were upregulated in response to long-term treatment with IFNγ but not IL-17, while surface CD73 expression was not affected, highlighting CD39 as a limiting factor in ATP degradation by astrocytes and indicating that this protective response may be elicited preferentially by Th1 cells. It is however noteworthy that both IFNγ and IL-17, and to an even greater extent conditioned media from encephalitogenic T cells, increase the abundance of a $CD39^+$ astrocyte subpopulation that co-expresses CD73, which may account for the increased ATP-degrading activity detected under these conditions. This finding supports the notion that astrocytes shift toward an immunosuppressive phenotype in a Th1/Th17-conditioned microenvironment. Of note, transcription of the gene encoding CD39 has been reported to be activated by cAMP (50). Taking into account the fact that astrocytes are able to promote CD39 upregulation on co-cultured activated T cells (8), a possible scenario is that the resulting adenosine-generating activity of T cells may trigger adenosine signaling on astrocytes, thereby promoting cAMP accumulation and transcriptional activation of CD39, which would in turn result in suppressive adenosine-mediated signaling in T cells. ROS-dependent upregulation of CD39 has been recently reported in CD8 T cells (51). While the impact of ShcC/Rai on ROS production has as yet not been investigated, our finding that surface CD39 expression was upregulated in response to long-term treatment with IFNγ opens the possibility that enhanced ROS generation may account for the higher CD39 expression also in astrocytes.

Our results identify Rai as a negative regulator of astrocyte-mediated, adenosine-dependent T-cell suppression. Indeed, the T cell suppressive effects of conditioned media from IFNγ-treated astrocytes were enhanced by Rai deficiency. This results both from the enhanced ability of $Rai^{-/-}$ astrocytes to degrade eATP to adenosine in response to short-term IFNγ treatment and from the greater increase in CD39 expression and frequency of the $CD39^+CD73^+$ subpopulation after long-term IFNγ treatment compared to their wild-type counterparts. These results provide insights into the mechanisms responsible for the protective effect of Rai deficiency in astrocytes from encephalitogenic T cell-dependent neurodegeneration (23). Rai was initially identified as a molecular adaptor that couples the receptor tyrosine kinase Ret to Akt in neuronal cells (52). We showed that in T cells Rai limits antigen receptor signaling by impairing ZAP-70 recruitment to the activated TCR (53). The restraining effects of Rai on IFNγ-dependent CD39 expression and activity could be hypothesized to result from a similar mechanism involving the ability of Rai to exploit its adaptor function to interfere with IFNγR signaling.

That Rai is able to modulate the activity CD39 is intriguing. Studies on this ectoenzyme have been largely focused on the extracellular domain, which represents the most conspicuous part of the protein (54). Interestingly, recent evidence indicates that the short cytosolic tail is also implicated in the regulation of CD39 activity. Namely, RanBPM, an interactor of the small GTPase Ran, has been shown to associate with the cytosolic

tail of CD39, which negatively regulates its activity, in B cells (28). RanBPM acts as a scaffolding protein, interacting with a variety of membrane proteins and receptors (55). Here we demonstrate that Rai forms a complex with RanBPM and promotes IFNγ-dependent recruitment of RanBMP to CD39, thereby restraining its function, which places Rai in the negative regulatory circuitry of CD39, accounting for the enhanced CD39 activity in $Rai^{-/-}$ astrocytes.

Reactive astrocytes may adopt two distinct phenotypes, A1 and A2, with A1 astrocytes being neurotoxic and A2 astrocytes neuroprotective (11). Although astrocyte conversion to the A1 phenotype has been shown to be modulated by activated microglia in human neurodegenerative diseases including multiple sclerosis (11), the underlying mechanism and the impact of encephalitogenic T cells on this process remain unknown. Our data provide evidence for a new role of Rai as a negative regulator of astrocyte polarization to the A2 phenotype, highlighting an additional mechanism involving astrocytes that contributes to attenuating EAE severity in $Rai^{-/-}$ mice (23).

In conclusion, the results presented in this report show a reciprocal interplay whereby pathogenic T cells trigger CD39 expression and activity on astrocytes, highlighting this ectonucleotidase as a hub where signals from T cells and astrocytes converge to modulate the pathogenic activity of T cells in the CNS. They moreover identify astrocytic Rai as a central player in this cross-talk which unleashes the pathogenic effects of infiltrated encephalitogenic T cells in the CNS by negatively regulating a protective CD39-based T cell suppression circuitry. Finally, they provide evidence that Rai negatively regulates the polarization of reactive astrocytes toward a neuroprotective A2 phenotype. Both the enhanced T cell suppressive activity of Rai-deficient astrocytes and their enhanced A2 polarization are likely to account for our finding that Rai deficiency in astrocytes prevents reactive astrogliosis and ameliorates EAE (23).

ETHICS STATEMENT

This study was carried out in accordance with the recommendations on the protection of animals used for scientific purposes, Directive 2010/63 EU of the European Parliament and of the Council. The protocol was approved by the Italian Ministry of Health.

AUTHOR CONTRIBUTIONS

CTB, CU, CB, GP, and MMD contributed conception and design of the study. CU, DD, and FF performed the experiments. CTB, CU, and DD wrote the first draft of the manuscript. BO, GP, CB, and MMD provided key reagents and expertise. All authors contributed to manuscript revision, read, and approved the submitted version.

FUNDING

This work was supported by Fondazione Italiana Sclerosi Multipla Grant # 2014/R/3 to CTB.

SUPPLEMENTARY MATERIAL

The Supplementary Material for this article can be found online at: https://www.frontiersin.org/articles/10.3389/fimmu.2019.01041/full#supplementary-material

REFERENCES

1. Goverman J. Autoimmune T cell responses in the central nervous system. *Nat Rev Immunol.* (2009) 9:393–407. doi: 10.1038/nri2550
2. Engelhardt B, Ransohoff RM. Capture, crawl, cross: the T cell code to breach the blood-brain barriers. *Trends Immunol.* (2012) 33:579–89. doi: 10.1016/j.it.2012.07.004
3. Zeinstra E, Wilczak N, Chesik D, Glazenburg L, Kroese FG, De Keyser J. Simvastatin inhibits interferon-gamma-induced MHC class II up-regulation in cultured astrocytes. *J Neuroinflammation.* (2006) 3:16. doi: 10.1186/1742-2094-3-16
4. Zeinstra E, Wilczak N, De Keyser J. Reactive astrocytes in chronic active lesions of multiple sclerosis express co-stimulatory molecules B7–1 and B7–2. *J Neuroimmunol.* (2003) 135:166–71. doi: 10.1016/S0165-5728(02)00462-9
5. Zeinstra E, Wilczak N, Streefland C, De Keyser J. Astrocytes in chronic active multiple sclerosis plaques express MHC class II molecules. *Neuroreport.* (2000) 11:89–91. doi: 10.1097/00001756-200001170-00018
6. Cornet A, Bettelli E, Oukka M, Cambouris C, Avellana-Adalid V, Kosmatopoulos K, et al. Role of astrocytes in antigen presentation and naive T-cell activation. *J Neuroimmunol.* (2000) 106:69–77. doi: 10.1016/S0165-5728(99)00215-5
7. Gimsa U, ØRen A, Pandiyan P, Teichmann D, Bechmann I, Nitsch R, et al. Astrocytes protect the CNS: antigen-specific T helper cell responses are inhibited by astrocyte-induced upregulation of CTLA-4 (CD152). *J Mol Med.* (2004) 82:364–72. doi: 10.1007/s00109-004-0531-6
8. Filipello F, Pozzi D, Proietti M, Romagnani A, Mazzitelli S, Matteoli M, et al. Ectonucleotidase activity and immunosuppression in astrocyte-CD4 T cell bidirectional signaling. *Oncotarget.* (2016) 7:5143–56. doi: 10.18632/oncotarget.6914
9. Beurel E, Harrington LE, Buchser W, Lemmon V, Jope RS. Astrocytes modulate the polarization of CD4+ T cells to Th1 cells. *PLoS ONE.* (2014) 9:e86257. doi: 10.1371/journal.pone.0086257
10. Xie L, Choudhury GR, Winters A, Yang SH, Jin K. Cerebral regulatory T cells restrain microglia/macrophage-mediated inflammatory responses via IL-10. *Eur J Immunol.* (2015) 45:180–91. doi: 10.1002/eji.201444823
11. Liddelow SA, Barres BA. Reactive astrocytes: production, function, and therapeutic potential. *Immunity.* (2017) 46:957–67. doi: 10.1016/j.immuni.2017.06.006
12. Lee M, McGeer E, McGeer PL. Neurotoxins released from interferon-gamma-stimulated human astrocytes. *Neuroscience.* (2013) 229:164–75. doi: 10.1016/j.neuroscience.2012.10.033
13. Kang Z, Altuntas CZ, Gulen MF, Liu C, Giltiay N, Qin H, et al. Astrocyte-restricted ablation of interleukin-17-induced Act1-mediated signaling ameliorates autoimmune encephalomyelitis. *Immunity.* (2010) 32:414–25. doi: 10.1016/j.immuni.2010.03.004
14. Rothhammer V, Quintana FJ. Control of autoimmune CNS inflammation by astrocytes. *Semin Immunopathol.* (2015) 37:625–38. doi: 10.1007/s00281-015-0515-3
15. Prajeeth CK, Kronisch J, Khorooshi R, Knier B, Toft-Hansen H, Gudi V, et al. Effectors of Th1 and Th17 cells act on astrocytes and augment their neuroinflammatory properties. *J Neuroinflammation.* (2017)14:204. doi: 10.1186/s12974-017-0978-3
16. Safarzadeh E, Jadidi-Niaragh F, Motallebnezhad M, Yousefi M. The role of adenosine and adenosine receptors in the immunopathogenesis of multiple sclerosis. *Inflamm Res.* (2016) 65:511–20. doi: 10.1007/s00011-016-0936-z
17. Bours MJ, Dagnelie PC, Giuliani AL, Wesselius A, Di Virgilio F. P2 receptors and extracellular ATP: a novel homeostatic pathway in inflammation. *Front Biosci.* (2011) 3:1443–56. doi: 10.2741/s235

18. Antonioli L, Pacher P, Vizi ES, Haskó G. CD39 and CD73 in immunity and inflammation. *Trends Mol Med*. (2013)19:355–67. doi: 10.1016/j.molmed.2013.03.005
19. Mills JH, Kim DG, Krenz A, Chen JF, Bynoe MS. A2A adenosine receptor signaling in lymphocytes and the central nervous system regulates inflammation during experimental autoimmune encephalomyelitis. *J Immunol.* (2012) 188:5713–22. doi: 10.4049/jimmunol.1200545
20. Liu Y, Zou H, Zhao P, Sun B, Wang J, Kong Q, et al. Activation of the adenosine A2A receptor attenuates experimental autoimmune encephalomyelitis and is associated with increased intracellular calcium levels. *Neuroscience.* (2016) 330:150–61. doi: 10.1016/j.neuroscience.2016.05.028
21. Yao SQ, Li ZZ, Huang QY, Li F, Wang ZW, Augusto E, et al. Genetic inactivation of the adenosine A(2A) receptor exacerbates brain damage in mice with experimental autoimmune encephalomyelitis. *J Neurochem.* (2012) 123:100–12. doi: 10.1111/j.1471-4159.2012.07807.x
22. Junqueira SC, Dos Santos Coelho I, Lieberknecht V, Cunha MP, Calixto JB, Rodrigues ALS, et al. Inosine, an endogenous purine nucleoside, suppresses immune responses and protects mice from experimental autoimmune encephalomyelitis: a role for A2A adenosine receptor. *Mol Neurobiol.* (2017) 54:3271–85. doi: 10.1007/s12035-016-9893-3
23. Ulivieri C, Savino MT, Luccarini I, Fanigliulo E, Aldinucci A, Bonechi E, et al. The adaptor protein Rai/ShcC promotes astrocyte-dependent inflammation during experimental autoimmune encephalomyelitis. *J Immunol.* (2016) 197:480–90. doi: 10.4049/jimmunol.1502063
24. Sakai R, Henderson JT, O'Bryan JP, Elia AJ, Saxton TM, Pawson T. The mammalian ShcB and ShcC phosphotyrosine docking proteins function in the maturation of sensory and sympathetic neurons. *Neuron.* (2000) 28:819–33. doi: 10.1016/S0896-6273(00)00156-2
25. Savino MT, Ortensi B, Ferro M, Ulivieri C, Fanigliulo D, Paccagnini E, et al. Rai acts as a negative regulator of autoimmunity by inhibiting antigen receptor signaling and lymphocyte activation. *J Immunol.* (2009) 182:301–8. doi: 10.4049/jimmunol.182.1.301
26. Stromnes IM, Goverman JM. Active induction of experimental allergic encephalomyelitis. *Nat Protoc.* (2006) 1:1810–9. doi: 10.1038/nprot.2006.285
27. Colombo E, Cordiglieri C, Melli G, Newcombe J, Krumbholz M, Parada LF, et al. Stimulation of the neurotrophin receptor TrkB on astrocytes drives nitric oxide production and neurodegeneration. *J Exp Med*. (2012) 209:521–35. doi: 10.1084/jem.20110698
28. Wu Y, Sun X, Kaczmarek E, Dwyer KM, Bianchi E, Usheva A, et al. RanBPM associates with CD39 and modulates ecto-nucleotidase activity. *Biochem J.* (2006) 396:23–30. doi: 10.1042/BJ20051568
29. Cekic C, Linden J. Purinergic regulation of the immune system. *Nat Rev Immunol.* (2016) 16:177–92. doi: 10.1038/nri.2016.4
30. Gaud G, Lesourne R, Love PE. Regulatory mechanisms in T cell receptor signalling. *Nat Rev Immunol.* (2018) 18:485–97. doi: 10.1038/s41577-018-0020-8
31. Ohta A, Kini R, Subramanian M, Madasu M, Sitkovsky M. The development and immunosuppressive functions of CD4(+) CD25(+) FoxP3(+) regulatory T cells are under influence of the adenosine-A2A adenosine receptor pathway. *Front Immunol*. (2012) 3:190. doi: 10.3389/fimmu.2012.00190
32. Vendetti S, Riccomi A, Sacchi A, Gatta L, Pioli C, De Magistris MT. Cyclic adenosine 5'-monophosphate and calcium induce CD152 (CTLA-4) up-regulation in resting CD4+ T lymphocytes. *J Immunol*. (2002) 169:6231–5. doi: 10.4049/jimmunol.169.11.6231
33. Walker LS, Sansom DM. Confusing signals: recent progress in CTLA-4 biology. *Trends Immunol.* (2015) 36:63–70. doi: 10.1016/j.it.2014.12.001
34. Li H, Edin ML, Gruzdev A, Cheng J, Bradbury JA, Graves JP, et al. Regulation of T helper cell subsets by cyclooxygenases and their metabolites. *Prostaglandins Other Lipid Mediat.* (2013) 104–105:74–83. doi: 10.1016/j.prostaglandins.2012.11.002
35. Oaks MK, Hallett KM. Cutting edge: a soluble form of CTLA-4 in patients with autoimmune thyroid disease. *J Immunol*. (2000) 164:5015–8. doi: 10.4049/jimmunol.164.10.5015
36. Ward FJ, Dahal LN, Wijesekera SK, Abdul-Jawad SK, Kaewarpai T, Xu H, et al. The soluble isoform of CTLA-4 as a regulator of T-cell responses. *Eur J Immunol*. (2013) 43:1274–85. doi: 10.1002/eji.201242529
37. Mayo L, Cunha AP, Madi A, Beynon V, Yang Z, Alvarez JI, et al. IL-10-dependent Tr1 cells attenuate astrocyte activation and ameliorate chronic central nervous system inflammation. *Brain*. (2016) 139:1939–57. doi: 10.1093/brain/aww113
38. Jensen CJ, Massie A, De Keyser J. Immune players in the CNS: the astrocyte. *J Neuroimmune Pharmacol*. (2013) 8:824–39. doi: 10.1007/s11481-013-9480-6
39. Bechmann I, Steiner B, Gimsa U, Mor G, Wolf S, Beyer M, et al. Astrocyte-induced T cell elimination is CD95 ligand dependent. *J Neuroimmunol*. (2002) 132:60–5. doi: 10.1016/S0165-5728(02)00311-9
40. Aloisi F, Ria F, Columba-Cabezas S, Hess H, Penna G, Adorini L. Relative efficiency of microglia, astrocytes, dendritic cells and B cells in naive CD4+ T cell priming and Th1/Th2 cell restimulation. *Eur J Immunol*. (1999) 29:2705–14. doi: 10.1002/(SICI)1521-4141(199909)29:09<2705::AID-IMMU2705>3.0.CO;2-1
41. Takenaka MC, Robson S, Quintana FJ. Regulation of the T cell response by CD39. *Trends Immunol.* (2016) 37:427–39. doi: 10.1016/j.it.2016.04.009
42. Rodrigues RJ, Tomé AR, Cunha RA. ATP as a multi-target danger signal in the brain. *Front Neurosci.* (2015) 9:148. doi: 10.3389/fnins.2015.00148
43. Borsellino G, Kleinewietfeld M, Di Mitri D, Sternjak A, Diamantini A, Giometto R, et al. Expression of ectonucleotidase CD39 by Foxp3+ Treg cells: hydrolysis of extracellular ATP and immune suppression. *Blood.* (2007) 110:1225–32. doi: 10.1182/blood-2006-12-064527
44. Deaglio S, Dwyer KM, Gao W, Friedman D, Usheva A, Erat A, et al. Adenosine generation catalyzed by CD39 and CD73 expressed on regulatory T cells mediates immune suppression. *J Exp Med*. (2007) 204:1257–65. doi: 10.1084/jem.20062512
45. Álvarez-Sánchez N, Cruz-Chamorro I, Díaz-Sánchez M, Lardone PJ, Guerrero JM, Carrillo-Vico A. Peripheral CD39-expressing T regulatory cells are increased and associated with relapsing-remitting multiple sclerosis in relapsing patients. *Sci Rep*. (2019) 9:2302–9. doi: 10.1038/s41598-019-38897-w
46. Muls NG, Dang HA, Sindic CJ, van Pesch V. Regulation of Treg-associated CD39 in multiple sclerosis and effects of corticotherapy during relapse. *Mult Scler.* (2015) 21:1533–45. doi: 10.1177/1352458514567215
47. Peelen E, Damoiseaux J, Smolders J, Knippenberg S, Menheere P, Tervaert JW, et al. Th17 expansion in MS patients is counterbalanced by an expanded CD39+ regulatory T cell population during remission but not during relapse. *J Neuroimmunol.* (2011) 240–1:97–103. doi: 10.1016/j.jneuroim.2011.09.013
48. Bours MJ, Swennen EL, Di Virgilio F, Cronstein BN, Dagnelie PC. Adenosine 5′-triphosphate and adenosine as endogenous signaling molecules in immunity and inflammation. *Pharmacol Ther.* (2006) 112:358–404. doi: 10.1016/j.pharmthera.2005.04.013
49. Wehbi VL, Taskén K. Molecular Mechanisms for cAMP-mediated immunoregulation in T cells—role of anchored protein kinase A signaling units. *Front Immunol*. (2016) 7:222. doi: 10.3389/fimmu.2016.00222
50. Cui M, Ding H, Chen F, Zhao Y, Yang Q, Dong Q. Mdivi-1 protects against ischemic brain injury via elevating extracellular adenosine in a cAMP/CREB-CD39-dependent manner. *Mol Neurobiol.* (2016) 53:240–53. doi: 10.1007/s12035-014-9002-4
51. Bai A, Moss A, Rothweiler S, Longhi MS, Wu Y, Junger WG, et al. NADH oxidase-dependent CD39 expression by CD8(+) T cells modulates interferon gamma responses via generation of adenosine. *Nat Commun.* (2015) 6:8819–31. doi: 10.1038/ncomms9819
52. Pelicci G, Troglio F, Bodini A, Melillo RM, Pettirossi V, Coda L, et al. The neuron-specific Rai (ShcC) adaptor protein inhibits apoptosis by coupling Ret to the phosphatidylinositol 3-kinase/Akt signaling pathway. *Mol Cell Biol.* (2002) 22:7351–63. doi: 10.1128/MCB.22.20.7351-7363.2002

53. Ferro M, Savino MT, Ortensi B, Finetti F, Genovese L, Masi G, et al. The Shc family protein adaptor, Rai, negatively regulates T cell antigen receptor signaling by inhibiting ZAP-70 recruitment and activation. *PLoS ONE.* (2011) 6:e29899. doi: 10.1371/journal.pone.0029899
54. Robson SC, Sévigny J, Zimmermann H. The E-NTPDase family of ectonucleotidases: structure function relationships and pathophysiological significance. *Purinergic Signal*. (2006) 2:409–30. doi: 10.1007/s11302-006-9003-5
55. Suresh B, Ramakrishna S, Baek KH. Diverse roles of the scaffolding protein RanBPM. *Drug Discov Today*. (2012) 17:379–87. doi: 10.1016/j.drudis.2011.10.030

Conflict of Interest Statement: The authors declare that the research was conducted in the absence of any commercial or financial relationships that could be construed as a potential conflict of interest.

frontiers in Neurology

MINI REVIEW
published: 12 June 2019
doi: 10.3389/fneur.2019.00622

A Novel Sex-Dependent Target for the Treatment of Postoperative Pain: The NLRP3 Inflammasome

Ashley M. Cowie[1], *Bonnie N. Dittel*[2,3] *and Cheryl L. Stucky*[1]*

[1] *Department of Cell Biology, Neurobiology, and Anatomy, Medical College of Wisconsin, Milwaukee, WI, United States,* [2] *Blood Research Institute, Versiti, Milwaukee, WI, United States,* [3] *Department of Microbiology and Immunology, Medical College of Wisconsin, Milwaukee, WI, United States*

In recent years the innate immune system has been shown to be crucial for the pathogenesis of postoperative pain. The mediators released by innate immune cells drive the sensitization of sensory neurons following injury by directly acting on peripheral nerve terminals at the injury site. The predominate sensitization signaling pathway involves the proinflammatory cytokine interleukin-1β (IL-1β). IL-1β is known to cause pain by directly acting on sensory neurons. Evidence demonstrates that blockade of IL-1β signaling decreases postoperative pain, however complete blockade of IL-1β signaling increases the risk of infection and decreases effective wound healing. IL-1β requires activation by an inflammasome; inflammasomes are cytosolic receptors of the innate immune system. NOD-like receptor protein 3 (NLRP3) is the predominant inflammasome activated by endogenous molecules that are released by tissue injury such as that which occurs during neuropathic and inflammatory pain disorders. Given that selective inhibition of NLRP3 alleviates postoperative mechanical pain, its selective targeting may be a novel and effective strategy for the treatment of pain that would avoid complications of global IL-1β inhibition. Moreover, NLRP3 is activated in pain in a sex-dependent and cell type-dependent manner. Sex differences in the innate immune system have been shown to drive pain and sensitization through different mechanisms in inflammatory and neuropathic pain disorders, indicating that it is imperative that both sexes are studied when researchers investigate and identify new targets for pain therapeutics. This review will highlight the roles of the innate immune response, the NLRP3 inflammasome, and sex differences in neuropathic and inflammatory pain.

Keywords: NLRP3, interleukin-1β, sex differences, pain, tissue injury, innate immunity

OPEN ACCESS

Edited by:
Craig Stephen Moore, Memorial University of Newfoundland, Canada

Reviewed by:
Bradley Kerr, University of Alberta, Canada
Nader Ghasemlou, Queen's University, Canada

***Correspondence:**
Cheryl L. Stucky
cstucky@mcw.edu

Specialty section:
This article was submitted to Multiple Sclerosis and Neuroimmunology, a section of the journal Frontiers in Neurology

Received: *29 March 2019*
Accepted: *28 May 2019*
Published: *12 June 2019*

Citation:
Cowie AM, Dittel BN and Stucky CL (2019) A Novel Sex-Dependent Target for the Treatment of Postoperative Pain: The NLRP3 Inflammasome. Front. Neurol. 10:622. doi: 10.3389/fneur.2019.00622

INTRODUCTION

A unique combination of molecular and cellular factors can lead to acute and chronic pain conditions with varying pathologies. Despite this, pain is categorized into the following broad categories: inflammatory, neuropathic, and syndrome-based (e.g., fibromyalgia). There is overlap between these generalized categories. For example, inflammation can result in nerve damage, nerve injury involves inflammation, and syndrome-based pain can be neuropathic or inflammatory or both. Inflammatory pain occurs with

peripheral tissue damage and the resulting tissue inflammation. Alternatively, neuropathic pain results from direct damage to nerves in the peripheral or central nervous systems. Postoperative pain has both inflammatory and neuropathic qualities (1). It is widely recognized that postoperative pain occurs as a result of the direct cutting of tissues and peripheral nerves at the surgical site.

Rodent models of postoperative pain have been consistently used to study the underlying causes of postoperative pain. Rodent models of surgical pain are strong preclinical models because the injury induced in the animal and human is similar, and therefore, these models likely recapitulate patient phenotypes and mechanisms (1–3). The most common postoperative pain model involves cutting through the skin and underlying muscle (flexor digitorum brevis), which reliably produces mechanical and heat hyperalgesia at the incision site (4–9). There is a robust immune response in this model that includes infiltration of neutrophils, macrophages, and lymphocytes. The immune response aids in wound healing, but also results in sensitization of sensory neurons to mechanical and heat stimuli (1, 10–13). The immune response begins at the incision site or site of tissue damage and moves proximally to the dorsal root ganglia and spinal cord.

There is a rapidly growing body of evidence demonstrating that the development and maintenance of postoperative pain are not solely dependent on the increased excitability of sensory neurons alone at the incision site, but they also depend on immune cell interactions with sensory neurons and activation of canonical immune receptors expressed by sensory neurons. Components of the innate immune system have emerged as crucial mediators in the development and maintenance of hypersensitivity following incision. Pattern-recognition receptors (PRRs) are part of the innate immune system and are among the first to be activated in response to tissue damage; their activation is important for the induction of immune responses leading to pathogen elimination and subsequent tissue repair (14). PRRs include cytosolic NOD-like receptors (NLRs) which, when activated, form inflammasomes. The NLR protein 3 (NLRP3) inflammasome is the best characterized NLR and has been shown to be critical in driving the immune response to sterile tissue damage (15), the type of inflammation that occurs with surgical incision. Additionally, NLRP3 is known to play a role in several painful conditions that arise from sterile tissue damage (16–30). Since the immune system is known to be sexually dimorphic, much recent attention has been given to understanding the sex differences and their causative factors that underlie painful conditions. However, little is known about the effects of sex on NLRP3 or the role of NLRP3 in postoperative pain. Therefore, this review provides a new insight into the relationship between NLRP3 and postoperative pain. Here we discuss the current understanding of sexual dimorphism in the innate immune system response to tissue injury and the role it plays in inflammatory and neuropathic pain conditions by focusing on the NLRP3 inflammasome.

THE IMMUNE RESPONSE TO INCISIONAL INJURY

Immune Cell Involvement

Surgical incision results in local tissue injury, which destroys physical barriers between the body and environment, and increases the risk of exposure to environmental and commensal microbes. These consequences of surgery all lead to activation of the innate immune system and local inflammation. Inflammation occurs immediately following tissue injury as an attempt to clear debris and initiate healing. Initially immune cells such as mast cells, neutrophils, and monocytes/macrophages are recruited to the injury site by mediators that are released in tissues, by neurons and by tissue-resident immune cells (12, 31–34). Recruitment and activation of different immune cells following injury occurs in the same sequence in both sexes. First, dermal mast cells regulate inflammation immediately following cutaneous wounding by releasing inflammatory mediators, thereby increasing vascular permeability and recruiting neutrophils (35, 36). The neutrophil recruitment is generally followed by monocyte/macrophage recruitment, which occurs 1–2 days following injury (12, 34, 37, 38). Macrophages play a dual role in wound healing, where initially they promote inflammation and then later, they switch to a reverse role where they promote the resolution of inflammation (34). Lastly, during the resolution of inflammation phase, T cells infiltrate the wound to aid in healing (34, 39).

The NLRP3 Inflammasome and Interleukin-1β Production

Surgical trauma is aseptic and causes the release of damage-associated molecular patterns (DAMPs) (40). DAMPs are endogenous molecules that are released from damaged or dying cells and serve as a signal for tissue damage (41). Soluble DAMPs that are released as a result of incision include: heparan sulfate (42, 43), fibronectin (44, 45), hyaluronan (46–48), β-defensins (49–51), heat shock protein 70 (Hsp70) (52), and high mobility group box-1 (HMGB1) (53, 54). These DAMPs then bind to PRRs such as Toll-like Receptors (TLRs) on innate immune cells (mast cells, neutrophils, monocytes/macrophages) and sensory neurons, specifically Toll-like Receptor 4 (TLR4) (18, 49, 55–58). Stimulation of TLR4 leads to activation of the transcription factor NF-κB and upregulation of the synthesis of pro-inflammatory cytokines like interleukin-1β (IL-1β) (59). Stimulation of TLR4 also serves as the priming signal for NLRP3, the activator of IL-1β (59).

NLRP3 is predominately expressed by cells in lymphoid organs and tissues that are highly populated by immune cells. These cells include but are not limited to mast cells, neutrophils, macrophages, monocytes, dendritic cells, and neurons in both the peripheral and central nervous systems (29, 60–62). The expression of NLRP3 in these cell types must be induced by inflammatory stimuli, which prevents uncontrolled release of IL-1β. NLRP3 requires two signals for canonical activation and for IL-1β secretion: the first signal primes the cell to express NLRP3 and pro-IL-1β, and the second signal induces inflammasome assembly and activation (41, 63, 64). NLRP3

forms a scaffold with apoptosis-associated speck-like protein containing a CARD (ASC) to provide a molecular platform for activation of pro-caspase-1, which collectively comprises the inflammasome (65). Activated caspase-1 cleaves pro-IL-1β into active IL-1β, which is secreted. Several DAMPs that are present after incision and that can serve as the activation signal for NLRP3 inflammasome assembly include: ATP (66, 67), reactive oxygen species (ROS) (68, 69), and low pH (70–72). The activation cascade for NLRP3 is summarized in **Figure 1**. Indeed, the presence of priming and activating DAMPs for NLRP3 activation after aseptic tissue injury implicate a role for NLRP3 in mediating the postoperative pain phenotype. We recently showed that NLRP3 is upregulated at the surgical site and drives postoperative mechanical pain-like behaviors in male mice, but not in female mice (13). This study provided the first evidence that NLRP3 drives postoperative pain and revealed that the immune-mediated mechanisms that underlie postoperative pain are sex-specific.

SEXUAL DIMORPHISM IN THE IMMUNE RESPONSE

The importance of taking sex into consideration when studying painful injuries and their underlying mechanisms was recently highlighted when it was revealed by Sorge et al. that male mice require microglia and TLR4, whereas female mice require T cells to mediate chronic neuropathic pain (73, 74). In addition, hormones significantly contribute to sex-based differences in the immune response (75). Estradiol, progesterone, and testosterone are the primary hormones that affect the immune response. Female vertebrates have higher baseline estrogen and progesterone levels whereas male vertebrates have higher baseline testosterone levels. Estrogen, progesterone, and testosterone receptors are expressed on both adaptive (T cells and B cells) and innate (macrophages, dendritic cells, neutrophils, and natural killer cells) immune cells; the effects of hormones on these receptors are dose-dependent (76). Consequently, there are alterations in immune system function during pregnancy, menses, and menopause. Each of the three hormones mentioned above affects the immune system during injury or disease states in different ways, and therefore, the immune response to injury differs between males and females.

The level of immune cell infiltration and the extent of the innate immune response at an injury site are both affected by sex hormones. Estrogen suppresses mast cell release of histamine and as a result, fewer neutrophils are recruited to a wound site in females (77, 78). In regards to the effects of estrogen on the macrophage response to injury, Price et al. recently showed that a reduced number of macrophages is recruited to a postoperative tissue site in female mice compared to male mice (79). Additionally, high estrogen levels skew macrophages toward the M2 phenotype (anti-inflammatory) while high testosterone levels promote the M1 phenotype (proinflammatory). As a consequence of the M1 phenotype, males have higher expression of TLR4, NLRP3, and produce more IL-1β than females (75, 80–83). However, chronic estrogen exposure induces increased TLR4-mediated production of IL-1β in macrophages (84). Despite the lower levels of immune cell infiltrate within a wound in females as compared to males, cytokine levels in females are sustained longer than in males, and females have more tissue-resident immune cells than males (75, 78). Furthermore, data from our laboratory demonstrated that males have more IL-1β protein at the peri-incisional site than females (13). Whereas, we showed that NLRP3 mRNA was upregulated by incision to a similar extent in males and females, global deletion of NLRP3 decreased IL-1β levels and sensitization to mechanical stimuli only in males. This suggested that NLRP3 may be differentially regulated post-transcriptionally in males and females following tissue incision, where in females, the IL-1β production occurs independent of NLRP3. The activation pathway for NLRP3 has been suggested to differ in macrophages from male and female Systemic Lupus Erythematosus patients as well (85). In addition, males and females utilize TLR4 in a cell-specific manner. Stimulation of TLR4 on macrophages drives pain in male mice whereas stimulation of TLR4 on sensory neurons drives pain in female mice (86, 87). Furthermore, fibroblasts which play critical roles in the immune response and local environment during tissue injury, also produce IL-1β, and fibroblast IL-1β levels are differentially affected by testosterone and estrogen treatment (88). Considering all of the evidence above for sex-driven differences in the immune response to injury and the resulting differences in sensory neurons, it is imperative to take the sex of an individual into account when selecting and assessing the efficacy of pain interventions.

PROINFLAMMATORY IL-1β AND POSTOPERATIVE PAIN

The primary function of IL-1β is to elicit a pro-inflammatory response to DAMPs (41). IL-1β is expressed by macrophages, monocytes, neutrophils, mast cells, glial cells, and sensory neurons (89–91). Secreted IL-1β exerts its proinflammatory effects through various mechanisms. These include increasing production of other inflammatory mediators via rapidly inducing their mRNA expression, increasing vascular permeability, recruiting immune cells, directly eliciting pain via binding of the IL-1β receptor on sensory neurons, and inducing neurogenic inflammation through sensory neuron sensitization and increased production of calcitonin gene-related peptide alpha (CGRPα) (91–94). IL-1β acts through its receptor type I IL-1 receptor (IL-1R1), which is ubiquitously expressed on neurons of the peripheral and central nervous systems (95, 96). When IL-1R1 binds IL-1β, the accessory protein IL-1R3 is recruited to induce intracellular signaling cascades via association of their intracellular Toll- and IL-1R-like (TIR) domains with signaling proteins (97). The cascade begins with the association of myeloid differentiation primary response gene 88 (MYD88) and interleukin-1 receptor–activated protein kinase (IRAK) 4 with the TIR domains. This leads to complex formation of IRAK1, IRAK2, and tumor necrosis factor–associated factor (TRAF) six and subsequent activation of transcription factors such as NF-κB to upregulate inflammatory genes.

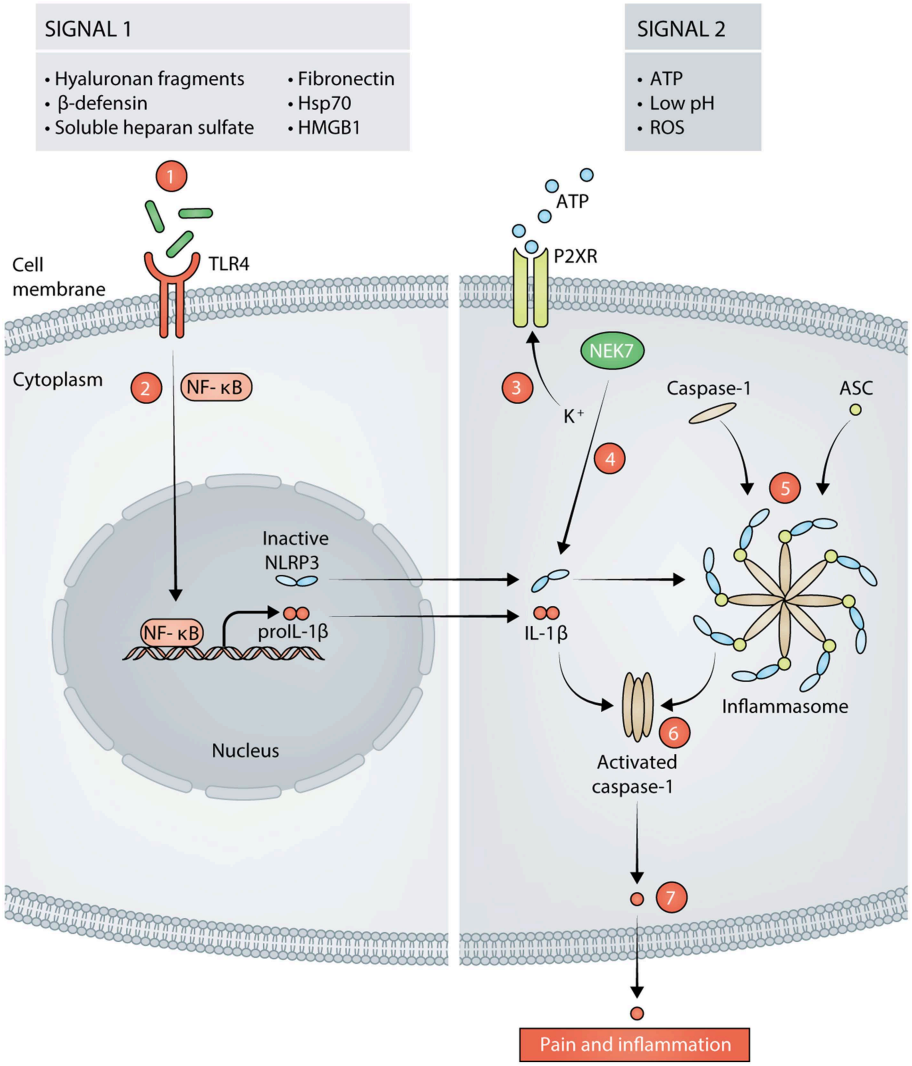

FIGURE 1 | Signals in response to tissue damage activate the NLRP3 inflammasome (signal 1 and signal 2). Hyaluronan fragments, β-defensins, soluble heparan sulfate, fibronectin, 70 kilodalton heat shock proteins (Hsp70), and high mobility group box 1 (HMGB1) are released following incision and act as signal 1 for NLRP3 by stimulating TLR4 on the cell membrane (1). Stimulation of TLR4 leads to activation of NF-κB and transcription of proIL-1β and NLRP3 (2). Adenosine Triphosphate (ATP), reactive oxygen species (ROS), and low pH can then act as signal 2 for NLRP3. ATP acts on purinergic ion channel receptors (P2XR) such as P2X7 or P2X4 which results in potassium (K^+) efflux from the cell (3). The decrease in K^+ concentration is sensed by NIMA Related Kinase 7 (NEK7). NEK7 associates with inactive NLRP3, thereby activating it (4). Active NLRP3 then forms a scaffold with caspase-1 and apoptosis-associated speck-like protein containing a CARD (ASC), thus, forming the inflammasome (5). Caspase-1 is activated by the formation of the inflammasome (6). Activated caspase-1 cleaves proIL- into mature IL-1β that is released from the cell and subsequently, results in pain and inflammation (7).

Postoperative pain is characterized by persistent acute pain at the incisional site which is associated with release of proinflammatory cytokines, including IL-1β. Studies have found that IL-1β is significantly upregulated at the incision site (12, 13, 32, 98–101). Wolf et al. demonstrated that either systemic inhibition of IL-1β signaling by its receptor antagonist IL-1ra or deletion of IL-1R1 prevented the development and maintenance of postoperative mechanical hypersensitivity at the incision site (102). Other groups further demonstrated that inhibition of IL-1β signaling through antagonism of its receptor significantly decreased postoperative pain-like behavior in rodents (32, 98, 100). Furthermore, additional research has established that inhibition of the upstream mediators of IL-1β, such as TLR4 (98, 103), NF-κB (103), caspase-1 (104), or NLRP3 (13), decreases postoperative pain-like behaviors in rodents. General blockade of IL-1β signaling, like that obtained with FDA approved Anakinra (IL-1R1 antagonist), increases the rate of infections due to the necessity of IL-1β for bacterial infection clearance (105, 106). Whereas, inhibition of TLR4, NF-κB, and caspase-1 is more ubiquitous, inhibition of one inflammasome is more specific. Therefore, reduction of IL-1β but not complete depletion, through inhibition of only NLRP3 may avoid these complications while decreasing postoperative pain. However, inhibition of NLRP3 alone may only be effective in males but not females

(13). Not only are sex differences prevalent in mice that received surgery, but they are present in human postoperative pain as well. For instance, a predicative factor of chronic postoperative pain is female sex (107–109). Thus, a therapeutic for the treatment of postoperative pain in females must target the unique factors that are required for the development of postoperative pain in females.

THE ROLE OF NLRP3 IN PAIN DISORDERS

Much is yet to be learned about NLRP3 and postoperative pain, however a role for NLRP3 in pain disorders is emerging (13). NLRP3 has been shown to be involved in the pathogenesis of both inflammatory and neuropathic pain conditions. Inflammatory pain depends on the sensitization of nociceptive neurons by proinflammatory mediators such as IL-1β (110, 111). In an acute model of dural inflammation, the injection of an "inflammatory soup" (comprised of histamine, serotonin, bradykinin, and prostaglandin E2 at pH 5.5) resulted in activated NLRP3 and caspase-1, and increased IL-1β expression in C fiber type neurons of the trigeminal ganglia (29). The inflammatory soup injection also resulted in pain-like behaviors which were alleviated by a caspase-1 inhibitor. In another inflammatory pain model, the complete Freund's adjuvant (CFA) model, NLRP3 was shown to be activated in the skin of rats (28). Electroacupuncture following CFA injection attenuated the expression of NLRP3 and ultimately eliminated the pain-like behavior (28). Additionally, NLRP3 has been demonstrated to be crucial for the pathogenesis of rheumatoid arthritis in both humans and rodents (27, 112, 113). Further, upregulation of NLRP3 has been shown to occur in rodent models of gout, and its inhibition or deletion ameliorated the pathology and pain (24, 25, 114–116). Collectively, these data point to a key role for NLRP3 in inflammatory pain.

Neuropathic pain involves direct damage to nerves from injury or disease. IL-1β significantly contributes to traumatic neuropathic pain where its expression is upregulated in the dorsal root ganglia and spinal cord, as well as in damaged nerves in rodent models of neuropathic pain and in patients with neuropathic pain (18, 117–119). NLRP3 plays a role in various rodent models of neuropathic pain. Alleviation of sciatic nerve ligation neuropathic pain with miR-23a overexpression, or CXCR4 knockdown results in decreased NLRP3 expression (16). A study utilizing the chronic constriction sciatic nerve injury model of neuropathic pain demonstrated that NLRP3 is upregulated by nerve injury and that treatment with Peptide5, a Connexin 43 mimetic peptide that blocks hemichannels, decreased NLRP3 expression and mechanical pain-like behavior (17). In addition, chemotherapy-induced neuropathy models of neuropathic pain revealed that NLRP3 is upregulated in both oxaliplatin-induced nerve injury (19) and paclitaxel-induced nerve injury (20) models, and inhibition of NLRP3 decreased the mechanical pain-like behaviors in both models. In contrast to these findings, it was demonstrated that global knockout of NLRP3 had no effect on neuropathic pain in the spared nerve injury model of neuropathic pain (120). This is consistent with discrepant findings that challenge the view that microglia drive neuropathic pain exclusively in males (121–123). When compared, these studies demonstrate that different models of neuropathic pain (spared nerve injury, spinal nerve transection, spinal nerve ligation, and partial nerve ligation) do not produce the same findings. Together, these studies suggest that while NLRP3 contributes to a variety of etiologies of neuropathic pain it is dependent on the type of injury and the diverse factors that are likely involved in different injuries.

Although much remains to be discovered about the mechanistic causes of body-wide pain syndromes such as fibromyalgia, several studies have indicated a role for NLRP3 in fibromyalgia-associated pain, and NLRP3 was found to be upregulated in patients with fibromyalgia (21–23). Further research is needed in animal models of fibromyalgia and tissues from patients with fibromyalgia.

CONCLUSION

The discovery of inflammasomes has provided new insights into the molecular mechanisms underlying the innate immune system activation in inflammatory and neuropathic pain conditions. As discussed here, many inflammatory and neuropathic pain conditions, and specifically postoperative pain, involve the innate immune system and NLRP3. Therefore, modulators of NLRP3 may provide a novel, selective, and effective pain therapeutic target. Notwithstanding, our understanding of the functional roles and the mechanisms of activation of the NLRP3 inflammasome in pain conditions is in its infancy. Additionally, it is imperative that further research be conducted on the effect of the sex of an individual on NLRP3 function since all of the rodent studies on NLRP3 in the pain conditions discussed here, except for the report by our group (13), were performed in males only. In our study we revealed that there are significant sex differences when NLRP3 is deleted, suggesting that NLRP3 plays different roles in males and females following tissue injury (13). Additionally, the literature concerning the specific immune responses to perioperative incision in males and females is insufficient and far more studies that include females must be done. Therefore, we conclude that targeting NLRP3 may provide a novel approach to control pain, but that further research needs to uncover the mechanistic differences and roles of NLRP3 in wound healing following surgery in females and males.

DATA AVAILABILITY

No datasets were generated or analyzed for this study.

AUTHOR CONTRIBUTIONS

AMC wrote and edited the manuscript. CLS and BND edited the manuscript.

FUNDING

This work was supported by the National Institute of Neurological Disorders and Stroke grants NS040538 and NS070711 to CLS and F31GM123778 to AMC. The Research and Education Component of the Advancing a Healthier Wisconsin Endowment at the Medical College of Wisconsin provided partial support.

ACKNOWLEDGMENTS

The authors thank Neil Smith, freelance illustrator, for creation of **Figure 1**.

REFERENCES

1. Pogatzki-Zahn EM, Segelcke D, Schug SA. Postoperative pain—from mechanisms to treatment. *PAIN Rep.* (2017) 2:e588. doi: 10.1097/PR9.0000000000000588
2. Brennan TJ. Pathophysiology of postoperative pain. *Pain.* (2011) 152:S33–40. doi: 10.1016/j.pain.2010.11.005
3. Mogil JS. Animal models of pain: progress and challenges. *Nat Rev Neurosci.* (2009) 10:283–94. doi: 10.1038/nrn2606
4. Barabas ME, Stucky CL. TRPV1, but not TRPA1, in primary sensory neurons contributes to cutaneous incision-mediated hypersensitivity. *Mol Pain.* (2013) 9:1–14. doi: 10.1186/1744-8069-9-9
5. Zahn PK, Brennan TJ. Primary and secondary hyperalgesia in a rat model for human postoperative pain. *Anesthesiology.* (1999) 90:863–872.
6. Cowie AM, Moehring F, O'Hara C, Stucky CL. Optogenetic inhibition of CGRPα sensory neurons reveals their distinct roles in neuropathic and incisional pain. *J Neurosci.* (2018) 38:5807–25. doi: 10.1523/JNEUROSCI.3565-17.2018
7. Brennan TJ, Vandermeulen EP, Gebhart GF. Characterization of a rat model of incisional pain. *Pain.* (1996) 64:493–501. doi: 10.1016/0304-3959(95)01441-1
8. Pogatzki EM, Raja SN. A mouse model of incisional pain. *Anesthesiology.* (2003) 99:1023–7. doi: 10.1097/00000542-200310000-00041
9. Cowie AM, Stucky CL. A mouse model of postoperative pain. *Bio Protocol.* (2019) 9:3140. doi: 10.21769/BioProtoc.3140
10. Raoof R, Willemen HLD, Eijkelkamp N. Divergent roles of immune cells and their mediators in pain. *Rheumatology.* (2018) 57:429–40. doi: 10.1093/rheumatology/kex308
11. Beilin B, Shavit Y, Trabekin E, Mordashev B, Mayburd E, Zeidel A, et al. The effects of postoperative pain management on immune response to surgery. *Anesth Analg.* (2003) 97:822–7. doi: 10.1213/01.ANE.0000078586.82810.3B
12. Ghasemlou N, Chiu IM, Julien J-P, Woolf CJ. CD11b+Ly6G– myeloid cells mediate mechanical inflammatory pain hypersensitivity. *Proc Natl Acad Sci.* (2015) 112:E6808-17. doi: 10.1073/pnas.1501372112
13. Cowie AM, Menzel AD, O'Hara C, Lawlor MW, Stucky CL. NOD-like receptor protein 3 inflammasome drives postoperative mechanical pain in a sex-dependent manner. *Pain.* (2019). doi: 10.1097/j.pain.0000000000001555. [Epub ahead of print].
14. Ye Z, Ting JPY. NLR, the nucleotide-binding domain leucine-rich repeat containing gene family. *Curr Opin Immunol.* (2008) 20:3–9. doi: 10.1016/j.coi.2008.01.003
15. Cassel SL, Sutterwala FS. Sterile inflammatory responses mediated by the NLRP3 inflammasome. *Eur J Immunol.* (2010) 40:607–11. doi: 10.1002/eji.200940207
16. Pan Z, Shan Q, Gu P, Wang XM, Tai LW, Sun M, et al. miRNA-23a/CXCR4 regulates neuropathic pain via directly targeting TXNIP/NLRP3 inflammasome axis. *J Neuroinflammation.* (2018) 15:1–19. doi: 10.1186/s12974-018-1073-0
17. Tonkin RS, Bowles C, Perera CJ, Keating BA, Makker PGS, Duffy SS, et al. Attenuation of mechanical pain hypersensitivity by treatment with Peptide5, a connexin-43 mimetic peptide, involves inhibition of NLRP3 inflammasome in nerve-injured mice. *Exp Neurol.* (2018) 300:1–12. doi: 10.1016/j.expneurol.2017.10.016
18. Grace PM, Strand KA, Galer EL, Rice KC, Maier SF, Watkins LR. Protraction of neuropathic pain by morphine is mediated by spinal damage associated molecular patterns (DAMPs) in male rats. *Brain Behav Immun.* (2018) 72:45–50. doi: 10.1016/j.bbi.2017.08.018
19. Wahlman C, Doyle TM, Little JW, Luongo L, Janes K, Chen Z, et al. Chemotherapy-induced pain is promoted by enhanced spinal adenosine kinase levels through astrocyte-dependent mechanisms. *Pain.* (2018) 159:1025–34. doi: 10.1097/j.pain.0000000000001177
20. Jia M, Wu C, Gao F, Xiang H, Sun N, Peng P, et al. Activation of NLRP3 inflammasome in peripheral nerve contributes to paclitaxel-induced neuropathic pain. *Mol Pain.* (2017) 13:1744806917719804. doi: 10.1177/1744806917719804
21. Cordero MD, Alcocer-Gómez E, Culic O, Carrión AM, de Miguel M, Díaz-Parrado E, et al. NLRP3 inflammasome is activated in fibromyalgia: the effect of coenzyme Q10. *Antioxid Redox Signal.* (2014) 20:1169–80. doi: 10.1089/ars.2013.5198
22. Cordero MD, Alcocer-Gómez E, Marín-Aguilar F, Rybkina T, Cotán D, Pérez-Pulido A, et al. Mutation in cytochrome b gene of mitochondrial DNA in a family with fibromyalgia is associated with NLRP3-inflammasome activation. *J Med Genet.* (2015) 53:113–22. doi: 10.1136/jmedgenet-2015-103392
23. Bullón P, Alcocer-Gómez E, Carrión AM, Marín-Aguilar F, Garrido-Maraver J, Román-Malo L, et al. AMPK phosphorylation modulates pain by activation of NLRP3 inflammasome. *Antioxid Redox Signal.* (2016) 24:157–70. doi: 10.1089/ars.2014.6120
24. Goldberg EL, Asher JL, Molony RD, Shaw AC, Zeiss CJ, Wang C, et al. β-hydroxybutyrate deactivates neutrophil NLRP3 inflammasome to relieve gout flares. *Cell Rep.* (2017) 18:2077–87. doi: 10.1016/j.celrep.2017.02.004
25. Liu HJ, Pan XX, Liu BQ, Gui X, Hu L, Jiang CY, et al. Grape seed-derived procyanidins alleviate gout pain via NLRP3 inflammasome suppression. *J Neuroinflamm.* (2017) 14:74. doi: 10.1186/s12974-017-0849-y
26. Marchetti C, Swartzwelter B, Gamboni F, Neff CP, Richter K, Azam T, et al. OLT1177, a β-sulfonyl nitrile compound, safe in humans, inhibits the NLRP3 inflammasome and reverses the metabolic cost of inflammation. *Proc Natl Acad Sci USA.* (2018) 115:E1530–9. doi: 10.1073/pnas.1716095115
27. Guo C, Fu R, Wang S, Huang Y, Li X, Zhou M, et al. NLRP3 inflammasome activation contributes to the pathogenesis of rheumatoid arthritis. *Clin Exp Immunol.* (2018) 194:231–43. doi: 10.1111/cei.13167
28. Gao F, Xiang H-C, Li H, Jia M, Pan X, Pan H-L, et al. Electroacupuncture inhibits NLRP3 inflammasome activation through CB2 receptors in inflammatory pain. *Brain Behav Immun.* (2018) 67:91–100. doi: 10.1016/j.bbi.2017.08.004
29. Chen L, Li X, Huang L, Wu Q, Chen LE, Wan Q. Chemical stimulation of the intracranial dura activates NALP3 inflammasome in trigeminal ganglia neurons. *Brain Res.* (2014) 1566:1–11. doi: 10.1016/j.brainres.2014.04.019
30. Zhang H, Li F, Li WW, Stary C, Clark JD, Xu S, et al. The inflammasome as a target for pain therapy. *Br J Anaesth.* (2016) 117:693–707. doi: 10.1093/bja/aew376
31. Hu Y, Liang D, Li X, Liu HH, Zhang X, Zheng M, et al. The role of interleukin-1 in wound biology. part I: murine *in silico* and *in vitro* experimental analysis. *Anesth Analg.* (2010) 111:1525–33. doi: 10.1213/ANE.0b013e3181f5ef5a
32. Hu Y, Liang D, Li X, Liu HH, Zhang X, Zheng M, et al. The role of interleukin-1 in wound biology. part II: *in vivo* and human translational studies. *Anesth Analg.* (2010) 111:1534–42. doi: 10.1213/ANE.0b013e3181f691eb
33. Martin P, D'Souza D, Martin J, Grose R, Cooper L, Maki R, et al. Wound healing in the PU.1 null mouse: tissue repair is not dependent on inflammatory cells. *Curr Biol.* (2003) 13:1122–8. doi: 10.1016/S0960-9822(03)00396-8

34. Baum CL, Arpey CJ. Normal cutaneous wound healing: clinical correlation with cellular and molecular events. *Dermatologic Surg.* (2005) 31:674–86. doi: 10.1097/00042728-200506000-00011
35. Nakamura Y, Kambe N, Saito M, Nishikomori R, Kim Y-G, Murakami M, et al. Mast cells mediate neutrophil recruitment and vascular leakage through the NLRP3 inflammasome in histamine-independent urticaria. *J Exp Med.* (2009) 206:1037–46. doi: 10.1084/jem.20082179
36. Wulff BC, Wilgus TA. Mast cell activity in the healing wound: more than meets the eye? *Exp Dermatol.* (2013) 22:507–10. doi: 10.1111/exd.12169
37. Delavary BM, van der Veer WM, van Egmond M, Niessen FB, Beelen RHJ. Macrophages in skin injury and repair. *Immunobiology.* (2011) 216:753–62. doi: 10.1016/j.imbio.2011.01.001
38. Serhan CN, Savill J. Resolution of inflammation: the beginning programs the end. *Nat Immunol.* (2005) 6:1191–7. doi: 10.1038/ni1276
39. Larouche J, Sheoran S, Maruyama K, Martino MM. Immune regulation of skin wound healing: mechanisms and novel therapeutic targets. *Adv Wound Care.* (2018) 7:209–31. doi: 10.1089/wound.2017.0761
40. Zhang Q, Raoof M, Chen Y, Sumi Y, Sursal T, Junger W, et al. Circulating mitochondrial DAMPs cause inflammatory responses to injury. *Nature.* (2010) 464:104–7. doi: 10.1038/nature08780
41. Martinon F, Mayor A, Tschopp J. The inflammasomes: guardians of the body. *Annu Rev Immunol.* (2009) 27:229–65. doi: 10.1146/annurev.immunol.021908.132715
42. Oksala O, Salo T, Tammi R, Häkkinen L, Jalkanen M, Inki P, et al. Expression of proteoglycans and hyaluronan during wound healing. *J Histochem Cytochem.* (1995) 43:125–35. doi: 10.1177/43.2.7529785
43. Johnson GB, Brunn GJ, Kodaira Y, Platt JL. Receptor-mediated monitoring of tissue well-being via detection of soluble heparan sulfate by toll-like receptor 4. *J Immunol.* (2002) 168:5233–9. doi: 10.4049/jimmunol.168.10.5233
44. Tscharntke M, Pofahl R, Chrostek-Grashoff A, Smyth N, Niessen C, Niemann C, et al. Impaired epidermal wound healing *in vivo* upon inhibition or deletion of Rac1. *J Cell Sci.* (2007) 120:1480–90. doi: 10.1242/jcs.03426
45. Gauperaa T, Gierckskey K, Revhaug A, Rekvig O. Fibronectin, complement and immunoglobulins in serum after surgery. *Br J Surg.* (1985) 72:59–62. doi: 10.1002/bjs.1800720123
46. Taylor KR, Yamasaki K, Radek KA, Di Nardo A, Goodarzi H, Golenbock D, et al. Recognition of hyaluronan released in sterile injury involves a unique receptor complex dependent on toll-like receptor 4, CD44, and MD-2. *J Biol Chem.* (2007) 282:18265–75. doi: 10.1074/jbc.M606352200
47. Litwiniuk M, Krejner A, Grzela T. Hyaluronic acid in inflammation and tissue regeneration. *Wounds.* (2016) 28:78–88.
48. Maharjan AS, Pilling D, Gomer RH. High and low molecular weight hyaluronic acid differentially regulate human fibrocyte differentiation. *PLoS ONE.* (2011) 6:e26078. doi: 10.1371/journal.pone.0026078
49. Gariboldi S, Palazzo M, Zanobbio L, Selleri S, Sommariva M, Sfondrini L, et al. Low molecular weight hyaluronic acid increases the self-defense of skin epithelium by induction of β-defensin 2 via TLR2 and TLR4. *J Immunol.* (2008) 181:2103–10. doi: 10.4049/jimmunol.181.3.2103
50. Bayer A, Lammel J, Tohidnezhad M, Lippross S, Behrendt P, Klüter T, et al. The antimicrobial peptide human β-defensin-3 is induced by platelet-released growth factors in primary keratinocytes. *Mediators Inflamm.* (2017) 2017:6157491. doi: 10.1155/2017/6157491
51. Carter JG, West SK, Painter S, Haynes RJ, Churchill AJ. β-defensin 1 haplotype associated with postoperative endophthalmitis. *Acta Ophthalmol.* (2010) 88:786–90. doi: 10.1111/j.1755-3768.2009.01534.x
52. Dybdahl B, Wahba A, Lien E, Flo TH, Waage A, Qureshi N, et al. Inflammatory response after open heart surgery: release of heat-shock protein 70 and signaling through toll-like receptor-4. *Circulation.* (2002) 105:685–90. doi: 10.1161/hc0602.103617
53. Vacas S, Degos V, Tracey KJ, Maze M. High-mobility group box 1 protein initiates postoperative cognitive decline by engaging bone marrow-derived macrophages. *Anesthesiology.* (2014) 120:1160–7. doi: 10.1097/ALN.0000000000000045
54. Mollen KP, Prince JM, Billiar TR, Liu S, Kaczorowski DJ, Hackam DJ, et al. Systemic inflammation and remote organ injury following trauma require HMGB1. *Am J Physiol Integr Comp Physiol.* (2007) 293:R1538–44. doi: 10.1152/ajpregu.00272.2007
55. Dusio GF, Cardani D, Zanobbio L, Mantovani M, Luchini P, Battini L, et al. Stimulation of TLRs by LMW-HA induces self-defense mechanisms in vaginal epithelium. *Immunol Cell Biol.* (2011) 89:630–9. doi: 10.1038/icb.2010.140
56. Zhang J, Wang H, Xiao Q, Liang H, Li Z, Jiang C, et al. Hyaluronic acid fragments evoke Kupffer cells via TLR4 signaling pathway. *Sci China Ser C Life Sci.* (2009) 52:147–54. doi: 10.1007/s11427-009-0002-y
57. Vabulas RM, Ahmad-Nejad P, Ghose S, Kirschning CJ, Issels RD, Wagner H. HSP70 as endogenous stimulus of the toll/interleukin-1 receptor signal pathway. *J Biol Chem.* (2002) 277:15107–12. doi: 10.1074/jbc.M111204200
58. Okamura Y, Watari M, Jerud ES, Young DW, Ishizaka ST, Rose J, et al. The extra domain a of fibronectin activates toll-like receptor 4. *J Biol Chem.* (2001) 276:10229–33. doi: 10.1074/jbc.M100099200
59. Tschopp J, Schroder K. NLRP3 inflammasome activation: the convergence of multiple signalling pathways on ROS production? *Nat Rev Immunol.* (2010) 10:210–5. doi: 10.1038/nri2725
60. Guarda G, Zenger M, Yazdi AS, Schroder K, Ferrero I, Menu P, et al. Differential expression of NLRP3 among hematopoietic cells. *J Immunol.* (2011) 186:2529–34. doi: 10.4049/jimmunol.1002720
61. Zhang A, Wang K, Ding L, Bao X, Wang X, Qiu X, et al. Bay11-7082 attenuates neuropathic pain via inhibition of nuclear factor-kappa B and nucleotide-binding domain-like receptor protein 3 inflammasome activation in dorsal root ganglions in a rat model of lumbar disc herniation. *J Pain Res.* (2017) 10:375–82. doi: 10.2147/JPR.S119820
62. Fann DY-W, Lim Y-A, Cheng Y-L, Lok K-Z, Chunduri P, Baik S-H, et al. Evidence that NF-κB and MAPK signaling promotes NLRP inflammasome activation in neurons following ischemic stroke. *Mol Neurobiol.* (2017) 55:1082–96. doi: 10.1007/s12035-017-0394-9
63. He Y, Hara H, Nunez G. Mechanism and regulation of NLRP3 inflammasome activation. *Trends Biochem Sci.* (2016) 41:1012–21. doi: 10.1016/j.tibs.2016.09.002
64. Schroder K, Tschopp J. The Inflammasomes. *Cell.* (2010) 140:821–32. doi: 10.1016/j.cell.2010.01.040
65. Martinon F, Burns K, Tschopp J. The inflammasome. *Mol Cell.* (2002) 10:417–26. doi: 10.1016/S1097-2765(02)00599-3
66. Tsuda M, Koizumi S, Inoue K. Role of endogenous ATP at the incision area in a rat model of postoperative pain. *Neuroreport.* (2001) 12:1701–4. doi: 10.1097/00001756-200106130-00036
67. Riteau N, Baron L, Villeret B, Guillou N, Savigny F, Ryffel B, et al. ATP release and purinergic signaling: a common pathway for particle-mediated inflammasome activation. *Cell Death Dis.* (2012) 3:e403. doi: 10.1038/cddis.2012.144
68. Sugiyama D, Kang S, Brennan TJ. Muscle reactive oxygen species (ROS) contribute to post-incisional guarding via the TRPA1 receptor. *PLoS ONE.* (2017) 12:e0170410. doi: 10.1371/journal.pone.0170410
69. Dai J, Zhang X, Wang Y, Chen H, Chai Y. ROS-activated NLRP3 inflammasome initiates inflammation in delayed wound healing in diabetic rats. *Int J Clin Exp Pathol.* (2017) 10:9902–9.
70. Woo YC, Park SS, Subieta AR, Brennan TJ. Changes in tissue pH and temperature after incision indicate acidosis may contribute to postoperative pain. *Anesthesiology.* (2004) 101:468–75. doi: 10.1097/00000542-200408000-00029
71. Rajamäki K, Nordström T, Nurmi K, Åkerman KEO, Kovanen PT, Öörni K, et al. Extracellular acidosis is a novel danger signal alerting innate immunity via the NLRP3 inflammasome. *J Biol Chem.* (2013) 288:13410–9. doi: 10.1074/jbc.M112.426254
72. Takenouchi T, Tsukimoto M, Hashimoto M, Kitani H. Inflammasome activation by danger signals: extracellular ATP and pH. *Inflammasome.* (2014) 1:76–80. doi: 10.2478/infl-2014-0008
73. Sorge RE, Mapplebeck JCS, Rosen S, Beggs S, Taves S, Alexander JK, et al. Different immune cells mediate mechanical pain hypersensitivity in male and female mice. *Nat Neurosci.* (2015) 18:1081–3. doi: 10.1038/nn.4053
74. Sorge RE, Lacroix-fralish ML, Tuttle AH, Sotocinal SG, Austin J, Ritchie J, et al. Spinal cord Toll-like receptor 4 mediates inflammatory and neuropathic hypersensitivity in male but not female mice. *J Neurosci.* (2011) 31:15450–4. doi: 10.1523/JNEUROSCI.3859-11.2011

75. Jaillon S, Berthenet K, Garlanda C. Sexual dimorphism in innate immunity. *Clin Rev Allergy Immunol.* (2017). doi: 10.1007/s12016-017-8648-x. [Epub ahead of print].
76. Klein SL, Marriott I, Fish EN. Sex-based differences in immune function and responses to vaccination. *Trans R Soc Trop Med Hyg.* (2015) 109:9–15. doi: 10.1093/trstmh/tru167
77. Atkins PC, von Allman C, Valenzano M, Zweiman B. The effects of gender on allergen-induced histamine release in ongoing allergic cutaneous reactions. *J Allergy Clin Immunol.* (1993) 91:1031–4. doi: 10.1016/0091-6749(93)90216-3
78. Bird MD, Karavitis J, Kovacs EJ. Sex differences and estrogen modulation of the cellular immune response after injury. *Cell Immunol.* (2008) 252:57–67. doi: 10.1016/j.cellimm.2007.09.007
79. Herneisey M, Mejia G, Pradhan G, Dussor G, Price T, Janjic J. Resveratrol nanoemulsions target inflammatory macrophages to prevent. *J Pain.* (2018) 19:S75–6. doi: 10.1016/j.jpain.2017.12.173
80. Cheng C, Wu H, Wang M, Wang L, Zou H, Li S, et al. Estrogen ameliorates allergic airway inflammation via regulating the activation of NLRP3 inflammasome in mice. *Biosci Rep.* (2018) 39:BSR20181117. doi: 10.1042/BSR20181117
81. Keselman A, Fang X, White PB, Heller NM. Estrogen signaling contributes to sex differences in macrophage polarization during asthma. *J Immunol.* (2017) 199:1573–83. doi: 10.4049/jimmunol.1601975
82. Martinez FO, Gordon S. The M1 and M2 paradigm of macrophage activation: time for reassessment. *F1000Prime Rep.* (2014) 6:1–13. doi: 10.12703/P6-13
83. Zendedel A, Mönnink F, Hassanzadeh G, Zaminy A, Ansar MM, Habib P, et al. Estrogen attenuates local inflammasome expression and activation after spinal cord injury. *Mol Neurobiol.* (2018) 55:1364–75. doi: 10.1007/s12035-017-0400-2
84. Calippe B, Douin-Echinard V, Delpy L, Laffargue M, Lélu K, Krust A, et al. 17β-estradiol promotes TLR4-triggered proinflammatory mediator production through direct estrogen receptor α signaling in macrophages *in vivo*. *J Immunol.* (2010) 185:1169–76. doi: 10.4049/jimmunol.0902383
85. Yang C-A, Huang S-T, Chiang BL. Sex-dependent differential activation of NLRP3 and AIM2 inflammasomes in SLE macrophages. *Rheumatology.* (2015) 54:324–31. doi: 10.1093/rheumatology/keu318
86. Burton M, Szabo-Pardi T, Garner K, Tierney J, Price T. Uncovering cell-specific mechanisms in sex differences in TLR4-dependent pain. *J Pain.* (2019) 20:S1. doi: 10.1016/j.jpain.2019.01.016
87. Burton M, Szabo-Pardi T, Garner K, Asiedu M, Mejia G, Megat S, et al. (131) TLR4-dependent pain depends on different cell types in males and females. *J Pain.* (2017) 18:S9. doi: 10.1016/j.jpain.2017.02.037
88. Ganesan K, Balachandran C, Manohar BM, Puvanakrishnan R. Effects of testosterone, estrogen and progesterone on TNF-α mediated cellular damage in rat arthritic synovial fibroblasts. *Rheumatol Int.* (2012) 32:3181–8. doi: 10.1007/s00296-011-2146-x
89. Dinarello CA. Immunological and inflammatory functions of the interleukin-1 family. *Annu Rev Immunol.* (2009) 27:519–50. doi: 10.1146/annurev.immunol.021908.132612
90. Copray JCVM, Mantingh I, Brouwer N, Biber K, Küst BM, Liem RSB, et al. Expression of interleukin-1 β in rat dorsal root ganglia. *J Neuroimmunol.* (2001) 118:203–11. doi: 10.1016/S0165-5728(01)00324-1
91. Verri WA, Cunha TM, Parada CA, Poole S, Cunha FQ, Ferreira SH. Hypernociceptive role of cytokines and chemokines: targets for analgesic drug development? *Pharmacol Ther.* (2006) 112:116–38. doi: 10.1016/j.pharmthera.2006.04.001
92. Hou L, Li W, Wang X. Mechanism of interleukin-1β-induced calcitonin gene-related peptide production from dorsal root ganglion neurons of neonatal rats. *J Neurosci Res.* (2003) 73:188–97. doi: 10.1002/jnr.10651
93. Jura J, Wegrzyn P, Korostynski M, Guzik K, Oczko-Wojciechowska M, Jarzab M, et al. Identification of interleukin-1 and interleukin-6-responsive genes in human monocyte-derived macrophages using microarrays. *Biochim Biophys Acta.* (2008) 1779:383–89. doi: 10.1016/j.bbagrm.2008.04.006
94. Weber A, Wasiliew P, Kracht M. Interleukin-1β (IL-1β) processing pathway. *Sci Signal.* (2010) 3:cm2. doi: 10.1126/scisignal.3105cm2
95. Boraschi D, Tagliabue A. The interleukin-1 receptor family. *Semin Immunol.* (2013) 25:394–407. doi: 10.1016/j.smim.2013.10.023
96. Song A, Zhu L, Gorantla G, Berdysz O, Amici SA, Guerau-de-Arellano M, et al. Salient type 1 interleukin 1 receptor expression in peripheral non-immune cells. *Sci Rep.* (2018) 8:1–14. doi: 10.1038/s41598-018-19248-7
97. Weber A, Wasiliew P, Kracht M. Interleukin-1 (IL-1) pathway. *Sci Signal.* (2010) 3:cm1. doi: 10.1126/scisignal.3105cm1
98. Chen H, Jiang YS, Sun Y, Xiong YC. P38 and interleukin-1 β pathway via toll-like receptor 4 contributed to the skin and muscle incision and retraction-induced allodynia. *J Surg Res.* (2015) 197:339–47. doi: 10.1016/j.jss.2015.04.061
99. Spofford CM, Brennan TJ. Gene expression in skin, muscle, and dorsal root ganglion after plantar incision in the rat. *Anesthesiology.* (2012) 117:161–72. doi: 10.1097/ALN.0b013e31825a2a2b
100. Loram LC, Themistocleous AC, Fick LG, Kamerman PR. The time course of inflammatory cytokine secretion in a rat model of postoperative pain does not coincide with the onset of mechanical hyperalgesia. *Can J Physiol Pharmacol.* (2007) 85:613–20. doi: 10.1139/Y07-054
101. Liang D, Shi X, Qiao Y, Angst MS, Yeomans DC, Clark JD. Chronic morphine administration enhances nociceptive sensitivity and local cytokine production after incision. *Mol Pain.* (2008) 4:7. doi: 10.1186/1744-8069-4-7
102. Wolf G, Livshits D, Beilin B, Yirmiya R, Shavit Y. Interleukin-1 signaling is required for induction and maintenance of postoperative incisional pain: genetic and pharmacological studies in mice. *Brain Behav Immun.* (2008) 22:1072–7. doi: 10.1016/j.bbi.2008.03.005
103. Xing F, Zhang W, Wen J, Bai L, Gu H, Li Z, et al. TLR4/NF-κB signaling activation in plantar tissue and dorsal root ganglion involves in the development of postoperative pain. *Mol Pain.* (2018) 14:1744806918807050. doi: 10.1177/1744806918807050
104. Liang D-Y, Li X, Li W-W, Fiorino D, Qiao Y, Sahbaie P, et al. Caspase-1 modulates incisional sensitization and inflammation. *Anesthesiology.* (2010) 113:945–56. doi: 10.1097/ALN.0b013e3181ee2f17
105. Cabral VP, de Andrade CAF, Passos SRL, Martins M de FM, Hökerberg YHM. Severe infection in patients with rheumatoid arthritis taking anakinra, rituximab, or abatacept: a systematic review of observational studies. *Rev Bras Reumatol.* (2016) 56:543–50. doi: 10.1016/j.rbre.2016.10.001
106. Sahoo M, Ceballos-Olvera I, Del Barrio L, Re F. Role of the inflammasome, IL-1β, and IL-18 in bacterial infections. *Sci World J.* (2011) 11:2037–50. doi: 10.1100/2011/212680
107. Van Gulik L, Janssen LI, Ahlers SJGM, Bruins P, Driessen AHG, Van Boven WJ, et al. Risk factors for chronic thoracic pain after cardiac surgery via sternotomy. *Eur J Cardio Thor Surg.* (2011) 40:1309–13. doi: 10.1016/j.ejcts.2011.03.039
108. Caumo W, Schmidt AP, Schneider CN, Bergmann J, Iwamoto CW, Adamatti LC, et al. Preoperative predictors of moderate to intense acute postoperative pain in patients undergoing abdominal surgery. *Acta Anaesthesiol Scand.* (2002) 46:1265–71. doi: 10.1034/j.1399-6576.2002.461015.x
109. Katz J, Poleshuck EL, Andruse CH, Hogan LA, Jung BF, Kulick DI, et al. Risk factors for acute pain and its persistence following breast cancer surgery. *Pain.* (2005) 119:16–25. doi: 10.1016/j.pain.2005.09.008
110. Braddock M, Quinn A. Targeting IL-1 in inflammatory disease: new opportunities for therapeutic intervention. *Nat Rev Drug Discov.* (2004) 3:330–40. doi: 10.1038/nrd1342
111. Pillarisetti S. Targeting interleukin-1b for pain. *CNS Neurol Disord Drug Targets.* (2011) 10:571–5. doi: 10.2174/187152711796234998
112. Vande Walle L, Van Opdenbosch N, Jacques P, Fossoul A, Verheugen E, Vogel P, et al. Negative regulation of the NLRP3 inflammasome by A20 protects against arthritis. *Nature.* (2014) 512:69–73. doi: 10.1038/nature13322
113. Choulaki C, Papadaki G, Repa A, Kampouraki E, Kambas K, Ritis K, et al. Enhanced activity of NLRP3 inflammasome in peripheral blood cells of patients with active rheumatoid arthritis. *Arthritis Res Ther.* (2015) 17:1–11. doi: 10.1186/s13075-015-0775-2
114. Martinon F, Pétrilli V, Mayor A, Tardivel A, Tschopp J. Gout-associated uric acid crystals activate the NALP3 inflammasome. *Nature.* (2006) 440:237–41. doi: 10.1038/nature04516
115. Hoffman HM, Scott P, Mueller JL, Misaghi A, Stevens S, Yancopoulos GD, et al. Role of the leucine-rich repeat (LRR) domain of cryopyrin/ NALP3

in monosodium urate crystal-induced inflammation. *Arthritis Rheumatol.* (2010) 62:2170–9. doi: 10.1002/art.27456
116. Amaral FA, Costa VV, Tavares LD, Sachs D, Coelho FM, Fagundes CT, et al. NLRP3 inflammasome-mediated neutrophil recruitment and hypernociception depend on leukotriene B4 in a murine model of gout. *Arthritis Rheum.* (2012) 64:474–84. doi: 10.1002/art.33355
117. Garcia MA, Daemen MA, Steinbusch HW, Visser-Vandewalle V, Andrade P, Hoogland G. Elevated IL-1β and IL-6 levels in lumbar herniated discs in patients with sciatic pain. *Eur Spine J.* (2013) 22:714–20. doi: 10.1007/s00586-012-2502-x
118. Thacker MA, Clark AK, Marchand F, McMahon SB. Pathophysiology of peripheral neuropathic pain: immune cells and molecules. *Anesth Analg.* (2007) 105:838–47. doi: 10.1213/01.ane.0000275190.42912.37
119. Gui W-S, Wei X, Mai C-L, Murugan M, Wu L-J, Xin W-J, et al. Interleukin-1β overproduction is a common cause for neuropathic pain, memory deficit, and depression following peripheral nerve injury in rodents. *Mol Pain.* (2016) 12:1–15. doi: 10.1177/1744806916646784
120. Curto-Reyes V, Kirschmann G, Pertin M, Drexler SK, Decosterd I, Suter MR. Neuropathic pain phenotype does not involve the NLRP3 inflammasome and its end product interleukin-1βin the Mice spared nerve injury model. *PLoS ONE.* (2015) 10:e0133707. doi: 10.1371/journal.pone.0133707
121. Denk F, Crow M, Didangelos A, Lopes DM, McMahon SB. Persistent alterations in microglial enhancers in a model of chronic pain. *Cell Rep.* (2016) 15:1771–81. doi: 10.1016/j.celrep.2016.04.063
122. Peng J, Gu N, Zhou L, Eyo BU, Murugan M, Gan WB, et al. Microglia and monocytes synergistically promote the transition from acute to chronic pain after nerve injury. *Nat Commun.* (2016) 7:12029. doi: 10.1038/ncomms12029
123. Batti L, Sundukova M, Murana E, Pimpinella S, De Castro Reis F, Pagani F, et al. TMEM16F regulates spinal microglial function in neuropathic pain states. *Cell Rep.* (2016) 15:2608–15. doi: 10.1016/j.celrep.2016.05.039

Conflict of Interest Statement: The authors declare that the research was conducted in the absence of any commercial or financial relationships that could be construed as a potential conflict of interest.

frontiers in Immunology

ORIGINAL RESEARCH
published: 14 June 2019
doi: 10.3389/fimmu.2019.01360

Melatonin Suppresses Microglial Necroptosis by Regulating Deubiquitinating Enzyme A20 After Intracerebral Hemorrhage

Jianan Lu[1†], Zeyu Sun[1†], Yuanjian Fang[1†], Jingwei Zheng[1], Shenbin Xu[1], Weilin Xu[1], Ligen Shi[1], Shuhao Mei[1], Haijian Wu[1], Feng Liang[1] and Jianmin Zhang[1,2,3*]*

[1] Department of Neurosurgery, The Second Affiliated Hospital, School of Medicine, Zhejiang University, Hangzhou, China, [2] Brain Research Institute, Zhejiang University, Hangzhou, China, [3] Collaborative Innovation Center for Brain Science, Zhejiang University, Hangzhou, China

OPEN ACCESS

Edited by:
Antje Kroner,
Medical College of Wisconsin,
United States

Reviewed by:
Geert Van Loo,
Flanders Institute for Biotechnology,
Belgium
Jorge Tolivia,
Universidad de Oviedo, Spain

***Correspondence:**
Feng Liang
frankfeng@zju.edu.cn
Jianmin Zhang
zjm135@zju.edu.cn

[†]These authors have contributed equally to this work

Specialty section:
This article was submitted to Multiple Sclerosis and Neuroimmunology, a section of the journal Frontiers in Immunology

Received: 01 March 2019
Accepted: 29 May 2019
Published: 14 June 2019

Citation:
Lu J, Sun Z, Fang Y, Zheng J, Xu S, Xu W, Shi L, Mei S, Wu H, Liang F and Zhang J (2019) Melatonin Suppresses Microglial Necroptosis by Regulating Deubiquitinating Enzyme A20 After Intracerebral Hemorrhage. Front. Immunol. 10:1360. doi: 10.3389/fimmu.2019.01360

Cell death is deeply involved in pathophysiology of brain injury after intracerebral hemorrhage (ICH). Necroptosis, one of the recently discovered forms of cell death, plays an important role in various diseases, including ICH. Previous studies have suggested that a considerable number of neurons undergoes necroptosis after ICH. However, necroptosis of microglia after ICH has not been reported to date. The present study demonstrated for the first time that necroptosis occurred in the microglia surrounding the hematoma after ICH in C57 mice, and melatonin, a hormone that is predominantly synthesized in and secreted from the pineal gland, exerted a neuroprotective effect by suppressing this process. When we further explored the potential underlying mechanism, we found that melatonin inhibits RIP3-mediated necroptosis by regulating the deubiquitinating enzyme A20 (also known as TNFAIP3) expression after ICH. In summary, we have demonstrated the role of microglial necroptosis in the pathogenesis of ICH. More importantly, A20 was identified as a novel target of melatonin, which opens perspectives for future research.

Keywords: intracerebral hemorrhage (ICH), necroptosis, microglia, melatonin, A20

INTRODUCTION

Intracerebral hemorrhage (ICH) is a significant cause of morbidity and mortality worldwide. As one of the most serious forms of stroke, ICH affects ∼2 million people worldwide each year (1–3). Primary injuries after ICH are usually caused by the mechanical damage of the hematoma to the surrounding brain tissues. Following the primary injuries, secondary injuries, including inflammation and cell death, are extensively involved in the pathological processes following hemorrhagic events (4). Treatment of secondary injuries is one of the important interventions after ICH.

Cell death is a hallmark of secondary brain injury after ICH (5). Numerous experimental and clinical observations indicate a variety of cell death forms and mechanisms take place during hemorrhagic stroke (6). Among them, programmed cell death is highly correlated with the homeostatic mechanisms of the nervous system. Necroptosis, also known as programmed necrosis, shares upstream signaling elements with apoptosis, such as tumor necrosis factor (TNF), Fas-associated death domain (FADD), and Toll-like receptor (TLR) (7). However, apoptosis and necroptosis have distinct outcomes.

Apoptotic cells usually induce a non-inflammatory response, whereas necroptosis triggers an inflammatory response (8) due to the rapid loss of plasma membrane integrity prior to the exposure of phagocytic signal (9), which in turn causes the release of intracellular damage-associated molecular patterns (10), which induce inflammation. Microglia, which are primary immune cells of the central nervous system (CNS), undergo necroptosis in various pathological processes, such as ischemic stroke (11), retinal degeneration (12), and spinal cord injury (12). Therefore, it may be beneficial to inhibit necroptosis to reduce neuroinflammation and improve neuronal survival in the context of disease, particularly in microglia (13).

Melatonin (N-acetyl-5-methoxytryptamine) is a hormone that is predominantly synthesized in and secreted from the pineal gland. (14) In 1958, Lerner et al. were the first to isolate melatonin from bovine pineal gland extracts and named it according to its ability to aggregate melanin granules (15). Initial research on melatonin was focused on its regulation of circadian and circannual cycles (16). Later, the multifunctional roles of melatonin were further explored. Melatonin serves as an effective antioxidant in scavenging the highly toxic hydroxyl radical and other oxygen-centered radicals (17), and it promotes the immune response (18). No serious side effects or risks have been reported in association with the ingestion of melatonin (17). These findings suggest that melatonin might play a protective role in various pathological conditions. Therapeutic effects of melatonin in various diseases, including diabetes (19), cancers (20), cardiovascular diseases (21, 22), and CNS diseases (23) have been reported.

In CNS diseases, melatonin has been shown to contribute to the maintenance of cell homeostasis and survival by regulating inflammation, apoptosis, or autophagy after different types of brain injury (24). Melatonin reportedly has a neuroprotective effect after stroke, either ischemic (25, 26) or hemorrhagic (27). Melatonin has also been shown to inhibit necroptosis during myocardial ischemia and liver fibrosis (28–30), and this mechanism might explain its therapeutic effects after stroke. However, whether melatonin can inhibit necroptosis of microglia after ICH and how much protection can be achieved by inhibiting this process remain to be elucidated.

Serine/threonine kinase receptor interacting protein 1 (RIP1) and receptor-interacting protein 3 (RIP3) are important molecules in the process of necroptosis (7). A previous study revealed that RIP1 expression was significantly increased 1–3 days after ICH (31), suggesting that necroptosis occurs in the acute phase after ICH. Upon inhibition of caspase activity, especially that of caspase 8 by genetic or chemical methods, RIP1 forms a necrosome with RIP3 by interacting via their homotypic interaction motif domains and activates their kinase activities (32–34). Subsequently, the pseudokinase mixed lineage kinase domain-like protein (MLKL), is activated as an executive molecule of necroptosis (35). In turn, MLKL translocates to the plasma membrane, where it forms pores and disrupts the plasma membrane integrity (36). Although the necrosome, the characteristic complex of necroptosis, is composed of both RIP1 and RIP3, RIP3 is considered to have a more critical role than RIP1 in the process of necroptosis (37–39). Previous studies have suggested that melatonin inhibits necroptosis mainly by inhibiting the kinase activity of RIP3 (28, 29). However, the specific mechanism of RIP3 regulation by melatonin has not been elucidated.

A20, also known as TNFAIP3, is a deubiquitinating enzyme (40). A20 is widely recognized as a potent anti-inflammatory protein linked to multiple human brain autoimmune diseases, neuro-degenerative diseases, and brain tumors, as well as stroke (41–44). Voet et al. reported that A20 controls microglial activation to regulate neuroinflammation, a function closely related to inhibition of NLR family pyrin domain-containing protein 3 (NLRP3) (45). Moreover, Onizawa et al. discovered that A20 restricts RIP3-dependent necroptosis (46). Thus, we hypothesized that melatonin can upregulate the expression of A20 in the brain, especially in microglia, after ICH, which in turn inhibits the expression of RIP3, thereby exerting a protective effect by inhibiting necroptosis.

In this study, we aimed to demonstrate the occurrence of microglial necroptosis after ICH and to evaluate the effect of melatonin on this process as well as the underlying mechanism, to improve the recovery of neurological function after ICH.

MATERIALS AND METHODS

Animals

C57 mice were purchased from SLAC Laboratory Animal Company Limited (Shanghai, China). In total, 214 male mice (8–10 weeks, 20–25 g) were used in this study. The mice were housed in a temperature- and humidity-controlled room under a standard 12-h light/dark cycle and had free access to food and water. The animal protocol was approved by the Institutional Ethics Committee of the Second Affiliated Hospital, Zhejiang University School of Medicine. The procedures were conducted according to the National Institutes of Health's Guide for the Care and the Use of Laboratory Animals and the ARRIVE (Animal Research: Reporting *in vivo* Experiments) guidelines. Experimental grouping was shown in **Supplementary Figure S1**.

ICH Model

The ICH model was established as previously described (47) (**Figure 1A**). Briefly, mice were anesthetized with 40 mg/kg 1% pentobarbital sodium via intraperitoneal injection. Under stereotactic guidance, a small cranial burr hole was made at a precise location (bregma coordinates: 0.5 mm anterior and 2.5 mm lateral to the midline). Autologous blood (30 μL) from the femoral artery was injected 3.5 mm deep into the right basal ganglia at a rate of 3 μL/min using a microinfusion pump, and the syringe was pulled out after 10 min.

Drug Administration

As described previously (48, 49), melatonin (Sigma, USA) was dissolved in dimethyl sulfoxide (DMSO) and diluted with 0.9% normal saline. A dose of melatonin (20 mg/kg) or vehicle (5% DMSO) was given to mice randomly via intraperitoneal injection 30 min before ICH induction.

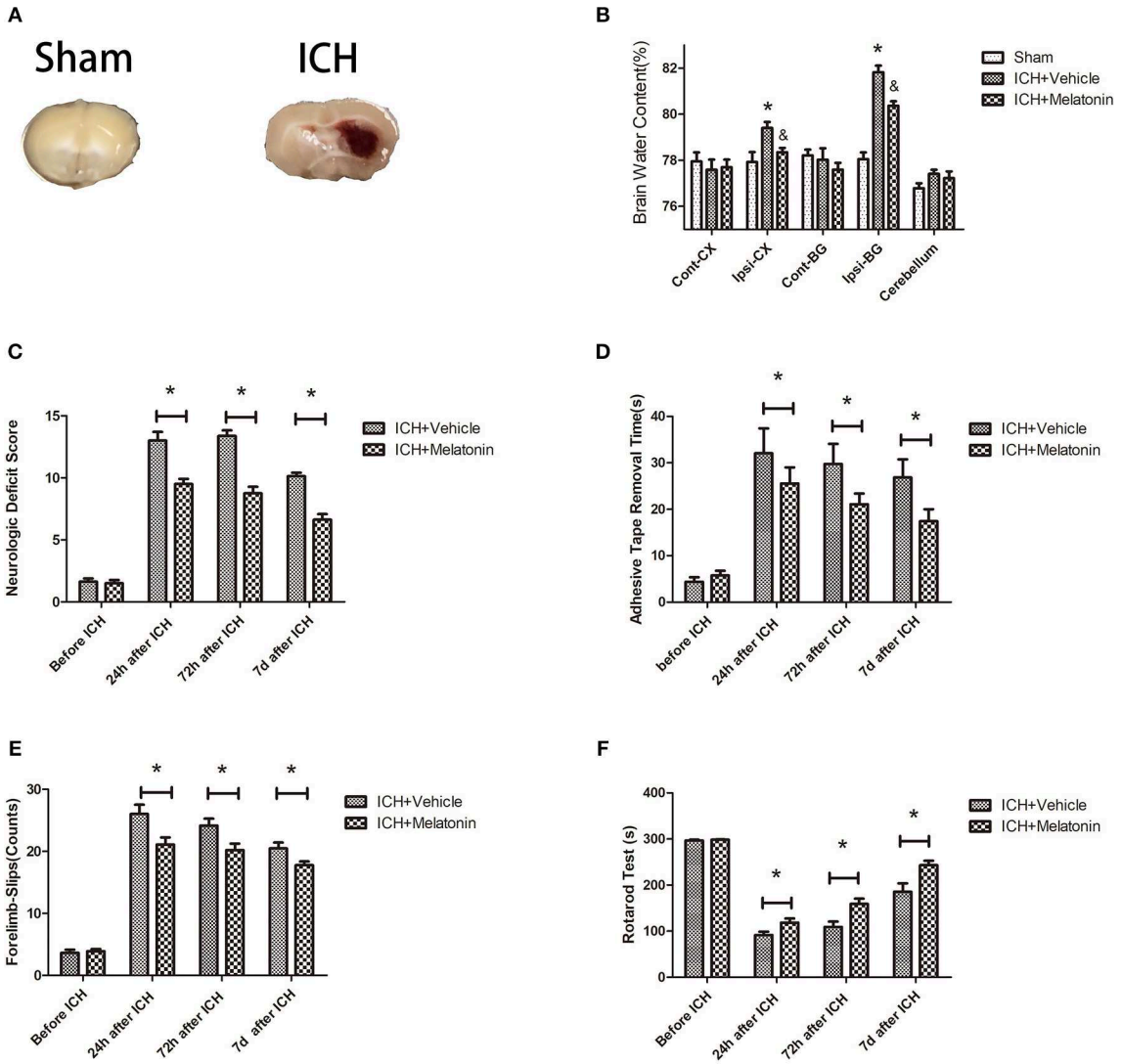

FIGURE 1 | Effects of melatonin on neurologic deficit score, neurological functions, and brain edema. **(A)** Representative photographs of brain slices in the sham and ICH groups (72 h after ICH). **(B)** Quantification of brain water content at 72 h after ICH. $^{*}P < 0.05$ vs. sham group, $^{\&}P < 0.05$ vs. ICH+vehicle group ($n = 6$ in each group). **(C)** Comparison of neurologic deficit scores among ICH+vehicle and ICH+melatonin groups before ICH and at 1, 3, and 7 days after ICH. **(D)** Comparison of adhesive removal test results among the ICH+vehicle and ICH+melatonin groups before ICH and at 1, 3, 7 days after ICH. **(E)** Comparison of foot-fault test results among the ICH+vehicle and ICH+melatonin groups before ICH and at 1, 3, 7 days after ICH. **(F)** Comparison of rotarod test results among the ICH+vehicle and ICH+melatonin groups before ICH and at 1, 3, 7 days after ICH. $^{*}P < 0.05$.

Neurobehavioral Function Assessment

Four evaluation methods were used to assess the voluntary activities and motor function of mice at 24 h, 72 h, and 7 days after ICH impairment.

Neurologic function was tested before and 1, 3, 7 days after ICH by assessing body symmetry, gait, climbing, circling behavior, front limb symmetry, and compulsory circling (50). Each test result was graded from 0 to 4, with a maximum deficit score of 24.

An adhesive removal test was conducted as previously described (51). Briefly, mice were accustomed to the experimental environment for 30 min. Then, an adhesive tape strip was placed on the left hairless part of the forepaws of the mice. Mice were then put into the testing cage and the time to feel and time to remove the strip by any behavior of the mice were recorded.

For the foot-fault test, mice were individually placed on a wired grid (50 × 55 × 52 cm length/width/height) with their paws. Behavior of the mice while they were moving was recorded for 1 min. Each successful foot placement onto the bar was recorded as a step. A foot fault was recorded when a paw slipped through the grid hole. The percentage of foot faults was calculated as: 100 × faults/(successful steps + faults) (52).

A rotarod test was performed as previously described (53). Mice were placed on a Rotamex 5 apparatus (Columbus Instruments). During the test, the speed was increased from 4 rpm to 40 rpm within 5 min. After adaptation for two consecutive days, mice were tested twice daily with at least 30 min between tests. The period to fall off the rotating rod was recorded, and the data were expressed as the mean from three trials.

Brain Water Content

We used a wet–dry method as previously described (54) to evaluate the brain water content at 72 h after ICH. Briefly, after euthanasia, mice ($n = 6$/group) were sacrificed and the brain hemispheres were collected and weighed immediately (wet weight). They were then dried at 100 °C for 48 h and weighed again to obtain the dry weight. The brain water content was calculated as follows: [(wet weight—dry weight)/(wet weight)] × 100% (55).

Propidium Iodide (PI) Staining *in vivo*

PI staining *in vivo* to identify microglial necroptosis was conducted as previously described (31). For all experiments, PI (Beyotime, Shanghai, China) was administered intraperitoneally (10 mg/kg) 1 h before the mice were sacrificed. The brain tissue was cryoprotected by immersion in 15 and 30% sucrose solution. Then, brain sections (10 μm) were cut along the anterior–posterior lesion and placed on poly-L-lysine-coated glass slides. Sections were visualized under a fluorescence microscope (OLYMPUS BX50/BX-FLA/DP70; Olympus Co.). PI+/Iba-1+ cells were counted by observers blinded to the experimental groups. Necroptotic microglia were counted in six microscopic fields per section, and the average number in each section was calculated.

Immunofluorescence

After the mice were anesthetized, transcardial perfusion was performed with 0.1 M PBS, followed by perfusion with 4% paraformaldehyde. The whole brain was immersed in 4% paraformaldehyde for 24 h, then cryoprotected in serial 15 and 30% sucrose solutions. The brain samples were then cut into coronal slices (9 μm) and fixed on slides. After preprocessing with 5% BSA and 0.3% triton X-100, the sections were incubated at 4°C overnight with primary antibodies, including anti-Iba-1 antibody (1:500, Abcam, Cambridge, UK, ab5079), anti-RIP1 antibody (1:200, Cell Signaling Technology, Danvers, MA, USA, CST#D94C12), anti-RIP3 antibody (1:200, Cell Signaling Technology, CST#D4G2A), anti-MLKL antibody (1:100, Santa Cruz Biotechnology, Santa Cruz, CA, USA sc-293201), anti-TNFAIP3 (A20) antibody (1:250, Abcam, ab13597). Then, the cryosections were incubated with secondary antibody [1:300, Thermo Fisher Scientific, Donkey anti-Goat IgG (H+L) Alexa Fluor 488, A32814; Donkey anti-Mouse IgG (H+L) Alexa Fluor 594, A32744; Goat anti-Rabbit IgG (H+L) Alexa Fluor 594, A-11037] at 37°C for 1 h and washed three times with PBST. Finally, the sections were observed and analyzed using a fluorescence microscope (Olympus Co., Tokyo, Japan).

Western Blot Analysis

Brain samples around the hematoma were collected and lysed in RIPA lysis buffer (Beyotime, Shanghai, China). Western blotting was performed as previously described (56). Protein samples (40 μg/lane) were separated by 10% sodium dodecyl sulfate polyacrylamide gel and electrotransferred to polyvinylidene fluoride membranes (Millipore, Burlington, MA, USA). The membranes were blocked at room temperature for 1 h and then incubated overnight with primary antibodies, including: anti-RIP1 antibody (1:1000, Cell Signaling Technology, CST#D94C12), anti-RIP3 antibody (1:1000, Cell Signaling Technology, CST#D4G2A), anti-MLKL antibody (1:200, Santa Cruz Biotechnology, sc-293201), anti-TNFAIP3 (A20) antibody (1:1000, Abcam, ab13597), anti-RIP3 (phospho S232) antibody (1:1000, Abcam, ab195117), anti-MLKL (phosphor S345) antibody (1:1000, Abcam, ab196436), anti-NLRP3 (1:1000, Abcam, ab98151).

Small Interfering (si)RNA and Intracerebroventricular Injection

A20 siRNA or scramble siRNA (Genomeditech, Shanghai, China) mixed with transfection reagent (Engreen Biosystem, Auckland, New Zealand) was delivered via intracerebroventricular injection as previously described (57). Briefly, the injections into the right ventricle were performed using the following coordinates relative to bregma (0.2 mm posterior, 1.0 mm lateral, and 2.0 mm deep) at 48 h prior to surgery. After the injection was completed, the needle was left in the brain for 10 min, and the burr hole was blocked with bone wax.

Single Cell Sorting

Single cell sorting was performed as described previously (58). In brief, brain samples were fixed by transcardial perfusion with PBS before extraction. After dissociation, cells were separated by 30% Percoll density gradient separation by centrifugation at 800 ×*g* for 30 min at 18°C. Then, the cells were passed through a 70-μm nylon mesh. Cell populations were sorted on an Aria SORP instrument (BD Biosciences, San Jose, CA, USA). The gating strategy is shown in **Supplementary Figure S2**. CD45+ (PerCP CD45, 1:200, BD Biosciences, 557235) and CD11b+ (FITC CD11b, 1:200, BD Biosciences, 557396) cells were isolated as microglia. Immediately after sorting, the cells were stored at −80°C until processed.

Cell Lines and Coculture

The mouse microglial cell line BV2 and the mouse hippocampal cell line HT22 were cultured (37°C, 5% CO_2) in Dulbecco's modified Eagle's medium with 10% fetal bovine serum, 100 U/ml penicillin and 100 μg/ml streptomycin. As secondary damage in ICH is mainly caused by oxidized hemoglobin, we used 100 μM OxyHb to simulate the pathological process of ICH *in vitro,* as previously described (31). Melatonin was used at 1 mM to study the effect of melatonin on necroptosis *in vitro*. A Transwell coculture system was used to investigate the effect of BV2 cells on HT22 cells. BV2 cells were cultured at a density of 5×10^4 in Transwell inserts (pore size 0.4 μm; Corning, Corning, NY, USA) placed above the HT22 neuronal layer.

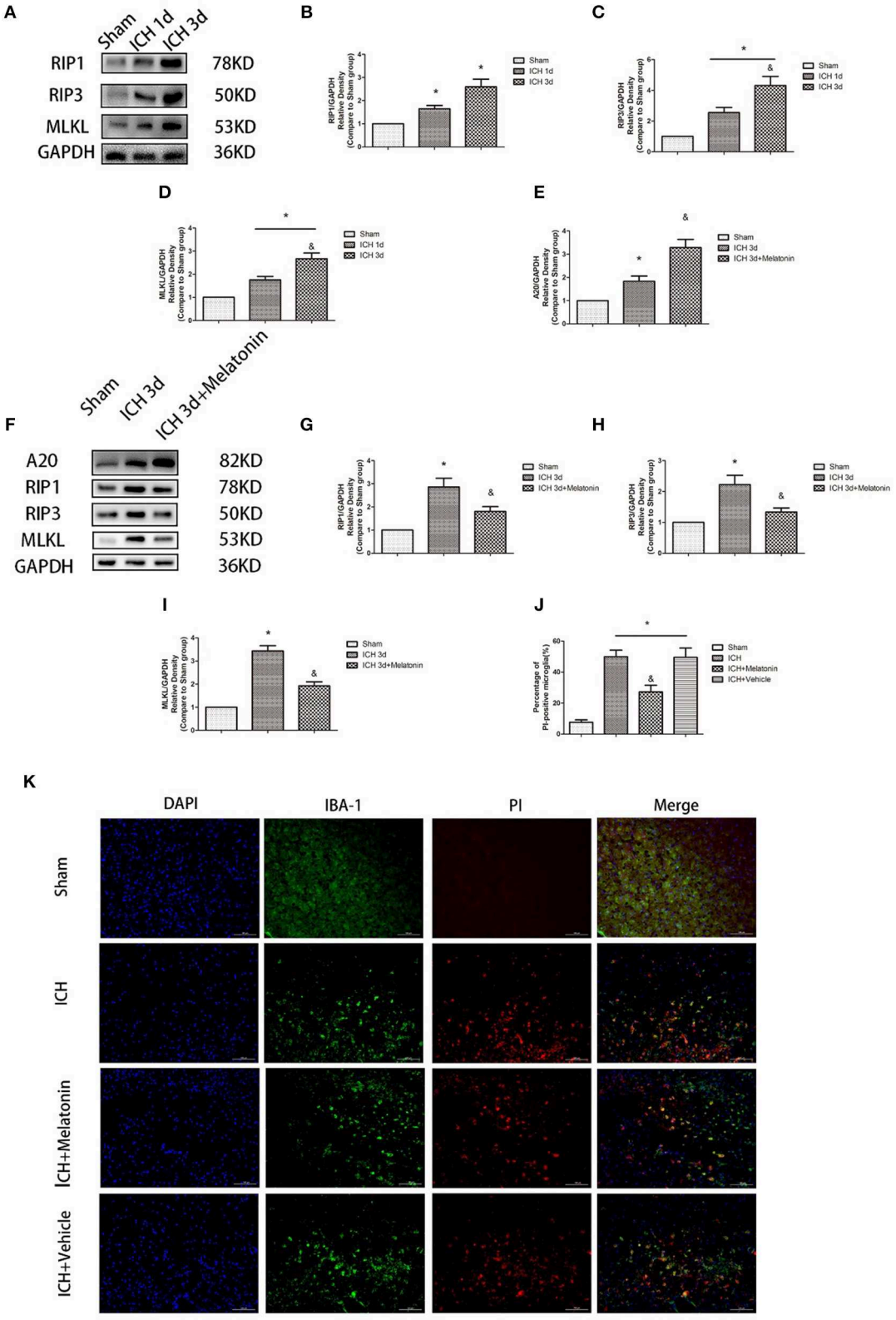

FIGURE 2 | Melatonin suppresses necroptosis in microglia after ICH. **(A)** RIP1, RIP3, and MLKL protein expression was significantly enhanced at 1 and 3 days after ICH. **(B)** RIP1 expression, $^{*}P < 0.05$ vs. sham group ($n = 6$/group). **(C)** RIP3 expression. $^{*}P < 0.05$ vs. sham group ($n = 6$/group), $^{\&}P < 0.05$ vs. ICH 1-day group

(Continued)

FIGURE 2 | ($n = 6$/group). **(D)** MLKL expression. $^{*}P < 0.05$ ($n = 6$ in each group), $^{\&}P < 0.05$ vs. ICH 1-day group ($n = 6$/group). **(E,K)** PI staining around ICH hematoma. A significant increase in PI+ microglia was observed in the ICH group. $^{*}P < 0.05$ vs. sham group ($n = 6$/group). Melatonin treatment significantly decreased PI+ microglia compared with the levels in the ICH+vehicle group. $^{\&}P < 0.05$ vs. ICH+vehicle group ($n = 6$/group). **(F)** Expression of A20, RIP1, RIP3, and MLKL proteins in sorted microglia of each group. **(G)** A20 expression. **(H)** RIP1 expression. **(I)** RIP3 expression. **(J)** MLKL expression. $^{*}P < 0.05$ vs. sham group ($n = 6$/group), $^{\&}P < 0.05$ vs. ICH 3-day group ($n = 6$/group).

Cell Viability Assay and Cytotoxicity Assay

As necroptosis is a type of cell death, cell viability and cytotoxicity can reflect its occurrence *in vitro*. Cells were cultured in 96-well plates. The CCK-8 cell counting kit (Beyotime, Shanghai, China) was used to evaluate cell viability according to the manufacturer's instructions. Twenty microliters of CCK-8 solution was added to 200 μl of cell culture medium, after which the plates were incubated at 37°C for 2 h. Then, the absorbance at 450 nm was measured. Cytotoxicity was evaluated using an LDH lactate dehydrogenase cytotoxicity test kit (Beyotime). Briefly, cells were cultured in serum-free medium for 24 h. Then, the plates were centrifuged at 400 ×*g* for 5 min. One hundred twenty microliters of supernatant of each well was transferred to a new 96-well plate, and the absorbance at 490 nm was measured immediately.

ELISA

To explore changes in inflammatory factors, a TNF ELISA KIT (Abcam, ab100747) was used according to the manufacturer's instructions to quantify the levels of TNF in BV2 cell supernatant.

Reactive Oxygen Species (ROS) Assay

ROS can be both an inducer and a product of necroptosis. ROS levels in cells were examined using a ROS Assay Kit (JianCheng, Nanjing, China) according to the manufacturer's instructions. In brief, cells were trypsinized, collected, and incubated with 10 μM 2′,7′-dichlorodihydrofluorescein diacetate at room temperature for 30 min. After two washes, intracellular ROS production was measured by fluorescence detection using a microplate reader at an excitation wavelength of 485 nm and an emission wavelength of 535 nm. Protein levels in the cells were measured using a detergent-compatible protein assay kit (Bio-Rad, Hercules, CA, USA). ROS levels are reported as fluorescence/mg protein.

Annexin V and PI Staining *in vitro*

Cells were cultured in six-well plates and subjected to melatonin treatment. Cells were trypsinized with 0.25% trypsin (without EDTA) and centrifuged at 1000 ×*g* for 5 min and resuspended in 300 μl of binding buffer. Subsequently, 1 μl of Annexin V and 1 μl of PI (Becton Dickinson, Franklin Lanes, NJ, USA) were added to the cell suspension. After 30 min of incubation at 37°C in the dark, the cells were analyzed by flow cytometry (FACSCalibur; BD Biosciences, San Diego, CA, USA). Cells were first gated based on forward and side scatter, and necroptotic cells were determined as FITC+/PI+.

Measurement of Mitochondrial Membrane Potential ($\Delta\psi$m)

BV2 cells were cultured in a six-well plate. The $\Delta\psi m$ was measured using a JC-1 kit (Beyotime, Shanghai, China) following the manufacturer's instructions. After rinsing with PBS, cells were incubated with JC-1 staining solution at 37°C for 20 min, then washed with JC-1 staining buffer. Then, the cells were imaged using a fluorescence microscope (Olympus, Tokyo, Japan). The fluorescence intensity was measured using a fluorometric microplate reader (FilterMax F5, Molecular Devices, Sunnyvale, USA) at dual wavelengths: excitation and emission at 485 and 530 nm (to detect JC-1 monomer) and at 530 and 590 nm (to detect JC-1 polymer).

Transmission Electron Microscopy

Mice were sacrificed and perfused with 0.9% saline and 4% PFA. Fragments of peri-hematoma tissues (∼1 mm^3) were collected and immersed in glutaraldehyde (2.5%) at 4°C overnight. The tissues were preprocessed as previously described (59, 60). The samples were sliced into 100-nm sections and stained with 4% uranyl acetate and 0.5% lead citrate. The ultrastructure of the tissues was evaluated by transmission electron microscopy (Philips Tecnai 10, Netherlands).

Statistical Analysis

All data are expressed as the mean ± standard deviation (SD) and were analyzed in GraphPad Prism v. 6.0. Data were tested for normality of distribution by the Kolmogorov-Smirnov test. One-way ANOVA was applied for comparing multiple groups. The analyses were conducted in SPSS v. 22.0 (SPSS Inc.). Statistical significance was defined as $P < 0.05$.

RESULTS

Melatonin Reduces Brain Edema, Improves Neurological and Motor Function After ICH

We evaluated the brain water content to explore the effects of melatonin treatment on ICH-induced brain edema. No significant differences were noted in the contralateral cortex, contralateral basal ganglia, or cerebellum between sham, ICH+vehicle, and ICH+melatonin groups. However, compared to the sham group, the brain water content was increased in the ipsilateral cortex and ipsilateral basal ganglia of mice in the ICH+vehicle group, whereas melatonin treatment significantly reduced the brain water content (**Figure 1B**). To explore the effect of melatonin on the neurological function of mice after ICH, we carried out various neurological tests before ICH and at 24 h, 72 h, and 7 days after ICH. Melatonin or vehicle (5% DMSO) was given to mice randomly via intraperitoneal injection 30 min before ICH induction. The neurological deficit scores were significantly increased after ICH and peaked at 72 h, whereas melatonin significantly improved neurological function (**Figure 1C**). The results of motor function assessment showed trends similar to those of neurological deficit scores (**Figures 1D–F**).

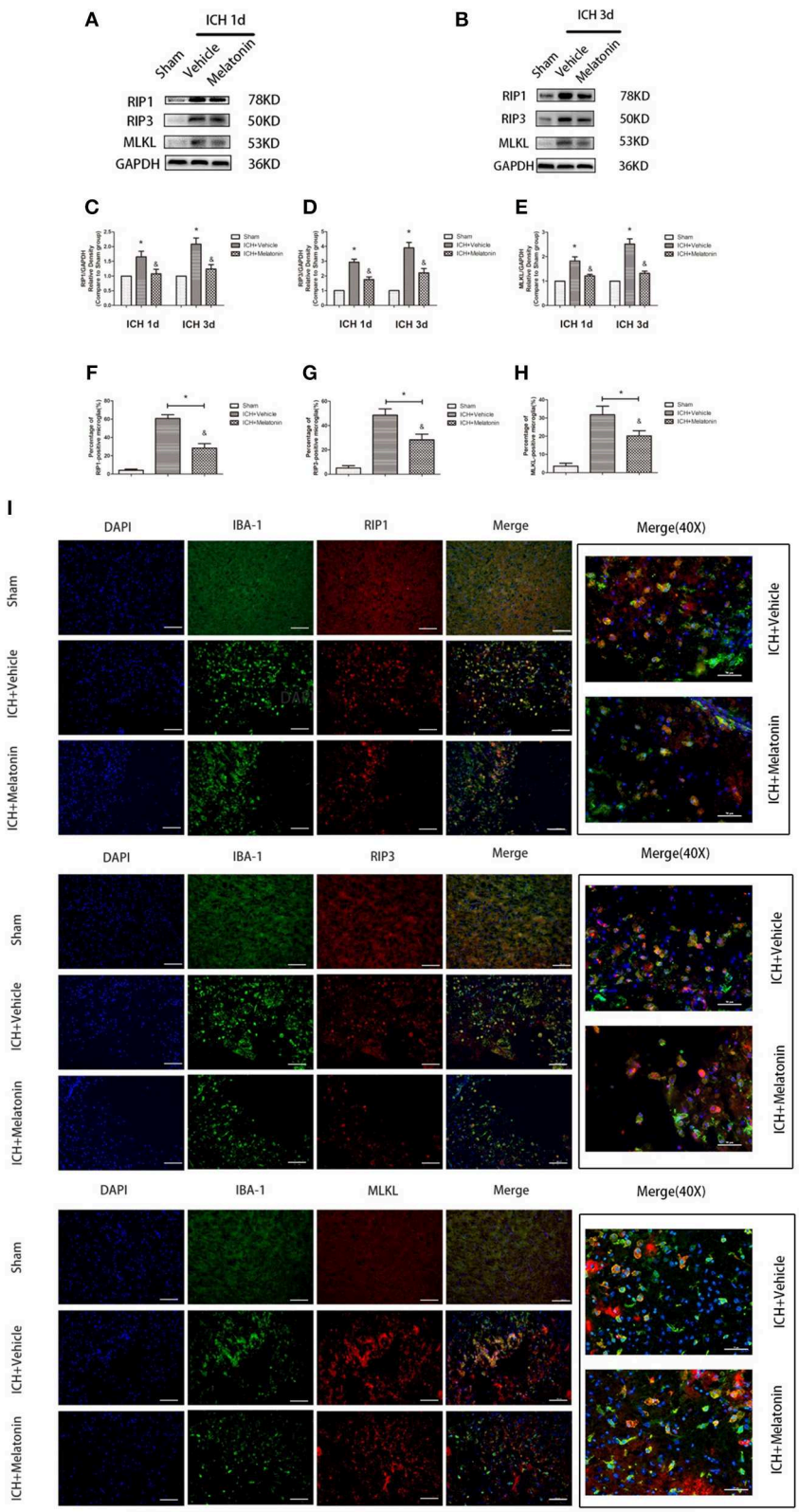

FIGURE 3 | Melatonin suppresses microglial necroptosis at the early stage after ICH. **(A,B)** Western blots for RIP1, RIP3, and MLKL proteins in mice pretreated or not with melatonin via intraperitoneal injection, at 1 day and 3 days after ICH. **(C)** RIP1 expression. *$P < 0.05$ vs.

(Continued)

FIGURE 3 | corresponding sham group ($n = 6$/group), $^{\&}P < 0.05$ vs. corresponding ICH+vehicle group ($n = 6$/group). **(D)** RIP3 expression. $^{*}P < 0.05$ vs. corresponding sham group ($n = 6$/group), $^{\&}P < 0.05$ vs. corresponding ICH+vehicle group. **(E)** MLKL expression. $^{*}P < 0.05$ vs. corresponding sham group ($n = 6$/group), $^{\&}P < 0.05$ vs. corresponding ICH+vehicle group. **(F–I)** Immunofluorescence staining showing the distribution of RIP1/RIP3/MLKL+ microglia surrounding hematoma at 3 days after ICH. Corresponding individually stained fluorescence images of higher magnification (40×) are shown in **Supplementary Figure S3**. $^{*}P < 0.05$ vs. sham group ($n = 6$/group), $^{\&}P < 0.05$ vs. ICH+vehicle group ($n = 6$/group).

Microglia Undergo Necroptosis After ICH

To explore the involvement of necroptosis of microglia after ICH, we performed a series of experiments. The expression of RIP1, RIP3, MLKL, which are executive molecules in necroptosis, was significantly increased at 24 h and 72 h after ICH ($P<0.05$ vs. sham group; **Figures 2A–D**). Correspondingly, cells that were costained for these molecules and Iba-1 were also remarkably increased at 72 h after ICH ($P < 0.05$ vs. sham group; **Figures 3F–I**). To further illustrate the occurrence of microglial necroptosis after ICH, we isolated microglia, and we found that at 3 days after ICH, the expression of necroptosis-related proteins (RIP1, RIP3, MLKL) in microglia was significantly higher than that in sham group ($P < 0.05$ vs. sham group; **Figures 2F–I**). We also counted PI+ microglia in frozen brain sections at 72 h after ICH. PI+/Iba-1+ cells were remarkably increased in brain tissues surrounding hematomas after ICH ($P < 0.05$ vs. sham group; **Figures 2J,K**). These results demonstrated that necroptosis occurred in microglia surrounding the hematoma after ICH.

Melatonin Plays a Protective Role by Suppressing Necroptosis in Microglia

To explore the effects of melatonin on necroptosis after ICH, the protein levels of RIP1, RIP3 and MLKL were detected by western blot analysis at 24 h and 72 h after ICH. As shown in **Figures 3A–E**, the expression of these proteins was significantly increased in the ICH+vehicle group compared to the sham group ($P < 0.05$), whereas melatonin treatment significantly suppressed the increases ($P < 0.05$ vs. ICH+vehicle group). Immunofluorescence staining revealed that cells costained for these molecules and Iba-1 were decreased in the ICH+melatonin compared to the ICH+vehicle group ($P < 0.05$; **Figures 3F–I**). Further, melatonin significantly reduced the expression of necroptosis-related proteins (RIP1, RIP3, MLKL) at 3 days after ICH in microglia ($P < 0.05$ vs. ICH 3-day group; **Figures 2F–I**). These results indicated that melatonin suppresses necroptosis of microglia in brain tissues after ICH.

Melatonin Reduces Mitochondrial Damage in Microglia After ICH

Mitochondrial damage has been shown to be involved in necroptosis (8, 61). Therefore, we used TEM to detect mitochondrial damage at 72 h after ICH. In the brain tissues of the ICH group, mitochondria with obvious vacuolization and swelling were observed (**Figure 4A**). Next, we determined the $\Delta\psi m$ of BV2 cells *in vitro* by JC-1 staining. As shown in **Figure 4B**, the green fluorescence intensity was increased in OxyHb+vehicle group compared to the sham group, indicating a decline of $\Delta\psi m$; however, pre-incubation with melatonin attenuated the OxyHb-induced collapse of the $\Delta\psi m$ ($P < 0.05$). A microplate fluorescence read-out yielded similar results (**Figure 4C**). These results suggested that melatonin reduces mitochondrial damage after ICH by suppressing necroptosis.

Melatonin Prevents Cytotoxic and ROS Production-Enhancing Effects of OxyHb *in vitro*

Figure 5A shows representative photographs of OxyHb-treated and control BV2 cells. Swollen cells with ruptured plasma membrane can be observed in the OxyHb-treated group. We examined the effects of melatonin on necroptosis *in vitro* by cell viability and cytotoxicity assays. As shown in **Figures 5B,C**, cell viability was decreased in the OxyHb+vehicle group as compared to the control group ($P < 0.05$), whereas pretreatment with melatonin significantly improved cell viability ($P < 0.05$). The cytotoxicity assays suggested that OxyHb had a cytotoxic effect on BV2 cells ($P < 0.05$), which was prevented by melatonin pretreatment ($P < 0.05$). ROS were measured to investigate the effects of melatonin on ROS production in BV2 cells. As shown in **Figure 5D**, treatment with OxyHb remarkably promoted ROS production, which was suppressed by pretreatment with melatonin ($P < 0.05$). The above results indicated that melatonin improves BV2 cell viability and reduces cytotoxicity and ROS generation *in vitro*.

Melatonin Suppresses TNF Secretion by Microglia, Thus Reducing Neuronal Necroptosis

As the main immune cells in the nervous system, changes in microglia would affect the homeostasis of other cells, such as neurons. We firstly explored whether the inflammatory factor TNF, a common inducer of necroptosis, is involved in this process. The concentration of TNF was significantly higher in the culture medium of BV2 cells treated with OxyHb than that in that of the control group, whereas melatonin pretreatment significantly reduced TNF production (**Figure 5E**, $P < 0.05$). Next, we explored the effects of necroptotic microglia on neurons after ICH by using a Transwell system. HT-22 neurons were cocultured with BV2 cells exposed to various treatments. The neurons were then stained with Annexin V and PI and analyzed by flow cytometry. The necroptotic population (defined as Annexin V−/PI+) was increased in neurons cocultured with BV2 cells treated with OxyHb when compared with the control group, whereas pretreatment with melatonin suppressed this increase (**Figures 5F–H**; $P < 0.05$). These results indicated that melatonin suppresses TNF secretion by reducing microglial necroptosis, which in turn reduces neuronal necroptosis.

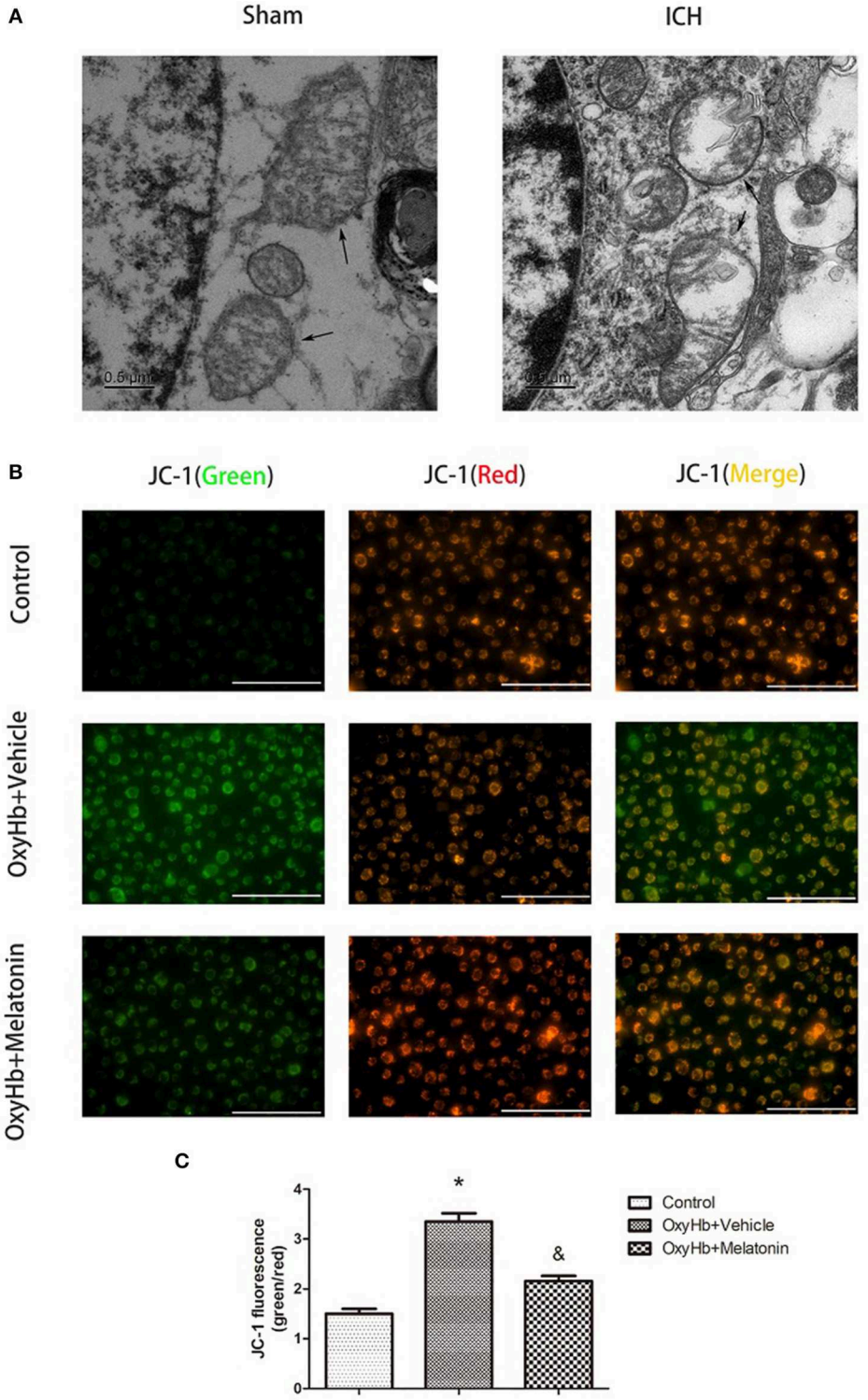

FIGURE 4 | Mitochondrial damage after ICH. **(A)** TEM images of mitochondrial ultrastructure (black arrow) in basal ganglion area. **(B)** Representative photographs of JC-1-staied BV2 cells. **(C)** Quantification of JC-1 fluorescence intensity using a fluorometric microplate reader at dual wavelengths. Treatment with 10 μM OxyHb significantly decreased the $\Delta\psi$m of BV2 cells, whereas pre-incubation with melatonin attenuated the OxyHb-induced collapse of the $\Delta\psi$m. $^{*}P < 0.05$ vs. control group (n= 6 in each group), $^{\&}P < 0.05$ vs. OxyHb+vehicle group (n = 6/group).

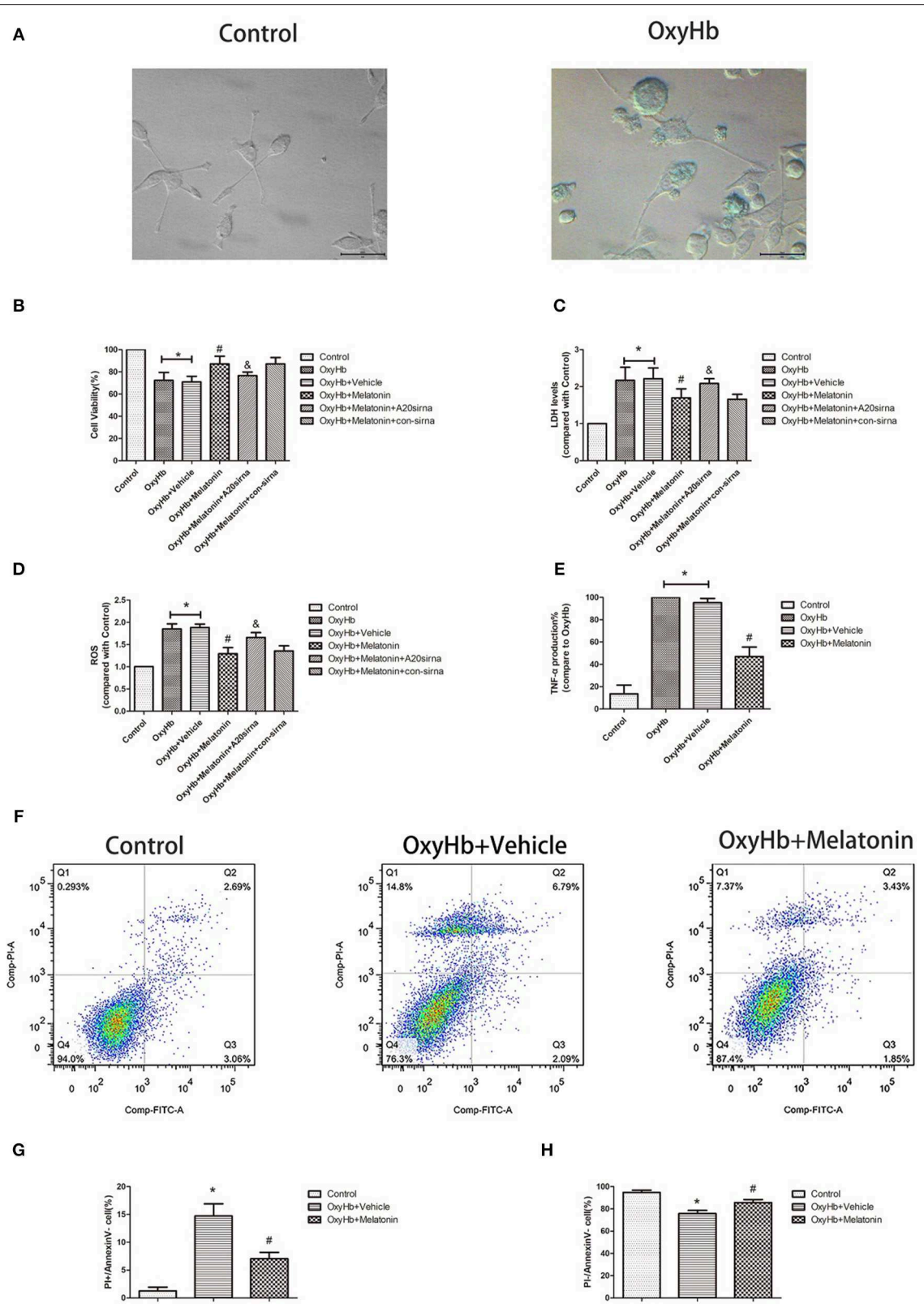

FIGURE 5 | OxyHb decreases cell viability, exerts cytotoxicity, and promotes inflammatory factor production in BV2 cells, thus inducing necroptosis in HT22 cells. Pre-incubation with melatonin effectively reduces the occurrence of these effects. **(A)** Representative photographs of BV2 cells in the control and OxyHb group (72 h).

(Continued)

FIGURE 5 | BV2 cells in the OxyHb group showed cell swelling and plasma membrane rupture. **(B)** Results of cell viability assay. **(C)** Result of LDH assay. **(D)** Results of ROS production assay. **(E)** Results of TNF production assay in BV2 cell supernatant. OxyHb increased TNF production in BV2 cells, whereas melatonin significantly suppressed this. **(F–H)** Flow-cytometric analysis of HT22 cells cocultured with BV2 cells exposed to different treatments. HT22 cells cocultured with BV2 cells treated with OxyHb showed a higher necroptotic population (defined as PI+/FITC−), whereas melatonin significantly reduced the necroptotic population. $^{*}P < 0.05$ vs. control group ($n = 6$/group), $^{\#}P < 0.05$ vs. OxyHb+vehicle group ($n = 6$/group), $^{\&}P < 0.05$ vs. OxyHb+melatonin+con-siRNA group.

A20 Is Expressed in the Acute Phase in Microglia After ICH, and Melatonin Promotes Its Expression and Thus Plays a Protective Role

We analyzed the expression of A20 at 72 h after ICH; A20 expression was significantly increased after ICH (**Figures 6A,B**; $P < 0.05$ vs. sham group). Treatment with melatonin significantly enhanced the expression of A20 after ICH (**Figures 6A,B**; $P < 0.05$ vs. ICH+vehicle group). Accordingly, immunofluorescence analysis revealed that A20 was expressed in the microglia surrounding the hematoma after ICH, and A20 expression was significantly increased after treatment with melatonin (**Figures 6C,D**, $P < 0.05$). To verify the above results, we measured A20 expression in microglia at 3 days after ICH. The results showed that A20 expression was significantly enhanced when compared with the sham group (**Figures 2E,F**; $P < 0.05$ vs. sham group). In line with the above results, melatonin treatment remarkably increased A20 expression after ICH (**Figures 2E,F**; $P < 0.05$ vs. ICH 3-day group). We investigated the relationship between A20 and RIP3-dependent necroptosis after ICH further by using A20 siRNA. As shown in **Figure 6E**, A20 siRNA transfection blocked the activating effect of melatonin on A20 expression ($P < 0.05$ vs. ICH+melatonin+con-siRNA group). Moreover, A20 siRNA blocked the effects of melatonin on RIP1, RIP3, MLKL expression ($P < 0.05$ vs. ICH+melatonin+con-siRNA group). Melatonin reduced the phosphorylation of RIP3 and MLKL, which was prevented by A20 siRNA transfection (**Figures 6E–L**; $P < 0.05$). *In vitro*, A20 siRNA abolished the effects of melatonin on viability and ROS production in BV2 cells (**Figures 5B–D**). As A20 is generally considered to be a negative regulator of NLRP3, we also detected NLRP3 expression. The results showed that A20 siNRA lowered the promotive effect of melatonin on NLRP3 expression (**Figures 6E–L**; $P < 0.05$). These results indicated that melatonin inhibits RIP3-mediated necrotic apoptosis following ICH by regulating A20 expression.

DISCUSSION

In this study, we demonstrated that melatonin inhibits necroptosis of microglia after ICH, thereby reducing brain edema and improving neurological function in the acute phase of ICH. In addition, we uncovered the potential underlying mechanism, in which melatonin regulates A20, thus affecting RIP3-dependent necroptosis (**Figure 7**).

Increasing evidence indicates that necroptosis plays a crucial role in the pathogenesis of several diseases with an inflammatory component (13). Shen et al. (31) found that necroptosis is an important mechanism of neuronal death after ICH, and treatment with necrostatin-1, a specific inhibitor of RIP1, could rescue the neurons from necroptosis, revealing a potential therapeutic target for ICH. Microglia are associated with necroptosis in different disease models (62–64); however, the exact underlying mechanism remained unclear. Moreover, there are no reports on microglial necroptosis after ICH. This study for the first time demonstrated that a significant amount of microglia around the hematoma did undergo necroptosis around 24 and 72 h after ICH. Although the relationship between necroptosis and inflammation has not been fully elucidated, necroptosis is generally thought to induce inflammation as, unlike apoptosis, it is essentially a type of necrotic cell death. In addition to inflammation, necroptosis causes some other cascade reactions, including mitochondrial damage, which exacerbates the release of ROS (32), which induce necroptosis. In line with previous experimental results (65), the present study suggested that mitochondrial damage and ROS accumulation after ICH might be caused by necroptosis. Therefore, necroptosis can play an intermediate role in the induction of inflammation by microglia after ICH. As resident macrophages in the CNS, microglia exert a variety of neuroprotective functions, such as phagocytosis and elimination, secretion of anti-inflammatory factors, growth factors, and promotion of the recovery of neurological function (66, 67). Thus, although microglia account for only approximately 10% of cells in the CNS, their death after ICH aggravates outcome. Therefore, we hypothesized that necroptosis plays an important role in the pathological processes after ICH.

A previous study revealed that A20 expression was increased after ICH and was associated with anti-inflammatory effects by inhibiting NF-κB activation (44). In addition to its NF-κB-regulatory function, A20 is a ubiquitin-regulating enzyme, and increasing evidence shows that the central importance of its functions can be attributed to its ability to modulate ubiquitin-dependent signaling cascades (42). Ubiquitination is one of most prevalent post-translational protein modifications that regulate a variety of important physiological functions. During ubiquitination, ubiquitin, a highly conserved 76-amino-acid protein, is conjugated to lysine residues of diverse cellular proteins (66, 68). The E3 ubiquitin ligase activity of A20 has been shown to directly ubiquitinate RIP1, thus triggering proteasomal degradation of RIP1, which in turn inhibits TNF-induced NF-κB activation (69). Therefore, in the present study, we mainly focused on the role of A20 as a deubiquitinating enzyme. As RIP1 is involved in apoptosis, it seems plausible that A20 could inhibit cellular apoptosis by promoting RIP1 degradation. However, a previous studies indicated that its anti-apoptotic effect is cell type- and stimulus-specific; thus, its protective effect is controversial (70). One study reported that A20 tends

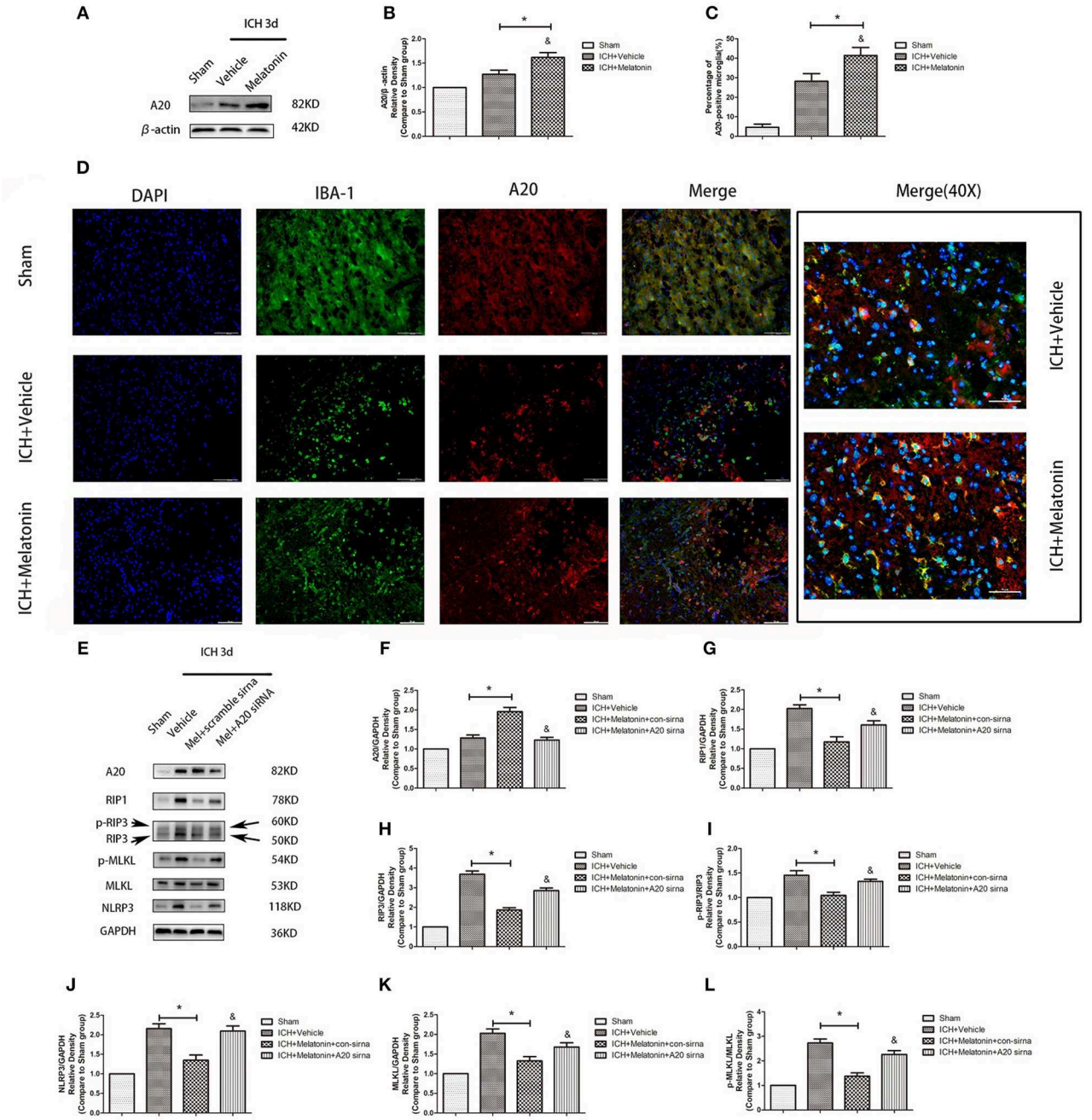

FIGURE 6 | Role of A20 in the regulation of necroptosis after ICH by melatonin. **(A)** Western blots for A20 proteins in mice pretreated or not with melatonin via intraperitoneal injection, at 3 day after ICH. **(B)** A20 expression. $^{*}P < 0.05$ vs. sham group ($n = 6$/group), $^{\&}P < 0.05$ vs. ICH+vehicle group ($n = 6$/group). **(C,D)** Immunofluorescence staining showing the distribution of A20+ microglia surrounding hematoma at 72 h after ICH. A significant increase in A20+/Iba-1+ cells was observed in the ICH+vehicle group. $^{*}P < 0.05$ vs. sham group ($n = 6$/group). Melatonin treatment significantly enhanced the increase in A20+/Iba-1+ cells. $^{\&}P < 0.05$ vs. ICH+vehicle group ($n = 6$/group). Corresponding individually stained fluorescence images of higher magnification (40×) are shown in **Supplementary Figure S3**. **(E)** A20 knockdown attenuated the inhibitory effects of melatonin on microglial necroptosis. **(F)** A20 expression, **(G)** RIP1 expression, **(H)** RIP3 expression, **(I)** p-RIP3 expression, **(J)** NLRP3 expression, **(K)** MLKL expression, and **(L)** p-MLKL expression. $^{*}P < 0.05$ vs. sham group ($n = 6$/group), $^{\&}P < 0.05$ vs. ICH+melatonin+con-siRNA group.

to inhibit apoptosis via various mechanisms (41); however, other results indicated that in certain pathological conditions, such as IBD, A20 binds to RIP1 to enhance TNF-induced apoptosis (71). We did not further explore the effect of A20 on microglial apoptosis in this study. However, regardless of promotive or inhibitory effects, A20 is considered to directly

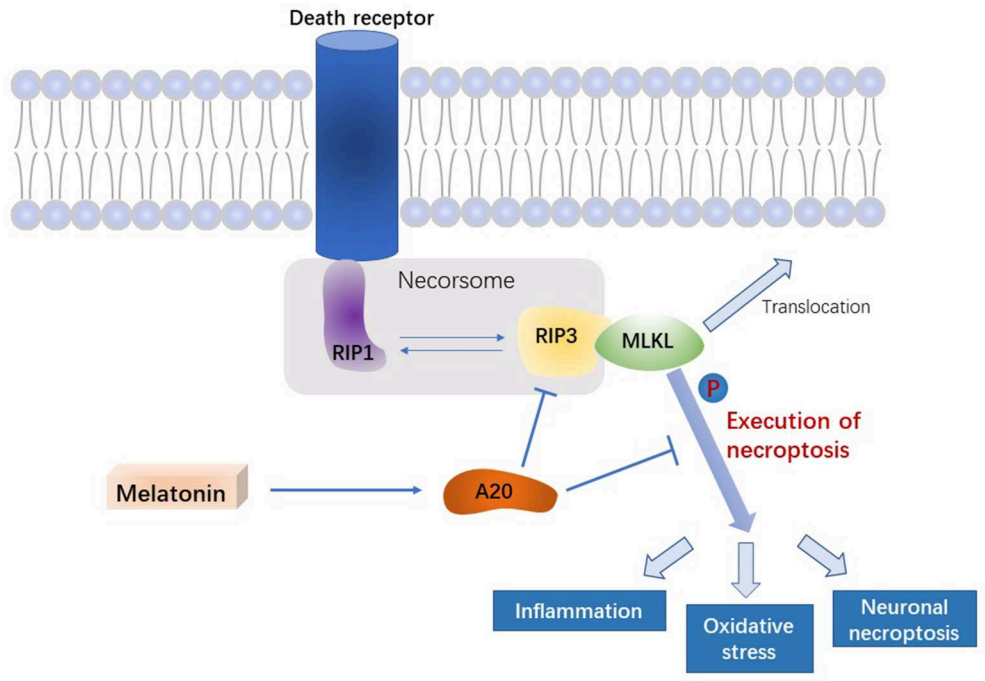

FIGURE 7 | Signal pathway underlying the effect of melatonin on microglial necroptosis after ICH. After ICH, by upregulating A20 protein expression, melatonin suppresses RIP3 phosphorylation in microglia, which in turn inhibits the activation of MLKL, the executive molecule of necroptosis, thereby inhibiting inflammation, reducing mitochondrial damage, and reducing oxidative stress, ultimately playing a neuroprotective role after ICH.

interact with RIP1 rather than via regulating NF-κB (71). As mentioned earlier, the necrosome is composed of both RIP1 and RIP3. Because RIP1 is involved in various biological processes, RIP3 is more valuable than RIP1 when studying necroptosis specifically. Moreover, RIP1 is not considered to be ubiquitinated in the necrosome, which suggests that A20 might regulate necroptosis by regulating RIP3. Furthermore, RIP3 has been regarded a specific activator of necroptosis because it regulates RIP1 phosphorylation (32) and switches TNF-induced cell death from apoptosis to necroptosis (33). The potential of A20 to suppress TNF-induced necroptosis by affecting RIP3 was observed in L929 cells and in primary mouse T cells (46, 72). In line herewith, in the present study, A20 regulated RIP3, thus inhibiting necroptosis.

Melatonin intervenes in different pathological processes through various mechanisms, e.g., it reduces inflammation (24, 73, 74), protects mitochondrial oxidoreductase and superoxide dismutase, thus improving ROS scavenging (75), and inhibits apoptosis (24, 76). In myocardial ischemia, melatonin inhibits necroptosis in cardiomyocytes by inhibiting RIP3 (29). In our study, melatonin inhibited necroptosis of microglia after ICH. We further explored the possible underlying mechanism. A20 is a regulatory protein of the NF-κB signaling pathway, with effects quite similar to those observed after treatment with melatonin. Accordingly, we found that melatonin inhibits RIP3-mediated necroptosis by promoting A20 expression. Interestingly, the NLRP3-regulatory effect of melatonin could be abolished by A20 siRNA transfection *in vitro*. This opens a new perspective for future exploration of NLRP3-mediated inflammation.

This study had some limitations that cannot be ignored. Firstly, melatonin might exert its neuroprotective effects after ICH by regulating various functions; the present study only explored its effect on necroptosis. Secondly, we only used cell lines for investigating the effect of melatonin on necroptosis *in vitro*; considering some subtle differences between cell lines and primary cells, out data would be more convincing had we used primary cells.

In conclusion, this study revealed that melatonin exerts neuroprotective effects after ICH. We demonstrated that melatonin inhibits microglial necroptosis via the A20/RIP3 pathway, in turn reducing cell death, inflammation, and mitochondrial damage. These findings implicate A20 as a novel potential therapeutic target for ICH.

DATA AVAILABILITY

The datasets generated for this study are available on request to the corresponding author.

ETHICS STATEMENT

The animal protocol was approved by the Institutional Ethics Committee of the Second Affiliated Hospital, Zhejiang University School of Medicine. The procedures were conducted according to the National Institutes of Health's Guide for the Care and the

Use of Laboratory Animals and the ARRIVE (Animal Research: Reporting *in vivo* Experiments) guidelines.

AUTHOR CONTRIBUTIONS

JiaZ is the principal investigator. JL, ZS, and FL contributed to the study design, performance, and manuscript draft. YF, JinZ, SX, and SM analyzed the experimental data. WX, LS, and HW revised the manuscript and polished the language.

FUNDING

This work was supported by grants of the Major Research and Development Project of Zhejiang Province (2017C03021) to JiaZ and the Youth Fund of the National Natural Science Fund project (81701214) to HW.

ACKNOWLEDGMENTS

We thank Susu Lou for support to JL.

SUPPLEMENTARY MATERIAL

The Supplementary Material for this article can be found online at: https://www.frontiersin.org/articles/10.3389/fimmu.2019.01360/full#supplementary-material

Supplementary Figure S1 | Experimental grouping.jpg. *In-vivo* and *in-vitro* experimental groups.

Supplementary Figure S2 | FACS gating strategy.jpg. Gating strategy used to isolate microglia.

Supplementary Figure S3 | Single-stained fluorescence.jpg. Single-stained high-magnification (40×) fluorescence images.

REFERENCES

1. Hemphill JC III, Greenberg SM, Anderson CS, Becker K, Bendok BR, Cushman M, et al. Guidelines for the management of spontaneous intracerebral hemorrhage: a guideline for healthcare professionals froma the american heart association/american stroke association. *Stroke*. (2015) 46:2032–60. doi: 10.1161/STR.0000000000000069
2. Krishnamurthi RV, Feigin VL, Forouzanfar MH, Mensah GA, Connor M, Bennett DA, et al. Global and regional burden of first-ever ischaemic and haemorrhagic stroke during 1990–2010: findings from the Global Burden of Disease Study 2010. *Lancet Global Health*. (2013) 1:e259–81. doi: 10.1016/S2214-109X(13)70089-5
3. Feigin VL, Lawes CM, Bennett DA, Barker-Collo SL, Parag V. Worldwide stroke incidence and early case fatality reported in 56 population-based studies: a systematic review. *Lancet Neurol*. (2009) 8:355–69. doi: 10.1016/S1474-4422(09)70025-0
4. Keep RF, Hua Y, Xi G. Intracerebral haemorrhage: mechanisms of injury and therapeutic targets. *Lancet Neurol*. (2012) 11:720–31. doi: 10.1016/S1474-4422(12)70104-7
5. Chu X, Wu X, Feng H, Zhao H, Tan Y, Wang L, et al. Coupling between interleukin-1R1 and necrosome complex involves in hemin-induced neuronal necroptosis after intracranial hemorrhage. *Stroke*. (2018) 49:2473–82. doi: 10.1161/STROKEAHA.117.019253
6. Fricker M, Tolkovsky AM, Borutaite V, Coleman M, Brown GC. Neuronal cell death. *Physiol Rev*. (2018) 98:813–80. doi: 10.1152/physrev.00011.2017
7. Linkermann A, Green DR. Necroptosis. *N Engl J Med*. (2014) 370:455–65. doi: 10.1056/NEJMra1310050
8. Maeda A, Fadeel B. Mitochondria released by cells undergoing TNF-alpha-induced necroptosis act as danger signals. *Cell Death Dis*. (2014) 5:e1312. doi: 10.1038/cddis.2014.277
9. Golstein P, Kroemer G. Cell death by necrosis: towards a molecular definition. *Trends Biochem Sci*. (2007) 32:37–43. doi: 10.1016/j.tibs.2006.11.001
10. Zhang Y, Chen X, Gueydan C, Han J. Plasma membrane changes during programmed cell deaths. *Cell Res*. (2018) 28:9–21. doi: 10.1038/cr.2017.133
11. Yang J, Zhao Y, Zhang L, Fan H, Qi C, Zhang K, et al. RIPK3/MLKL-mediated neuronal necroptosis modulates the M1/M2 polarization of microglia/macrophages in the ischemic cortex. *Cerebral Cortex*. (2018) 28:2622–35. doi: 10.1093/cercor/bhy089
12. Fan H, Zhang K, Shan L, Kuang F, Chen K, Zhu K, et al. Reactive astrocytes undergo M1 microglia/macrohpages-induced necroptosis in spinal cord injury. *Mol Neurodegener*. (2016) 11:14. doi: 10.1186/s13024-016-0081-8
13. Oliveira SR, Amaral JD, Rodrigues CMP. Mechanism and disease implications of necroptosis and neuronal inflammation. *Cell Death Dis*. (2018) 9:903. doi: 10.1038/s41419-018-0872-7
14. Hu J, Zhang L, Yang Y, Guo Y, Fan Y, Zhang M, et al. Melatonin alleviates postinfarction cardiac remodeling and dysfunction by inhibiting Mst1. *J Pineal Res*. (2017) 62:e12368. doi: 10.1111/jpi.12368
15. Lerner AB, Case JD, Takahashi Y. Isolation of melatonin and 5-methoxyindole-3-acetic acid from bovine pineal glands. *J Biol Chem*. (1960) 235:1992–7.
16. Reiter RJ. Pineal melatonin: cell biology of its synthesis and of its physiological interactions. *Endocr Rev*. (1991) 12:151–80. doi: 10.1210/edrv-12-2-151
17. Brzezinski A. Melatonin in humans. *N Engl J Med*. (1997) 336:186–95. doi: 10.1056/NEJM199701163360306
18. Maestroni GJ. The immunoneuroendocrine role of melatonin. *J Pineal Res*. (1993) 14:1–10. doi: 10.1111/j.1600-079X.1993.tb00478.x
19. Rubio-Sastre P, Scheer FA, Gómez-Abellán P, Madrid JA, Garaulet M. Acute melatonin administration in humans impairs glucose tolerance in both the morning and evening. *Sleep*. (2014) 37:1715–9. doi: 10.5665/sleep.4088
20. Su SC, Hsieh MJ, Yang WE, Chung WH, Reiter RJ, Yang SF. Cancer metastasis: mechanisms of inhibition by melatonin. *J Pineal Res*. (2017) 62:e12370. doi: 10.1111/jpi.12370
21. Simko F, Baka T, Paulis L, Reiter RJ. Elevated heart rate and nondipping heart rate as potential targets for melatonin: a review. *J Pineal Res*. (2016) 61:127–37. doi: 10.1111/jpi.12348
22. Dominguez-Rodriguez A, Abreu-Gonzalez P, Sanchez-Sanchez JJ, Kaski JC, Reiter RJ. Melatonin and circadian biology in human cardiovascular disease. *J Pineal Res*. (2010) 49:14–22. doi: 10.1111/j.1600-079X.2010.00773.x
23. Pandi-Perumal SR, Trakht I, Srinivasan V, Spence DW, Maestroni GJ, Zisapel N, et al. Physiological effects of melatonin: role of melatonin receptors and signal transduction pathways. *Progress Neurobiol*. (2008) 85:335–53. doi: 10.1016/j.pneurobio.2008.04.001
24. Fernandez A, Ordonez R, Reiter RJ, Gonzalez-Gallego J, Mauriz JL. Melatonin and endoplasmic reticulum stress: relation to autophagy and apoptosis. *J Pineal Res*. (2015) 59:292–307. doi: 10.1111/jpi.12264
25. Macleod MR, O'Collins T, Horky LL, Howells DW, Donnan GA. Systematic review and meta-analysis of the efficacy of melatonin in experimental stroke. *J Pineal Res*. (2005) 38:35–41. doi: 10.1111/j.1600-079X.2004.00172.x
26. Ramos E, Patiño P, Reiter RJ, Gil-Martín E, Marco-Contelles J, Parada E, et al. Ischemic brain injury: new insights on the protective role of melatonin. *Free Radical Biol Med*. (2017) 104:32–53. doi: 10.1016/j.freeradbiomed.2017.01.005
27. Wu HJ, Wu C, Niu HJ, Wang K, Mo LJ, Shao AW, et al. Neuroprotective mechanisms of melatonin in hemorrhagic stroke. *Cell Mol Neurobiol*. (2017) 37:1173–85. doi: 10.1007/s10571-017-0461-9
28. Yang Z, Li C, Wang Y, Yang J, Yin Y, Liu M, et al. Melatonin attenuates chronic pain related myocardial ischemic susceptibility through inhibiting RIP3-MLKL/CaMKII dependent necroptosis. *J Mol Cell Cardiol*. (2018) 125:185–94. doi: 10.1016/j.yjmcc.2018.10.018
29. Zhou H, Li D, Zhu P, Ma Q, Toan S, Wang J, et al. Inhibitory effect of melatonin on necroptosis via repressing the Ripk3-PGAM5-CypD-mPTP

pathway attenuates cardiac microvascular ischemia-reperfusion injury. *J Pineal Res.* (2018) 65:e12503. doi: 10.1111/jpi.12503
30. Choi HS, Kang JW, Lee SM. Melatonin attenuates carbon tetrachloride-induced liver fibrosis via inhibition of necroptosis. *Transl Res*. (2015) 166:292–303. doi: 10.1016/j.trsl.2015.04.002
31. Shen H, Liu C, Zhang D, Yao X, Zhang K, Li H, et al. Role for RIP1 in mediating necroptosis in experimental intracerebral hemorrhage model both *in vivo* and *in vitro*. *Cell Death Dis*. (2017) 8:e2641. doi: 10.1038/cddis.2017.58
32. Cho YS, Challa S, Moquin D, Genga R, Ray TD, Guildford M, et al. Phosphorylation-driven assembly of the RIP1-RIP3 complex regulates programmed necrosis and virus-induced inflammation. *Cell*. (2009) 137:1112–23. doi: 10.1016/j.cell.2009.05.037
33. Zhang DW, Shao J, Lin J, Zhang N, Lu BJ, Lin SC, et al. RIP3, an energy metabolism regulator that switches TNF-induced cell death from apoptosis to necrosis. *Science*. (2009) 325:332–6. doi: 10.1126/science.1172308
34. He S, Wang L, Miao L, Wang T, Du F, Zhao L, et al. Receptor interacting protein kinase-3 determines cellular necrotic response to TNF-alpha. *Cell*. (2009) 137:1100–11. doi: 10.1016/j.cell.2009.05.021
35. Sun L, Wang H, Wang Z, He S, Chen S, Liao D, et al. Mixed lineage kinase domain-like protein mediates necrosis signaling downstream of RIP3 kinase. *Cell*. (2012) 148:213–27. doi: 10.1016/j.cell.2011.11.031
36. Vanden Berghe T, Linkermann A, Jouan-Lanhouet S, Walczak H, Vandenabeele P. Regulated necrosis: the expanding network of non-apoptotic cell death pathways. *Nat Rev. Mol Cell Biol*. (2014) 15:135–47. doi: 10.1038/nrm3737
37. Mandal P, Berger SB, Pillay S, Moriwaki K, Huang C, Guo H, et al. RIP3 induces apoptosis independent of pronecrotic kinase activity. *Mol Cell*. (2014) 56:481–95. doi: 10.1016/j.molcel.2014.10.021
38. Kaiser WJ, Daley-Bauer LP, Thapa RJ, Mandal P, Berger SB, Huang C, et al. RIP1 suppresses innate immune necrotic as well as apoptotic cell death during mammalian parturition. *Proc Natl Acad Sci USA*. (2014) 111:7753–8. doi: 10.1073/pnas.1401857111
39. Kaiser WJ, Sridharan H, Huang C, Mandal P, Upton JW, Gough PJ, et al. Toll-like receptor 3-mediated necrosis via TRIF, RIP3, and MLKL. *J Biol Chem*. (2013) 288:31268–79. doi: 10.1074/jbc.M113.462341
40. Boone DL, Turer EE, Lee EG, Ahmad RC, Wheeler MT, Tsui C, et al. The ubiquitin-modifying enzyme A20 is required for termination of Toll-like receptor responses. *Nat Immunol*. (2004) 5:1052–60. doi: 10.1038/ni1110
41. Abbasi A, Forsberg K, Bischof F. The role of the ubiquitin-editing enzyme A20 in diseases of the central nervous system and other pathological processes. *Front Mol Neurosci*. (2015) 8:21. doi: 10.3389/fnmol.2015.00021
42. Catrysse L, Vereecke L, Beyaert R, van Loo G. A20 in inflammation and autoimmunity. *Trends Immunol*. (2014) 35:22–31. doi: 10.1016/j.it.2013.10.005
43. Ma A, Malynn BA. A20: linking a complex regulator of ubiquitylation to immunity and human disease. *Nat Rev Immunol*. (2012) 12:774–85. doi: 10.1038/nri3313
44. Meng Z, Zhao T, Zhou K, Zhong Q, Wang Y, Xiong X, et al. A20 ameliorates intracerebral hemorrhage-induced inflammatory injury by regulating TRAF6 polyubiquitination. *J Immunol*. (2017) 198:820–31. doi: 10.4049/jimmunol.1600334
45. Voet S, Mc Guire C, Hagemeyer N, Martens A, Schroeder A, Wieghofer P, et al. A20 critically controls microglia activation and inhibits inflammasome-dependent neuroinflammation. *Nat Commun*. (2018) 9:2036. doi: 10.1038/s41467-018-04376-5
46. Onizawa M, Oshima S, Schulze-Topphoff U, Oses-Prieto JA, Lu T, Tavares R, et al. The ubiquitin-modifying enzyme A20 restricts ubiquitination of the kinase RIPK3 and protects cells from necroptosis. *Nat Immunol*. (2015) 16:618–27. doi: 10.1038/ni.3172
47. Rynkowski MA, Kim GH, Komotar RJ, Otten ML, Ducruet AF, Zacharia BE, et al. A mouse model of intracerebral hemorrhage using autologous blood infusion. *Nat Protocols*. (2008) 3:122–8. doi: 10.1038/nprot.2007.513
48. Lekic T, Hartman R, Rojas H, Manaenko A, Chen W, Ayer R, et al. Protective effect of melatonin upon neuropathology, striatal function, and memory ability after intracerebral hemorrhage in rats. *J Neurotrauma*. (2010) 27:627–37. doi: 10.1089/neu.2009.1163
49. Wang Z, Zhou F, Dou Y, Tian X, Liu C, Li H, et al. Melatonin alleviates intracerebral hemorrhage-induced secondary brain injury in rats via suppressing apoptosis, inflammation, oxidative stress, DNA damage, and mitochondria injury. *Transl Stroke Res*. (2018) 9:74–91. doi: 10.1007/s12975-017-0559-x
50. Wu H, Wu T, Han X, Wan J, Jiang C, Chen W, et al. Cerebroprotection by the neuronal PGE2 receptor EP2 after intracerebral hemorrhage in middle-aged mice. *J Cerebral Blood Flow Metabol*. (2017) 37:39–51. doi: 10.1177/0271678X15625351
51. Bouet V, Boulouard M, Toutain J, Divoux D, Bernaudin M, Schumann-Bard P, et al. The adhesive removal test: a sensitive method to assess sensorimotor deficits in mice. *Nat Protocols*. (2009) 4:1560–4. doi: 10.1038/nprot.2009.125
52. Paes-Branco D, Abreu-Villaca Y, Manhaes AC, Filgueiras CC. Unilateral hemispherectomy at adulthood asymmetrically affects motor performance of male Swiss mice. *Experi Brain Res*. (2012) 218:465–76. doi: 10.1007/s00221-012-3034-7
53. Liu X, Liu J, Zhao S, Zhang H, Cai W, Cai M, et al. Interleukin-4 is essential for microglia/macrophage m2 polarization and long-term recovery after cerebral ischemia. *Stroke*. (2016) 47:498–504. doi: 10.1161/STROKEAHA.115.012079
54. Wu J, Zhang Y, Yang P, Enkhjargal B, Manaenko A, Tang J, et al. Recombinant osteopontin stabilizes smooth muscle cell phenotype via integrin receptor/integrin-linked Kinase/Rac-1 pathway after subarachnoid hemorrhage in rats. *Stroke*. (2016) 47:1319–27. doi: 10.1161/STROKEAHA.115.011552
55. Chen M, Li X, Zhang X, He X, Lai L, Liu Y, et al.Chen M, et al. The inhibitory effect of mesenchymal stem cell on blood-brain barrier disruption following intracerebral hemorrhage in rats: contribution of TSG-6. *J Neuroinflamm*. (2015) 12:61. doi: 10.1186/s12974-015-0284-x
56. Pariente R, Pariente JA, Rodríguez AB, Espino J. Melatonin sensitizes human cervical cancer HeLa cells to cisplatin-induced cytotoxicity and apoptosis: effects on oxidative stress and DNA fragmentation. *J Pineal Res*. (2016) 60:55–64. doi: 10.1111/jpi.12288
57. Zhao L, Chen S, Sherchan P, Ding Y, Zhao W, Guo Z, et al. Recombinant CTRP9 administration attenuates neuroinflammation via activating adiponectin receptor 1 after intracerebral hemorrhage in mice. *J Neuroinflam*. (2018) 15:215. doi: 10.1186/s12974-018-1256-8
58. Keren-Shaul H, Spinrad A, Weiner A, Matcovitch-Natan O, Dvir-Szternfeld R, Ulland TK, et al. A unique microglia type associated with restricting development of alzheimer's disease. *Cell*. (2017) 169:1276–90 e1217. doi: 10.1016/j.cell.2017.05.018
59. Fan LF, He PY, Peng YC, Du QH, Ma YJ, Jin JX, et al. Mdivi-1 ameliorates early brain injury after subarachnoid hemorrhage via the suppression of inflammation-related blood-brain barrier disruption and endoplasmic reticulum stress-based apoptosis. *Free Radical Biol Med*. (2017) 112:336–49. doi: 10.1016/j.freeradbiomed.2017.08.003
60. Zheng J, Shi L, Liang F, Xu W, Li T, Gao L, et al. Sirt3 Ameliorates oxidative stress and mitochondrial dysfunction after intracerebral hemorrhage in diabetic rats. *Front Neurosci*. (2018) 12:414. doi: 10.3389/fnins.2018.00414
61. Matsuzawa-Ishimoto Y, Shono Y, Gomez LE, Hubbard-Lucey VM, Cammer M, Neil J, et al. Autophagy protein ATG16L1 prevents necroptosis in the intestinal epithelium. *J Experi Med*. (2017) 214:3687–705. doi: 10.1084/jem.20170558
62. Kim SJ, Li J. Caspase blockade induces RIP3-mediated programmed necrosis in Toll-like receptor-activated microglia. *Cell Death Dis*. (2013) 4:e716. doi: 10.1038/cddis.2013.238
63. Fricker M, Vilalta A, Tolkovsky AM, Brown GC. Caspase inhibitors protect neurons by enabling selective necroptosis of inflamed microglia. *J Biol Chem*. (2013) 288:9145–52. doi: 10.1074/jbc.M112.427880
64. Huang Z, Zhou T, Sun X, Zheng Y, Cheng B, Li M, et al. Necroptosis in microglia contributes to neuroinflammation and retinal degeneration through TLR4 activation. *Cell Death Different*. (2018) 25:180–9. doi: 10.1038/cdd.2017.141
65. Degterev A, Huang Z, Boyce M, Li Y, Jagtap P, Mizushima N, et al. Chemical inhibitor of nonapoptotic cell death with therapeutic potential for ischemic brain injury. *Nat Chem Biol*. (2005) 1:112–9. doi: 10.1038/nchembio711
66. Colonna M, Butovsky O. Microglia function in the central nervous system during health and neurodegeneration. *Ann Rev Immunol*. (2017) 35:441–68. doi: 10.1146/annurev-immunol-051116-052358

67. Ma Y, Wang J, Wang Y, Yang GY. The biphasic function of microglia in ischemic stroke. *Progress Neurobiol*. (2017) 157:247–72. doi: 10.1016/j.pneurobio.2016.01.005
68. Hershko A, Ciechanover, A. The ubiquitin system. *Ann Rev Biochem*. (1998) 67:425–79. doi: 10.1146/annurev.biochem.67.1.425
69. Wertz IE, O'Rourke KM, Zhou H, Eby M, Aravind L, Seshagiri S, et al. De-ubiquitination and ubiquitin ligase domains of A20 downregulate NF-kappaB signalling. *Nature*. (2004) 430:694–9. doi: 10.1038/nature02794
70. Daniel S, Arvelo MB, Patel VI, Longo CR, Shrikhande G, Shukri T, et al. A20 protects endothelial cells from TNF-, Fas-, and NK-mediated cell death by inhibiting caspase 8 activation. *Blood*. (2004) 104:2376–84. doi: 10.1182/blood-2003-02-0635
71. Garcia-Carbonell R, Wong J, Kim JY, Close LA, Boland BS, Wong TL, et al. Elevated A20 promotes TNF-induced and RIPK1-dependent intestinal epithelial cell death. *Proc Natl Acad Sci USA*. (2018) 115:E9192–200. doi: 10.1073/pnas.1810584115
72. Vanlangenakker N, Vanden Berghe T, Bogaert P, Laukens B, Zobel K, Deshayes K, et al. cIAP1 and TAK1 protect cells from TNF-induced necrosis by preventing RIP1/RIP3-dependent reactive oxygen species production. *Cell Death Different*. (2011) 18:656–65. doi: 10.1038/cdd.2010.138
73. Sun CK, Lee FY, Kao YH, Chiang HJ, Sung PH, Tsai TH, et al. Systemic combined melatonin-mitochondria treatment improves acute respiratory distress syndrome in the rat. *J Pineal Res*. (2015) 58:137–50. doi: 10.1111/jpi.12199
74. Sagrillo-Fagundes L, Assunção Salustiano EM, Ruano R, Markus RP, Vaillancourt C. Melatonin modulates autophagy and inflammation protecting human placental trophoblast from hypoxia/reoxygenation. *J Pineal Res*. (2018) 65:e12520. doi: 10.1111/jpi.12520
75. Reiter RJ, Mayo JC, Tan DX, Sainz RM, Alatorre-Jimenez M, Qin L. Melatonin as an antioxidant: under promises but over delivers. *J Pineal Res*. (2016) 61:253–78. doi: 10.1111/jpi.12360
76. Hosseinzadeh A, Kamrava SK, Joghataei MT, Darabi R, Shakeri-Zadeh A, Shahriari M, et al. Apoptosis signaling pathways in osteoarthritis and possible protective role of melatonin. *J Pineal Res*. (2016) 61:411–25. doi: 10.1111/jpi.12362

Conflict of Interest Statement: The authors declare that the research was conducted in the absence of any commercial or financial relationships that could be construed as a potential conflict of interest.

frontiers in Molecular Neuroscience

ORIGINAL RESEARCH
published: 27 August 2019
doi: 10.3389/fnmol.2019.00190

Mucosal Administration of E-selectin Limits Disability in Models of Multiple Sclerosis

Jacqueline A. Quandt[1]*, *Pierre Becquart*[1], *Emily Kamma*[1] and *John Hallenbeck*[2]

[1]Department of Pathology and Laboratory Medicine, University of British Columbia, Vancouver, BC, Canada, [2]Stroke Branch, National Institute of Neurological Disorders and Stroke, National Institutes of Health, Bethesda, MD, United States

E-selectin plays an important role in mediating the rolling of leukocytes along and thus, the subsequent extravasation across activated endothelial cells comprising the microvasculature of the blood brain barrier (BBB). In multiple sclerosis (MS) and other inflammatory disorders of the central nervous system (CNS), the microvasculature is altered and immune cells infiltrate the brain and spinal cord contributing to damage, demyelination and ultimately disability. While mucosal administration is typically used to affect lymphocyte hyporesponsiveness or tolerance to suspect autoantigens, intranasal administration to E-selectin has previously been shown to protect against CNS inflammatory insults. We characterized the potential for mucosal administration of E-selectin to modulate CNS autoimmunity in the experimental autoimmune encephalomyelitis (EAE) model of MS. Intranasally administered E-selectin reduced swelling by as much as 50% in delayed-type hypersensitivity reactions compared to ovalbumin-tolerized controls. Intranasal E-selectin delivery prior to disease induction with myelin oligodendrocyte glycoprotein $(MOG)_{35–55}$ reduced disease severity and total disease burden by more than 50% compared to PBS-tolerized animals; this protection was not associated with differences in the magnitude of the autoimmune response. Examination after the onset of disease showed that protection was associated with significant reductions in inflammatory infiltrates throughout the spinal cord. Tolerization to E-selectin did not influence encephalitogenic characteristics of autoreactive T cells such as IFN-gamma or IL-17 production. Clinical disease was also significantly reduced when E-selectin was first delivered after the onset of clinical symptoms. Splenic and lymph node (LN) populations from E-selectin-tolerized animals showed E-selectin-specific T cell responses and production of the immunomodulatory cytokine IL-10. Transfer of enriched CD4+ T cells from E-selectin tolerized mice limited disability in the passive SJL model of relapsing remitting MS. These results suggest a role for influencing E-selectin specific responses to limit neuroinflammation that warrants further exploration and characterization to better understand its potential to mitigate neurodegeneration in disorders such as MS.

Keywords: multiple sclerosis, E-selectin, mucosal tolerance, experimental autoimmune encephalomyelitis, neuroinflammation

OPEN ACCESS

Edited by:
Craig Stephen Moore, Memorial University of Newfoundland, Canada

Reviewed by:
Denis Gris, Université de Sherbrooke, Canada
Manu Rangachari, Laval University, Canada

***Correspondence:**
Jacqueline A. Quandt
jquandt@pathology.ubc.ca

Received: *04 June 2019*
Accepted: *22 July 2019*
Published: *27 August 2019*

Citation:
Quandt JA, Becquart P, Kamma E and Hallenbeck J (2019) Mucosal Administration of E-selectin Limits Disability in Models of Multiple Sclerosis. Front. Mol. Neurosci. 12:190. doi: 10.3389/fnmol.2019.00190

INTRODUCTION

Multiple sclerosis (MS) is amongst the most common neurological diseases in young adults, with symptoms such as altered balance, vision or speech, weakness or paralysis, as well as extreme fatigue, depression and cognitive dysfunction. MS is a chronic inflammatory neurodegenerative disorder characterized histologically by vascular changes, immune infiltrates, loss of myelin and oligodendrocytes, and damage or loss of axons (Frohman et al., 2006). Ultimately, chronic disability is closely linked to neurodegeneration and irreversible axonal loss (Bjartmar and Trapp, 2003). Oligodendrocytes, myelin, neurons and axons are all damaged (Frischer et al., 2009) in MS and its primary animal model, experimental autoimmune encephalomyelitis (EAE). The demyelination and axonal injury observed in acute inflammatory lesions (Trapp et al., 1998; Kuhlmann et al., 2002) is thought to be driven by mechanisms distinct from those driving diffuse-axonal degeneration and atrophy associated with disease progression (Ingle et al., 2003; Kutzelnigg et al., 2005). Relapsing-remitting (RRMS) presents with alternating clinical attacks and periods of stability that transition into secondary progressive MS (SPMS) with progressive deterioration. Approved disease modifying therapies (DMT) for MS target inflammatory processes and have demonstrated significant benefit in studies of RRMS (Yong et al., 2018), yet only recently have DMT been approved to give modest but significant benefits in progressive or primary progressive MS (PPMS). Specifically, the B-cell depleting antibody, ocrelizumab, has been shown to significantly reduce the confirmed disability progression over 12 weeks in ocrelizumab patients compared to those taking placebo (Montalban et al., 2017). Siponimod, a compound which traps B and T cells in the body's immune organs has also shown evidence of slowing disability progression and has recently been approved for patients with active SPMS (Kappos et al., 2018).

Focal lesions are attributed to activated T cells that travel to the central nervous system (CNS) and trigger an inflammatory cascade as they encounter antigen (Bar-Or, 2008). CD4 and CD8 T cells may contribute directly and indirectly to disease but have been postulated to have both pathogenic and suppressive/regulatory roles over the disease course (Hauser et al., 2008; Racke, 2009; Johnson et al., 2010). Cells that induce EAE have a proinflammatory phenotype (Th1) producing interferon-γ (IFN-γ), tumor necrosis factor-α (TNF-α), and granulocyte macrophage colony stimulating factor (GM-CSF), in contrast to any of the immunosuppressive cytokines interleukin-4 (IL-4), IL-5, IL-9 or IL-10 (Gor et al., 2003; Sospedra and Martin, 2005). Additionally, the role of IL-17 producing T helper cells (Th17), as key drivers of pathogenic autoimmunity has been highlighted in EAE (Aranami and Yamamura, 2008). Yet, a balance seems to exist over the course of disease between effector T cells and regulatory T cells (Korn et al., 2007). Regulatory T cells (Treg) are capable of limiting immunity either by interacting directly with pathogenic cells, or by synthesis of immunosuppressive factors including IL-10 or transforming growth factor-β (TGF-β; Banham et al., 2006). Specifically, Treg cells expressing forkhead transcription factor FoxP3 are key cells capable of preventing disease in animal models of autoimmunity (Sakaguchi et al., 2008). Several factors in the local tissue environment can influence the phenotype of a T cell; inflammatory mediators or other cytokines, as well as the nature of the antigen presenting cell (APC), can greatly influence the properties of effector cells. Autoimmunity is typically reduced or even prevented if the generation of these pathogenic cytokine-producing cells deviates to a more immunosuppressive phenotype (Zamvil and Steinman, 1990; Segal and Shevach, 1998). As such, therapies which are able to reduce the development of autoreactive T cells, alter the pathogenic profile of these cells, or encourage the generation of regulatory T cells hold promise.

Mucosal tolerance describes the phenomenon of limiting immune responsiveness to antigens delivered *via* oral or nasal routes that would typically be considered non-pathogenic (i.e., food). Tolerance induction has been demonstrated *via* the intranasal route and is thought to involve active suppression as it can be transferred with adoptive transfer of splenocytes (Unger et al., 2003). In this regard, antigens delivered to the nasal mucosa spurs activation after draining into the cervical lymph nodes (CLN) and spleen which leads to tolerance; the internal jugular superficial cervical lymph nodes (SCLN) are also key in mediating tolerance (Wolvers et al., 1999; Li et al., 2011). Intranasal and oral delivery of antigen for tolerization has been effective in animal models of autoimmunity, atherosclerosis, transplant rejection, and allergy (Maron et al., 2002; George et al., 2004; Mayer and Shao, 2004; van Puijvelde et al., 2006; Broere et al., 2008; Klingenberg et al., 2010).

E-selectin is a cell surface adhesion molecule rapidly and specifically induced on activated endothelium which along with P-selectin, mediates tethering and rolling of immune cells *in vivo* and *in vitro* (Lawrence and Springer, 1991, 1993; Frenette et al., 1996). E-selectin has been implicated in processes of rolling and recruitment in EAE (Engelhardt et al., 1997; Doring et al., 2007), and soluble plasma levels have been associated with inflammatory activity in MS (Kuenz et al., 2005). Nasal instillation of E-selectin was previously shown to limit damage secondary to both ischemic and hemorrhagic strokes and to be protective in a vascular cognitive impairment model (Takeda et al., 2002, 2004; Wakita et al., 2008). E-selectin administration gave rise to a cell-mediated protection in models of stroke (Chen et al., 2003) as well as limiting atherosclerosis in susceptible $Apoe^{-/-}$ animals (Li et al., 2011). This study was designed to test whether tolerization to human E-selectin *via* intranasal administration could alter the course and severity of disease in EAE as a model of MS.

MATERIALS AND METHODS

Intranasal Administration of E-selectin

Experiments were approved and conducted in accordance with the Guide for the Care and Use of Laboratory Animal Resources (1996) and the Canadian Council on Animal Care guidelines, with approval by the NINDS Animal Care and Use and UBC Animal Care Committees. Intranasal instillations were

as follows: (1) PBS (Biowhittaker, Walkersville, MD, USA); and (2) recombinant human (hu) or mouse (m) E-selectin (**Supplementary Figure S1**) synthesized with a Baculovirus expression system with lectin and epidermal growth factor domains (prepared and provided by Novavax Pharmaceuticals, Rockville, MD, USA). Instillations were carried out with the animals under brief anesthesia with 4% isoflurane using a 10 μl pipette tip and micropipettor.

The tolerization regimens changed over the course of the study (**Figure 1**) depending on whether it was administration of E-selectin to limit delayed-type hypersensitivity (DTH; **Figure 1A**), prophylactic administration of E-selectin prior to active EAE induction to prevent EAE (**Figure 1B**), or therapeutic administration of E-selectin after the onset of clinical symptoms (**Figure 1C**) PBS (10 μl), E-selectin or ovalbumin (Ova; varied doses in 10 μl) were instilled into each nostril every other day for 10 days (total of five administrations), designated as a single-course regimen. For EAE studies, a repetitive (booster) regimen was also applied, where the booster would be repeated at 3-week intervals.

Delayed-Type Hypersensitivity Reactions (DTH)

DTH was assessed in C57BL/6 animals receiving a single-course tolerization regimen (five administrations every other day over a total of 10 days per regimen) as previously described (Li et al., 2011). Fourteen days later, the animals were immunized in four spots on the flank with 55 μg E-selectin/200 μl of 0.5mg/ml complete Freund's adjuvant in PBS (Difco Laboratories, Detroit, MI, USA). Fourteen days later, ear thickness was measured with microcalipers and animals were subsequently re-challenged with 5 μg E-selectin/10 μl PBS injected subcutaneously into the ear. Ear thickness increase over baseline was measured 2 days later and presented as percentage increase and compared to increases following a PBS injection in the alternate ear.

EAE Induction

For active disease, female 8–10-week-old C57BL6/J mice (Jackson Labs) were immunized with 200 μg myelin oligodendrocyte glycoprotein $(MOG)_{35–55}$ (MEVGWYRSPF SRVVHLYRNGK; Stanford Pan Facility, Stanford, CA, USA; Quandt et al., 2012). For passive disease, SJL/J mice (Harlan Laboratories) were immunized with 75 μg PLP139–151 (HCLG KWLGHPDKF, Stanford Pan Facility) and draining LN cells enriched with PLP for 3 days in culture before the transfer of 1.5 million blasted cells to healthy recipients as described (Anderson et al., 2004). Animals were monitored by a blinded assessor daily for clinical signs through the onset of disease and through recovery (typically day 30–35) or longer in chronic studies to day 45 or 60 according to the following: 0–0.5 indicated no disease/distal limp tail, 1.0 limp tail, 2.0 mild weakness in one or 2.25 in two hindlimbs/slipping on cage insert bars, 2.5 moderate-severe weakness in one or in 2.75 two hind limbs/getting stuck on cage insert bars, 3.0 paralysis in one or 3.5 both hind limbs, 4.0 hind limb paralysis plus weakness in one or in 4.5 both forelimbs, and five for moribund animals.

Isolation of Immune Populations for Transfer or T Cell Proliferation and Cytokine Assays

The spleens or SCLN were aseptically removed from mice following CO_2 inhalation and euthanasia and transferred to cold sterile PBS and pressed through a sterile 40 μm filter to prepare a single-cell suspension. For transfer, cells were resuspended in a sterile PBS buffer and incubated with antibodies specific for non-T cell populations to prepare CD4+ T cell-enriched populations by negative selection (Miltenyi Biotec, Gladbach, Germany); a small sample was kept for characterization by flow cytometry which showed CD4+ T cell purities ranged from 93% to 96% in each experiment. Five million cells from tolerized animals were immediately transferred retroorbitally to recipient animals which had been induced for passive EAE as above. For analyses of immune responses or priming, $2–4 \times 10^5$ spleen or LN cells in serum-free X-vivo 15 media (BioWhittaker, Walkersville, MD, USA) were incubated with varying doses of E-selectin, control culture media, or concanavalin A (Con A; final concentration 2 μg/ml, Sigma, MO, USA) in 96-well round bottom plates for 48 h at 37°C when tissue culture supernatants were harvested. Thymidine (1 mCi of $[^3H]$-thymidine) was added for 16 h prior to harvesting the cells at 72 h and measurement of incorporated radioactivity. Cytokine analysis was performed using anti-mouse IFN-γ IL-10-, IL-17 or TGF-β-specific DuoSet kits from R&D Systems (Minneapolis, MN, USA) per protocol directions.

Serum Analyses

Blood was collected from the tail vein *via* sterile scalpel from mice anesthetized under 4% isoflurane. Samples sat at room temperature for 30 min in a Serum Gel Z/1.1 tube (Sarstedt, Numbrech, Germany) prior to processing per manufacturer's recommendations and frozen at −80°C until assay. Serum E-selectin was measured using a mouse E-selectin-specific Duoset kit from R&D Systems as above and $MOG_{35–55}$ specific IgG1 and IgG2a/c antibodies were detected as previously described (Neil et al., 2017).

Immunohistochemistry of EAE Tissues

Mice were deeply anesthetized with a ketamine/xylazine cocktail prior to transcardial perfusion with PBS followed by 10% buffered formalin and processed for immunohistochemistry (IHC; Quandt et al., 2012). Immunofluorescence with antibodies to SMI-32 (to hypophosphorylated neurofilament, Biolegend, San Diego, CA, USA) and myelin basic protein (MBP, Santa Cruz Biotechnology, Dallas, TX, USA) were used to assess infiltration, axonal damage as well as demyelination in the spinal cord. Tissue sections were examined with a Zeiss Axio Vert 200 Inverted Fluorescence Microscope (Oberkochen, DE, Germany), equipped with an Axiocam 506 monochrome camera at 20× with matched light intensity and exposure times across the entire experimental set. Analysis was performed with Zeiss software Zen (Version 2.3). Immunostained sections from each EAE mouse spinal cord were analyzed (n = 5 per treatment, three levels per mouse corresponding to the T8/T9, T12,

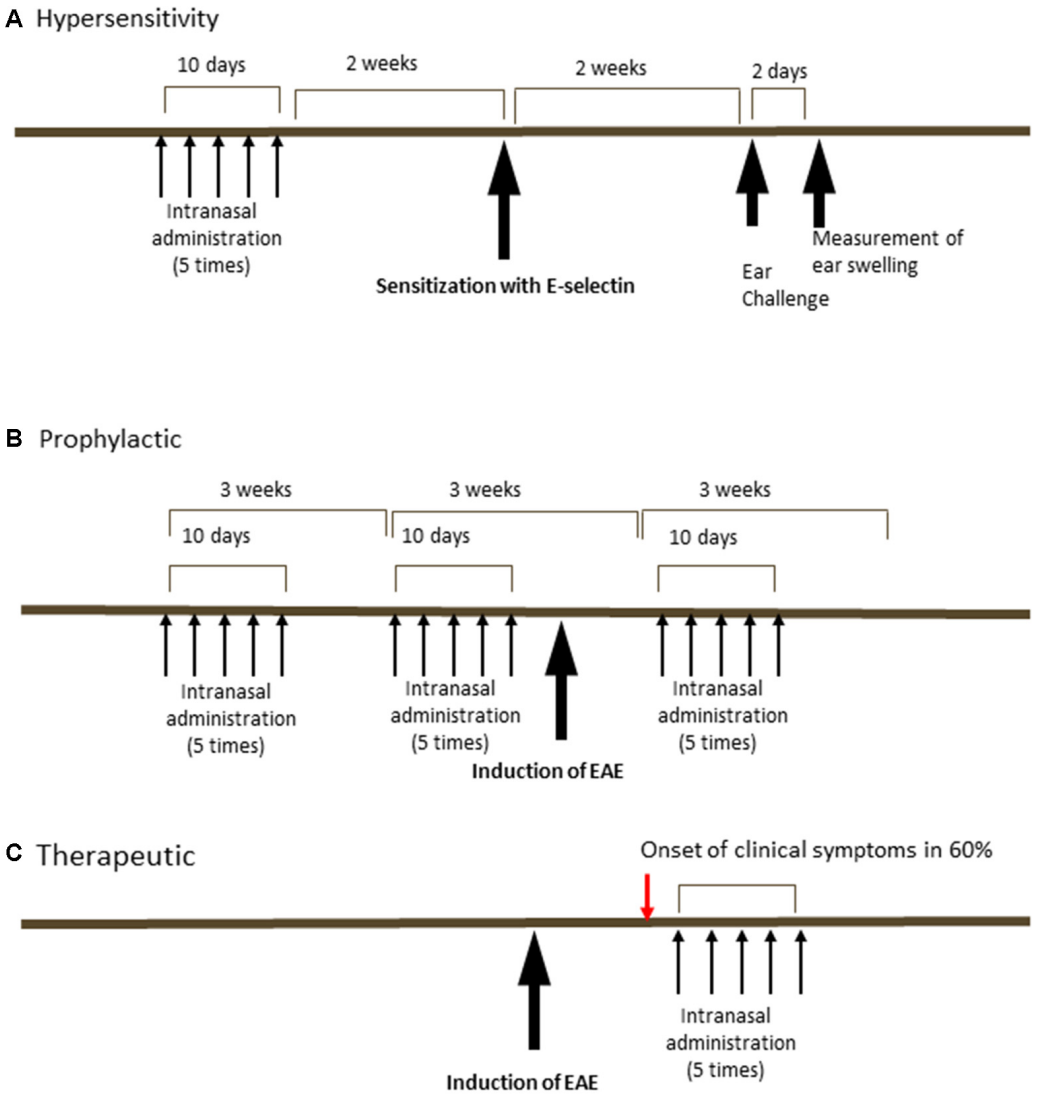

FIGURE 1 | Schedules of intranasal delivery of E-selectin in delayed-type hypersensitivity (DTH) assays or prophylactic or therapeutic regimens in experimental autoimmune encephalomyelitis (EAE). **(A)** In a DTH reaction, animals received varying doses of ovalbumin or E-selectin in 10 μl PBS every other day for 10 days ending 2 weeks prior to sensitization with E-selectin. Animals were challenged in the ears 2 weeks later and swelling measured 48 h later. **(B)** In a prophylactic regimen, animals received E-selectin or ovalbumin over two periods prior to the induction of EAE and again 9 days after the induction of EAE. **(C)** In a therapeutic regimen, E-selectin was administered intranasally starting 2 days after the onset of clinical symptoms in EAE mice (red arrow, typically onset was day 14, with administration started at day 16 and delivered for 10 days).

and L4/5 levels of the spinal cord for a total of 15 levels per treatment group examined). The sections were assessed for the degree of inflammatory infiltration by outlining and pooling the area of all infiltrates per section and calculating the percentage of white matter (WM) infiltrated by immune cells by taking this as a fraction of the WM area in that section. SMI32-positive regions of interest typically resembling spheroids with a staining intensity above the threshold set by averaging regions of WM in healthy animals were used to report the number of SMI32+ spheroids per square millimeter of WM.

Statistical Analysis

GraphPad Prism (version 7, La Jolla, CA, USA) was used for all analyses. A repeated-measures one-way analysis of variance (ANOVA) was used for normally distributed data or a repeated measures ANOVA on ranks (Friedman test) was performed when comparing multiple treatments. In EAE comparisons of multiple doses over time, a two-way ANOVA on ranks was performed followed by a Tukey multiple comparisons test vs. PBS-treated controls. Values represent mean ± standard deviation unless otherwise indicated. A Mann-Whitney comparisons test was performed in comparisons of EAE to

healthy or sham/CFA immunized mice and significance reported at $p < 0.05$.

RESULTS

Intranasal Administration of E-selectin Specifically Limits Inflammation Secondary to Immunization With E-selectin or EAE Induction With MOG

In C57BL/6J mice, animals sensitized and later undergoing recall to either human or mouse E-selectin *in vivo* in a DTH assay (**Figure 1A**) showed similar responses: the average increase of ear thickness in mice sensitized with hE-selectin and recalled later with hE-selectin was 0.331 ± 0.02 mm and was similar to mice sensitized with msE-selectin and later challenged with mE-selectin at 0.324 ± 0.06 mm. In animals sensitized to huE-selectin, intranasal administration of huE-selectin limited swelling to 57.9 ± 4.2% compared to 128.5 ± 3.8% observed in animals receiving Ova intranasally (**Figure 2A**, 5 μg dose; $p < 0.0001$). Similarly, intranasal msE-selectin limited swelling in msE-selectin-sensitized mice although to a lesser degree (94.7 ± 5.4% vs. 126.2 ± 7.4% in Ova-tolerized animals **Figure 2B**; $p = 0.02$). A lower dose of 1 μg still significantly reduced hE-selectin responses whereas 1 μg of mouse E-selectin was not effective (data not shown). Notably, human and mouse E-selectin proteins share 81% amino acid similarity.

We next administered hE-selectin intranasally to test its potential to limit autoimmunity and clinical disease in the actively induced $MOG_{35–55}$ chronic model of EAE. Animals received 0.1–10 μg of hE-selectin in three sessions which precede and span the induction of EAE as in **Figure 1B**. Compared to intranasal PBS, 5 μg of hE-selectin reduced clinical disability in animals to the greatest degree, although 0.1 and 10 μg doses were also effective (**Figure 2C**). Intranasal administration of 5 μg hE-selectin significantly reduced the cumulative disease burden over the study (37.1 ± 9.4 vs. 70.3 ± 13.7 in PBS, $p = 0.05$) and the average disease severity (1.16 ± 0.27 vs. 2.141 ± 0.42 in PBS, $p = 0.05$). Comparisons of the disease score over time showed that the means of each treatment were significantly different to PBS (PBS vs. 0.1 μg, $p < 0.0001$, PBS vs. 1 μg, $p = 0.0002$, PBS vs. 5 μg, $p < 0.0001$, PBS vs. 10 μg, $p = 0.0007$). We postulated that intranasal administration of E-selectin may limit the magnitude of a response to MOG in these animals, and examined spleens from animals culled at day 45 and tested recall *ex vivo* to both MOG and hE-selectin. Notably, stimulation indices to MOG were not significantly different between the two groups (**Figure 2D**). Furthermore, hE-selectin-specific responses could only be detected in populations derived from E-selectin tolerized animals. Notably, we have found that the isotype of antibody responses to $MOG_{35–55}$ can be a sensitive means of detecting shifts in Th1 or Th2 profiles (Neil et al., 2017) and found that IgG1 and IgG2a antibody responses to $MOG_{35–55}$ were comparable in PBS and hE-selectin serum from mice examined at day 45 tolerized with the regimen in **Figure 2C** (data not shown). To determine whether or not E-selectin tolerization interfered with the initial priming of encephalitogenic T cells, draining inguinal, axillary and brachial LN populations were isolated from animals receiving one round of intranasal PBS or E-selectin and actively immunized to induce EAE. Animals were culled 12 days after immunization and tested for proliferative responses to MOG, hE-selectin, and anti-CD3 as well cytokine production over 48–72 h. Proliferation responses measured by stimulation

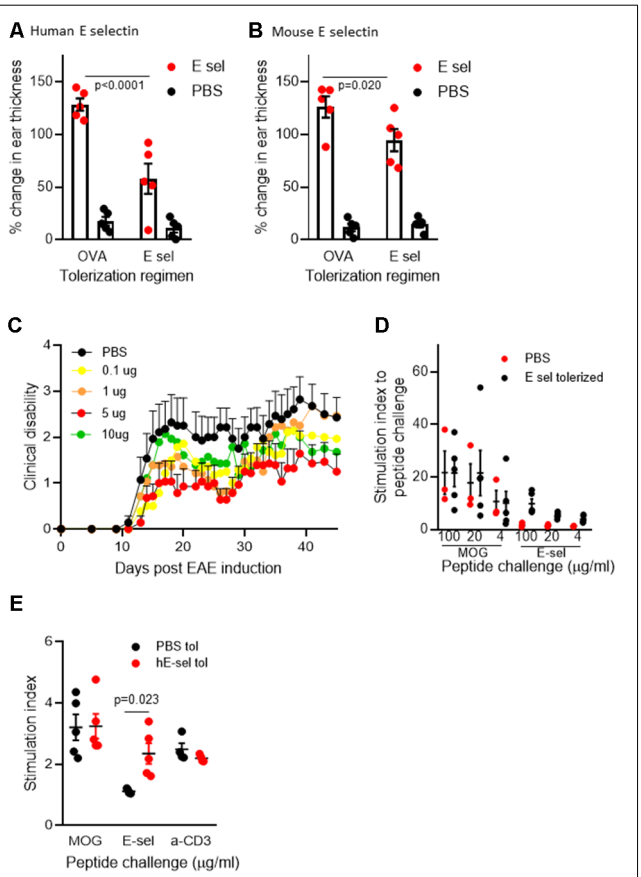

FIGURE 2 | Intranasal E-selectin limits DTH responses and limits clinical disability in EAE. **(A)** Percentage change in ear thickness in animals sensitized to huE-selectin after intranasal administration of 5 μg E-selectin or Ova and challenged with PBS or huE-selectin in opposite ears. **(B)** Percentage change in ear thickness in animals sensitized to mE-selectin after intranasal delivery of mE-selectin or Ova. No differences in ear thickness were observed between ears receiving PBS challenge following either regimen. $n = 5$ mice per treatment group, bars represent the SEM. Mann-Whitney *T*-test comparing Ova to E-selectin tolerization. **(C)** huE-selectin was administered per the regimen in **Figure 1B** spanning the active induction of chronic EAE. 0.1 up to 10 μg of huE-selectin were administered and results represent the mean ± SEM of the animals over time. **(D)** Splenocytes isolated from animals at D.45 post-EAE induction were challenged *ex vivo* with different doses of $MOG_{35–55}$ or huE-selectin for 72 h to examine the proliferation relative to untreated samples (stimulation index or SI). $n = 3–4$ animals per group, dots and error bars represent the average SI of responses from PBS (black) or huE-selectin tolerized (red) animals ± SD. Responses to huE-selectin in PBS tolerized animals were negligible. **(E)** Cells isolated from the draining axillary, brachial and inguinal lymph node (LN) 12 days after EAE induction were tested for proliferative responses to $MOG_{35–55}$ (20 μg/ml), E-selectin (10 μg/ml) and anti-CD3 combined with anti-CD28 ($n = 4–5$ mice per group, stimulation index (SI) is proliferation relative to untreated samples from PBS—black or E-selectin-red-tolerized animals ± SEM).

indices to MOG_{35-55} and anti-CD3 were similar between PBS and E-selectin tolerized animals (**Figure 2E**); however, proliferation in response to E-selectin was only detected when E-selectin had previously been administered ($p = 0.023$). Both IL-17 and IFN-γ production, in response to 20 μg/ml of MOG_{35-55}, was similar in cells derived from E-selectin tolerized LN as from those receiving PBS (596 ± 84.3 pg/ml vs. 654.8 ± 189 pg/ml and 426 ± 64.8 vs. 502 ± 72.1 pg/ml respectively). Polyclonal T cell activation with anti-CD3 and CD28 also yielded similar IL-17 and IFN-γ amounts from the two different treatment groups ($n = 5$ mice per treatment group). No IL-17 or IFN-γ was detected in either group in response to E-selectin and production of TGF-β was negligible across all tolerization and stimulation groups (data not shown). IL-10 levels were near the lower limit of detection (0–16 pg/ml) and was not significantly different between PBS and E-selectin tolerized populations no matter the stimulus. At day 12, animals receiving PBS scored at 0, 2, 1.5, 1 and 2.5; animals receiving huE-selectin scored at 0, 0, 0, 0 and 2.75. Examination of three levels of spinal cord showed that animals which received intranasal E-selectin had inflammatory infiltrates in less than 1/3 of the tissue observed in PBS tolerized mice (**Figure 3A**; 1.12% ± 0.5 of the tissues vs. 4.27% ± 1.6 of the tissue, $p = 0.012$). No significant differences in the accumulation of SMI-32+ spheroids as a marker of axonal damage were observed at this time point (**Figures 3B–G**; data not shown).

Therapeutic Potential of E-selectin Tolerization and Immune Responsiveness

Administration of huE-selectin after the onset of disease symptoms was tested for the potential to treat disease in chronic EAE. Administration of huE-selectin after the onset of disease (starting on day 13 for 10 days as in **Figures 1C**, **4A**) reduced the average disease score over the study period (2.60 ± 0.13 vs. 2.12 ± 0.09, $p = 0.0006$). To characterize the specificity of the immune response to E-selectin, superficial cervical LN and splenic populations were examined from mice at the end of the study period (d.45 post-immunization) for recall to E-selectin and compared to the T cell mitogen Con A (**Figure 4B**). E-selectin-specific responses were only detected in animals that had been tolerized to E-selectin. Likely consistent with fewer T cells in the spleen than LN, the splenic responses to E-selectin were less than those observed in the LN (1.58 ± 0.18 vs. 5.72 ± 2.45, $p = 0.03$). Responses to Con A were similarly lower in spleens than LN in both groups of tolerized animals, and no differences were observed between the proliferative responses of cells derived from the PBS vs. E-selectin tolerized animals. Supernatants from spleen cells and LN cells isolated from PBS or E-selectin tolerized animals were tested for IL-10 production; IL-10 production in response to E-selectin was only detected in animals that had received E-selectin (**Figures 4C,D**) where it was significantly greater ($p < 0.05$) than that observed in PBS-tolerized animals. Notably, IL-10 production in response to Con A was similar from both PBS and E-selectin tolerized animals.

Our group had previously shown that transfer of splenic cells from E-selectin tolerized cells was able to confer protection in

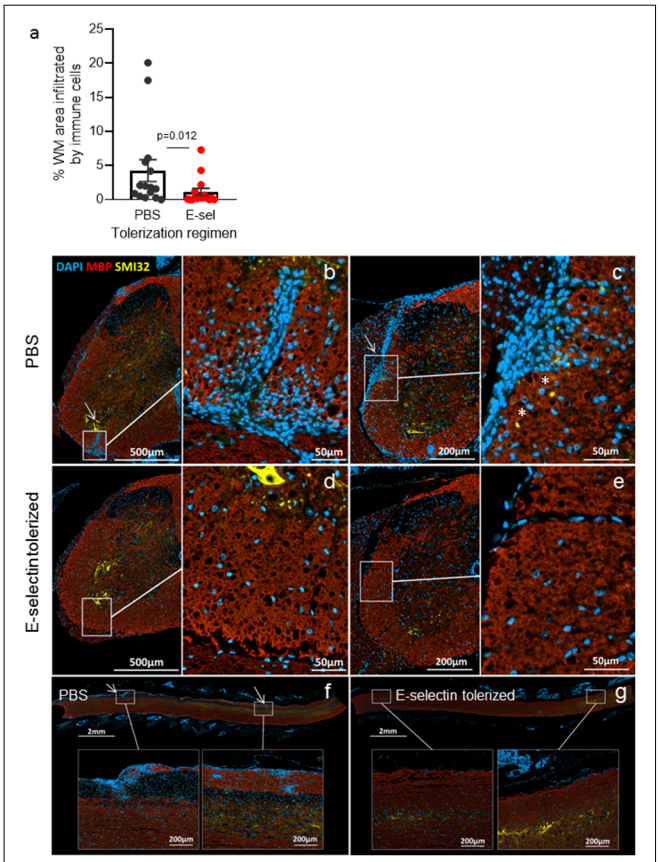

FIGURE 3 | Immune infiltrates are significantly reduced in E-selectin tolerized mice. **(A)** Animals receiving PBS (black) or huE-selectin (red) for one round prior to EAE induction were euthanized after the onset of disease (D.12) to examine the percentage of white matter (WM) infiltration by immune cells in the spinal cord. $N = 5$ mice analyzed at three levels per treatment group; bars represent the mean and error bars the SEM of 15 levels per treatment group. Representative images from mice in panel **(A)** are shown. Images and insets were taken from different levels of PBS tolerized **(B,C)** and E-selectin-tolerized **(D,E)** animals. Arrows highlight regions of extensive immune infiltrate from the meninges that extend into the parenchyma that were typically only present in animals receiving PBS intranasally. MBP (red) loss was detected in PBS-tolerized animals in heavily infiltrated areas, as were SMI-32+ ovoids reflecting axonal damage (*). Longitudinal sections also demonstrate the extensive inflammatory infiltrates detected in animals receiving intranasal PBS **(F)** vs. E-selectin **(G)**.

experimental models of disease and we sought to test the same in EAE (**Figure 5**). To focus on CD4+ T effector populations, we purified CD4+ T cells from the superficial cervical LN or spleens of animals that had undergone two rounds of intranasal administration (per **Figure 1**) with PBS, OVA or E-selectin and transferred them into animals induced passively for $PLP_{139-151}$ EAE.

Animals receiving splenic cells from huE-selectin or Ova-tolerized animals or LN cells from Ova-tolerized animals all had similar average disease severities over the study period to PBS-tolerized animals (1.87 ± 0.30, 1.84 ± 0.31, 2.05 ± 0.31 and 1.95 ± 0.32); only animals receiving LN cells from E-selectin tolerized mice were different at 1.611 ± 0.25 ($p < 0.05$ over the disease course; **Figure 5A**). In a replicate of the study over

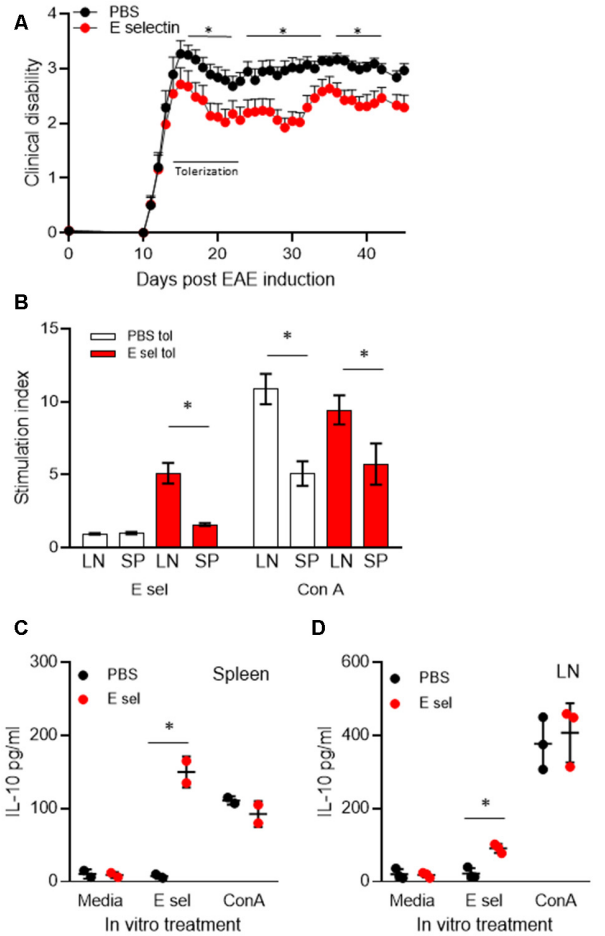

FIGURE 4 | Administration of E-selectin treats disability in chronic EAE and generates E-selectin-specific populations in immune organs. **(A)** Mice were immunized with myelin oligodendrocyte glycoprotein $(MOG)_{35–55}$ to actively induce EAE. Once more than half the animals exhibited a limp tail (day 13) huE-selectin tolerization was initiated every other day for 10 days. Animals were followed to day 45. Average disease scores were significantly reduced over the treatment study, $*p < 0.05$ *t*-tests vs. PBS-treated mice indicated those days which were significant. $n = 13$ and 14 for the PBS and E-selectin groups respectively. One of three representative experiments is shown. **(B)** Superficial LN and splenic populations were isolated from the mice in **(A)** at day 45 and challenged *ex vivo* with E-selectin or Con A to assess the response to antigen. Proliferative responses over 72 h to 20 μg/ml huE-selectin (left panel) were only observed in LN and spleen populations which had received E-selectin intranasally (red bars). Data represents spleen and cervical lymph nodes (CLN) from three mice per treatment group, average ± SD. **(C,D)** Supernatants from the splenic and LN populations isolated from animals undergoing E-selectin tolerization were examined for IL-10 production, PBS or huE-selectin. Spleens from $n = 2$ or from LN $n = 3$ mice were assayed per regimen treatment group, bars represent the average produced from duplicate or triplicate wells, error bars represent the SD. $p < 0.05$.

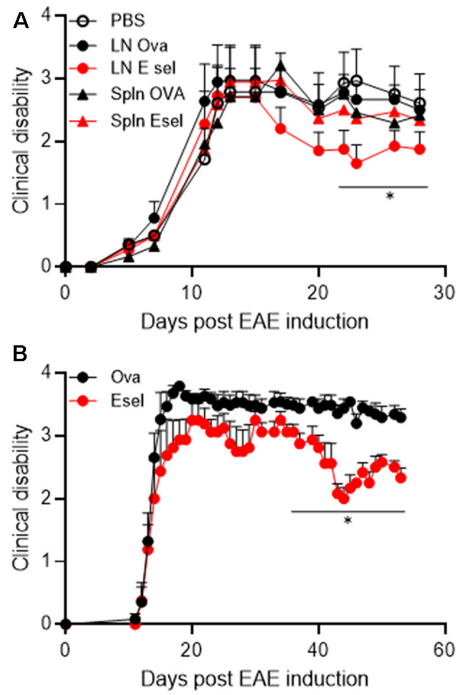

FIGURE 5 | (A) Superficial cervical LN populations protect against passive EAE in SJL mice. SJL animals received 1.5 million blasted $PLP_{139–151}$-specific T cells intraperitoneally to induce disease. Purified CD4+ T cells isolated from Ova (black) or huE-selectin (red) tolerized animals (two rounds) were transferred 5 days later. Clinical scores were assessed daily until day 30. Points represent the average clinical score of $n = 8–11$ mice per group, errors bars the SEM. $*p < 0.05$ compared to animals receiving PBS. **(B)** A replicate of the experiment in panel **(A)** where CLN cells from OVA or huE-selectin tolerized mice were transferred after CD4+ T cell purification. Points represent the average clinical score of $n = 5$ and 6 mice per group, errors bars the SEM. $*p < 0.05$ compared to Ova-tolerized animals.

60 days, LN cells from huE-selectin tolerized animals had a significantly lower disease score over the study than cells from Ova tolerized animals (3.16 ± 0.15 vs. 2.51 ± 0.13, $p < 0.0001$; **Figure 5B**). LN populations were assessed by flow cytometry prior to transfer in each experiment, with 94.3%–96.5% CD4 T cell purity and within that population 10.3%–12.6% $FoxP_3$+/CD25+ cells in the Ova vs. huE-selectin transferred populations, showing no significant difference in T reg numbers between the two transferred populations.

DISCUSSION

The microvasculature of the brain exhibits specialized tight junctions, low levels of vesicular trafficking and limited cell adhesion molecule (CAM) expression that otherwise enables immune cell movement out of the vessel (Reese and Karnovsky, 1967; Risau et al., 1998). Therapies which limit endothelial cell activation or immune cell recruitment across the blood brain barrier (BBB) offer promise in MS. Indeed, natalizumab, an antibody to α4 integrin the ligand for vascular CAM-1 (VCAM-1), was extremely effective in treating EAE (Zhang et al., 2003) and went on to show the ability to reduce relapses in MS patients by 68% compared to placebo, which far exceeded results for approved MS therapies at that time (Polman et al., 2006). However, this, and more recently approved efficacious therapies, have an increased risk profile, where depleting immune cell subsets or reducing immune surveillance with monoclonal

antibodies were associated in rare instances with multifocal leukoencephalopathy (PML) as a rare yet serious adverse event (Piehl et al., 2011; Yong et al., 2018).

The current study uses a novel approach enabling expression of E-selectin under inflammatory conditions to localize and perpetuate an immunoregulatory response. Intranasal administration of E-selectin was a driver of specific immune responses in both the SCLN and spleen which were associated with the expression of the immunomodulatory cytokine IL-10 (Li et al., 2011), as previously described.

In our studies, we compared the efficacy of purified CD4+ T cells from SCLN to splenic populations and found E-selectin-specific cells derived from SCLN after two rounds of priming had efficacy. Many studies have reported intranasal antigen administration as a means to regulate CD4+ T cell function and have linked IL-10 to subsequent immune tolerance (Hoyne et al., 1996; Burkhart et al., 1999; Laliotou and Dick, 1999). In an experimental autoimmune uveitis model, authors showed a transfer of tolerance with a regulatory population of spleen cells (Burkhart et al., 1999; Laliotou and Dick, 1999). Studies have implicated APCs as key mediators of tolerance, particularly those in the regional drainage lymph nodes; a single intranasal administration was rapidly followed by T cell proliferation secondary to signaling networks in both SCLN and spleen (Wolvers et al., 1999). It may be that the multiplicity and boosting of these administrations in our model contributed to the increased efficacy observed upon transfer of SCLN-derived populations, which was also apparent in the increased proliferative responses observed when comparing E-selectin responses between the two immune organs.

The administration of E-selectin repeatedly, as with any antigen, has the capacity to generate both T and B cell responses specific to E-selectin. Although we previously showed that antibodies specific for E-selectin are generated using this approach, we showed that they are indeed of the IgG1 isotype, and are therefore a more immunsuppressive than inflammatory phenotype. This, combined with previous observations from other groups which show that neutralization of E-selectin with antibodies does not reduce the severity of EAE, suggests that the primary mechanisms of action here are not attributable to antibodies generated from T cell-aided B cell responses. It is well known that administration of antigens through mucosal routes rapidly generates T cell populations, immunomodulatory in nature, which, through their production of cytokines such as IL-10, can limit inflammation. Numerous reports have outlined the relative success of antigen-specific tolerance to limit EAE based on the administration of the candidate autoantigen driving the disease, although discussion surrounds the safety and also reliability of mucosal administration of antigen to suppress ongoing active disease (Burkhart et al., 1999). To test the efficacy of E-selectin administration in the most robust manner, we tested the approach prophylactically and therapeutically in active and passive models of chronic and relapsing-remitting MS, to overcome previous concerns that only in more of the milder relapsing disease settings would tolerance approaches have success (Liu and Wraith, 1995; Bai et al., 1997; Thurau et al., 1997).

The very nature of the tolerizing antigen in our approach may be the key to the success here; rather than having to energize or deviate the full weight of the immune response to the candidate autoantigen, E-selectin tolerization and the potential of E-selectin specific cells to act at the specific site of inflammatory responses and damage may significantly augment its potential to limit disease, without the risk of overt immunosuppression. Furthermore, in the case of MS where the definitive putative autoantigen remains elusive, the specific autoantigen need not be identified for this approach to yield benefit. Here, we target immunosuppressive cell populations towards the activated microvasculature and/or local immune organs; the specific sites remain to be identified. Future studies will be important to establish the site where these cells act to afford protection. There is indeed the possibility that the human E-selectin gives a more robust response as seen in the DTH because it differs from the mouse protein in sequence. It is also possible that any differences observed in the glycosylation patterns of otherwise homologous regions of the protein may be enhancing immunogenicity following intranasal administration. It is possible that E-selectin from another species from human may be more potent in humans, but may increase the potential for autoimmunity if high avidity cells specific for a non-human protein that have not been depleted through tolerance to self (human) antigen are indeed activated. Because self into self in our model was not a clear driver of autoimmunity, yet showed efficacy albeit lower than that observed with that from a different species, we believe a homologous system is a safe approach to consider in driving antigen-specific tolerance to E-selectin.

Despite E-selectin upregulation in association with activation of the vasculature in a variety of CNS insults or inflammatory settings and their models, a specific requirement for E-selectin in EAE development has been discounted. Intravital microscopy experiments showed that E-selectin is localized to regions of immune cell rolling and interactions with the superficial CNS microvasculature (Kerfoot et al., 2006); moreover, E- and P-selectin mediate early cerebrovascular T cell/endothelial interactions in EAE, and P-selectin glycoprotein ligand-1 (PSGL-1, one ligand for E- and P-selectin) is a primary mediator of E- and P-selectin-mediated T cell rolling in the spinal cord (Sathiyanadan et al., 2014). In contrast, studies have: (a) failed to localize E-selectin to parenchymal vessels over the course of EAE development; and (b) have shown that neutralization of E-selectin with antibodies or E-selectin knockout models show no differences in clinical disease or infiltrate composition compared to their wildtype counterparts (Engelhardt et al., 1997). In this regard, one concludes such rolling of T cells is not required for the initiation of EAE. However, elegant studies in relapsing and remitting remodels of disease have shown an important role for neo-epitope generation in potentiating disease through antigen presentation and the potentiation of immune responses to newly generated antigens within the CNS as proposed in antigenic "spread" (McMahon et al., 2005). Notably, relapse in chronic-relapsing EAE is less severe where CNS-draining lymph nodes have been removed (van Zwam et al., 2009). E-selectin draining to these lymph nodes during EAE or MS may be the driver for IL-10 responses that limit immune responses here, and

foreseeably further potentiation. Future experiments will build on this initial study, and look to further characterize E-selectin-specific populations and their potential to limit inflammation both *in vitro* and *in vivo*.

In vitro models and the postulated pathogenesis of MS suggest that the BBB is not restrictive to trafficking of activated lymphocytes (Goverman, 2009). In our model, where T cells specific for E-selectin are generated and repeatedly challenged, this may lead to E-selectin specific cells that can gain entry to the CNS, even when the BBB has not been compromised. If these cells access the CNS and can go on through the cerebrospinal fluid to the recently characterized CNS meningeal lymphatics which then drain to cervical lymph nodes (Louveau et al., 2015), exposure here to E-selectin may drive their production of immunomodulatory factors such as IL-10 which may help to limit antigenic spread and the potentiation of immune responses that are more likely to start within the CNS. Additional studies are required to titer as well to localize E-selectin-specific T cells in our model over the course of EAE to better understand their full potential to actively and passively protect against and treat established disease in our models.

While rapid expression of E-selectin at the CNS microvasculature surface at a specified point in the disease process may be the most robust signal of inflammation in acute settings such as stroke, perhaps equally as important is the shedding of E-selectin. While not characterized over the course of disease, we did detect mouse E-selectin in the serum of animals undergoing acute attacks of EAE (ranging from 250 to 300 pg/ml); notably, these levels were highest in animals undergoing EAE that had been tolerized with Ova; levels were significantly lower in animals that had been tolerized with human E-selectin suggesting that the relative level of serum E-selectin may be linked to the severity of disease and/or inflammation. In our therapeutic studies of E-selectin administration after the onset of disease, we saw no difference in serum E-selectin levels between animals receiving PBS or E-selectin 1 month (588.0 $\pm$ 15.1 vs. 566.6 $\pm$ 11.9 ng/ml) or 2 months (310.5 $\pm$ 12.1 vs. 366.5 $\pm$ 13.3 ng/ml) after disease induction, although soluble E-selectin had clearly dropped by almost half over that time. Notably, sE-selectin is markedly increased in RRMS patients during an exacerbation or those with chronic progressive MS in comparison to controls (Tsukada et al., 1995). Notably, MS was distinct from HTLV-1 associated myelopathy (HAM) in this regard where levels of sE-selectin were similar between patients with HAM and controls (Tsujino et al., 1998). Authors also frequently found sE-selectin in the CSF during exacerbations in RRMS, supporting a role for E-selectin–mediated responses to endothelial cell activation or damage during an exacerbation (Droogan et al., 1996). In contrast, others found CSF and serum sE-selectin levels were similar between patients in relapse and those with other inflammatory (IND) and non-inflammatory neurological disease (NIND). Another report sought to determine whether concentrations of sE-selectin correlated with gadolinium-DPTA enhancement (a marker of enhanced BBB permeability) on MRI in patients with MS. Authors found levels of sE-selectin were significantly increased in PPMS patients compared to the near control levels of sE-selectin detected in RRMS and SPMS patients. Interestingly, 5 of the 10 primary progressive patients with high levels of sE-selectin showed very low activity on MRI scans. While there was no correlation between sE-selectin concentrations and contrast-enhancing lesions on MRI, a close correlation was observed between TNF-α and sE-selectin (Giovannoni et al., 1996). Other groups have documented the same high levels of serum sE-selectin in PPMS compared with RRMS and SPMS (McDonnell et al., 1999) and provide evidence for significant immunological heterogeneity in MS related to immune/endothelial cell interactions in different types of MS. It also goes against the dogma of lesser inflammatory involvement that has previously characterized PPMS. This unique association between serum E-selectin and PPMS may indeed highlight the importance of advancing the therapeutic consideration of E-selectin tolerization to limit neurodegeneration in MS, with relevance to particularly acute and active processes such as those implicated in PPMS.

DATA AVAILABILITY

All datasets generated for this study are included in the manuscript and/or the **Supplementary Files**.

ETHICS STATEMENT

Animal Subjects

All experiments were carried out in compliance with the Guide for the Care and Use of Laboratory Animal Resources (1996), the Canadian Council on Animal Care guidelines and approved by the NINDS Animal Care and Use and UBC Animal Care Committees.

AUTHOR CONTRIBUTIONS

JQ performed EAE induction, scoring, data collection, analyses, immunoassays, cell culture, tissue isolation and preparation, prepared the first and subsequent versions of the manuscript, formulated the research plan and series of experiments with input from JH; and oversaw the experimental approach and design, reviewed data and analyses and prepared the manuscript including revising the manuscript critically for technical and scientific accuracy with JH. PB and EK performed immunohistochemistry and analyses of that data. All authors have reviewed the manuscript in entirety and are in agreement with the content of this work.

FUNDING

This study was supported by funds from the Intramural Research Program of the Neuroimmunology Branch at the National Institutes of Health and post-doctoral support to Xinhui Li. JQ was supported by an MS Society of Canada Donald Paty Career Development Award and additional support was provided by philanthropic funds for our MS Neuroprotection Research Program through the UBC Hospital and VGH foundation.

ACKNOWLEDGMENTS

We would like to thank Jaebong Huh and Xinhui Li for technical assistance with aspects of EAE scoring, immunoassays and data analyses.

SUPPLEMENTARY MATERIAL

The Supplementary Material for this article can be found online at: https://www.frontiersin.org/articles/10.3389/fnmol.2019.00190/full#supplementary-material

REFERENCES

Anderson, S. A., Shukaliak-Quandt, J., Jordan, E. K., Arbab, A. S., Martin, R., McFarland, H., et al. (2004). Magnetic resonance imaging of labeled T-cells in a mouse model of multiple sclerosis. *Ann. Neurol.* 55, 654–659. doi: 10.1002/ana.20066

Aranami, T., and Yamamura, T. (2008). Th17 Cells and autoimmune encephalomyelitis (EAE/MS). *Allergol. Int.* 57, 115–120. doi: 10.2332/allergolint.r-07-159

Bai, X. F., Shi, F. D., Xiao, B. G., Li, H. L., van der Meide, P. H., and Link, H. (1997). Nasal administration of myelin basic protein prevents relapsing experimental autoimmune encephalomyelitis in DA rats by activating regulatory cells expressing IL-4 and TGF-β mRNA. *J. Neuroimmunol.* 80, 65–75. doi: 10.1016/s0165-5728(97)00133-1

Banham, A. H., Powrie, F. M., and Suri-Payer, E. (2006). FOXP3$^+$ regulatory T cells: current controversies and future perspectives. *Eur. J. Immunol.* 36, 2832–2836. doi: 10.1002/eji.200636459

Bar-Or, A. (2008). The immunology of multiple sclerosis. *Semin Neurol.* 28, 29–45. doi: 10.1055/s-2007-1019124

Bjartmar, C., and Trapp, B. D. (2003). Axonal degeneration and progressive neurologic disability in multiple sclerosis. *Neurotox. Res.* 5, 157–164. doi: 10.1007/bf03033380

Broere, F., Wieten, L., Klein Koerkamp, E. I., van Roon, J. A., Guichelaar, T., Lafeber, F. P., et al. (2008). Oral or nasal antigen induces regulatory T cells that suppress arthritis and proliferation of arthritogenic T cells in joint draining lymph nodes. *J. Immunol.* 181, 899–906. doi: 10.4049/jimmunol.181.2.899

Burkhart, C., Liu, G. Y., Anderton, S. M., Metzler, B., and Wraith, D. C. (1999). Peptide-induced T cell regulation of experimental autoimmune encephalomyelitis: a role for IL-10. *Int. Immunol.* 11, 1625–1634. doi: 10.1093/intimm/11.10.1625

Chen, Y., Ruetzler, C., Pandipati, S., Spatz, M., McCarron, R. M., Becker, K., et al. (2003). Mucosal tolerance to E-selectin provides cell-mediated protection against ischemic brain injury. *Proc. Natl. Acad. Sci. U S A* 100, 15107–15112. doi: 10.1073/pnas.2436538100

Doring, A., Wild, M., Vestweber, D., Deutsch, U., and Engelhardt, B. (2007). E- and P-selectin are not required for the development of experimental autoimmune encephalomyelitis in C57BL/6 and SJL mice. *J. Immunol.* 179, 8470–8479. doi: 10.4049/jimmunol.179.12.8470

Droogan, A. G., McMillan, S. A., Douglas, J. P., and Hawkins, S. A. (1996). Serum and cerebrospinal fluid levels of soluble adhesion molecules in multiple sclerosis: predominant intrathecal release of vascular cell adhesion molecule-1. *J. Neuroimmunol.* 64, 185–191. doi: 10.1016/0165-5728(95)00174-3

Engelhardt, B., Vestweber, D., Hallmann, R., and Schulz, M. (1997). E- and P-selectin are not involved in the recruitment of inflammatory cells across the blood-brain barrier in experimental autoimmune encephalomyelitis. *Blood* 90, 4459–4472.

Frenette, P. S., Mayadas, T. N., Rayburn, H., Hynes, R. O., and Wagner, D. D. (1996). Susceptibility to infection and altered hematopoiesis in mice deficient in both P- and E-selectins. *Cell* 84, 563–574. doi: 10.1016/s0092-8674(00)81032-6

Frischer, J. M., Bramow, S., Dal-Bianco, A., Lucchinetti, C. F., Rauschka, H., Schmidbauer, M., et al. (2009). The relation between inflammation and neurodegeneration in multiple sclerosis brains. *Brain* 132, 1175–1189. doi: 10.1093/brain/awp070

Frohman, E. M., Racke, M. K., and Raine, C. S. (2006). Multiple sclerosis—the plaque and its pathogenesis. *N Engl. J. Med.* 354, 942–955. doi: 10.1056/NEJMra052130

George, J., Yacov, N., Breitbart, E., Bangio, L., Shaish, A., Gilburd, B., et al. (2004). Suppression of early atherosclerosis in LDL-receptor deficient mice by oral tolerance with β 2-glycoprotein I. *Cardiovasc Res.* 62, 603–609. doi: 10.1016/s0008-6363(04)00066-5

Giovannoni, G., Thorpe, J. W., Kidd, D., Kendall, B. E., Moseley, I. F., Thompson, A. J., et al. (1996). Soluble E-selectin in multiple sclerosis: raised concentrations in patients with primary progressive disease. *J. Neurol. Neurosurg. Psychiatry* 60, 20–26. doi: 10.1136/jnnp.60.1.20

Gor, D. O., Rose, N. R., and Greenspan, N. S. (2003). TH1-TH2: a procrustean paradigm. *Nat. Immunol.* 4, 503–505. doi: 10.1038/ni0603-503

Goverman, J. (2009). Autoimmune T cell responses in the central nervous system. *Nat. Rev. Immunol.* 9, 393–407. doi: 10.1038/nri2550

Hauser, S. L., Waubant, E., Arnold, D. L., Vollmer, T., Antel, J., Fox, R. J., et al. (2008). B-cell depletion with rituximab in relapsing-remitting multiple sclerosis. *N Engl. J. Med.* 358, 676–688. doi: 10.1056/NEJMoa0706383

Hoyne, G. F., Askonas, B. A., Hetzel, C., Thomas, W. R., and Lamb, J. R. (1996). Regulation of house dust mite responses by intranasally administered peptide: transient activation of CD4$^+$ T cells precedes the development of tolerance *in vivo*. *Int. Immunol.* 8, 335–342. doi: 10.1093/intimm/8.3.335

Ingle, G. T., Stevenson, V. L., Miller, D. H., and Thompson, A. J. (2003). Primary progressive multiple sclerosis: a 5-year clinical and MR study. *Brain* 126, 2528–2536. doi: 10.1093/brain/awg261

Johnson, T. A., Jirik, F. R., and Fournier, S. (2010). Exploring the roles of CD8$^+$ T lymphocytes in the pathogenesis of autoimmune demyelination. *Semin. Immunopathol.* 32, 197–209. doi: 10.1007/s00281-010-0199-7

Kappos, L., Bar-Or, A., Cree, B. A. C., Fox, R. J., Giovannoni, G., Gold, R., et al. (2018). Siponimod versus placebo in secondary progressive multiple sclerosis (EXPAND): a double-blind, randomised, phase 3 study. *Lancet* 391, 1263–1273. doi: 10.1016/S0140-6736(18)30475-6

Kerfoot, S. M., Norman, M. U., Lapointe, B. M., Bonder, C. S., Zbytnuik, L., and Kubes, P. (2006). Reevaluation of P-selectin and α 4 integrin as targets for the treatment of experimental autoimmune encephalomyelitis. *J. Immunol.* 176, 6225–6234. doi: 10.4049/jimmunol.176.10.6225

Klingenberg, R., Lebens, M., Hermansson, A., Fredrikson, G. N., Strodthoff, D., Rudling, M., et al. (2010). Intranasal immunization with an apolipoprotein B-100 fusion protein induces antigen-specific regulatory T cells and reduces atherosclerosis. *Arterioscler. Thromb. Vasc. Biol.* 30, 946–952. doi: 10.1161/ATVBAHA.109.202671

Korn, T., Anderson, A. C., Bettelli, E., and Oukka, M. (2007). The dynamics of effector T cells and Foxp3+ regulatory T cells in the promotion and regulation of autoimmune encephalomyelitis. *J. Neuroimmunol.* 191, 51–60. doi: 10.1016/j.jneuroim.2007.09.009

Kuenz, B., Lutterotti, A., Khalil, M., Ehling, R., Gneiss, C., Deisenhammer, F., et al. (2005). Plasma levels of soluble adhesion molecules sPECAM-1, sP-selectin and sE-selectin are associated with relapsing-remitting disease course of multiple sclerosis. *J. Neuroimmunol.* 167, 143–149. doi: 10.1016/j.jneuroim.2005.06.019

Kuhlmann, T., Lingfeld, G., Bitsch, A., Schuchardt, J., and Bruck, W. (2002). Acute axonal damage in multiple sclerosis is most extensive in early disease stages and decreases over time. *Brain* 125, 2202–2212. doi: 10.1093/brain/awf235

Kutzelnigg, A., Lucchinetti, C. F., Stadelmann, C., Brück, W., Rauschka, H., Bergmann, M., et al. (2005). Cortical demyelination and diffuse white matter injury in multiple sclerosis. *Brain* 128, 2705–2712. doi: 10.1093/brain/awh641

Laliotou, B., and Dick, A. D. (1999). Modulating phenotype and cytokine production of leucocytic retinal infiltrate in experimental autoimmune uveoretinitis following intranasal tolerance induction with retinal antigens. *Br. J. Ophthalmol.* 83, 478–485. doi: 10.1136/bjo.83.4.478

Lawrence, M. B., and Springer, T. A. (1991). Leukocytes roll on a selectin at physiologic flow rates: distinction from and prerequisite for adhesion through integrins. *Cell* 65, 859–873. doi: 10.1016/0092-8674(91)90393-d

Lawrence, M. B., and Springer, T. A. (1993). Neutrophils roll on E-selectin. *J. Immunol.* 151, 6338–6346.

Li, X., Johnson, K. R., Bryant, M., Elkahloun, A. G., Amar, M., Remaley, A. T., et al. (2011). Intranasal delivery of E-selectin reduces atherosclerosis in ApoE−/− mice. *PLoS One* 6:e20620. doi: 10.1371/journal.pone.0020620

Liu, G. Y., and Wraith, D. C. (1995). Affinity for class II MHC determines the extent to which soluble peptides tolerize autoreactive T cells in naive and primed adult mice—implications for autoimmunity. *Int. Immunol.* 7, 1255–1263. doi: 10.1093/intimm/7.8.1255

Louveau, A., Smirnov, I., Keyes, T. J., Eccles, J. D., Rouhani, S. J., Peske, J. D., et al. (2015). Structural and functional features of central nervous system lymphatic vessels. *Nature* 523, 337–341. doi: 10.1038/nature14432

Maron, R., Sukhova, G., Faria, A. M., Hoffmann, E., Mach, F., Libby, P., et al. (2002). Mucosal administration of heat shock protein-65 decreases atherosclerosis and inflammation in aortic arch of low-density lipoprotein receptor-deficient mice. *Circulation* 106, 1708–1715. doi: 10.1161/01.cir.0000029750.99462.30

Mayer, L., and Shao, L. (2004). Therapeutic potential of oral tolerance. *Nat. Rev. Immunol.* 4, 407–419. doi: 10.1038/nri1370

McDonnell, G. V., McMillan, S. A., Douglas, J. P., Droogan, A. G., and Hawkins, S. A. (1999). Serum soluble adhesion molecules in multiple sclerosis: raised sVCAM-1, sICAM-1 and sE-selectin in primary progressive disease. *J. Neurol.* 246, 87–92. doi: 10.1007/s004150050313

McMahon, E. J., Bailey, S. L., Castenada, C. V., Waldner, H., and Miller, S. D. (2005). Epitope spreading initiates in the CNS in two mouse models of multiple sclerosis. *Nat. Med.* 11, 335–339. doi: 10.1038/nm1202

Montalban, X., Hauser, S. L., Kappos, L., Arnold, D. L., Bar-Or, A., Comi, G., et al. (2017). Ocrelizumab versus placebo in primary progressive multiple sclerosis. *N Engl. J. Med.* 376, 209–220. doi: 10.1056/NEJMoa1606468

Neil, S., Huh, J., Baronas, V., Li, X., McFarland, H. F., Cherukuri, M., et al. (2017). Oral administration of the nitroxide radical TEMPOL exhibits immunomodulatory and therapeutic properties in multiple sclerosis models. *Brain Behav. Immun.* 62, 332–343. doi: 10.1016/j.bbi.2017.02.018

Piehl, F., Holmen, C., Hillert, J., and Olsson, T. (2011). Swedish natalizumab (Tysabri) multiple sclerosis surveillance study. *Neurol Sci.* 31, 289–293. doi: 10.1007/s10072-010-0345-y

Polman, C. H., O'Connor, P. W., Havrdova, E., Hutchinson, M., Kappos, L., Miller, D. H., et al. (2006). A randomized, placebo-controlled trial of natalizumab for relapsing multiple sclerosis. *N Engl. J. Med.* 354, 899–910. doi: 10.1056/NEJMoa044397

Quandt, J. A., Huh, J., Baig, M., Yao, K., Ito, N., Bryant, M., et al. (2012). Myelin basic protein-specific TCR/HLA-DRB5*01:01 transgenic mice support the etiologic role of DRB5*01:01 in multiple sclerosis. *J. Immunol.* 189, 2897–2908. doi: 10.4049/jimmunol.1103087

Racke, M. K. (2009). Immunopathogenesis of multiple sclerosis. *Ann. Indian Acad. Neurol.* 12, 215–220. doi: 10.4103/0972-2327.58274

Reese, T. S., and Karnovsky, M. J. (1967). Fine structural localization of a blood-brain barrier to exogenous peroxidase. *J. Cell Biol.* 34, 207–217. doi: 10.1083/jcb.34.1.207

Risau, W., Esser, S., and Engelhardt, B. (1998). Differentiation of blood-brain barrier endothelial cells. *Pathol. Biol.* 46, 171–175.

Sakaguchi, S., Yamaguchi, T., Nomura, T., and Ono, M. (2008). Regulatory T cells and immune tolerance. *Cell.* 133, 775–787. doi: 10.1016/j.cell.2008.05.009

Sathiyanadan, K., Coisne, C., Enzmann, G., Deutsch, U., and Engelhardt, B. (2014). PSGL-1 and E/P-selectins are essential for T-cell rolling in inflamed CNS microvessels but dispensable for initiation of EAE. *Eur. J. Immunol.* 44, 2287–2294. doi: 10.1002/eji.201344214

Segal, B. M., and Shevach, E. M. (1998). The straight talk on immune deviation. *Clin. Immunol. Immunopathol.* 88, 1–3. doi: 10.1006/clin.1998.4559

Sospedra, M., and Martin, R. (2005). Immunology of multiple sclerosis. *Annu. Rev. Immunol.* 23, 683–747. doi: 10.1146/annurev.immunol.23.021704.115707

Takeda, H., Spatz, M., Ruetzler, C., McCarron, R., Becker, K., and Hallenbeck, J. (2002). Induction of mucosal tolerance to E-selectin prevents ischemic and hemorrhagic stroke in spontaneously hypertensive genetically stroke-prone rats. *Stroke* 33, 2156–2163. doi: 10.1161/01.str.0000029821.82531.8b

Takeda, H., Spatz, M., Ruetzler, C., McCarron, R., Becker, K., and Hallenbeck, J. (2004). "Induction of mucosal tolerance to E-selectin targets immunomodulation to activating vessel segments and prevents ischemic and hemorrhagic stroke," in *Neuroinflammation in Stroke. Ernst Schering Research Foundation Workshop* (Vol. 47), eds U. Dirnagl and B. Elger (Berlin, Heidelberg: Springer), 117–132.

Thurau, S. R., Chan, C. C., Nussenblatt, R. B., and Caspi, R. R. (1997). Oral tolerance in a murine model of relapsing experimental autoimmune uveoretinitis (EAU): induction of protective tolerance in primed animals. *Clin. Exp. Immunol.* 109, 370–376. doi: 10.1046/j.1365-2249.1997.4571356.x

Trapp, B. D., Peterson, J., Ransohoff, R. M., Rudick, R., Mork, S., and Bo, L. (1998). Axonal transection in the lesions of multiple sclerosis. *N Engl. J. Med.* 338, 278–285. doi: 10.1056/nejm199801293380502

Tsujino, A., Nakamura, T., Furuya, T., Goto, H., Nishiura, Y., Shirabe, S., et al. (1998). Elevated serum levels of soluble E- and L-selectin in patients with human T-cell lymphotropic virus type I-associated myelopathy. *J. Neurol. Sci.* 155, 76–79. doi: 10.1016/s0022-510x(97)00264-5

Tsukada, N., Miyagi, K., Matsuda, M., and Yanagisawa, N. (1995). Soluble E-selectin in the serum and cerebrospinal fluid of patients with multiple sclerosis and human T-lymphotropic virus type 1-associated myelopathy. *Neurology* 45, 1914–1918. doi: 10.1212/wnl.45.10.1914

Unger, W. W., Jansen, W., Wolvers, D. A., van Halteren, A. G., Kraal, G., and Samsom, J. N. (2003). Nasal tolerance induces antigen-specific $CD4^+CD25^-$ regulatory T cells that can transfer their regulatory capacity to naive $CD4^+$ T cells. *Int. Immunol.* 15, 731–739. doi: 10.1093/intimm/dxg069

van Puijvelde, G. H., Hauer, A. D., de Vos, P., van den Heuvel, R., van Herwijnen, M. J., van der Zee, R., et al. (2006). Induction of oral tolerance to oxidized low-density lipoprotein ameliorates atherosclerosis. *Circulation* 114, 1968–1976. doi: 10.1161/circulationaha.106.615609

van Zwam, M., Huizinga, R., Heijmans, N., van Meurs, M., Wierenga-Wolf, A. F., Melief, M. J., et al. (2009). Surgical excision of CNS-draining lymph nodes reduces relapse severity in chronic-relapsing experimental autoimmune encephalomyelitis. *J. Pathol.* 217, 543–551. doi: 10.1002/path.2476

Wakita, H., Ruetzler, C., Illoh, K. O., Chen, Y., Takanohashi, A., Spatz, M., et al. (2008). Mucosal tolerization to E-selectin protects against memory dysfunction and white matter damage in a vascular cognitive impairment model. *J. Cereb. Blood Flow Metab.* 28, 341–353. doi: 10.1038/sj.jcbfm.9600528

Wolvers, D. A., Coenen-de Roo, C. J., Mebius, R. E., van der Cammen, M. J., Tirion, F., Miltenburg, A. M., et al. (1999). Intranasally induced immunological tolerance is determined by characteristics of the draining lymph nodes: studies with OVA and human cartilage gp-39. *J. Immunol.* 162, 1994–1998.

Yong, H., Chartier, G., and Quandt, J. (2018). Modulating inflammation and neuroprotection in multiple sclerosis. *J. Neurosci. Res.* 96, 927–950. doi: 10.1002/jnr.24090

Zamvil, S. S., and Steinman, L. (1990). The T lymphocyte in experimental allergic encephalomyelitis. *Annu. Rev. Immunol.* 8, 579–621. doi: 10.1146/annurev.iy.08.040190.003051

Zhang, X., Hupperts, R., and De Baets, M. (2003). Monoclonal antibody therapy in experimental allergic encephalomyelitis and multiple sclerosis. *Immunol. Res.* 28, 61–78. doi: 10.1385/ir:28:1:61

Conflict of Interest Statement: The authors declare that the research was conducted in the absence of any commercial or financial relationships that could be construed as a potential conflict of interest.

frontiers in Molecular Neuroscience

REVIEW
published: 19 September 2019
doi: 10.3389/fnmol.2019.00225

Central Nervous System Remyelination: Roles of Glia and Innate Immune Cells

*Charbel S. Baaklini[1], Khalil S. Rawji[2], Greg J. Duncan[3], Madelene F. S. Ho[1] and Jason R. Plemel[1]**

[1]Department of Medicine, Division of Neurology, Neuroscience and Mental Health Institute, Faculty of Medicine & Dentistry, University of Alberta, Edmonton, AB, Canada, [2]Wellcome Trust-Medical Research Council, Cambridge Stem Cell Institute, Cambridge Biomedical Campus, University of Cambridge, Cambridge, United Kingdom, [3]Department of Neurology, Jungers Center for Neurosciences Research, Oregon Health and Science University, Portland, OR, United States

In diseases such as multiple sclerosis (MS), inflammation can injure the myelin sheath that surrounds axons, a process known as demyelination. The spontaneous regeneration of myelin, called remyelination, is associated with restoration of function and prevention of axonal degeneration. Boosting remyelination with therapeutic intervention is a promising new approach that is currently being tested in several clinical trials. The endogenous regulation of remyelination is highly dependent on the immune response. In this review article, we highlight the cell biology of remyelination and its regulation by innate immune cells. For the purpose of this review, we discuss the roles of microglia, and also astrocytes and oligodendrocyte progenitor cells (OPCs) as they are being increasingly recognized to have immune cell functions.

Keywords: remyelination, microglia, oligodendrocyte, oligodendrocyte progenitor cells, astrocytes, white matter disease, aging

OPEN ACCESS

Edited by:
Craig Stephen Moore, Memorial University of Newfoundland, Canada

Reviewed by:
Andrew David Greenhalgh, INRA UMR1286 Laboratoire NutriNeuro, France
Samaneh Maysami, University of Manchester, United Kingdom

****Correspondence:***
Jason R. Plemel
jrplemel@ualberta.ca

Received: *28 June 2019*
Accepted: *04 September 2019*
Published: *19 September 2019*

Citation:
Baaklini CS, Rawji KS, Duncan GJ, Ho MFS and Plemel JR (2019) Central Nervous System Remyelination: Roles of Glia and Innate Immune Cells. Front. Mol. Neurosci. 12:225. doi: 10.3389/fnmol.2019.00225

INTRODUCTION

Demyelination is a common feature of disease occurring after conditions such as spinal cord injury (SCI; Crowe et al., 1997; Powers et al., 2012; Plemel et al., 2014), multiple sclerosis (MS; Franklin and Ffrench-Constant, 2008; Plemel et al., 2017), stroke (Rosenzweig and Carmichael, 2015; Khodanovich et al., 2018), and traumatic brain injury (Mierzwa et al., 2015; Armstrong et al., 2016). Moreover, white matter loss occurs in Alzheimer's disease (Mitew et al., 2010; Carmeli et al., 2013; Zhan et al., 2014; Bejanin et al., 2017) and is a feature of aging that is correlated with cognitive decline (Bartzokis et al., 2012; Yeatman et al., 2014; Li et al., 2017). With age, myelin shows increasing signs of damage while at the same time myelin debris accumulates within microglia (Safaiyan et al., 2016; Hill et al., 2018), which can trigger cholesterol crystal formation and inflammasome activation (Cantuti-Castelvetri et al., 2018). In MS, more remyelination is associated with less disability (Bramow et al., 2010; Bodini et al., 2016), suggesting that enhancing remyelination is a viable therapeutic strategy that is only recently showing benefits in clinical trials (Plemel et al., 2017). However, for those with MS, remyelination is variable and prone to failure (Prineas et al., 1993; Patrikios et al., 2006; Patani et al., 2007; Bramow et al., 2010), especially in the context of aging which is known to slow the rate of remyelination (Shields et al., 1999; Goldschmidt et al., 2009; Ruckh et al., 2012; Brown et al., 2014; Frischer et al., 2015). In this review article, we focus on the innate immune cells of the central nervous system (CNS) and their role during remyelination. We include microglia as the primary CNS innate immune cells, but also recognize that other glia such as astrocytes and oligodendrocyte progenitor cells (OPCs) may sculpt the innate immune response.

CELL BIOLOGY OF REMYELINATION

Importance of Remyelination

Demyelination, or the loss of myelin, can be induced due to injury or disease. MS is characterized by inflammatory demyelination, possibly induced by monocytes, macrophage/microglia, and T-cells. For example, microglia/macrophage-derived oxidative species cause damage by inducing myelin and axonal injury (Haider et al., 2011; Nikic et al., 2011; Witte et al., 2019). The immune system produces demyelination by many other mechanisms, but this is not the focus of this review (Mayo et al., 2012; Lassmann and van Horssen, 2016; Mishra and Yong, 2016; Davies and Miron, 2018). Demyelination slows axonal conduction, and as suggested by computer simulations (Koles and Rasminsky, 1972; Waxman and Brill, 1978), may even result in a failure to propagate the signal past the demyelinated segment (Koles and Rasminsky, 1972; Waxman and Brill, 1978). The conduction block associated with demyelination is thought to relate to ionic disbalance once the myelin is removed. The loss of myelin unmasks potassium channels underneath the myelin sheath that can act as a current sink (Schauf and Davis, 1974; Bostock et al., 1978, 1981; Sherratt et al., 1980; Wang et al., 1993, 1995). To compensate, axons can upregulate voltage-gated sodium channels along their length (Foster et al., 1980; England et al., 1991; Black et al., 2007; Hamada and Kole, 2015). Potentially due to this upregulation or redistribution of voltage-gated sodium channels, it is possible to propagate the signal along a demyelinated segment, albeit more slowly (Felts et al., 1997). Associated with the axonal conduction block is a corresponding functional loss or alteration. For example, demyelination of the ventral medial geniculate nucleus (vMGN) or A1 region in the auditory cortex in mice results in both impaired sound frequency-specific responses and an increase in latency in auditory responses (Narayanan et al., 2018). Importantly, while remyelination may speed axonal propagation, it is not always linked to functional recovery (Duncan et al., 2009, 2018; Mozafari et al., 2010; Assinck et al., 2017a; Narayanan et al., 2018). Both the extent and severity of demyelination may dictate the functional consequences. For example, in an experimental murine model of SCI where demyelination is confined to the lesion, preventing remyelination did not change the spontaneous recovery, potentially because after SCI conduction is not sufficiently disrupted (Felts et al., 1997; Duncan et al., 2017, 2018).

Remyelination also maintains axonal integrity and attenuates axonal degeneration. If remyelination is slowed using irradiation to ablate OPCs in mice, there is more axonal degeneration (Irvine and Blakemore, 2008). However, this study is confounded by off-target effects of irradiation including blood-brain barrier (BBB) disruption (Diserbo et al., 2002), enhanced astrogliosis (Wilson et al., 2009), and activation of microglia (Hwang et al., 2006; Irvine and Blakemore, 2008). More specifically, if remyelination is accelerated by promoting oligodendrocyte differentiation in a cell-type specific manner, more axons are preserved (Mei et al., 2016). How might myelin protect axons? One likely mechanism is *via* the buffering of potassium through the potassium channel KIR4.1, expressed in oligodendrocytes (Schirmer et al., 2018). Potassium is released from axons as part of their action potential and conditional oligodendrocyte-specific removal of this KIR4.1 buffering results in late-onset axonal degeneration, suggesting that myelinic potassium buffering maintains axonal integrity. Oligodendrocytes also support axons by providing them with glycolytic metabolites *via* the myelin sheath (Fünfschilling et al., 2012; Saab et al., 2016; Micu et al., 2017). Even the myelin sheath may itself can act as a protective barrier by surrounding the axon from toxic reactive oxygen species (Nikic et al., 2011; Witte et al., 2019). The myelin sheath also shifts some of the metabolic demands from the axon to the oligodendrocyte. For example, when an axon is myelinated there is less sodium released for an axon potential, and therefore less energy is required to repolarize its membrane, yet the production of myelin is energetically expensive (Harris and Attwell, 2012). Other possible mechanisms of axonal support by oligodendrocytes include the release of oligodendrocyte-derived exosomes or ribosomes (Frühbeis et al., 2013; Shakhbazau et al., 2016). Oligodendrocytes can also secrete many other factors to boost neuronal health or survival in culture such as insulin-like growth factor 1 (IGF-1) and glial cell-derived neurotrophic factor (GDNF; Wilkins et al., 2001, 2003; Dai et al., 2003), which may support axons *in vivo*.

An analogous relationship between glial cells and axons exists in the peripheral nervous system (PNS). Schwann cells (SCs) are glial cells generally restricted to the PNS that arise from neural crest-derived SC precursors (Monk et al., 2015). Under normal conditions, SCs myelinate axons in the PNS. However, there is evidence that SCs can remyelinate in the CNS under inflammatory conditions. In fact, P_0 staining—a marker for SC-derived myelin sheaths—was observed in MS spinal cord lesions (Itoyama et al., 1983). Indeed, fate-mapping revealed that in LPC-demyelinated lesions, PDGFRa and NG2-expressing progenitor cells in the CNS produce the myelinating oligodendrocytes and SCs (Zawadzka et al., 2010).

Process of Remyelination

Remyelination is a regenerative process that requires the sequential activation and recruitment of OPCs to areas of demyelination, followed by their differentiation into new oligodendrocytes—but also less frequently into SCs—and subsequent myelin deposition around demyelinated axons (Franklin and Ffrench-Constant, 2008, 2017; Zawadzka et al., 2010; Plemel et al., 2017). OPCs are found throughout the adult mouse brain white matter and gray matter (Dimou et al., 2008; Rivers et al., 2008; Kang et al., 2010). After a demyelinating insult, OPCs transition to a reactive state with the upregulation of key transcription factors such as Nkx2.2, Olig2 and Sox2 (Levine and Reynolds, 1999; Fancy et al., 2004; Zhao et al., 2015). In the lesion, there is a release of many growth factors such as platelet-derived growth factor (PDGF) and fibroblast growth factor (FGF; Hinks and Franklin, 1999; Messersmith et al., 2000). These factors and others are thought to regulate OPC lineage progression by increasing proliferation and migration towards the lesion (Messersmith et al., 2000; Murtie et al., 2005; Dehghan et al., 2012). OPCs proliferate and migrate in the days following demyelination or injury, as part

of their recruitment (Redwine and Armstrong, 1998; Hughes et al., 2013). Following OPC recruitment, they differentiate and mature into myelinating oligodendrocytes, which involves the ensheathment and enwrapping of the denuded axon with a new myelin sheath (Tripathi et al., 2010; Zawadzka et al., 2010; Crawford et al., 2016b). Differentiated oligodendrocytes start expressing myelin proteins such as myelin basic protein (MBP), which allows for the compaction of myelin membranes (Kimura et al., 1989; Watanabe et al., 2002; Polito and Reynolds, 2005; Snaidero et al., 2014). Much of the process of oligodendrocyte differentiation is due to key transcription factors. For example, the transcription factor myelin regulatory factor (MyRF) is required for oligodendrocyte maturation and myelination (Emery et al., 2009) and effective remyelination in adulthood (Duncan et al., 2017). MyRF binds to enhancer sequences and directly drives the expression of myelin genes (Bujalka et al., 2013); it is necessary for remyelination after chemical and traumatic demyelinating injuries (Duncan et al., 2017, 2018). Remyelinating oligodendrocytes can adopt different phenotypes, as shown by single-nucleus RNA sequencing (Jäkel et al., 2019). Interestingly, oligodendrocytes in the white matter of MS patients compared to non-diseased controls have different subclustering based on their transcriptomes. This shift in oligodendrocyte phenotypes may reflect an impaired capacity to remyelinate but the functional consequences of these different phenotypes have not yet been directly determined.

Much of the research on remyelination is conducted on demyelinating rodent models. Using these models, it has been shown that OPCs, and not mature oligodendrocytes, are the cells most responsible for remyelination (Crawford et al., 2016a). Transplantation of mature oligodendrocytes into demyelinated lesions do not remyelinate denuded axons (Targett et al., 1996). Oligodendrocyte fate-mapping in mice also demonstrated that mature oligodendrocytes do not engage in remyelination (Crawford et al., 2016a). Surprisingly, new data provides evidence that mature oligodendrocytes can remyelinate in larger mammals. Duncan et al. (2018) find the presence of oligodendrocytes with both thick and thin myelin sheaths using a feline irradiated food-induced demyelination (FIDID) model and vitamin B12 deficiency and in a non-human primate model. Given that remyelination is typically, but not always associated with thin myelin sheaths (Blakemore, 1974; Duncan et al., 2017), one explanation for these results is that spared oligodendrocytes with a thick, unaffected, myelin sheath can re-extend their processes and remyelinate adjacent denuded axons (Duncan et al., 2018). An alternative possibility with this study is that myelin sheath thickness may be differentially regulated by the axon. In a recent study, Yeung et al. (2019) investigated oligodendrogenesis in humans with MS using a specific carbon dating strategy. After cell division, the daughter cell's DNA will have a radioactive carbon concentration that is proportional to concentration of radioactive carbon in the atmosphere. As a result of atomic bomb testing starting in the mid-late 1940s, the atmospheric radioactive carbon increased making it possible to date daughter cells after the 1940s based on the nuclear radioactive carbon levels. Using this strategy, Yeung et al. (2019) measured new oligodendrocyte production in shadow plaques, which are regions of intermediate lipid staining that are thought to be remyelinated. Surprisingly, they found that new oligodendrocyte production was similar in shadow plaques to those found in the non-diseased brain, suggesting that in humans the mature oligodendrocytes can remyelinate denuded axons. However, in this one study, these conclusions are based off of 11 samples. Moreover, this study found that OPCs did turn over in shadow plaques, but due to the levels of atmospheric radioactive carbon, this was only apparent for those born in the mid-1960s onwards. Only one shadow plaque was measured for oligodendrocyte carbon after this critical mid-1960s period. The question of whether adult oligodendrocytes can remyelinate will, therefore, require further validation in future studies.

ROLES OF MICROGLIA AND INFILTRATING MACROPHAGES IN REMYELINATION

Microglia are immunocompetent glial cells of the CNS (Streit, 2002). They are the CNS parenchymal macrophages that arise developmentally from erythromyeloid precursors in the yolk sac (Ginhoux et al., 2010; Kierdorf et al., 2013). They are unevenly distributed according to the CNS region and range from 5 to 12% of glia in the mouse brain and 0.5%–16.6% of human brain parenchymal cells (Lawson et al., 1990; Mittelbronn et al., 2001). They are important for controlling many neurodevelopmental processes. For example, neural precursor cells proliferate in the presence of microglia *in vitro* (Antony et al., 2011). Also, microglia conditioned media promotes the differentiation of neural precursor cells into neurons as well as astrocytes (Nakanishi et al., 2007; Antony et al., 2011). Microglial ablation results in neuronal apoptosis and a decrease in spine density in young mice indicating microglia promote synaptogenesis and the survival of neurons (Ueno et al., 2013; Miyamoto et al., 2016). Microglia also regulate myelinogenesis through the secretion of growth factors like IGF-1, which is critical for *Mbp* expression in young mice (Wlodarczyk et al., 2017).

Microglia Response to Injury

Microglia regulate homeostasis by surveying their microenvironment but are highly responsive to injury or disease as laser-induced injury in the mouse neocortex results in microglial extensions surrounding the site of injury (Davalos et al., 2005; Nimmerjahn et al., 2005). When there is more damage over a longer period of time, for example following focal demyelination with LPC, microglia can retract their processes and become more spheroidal (Plemel et al., 2018). These morphological attributes of activated microglia, as well as similar expression patterns, have made it difficult to differentiate microglia from other macrophages such as border-associated macrophages in the CNS that include meningeal, choroid plexus and perivascular macrophages (Goldmann et al., 2016; Mrdjen et al., 2018), as well as monocyte-derived macrophages (Butovsky et al., 2014). Most studies do not differentiate between these cell types. As such, in this review article, these cells will be referred to as microglia/macrophages.

Microglia are surveillant cells that are highly responsive to environmental cues. In adults, microglia self-renew with modest

proliferation (Nimmerjahn et al., 2005; Elmore et al., 2014; Kawabori and Yenari, 2015). In the uninjured state of the CNS, *in vivo* imaging revealed that ramified microglia continuously scan their microenvironment by undergoing structural changes including filopodia extension and retraction (Nimmerjahn et al., 2005; Bernier et al., 2019). By this surveillance mechanism, using two-photon microscopy of living murine microglia, Davalos et al. (2005) demonstrate that they detect and act accordingly to damage-associated molecular patterns (DAMPs). Microglia respond to disease conditions through a combination of receptors such as pattern recognition receptors, purinergic and fractalkine receptors, and cytokine receptors (Hickman et al., 2013). Microglia likely responds to hundreds, if not thousands of molecules, many in undefined ways. Certain molecules elicit specific responses, for example, the subsequent activation of purinergic receptors leads to the activation of the phagocytic pathway in rat microglia, that involves the clearance of apoptotic cells, both *in vitro* and *in vivo* (Davalos et al., 2005; Haynes et al., 2006; Koizumi et al., 2007; Bernier et al., 2019).

Microglia During Remyelination

In the context of remyelination, microglia/macrophages can have many beneficial roles. However, these cells also contribute to autoimmune-related toxicity (Heppner et al., 2005; Ajami et al., 2011; Goldmann et al., 2013; Rothhammer et al., 2018). The dichotomous nature of microglia and macrophages is incompletely understood. One important function of microglia/macrophages following demyelination is the removal of inhibitory myelin debris present in the lesion. This myelin debris has been shown to negatively regulate OPC lineage progression (Syed et al., 2008; Plemel et al., 2013) and consequently, remyelination (Kotter et al., 2006). As microglia are phagocytotic cells, they contribute to myelin debris clearance (Sosa et al., 2013; Rawji et al., 2018). This phagocytosis is reflected by the presence of myelin proteins such as MBP in microglia/macrophages in the white matter following demyelination (Sosa et al., 2013).

Microglia also secrete an array of signaling molecules, including cytokines, chemokines and growth factors; many of these factors signal *via* receptors on oligodendrocyte lineage cells. For instance, the proinflammatory cytokine tumor necrosis factor-α (TNF-α), secreted by microglia/macrophages as well as astrocytes in mouse cuprizone-induced lesions, promotes OPC expansion and remyelination through TNF receptor 2 (TNFR2) on $NG2^+$ cells (Arnett et al., 2001; Voss et al., 2012). Interleukin-1β (IL-1β), also secreted by microglia/macrophages and astrocytes, is important for remyelination potentially by controlling oligodendrocyte lineage cell's survival by stimulating IGF-1 secretion from microglia/macrophages in cuprizone-treated mice (Mason et al., 2001). Recently, it was shown microglia can modulate remyelination through the secreted enzyme transglutaminase 2 (TG2). TG2 interacts with OPC-specific Adhesion G Protein-Coupled Receptor G1 (ADGRG1) to promote OPC proliferation. Either, microglia-specific loss of TG2 or OPC-specific loss of ADGRG1 impairs remyelination in two murine demyelination models (Giera et al., 2018). As microglia/macrophages transition from a more pro-inflammatory state in the days after demyelination to a more immunoregulatory phenotype at a later time point, they secrete Activin-A in mouse lesions (Miron et al., 2013). Activin-A release, in turn, interacts with activin receptors on OPCs, which are required for developmental myelination and remyelination (Dillenburg et al., 2018).

It is important to note that some of the cytokines that have pro-remyelinating roles can be implicated in mediating pathogenesis, including, for example, TNF-α that is required for autoimmune demyelination (Ruddle et al., 1990; Selmaj et al., 1991; Baker et al., 1994; Steeland et al., 2017). In addition, IL-1β from neutrophils and monocyte-derived macrophages drives neuroinflammation in EAE mice (Lévesque et al., 2016; Paré et al., 2018). Indeed, in autoimmune demyelination the removal of a key NF-kB regulator, TAK1, from microglia and CNS macrophages prevents EAE, suggesting an important role of these cells in the execution of autoimmune demyelination (Goldmann et al., 2013).

Microglia Response Is Heterogeneous

Recent transcriptomic analyses in both mice and humans revealed that the microglia response to acute demyelination is more heterogeneous than previously thought (Hammond et al., 2019; Masuda et al., 2019). In the resting state, microglia typically adopt a homeostatic phenotype characterized by the expression of such markers as CX3CR1, the purinergic receptor P2RY12, and TMEM119 (Krasemann et al., 2017; Masuda et al., 2019). As microglia become activated, they shift their phenotype. One recently characterized microglia phenotype is the damage-associated microglia (DAM), which are a subset of microglia revealed by single-cell RNA sequencing in Alzheimer's Disease transgenic mice (Keren-Shaul et al., 2017). DAM are linked to neurodegeneration and are characterized by the upregulation TREM2, a phagocytic marker (Deczkowska et al., 2018). Many of these markers associated with DAM are also upregulated in microglia following demyelination such as *Lpl, Cst7* and *Apoe*, suggesting that there is an overlapping response between neurodegeneration and demyelination (Keren-Shaul et al., 2017; Hammond et al., 2019). The transition to a less pro-inflammatory microglia/macrophage phenotype is promoted by the secreted enzyme, interleukin 4 induced 1, which is induced in microglia in response to interleukin 4 (Psachoulia et al., 2016). Recently, it was shown that necroptosis of microglia/macrophages is important in the phenotypic shift during remyelination, suggesting that microglia/macrophages may not transition between phenotypes but instead die, only to be replaced by alternative phenotypes (Lloyd et al., 2019).

Infiltrating Macrophages During Remyelination

The functional overlap of monocytes-derived macrophages and microglia during remyelination is still unclear. Monocyte-derived macrophages are mononuclear phagocytic cells of the hematopoeitic stem cell lineage (Jakubzick et al., 2017). Under inflammatory conditions in the CNS, circulating monocytes cross the BBB and mature into macrophages (King et al., 2009; Caravagna et al., 2018). These infiltrating macrophages

are evident in both MS lesions and in the different models of demyelination/remyelination such as EAE, LPC and cuprizone-treated animal models (Hiremath et al., 1998; Trebst et al., 2001; King et al., 2009; Miron et al., 2013; Vogel et al., 2013; Kuhlmann et al., 2017). Monocytes that express C-C Motif Chemokine Receptor (CCR2), known as inflammatory monocytes, migrate into the CNS in response to C-C Motif Chemokine Ligand 2 (CCL2). Following cuprizone toxicity or in aged mice following focal demyelination, the vast majority of monocytes require CCR2 for their entry (Ruckh et al., 2012; Lampron et al., 2015). CCR2-knockout mice are resistant to EAE (Fife et al., 2000) and blocking monocyte infiltration prevents EAE in mice (Ajami et al., 2011) suggesting that monocytes are required for autoimmune-mediated demyelination in part by the production of reactive oxygen species (Nikic et al., 2011; Locatelli et al., 2018).

The roles of monocyte-derived macrophages are just beginning to be characterized during remyelination and can be difficult to delineate from microglia as experimentally manipulating these cells while leaving the microglial response intact is challenging. During remyelination, the early use of clodronate liposomes reduces remyelination. Clodronate liposomes are artificial lipid vesicles that are taken up preferentially by phagocytic cells and kill circulating monocytes and macrophages (van Rooijen, 1992; Van Rooijen and Sanders, 1994; Popovich et al., 1999; Kotter et al., 2006; Döring et al., 2015), but they can also ablate microglia (Kumamaru et al., 2012; Han et al., 2019). It is, therefore, still unclear whether clodronate liposomes impair remyelination by killing microglia or macrophages or both. One important correlate of remyelination is the removal of inhibitory myelin debris for which young monocyte-derived macrophages participate (Ruckh et al., 2012). However, it is still unclear whether microglia or macrophages predominate during myelin debris phagocytosis. Taken together, CNS-infiltrating macrophages promote demyelination, but the overlap in functions between microglia and macrophages during remyelination is less clear.

Taken together, microglia and macrophage likely possess overlapping functions that are not completely defined, which as a whole are required for remyelination (**Figure 1**). One critical function is the phagocytosis of inhibitory myelin debris, but other key roles of these cells include secretion of growth factors and the regulation of the immune response through cytokines and other immunoregulatory molecules. The response of these cells is heterogeneous and exciting new technologies such as single-cell RNA sequencing will allow for the characterization of their response during the continuum of remyelination.

ROLES OF OTHER INNATE IMMUNE CELLS DURING REMYELINATION

Following demyelination microglia/macrophages predominate, but other innate immune cells could potentially participate in remyelination. The other cells of the innate immune system include natural killer cells, mast cells, eosinophils, basophils, neutrophils, and dendritic cells. Many of these innate immune cells can inflict tissue damage (Mayo et al., 2012; Boutajangout and Wisniewski, 2013; Courties et al., 2014), but little is known about their role in remyelination. In the context of demyelinating diseases, several of these innate immune cells have a described role during demyelination. For instance, neutrophils are important players in disease pathogenesis as mice lacking the key neutrophils chemokine receptor, C-X-C motif chemokine receptor 2 (CXCR2), are resistant to cuprizone-induced oligodendrocyte cell death and demyelination (Liu et al., 2010). Eosinophils also contribute to demyelination as preventing their infiltration into the CNS in EAE mice decreases disease severity (Gladue et al., 1996). Mast cells, which are found in MS lesions, are also important in disease pathogenesis as blocking their ability to degranulate in EAE rats reduces disease severity (Olsson, 1974; Dimitriadou et al., 2000). To date, less is known about how eosinophils, basophils and neutrophils regulate remyelination. Dendritic cells, which are professional antigen producing cells, may have pro-remyelinating roles (Pusic et al., 2014). Dendritic cells challenged with interferon γ (IFNγ) release exosomes containing microRNA such as miR-219. These dendritic cell-derived exosomes improve remyelination in cultured rat hippocampal slices *ex vivo*, however, it is still unclear how dendritic cells regulate remyelination *in vivo*. Given the complex interplay between various innate immune cells and their known involvement in repair of other systems, such as during wound healing (MacLeod and Mansbridge, 2016), there are likely other unknown roles for these cells during remyelination.

ROLES OF ASTROCYTES IN REMYELINATION

Astrocytes have important roles in both CNS development and homeostasis such as during synaptogenesis, neurotransmission, BBB formation and maintenance, among other roles (Sofroniew and Vinters, 2010; Molofsky and Deneen, 2015). In response to neuroinflammation, astrocytes respond in a process called reactive astrogliosis (Zamanian et al., 2012). Reactive astrocytes have both potentially beneficial and detrimental roles during remyelination; indeed, these functions may relate to a particular phenotype that the astrocytes adopt (Liddelow and Barres, 2017; Liddelow et al., 2017). Astrocytes may promote/inhibit remyelination directly, but could also signal through microglia to promote remyelination. For example, the ablation of reactive astrocytes in cuprizone-treated mice impairs recruitment of microglia to the demyelinating lesion (Skripuletz et al., 2013). Lowered microglia recruitment is associated with reduced clearance of inhibitory myelin debris, which impairs oligodendrocyte maturation (Syed et al., 2008; Plemel et al., 2013) and remyelination (Kotter et al., 2006). The inverse is likely also true, whereby microglia can regulate astrocyte function. Microglia activated by a TLR4 agonist, LPS, induces a newly identified neurotoxic phenotype of astrocytes. The neurotoxic astrocyte may be detrimental for OPC maturation as it has been shown to induce oligodendrocyte and neuronal apoptosis (Liddelow et al., 2017). As microglia/macrophages display a temporal shift from a predominantly pro-inflammatory phenotype to an

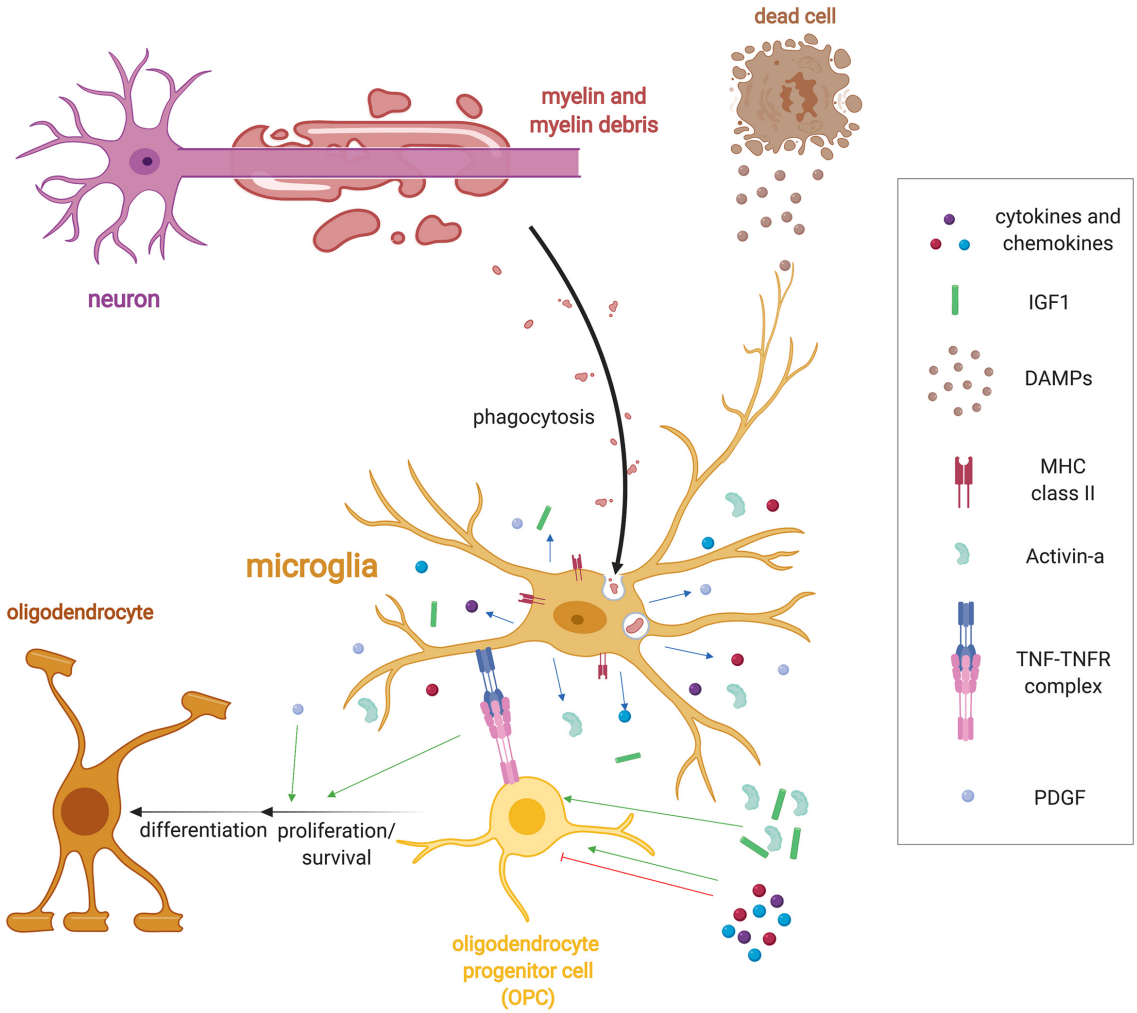

FIGURE 1 | Microglia regulation of remyelination. Following demyelination, microglia detect injury in the form of damage associated molecular patterns (DAMPs) *via* a variety of receptor classes such as pattern recognition receptors, purinergic and fractalkine receptors, and cytokine receptors. DAMPS induce a wide range of functions including the activation of microglia to phagocytose myelin and cellular debris. Microglia also upregulate a host of immune molecules when activated such as MHC-II expression and release cytokines, chemokines and growth factors such as Activin-A, platelet-derived growth factor (PDGF), IL-1β, and IGF-1 that regulate oligodendrocyte progenitor cell (OPC) lineage progression. They also express tumor necrosis factor-α (TNF-α), which binds to TNF receptor 2 (TNFR2) to promote remyelination.

anti-inflammatory phenotype (Miron et al., 2013), it is unknown whether the astrocytes within a demyelinating lesion adopt a similar temporal shift in phenotype and whether this may in turn yield a spectrum of beneficial or detrimental functions for remyelination.

One role of astrocytes is mediated by endothelin-1, a peptide that has been characterized to potently induce vasoconstriction. Following demyelination in animal models and in MS patients' lesions, astrocytes begin expressing endothelin-1 (ET-1; Hammond et al., 2014). ET-1 is secreted by astrocytes and endothelial cells and acts in paracrine and autocrine manners in the CNS (Hostenbach et al., 2016). ET-1 can activate receptors on vascular smooth muscle cells, inducing vasoconstriction and leading to cerebral hypoperfusion, which is commonly observed in MS patients (Law et al., 2004; Varga et al., 2009). Low oxygen tension, at least during development in mice, also impairs OPC maturation (Yuen et al., 2014). Following acute demyelination, astrocytes respond to ET-1 *via* their endothelin receptor B by upregulating the Notch1 receptor ligand, jagged1 (Hammond et al., 2014, 2015). Astrocyte-induced Notch1 activation is known to inhibit OPC differentiation and remyelination. Interestingly, this astrocyte jagged1-Notch1 interaction resolves to allow OPC differentiation after a period of OPC expansion. Astrocytes could, therefore, be delaying OPC differentiation to allow sufficient proliferation of OPCs (Zhang et al., 2009; Hammond et al., 2014). This notch-mediated interaction may be relevant to MS considering a histological analysis of lesions shows that astrocytes express jagged1 and OPCs express Notch1 (John et al., 2002). This is important as it is thought that a differentiation and maturation failure of OPCs is a significant contributor to

remyelination failure in MS lesions (Kuhlmann et al., 2008; Duncan et al., 2017).

Astrocytes as Regulators of the Extracellular Matrix (ECM)

Astrocytes are also major modulators of the extracellular matrix (ECM). The ECM is composed of several molecules which can influence OPC function (Pu et al., 2018). Astrocytes are major producers of the ECM molecules high molecular weight hyaluronan (Back et al., 2005), Tenascin-C (Gutowski et al., 1999), fibronectin (Stoffels et al., 2013), and various members of the chondroitin sulfate proteoglycan family (Jones et al., 2003; Siebert et al., 2014). In addition to providing chemical signals, the mechanical stiffness of the ECM significantly influences the proliferation and differentiation of OPCs *in vivo*. It was recently shown that aging rodents have a stiffer ECM, resulting in decreased OPC proliferation and differentiation (Segel et al., 2019). When the mechanosensitive ion channel PIEZO1 is inhibited, OPCs are able to restore their loss of function in proliferation and differentiation. In addition to inhibiting OPC maturation and axon regeneration, these molecules exert immunomodulatory effects on several members of the immune system (Stephenson et al., 2018). For example, when chondroitin sulfate proteoglycans are added to murine macrophages *in vitro*, these cells significantly upregulate their production of pro-inflammatory cytokines, matrix metalloproteinases, as well as displaying an increase in migration (Stephenson et al., 2018). In this study, these ECM molecules were observed around perivascular cuffs in the EAE model. Pharmacologically inhibiting the synthesis of these molecules in this model resulted in reduced immune cell infiltration and decreased clinical severity (Stephenson et al., 2019). Although not yet addressed, the production of such inhibitory molecules may be influenced by the phenotypic state adopted by astrocytes.

Astrocyte Role in Lipid Metabolism

Astrocytes play a central role in lipid metabolism. As the BBB limits the entry of several lipoproteins from the peripheral circulation, the CNS has developed a tightly regulated system in which to regulate the production of lipid species such as arachidonic acid, docosahexanoic acid, and cholesterol (Moore, 2001; Dietschy, 2009). Astrocytes are the major producers of cholesterol and the cholesterol carrier, apolipoprotein E (APOE) under homeostatic conditions (Boyles et al., 1985). Cholesterol is a major constituent of cell membranes and myelin and is therefore critical in normal CNS functioning (Linton et al., 1991). Rodent neurons do not readily synthesize cholesterol and depend on astrocytes for their source of cholesterol (Nieweg et al., 2009). As astrocyte-derived cholesterol is important for normal neuronal functioning, it is likely that transport of cholesterol to oligodendrocytes from astrocytes or other glial cells such as microglia is important in myelin synthesis. Indeed, it was recently shown that demyelinated white matter lesions from aging mice have deficient reverse cholesterol transport that was associated with reduced remyelination (Cantuti-Castelvetri et al., 2018). Cantuti-Castelvetri et al. (2018) found that stimulating reverse cholesterol transport enhanced remyelination in the aging CNS, highlighting the role of lipid metabolism in myelin synthesis. Whether cholesterol exported by astrocytes and macrophages/microglia can be directly taken up by OPCs responding to a demyelinated lesion was not addressed in this study and is yet to be determined. This area is of direct importance as several small molecules capable of stimulating oligodendrogenesis act on the cholesterol biosynthesis pathways (Hubler et al., 2018). Importantly GFAP-expressing reactive astrocytes in EAE mice have decreased cholesterol synthesis, which may limit remyelination efficiency (Itoh et al., 2018), suggesting that autoimmunity may impair cholesterol synthesis.

Medications used to treat hypercholesterolemia (statins) seem to show some benefit in secondary progressive MS (Chataway et al., 2014). High-dose statin treatment resulted in a 43% reduction in brain atrophy compared to placebo. As statins have effects on the immune system, it is unclear whether the therapeutic efficacy of statins in secondary progressive MS are mediated through cholesterol modulation or other indirect mechanisms (Eshaghi et al., 2019). It is important to note that statins did not influence relapse risk, disease progression or disability scores in people with MS in combination with interferon therapy (Bhardwaj et al., 2012).

Astrocytes Regulate CNS Schwann Cell Myelin and Secrete Growth Factors

Astrocytes are thought to regulate the degree to which remyelination is favored by OPC-derived oligodendrocytes or SCs (Zawadzka et al., 2010; Monteiro de Castro et al., 2015). In the absence of astrocytes, more SC remyelination is observed. The mechanism by which astrocytes regulate the fate choice of OPCs is unclear but may be due to interactions in BMP/Wnt signaling within the lesion microenvironment (Ulanska-Poutanen et al., 2018). Although SCs remyelination appears to re-establish conduction capacity within CNS axons (Smith et al., 1979; Blight and Young, 1989), it is not yet clear whether SCs differ from oligodendrocytes in the provision of metabolic support to axons. Similarly, it is unclear how different myelin sheath thicknesses between oligodendrocytes and SCs affect the timing of axonal conduction.

Astrocyte secretion of neurotrophins, a class of proteins that induce the growth and survival of neuronal cells, are involved in remyelination. For example, astrocytes can regulate myelin protein synthesis by the release of brain-derived neurotrophic factor (BDNF; Fulmer et al., 2014). In the cuprizone model of demyelination, the activation of OPC-expressed BDNF receptor TrkB promotes remyelination as reflected by an increase in OPC differentiation, the number of remyelinated axons and myelin sheath thickness (Fletcher et al., 2018). Furthermore, astrocytes secrete the mitogen platelet-derived growth factor-A (PDGF-A) to act on OPCs, which can promote proliferation (Wolswijk and Noble, 1992; Redwine and Armstrong, 1998; Frost et al., 2003). Lesions from MS also display PDGFRα expression on proliferating cells (Maeda et al., 2001). Astrocytes are also thought to produce leukemia inhibitory factor, ciliary neurotrophic factor, and insulin-like growth factor-1, all of which have been implicated in supporting OPC maturation (Moore et al., 2011).

Taken together, the role of astrocytes during remyelination is complex and incompletely understood (**Figure 2**). Release of growth factors and lipid metabolism is required for remyelination, yet astrocytes also produce several inhibitory ECM molecules that impair remyelination. The expression of notch ligands by astrocytes also serves as a break for remyelination. How astrocytes are regulated through the continuum of remyelination is yet to be defined, but may provide an explanation for their diverse roles during remyelination.

NON-MYELINATING ROLES OF OLIGODENDROCYTE LINEAGE CELLS DURING REMYELINATION

The non-myelinating roles of oligodendrocyte lineage cells are being increasingly realized and may provide new avenues for therapeutic intervention. During development and into adulthood, OPC differentiation is restricted to forming mature oligodendrocytes (Kang et al., 2010; Young et al., 2013; Huang et al., 2019) but during traumatic injury or demyelination OPCs act as multipotent progenitor cells (Richardson et al., 2011; Crawford et al., 2014) capable of differentiating into other neural lineage cells such as astrocytes and SCs (Zawadzka et al., 2010; Assinck et al., 2017b; Hackett et al., 2018; Huang et al., 2018). Beyond differentiating into other lineages, OPCs respond to disruptions in tissue homeostasis in a manner reminiscent of microglia. For example, OPCs proliferate and extend their processes to surround local injury sites (Hughes et al., 2013), albeit the kinetics of this process extension are slower than microglia (Davalos et al., 2005; Nimmerjahn et al., 2005). OPCs also migrate to areas of injury and proliferate to compensate for the loss of adjacent OPCs, again reminiscent of microglia. The high proliferative capacity and robust response to tissue injury suggest OPCs themselves may be major regulators of repair. Indeed a number of studies now indicate that the response of OPCs is critical for modulating inflammation, altering glial scarring and potentially regulating angiogenesis. The subsequent sections will review the evidence that OPCs are subverted to directly perform additional functions in CNS repair with an emphasis on how modulating these functions may offer new therapeutic strategies.

Inflammatory Nature of Oligodendrocyte Progenitor Cells

The rapid proliferation and migration to areas of tissue damage leave OPCs ideally situated to regulate subsequent immune responses. OPCs express many microglia-enriched genes but often at lower levels. For example, the homeostatic microglia marker CX3CR1 is expressed by OPCs (Voronova et al., 2017). Accordingly, OPCs express a number of critical modulators of the inflammatory response including IL-33 and the low-affinity Fc receptor (Fcgr2b) during EAE (Falcão et al., 2018), the latter of which is normally only expressed by microglia (Zhang et al., 2014). Transcriptomic analyses of OPCs reveal an increase in expression of the inflammasome-associated cytokines IL-1β and the chemokine CCL2 during demyelination (Moyon et al., 2015). It should be noted, however, that OPCs were isolated by Moyon et al. (2015) based on PDGFRα expression, which is also enriched in a population of pericytes (Assinck et al., 2017b), so these results should be interpreted with caution. However, recent single-cell RNA sequencing of OPCs during EAE (Falcão et al., 2018) and in MS (Jakubzick et al., 2017) confirms that these cells express a number of proinflammatory genes typically restricted to microglia/macrophages (Butovsky et al., 2014; Zhang et al., 2014). For example in response to IFNγ, OPCs go on to express the antigen presentation molecules MHC-I/II (Falcão et al., 2018). OPCs use MHCI/II to activate T-cells both *in vivo* and *in vitro* (Falcão et al., 2018; Kirby et al., 2018), and the capacity to cross-present antigens to CD8 T-cells was confirmed *in vivo* (Kirby et al., 2018). Taken together, inflammatory demyelination triggers OPCs to express pro-inflammatory cytokines and subsequently present antigens to T-cells.

Given that OPCs can perpetuate an inflammatory response raises the possibility that they might directly induce damage in autoimmune disease. Indeed, the induction of pro-inflammatory genes in OPCs during autoimmune demyelination may be necessary for subsequent demyelination. Blocking the activation of NF-κB by deleting Act1 in NG2+ glia blocks the development of EAE-induced demyelination and diminishes inflammatory gene expression following the adoptive transfer of $MOG_{35–55}$ Th-17 cells (Kang et al., 2013). Thus, the co-option of OPCs into a pro-inflammatory phenotype during Th-17-mediated autoimmune disease likely drives subsequent tissue damage. Additionally, the co-opting of OPCs to perpetuate an inflammatory response may leave them unable to adequately differentiate into new remyelinating oligodendrocytes, a possibility that remains to be proven. Indeed, the adoptive transfer of autoimmune T-cells (Baxi et al., 2015) or engraftment of lymphocytes from people with MS into mice with LPC-induced lesions (El Behi et al., 2017) slows remyelination, which is consistent with OPC immune activities impairing their differentiation. Likewise, following cuprizone demyelination, the transfer of effector T cells or IFNγ impairs oligodendrocyte differentiation and is associated with the increased presentation of antigens by OPCs to CD8+ T cells (Kirby et al., 2018).

This co-option of OPCs into an inflammatory phenotype during autoimmune demyelination raises the intriguing possibility that the pro-inflammatory OPC phenotype likely drives tissue damage and may impair effective remyelination. Current FDA-approved therapeutics for MS target autoimmune damage in the CNS, and as such, they may have an unexpected benefit to diminish the co-option of OPCs, therefore, "freeing" them so that they can effectively remyelinate. In accordance, both the switch of microglia to a less inflammatory phenotype (Miron et al., 2013) and the transfer of regulatory T-cells promote remyelination following chemical demyelination (Dombrowski et al., 2017).

Oligodendrocyte Lineage Cells During Glial Scarring

When the extent of trauma or tissue injury necessitates glial scar formation, OPCs' role is to modify other cells that contribute to scar formation such as astrocytes or pericytes

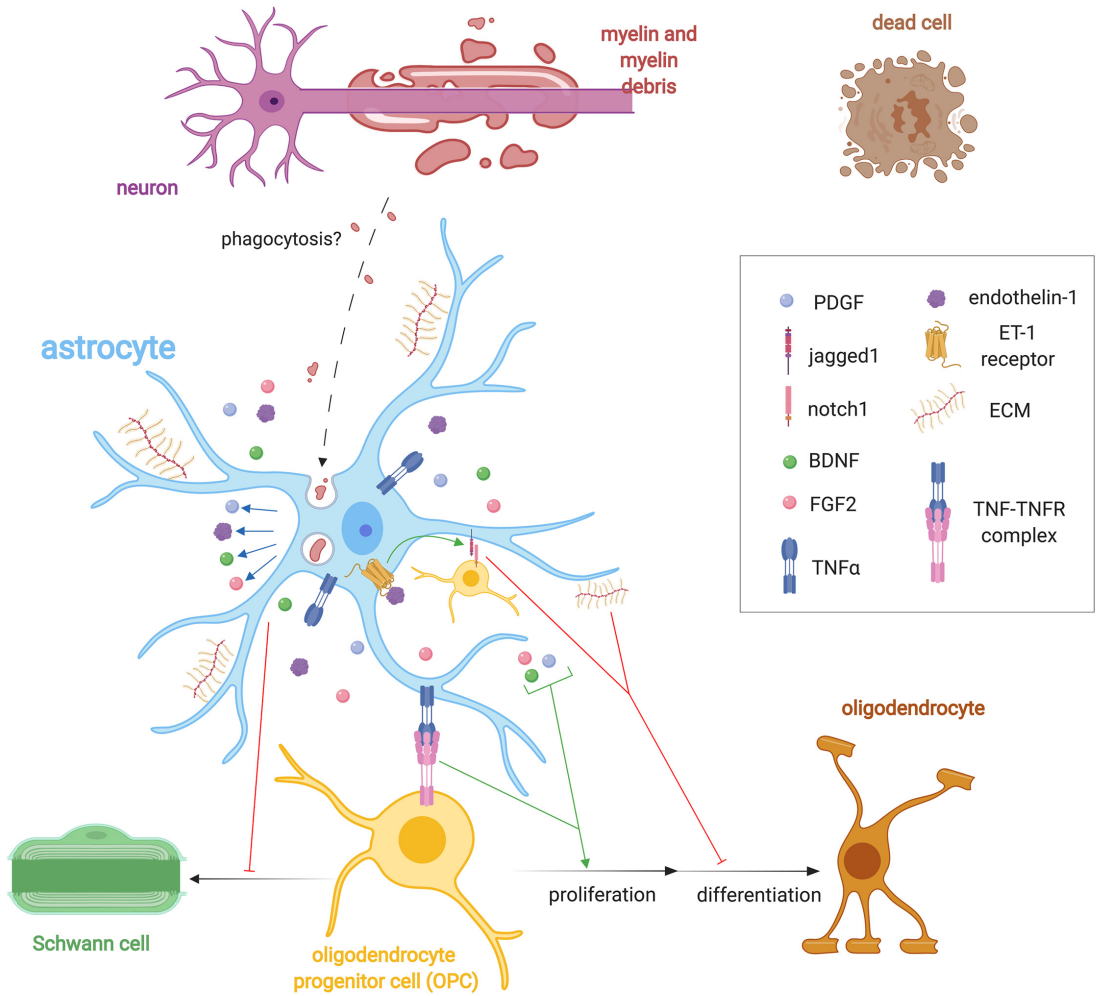

FIGURE 2 | Importance of astrocyte regulation of remyelination. Following demyelination, astrocytes help regulate OPC behavior *via* the expression of extracellular matrix (ECM) molecules such as CSPGs, hyluronan, fibronectin, and tenacin C, endothelin-1 and growth factor secretion such as FGF2, brain-derived neurotrophic factor (BDNF), and PDGF. Endothelin-1, through autocrine and paracrine signaling, stimulates the expression of the notch ligand jagged1 that antagonizes remyelination. Astrocytes control the fate choice of OPCs following demyelination by antagonizing their differentiation into Schwann cells (SCs). Astrocytes may phagocytose myelin debris, but this has only been validated *in vitro*. They also express TNF-α, which binds to TNFR2 to promote remyelination.

(Hackett et al., 2016; Huang et al., 2018) and in some cases directly such as astrocytes (Rodriguez et al., 2014; Hesp et al., 2018). With a milder injury, OPCs have a much-reduced capacity to differentiate into astrocytes (Zawadzka et al., 2010). If proliferating NG2+ cells—which are composed of OPCs, pericytes, SCs and activated microglia/macrophage following traumatic SCI (McTigue et al., 2006)—are depleted, glial scar formation is dramatically impaired (Hesp et al., 2018). The result of NG2+ cell depletion is prolonged hemorrhage, larger lesions, and more pronounced edema (Hesp et al., 2018). Taken together, the proliferation and activation of NG2+ glia, which prominently includes OPCs, is necessary for proper formation of the glial scar that restricts ongoing secondary damage to tissue following traumatic injury. Given that scar formation is associated with ECM molecules inhibitory to remyelination, this raises the intriguing possibility that OPCs indirectly regulate ECM molecules known to inhibit remyelination.

Oligodendrocyte Lineage Cells Interact With and Regulate the Vasculature

During development, OPCs migrate along blood vessels in order to successfully distribute throughout the parenchyma, a step that is necessary for their subsequent differentiation into myelinating oligodendrocytes (Tsai et al., 2016). The secretion of stromal cell-derived factor 1 (SDF1) by endothelial cells attracts OPCs by binding to CXCR4, which is abundantly expressed on OPCs when Wnt-tone is high (Tsai et al., 2016). However, signaling between OPCs and endothelial cells is bidirectional, and given OPCs' location along blood vessels in development (Tsai et al., 2016), they are ideally positioned to sense oxygen

levels and regulate angiogenesis. OPCs sense oxygen tension within the parenchyma *via* HIF1/2α (Yuen et al., 2014), a protein sensor that is stabilized under hypoxic conditions (Wang et al., 1995; Majmundar et al., 2010). Experimentally stabilizing HIF in OPCs—and therefore mimicking hypoxia for these cells—promotes angiogenesis in both the cortex and corpus callosum likely through the secretion of soluble factors (Yuen et al., 2014). A mechanism emerges in which endothelial cells are necessary for the initial migration of OPCs throughout the parenchyma, which in turn, drive angiogenesis until oxygen tension is sufficient to support proper oligodendrocyte differentiation and myelination (Yuen et al., 2014; Tsai et al., 2016). Paracrine signaling between OPCs and endothelial cells is therefore critical for proper developmental myelination.

Interestingly, recent studies suggest the angiogenic activities of OPCs can be subverted under pathological conditions. In development, heightened OPC clustering along blood vessels disrupts BBB function resulting in lymphocyte trafficking in the CNS parenchyma. Like development (Tsai et al., 2016), OPCs migrate along blood vessels during remyelination (Niu et al., 2019). In active MS lesions, OPCs become trapped and cluster along blood vessels. It is unclear if this heightened clustering is due to local hypoxia within MS lesions or inflammation. Cytokines like IL-1β stimulates OPCs to secrete factors that promote angiogenesis *in vitro*, suggesting inflammation may also regulate OPC-dependent angiogenesis. Excessive Wnt signaling in OPCs not only induced clustering of OPCs but also increased the expression of Wif1, which suppresses tight junction formation in endothelial cells (Niu et al., 2019). Indeed hypoperfusion are present in both the NAWM and NAGM in MS potentially inducing a hypoxic environment (Law et al., 2004; Varga et al., 2009). Inflammation may also subvert OPCs to associate with blood vessels and block their ability to fully differentiate in MS. Given that excessive interactions between OPCs and blood vessels during development are sufficient to trigger pathological immunity, it will be interesting to examine if this interaction promotes pathology in models of inflammatory demyelination like EAE.

Taken together, OPCs are increasingly being recognized for their roles other than differentiating into oligodendrocytes during remyelination (**Figure 3**). OPCs morphologically respond to injury in a way comparable to microglia, they secrete cytokines, and they regulate scar formation. In these capacities OPCs are an alternative CNS-innate immune cell. OPCs are also responsive to oxygen levels and are important regulators of angiogenesis.

REMYELINATION DECLINES WITH AGE

Remyelination, as with any regenerative process, declines in efficiency with age (Shields et al., 1999; Sim et al., 2002; Ruckh et al., 2012). OPC proliferation and differentiation, which are necessary processes for remyelination, are reduced with age (Sim et al., 2002). In fact, dorsally-derived OPCs in the spinal cord are the predominant source of remyelination in young mice, but contribute less in aged animals (Crawford et al., 2016b). Age can intrinsically alter OPCs directly as old OPCs display a different global DNA methylation profile that alters and/or diminishes their response to pro-remyelinating factors (Zhou et al., 2019). Aging also decreases the recruitment of histone deacetylases (HDACs) in OPCs—epigenetic regulators of gene expression—that leads to a decrease in remyelination efficiency. In OPCs, HDACs downregulate the expression of many transcription factors that inhibit OPC differentiation, including Hes5 and Sox2. They, therefore, regulate remyelination by controlling OPC differentiation (Liu et al., 2006; Shen et al., 2008).

Age-impaired remyelination is also due to impaired innate immune cell function. The removal of inhibitory myelin debris by microglia/macrophages is impaired by aging (Natrajan et al., 2015; Safaiyan et al., 2016; Cantuti-Castelvetri et al., 2018; Rawji et al., 2018). In LPC-induced lesions, aging microglia/macrophages display a decrease in microenvironment surveillance activity and a decrease in phagocytic activity (Rawji et al., 2018). Furthermore, aging microglia/macrophage lysosomal degradation of myelin is diminished as reflected by the accumulation of myelin proteins in microglial lysosomes of aging mice (Safaiyan et al., 2016). This accumulation of myelin debris inside of microglia could be due to a deficiency in reverse cholesterol transport as remyelination efficiency increased when mice with LPC-induced focal demyelination were treated with HβCD, a drug that stimulates cholesterol efflux from cells (Cantuti-Castelvetri et al., 2018). These findings raise the possibility that targeting the phagocytic pathway of microglia/macrophages could improve the efficiency of the myelin debris clearance.

Why myelin debris clearance declines are likely multifaceted? Recently, a CRISPR-Cas9 knockout screen identified CD22 as a negative regulator of microglia phagocytosis that increases with age (Pluvinage et al., 2019). Many factors, such as Retinoid-X-Receptor-α (RXR-α), fractalkine receptor CX3CR1 and Galectin-3 (Gal-3) can also influence the ability of microglia to phagocytose (Lampron et al., 2015; Natrajan et al., 2015; Reichert and Rotshenker, 2019). RXR-α is a ligand-activated transcription factor that controls a variety of genetic programs, including immune cell-related functions (Dawson and Xia, 2012). Natrajan et al. (2015) demonstrate that RXR-α knockout from young macrophages in mice LPC-induced lesion delays myelin debris clearance and remyelination, and also that stimulating RXR-α in monocytes from MS patients *in vitro* improves this normally inefficient myelin debris phagocytosis. There is now an ongoing clinical trial using an RXR-α agonist (EudraCT number: 2014-003145-99). Similarly, the chemokine receptor CX3CR1—enriched in microglia—is critical for myelin debris clearance following cuprizone-induced demyelination (Lampron et al., 2015). Ruckh et al. (2012) found that in the LPC-induced demyelination model, the systemic circulatory system of young mice can restore the efficiency of OPC proliferation, differentiation, and remyelination in aged mice to levels near those observed in young mice. They were able to show these differences by joining the circulatory systems of young and old mice in pairs through heterochronic parabiosis. This rejuvenation of remyelination suggests that reversing the peripheral immune system can partially restore

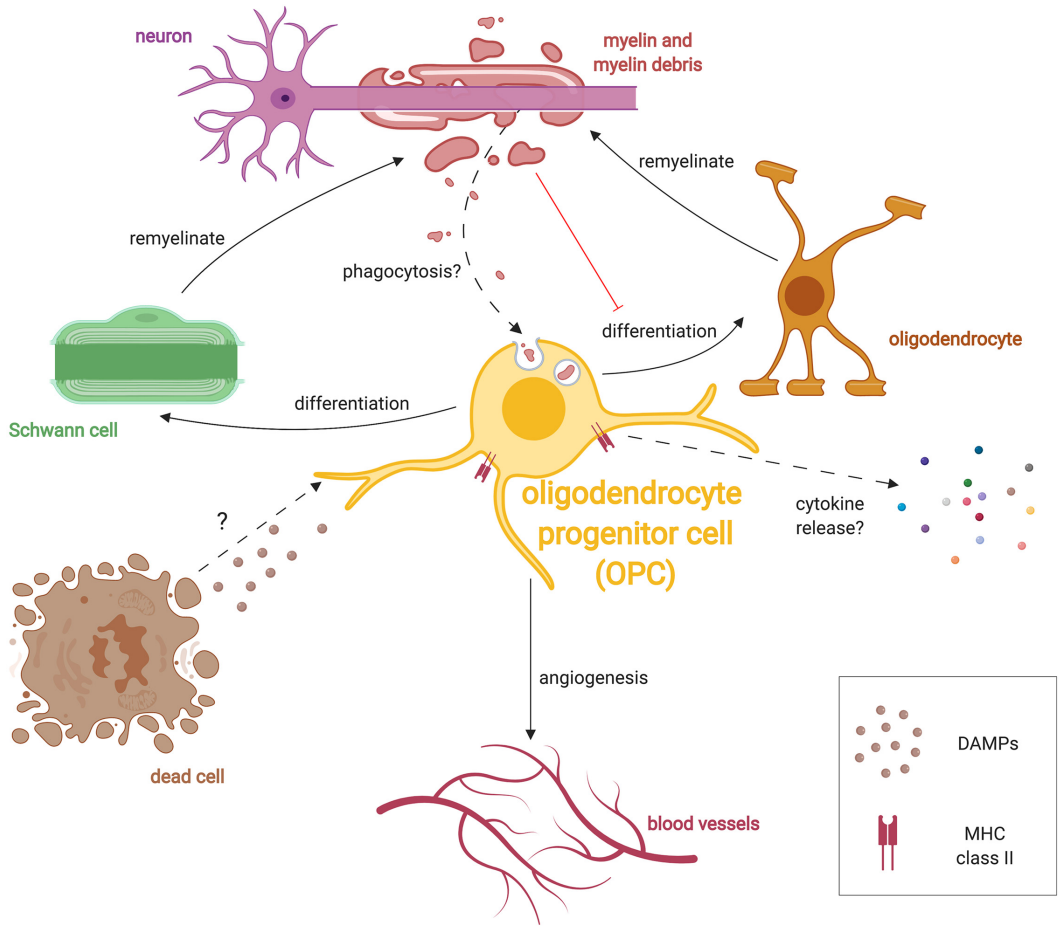

FIGURE 3 | Multiple roles of OPCs during remyelination. After damage, OPCs respond to injury by extending processes, migrating and proliferating following injury presumably in response to unknown DAMPs. OPCs can differentiate into either oligodendrocytes or SCs following demyelination. OPCs also respond to hypoxic conditions and promote angiogenesis. Similar to microglia, OPCs have been shown to phagocytose debris in culture, and may also do so *in vivo*. Given that myelin debris inhibits OPC lineage progression, phagocytosis of debris may subvert OPCs until debris clearance is completed. OPCs in the diseased state are also known to express the antigen-presenting protein, MHC-II, and presumably release specific cytokines which alter the immune response.

age-dependent decline in remyelination potential. In fact, several human trials such as the Stanford Parkinson's Disease Plasma Study (NCT02968433) infuse plasma from young people to diseased patients. However, a proper evaluation of the blood-borne rejuvenating factors is needed before any similar trial can be conducted for demyelinating diseases such as MS.

Peripheral changes during aging can also impart effects onto innate immune cells such as microglia. For example, peripheral blood from aged mice is sufficient to lower the levels of type II interferon in the choroid plexus, which is linked to cognitive decline, a common symptom observed in MS patients (Franklin et al., 1989; Baruch et al., 2014). Microglia also have interferon phenotypic changes during aging, in this case, driven in part by higher levels of IFN-I cytokines (Deczkowska et al., 2017) that likely come from peripheral sources. Furthermore, retro-orbital injection of plasma from aging mice to young mice is sufficient to activate microglia (Yousef et al., 2019). Peripheral immune changes are therefore important in regulating the innate immune system in the CNS.

CONCLUSION

Remyelination involves a complex interplay between the oligodendrocyte lineage cells that produce the myelin, the astrocytes and the other innate immune cells that regulate the microenvironment of remyelination. Microglia and CNS-infiltrating macrophages regulate the lesion environment and make it suitable for remyelination by activities such as the removal of inhibitory myelin debris. Astrocytes secrete growth factors and provide key lipids species, but also produce inhibitory ECM molecules and the Notch ligand Jagged. OPCs are the key source of remyelinating oligodendrocytes but are now recognized to also regulate angiogenesis, respond to injury and secrete cytokines suggesting they may also be a brain resident immune cell. Given that boosting remyelination

spares venerable axons (Mei et al., 2016), more work is required to examine how these cells interact with one another during remyelination.

AUTHOR CONTRIBUTIONS

CB, KR, GD and JP drafted and reviewed this manuscript. MH and CB constructed the figures. JP supervised the drafting of this manuscript.

FUNDING

KR is supported by the MS Society of Canada. GD is supported by a National Multiple Sclerosis Society fellowship. This work was funded by the University of Alberta, the University Hospital Foundation Medical Research Competition, the Azrieli Foundation and Brain Canada, through the Canada Brain Research fund, with support of Health Canada and the Funding Partner(s).

REFERENCES

Ajami, B., Bennett, J. L., Krieger, C., McNagny, K. M., and Rossi, F. M. (2011). Infiltrating monocytes trigger EAE progression, but do not contribute to the resident microglia pool. *Nat. Neurosci.* 14, 1142–1149. doi: 10.1038/nn.2887

Antony, J. M., Paquin, A., Nutt, S. L., Kaplan, D. R., and Miller, F. D. (2011). Endogenous microglia regulate development of embryonic cortical precursor cells. *J. Neurosci. Res.* 89, 286–298. doi: 10.1002/jnr.22533

Armstrong, R. C., Mierzwa, A. J., Sullivan, G. M., and Sanchez, M. A. (2016). Myelin and oligodendrocyte lineage cells in white matter pathology and plasticity after traumatic brain injury. *Neuropharmacology* 110, 654–659. doi: 10.1016/j.neuropharm.2015.04.029

Arnett, H. A., Mason, J., Marino, M., Suzuki, K., Matsushima, G. K., and Ting, J. P. (2001). TNF-α promotes proliferation of oligodendrocyte progenitors and remyelination. *Nat. Neurosci.* 4, 1116–1122. doi: 10.1038/nn738

Assinck, P., Duncan, G. J., Hilton, B. J., Plemel, J. R., and Tetzlaff, W. (2017a). Cell transplantation therapy for spinal cord injury. *Nat. Neurosci.* 20, 637–647. doi: 10.1038/nn.4541

Assinck, P., Duncan, G. J., Plemel, J. R., Lee, M. J., Stratton, J. A., Manesh, S. B., et al. (2017b). Myelinogenic plasticity of oligodendrocyte precursor cells following spinal cord contusion injury. *J. Neurosci.* 37, 8635–8654. doi: 10.1523/jneurosci.2409-16.2017

Back, S. A., Tuohy, T. M., Chen, H., Wallingford, N., Craig, A., Struve, J., et al. (2005). Hyaluronan accumulates in demyelinated lesions and inhibits oligodendrocyte progenitor maturation. *Nat. Med.* 11, 966–972. doi: 10.1038/nm1279

Baker, D., Butler, D., Scallon, B. J., O'Neill, J. K., Turk, J. L., and Feldmann, M. (1994). Control of established experimental allergic encephalomyelitis by inhibition of tumor necrosis factor (TNF) activity within the central nervous system using monoclonal antibodies and TNF receptor-immunoglobulin fusion proteins. *Eur. J. Immunol.* 24, 2040–2048. doi: 10.1002/eji.1830240916

Bartzokis, G., Lu, P. H., Heydari, P., Couvrette, A., Lee, G. J., Kalashyan, G., et al. (2012). Multimodal magnetic resonance imaging assessment of white matter aging trajectories over the lifespan of healthy individuals. *Biol. Psychiatry* 72, 1026–1034. doi: 10.1016/j.biopsych.2012.07.010

Baruch, K., Deczkowska, A., David, E., Castellano, J. M., Miller, O., Kertser, A., et al. (2014). Aging-induced type I interferon response at the choroid plexus negatively affects brain function. *Science* 346, 89–93. doi: 10.1126/science.1252945

Baxi, E. G., DeBruin, J., Tosi, D. M., Grishkan, I. V., Smith, M. D., Kirby, L. A., et al. (2015). Transfer of myelin-reactive th17 cells impairs endogenous remyelination in the central nervous system of cuprizone-fed mice. *J. Neurosci.* 35, 8626–8639. doi: 10.1523/jneurosci.3817-14.2015

Bejanin, A., Desgranges, B., Joie La, R., Landeau, B., Perrotin, A., Mezenge, F., et al. (2017). Distinct white matter injury associated with medial temporal lobe atrophy in Alzheimer's versus semantic dementia. *Hum. Brain Mapp.* 38, 1791–1800. doi: 10.1002/hbm.23482

Bernier, L. P., Bohlen, C. J., York, E. M., Choi, H. B., Kamyabi, A., Dissing-Olesen, L., et al. (2019). Nanoscale surveillance of the brain by microglia *via* cAMP-regulated filopodia. *Cell Rep.* 27, 2895.e4–2908.e4. doi: 10.1016/j.celrep.2019.05.010

Bhardwaj, S., Coleman, C. I., and Sobieraj, D. M. (2012). Efficacy of statins in combination with interferon therapy in multiple sclerosis: a meta-analysis. *Am. J. Health Syst. Pharm.* 69, 1494–1499. doi: 10.2146/ajhp110675

Black, J. A., Newcombe, J., Trapp, B. D., and Waxman, S. G. (2007). Sodium channel expression within chronic multiple sclerosis plaques. *J. Neuropathol. Exp. Neurol.* 66, 828–837. doi: 10.1097/nen.0b013e3181462841

Blakemore, W. F. (1974). Pattern of remyelination in the CNS. *Nature* 249, 577–578. doi: 10.1038/249577a0

Blight, A. R., and Young, W. (1989). Central axons in injured cat spinal cord recover electrophysiological function following remyelination by Schwann cells. *J. Neurol. Sci.* 91, 15–34. doi: 10.1016/0022-510x(89)90073-7

Bodini, B., Veronese, M., García-Lorenzo, D., Battaglini, M., Poirion, E., Chardain, A., et al. (2016). Dynamic imaging of individual remyelination profiles in multiple sclerosis. *Ann. Neurol.* 79, 726–738. doi: 10.1002/ana.24620

Bostock, H., Sears, T. A., and Sherratt, R. M. (1981). The effects of 4-aminopyridine and tetraethylammonium ions on normal and demyelinated mammalian nerve fibres. *J. Physiol.* 313, 301–315. doi: 10.1113/jphysiol.1981.sp013666

Bostock, H., Sherratt, R. M., and Sears, T. A. (1978). Overcoming conduction failure in demyelinated nerve fibres by prolonging action potentials. *Nature* 274, 385–387. doi: 10.1038/274385a0

Boutajangout, A., and Wisniewski, T. (2013). The innate immune system in Alzheimer's disease. *Int. J. Cell Biol.* 2013:576383. doi: 10.1155/2013/576383

Boyles, J. K., Pitas, R. E., Wilson, E., Mahley, R. W., and Taylor, J. M. (1985). Apolipoprotein E associated with astrocytic glia of the central nervous system and with nonmyelinating glia of the peripheral nervous system. *J. Clin. Invest.* 76, 1501–1513. doi: 10.1172/jci112130

Bramow, S., Frischer, J. M., Lassmann, H., Koch-Henriksen, N., Lucchinetti, C. F., Sørensen, P. S., et al. (2010). Demyelination versus remyelination in progressive multiple sclerosis. *Brain* 133, 2983–2998. doi: 10.1093/brain/awq250

Brown, R. A., Narayanan, S., Banwell, B., Arnold, D. L., and Canadian Pediatric Demyelinating Disease Network. (2014). Magnetization transfer ratio recovery in new lesions decreases during adolescence in pediatric-onset multiple sclerosis patients. *Neuroimage Clin.* 6, 237–242. doi: 10.1016/j.nicl.2014.09.003

Bujalka, H., Koenning, M., Jackson, S., Perreau, V. M., Pope, B., Hay, C. M., et al. (2013). MYRF is a membrane-associated transcription factor that autoproteolytically cleaves to directly activate myelin genes. *PLoS Biol.* 11:e1001625. doi: 10.1371/journal.pbio.1001625

Butovsky, O., Jedrychowski, M. P., Moore, C. S., Cialic, R., Lanser, A. J., Gabriely, G., et al. (2014). Identification of a unique TGF-β-dependent molecular and functional signature in microglia. *Nat. Neurosci.* 17, 131–143. doi: 10.1038/nn.3599

Cantuti-Castelvetri, L., Fitzner, D., Bosch-Queralt, M., Weil, M. T., Su, M., Sen, P., et al. (2018). Defective cholesterol clearance limits remyelination in the aged central nervous system. *Science* 359, 684–688. doi: 10.1126/science.aan4183

Caravagna, C., Jaouën, A., Desplat-Jégo, S., Fenrich, K. K., Bergot, E., Luche, H., et al. (2018). Diversity of innate immune cell subsets across spatial and temporal scales in an EAE mouse model. *Sci. Rep.* 8:5146. doi: 10.1038/s41598-018-22872-y

Carmeli, C., Donati, A., Antille, V., Viceic, D., Ghika, J., Gunten von, A., et al. (2013). Demyelination in mild cognitive impairment suggests progression path to Alzheimer's disease. *PLoS One* 8:e72759. doi: 10.1371/journal.pone.0072759

Chataway, J., Schuerer, N., Alsanousi, A., Chan, D., MacManus, D., Hunter, K., et al. (2014). Effect of high-dose simvastatin on brain atrophy and disability in secondary progressive multiple sclerosis (MS-STAT): a randomised, placebo-controlled, phase 2 trial. *Lancet* 383, 2213–2221. doi: 10.1016/S0140-6736(13)62242-4

Courties, G., Moskowitz, M. A., and Nahrendorf, M. (2014). The innate immune system after ischemic injury: lessons to be learned from the heart and brain. *JAMA Neurol.* 71, 233–236. doi: 10.1001/jamaneurol.2013.5026

Crawford, A. H., Stockley, J. H., Tripathi, R. B., Richardson, W. D., and Franklin, R. J. (2014). Oligodendrocyte progenitors: adult stem cells of the central nervous system? *Exp. Neurol.* 260, 50–55. doi: 10.1016/j.expneurol.2014.04.027

Crawford, A. H., Tripathi, R. B., Foerster, S., McKenzie, I., Kougioumtzidou, E., Grist, M., et al. (2016a). Pre-existing mature oligodendrocytes do not contribute to remyelination following toxin-induced spinal cord demyelination. *Am. J. Pathol.* 186, 511–516. doi: 10.1016/j.ajpath.2015.11.005

Crawford, A. H., Tripathi, R. B., Richardson, W. D., and Franklin, R. J. M. (2016b). Developmental origin of oligodendrocyte lineage cells determines response to demyelination and susceptibility to age-associated functional decline. *Cell Rep.* 15, 761–773. doi: 10.1016/j.celrep.2016.03.069

Crowe, M. J., Bresnahan, J. C., Shuman, S. L., Masters, J. N., and Beattie, M. S. (1997). Apoptosis and delayed degeneration after spinal cord injury in rats and monkeys. *Nat. Med.* 3, 73–76. doi: 10.1038/nm0197-73

Dai, X., Lercher, L. D., Clinton, P. M., Du, Y., Livingston, D. L., Vieira, C., et al. (2003). The trophic role of oligodendrocytes in the basal forebrain. *J. Neurosci.* 23, 5846–5853. doi: 10.1523/jneurosci.23-13-05846.2003

Davalos, D., Grutzendler, J., Yang, G., Kim, J. V., Zuo, Y., Jung, S., et al. (2005). ATP mediates rapid microglial response to local brain injury *in vivo*. *Nat. Neurosci.* 8, 752–758. doi: 10.1038/nn1472

Davies, C. L., and Miron, V. E. (2018). Distinct origins, gene expression and function of microglia and monocyte-derived macrophages in CNS myelin injury and regeneration. *Clin. Immunol.* 189, 57–62. doi: 10.1016/j.clim.2016.06.016

Dawson, M. I., and Xia, Z. (2012). The retinoid X receptors and their ligands. *Biochim. Biophys. Acta* 1821, 21–56. doi: 10.1016/j.bbalip.2011.09.014

Deczkowska, A., Keren-Shaul, H., Weiner, A., Colonna, M., Schwartz, M., and Amit, I. (2018). Disease-associated microglia: a universal immune sensor of neurodegeneration. *Cell* 173, 1073–1081. doi: 10.1016/j.cell.2018.05.003

Deczkowska, A., Matcovitch-Natan, O., Tsitsou-Kampeli, A., Ben-Hamo, S., Dvir-Szternfeld, R., Spinrad, A., et al. (2017). Mef2C restrains microglial inflammatory response and is lost in brain ageing in an IFN-I-dependent manner. *Nat. Commun.* 8:717. doi: 10.1038/s41467-017-00769-0

Dehghan, S., Javan, M., Pourabdolhossein, F., Mirnajafi-Zadeh, J., and Baharvand, H. (2012). Basic fibroblast growth factor potentiates myelin repair following induction of experimental demyelination in adult mouse optic chiasm and nerves. *J. Mol. Neurosci.* 48, 77–85. doi: 10.1007/s12031-012-9777-6

Dietschy, J. M. (2009). Central nervous system: cholesterol turnover, brain development and neurodegeneration. *Biol. Chem.* 390, 287–293. doi: 10.1515/bc.2009.035

Dillenburg, A., Ireland, G., Holloway, R. K., Davies, C. L., Evans, F. L., Swire, M., et al. (2018). Activin receptors regulate the oligodendrocyte lineage in health and disease. *Acta Neuropathol.* 135, 887–906. doi: 10.1007/s00401-018-1813-3

Dimitriadou, V., Pang, X., and Theoharides, T. C. (2000). Hydroxyzine inhibits experimental allergic encephalomyelitis (EAE) and associated brain mast cell activation. *Int. J. Immunopharmacol.* 22, 673–684. doi: 10.1016/s0192-0561(00)00029-1

Dimou, L., Simon, C., Kirchhoff, F., Takebayashi, H., and Gotz, M. (2008). Progeny of Olig2-expressing progenitors in the gray and white matter of the adult mouse cerebral cortex. *J. Neurosci.* 28, 10434–10442. doi: 10.1523/jneurosci.2831-08.2008

Diserbo, M., Agin, A., Lamproglou, I., Mauris, J., Staali, F., Multon, E., et al. (2002). Blood-brain barrier permeability after γ whole-body irradiation: an *in vivo* microdialysis study. *Can. J. Physiol. Pharmacol.* 80, 670–678. doi: 10.1139/y02-070

Dombrowski, Y., O'Hagan, T., Dittmer, M., Penalva, R., Mayoral, S. R., Bankhead, P., et al. (2017). Regulatory T cells promote myelin regeneration in the central nervous system. *Nat. Neurosci.* 20, 674–680. doi: 10.1038/nn.4528

Döring, A., Sloka, S., Lau, L., Mishra, M., Minnen van, J., Zhang, X., et al. (2015). Stimulation of monocytes, macrophages and microglia by amphotericin B and macrophage colony-stimulating factor promotes remyelination. *J. Neurosci.* 35, 1136–1148. doi: 10.1523/jneurosci.1797-14.2015

Duncan, G. J., Manesh, S. B., Hilton, B. J., Assinck, P., Liu, J., Moulson, A., et al. (2018). Locomotor recovery following contusive spinal cord injury does not require oligodendrocyte remyelination. *Nat. Commun.* 9:3066. doi: 10.1038/s41467-018-05473-1

Duncan, I. D., Brower, A., Kondo, Y., Curlee, J. F., and Schultz, R. D. (2009). Extensive remyelination of the CNS leads to functional recovery. *Proc. Natl. Acad. Sci. U S A* 106, 6832–6836. doi: 10.1073/pnas.0812500106

Duncan, I. D., Marik, R. L., Broman, A. T., and Heidari, M. (2017). Thin myelin sheaths as the hallmark of remyelination persist over time and preserve axon function. *Proc. Natl. Acad. Sci. U S A* 114, E9685–E9691. doi: 10.1073/pnas.1714183114

Duncan, G. J., Plemel, J. R., Assinck, P., Manesh, S. B., Muir, F. G. W., Hirata, R., et al. (2017). Myelin regulatory factor drives remyelination in multiple sclerosis. *Acta Neuropathol.* 134, 403–422. doi: 10.1007/s00401-017-1741-7

Duncan, I. D., Radcliff, A. B., Heidari, M., Kidd, G., August, B. K., and Wierenga, L. A. (2018). The adult oligodendrocyte can participate in remyelination. *Proc. Natl. Acad. Sci. U S A* 115, E11807–E11816. doi: 10.1073/pnas.1808064115

El Behi, M., Sanson, C., Bachelin, C., Guillot-Noel, L., Fransson, J., Stankoff, B., et al. (2017). Adaptive human immunity drives remyelination in a mouse model of demyelination. *Brain* 140, 967–980. doi: 10.1093/brain/awx008

Elmore, M. R., Najafi, A. R., Koike, M. A., Dagher, N. N., Spangenberg, E. E., Rice, R. A., et al. (2014). Colony-stimulating factor 1 receptor signaling is necessary for microglia viability, unmasking a microglia progenitor cell in the adult brain. *Neuron* 82, 380–397. doi: 10.1016/j.neuron.2014.02.040

Emery, B., Agalliu, D., Cahoy, J. D., Watkins, T. A., Dugas, J. C., Mulinyawe, S. B., et al. (2009). Myelin gene regulatory factor is a critical transcriptional regulator required for CNS myelination. *Cell* 138, 172–185. doi: 10.1016/j.cell.2009.04.031

England, J. D., Gamboni, F., and Levinson, S. R. (1991). Increased numbers of sodium channels form along demyelinated axons. *Brain Res.* 548, 334–337. doi: 10.1016/0006-8993(91)91144-p

Eshaghi, A., Kievit, R. A., Prados, F., Sudre, C. H., Nicholas, J., Cardoso, M. J., et al. (2019). Applying causal models to explore the mechanism of action of simvastatin in progressive multiple sclerosis. *Proc. Natl. Acad. Sci. U S A* 116, 11020–11027. doi: 10.1073/pnas.1818978116

Falcão, A. M., Bruggen van, D., Marques, S., Meijer, M., Jakel, S., Agirre, E., et al. (2018). Disease-specific oligodendrocyte lineage cells arise in multiple sclerosis. *Nat. Med.* 24, 1837–1844. doi: 10.1038/s41591-018-0236-y

Fancy, S. P., Zhao, C., and Franklin, R. J. (2004). Increased expression of Nkx2.2 and Olig2 identifies reactive oligodendrocyte progenitor cells responding to demyelination in the adult CNS. *Mol. Cell. Neurosci.* 27, 247–254. doi: 10.1016/j.mcn.2004.06.015

Felts, P. A., Baker, T. A., and Smith, K. J. (1997). Conduction in segmentally demyelinated mammalian central axons. *J. Neurosci.* 17, 7267–7277. doi: 10.1523/jneurosci.17-19-07267.1997

Fife, B. T., Huffnagle, G. B., Kuziel, W. A., and Karpus, W. J. (2000). CC chemokine receptor 2 is critical for induction of experimental autoimmune encephalomyelitis. *J. Exp. Med.* 192, 899–905. doi: 10.1084/jem.192.6.899

Fletcher, J. L., Wood, R. J., Nguyen, J., Norman, E. M. L., Jun, C. M. K., Prawdiuk, A. R., et al. (2018). Targeting TrkB with a brain-derived neurotrophic factor mimetic promotes myelin repair in the brain. *J. Neurosci.* 38, 7088–7099. doi: 10.1523/jneurosci.0487-18.2018

Foster, R. E., Whalen, C. C., and Waxman, S. G. (1980). Reorganization of the axon membrane in demyelinated peripheral nerve fibers: morphological evidence. *Science* 210, 661–663. doi: 10.1126/science.6159685

Franklin, R. J. M., and Ffrench-Constant, C. (2017). Regenerating CNS myelin-from mechanisms to experimental medicines. *Nat. Rev. Neurosci.* 18, 753–769. doi: 10.1038/nrn.2017.136

Franklin, R. J., and Ffrench-Constant, C. (2008). Remyelination in the CNS: from biology to therapy. *Nat. Rev. Neurosci.* 9, 839–855. doi: 10.1038/nrn2480

Franklin, G. M., Nelson, L. M., Filley, C. M., and Heaton, R. K. (1989). Cognitive loss in multiple sclerosis. Case reports and review of the literature. *Arch. Neurol.* 46, 162–167. doi: 10.1001/archneur.1989.00520380066014

Frischer, J. M., Weigand, S. D., Guo, Y., Kale, N., Parisi, J. E., Pirko, I., et al. (2015). Clinical and pathological insights into the dynamic nature of the white matter multiple sclerosis plaque. *Ann. Neurol.* 78, 710–721. doi: 10.1002/ana.24497

Frost, E. E., Nielsen, J. A., Le, T. Q., and Armstrong, R. C. (2003). PDGF and FGF2 regulate oligodendrocyte progenitor responses to demyelination. *J. Neurobiol.* 54, 457–472. doi: 10.1002/neu.10158

Frühbeis, C., Fröhlich, D., Kuo, W. P., Amphornrat, J., Thilemann, S., Saab, A. S., et al. (2013). Neurotransmitter-triggered transfer of exosomes mediates oligodendrocyte-neuron communication. *PLoS Biol.* 11:e1001604. doi: 10.1371/journal.pbio.1001604

Fulmer, C. G., VonDran, M. W., Stillman, A. A., Huang, Y., Hempstead, B. L., and Dreyfus, C. F. (2014). Astrocyte-derived BDNF supports myelin protein synthesis after cuprizone-induced demyelination. *J. Neurosci.* 34, 8186–8196. doi: 10.1523/jneurosci.4267-13.2014

Fünfschilling, U., Supplie, L. M., Mahad, D., Boretius, S., Saab, A. S., Edgar, J., et al. (2012). Glycolytic oligodendrocytes maintain myelin and long-term axonal integrity. *Nature* 485, 517–521. doi: 10.1038/nature11007

Giera, S., Luo, R., Ying, Y., Ackerman, S. D., Jeong, S. J., Stoveken, H. M., et al. (2018). Microglial transglutaminase-2 drives myelination and myelin repair *via* GPR56/ADGRG1 in oligodendrocyte precursor cells. *Elife* 7:e33385. doi: 10.7554/elife.33385

Ginhoux, F., Greter, M., Leboeuf, M., Nandi, S., See, P., Gokhan, S., et al. (2010). Fate mapping analysis reveals that adult microglia derive from primitive macrophages. *Science* 330, 841–845. doi: 10.1126/science.1194637

Gladue, R. P., Carroll, L. A., Milici, A. J., Scampoli, D. N., Stukenbrok, H. A., Pettipher, E. R., et al. (1996). Inhibition of leukotriene B4-receptor interaction suppresses eosinophil infiltration and disease pathology in a murine model of experimental allergic encephalomyelitis. *J. Exp. Med.* 183, 1893–1898. doi: 10.1084/jem.183.4.1893

Goldmann, T., Wieghofer, P., Jordao, M. J., Prutek, F., Hagemeyer, N., Frenzel, K., et al. (2016). Origin, fate and dynamics of macrophages at central nervous system interfaces. *Nat. Immunol.* 17, 797–805. doi: 10.1038/ni.3423

Goldmann, T., Wieghofer, P., Muller, P. F., Wolf, Y., Varol, D., Yona, S., et al. (2013). A new type of microglia gene targeting shows TAK1 to be pivotal in CNS autoimmune inflammation. *Nat. Neurosci.* 16, 1618–1626. doi: 10.1038/nn.3531

Goldschmidt, T., Antel, J., Konig, F. B., Bruck, W., and Kuhlmann, T. (2009). Remyelination capacity of the MS brain decreases with disease chronicity. *Neurology* 72, 1914–1921. doi: 10.1212/WNL.0b013e3181a8260a

Gutowski, N. J., Newcombe, J., and Cuzner, M. L. (1999). Tenascin-R and C in multiple sclerosis lesions: relevance to extracellular matrix remodelling. *Neuropathol. Appl. Neurobiol.* 25, 207–214. doi: 10.1046/j.1365-2990.1999.00176.x

Hackett, A. R., Lee, D. H., Dawood, A., Rodriguez, M., Funk, L., Tsoulfas, P., et al. (2016). STAT3 and SOCS3 regulate NG2 cell proliferation and differentiation after contusive spinal cord injury. *Neurobiol. Dis.* 89, 10–22. doi: 10.1016/j.nbd.2016.01.017

Hackett, A. R., Yahn, S. L., Lyapichev, K., Dajnoki, A., Lee, D. H., Rodriguez, M., et al. (2018). Injury type-dependent differentiation of NG2 glia into heterogeneous astrocytes. *Exp. Neurol.* 308, 72–79. doi: 10.1016/j.expneurol.2018.07.001

Haider, L., Fischer, M. T., Frischer, J. M., Bauer, J., Hoftberger, R., Botond, G., et al. (2011). Oxidative damage in multiple sclerosis lesions. *Brain* 134, 1914–1924. doi: 10.1093/brain/awr128

Hamada, M. S., and Kole, M. H. (2015). Myelin loss and axonal ion channel adaptations associated with gray matter neuronal hyperexcitability. *J. Neurosci.* 35, 7272–7286. doi: 10.1523/jneurosci.4747-14.2015

Hammond, T. R., Dufort, C., Dissing-Olesen, L., Giera, S., Young, A., Wysoker, A., et al. (2019). Single-cell RNA sequencing of microglia throughout the mouse lifespan and in the injured brain reveals complex cell-state changes. *Immunity* 50, 253.e6–271.e6. doi: 10.1016/j.immuni.2018.11.004

Hammond, T. R., Gadea, A., Dupree, J., Kerninon, C., Nait-Oumesmar, B., Aguirre, A., et al. (2014). Astrocyte-derived endothelin-1 inhibits remyelination through notch activation. *Neuron* 81, 588–602. doi: 10.1016/j.neuron.2013.11.015

Hammond, T. R., McEllin, B., Morton, P. D., Raymond, M., Dupree, J., and Gallo, V. (2015). Endothelin-B receptor activation in astrocytes regulates the rate of oligodendrocyte regeneration during remyelination. *Cell Rep.* 13, 2090–2097. doi: 10.1016/j.celrep.2015.11.002

Han, X., Li, Q., Lan, X., El-Mufti, L., Ren, H., and Wang, J. (2019). Microglial depletion with clodronate liposomes increases proinflammatory cytokine levels, induces astrocyte activation and damages blood vessel integrity. *Mol. Neurobiol.* 56, 6184–6196. doi: 10.1007/s12035-019-1502-9

Harris, J. J., and Attwell, D. (2012). The energetics of CNS white matter. *J. Neurosci.* 32, 356–371. doi: 10.1523/jneurosci.3430-11.2012

Haynes, S. E., Hollopeter, G., Yang, G., Kurpius, D., Dailey, M. E., Gan, W. B., et al. (2006). The P2Y12 receptor regulates microglial activation by extracellular nucleotides. *Nat. Neurosci.* 9, 1512–1519. doi: 10.1038/nn1805

Heppner, F. L., Greter, M., Marino, D., Falsig, J., Raivich, G., Hovelmeyer, N., et al. (2005). Experimental autoimmune encephalomyelitis repressed by microglial paralysis. *Nat. Med.* 11, 146–152. doi: 10.1038/nm1177

Hesp, Z. C., Yoseph, R. Y., Suzuki, R., Jukkola, P., Wilson, C., Nishiyama, A., et al. (2018). Proliferating NG2-cell-dependent angiogenesis and scar formation alter axon growth and functional recovery after spinal cord injury in mice. *J. Neurosci.* 38, 1366–1382. doi: 10.1523/jneurosci.3953-16.2017

Hickman, S. E., Kingery, N. D., Ohsumi, T. K., Borowsky, M. L., Wang, L. C., Means, T. K., et al. (2013). The microglial sensome revealed by direct RNA sequencing. *Nat. Neurosci.* 16, 1896–1905. doi: 10.1038/nn.3554

Hill, R. A., Li, A. M., and Grutzendler, J. (2018). Lifelong cortical myelin plasticity and age-related degeneration in the live mammalian brain. *Nat. Neurosci.* 21, 683–695. doi: 10.1038/s41593-018-0120-6

Hinks, G. L., and Franklin, R. J. (1999). Distinctive patterns of PDGF-A, FGF-2, IGF-I, and TGF-β1 gene expression during remyelination of experimentally-induced spinal cord demyelination. *Mol. Cell. Neurosci.* 14, 153–168. doi: 10.1006/mcne.1999.0771

Hiremath, M. M., Saito, Y., Knapp, G. W., Ting, J. P., Suzuki, K., and Matsushima, G. K. (1998). Microglial/macrophage accumulation during cuprizone-induced demyelination in C57BL/6 mice. *J. Neuroimmunol.* 92, 38–49. doi: 10.1016/s0165-5728(98)00168-4

Hostenbach, S., D'haeseleer, M., Kooijman, R., and De Keyser, J. (2016). The pathophysiological role of astrocytic endothelin-1. *Prog. Neurobiol.* 144, 88–102. doi: 10.1016/j.pneurobio.2016.04.009

Huang, W., Bai, X., Stopper, L., Catalin, B., Cartarozzi, L. P., Scheller, A., et al. (2018). During development NG2 glial cells of the spinal cord are restricted to the oligodendrocyte lineage, but generate astrocytes upon acute injury. *Neuroscience* 385, 154–165. doi: 10.1016/j.neuroscience.2018.06.015

Huang, W., Guo, Q., Bai, X., Scheller, A., and Kirchhoff, F. (2019). Early embryonic NG2 glia are exclusively gliogenic and do not generate neurons in the brain. *Glia* 67, 1094–1103. doi: 10.1002/glia.23590

Hubler, Z., Allimuthu, D., Bederman, I., Elitt, M. S., Madhavan, M., Allan, K. C., et al. (2018). Accumulation of 8,9-unsaturated sterols drives oligodendrocyte formation and remyelination. *Nature* 560, 372–376. doi: 10.1038/s41586-018-0360-3

Hughes, E. G., Kang, S. H., Fukaya, M., and Bergles, D. E. (2013). Oligodendrocyte progenitors balance growth with self-repulsion to achieve homeostasis in the adult brain. *Nat. Neurosci.* 16, 668–676. doi: 10.1038/nn.3390

Hwang, S. Y., Jung, J. S., Kim, T. H., Lim, S. J., Oh, E. S., Kim, J. Y., et al. (2006). Ionizing radiation induces astrocyte gliosis through microglia activation. *Neurobiol. Dis.* 21, 457–467. doi: 10.1016/j.nbd.2005.08.006

Irvine, K. A., and Blakemore, W. F. (2008). Remyelination protects axons from demyelination-associated axon degeneration. *Brain* 131, 1464–1477. doi: 10.1093/brain/awn080

Itoh, N., Itoh, Y., Tassoni, A., Ren, E., Kaito, M., Ohno, A., et al. (2018). Cell-specific and region-specific transcriptomics in the multiple sclerosis model: focus on astrocytes. *Proc. Natl. Acad. Sci. U S A* 115, E302–E309. doi: 10.1073/pnas.1716032115

Itoyama, Y., Webster, H. D., Richardson, E. P., and Trapp, B. D. (1983). Schwann cell remyelination of demyelinated axons in spinal cord multiple sclerosis lesions. *Ann. Neurol.* 14, 339–346. doi: 10.1002/ana.410140313

Jäkel, S., Agirre, E., Mendanha Falcão, A., Bruggen van, D., Lee, K. W., Knuesel, I., et al. (2019). Altered human oligodendrocyte heterogeneity in multiple sclerosis. *Nature* 566, 543–547. doi: 10.1038/s41586-019-0903-2

Jakubzick, C. V., Randolph, G. J., and Henson, P. M. (2017). Monocyte differentiation and antigen-presenting functions. *Nat. Rev. Immunol.* 17, 349–362. doi: 10.1038/nri.2017.28

John, G. R., Shankar, S. L., Shafit-Zagardo, B., Massimi, A., Lee, S. C., Raine, C. S., et al. (2002). Multiple sclerosis: re-expression of a developmental pathway that restricts oligodendrocyte maturation. *Nat. Med.* 8, 1115–1121. doi: 10.1038/nm781

Jones, L. L., Margolis, R. U., and Tuszynski, M. H. (2003). The chondroitin sulfate proteoglycans neurocan, brevican, phosphacan and versican are differentially regulated following spinal cord injury. *Exp. Neurol.* 182, 399–411. doi: 10.1016/s0014-4886(03)00087-6

Kang, S. H., Fukaya, M., Yang, J. K., Rothstein, J. D., and Bergles, D. E. (2010). NG2$^+$ CNS glial progenitors remain committed to the oligodendrocyte lineage in postnatal life and following neurodegeneration. *Neuron* 68, 668–681. doi: 10.1016/j.neuron.2010.09.009

Kang, Z., Wang, C., Zepp, J., Wu, L., Sun, K., Zhao, J., et al. (2013). Act1 mediates IL-17-induced EAE pathogenesis selectively in NG2$^+$ glial cells. *Nat. Neurosci.* 16, 1401–1408. doi: 10.1038/nn.3505

Kawabori, M., and Yenari, M. A. (2015). The role of the microglia in acute CNS injury. *Metab. Brain Dis.* 30, 381–392. doi: 10.1007/s11011-014-9531-6

Keren-Shaul, H., Spinrad, A., Weiner, A., Matcovitch-Natan, O., Dvir-Szternfeld, R., Ulland, T. K., et al. (2017). A unique microglia type associated with restricting development of Alzheimer's disease. *Cell* 169, 1276.e17–1290.e17. doi: 10.1016/j.cell.2017.05.018

Khodanovich, M. Y., Kisel, A. A., Akulov, A. E., Atochin, D. N., Kudabaeva, M. S., Glazacheva, V. Y., et al. (2018). Quantitative assessment of demyelination in ischemic stroke *in vivo* using macromolecular proton fraction mapping. *J. Cereb. Blood Flow Metab.* 38, 919–931. doi: 10.1177/0271678x18755203

Kierdorf, K., Erny, D., Goldmann, T., Sander, V., Schulz, C., Perdiguero, E. G., et al. (2013). Microglia emerge from erythromyeloid precursors *via* Pu.1- and Irf8-dependent pathways. *Nat. Neurosci.* 16, 273–280. doi: 10.1038/nn.3318

Kimura, M., Sato, M., Akatsuka, A., Nozawa-Kimura, S., Takahashi, R., Yokoyama, M., et al. (1989). Restoration of myelin formation by a single type of myelin basic protein in transgenic shiverer mice. *Proc. Natl. Acad. Sci. U S A* 86, 5661–5665. doi: 10.1073/pnas.86.14.5661

King, I. L., Dickendesher, T. L., and Segal, B. M. (2009). Circulating Ly-6C$^+$ myeloid precursors migrate to the CNS and play a pathogenic role during autoimmune demyelinating disease. *Blood* 113, 3190–3197. doi: 10.1182/blood-2008-07-168575

Kirby, L., Jin, J., Cardona, J. G., Smith, M. D., Martin, K. A., Wang, J., et al. (2018). Oligodendrocyte precursor cells are co-opted by the immune system to cross-present antigen and mediate cytotoxicity. *bioRxiv* [Preprint]. 461434. doi: 10.1101/461434

Koizumi, S., Shigemoto-Mogami, Y., Nasu-Tada, K., Shinozaki, Y., Ohsawa, K., Tsuda, M., et al. (2007). UDP acting at P2Y6 receptors is a mediator of microglial phagocytosis. *Nature* 446, 1091–1095. doi: 10.1038/nature05704

Koles, Z. J., and Rasminsky, M. (1972). A computer simulation of conduction in demyelinated nerve fibres. *J. Physiol.* 227, 351–364. doi: 10.1113/jphysiol.1972.sp010036

Kotter, M. R., Li, W. W., Zhao, C., and Franklin, R. J. (2006). Myelin impairs CNS remyelination by inhibiting oligodendrocyte precursor cell differentiation. *J. Neurosci.* 26, 328–332. doi: 10.1523/jneurosci.2615-05.2006

Krasemann, S., Madore, C., Cialic, R., Baufeld, C., Calcagno, N., Fatimy El, R., et al. (2017). The TREM2-APOE pathway drives the transcriptional phenotype of dysfunctional microglia in neurodegenerative diseases. *Immunity* 47, 566.e9–581.e9. doi: 10.1016/j.immuni.2017.08.008

Kuhlmann, T., Ludwin, S., Prat, A., Antel, J., Brück, W., and Lassmann, H. (2017). An updated histological classification system for multiple sclerosis lesions. *Acta Neuropathol.* 133, 13–24. doi: 10.1007/s00401-016-1653-y

Kuhlmann, T., Miron, V., Cui, Q., Cuo, Q., Wegner, C., Antel, J., et al. (2008). Differentiation block of oligodendroglial progenitor cells as a cause for remyelination failure in chronic multiple sclerosis. *Brain* 131, 1749–1758. doi: 10.1093/brain/awn096

Kumamaru, H., Saiwai, H., Kobayakawa, K., Kubota, K., Rooijen van, N., Inoue, K., et al. (2012). Liposomal clodronate selectively eliminates microglia from primary astrocyte cultures. *J. Neuroinflammation* 9:116. doi: 10.1186/1742-2094-9-116

Lampron, A., Larochelle, A., Laflamme, N., Prefontaine, P., Plante, M. M., Sanchez, M. G., et al. (2015). Inefficient clearance of myelin debris by microglia impairs remyelinating processes. *J. Exp. Med.* 212, 481–495. doi: 10.1084/jem.20141656

Lassmann, H., and van Horssen, J. (2016). Oxidative stress and its impact on neurons and glia in multiple sclerosis lesions. *Biochim. Biophys. Acta* 1862, 506–510. doi: 10.1016/j.bbadis.2015.09.018

Law, M., Saindane, A. M., Ge, Y., Babb, J. S., Johnson, G., Mannon, L. J., et al. (2004). Microvascular abnormality in relapsing-remitting multiple sclerosis: perfusion MR imaging findings in normal-appearing white matter. *Radiology* 231, 645–652. doi: 10.1148/radiol.2313030996

Lawson, L. J., Perry, V. H., Dri, P., and Gordon, S. (1990). Heterogeneity in the distribution and morphology of microglia in the normal adult mouse brain. *Neuroscience* 39, 151–170. doi: 10.1016/0306-4522(90)90229-w

Lévesque, S. A., Paré, A., Mailhot, B., Bellver-Landete, V., Kébir, H., Lécuyer, M. A., et al. (2016). Myeloid cell transmigration across the CNS vasculature triggers IL-1β-driven neuroinflammation during autoimmune encephalomyelitis in mice. *J. Exp. Med.* 213, 929–949. doi: 10.1084/jem.20151437

Levine, J. M., and Reynolds, R. (1999). Activation and proliferation of endogenous oligodendrocyte precursor cells during ethidium bromide-induced demyelination. *Exp. Neurol.* 160, 333–347. doi: 10.1006/exnr.1999.7224

Li, C., Zhang, L., Chao, F., Xiao, Q., Luo, Y., and Tang, Y. (2017). Stereological quantification of age-related changes in myelinated fibers of rat white matter. *Neuroreport* 28, 42–49. doi: 10.1097/wnr.0000000000000706

Liddelow, S. A., and Barres, B. A. (2017). Reactive astrocytes: production, function and therapeutic potential. *Immunity* 46, 957–967. doi: 10.1016/j.immuni.2017.06.006

Liddelow, S. A., Guttenplan, K. A., Clarke, L. E., Bennett, F. C., Bohlen, C. J., Schirmer, L., et al. (2017). Neurotoxic reactive astrocytes are induced by activated microglia. *Nature* 541, 481–487. doi: 10.1038/nature21029

Linton, M. F., Gish, R., Hubl, S. T., Butler, E., Esquivel, C., Bry, W. I., et al. (1991). Phenotypes of apolipoprotein B and apolipoprotein E after liver transplantation. *J. Clin. Invest.* 88, 270–281. doi: 10.1172/JCI115288

Liu, L., Belkadi, A., Darnall, L., Hu, T., Drescher, C., Cotleur, A. C., et al. (2010). CXCR2-positive neutrophils are essential for cuprizone-induced demyelination: relevance to multiple sclerosis. *Nat. Neurosci.* 13, 319–326. doi: 10.1038/nn.2491

Liu, A., Li, J., Marin-Husstege, M., Kageyama, R., Fan, Y., Gelinas, C., et al. (2006). A molecular insight of Hes5-dependent inhibition of myelin gene expression: old partners and new players. *EMBO J.* 25, 4833–4842. doi: 10.1038/sj.emboj.7601352

Lloyd, A. F., Davies, C. L., Holloway, R. K., Labrak, Y., Ireland, G., Carradori, D., et al. (2019). Central nervous system regeneration is driven by microglia necroptosis and repopulation. *Nat. Neurosci.* 22, 1046–1052. doi: 10.1038/s41593-019-0418-z

Locatelli, G., Theodorou, D., Kendirli, A., Jordão, M. J. C., Staszewski, O., Phulphagar, K., et al. (2018). Mononuclear phagocytes locally specify and adapt their phenotype in a multiple sclerosis model. *Nat. Neurosci.* 21, 1196–1208. doi: 10.1038/s41593-018-0212-3

MacLeod, A. S., and Mansbridge, J. N. (2016). The innate immune system in acute and chronic wounds. *Adv. Wound Care* 5, 65–78. doi: 10.1089/wound.2014.0608

Maeda, Y., Solanky, M., Menonna, J., Chapin, J., Li, W., and Dowling, P. (2001). Platelet-derived growth factor-α receptor-positive oligodendroglia are frequent in multiple sclerosis lesions. *Ann. Neurol.* 49, 776–785. doi: 10.1002/ana.1015

Majmundar, A. J., Wong, W. J., and Simon, M. C. (2010). Hypoxia-inducible factors and the response to hypoxic stress. *Mol. Cell* 40, 294–309. doi: 10.1016/j.molcel.2010.09.022

Mason, J. L., Suzuki, K., Chaplin, D. D., and Matsushima, G. K. (2001). Interleukin-1β promotes repair of the CNS. *J. Neurosci.* 21, 7046–7052. doi: 10.1523/JNEUROSCI.21-18-07046.2001

Masuda, T., Sankowski, R., Staszewski, O., Böttcher, C., Amann, L., Sagar, et al. (2019). Spatial and temporal heterogeneity of mouse and human microglia at single-cell resolution. *Nature* 566, 388–392. doi: 10.1038/s41586-019-0924-x

Mayo, L., Quintana, F. J., and Weiner, H. L. (2012). The innate immune system in demyelinating disease. *Immunol. Rev.* 248, 170–187. doi: 10.1111/j.1600-065x.2012.01135.x

McTigue, D. M., Tripathi, R., and Wei, P. (2006). NG2 colocalizes with axons and is expressed by a mixed cell population in spinal cord lesions. *J. Neuropathol. Exp. Neurol.* 65, 406–420. doi: 10.1097/01.jnen.0000218447.32320.52

Mei, F., Lehmann-Horn, K., Shen, Y. A., Rankin, K. A., Stebbins, K. J., Lorrain, D. S., et al. (2016). Accelerated remyelination during inflammatory demyelination prevents axonal loss and improves functional recovery. *Elife* 5:e18246. doi: 10.7554/elife.18246

Messersmith, D. J., Murtie, J. C., Le, T. Q., Frost, E. E., and Armstrong, R. C. (2000). Fibroblast growth factor 2 (FGF2) and FGF receptor expression in an experimental demyelinating disease with extensive remyelination. *J. Neurosci. Res.* 62, 241–256. doi: 10.1002/1097-4547(20001015)62:2<241::aid-jnr9>3.0.co;2-d

Micu, I., Plemel, J. R., Caprariello, A. V., Nave, K. A., and Stys, P. K. (2017). Axo-myelinic neurotransmission: a novel mode of cell signalling in the central nervous system. *Nat. Rev. Neurosci.* 19:58. doi: 10.1038/nrn.2017.128

Mierzwa, A. J., Marion, C. M., Sullivan, G. M., McDaniel, D. P., and Armstrong, R. C. (2015). Components of myelin damage and repair in the progression of white matter pathology after mild traumatic brain injury. *J. Neuropathol. Exp. Neurol.* 74, 218–232. doi: 10.1097/nen.0000000000000165

Miron, V. E., Boyd, A., Zhao, J.-W., Yuen, T. J., Ruckh, J. M., Shadrach, J. L., et al. (2013). M2 microglia and macrophages drive oligodendrocyte differentiation during CNS remyelination. *Nat. Neurosci.* 16, 1211–1218. doi: 10.1038/nn.3469

Mishra, M. K., and Yong, V. W. (2016). Myeloid cells—targets of medication in multiple sclerosis. *Nat. Rev. Neurol.* 12, 539–551. doi: 10.1038/nrneurol.2016.110

Mitew, S., Kirkcaldie, M. T., Halliday, G. M., Shepherd, C. E., Vickers, J. C., and Dickson, T. C. (2010). Focal demyelination in Alzheimer's disease and transgenic mouse models. *Acta Neuropathol.* 119, 567–577. doi: 10.1007/s00401-010-0657-2

Mittelbronn, M., Dietz, K., Schluesener, H. J., and Meyermann, R. (2001). Local distribution of microglia in the normal adult human central nervous system differs by up to one order of magnitude. *Acta Neuropathol.* 101, 249–255. doi: 10.1007/s004010000284

Miyamoto, A., Wake, H., Ishikawa, A. W., Eto, K., Shibata, K., Murakoshi, H., et al. (2016). Microglia contact induces synapse formation in developing somatosensory cortex. *Nat. Commun.* 7:12540. doi: 10.1038/ncomms12540

Molofsky, A. V., and Deneen, B. (2015). Astrocyte development: a guide for the perplexed. *Glia* 63, 1320–1329. doi: 10.1002/glia.22836

Monk, K. R., Feltri, M. L., and Taveggia, C. (2015). New insights on Schwann cell development. *Glia* 63, 1376–1393. doi: 10.1002/glia.22852

Monteiro de Castro, G., Deja, N. A., Ma, D., Zhao, C., and Franklin, R. J. (2015). Astrocyte activation *via* Stat3 signaling determines the balance of oligodendrocyte versus schwann cell remyelination. *Am. J. Pathol.* 185, 2431–2440. doi: 10.1016/j.ajpath.2015.05.011

Moore, S. A. (2001). Polyunsaturated fatty acid synthesis and release by brain-derived cells *in vitro*. *J. Mol. Neurosci.* 16, 195–200; discussion 215–221. doi: 10.1385/JMN:16:2-3:195

Moore, C. S., Abdullah, S. L., Brown, A., Arulpragasam, A., and Crocker, S. J. (2011). How factors secreted from astrocytes impact myelin repair. *J. Neurosci. Res.* 89, 13–21. doi: 10.1002/jnr.22482

Moyon, S., Dubessy, A. L., Aigrot, M. S., Trotter, M., Huang, J. K., Dauphinot, L., et al. (2015). Demyelination causes adult CNS progenitors to revert to an immature state and express immune cues that support their migration. *J. Neurosci.* 35, 4–20. doi: 10.1523/JNEUROSCI.0849-14.2015

Mozafari, S., Sherafat, M. A., Javan, M., Mirnajafi-Zadeh, J., and Tiraihi, T. (2010). Visual evoked potentials and MBP gene expression imply endogenous myelin repair in adult rat optic nerve and chiasm following local lysolecithin induced demyelination. *Brain Res.* 1351, 50–56. doi: 10.1016/j.brainres.2010.07.026

Mrdjen, D., Pavlovic, A., Hartmann, F. J., Schreiner, B., Utz, S. G., Leung, B. P., et al. (2018). High-dimensional single-cell mapping of central nervous system immune cells reveals distinct myeloid subsets in health, aging, and disease. *Immunity* 48, 380.e6–395.e6. doi: 10.1016/j.immuni.2018.01.011

Murtie, J. C., Zhou, Y. X., Le, T. Q., Vana, A. C., and Armstrong, R. C. (2005). PDGF and FGF2 pathways regulate distinct oligodendrocyte lineage responses in experimental demyelination with spontaneous remyelination. *Neurobiol. Dis.* 19, 171–182. doi: 10.1016/j.nbd.2004.12.006

Nakanishi, M., Niidome, T., Matsuda, S., Akaike, A., Kihara, T., and Sugimoto, H. (2007). Microglia-derived interleukin-6 and leukaemia inhibitory factor promote astrocytic differentiation of neural stem/progenitor cells. *Eur. J. Neurosci.* 25, 649–658. doi: 10.1111/j.1460-9568.2007.05309.x

Narayanan, V., Cerina, M., Göbel, K., Meuth, P., Herrmann, A. M., Fernandez-Orth, J., et al. (2018). Impairment of frequency-specific responses associated with altered electrical activity patterns in auditory thalamus following focal and general demyelination. *Exp. Neurol.* 309, 54–66. doi: 10.1016/j.expneurol.2018.07.010

Natrajan, M. S., de la Fuente, A. G., Crawford, A. H., Linehan, E., Nuñez, V., Johnson, K. R., et al. (2015). Retinoid X receptor activation reverses age-related deficiencies in myelin debris phagocytosis and remyelination. *Brain* 138, 3581–3597. doi: 10.1093/brain/awv289

Nieweg, K., Schaller, H., and Pfrieger, F. W. (2009). Marked differences in cholesterol synthesis between neurons and glial cells from postnatal rats. *J. Neurochem.* 109, 125–134. doi: 10.1111/j.1471-4159.2009.05917.x

Nikic, I., Merkler, D., Sorbara, C., Brinkoetter, M., Kreutzfeldt, M., Bareyre, F. M., et al. (2011). A reversible form of axon damage in experimental autoimmune encephalomyelitis and multiple sclerosis. *Nat. Med.* 17, 495–499. doi: 10.1038/nm.2324

Nimmerjahn, A., Kirchhoff, F., and Helmchen, F. (2005). Resting microglial cells are highly dynamic surveillants of brain parenchyma *in vivo*. *Science* 308, 1314–1318. doi: 10.1126/science.1110647

Niu, J., Tsai, H. H., Hoi, K. K., Huang, N., Yu, G., Kim, K., et al. (2019). Aberrant oligodendroglial-vascular interactions disrupt the blood-brain barrier, triggering CNS inflammation. *Nat. Neurosci.* 22, 709–718. doi: 10.1038/s41593-019-0369-4

Olsson, Y. (1974). Mast cells in plaques of multiple sclerosis. *Acta Neurol. Scand.* 50, 611–618. doi: 10.1111/j.1600-0404.1974.tb02806.x

Paré, A., Mailhot, B., Lévesque, S. A., Juzwik, C., Ignatius Arokia Doss, P. M., Lécuyer, M. A., et al. (2018). IL-1β enables CNS access to $CCR2^{hi}$ monocytes and the generation of pathogenic cells through GM-CSF released by CNS endothelial cells. *Proc. Natl. Acad. Sci. U S A* 115, E1194–E1203. doi: 10.1073/pnas.1714948115

Patani, R., Balaratnam, M., Vora, A., and Reynolds, R. (2007). Remyelination can be extensive in multiple sclerosis despite a long disease course. *Neuropathol. Appl. Neurobiol.* 33, 277–287. doi: 10.1111/j.1365-2990.2007.00805.x

Patrikios, P., Stadelmann, C., Kutzelnigg, A., Rauschka, H., Schmidbauer, M., Laursen, H., et al. (2006). Remyelination is extensive in a subset of multiple sclerosis patients. *Brain* 129, 3165–3172. doi: 10.1093/brain/awl217

Plemel, J. R., Keough, M. B., Duncan, G. J., Sparling, J. S., Yong, V. W., Stys, P. K., et al. (2014). Remyelination after spinal cord injury: is it a target for repair? *Prog. Neurobiol.* 117, 54–72. doi: 10.1016/j.pneurobio.2014.02.006

Plemel, J. R., Liu, W. Q., and Yong, V. W. (2017). Remyelination therapies: a new direction and challenge in multiple sclerosis. *Nat. Rev. Drug Discov.* 16, 617–634. doi: 10.1038/nrd.2017.115

Plemel, J. R., Manesh, S. B., Sparling, J. S., and Tetzlaff, W. (2013). Myelin inhibits oligodendroglial maturation and regulates oligodendrocytic transcription factor expression. *Glia* 61, 1471–1487. doi: 10.1002/glia.22535

Plemel, J. R., Michaels, N. J., Weishaupt, N., Caprariello, A. V., Keough, M. B., Rogers, J. A., et al. (2018). Mechanisms of lysophosphatidylcholine-induced demyelination: a primary lipid disrupting myelinopathy. *Glia* 66, 327–347. doi: 10.1002/glia.23245

Pluvinage, J. V., Haney, M. S., Smith, B. A. H., Sun, J., Iram, T., Bonanno, L., et al. (2019). CD22 blockade restores homeostatic microglial phagocytosis in ageing brains. *Nature* 568, 187–192. doi: 10.1038/s41586-019-1088-4

Polito, A., and Reynolds, R. (2005). NG2-expressing cells as oligodendrocyte progenitors in the normal and demyelinated adult central nervous system. *J. Anat.* 207, 707–716. doi: 10.1111/j.1469-7580.2005.00454.x

Popovich, P. G., Guan, Z., Wei, P., Huitinga, I., van Rooijen, N., and Stokes, B. T. (1999). Depletion of hematogenous macrophages promotes partial hindlimb recovery and neuroanatomical repair after experimental spinal cord injury. *Exp. Neurol.* 158, 351–365. doi: 10.1006/exnr.1999.7118

Powers, B. E., Lasiene, J., Plemel, J. R., Shupe, L., Perlmutter, S. I., Tetzlaff, W., et al. (2012). Axonal thinning and extensive remyelination without chronic demyelination in spinal injured rats. *J. Neurosci.* 32, 5120–5125. doi: 10.1523/JNEUROSCI.0002-12.2012

Prineas, J. W., Barnard, R. O., Kwon, E. E., Sharer, L. R., and Cho, E. S. (1993). Multiple sclerosis: remyelination of nascent lesions. *Ann. Neurol.* 33, 137–151. doi: 10.1002/ana.410330203

Psachoulia, K., Chamberlain, K. A., Heo, D., Davis, S. E., Paskus, J. D., Nanescu, S. E., et al. (2016). IL4I1 augments CNS remyelination and axonal protection by modulating T cell driven inflammation. *Brain* 139, 3121–3136. doi: 10.1093/brain/aww254

Pu, A., Stephenson, E. L., and Yong, V. W. (2018). The extracellular matrix: focus on oligodendrocyte biology and targeting CSPGs for remyelination therapies. *Glia* 66, 1809–1825. doi: 10.1002/glia.23333

Pusic, A. D., Pusic, K. M., Clayton, B. L., and Kraig, R. P. (2014). IFNγ-stimulated dendritic cell exosomes as a potential therapeutic for remyelination. *J. Neuroimmunol.* 266, 12–23. doi: 10.1016/j.jneuroim.2013.10.014

Rawji, K. S., Kappen, J., Tang, W., Teo, W., Plemel, J. R., Stys, P. K., et al. (2018). Deficient surveillance and phagocytic activity of myeloid cells within demyelinated lesions in aging mice visualized by *ex vivo* live multiphoton imaging. *J. Neurosci.* 38, 1973–1988. doi: 10.1523/JNEUROSCI.2341-17.2018

Redwine, J. M., and Armstrong, R. C. (1998). *In vivo* proliferation of oligodendrocyte progenitors expressing PDGFαR during early remyelination. *J. Neurobiol.* 37, 413–428. doi: 10.1002/(sici)1097-4695(19981115)37:3<413::aid-neu7>3.0.co;2-8

Reichert, F., and Rotshenker, S. (2019). Galectin-3 (MAC-2) controls microglia phenotype whether amoeboid and phagocytic or branched and non-phagocytic by regulating the cytoskeleton. *Front. Cell. Neurosci.* 13:90. doi: 10.3389/fncel.2019.00090

Richardson, W. D., Young, K. M., Tripathi, R. B., and McKenzie, I. (2011). NG2-glia as multipotent neural stem cells: fact or fantasy? *Neuron* 70, 661–673. doi: 10.1016/j.neuron.2011.05.013

Rivers, L. E., Young, K. M., Rizzi, M., Jamen, F., Psachoulia, K., Wade, A., et al. (2008). PDGFRA/NG2 glia generate myelinating oligodendrocytes and piriform projection neurons in adult mice. *Nat. Neurosci.* 11, 1392–1401. doi: 10.1038/nn.2220

Rodriguez, J. P., Coulter, M., Miotke, J., Meyer, R. L., Takemaru, K., and Levine, J. M. (2014). Abrogation of β-catenin signaling in oligodendrocyte precursor cells reduces glial scarring and promotes axon regeneration after CNS injury. *J. Neurosci.* 34, 10285–10297. doi: 10.1523/JNEUROSCI.4915-13.2014

Rosenzweig, S., and Carmichael, S. T. (2015). The axon-glia unit in white matter stroke: mechanisms of damage and recovery. *Brain Res.* 1623, 123–134. doi: 10.1016/j.brainres.2015.02.019

Rothhammer, V., Borucki, D. M., Tjon, E. C., Takenaka, M. C., Chao, C. C., Ardura-Fabregat, A., et al. (2018). Microglial control of astrocytes in response to microbial metabolites. *Nature* 557, 724–728. doi: 10.1038/s41586-018-0119-x

Ruckh, J. M., Zhao, J. W., Shadrach, J. L., van Wijngaarden, P., Rao, T. N., Wagers, A. J., et al. (2012). Rejuvenation of regeneration in the aging central nervous system. *Cell Stem Cell* 10, 96–103. doi: 10.1016/j.stem.2011.11.019

Ruddle, N. H., Bergman, C. M., McGrath, K. M., Lingenheld, E. G., Grunnet, M. L., Padula, S. J., et al. (1990). An antibody to lymphotoxin and tumor necrosis factor prevents transfer of experimental allergic encephalomyelitis. *J. Exp. Med.* 172, 1193–1200. doi: 10.1084/jem.172.4.1193

Saab, A. S., Tzvetavona, I. D., Trevisiol, A., Baltan, S., Dibaj, P., Kusch, K., et al. (2016). Oligodendroglial NMDA receptors regulate glucose import and axonal energy metabolism. *Neuron* 91, 119–132. doi: 10.1016/j.neuron.2016.05.016

Safaiyan, S., Kannaiyan, N., Snaidero, N., Brioschi, S., Biber, K., Yona, S., et al. (2016). Age-related myelin degradation burdens the clearance function of microglia during aging. *Nat. Neurosci.* 19, 995–998. doi: 10.1038/nn.4325

Schauf, C. L., and Davis, F. A. (1974). Impulse conduction in multiple sclerosis: a theoretical basis for modification by temperature and pharmacological agents. *J. Neurol. Neurosurg. Psychiatry* 37, 152–161. doi: 10.1136/jnnp.37.2.152

Schirmer, L., Mobius, W., Zhao, C., Cruz-Herranz, A., Haim Ben, L., Cordano, C., et al. (2018). Oligodendrocyte-encoded Kir4.1 function is required for axonal integrity. *Elife* 7:e36428. doi: 10.7554/elife.36428

Segel, M., Neumann, B., Hill, M. F. E., Weber, I. P., Viscomi, C., Zhao, C., et al. (2019). Niche stiffness underlies the ageing of central nervous system progenitor cells. *Nature* doi: 10.1038/s41586-019-1552-1 [Epub ahead of print].

Selmaj, K., Raine, C. S., and Cross, A. H. (1991). Anti-tumor necrosis factor therapy abrogates autoimmune demyelination. *Ann. Neurol.* 30, 694–700. doi: 10.1002/ana.410300510

Shakhbazau, A., Schenk, G. J., Hay, C., Kawasoe, J., Klaver, R., Yong, V. W., et al. (2016). Demyelination induces transport of ribosome-containing vesicles from glia to axons: evidence from animal models and MS patient brains. *Mol. Biol. Rep.* 43, 495–507. doi: 10.1007/s11033-016-3990-2

Shen, S., Sandoval, J., Swiss, V. A., Li, J., Dupree, J., Franklin, R. J., et al. (2008). Age-dependent epigenetic control of differentiation inhibitors is critical for remyelination efficiency. *Nat. Neurosci.* 11, 1024–1034. doi: 10.1038/nn.2172

Sherratt, R. M., Bostock, H., and Sears, T. A. (1980). Effects of 4-aminopyridine on normal and demyelinated mammalian nerve fibres. *Nature* 283, 570–572. doi: 10.1038/283570a0

Shields, S. A., Gilson, J. M., Blakemore, W. F., and Franklin, R. J. M. (1999). Remyelination occurs as extensively but more slowly in old rats compared to young rats following gliotoxin-induced CNS demyelination. *Glia* 28, 77–83. doi: 10.1002/(SICI)1098-1136(199910)28:1<77::AID-GLIA9>3.0.CO;2-F

Siebert, J. R., Conta Steencken, A., and Osterhout, D. J. (2014). Chondroitin sulfate proteoglycans in the nervous system: inhibitors to repair. *Biomed Res. Int.* 2014:845323. doi: 10.1155/2014/845323

Sim, F. J., Zhao, C., Penderis, J., and Franklin, R. J. (2002). The age-related decrease in CNS remyelination efficiency is attributable to an impairment of both oligodendrocyte progenitor recruitment and differentiation. *J. Neurosci.* 22, 2451–2459. doi: 10.1523/jneurosci.22-07-02451.2002

Skripuletz, T., Hackstette, D., Bauer, K., Gudi, V., Pul, R., Voss, E., et al. (2013). Astrocytes regulate myelin clearance through recruitment of microglia during cuprizone-induced demyelination. *Brain* 136, 147–167. doi: 10.1093/brain/aws262

Smith, K. J., Blakemore, W. F., and Mcdonald, W. I. (1979). Central remyelination restores secure conduction. *Nature* 280, 395–396. doi: 10.1038/280395a0

Snaidero, N., Möbius, W., Czopka, T., Hekking, L. H., Mathisen, C., Verkleij, D., et al. (2014). Myelin membrane wrapping of CNS axons by PI(3,4,5)P3-dependent polarized growth at the inner tongue. *Cell* 156, 277–290. doi: 10.1016/j.cell.2013.11.044

Sofroniew, M. V., and Vinters, H. V. (2010). Astrocytes: biology and pathology. *Acta Neuropathol.* 119, 7–35. doi: 10.1007/s00401-009-0619-8

Sosa, R. A., Murphey, C., Ji, N., Cardona, A. E., and Forsthuber, T. G. (2013). The kinetics of myelin antigen uptake by myeloid cells in the central nervous system during experimental autoimmune encephalomyelitis. *J. Immunol.* 191, 5848–5857. doi: 10.4049/jimmunol.1300771

Steeland, S., Van Ryckeghem, S., Van Imschoot, G., De Rycke, R., Toussaint, W., Vanhoutte, L., et al. (2017). TNFR1 inhibition with a Nanobody protects against EAE development in mice. *Sci. Rep.* 7:13646. doi: 10.1038/s41598-017-13984-y

Stephenson, E. L., Mishra, M. K., Moussienko, D., Laflamme, N., Rivest, S., Ling, C. C., et al. (2018). Chondroitin sulfate proteoglycans as novel drivers of leucocyte infiltration in multiple sclerosis. *Brain* 141, 1094–1110. doi: 10.1093/brain/awy033

Stephenson, E. L., Zhang, P., Ghorbani, S., Wang, A., Gu, J., Keough, M. B., et al. (2019). Targeting the chondroitin sulfate proteoglycans: evaluating fluorinated glucosamines and xylosides in screens pertinent to multiple sclerosis. *ACS Cent. Sci.* 5, 1223–1234. doi: 10.1021/acscentsci.9b00327

Stoffels, J. M., de Jonge, J. C., Stancic, M., Nomden, A., van Strien, M. E., Ma, D., et al. (2013). Fibronectin aggregation in multiple sclerosis lesions impairs remyelination. *Brain* 136, 116–131. doi: 10.1093/brain/aws313

Streit, W. J. (2002). Microglia as neuroprotective, immunocompetent cells of the CNS. *Glia* 40, 133–139. doi: 10.1002/glia.10154

Syed, Y. A., Baer, A. S., Lubec, G., Hoeger, H., Widhalm, G., and Kotter, M. R. (2008). Inhibition of oligodendrocyte precursor cell differentiation by myelin-associated proteins. *Neurosurg. Focus* 24:E5. doi: 10.3171/foc/2008/24/3-4/e4

Targett, M. P., Sussman, J., Scolding, N., O'Leary, M. T., Compston, D. A., and Blakemore, W. F. (1996). Failure to achieve remyelination of demyelinated rat axons following transplantation of glial cells obtained from the adult human brain. *Neuropathol. Appl. Neurobiol.* 22, 199–206. doi: 10.1046/j.1365-2990.1996.4398043.x

Trebst, C., Sørensen, T. L., Kivisäkk, P., Cathcart, M. K., Hesselgesser, J., Horuk, R., et al. (2001). CCR1+/CCR5+ mononuclear phagocytes accumulate in the central nervous system of patients with multiple sclerosis. *Am. J. Pathol.* 159, 1701–1710. doi: 10.1016/s0002-9440(10)63017-9

Tripathi, R. B., Rivers, L. E., Young, K. M., Jamen, F., and Richardson, W. D. (2010). NG2 glia generate new oligodendrocytes but few astrocytes in a murine

experimental autoimmune encephalomyelitis model of demyelinating disease. *J Neurosci* 30, 16383–16390. doi: 10.1523/jneurosci.3411-10.2010

Tsai, H. H., Niu, J., Munji, R., Davalos, D., Chang, J., Zhang, H., et al. (2016). Oligodendrocyte precursors migrate along vasculature in the developing nervous system. *Science* 351, 379–384. doi: 10.1126/science.aad3839

Ueno, M., Fujita, Y., Tanaka, T., Nakamura, Y., Kikuta, J., Ishii, M., et al. (2013). Layer V cortical neurons require microglial support for survival during postnatal development. *Nat. Neurosci.* 16, 543–551. doi: 10.1038/nn.3358

Ulanska-Poutanen, J., Mieczkowski, J., Zhao, C., Konarzewska, K., Kaza, B., Pohl, H. B., et al. (2018). Injury-induced perivascular niche supports alternative differentiation of adult rodent CNS progenitor cells. *Elife* 7:e30325. doi: 10.7554/elife.30325

van Rooijen, N. (1992). Liposome-mediated elimination of macrophages. *Res. Immunol.* 143, 215–219. doi: 10.1016/s0923-2494(92)80169-l

Van Rooijen, N., and Sanders, A. (1994). Liposome mediated depletion of macrophages: mechanism of action, preparation of liposomes and applications. *J. Immunol. Methods* 174, 83–93. doi: 10.1016/0022-1759(94)90012-4

Varga, A. W., Johnson, G., Babb, J. S., Herbert, J., Grossman, R. I., and Inglese, M. (2009). White matter hemodynamic abnormalities precede sub-cortical gray matter changes in multiple sclerosis. *J. Neurol. Sci.* 282, 28–33. doi: 10.1016/j.jns.2008.12.036

Vogel, D. Y., Vereyken, E. J., Glim, J. E., Heijnen, P. D., Moeton, M., van der Valk, P., et al. (2013). Macrophages in inflammatory multiple sclerosis lesions have an intermediate activation status. *J. Neuroinflammation* 10:35. doi: 10.1186/1742-2094-10-35

Voronova, A., Yuzwa, S. A., Wang, B. S., Zahr, S., Syal, C., Wang, J., et al. (2017). Migrating interneurons secrete fractalkine to promote oligodendrocyte formation in the developing mammalian brain. *Neuron* 94, 500.e9–516.e9. doi: 10.1016/j.neuron.2017.04.018

Voss, E. V., Škuljec, J., Gudi, V., Skripuletz, T., Pul, R., Trebst, C., et al. (2012). Characterisation of microglia during de- and remyelination: can they create a repair promoting environment? *Neurobiol. Dis.* 45, 519–528. doi: 10.1016/j.nbd.2011.09.008

Wang, H., Allen, M. L., Grigg, J. J., Noebels, J. L., and Tempel, B. L. (1995). Hypomyelination alters K^+ channel expression in mouse mutants shiverer and Trembler. *Neuron* 15, 1337–1347. doi: 10.1016/0896-6273(95)90012-8

Wang, G. L., Jiang, B. H., Rue, E. A., and Semenza, G. L. (1995). Hypoxia-inducible factor 1 is a basic-helix-loop-helix-PAS heterodimer regulated by cellular O2 tension. *Proc. Natl. Acad. Sci. U S A* 92, 5510–5514. doi: 10.1073/pnas.92.12.5510

Wang, H., Kunkel, D. D., Martin, T. M., Schwartzkroin, P. A., and Tempel, B. L. (1993). Heteromultimeric K^+ channels in terminal and juxtaparanodal regions of neurons. *Nature* 365, 75–79. doi: 10.1038/365075a0

Watanabe, M., Toyama, Y., and Nishiyama, A. (2002). Differentiation of proliferated NG2-positive glial progenitor cells in a remyelinating lesion. *J. Neurosci. Res.* 69, 826–836. doi: 10.1002/jnr.10338

Waxman, S. G., and Brill, M. H. (1978). Conduction through demyelinated plaques in multiple sclerosis: computer simulations of facilitation by short internodes. *J. Neurol. Neurosurg. Psychiatry* 41, 408–416. doi: 10.1136/jnnp.41.5.408

Wilkins, A., Chandran, S., and Compston, A. (2001). A role for oligodendrocyte-derived IGF-1 in trophic support of cortical neurons. *Glia* 36, 48–57. doi: 10.1002/glia.1094

Wilkins, A., Majed, H., Layfield, R., Compston, A., and Chandran, S. (2003). Oligodendrocytes promote neuronal survival and axonal length by distinct intracellular mechanisms: a novel role for oligodendrocyte-derived glial cell line-derived neurotrophic factor. *J. Neurosci.* 23, 4967–4974. doi: 10.1523/jneurosci.23-12-04967.2003

Wilson, C. M., Gaber, M. W., Sabek, O. M., Zawaski, J. A., and Merchant, T. E. (2009). Radiation-induced astrogliosis and blood-brain barrier damage can be abrogated using anti-TNF treatment. *Int. J. Radiat. Oncol. Biol. Phys.* 74, 934–941. doi: 10.1016/j.ijrobp.2009.02.035

Witte, M. E., Schumacher, A. M., Mahler, C. F., Bewersdorf, J. P., Lehmitz, J., Scheiter, A., et al. (2019). Calcium influx through plasma-membrane nanoruptures drives axon degeneration in a model of multiple sclerosis. *Neuron* 101, 615.e5–624.e5. doi: 10.1016/j.neuron.2018.12.023

Wlodarczyk, A., Holtman, I. R., Krueger, M., Yogev, N., Bruttger, J., Khorooshi, R., et al. (2017). A novel microglial subset plays a key role in myelinogenesis in developing brain. *EMBO J.* 36, 3292–3308. doi: 10.15252/embj.201696056

Wolswijk, G., and Noble, M. (1992). Cooperation between PDGF and FGF converts slowly dividing O-2Aadult progenitor cells to rapidly dividing cells with characteristics of O-2Aperinatal progenitor cells. *J. Cell Biol.* 118, 889–900. doi: 10.1083/jcb.118.4.889

Yeatman, J. D., Wandell, B. A., and Mezer, A. A. (2014). Lifespan maturation and degeneration of human brain white matter. *Nat. Commun.* 5:4932. doi: 10.1038/ncomms5932

Yeung, M. S. Y., Djelloul, M., Steiner, E., Bernard, S., Salehpour, M., Possnert, G., et al. (2019). Dynamics of oligodendrocyte generation in multiple sclerosis. *Nature* 566, 538–542. doi: 10.1038/s41586-018-0842-3

Young, K. M., Psachoulia, K., Tripathi, R. B., Dunn, S. J., Cossell, L., Attwell, D., et al. (2013). Oligodendrocyte dynamics in the healthy adult CNS: evidence for myelin remodeling. *Neuron* 77, 873–885. doi: 10.1016/j.neuron.2013.01.006

Yousef, H., Czupalla, C. J., Lee, D., Chen, M. B., Burke, A. N., Zera, K. A., et al. (2019). Aged blood impairs hippocampal neural precursor activity and activates microglia *via* brain endothelial cell VCAM1. *Nat. Med.* 25, 988–1000. doi: 10.1038/s41591-019-0440-4

Yuen, T. J., Silbereis, J. C., Griveau, A., Chang, S. M., Daneman, R., Fancy, S. P., et al. (2014). Oligodendrocyte-encoded HIF function couples postnatal myelination and white matter angiogenesis. *Cell* 158, 383–396. doi: 10.1016/j.cell.2014.04.052

Zamanian, J. L., Xu, L., Foo, L. C., Nouri, N., Zhou, L., Giffard, R. G., et al. (2012). Genomic analysis of reactive astrogliosis. *J. Neurosci.* 32, 6391–6410. doi: 10.1523/JNEUROSCI.6221-11.2012

Zawadzka, M., Rivers, L. E., Fancy, S. P., Zhao, C., Tripathi, R., Jamen, F., et al. (2010). CNS-resident glial progenitor/stem cells produce Schwann cells as well as oligodendrocytes during repair of CNS demyelination. *Cell Stem Cell* 6, 578–590. doi: 10.1016/j.stem.2010.04.002

Zhan, X., Jickling, G. C., Ander, B. P., Liu, D., Stamova, B., Cox, C., et al. (2014). Myelin injury and degraded myelin vesicles in Alzheimer's disease. *Curr. Alzheimer Res.* 11, 232–238. doi: 10.2174/1567205011666140131120922

Zhang, Y., Argaw, A. T., Gurfein, B. T., Zameer, A., Snyder, B. J., Ge, C., et al. (2009). Notch1 signaling plays a role in regulating precursor differentiation during CNS remyelination. *Proc. Natl. Acad. Sci. U S A* 106, 19162–19167. doi: 10.1073/pnas.0902834106

Zhang, Y., Chen, K., Sloan, S. A., Bennett, M. L., Scholze, A. R., O'Keeffe, S., et al. (2014). An RNA-sequencing transcriptome and splicing database of glia, neurons, and vascular cells of the cerebral cortex. *J. Neurosci.* 34, 11929–11947. doi: 10.1523/JNEUROSCI.1860-14.2014

Zhao, C., Ma, D., Zawadzka, M., Fancy, S. P., Elis-Williams, L., Bouvier, G., et al. (2015). Sox2 sustains recruitment of oligodendrocyte progenitor cells following CNS demyelination and primes them for differentiation during remyelination. *J. Neurosci.* 35, 11482–11499. doi: 10.1523/JNEUROSCI.3655-14.2015

Zhou, J., Wu, Y. C., Xiao, B. J., Guo, X. D., Zheng, Q. X., and Wu, B. (2019). Age-related changes in the global DNA methylation profile of oligodendrocyte progenitor cells derived from rat spinal cords. *Curr. Med. Sci.* 39, 67–74. doi: 10.1007/s11596-019-2001-y

Conflict of Interest: The authors declare that the research was conducted in the absence of any commercial or financial relationships that could be construed as a potential conflict of interest.

frontiers in Immunology

ORIGINAL RESEARCH
published: 25 September 2019
doi: 10.3389/fimmu.2019.02231

Mimicry of Central-Peripheral Immunity in Alzheimer's Disease and Discovery of Neurodegenerative Roles in Neutrophil

Joseph Park[1], *Sung Hoon Baik*[2], *Inhee Mook-Jung*[2], *Daniel Irimia*[3]* *and Hansang Cho*[1,3,4]*

[1] The Nanoscale Science Program, Department of Mechanical Engineering and Engineering Science, Department of Biological Sciences, Center for Biomedical Engineering and Science, University of North Carolina at Charlotte, Charlotte, NC, United States, [2] Department of Biochemistry and Biomedical Sciences, Seoul National University, Seoul, South Korea, [3] Department of Surgery, BioMEMS Resource Center, Harvard Medical School, Massachusetts General Hospital, Charlestown, MA, United States, [4] Department of Biophysics, Institute of Quantum Biology, Sungkyunkwan University, Suwon, South Korea

Neuroinflammatory roles of central innate immunity in brain parenchyma are well-regarded in the progression of neurodegenerative disorders including Alzheimer's disease (AD), however, the roles of peripheral immunity in central nervous system (CNS) diseases are less clear. Here, we created a microfluidic environment of human AD brains: microglial neuroinflammation induced by soluble amyloid-beta (Abeta), a signature molecule in AD and employed the environment to investigate the roles of neutrophils through the central-peripheral innate immunity crosstalk. We observed that soluble Abeta-activated human microglial cells produced chemoattractants for neutrophils including IL6, IL8, CCL2, CCL3/4, CCL5 and consequently induced reliable recruitment of human neutrophils. Particularly, we validated the discernable chemo-attractive roles of IL6, IL8, and CCL2 for neutrophils by interrupting the recruitment with neutralizing antibodies. Upon recruitment, microglia-neutrophils interaction results in the production of inflammatory mediators such as MIF and IL2, which are known to up-regulate neuroinflammation in AD. We envision that targeting the crosstalk between central-peripheral immune community is a potential strategy to reduce immunological burdens in other neuroinflammatory CNS diseases.

Keywords: neuroinflammation, neurodegeneration, Alzheimer's disease, microglia, neutrophil, chemotaxis, cellular interaction, microfluidics

OPEN ACCESS

Edited by:
Antje Kroner,
Medical College of Wisconsin,
United States

Reviewed by:
Andre Ortlieb Guerreiro Cacais,
Karolinska Institute (KI), Sweden
Yoshiro Ohara,
Kanazawa Medical University, Japan

***Correspondence:**
Daniel Irimia
daniel_irimia@hms.harvard.edu
Hansang Cho
h.cho@uncc.edu

Specialty section:
This article was submitted to Multiple Sclerosis and Neuroimmunology, a section of the journal Frontiers in Immunology

Received: *24 June 2019*
Accepted: *03 September 2019*
Published: *25 September 2019*

Citation:
Park J, Baik SH, Mook-Jung I, Irimia D and Cho H (2019) Mimicry of Central-Peripheral Immunity in Alzheimer's Disease and Discovery of Neurodegenerative Roles in Neutrophil. Front. Immunol. 10:2231. doi: 10.3389/fimmu.2019.02231

INTRODUCTION

Alzheimer's disease (AD) is the most common form of dementia. It affects more than 35 million people worldwide (1, 2). It is characterized by neuropathological features including amyloid-beta (Abeta) plaques, neurofibrillary tangles, and neuroinflammation that lead into synaptic dysfunction and a progressive deterioration of cognitive functions (2–5). A growing body of evidence suggests that neuroinflammation is the critical hallmark of AD and central innate immune cells (microglia and astrocytes) have the major roles of neuroinflammation in a central nervous system (CNS) (6–9). Particularly, microglia, a macrophage resident in brains, produce both beneficial neuroinflammatory responses and detrimental neurotoxic effects in the progression of AD (10–12). Therefore, the regulation of microglial activation has been proposed as a potential therapeutic approach in AD treatment (13).

In contrast to the field's increasing understanding of the neuroinflammatory roles of central innate immunity in AD, comparatively little is known about their interactions with peripheral immunity. Peripheral immune cells including T-cells, B-cells, monocytes, and neutrophils, have been found in the brains of AD human patients and corresponding AD animal models (14–17). Among them, neutrophils are the body's most abundant and frontline immune cells, respond with both central and peripheral immune effectors during the progression of AD (17). The migration of neutrophils is initiated by chemokine-triggered activation. Neutrophils actively crawl through the endothelium and accumulate in tissues where they released neutrophil extracellular traps (NETs) and IL-17 which are markers of sterile inflammation and toxic cytokines, respectively. Neutrophil depletion or inhibition of trafficking *via* LFA-1 blockade reduced Alzheimer's disease–like neuropathology and improved memory in mice showing cognitive dysfunction in transgenic Alzheimer's disease mouse models (18). However, the mechanism study of neutrophil recruitment and induction of neuropathological changes of AD still remains unclear. The challenge of the study is due to, in part, the limited readouts *in vivo*, the similar profiles of peripheral inflammatory roles compared to the central immunity by microglia and astrocytes, and inconsistent observation and/or variation in AD animal models. Recently, microfluidic organ-on-chips demonstrated successfully to provide feasible, regulated, accessible microenvironments to study multicellular interaction and/or multiorgan behaviors in quantitative, reproducible, and large-scaled manners (19).

Here, we present a microfluidic system mimicking central-peripheral innate immunity in AD for the first time. We identified IL6, IL8, CCL2, CCL3, and CCL5 as mediators released by soluble Abeta-stimulated microglia. We validated their contribution to neutrophil recruitment by inhibiting with neutralizing antibodies. Moreover, the recruited neutrophils induce the secretion of inflammatory factors such as MIF and IL2, which may further stimulate the glia cells. Taken together, these studies suggest that central innate immune cells have a critical role in recruiting peripheral immune cells and mitigating AD pathogenesis.

RESULTS

Replicated AD Microenvironment by Using a Chemotactic Microfluidic Platform

We established an *in vitro* system to study the crosstalk between microglia and neutrophils in the context of AD (**Figure 1**). The system consists of two compartments: central circular and surrounding annular compartments representing regions of cerebral tissues and blood streams, respectively. The two compartments are connected with microchannels ($10 \times 5 \times 500$ μm^3 in width, height, and length) representing a mechanical barrier between two regions, which only chemoattracted neutrophils can penetrate through. The long and thin migration channels serve as mechanical constraints to avoid spontaneous entrance of inactivated neutrophils and activated microglia. Firstly, we cultured human adult microglia cells in the central compartment in addition of soluble Abeta for 3 days to induce the release of microglial inflammatory mediators in the context of AD. Later, we plated freshly isolated human neutrophils on the annular compartment under effective gradients of microglial soluble factors from the central compartment. We tested 200 independent conditions on eight arrays of twenty-five devices in single well plates and measured neutrophil mobility at a single cell resolution in a real-time.

Assessment of Microglial Neuroinflammation Activated by Soluble Abeta

We assessed the status of microglial inflammation by measuring inflammatory cytokines. We found that proinflammatory mediators, CCL2, IL-6, and IL-8 increase significantly by 1.4-, 1.9-, and 2.3-folds, respectively and chemokines, e.g., CCL3/4, CCL5 released from activated microglia only under stimulation of Abeta (**Figures 2A,B**). Secretion of anti-inflammatory markers, such as IL-1RA, IL-4, IL-10, and TGF-ß were below the limit of detection. These data collectively suggest that soluble Abeta induces microglial proinflammation quantified by using our microfluidic platform.

To identify the microglial activation, Abeta-treated microglial cells were monitored for three days using a time-lapse imaging microscopy. At the early 24 h, microglia remained as branched filopodia in all directions, morphological features typically associated with "resting" microglia (**Figure 2C**, upper, −Abeta). At 48 h after cell seeding and Abeta incubation, microglia cells became larger (**Figure 2C**, lower, +Abeta) and transformed into an amoeboid shape while the length and area of microglial somata increased in all directions (**Figures 2C,D**). In addition, microglia treated with soluble Abeta showed up-regulation of microglial activation markers such as CD11b and CD68 (**Figures 2C,E**, **Supplementary Figure 1**).

Validation of Microfluidic Chemotaxis for Neutrophils

We induced gradients of chemoattractants for neutrophils from the central toward the annular compartments and validated the design of microchannels effective for measuring chemotactic activities of neutrophils. We defined a neutrophil recruitment index, R.I. (**Figure 3A**, **Supplementary Figure 2**), representing the fraction of neutrophils recruited to the central compartment by chemoattractants. We assessed the R.I. values under various conditions (fMLP: N-formyl-methionyl-leucyl-phenalanine, Abeta, and culturing medium) and observed discernable neutrophil recruitment only in addition of fMLP to the central compartment (**Figures 3A,B**). In this study, we used fMLP for a positive control as fMLP triggers p38 pathway overriding PI(3)K and is certain for effectiveness of neutrophil chemoattraction (20). However, neutrophil recruitment was not discernable with Abeta only and the medium during the observation for 6 h. The results successfully demonstrate that our platform can engage neutrophils with chemical cues actively while avoiding spontaneous entrance of neutrophils with the mechanical barriers. Neutrophil recruitment reached

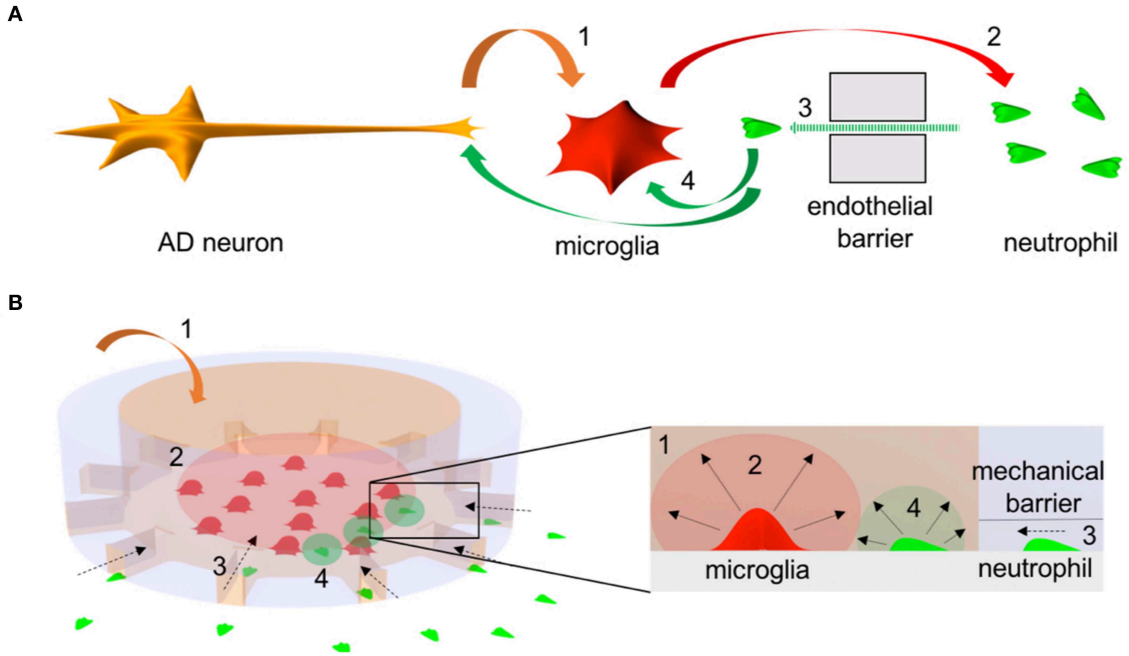

FIGURE 1 | Schematics of microglia-neutrophil crosstalk in Alzheimer's disease (AD) brains and a microfluidic mimicry. **(A)** Schematics describe orchestral and multicellular crosstal k in AD brains. AD neurons secrete pathological soluble factors (1) including Abeta peptides which activate microglial proinflammation. Microglial proinflammatory soluble factors (2) disrupt a cerebral endothelial barrier and induce neutrophil chemotaxis (3). Recruited neutrophils secrete proinflammatory factors (4) that affect microglia and/or AD neurons. **(B)** Schematics describe a mimicry of the crosstalk between central-peripheral innate immune cells in our microfluidic neuroinflammatory model. To reconstruct microenvironments in AD brains, a signature molecule in AD, soluble Abeta (1) is added to a central microglial microcompartment which represents a brain parenchyma and stimulates microglia to secrete neutrophil chemoattractants (2). As a result, neutrophils in an annular microcompartment migrate across a mechanical barrier (3) representing the endothelial barrier and release additional proinflammatory factors (4) in the microglial compartment after recruitment.

the peak activity at 18 ± 5 μm/min within the first 6 h (**Supplementary Figure 3**) and the activity was proportional to the concentration of fMLP, such as 1.6 times faster at 10 nM fMLP compared to 1 nM fMLP (**Figure 3B**).

We further analyzed the migratory activities of human neutrophils in a single cellular level. We found that 88.5 ± 3.8% of active neutrophils migrated forwards and 11.5 ± 1.7% migrated backward 10 nM fMLP, whereas 82.2 ± 3.4% migrated forward and 17.8 ± 2.8% backward 1 nM fMLP showing the persistent migration (**Figures 3C,D**). However, too much fMLP of 1 μM resulted in a 63 % reduction in the total fraction of migrating cells compared to 10 nM (**Supplementary Figure 4**).

Inducement of Neutrophil Recruitment by A-Beta Activated Microglia

To probe the crosstalk between microglia and neutrophils in the context of AD, we cultured microglia cells in the central compartment at various cell numbers (5,000, 10,000, 20,000 cells per device) with the treatment of soluble Abeta42 (22 nM) for 48 h, and then introduced neutrophils to the surrounding compartment. Microglia cells were pre-labeled with a red membrane dye to monitor their morphogenesis. Microglia were incubated alone for 24 h with reduced 1% FBS PrigrowIII medium without Abeta. Followed by microglial incubation with soluble Abeta, human neutrophil labeled with a green membrane dye were plated on the annular compartment. Neutrophil immediately started to migrate toward the central compartment of microglia of 5,000 with Abeta (**Figure 4A**). With the increase of microglia in the central compartment, neutrophil migration became more discernable and the number of recruited neutrophils increases proportional to the microglia, presuming that A-beta activated microglia release neutrophil chemoattractants. The responding neutrophils showed the enhanced polarity and distinct trailing edge toward microglial compartment with Abeta (**Figure 4A**, **Supplementary Figure 5**, **Supplementary Videos 1, 2**). However, neutrophil migration and the basal cell polarity were not noticeable in the conditions of microglia only, Abeta only, nor culture medium only (**Figure 4B**, **Supplementary Video 3**).

To confirm neutrophil activation, neutrophils co-cultured with microglial cells with or without Abeta for 5 min, were thoroughly washed away and the numbers of adherent neutrophils were counted. It showed that neutrophils co-cultured with Abeta-activated microglia enhanced cellular adhesion to the surface, confirming the neutrophil activation (**Supplementary Figure 6**).

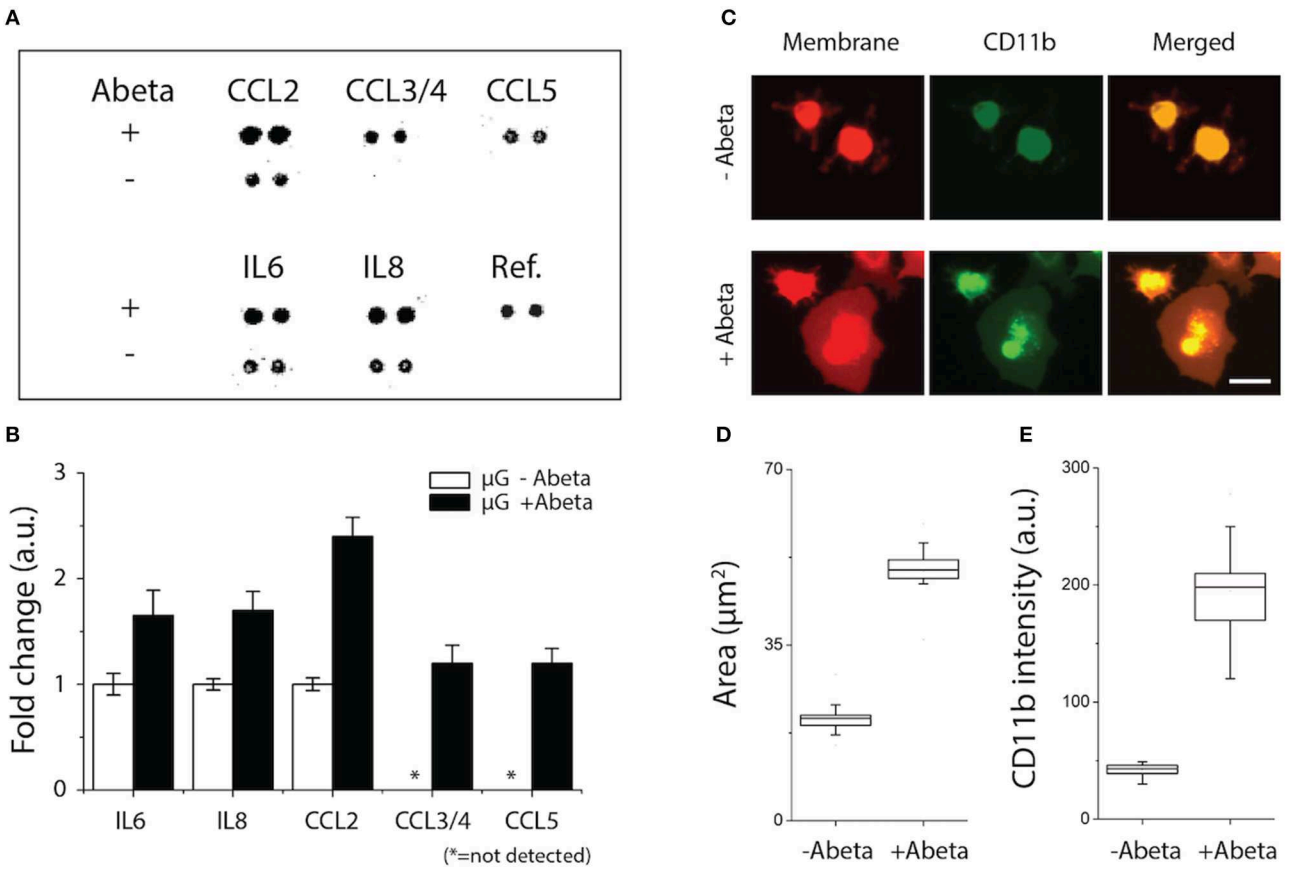

FIGURE 2 | Activation of microglial proinflammation with Abeta: chemokine release, morphogenesis, and marker expression. **(A,B)** Five chemokines among 29 membrane human cytokines measured were upregulated from microglia stimulated with Abeta at 22 nM for 24 h (upper row) compared to an unstimulated condition (lower row). **(C)** Membrane-staining (red) shows the discernable change in microglial morphology with Abeta stimulation from a branch-ramified shape (resting) to an amoeboid shape (activated). A microglia activation marker of CD11b (green) was upregulated with Abeta stimulation. Both the membrane area **(D)** and the amounts of expressed CD11b **(E)** increase in the activated microglia with Abeta. $n_{device} = 3$, $n_{cell} = 150$. Scale bars: 30 μm. All parameters are presented as mean ± SEM.

Identification of Microglial Chemoattractants That Induce Neutrophil Recruitment

We investigated which of microglial soluble factors are responsible for neutrophil recruitment. Firstly, we measured multiple cytokines in conditional media of Abeta-activated microglia and tested neutrophil chemotaxis for selected cytokines: IL-6, IL-8, CCL2, CCL3/4, and CCL5 (**Figure 4C**). We compared the recruitment activity by counting the neutrophil R.I. and found the significant recruitment by IL8 at 10 nM (R.I. = 12 ± 2.2), IL6 at 12 nM (R.I. = 8.7 ± 1.1) and discernable recruitment by CCL2 (R.I. = 5.1 ± 0.72), CCL3 (R.I. = 4.9 ± 0.51), CCL5 (R.I. = 4.2 ± 0.31) at 10 nM, respectively.

We also assessed the persistent movement of neutrophils by utilizing a single-cellular, high-resolution, and spatiotemporal imaging microscope. Neutrophils showed the highest persistent migration (∼92%) toward Abeta-stimulated microglial cells, compared to single soluble factors of IL8, IL6, CCL2, CCL3, and CCL5 (79.2, 75.2, 73.1, 64.2, and 51.2%, respectively) (**Figure 4D**). Such the high persistency was consistent with the variation in microglial cell numbers.

Validation of Microglial Chemoattractants That Induce Neutrophil Recruitment

To confirm the contribution of microglia-derived cytokines to neutrophil recruitment, we inhibited neutrophil migration toward Abeta-activated microglia by adding individual neutralizers for CCL2, CCL3/4, CCL5, IL6, and IL8 to the central compartment. We observed the discernable reduction of neutrophil recruitment by neutralizing antibodies against IL8, IL6, and CCL2 (**Figure 4E**). As reported in literature, IL8 appears to be the most dominant chemoattractant among others. IL8 neutralization reduced neutrophil recruitment most significantly by 50.2%, while IL6 (34.1%), CCL2 (22.1%), CCL3 (9.1%), and CCL5 (7.9%) neutralizers showed moderate reduction of neutrophil recruitment, respectively (**Figure 4E**).

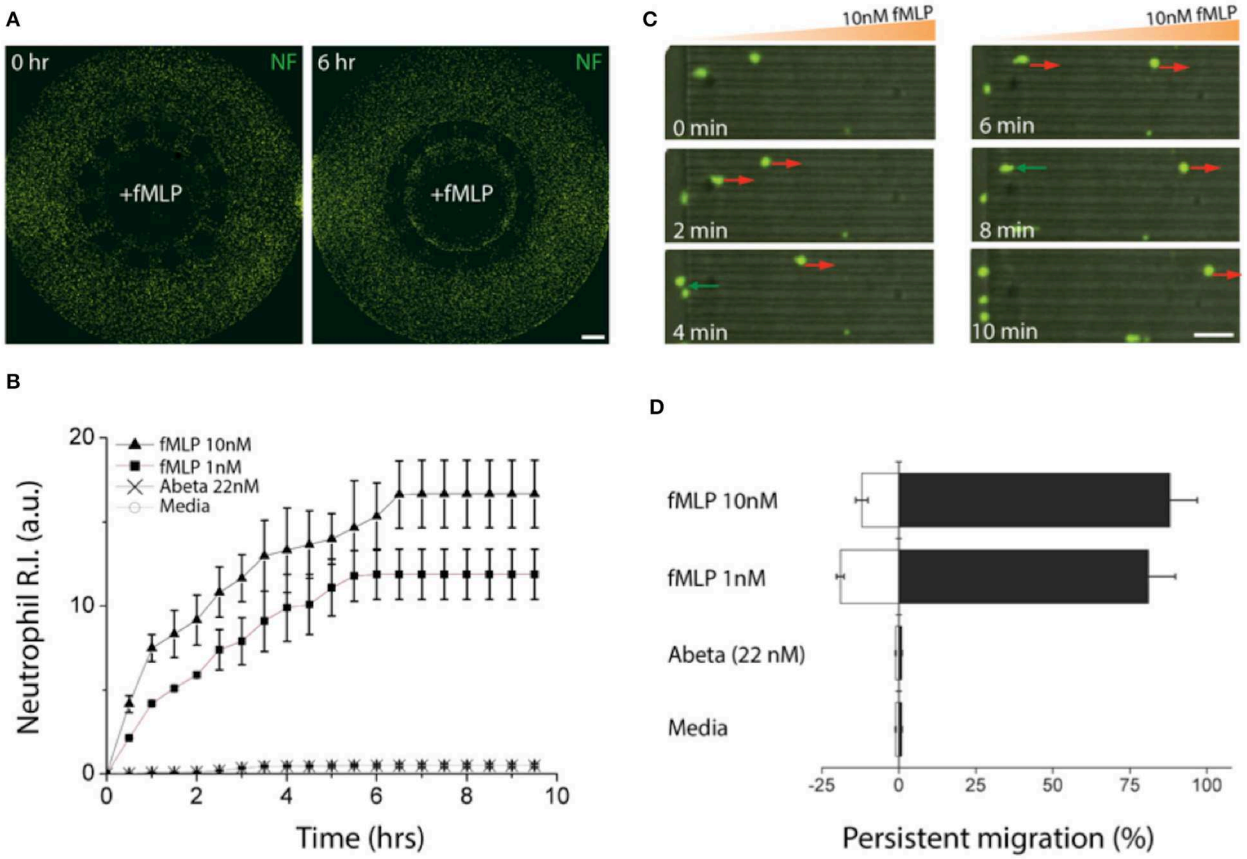

FIGURE 3 | Validation of a chemotactic microfluidics for neutrophils. **(A)** Neutrophils (green) instantly migrated through microchannels size-exclusive for activated neutrophils along a gradient of fMLP (10 nM) and accumulated in a central compartment, the source of fMLP. **(B)** Time-lapse images show chemotactic migration of neutrophils by fMLP on a single cellular level. The red arrows indicate persistent chemotaxis of neutrophils along the gradient of the chemoattractant and green arrows indicate the retrotaxis against the gradient. **(C)** Counting the accumulated neutrophils in the central compartment for the first 6 h shows persistent chemotactic behavior of neutrophils responding to fMLP (10 nM, 1 nM), Abeta (22 nM), and a negative control (medium). **(D)** Measuring the migration persistence for the first 1 h shows the dominancy of the forward migration of neutrophils. Combined data from $n_{device} = 3$, $n_{neutrophil} = 250$ independent experiments. Scale bars: **(A)** 500 μm, **(B)** 50 μm. Data represented as mean ± SEM.

Assessment of Neutrophil Inflammation Activated by Microglial Soluble Factors

To assess the roles of recruited neutrophils in the progression of AD pathology, we investigated neutrophil inflammation. We compared the morphology of neutrophils resting in the annular compartment (**Figure 5A** left) and activated in the central compartment (**Figure 5A** right). Microglia-activated neutrophils extended their bodies by 1.8 folds (**Figure 5B**). In a 37-human cytokine assay, we found two additional cytokines, MIF and IL2 (1.7-fold and 1.67-fold, respectively) from the recruited neutrophils compared to A-beta activated microglia only (**Figures 5D,E**). The other 5-soluble factors from Abeta-activated microglia remained unchanged after neutrophil recruitment. Other key proinflammatory and neurotoxic cytokines including interleukin 1β (IL-1β), interleukin 17 and tumor necrosis factor alpha (TNF-alpha) were below the detection limit of the kit used (**Figure 5C**). This measurement suggests that the recruitment of neutrophils may exacerbate microglial neuroinflammation activated by Abeta in AD.

DISCUSSION

Microglial cells are cerebral innate immune cells having neuroinflammatory roles for AD pathology. Based on our previous study of neutrophil accumulation on Abeta plaques in AD animal models (17), we hypothesized that neutrophils, the frontline of peripheral immune cells are engaged with neuroinflammation not directly with Abeta but mediated by microglia. Our microscale platforms enabled comprehensive studies of the crosstalk between central and peripheral immunity and overcame significant limitations of previous studies (21–23). For example, the study of neutrophil involvement in previous models lack control over the complex cellular interactions among multiple types of brain cells and leukocytes (23). Another

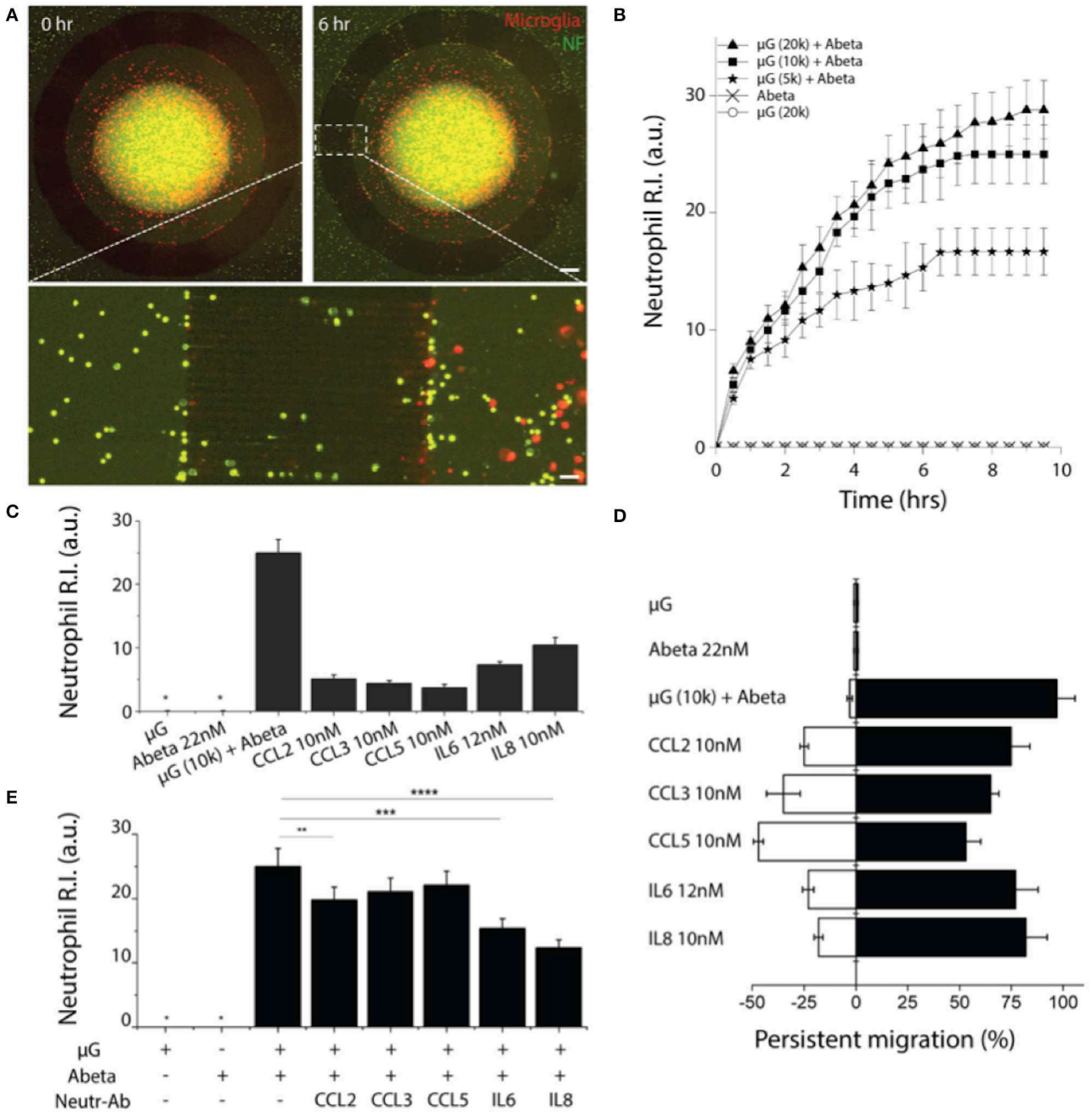

FIGURE 4 | Reconstruction of human neutrophil recruitment mediated by human microglia in AD**. (A)** Fluorescent images show discernable neutrophil recruitment (green) modulated by Abeta-stimulated microglia (red). **(B)** Measurement of single cellular migration shows instant activation and saturation of neutrophil migration responding to co-culturing conditions: microglia (μG) of 20,000 cells per device, 10,000 cells per device, 5,000 cells per device with Abeta at 22 nM, and negative controls (Abeta only, 20,000 microglia only). Neutrophil chemotaxis was assessed with various soluble factors: Abeta at 22 nM, CCL2 at 10 nM, CCL3 at 10 nM, CCL5 at 10 nM, IL6 at 12 nM, and IL8 at 10 nM by counting the accumulated neutrophils **(C)** and measuring the persistence **(D)**. **(E)** The effectiveness of microglia-derived chemokines was confirmed by showing the reduced neutrophil accumulation to Abeta-stimulated microglia in addition of neutralizing antibodies for individual chemokines. Statistical significance is denoted by $^{**}P < 0.20$, $^{***}P < 0.10$, $^{****}P < 0.01$ $n_{device} = 4$ **(B–E)**, $n_{device} = 3$, $n_{neutrophil} = 250$. Scale bars: 500 μm (upper right), 50 μm (lower pannel). All parameters are presented as mean ± SEM. *not detected.

key feature of our platform is the capability of isolating activated neutrophils from resting neutrophils, which allows selective monitoring the activities of interest in the AD progression (21) and on-chip investigation of drug efficacy, such as, inhibitor treatment against neutrophil recruitment and microglial inflammation (23).

One of the intriguing findings is that several mediators contribute to the robust recruitment of human neutrophils,

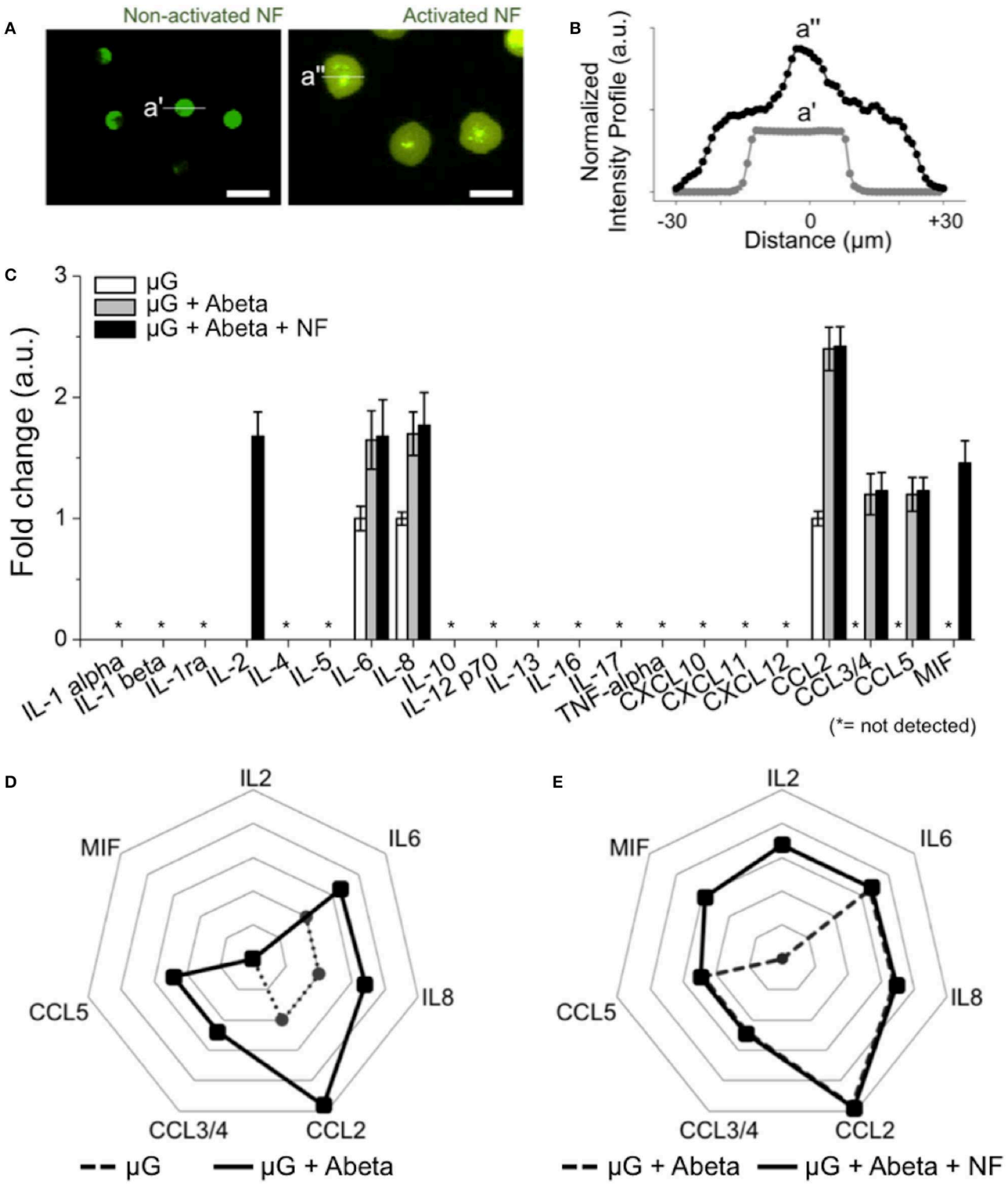

FIGURE 5 | Inducement of additional proinflammatory mediators from recruited human neutrophils. **(A)** Fluorescent images show the discernable morphology change of activated neutrophils (central compartment) compared to non-activated neutrophils (annular compartment). **(B)** Intensity profile shows the significantly enlarged neutrophils after recruitment (black dotted line) compared to non-activated ones (light gray dotted line). **(C)** 21 human cytokines/chemokines for inflammation-related soluble factors were measured. Among them, MIF and IL2 are the additional soluble factors secreted from recruited neutrophils in comparison with other conditions. **(D)** A radar plot highlights the increase of IL6, IL8, CCL2, CCL3/4, CCL5 from Abeta-stimulated microglia (dotted black line) in comparison with resting microglia (dotted gray line). **(E)** A radar plot highlights the increase of MIF and IL2 from Abeta-stimulated microglia and recruited neutrophil (dotted black line) in comparison with Abeta-stimulated microglia only (dotted gray line). $n_{device} = 5$ **(A–E)**. Scale bars: 25 μm. All parameters are presented as mean ± SEM. *: not detected.

which is similar to the findings in AD mouse models (24, 25). CCL3 has been found to be associated with AD (26, 27), reported as expressed by neurons and microglia in post-mortem brains from AD patients (28) and upregulated in experimental models mimicking both amyloid and Tau deposits (29). In addition, a CCL3 polymophism has been associated with AD (30) and CCL3 secretion was found dependent on apoplipoprotein ε4, the greatest genetic risk factor for sporadic AD (31). CCL5 is most commonly involved in AD neurodegenerative processes, which regulates the activities of normal T cells. During AD pathogenesis, an elevated level of the glial CCL5 chemokine is observed in the microcirculatory system of the brain (32). Its elevated levels contribute to the recruitment of immune-competent cells, which occurs concurrently with increased rates of neuronal deaths (33). In addition to these factors, we identified two proinflammatory-specific proteins released during the crosstalk in between activated microglia and neutrophils. IL2 and MIF are known to enhance human-neutrophil inflammatory activities (25). Especially, MIF (macrophage inhibitor factor), was observed in serial brain sections of transgenic APP AD mice and stained MIF immunolabeling in neutrophils in association with Abeta plaques in the transgenic mouse brain sections (34). In addition, functional studies in murine and human neuronal cell lines revealed that Abeta-induced toxicity could be reversed significantly by a small amount of MIF, showing the beneficial effect in AD mediated by microglia (25). Finally, MIF levels in the brain cytosol and cerebrospinal fluid (CSF) of AD patients showed marked increase compare to and age-matched controls. MIF are regarded as an important proinflammatory mediator by observing in the brain cytosol and cerebrospinal fluid (CSF) of AD patients and affecting tau hyper-phosphorylation, which is found in the late stage of AD (35). IL-2 was found to attenuate Abeta pathology and synaptic impairment in AD mice by engaging astrocytes for clearing Abeta and consequently improving synaptic plasticity (36).

CONCLUSION

We developed a microfluidic platform to explore the crosstalk between microglia and neutrophils in the context of AD and suggested how peripheral immune cells, neutrophils are involved in AD pathology mediated by Abeta-activated microglia to enhance the beneficial neuroinflammation. Our platform will serve as a physiologically relevant *in vitro* AD brain model for the study of neuroinflammation and a reliable tool for the validation of therapeutic strategy for neuroinflammatory immunotherapy.

METHODS

Cell Lines, Media, and Reagents

Immortalized human adult microglia cells (SV40-microglia) were created by a company (ABM Inc., Montreal, Canada). The cells were plated onto T25 cell culture flasks (BD Biosciences, San Jose, CA, USA) and maintained in Prigrow III Medium (ABM Inc) supplemented with 10 % FBS (Life Technologies) and 1 % Pen/Strep (Invitrogen) in a CO_2 cell culture incubator. The cell culture medium was changed every 3 days until cells were confluent.

For neutrophil isolation, human peripheral blood samples from healthy volunteers, aged 18 years and older, were collected by a company (Zen-Bio Inc., Research Triangle Park, NC, USA). Peripheral blood was drawn in a 10-mL tube containing a final concentration of 5 mM EDTA (Vacutainer; Becton Dickinson). Nucleated cells were isolated using a HetaSep gradient, followed by the EasySep Human Neutrophil Enrichment Kit (STEMCELL Technologies, Vancouver, Canada) according to the manufacturer's protocol.

Microfluidic Device Fabrication

Negative photoresists, SU-8 5 and SU-8 100 (MicroChem, Newton, MA, USA), were sequentially patterned using standard lithography on a 4" silicon wafer to create a mold for cell migration channels of 5 μm in height and chemokine compartments of 100 μm in height. A mixture of a base and a curing agent with a 10:1 weight ratio (SYLGARD 184 A/B, Dow corning, Midland, MI, USA) was poured onto the SU-8 mold and cured for 1 h at room temperature under vacuum and, subsequently, cured for more than 3 h in an oven at 80°C. The cured poly dimethyl-siloxane (PDMS) replica was peeled off from the mold and holes were punched for fluid reservoirs. Arrayed holes were also laser-cut (Zing 24, Epilog Laser, Golden, CO, USA) into an acrylic plate of 6 mm in thickness. The machined membrane and the plate were glued together using uncured PDMS and incubated at 80°C overnight. This assembly was irreversibly bonded first to the PDMS replica using oxygen plasma at 50 mW, 5 cm, for 30 s (PX-250, March Plasma Systems, Petersburg, FL, USA), and later to a glass-bottomed single well plate (P384G-1.5-10872-C, MatTek Corp., Ashland, MA, USA). Immediately after the bonding, 10 μL of poly (l-lysine) solution (PLL, M.W. 70,000–150,000, 1.0 mg/mL, Sigma-Aldrich Co. LLC) was injected into each platform and incubated for 2 h at a room temperature to promote cellular adhesion. PLL-treated surface was rinsed with autoclaved and 0.2 μm filtered water (AM9920, Life Technologies).

Membrane Staining of Microglia

Before the experiment, cells were washed using a serum-free medium and the cell membrane was labeled with red fluorescent dyes (PKH26PCL Red Fluorescent Cell Linker, Sigma-Aldrich). Briefly, after centrifugation (1,200 rpm.g for 5 min), the cells were re-suspended in 1 mL of Diluent C (G8278, Sigma-Aldrich) and immediately mixed with 4 μL of dye solution. The cell/dye mixture was incubated at room temperature for 4 min and periodically mixed by pipetting to achieve a bright, uniform, and reproducible labeling. After the incubation, the staining was stopped by adding an equal volume (1 mL) of 1 % BSA in PBS and incubating for 1 min to remove excess dye. Unbound dye was washed by centrifugation and suspending cells in culture medium (10^6 cells/mL). Ten μL of the cell suspension was injected into each platform and 100 μL of a culturing medium was added into side and central extra wells. The loaded micro-devices were then incubated at 37°C supplied with 5% CO_2.

Isolation and Membrane Staining of Neutrophils

Human neutrophils were isolated from fresh human blood samples within 2 h of blood collection by using EasySepHuman Neutrophil Enrichment Kits (STEMCELL Technologies) and following the manufacturer's instructions. After isolation, the neutrophils were washed using 1x PBS, and immediately mixed with 4 μL of dye solution (PKH67 Green Fluorescent Cell Linker, Sigma-Aldrich). The cell/dye mixture was incubated at room temperature for 4 min and periodically mixed by pipetting to achieve a bright, uniform, and reproducible labeling. After the incubation, the staining was stopped by adding an equal volume (1 mL) of 1% BSA in PBS and incubating for 1 min to remove excess dyes. Unbound dyes were washed by centrifugation and suspending cells in culture medium (10^6 cells/mL). Ten μL of the cell suspension was injected into each annular compartment. The loaded microfluidic-device were then incubated at 37°C supplied with 5% CO_2 in 10 min for the cell attachment and used later in microscope.

Time-Lapse Imaging

To track individual cells at a high throughput, we prepared 24 devices on a single-well plate and time-lapse imaged the entire devices in a large-area mode of 8 × 8 mm^2 with a 15 % stitching by using a fully automated microscope (Ti-E/NIS Elements, Nikon Inc.) integrated with a heated incubating stage (INU-TIZB-F1, Tokai Hit Co., Ltd., Shizuoka, Japan), set at 37.5°C and 5% CO_2 with moderate humidity. We imaged cells at every 15 min for 6 h in three channels—FITC, Cy5, and a bright field—with a 10x objective lens and a perfect focusing system in a phase contrast mode.

Immunostaining

Before immunofluorescent staining, we rinsed the cells twice with DPBS. To fix, cells were incubated in fresh 4% paraformaldehyde aqueous solution (157-4, ElectronMicroscopy Sciences) for more than 15 min at RT followed by rinsing twice with DPBS. To permeabilize, cells were incubated in 0.1% Triton X-100 in PBST (phosphate buffered saline with 0.1% tween®20) for 15 min at RT. To block, cells were incubated in 3% human serum albumin for overnight in PBST at 4°C. After incubating with the primary antibody solutions for 24 h at 4°C, the cells were washed five times. The following antibody (and dilutions) were used: anti-cd11b (1:100, Life Technologies).

Multiple Human Cytokine Array Kit

A human cytokine array kit was purchased from R&D Systems (Catalog # ARY005, Human Cytokine 37-membrane kit array) and utilized following the protocol provided by the manufacturer. Capture antibodies have been spotted in duplicate on nitrocellulose membranes. Cell culture supernatants are mixed with a cocktail of biotinylated detection antibodies. The sample/antibody mixture is then incubated with the array. Any cytokine/detection antibody complex present is bound by its cognate immobilized capture antibody on the membrane. Streptavidin-Horseradish Peroxidase and chemiluminescent detection reagents are added. A signal is produced, proportional with the amount of cytokine bound. Chemiluminescence is detected in the same manner as a Western blot and the resulting cytokine release profiles were quantified with ImageJ.

Microglial Stimulation by Soluble Abeta

After stabilizing microglia in the central compartment, the culturing medium was replaced by a medium containing Abeta 42 (PAM-4349-v, Amyloid Beta-Protein, Peptides International, Inc.) at 22 nM of 2% FBS and microglia were incubated for 72 h.

Statistical Analysis

Data, expressed as mean ± SEM, were compared using either a two-tailed Student's *t*-test when comparing two groups/conditions or one-way ANOVA followed by a *post hoc* test when comparing 3 or more groups/conditions. $P < 0.05$ was considered significant.

DATA AVAILABILITY

The datasets generated for this study are available on request to the corresponding author.

AUTHOR CONTRIBUTIONS

JP and HC designed, fabricated, and tested devices, designed experiments, performed immunostaining, statistical quantification, generated figures, wrote and edited the manuscript. JP, SB, IM-J, DI, and HC conceived the ideas and edited the manuscript. All authors read and edited the manuscript extensively.

FUNDING

This work was supported by the Pioneering Funding Award funded by Cure Alzheimer's Fund (CAF, HC), Duke Energy Special Initiatives funded by Charlotte Research Institute (CRI, HC) and Basic Science Research Program through the National Research Foundation of Korea (NRF) funded by the Ministry of Education (2015R1A6A3A03019848, JP), the National Institute of Health (AG059236-01A1, HC).

ACKNOWLEDGMENTS

We appreciate Dr. You Jung Kang (UNCC) for critical reviewing our manuscript.

SUPPLEMENTARY MATERIAL

The Supplementary Material for this article can be found online at: https://www.frontiersin.org/articles/10.3389/fimmu.2019.02231/full#supplementary-material

REFERENCES

1. Querfurth HW, LaFerla FM. Alzheimer's disease. *N Engl J Med*. (2010) 362:329–344. doi: 10.1056/NEJMra0909142
2. Wyss-Coray T. Inflammation in Alzheimer disease: driving force, bystander or beneficial response? *Nat Med*. (2006) 12:1005–15. doi: 10.1038/nm1484
3. Marcello E, Epis R, Saraceno C, Di Luca M. Synaptic dysfunction in Alzheimer's Disease. In: Kreutz MR, Sala C, editors. *Synaptic Plasticity Dynamics, Development and Disease*. Vienna: Springer-Verlag Wienõ. 573–601. doi: 10.1007/978-3-7091-0932-8_25
4. Seeman P, Seeman N. Alzheimer's disease: β-amyloid plaque formation in human brain. *Synapse*. (2011) 65:1289–97. doi: 10.1002/syn.20957
5. Binder LI, Guillozet-Bongaarts AL, Garcia-Sierra F, Berry RW. Tau, tangles, and Alzheimer's disease. *Biochim Biophys Acta*. (2005) 1739:216–23. doi: 10.1016/j.bbadis.2004.08.014
6. Wyss-Coray T, Rogers J. Inflammation in Alzheimer Disease—a brief review of the basic science and clinical literature. *Cold Spring Harb Perspect Med*. (2012) 2:a006346. doi: 10.1101/cshperspect.a006346
7. Schwartz M, Kipnis J, Rivest S, Prat A. How do immune cells support and shape the brain in health, disease, and aging? *J Neurosci*. (2013) 33:17587–96. doi: 10.1523/JNEUROSCI.3241-13.2013
8. Czirr E, Wyss-Coray T. The immunology of neurodegeneration. *J Clin Invest*. (2012) 122:1156–63. doi: 10.1172/JCI58656
9. Krstic D, Knuesel I. Deciphering the mechanism underlying late-onset Alzheimer disease. *Nat Rev Neurol*. (2013) 9:25–34. doi: 10.1038/nrneurol.2012.236
10. Prokop S, Miller KR, Heppner FL. Microglia actions in Alzheimer's disease. *Acta Neuropathol*. (2013) 126:461–77. doi: 10.1007/s00401-013-1182-x
11. Khoury El J, Toft M, Hickman SE, Means TK, Terada K, Geula C, Luster AD. Ccr2 deficiency impairs microglial accumulation and accelerates progression of Alzheimer-like disease. *Nat Med*. (2007) 13:432–8. doi: 10.1038/nm1555
12. Cagnin A, Brooks DJ, Kennedy AM, Gunn RN, Myers R, Turkheimer FE, Jones T, Banati RB. *In-vivo* measurement of activated microglia in dementia. *Lancet*. (2001) 358:461–7. doi: 10.1016/S0140-6736(01)05625-2
13. Block ML, Zecca L, Hong J-S. Microglia-mediated neurotoxicity: uncovering the molecular mechanisms. *Nat Rev Neurosci*. (2007) 8:57–69. doi: 10.1038/nrn2038
14. Togo T, Akiyama H, Iseki E, Kondo H, Ikeda K, Kato M, Oda T, Tsuchiya K, Kosaka K. Occurrence of T cells in the brain of Alzheimer's disease and other neurological diseases. *J Neuroimmunol*. (2002) 124:83–92. doi: 10.1016/S0165-5728(01)00496-9
15. Subramanian S, Ayala P, Wadsworth TL, Harris CJ, Vandenbark AA, Quinn JF, Offner H. CCR6: a biomarker for Alzheimer's-like disease in a triple transgenic mouse model. *J Alzheimers Dis*. (2010) 22:619–29. doi: 10.3233/JAD-2010-100852
16. Michaud J-P, Bellavance M-A, Préfontaine P, Rivest S. Real-time in vivo imaging reveals the ability of monocytes to clear vascular amyloid beta. *Cell Rep*. (2013) 5:646–53. doi: 10.1016/j.celrep.2013.10.010
17. Baik SH, Cha M-Y, Hyun Y-M, Cho H, Hamza B, Kim DK, et al. Migration of neutrophils targeting amyloid plaques in Alzheimer's disease mouse model. *Neurobiol Aging*. (2014) 35:1286–92. doi: 10.1016/j.neurobiolaging.2014.01.003
18. Zenaro E, Pietronigro E, Bianca VD, Piacentino G, Marongiu L, Budui S, et al. Neutrophils promote Alzheimer's disease–like pathology and cognitive decline via LFA-1 integrin. *Nat Med*. (2015) 21:880–6. doi: 10.1038/nm.3913
19. Park SE, Georgescu A, Huh D. Organoids-on-a-chip. *Science*. (2019) 364:960–5. doi: 10.1126/science.aaw7894
20. Cho H, Hamza B, Wong EA, Irimia D. On-demand, competing gradient arrays for neutrophil chemotaxis. *Lab Chip*. (2014) 14:972–8. doi: 10.1039/C3LC50959A
21. Reátegui E, Jalali F, Khankhel AH, Wong E, Cho H, Lee J, et al. Microscale arrays for the profiling of start and stop signals coordinating human-neutrophil swarming. *Nat Biomed Eng*. (2017) 1:94. doi: 10.1038/s41551-017-0094
22. Boneschansker L, Yan J, Wong E, Briscoe DM, Irimia D. Microfluidic platform for the quantitative analysis of leukocyte migration signatures. *Nat Commu*. (2014) 5:4787. doi: 10.1038/ncomms5787
23. Jones CN, Dalli J, Dimisko L, Wong E, Serhan CN, Irimia D. Microfluidic chambers for monitoring leukocyte trafficking and humanized nano-proresolving medicines interactions. *Proc Natl Acad Sci USA*. (2012) 109:20560–5. doi: 10.1073/pnas.1210269109
24. Akiyama H, Barger S, Barnum S, Bradt B, Bauer J, Cole GM, et al. Inflammation and Alzheimer's disease. *Neurobiol Aging*. (2000) 21:383–421. doi: 10.1016/S0197-4580(00)00124-X
25. Bacher M, Deuster O, Aljabari B, Egensperger R, Neff F, Jessen F, et al. The role of macrophage migration inhibitory factor in Alzheimer's Disease. *Mol Med*. (2010) 16:116–21. doi: 10.2119/molmed.2009.00123
26. Cartier L, Hartley O, Dubois-Dauphin M, Krause K-H. Chemokine receptors in the central nervous system: role in brain inflammation and neurodegenerative diseases. *Brain Res Brain Res Rev*. (2005) 48:16–42. doi: 10.1016/j.brainresrev.2004.07.021
27. Liu C, Cui G, Zhu M, Kang X, Guo H. Neuroinflammation in Alzheimer's disease: chemokines produced by astrocytes and chemokine receptors. *Int J Clin Exp Pathol*. (2014) 7:8342–55.
28. Xia MQ, Qin SX, Wu LJ, Mackay CR, Hyman BT. Immunohistochemical study of the beta-chemokine receptors CCR3 and CCR5 and their ligands in normal and Alzheimer's disease brains. *Am J Pathol*. (1998) 153:31–7. doi: 10.1016/S0002-9440(10)65542-3
29. Song M, Jin J, Lim J-E, Kou J, Pattanayak A, Rehman JA, et al. TLR4 mutation reduces microglial activation, increases Aβ deposits and exacerbates cognitive deficits in a mouse model of Alzheimer's disease. *J Neuroinflammation*. (2011) 8:92–14. doi: 10.1186/1742-2094-8-92
30. Li K, Dai D, Yao L, Gu X, Luan K, Tian W, et al. Association between the macrophage inflammatory protein-l alpha gene polymorphism and Alzheimer's disease in the Chinese population. *Neurosci Lett*. (2008) 433:125–8. doi: 10.1016/j.neulet.2008.01.002
31. Cudaback E, Yang Y, Montine TJ, Keene CD. APOE genotype-dependent modulation of astrocyte chemokine CCL3 production. *Glia*. (2015) 63:51–65. doi: 10.1002/glia.22732
32. Tripathy D, Thirumangalakudi L, Grammas P. RANTES upregulation in the Alzheimer's disease brain: a possible neuroprotective role. *Neurobiol Aging*. (2010) 31:8–16. doi: 10.1016/j.neurobiolaging.2008.03.009
33. Lumpkins K, Bochicchio GV, Zagol B, Ulloa K, Simard JM, Schaub S, et al. Plasma levels of the beta chemokine regulated upon activation, normal T cell expressed, and secreted (RANTES) correlate with severe brain injury. *J Trauma*. (2008) 64:358–61. doi: 10.1097/TA.0b013e318160df9b
34. Li S-Q, Yu Y, Han J-Z, Wang D, Liu J, Qian F, et al. Deficiency of macrophage migration inhibitory factor attenuates tau hyperphosphorylation in mouse models of Alzheimer's disease. *J Neuroinflammation*. (2015) 12:177–11. doi: 10.1186/s12974-015-0396-3
35. Popp J, Bacher M, Kölsch H, Noelker C, Deuster O, Dodel R, et al. Macrophage migration inhibitory factor in mild cognitive impairment and Alzheimer's disease. *J Psychiatr Res*. (2009) 43:749–53. doi: 10.1016/j.jpsychires.2008.10.006
36. Alves S, Churlaud G, Audrain M, Michaelsen-Preusse K, Fol R, Souchet B, et al. Interleukin-2 improves amyloid pathology, synaptic failure and memory in Alzheimer's disease mice. *Brain*. (2017) 140:826–42. doi: 10.1093/brain/aww330

Conflict of Interest Statement: The authors declare that the research was conducted in the absence of any commercial or financial relationships that could be construed as a potential conflict of interest.

frontiers in Immunology

ORIGINAL RESEARCH
published: 01 November 2019
doi: 10.3389/fimmu.2019.02558

Meningeal Foam Cells and Ependymal Cells in Axolotl Spinal Cord Regeneration

*Nathaniel Enos, Hidehito Takenaka, Sarah Scott, Hai V. N. Salfity†, Maia Kirk, Margaret W. Egar‡, Deborah A. Sarria, Denise Slayback-Barry, Teri Belecky-Adams and Ellen A. G. Chernoff**

Department of Biology, Indiana University-Purdue University Indianapolis, Indianapolis, IN, United States

OPEN ACCESS

Edited by:
Craig Stephen Moore, Memorial University of Newfoundland, Canada

Reviewed by:
Akira Satoh, Okayama University, Japan
Emanuele D'amico, University of Catania, Italy

***Correspondence:**
Ellen A. G. Chernoff
echernof@iupui.edu

†Present address:
Hai V. N. Salfity, Division of Thoracic Surgery, Cardiothoracic Department, Duke University Health Center, Durham, NC, United States

‡*Retired, Cleveland Heights, OH, United States*

Specialty section:
This article was submitted to Multiple Sclerosis and Neuroimmunology, a section of the journal Frontiers in Immunology

Received: *30 July 2019*
Accepted: *15 October 2019*
Published: *01 November 2019*

Citation:
Enos N, Takenaka H, Scott S, Salfity HVN, Kirk M, Egar MW, Sarria DA, Slayback-Barry D, Belecky-Adams T and Chernoff EAG (2019) Meningeal Foam Cells and Ependymal Cells in Axolotl Spinal Cord Regeneration. Front. Immunol. 10:2558. doi: 10.3389/fimmu.2019.02558

A previously unreported population of foam cells (foamy macrophages) accumulates in the invasive fibrotic meninges during gap regeneration of transected adult Axolotl spinal cord (salamander *Ambystoma mexicanum*) and may act beneficially. Multinucleated giant cells (MNGCs) also occurred in the fibrotic meninges. Actin-label localization and transmission electron microscopy showed characteristic foam cell and MNGC podosome and ruffled border-containing sealing ring structures involved in substratum attachment, with characteristic intermediate filament accumulations surrounding nuclei. These cells co-localized with regenerating cord ependymal cell (ependymoglial) outgrowth. Phase contrast-bright droplets labeled with Oil Red O, DiI, and DyRect polar lipid live cell label showed accumulated foamy macrophages to be heavily lipid-laden, while reactive ependymoglia contained smaller lipid droplets. Both cell types contained both neutral and polar lipids in lipid droplets. Foamy macrophages and ependymoglia expressed the lipid scavenger receptor CD36 (fatty acid translocase) and the co-transporter toll-like receptor-4 (TLR4). Competitive inhibitor treatment using the modified fatty acid Sulfo-N-succinimidyl Oleate verified the role of the lipid scavenger receptor CD36 in lipid uptake studies *in vitro*. Fluoromyelin staining showed both cell types took up myelin fragments *in situ* during the regeneration process. Foam cells took up DiI-Ox-LDL and DiI-myelin fragments *in vitro* while ependymoglia took up only DiI-myelin *in vitro*. Both cell types expressed the cysteine proteinase cathepsin K, with foam cells sequestering cathepsin K within the sealing ring adjacent to the culture substratum. The two cell types act as sinks for Ox-LDL and myelin fragments within the lesion site, with foamy macrophages showing more Ox-LDL uptake activity. Cathepsin K activity and cellular localization suggested that foamy macrophages digest ECM within reactive meninges, while ependymal cells act from within the spinal cord tissue during outgrowth into the lesion site, acting in complementary fashion. Small MNGCs also expressed lipid transporters and showed cathepsin K activity. Comparison of ^{3}H-glucosamine uptake in ependymal cells and foam cells showed that only ependymal cells produce glycosaminoglycan and proteoglycan-containing ECM, while the cathepsin studies showed both cell types remove ECM. Interaction of foam cells and ependymoglia *in vitro* supported the dispersion of ependymal outgrowth associated with tissue reconstruction in Axolotl spinal cord regeneration.

Keywords: foam cells, foamy macrophages, ependymal cells, meningeal fibrosis, spinal cord regeneration, axolotl regeneration, lipid uptake, myelin uptake

INTRODUCTION

This research examines a previously unidentified phenomenon in spinal cord regeneration involving the accumulation of foamy macrophages in fibrotic meninges during amphibian spinal cord regeneration. In the transected spinal cord, during gap regeneration, of the adult Axolotl (an aquatic salamander, *Ambystoma mexicanum*) foamy macrophages took up lesion site lipids and myelin while degrading ECM. These innate immune system cells were also found in close association with Axolotl ependymal cell (ependymoglial) outgrowth that remodels the cord following injury. The interaction of foamy macrophage with ependymal cells *in vitro* modified ependymal cell behavior related to mesenchymal outgrowth.

The role of ependymal cells has been investigated extensively in urodele spinal cord regeneration. Studies include ependymal growth factor and retinoid responses, ECM formation and removal, cytoskeletal changes, remodeling of radial processes and epithelial to mesenchymal transition, association with axonal outgrowth, stem cell properties and neurogenesis, and dorsal-ventral patterning of the regenerating cord (1–17). The role of a meningeal reaction in urodele spinal cord regeneration has a far less extensive body of work (5, 12, 13). The present research explores aspects of the urodele spinal meninges response complementary to the earlier studies.

Meningeal fibrosis occurs after penetrating spinal cord injury (SCI) in urodele amphibians (newts and salamanders), as it does in mammals [rev. (10, 15)]. Penetrating mammalian SCI induces a meningeal (fibrotic) scar that inhibits axonal regrowth directly and reinforces the astrocytic (gliotic) scar (18, 19). This dual scarring process forms a permanent barrier to axonal regrowth. In urodeles, fibrotic meninges is remodeled and excluded to the periphery of regenerating cord, a process that involves ependymal outgrowth and digestion of extracellular matrix (10, 12, 15, 20). Stensaas (5) and Zukor et al. (12) showed an intimate association of reactive meninges with multiple cell types in transected newt spinal cord. Reactive newt meninges and cord outgrowth were shown to contain macrophages that contact regenerating neurons and ependymoglia during the regenerative process (12).

Foamy macrophages, also known as foam cells, foamy phagocytes or foamy histiocytes, are of monocyte origin and distinguished by the "foamy" appearance of their extensive lipid inclusions in histological preparations (21, 22). They can fuse into "osteoclast-like" MNGCs (21, 23, 24). Foamy macrophages can serve as sinks for lipoproteins and myelin fragments in pathological neural conditions, such as multiple sclerosis (21, 25–27). They can be, at least transiently, beneficial in this pathology (22, 27).

Foamy macrophages form from monocyte-derived M2-macrophage (anti-inflammatory macrophage) precursors (26, 28, 29). Features of foam cells *in vivo* and *in vitro* include: clusters of lipid inclusions that are phase contrast bright, stain with Oil Red O or the indocarbocyanine dye DiI, production of the cysteine proteinase cathepsin K, activity of the lipid scavenger receptor CD36, uptake of oxidized low density lipoprotein (Ox-LDL), and uptake of myelin fragments. These features are characteristic of live cell lipid droplets, foam cells and osteoclast-like MNGCs derived from foam cells (21, 25–27, 30–33).

In mammalian SCI, foamy macrophages form only within injured spinal cord tissue, where they take up myelin and contribute to a pro-inflammatory environment (34). Accumulation of foamy macrophages has not been shown within injured mammalian spinal meninges (34, 35). Macrophages have been described within injured salamander spinal cord, as well, and many immune responsive genes are upregulated shortly after Axolotl SCI (12, 36, 37). However, foamy macrophages have not previously been reported in salamander cord or meninges.

Uptake of the toxic lipid metabolites after neural injury can be approximated *in vitro* by uptake of Ox-LDL (38). A common lipid transport mechanism involved in the uptake of Ox-LDL uses CD36, a class B scavenger receptor/fatty acid translocase (25, 39). In atherosclerosis and other pathological conditions, CD36 and Toll-like Receptor-4 (TLR4), along with TLR6, act together in lipid uptake and inflammatory behavior (40). CD 36 is also involved in fusion of macrophages to form MNGCs (23, 24). These studies suggest the use of an Ox-LDL uptake model and examination of the role of CD36 in Axolotl meningeal foam cell lipid transport.

In many neural pathologies, foamy macrophages and MNGCs also take up myelin sheath products by phagocytosis. Myelin debris persists for extended periods in mammalian spinal cord lesion sites and is sequestered in macrophages (41, 42). Extensive myelin fragment uptake by foamy macrophages occurs within active and chronic-active plaques in the CNS in multiple sclerosis (25–27, 43). In animal models of amyotrophic lateral sclerosis, foamy macrophages are involved in myelin uptake during Wallerian degeneration in the peripheral nerves, associated with loss of axons and neuromuscular synapses (44–46). In Charcot-Marie-Tooth disease, a group of peripheral nervous system (PNS) demyelinating disorders, foamy macrophages with myelin inclusions are found next to poorly myelinated or demyelinated axons (47). Foamy, myelin-containing macrophages are also found in association with peripheral nerve degeneration in aging mice (48). In some of these pathologies the literature is contradictory on the pro-inflammatory or anti-inflammatory nature of the foam cells involved in this processes, depending on the type of experimental system, stage of disease or the markers examined (27, 46, 47, 49–51). The question whether these foam cell effects are beneficial or harmful is even more complex. The work presented here showed uptake of myelin *in situ* and *in vitro* similar to that in seen in mammalian neural pathologies.

A third critical property of foamy macrophages in the nervous system, in addition to oxidized lipoprotein and myelin uptake, is their ability to degrade ECM (32). This process appears to be universal in foamy macrophages and occurs in osteoclast-like MNGCs associated with atherosclerosis and MNGC tumors (52, 53). Foamy macrophages and MNGCs digest ECM using cathepsin K and MMP9 as major secreted proteolytic factors (32, 52–55). Secreted proteases can be concentrated on the matrix within the sealing ring, a set of cytoskeletal and membrane specializations also seen in osteoclasts (24, 32). The examination of foamy macrophage and ependymal cathepsin K expression extends our prior studies of matrix proteinase activity from

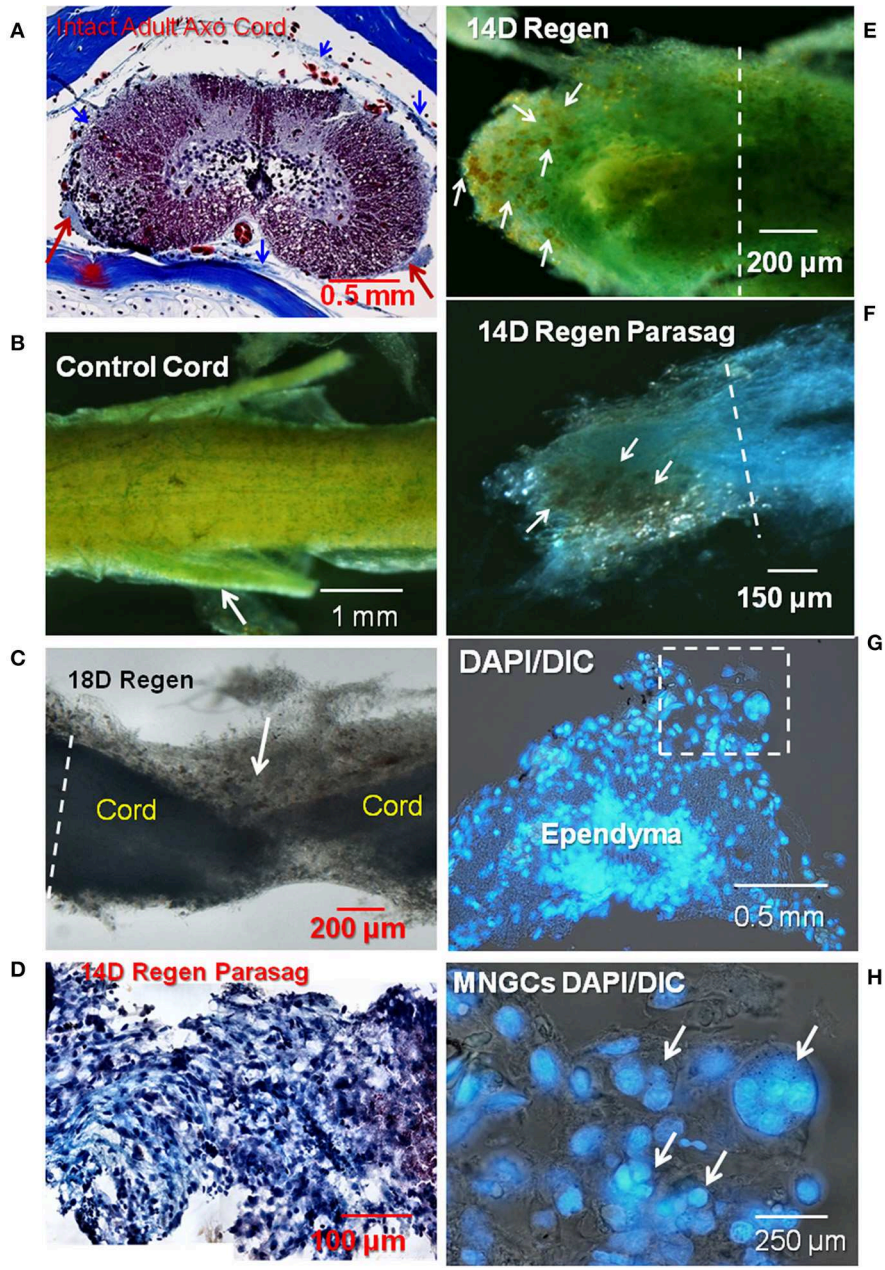

FIGURE 1 | Collagen and proteoglycan stains in regenerating and control adult axolotl spinal cord. **(A)** A cross-section of intact adult axolotl spinal cord labeled with trichrome stain. Red arrows show denticulate ligaments, a pial extension stained with aniline blue (collagen). Thin meningeal layers are present, collagen stained blue (blue arrowheads). **(B)** Spinal cord wholemount labeled with mentanil yellow (collagen) and alcian blue (acidic proteoglycans). Arrow shows a nerve root. **(C)** Unstained lesioned cord regenerated for 18 days, backlit stereoscopic view. Arrow shows a mass of ECM that joins the proximal and distal regenerating stumps. **(D)** Parasagittal paraffin section through 14D regenerating cord stained with trichrome. **(E)** Mentanil yellow and alcian blue label in 14D regenerating cord. The arrows indicate lipid-laden cells that appear orange against the stained ECM. **(F)** Regenerating spinal cord stained with alcian blue and the tissue dissected in the parasagittal plane. Lipid-laden cells in the fibrotic ECM are indicated by arrows. **(G)** Paraffin sections of a regenerating 14D cord with DAPI nuclear label. Stump region with reactive meninges. Dashed square indicates area at higher magnification in **(H)**. **(H)** DAPI-labeled nuclei in 14D regenerating cord. Arrows show a group of multinucleated cells present in the meninges. The white dashed lines in **(C,E,F)** indicate the site margin of harvested tissue for explants culture. Axo, axolotl; Regen, regenerating; Parasag, parasaggital; D, day; DIC, differential interference contrast. Magnification bar is shown in the lower portion of each image.

ependymal cells in Axolotl spinal cord regeneration by Chernoff et al. (20).

The studies reported here characterize distribution and functionality of foamy macrophages and some MNGCs in the injury-reactive Axolotl spinal cord meninges, starting at the histological level. In transected adult Axolotl body-region (non-tail) cord, transmission electron microscopic (TEM) morphological studies, plus collagen and proteoglycan staining,

show that interstitial meningeal ECM fills the lesion site and wraps the regenerating transected stumps. DiI labeling identify lipid-laden mononucleated cells attached to the fibrotic meningeal ECM. Within the lesion site, lipid-laden and multinucleated cells share ECM-filled space with the reactive ependymal cells that grow out from the spinal cord. Transmission electron microscope (TEM) studies show co-localization of foamy macrophages and reactive ependymal cells within lesion site fibrillar collagen. A primary tissue culture system uses lipid stains to identify neutral and polar lipids. Functional studies indicate that the foamy macrophages and some associated MNGCs take up lipid via the scavenger receptor CD36, co-expressed with toll-like receptor 4 (TLR4), and produce cathepsin K.

Our studies are the first to indicate that foamy macrophages are present in reactive Axolotl spinal cord meninges and participate in spinal cord regeneration.

METHODS AND MATERIALS

Surgery and Tissue Culture

Surgery

Axolotls were obtained from the Ambystoma Genetic Stock Center, University of Kentucky and maintained at 20–22°C in 20% Holtfreter's Salts Solution. Transdermal anesthetic tricaine methane sulfonate (Finquel; Syndel, Formerly Western Chemical) was used in 20% Holtfreter's Salts Solution, with thimerosal for disinfection of the surgical field (5 ml/L of a 20 g/L 88% ethanol thimerosal stock), adjusted to pH 7 with sodium bicarbonate. Finquel concentration was adjusted for the size of the animal. Animals were anesthetized in 0.5 g/l Finquel for adult; >20 cm, 2–3 years old; 0.3 g/L for juveniles; 10–15 cm, 6 months old. Before surgery, animals were injected with the antibiotic Amikacin (2.5 mg/ml, 0.75 ml for an adult; 0.5 ml for a juvenile). The lesioning procedure is described in detail in Chernoff et al. (56) and will not be repeated here. Post-surgically, lesioned-cord animals were treated in 20% Holtfreter's solution at 12°C in a BOD incubator for 3 days, with daily water changes and amikacin injections, then kept at 20–22°C in the vivarium through the regeneration process. All husbandry, surgery, analgesia, and euthanasia was performed following the IUPUI School of Science IACUC approved protocol SC 280R.

Tissue Culture

For these experiments sets of four to six animals, either sex, age matched, but any color morph, were lesioned. Explants were isolated following the procedure described in Chernoff et al. (56) and O'Hara and Chernoff (6). Two weeks outgrowth (see dashed lines in **Figure 1**) was isolated, cut to size and cultured on poly-D-lysine/fibronectin-coated dishes. Explants were divided among 2–3 dishes. Each experiment was repeated at least three times. Culture contained Leibovitz L-15 medium, 5 mM Hepes Buffer, and progesterone 20 nM. Finally a stock solution containing 5 μg/ml insulin, 100 μg/ml transferrin, 100 μM putrescine, and 30 nM selenium was added (Sigma Chemical). EGF 20 ng/ml, 1% axolotl serum, and 1% Pen-Strep/Fungizone (Gibco) was added to L-15 medium, which was used for the cultures. pH was adjusted to 7.6.

Culture Dish Preparation

Thirty-five millimeter polystyrene tissue culture dishes were coated with 100 μg/ml poly- D -lysine in HEPES-buffered saline solution, pH 7.4. The dishes were incubated at 37°C for at least 30 min, then rinsed twice with HEPES buffered saline pH 7.4. Fibronectin (75 μg/ml) was added to each dish and incubated at 37°C for 1 h and rinsed with HEPES buffered saline. HEPES buffered saline contains 0.01 M HEPES, 0.01 M KCl, and 0.013 M NaCl in water, adjusted to pH 7.4. The dishes were rinsed with medium prior to addition of explants.

Histological Stains

Wholemount

Animals were anesthetized and 3 cm spinal column segments were excised fixed in 4% paraformaldehyde, pH 7.4 on a rocker platform at room temperature for 20 min, then overnight at 4°C. After rinsing in Hanks' BSS, the tissue was incubated for 1 day in 0.5% neutral calcium chelator EGTA to soften bone, rinsed in HBSS and the spinal cord removed.

To identify the ECM collagen and proteoglycan wholemount segments of axolotl spinal cord were stained. Proteoglycan was stained with alcian blue alone. Collagen and proteoglycan were co-stained with metanil yellow and alcian blue. Samples were stained in alcian blue for 5 min, and in metanil yellow for 1 min. After staining, samples were rinsed briefly in three changes of 10% ethanol for 5 min to remove excess dye.

All samples were viewed and photographed in their whole-mount state using a Nikon stereomicrocope and photographed using a Nikon DXM-F digital camera system.

Trichrome Stain

Slides with paraffin sections were deparaffinized in xylene, twice for 5 min each. The slides were then placed in decreasing concentrations of ethanol, then distilled water for 30 s at each step. Deparaffinized slides were stained using Weigert's iron hematoxylin, followed by Biebrich scarlet-acid fuchin and phosphotungstic/phosphomolybdic acid following kit instructions (Sigma Chemical Co.). Slides were then soaked for 5 min in aniline blue. After the finally staining step, the slides are placed in 1% acetic acid for 2 min, twice, then rinsed in distilled water for 5 min, twice. Finally, slides are dehydrated and cleared in increasing concentrations of ethanol and finally xylene for 10 min in each solution. Histomount (Pella) permanent mounting medium is then used to mount the slides.

Transmission Electron Microscopy

Animals were anesthetized and either perfused, or spinal cord segments were fixed *in situ* for several minutes in cacodylate-buffered tri-aldehyde fixative (57). Tissue was removed and fixation continued in Kalt's fixative for 24 h. Tissue was post-fixed in buffered 2% osmium tetroxide, dehydrated, and embedded in araldite epoxy resin. Plastic-embedded tissue was sectioned on a Porter-Blum MT-2 ultra-microtome with glass knives for 1-micron sections, or with a diamond knife for thin sections.

Thick sections were collected on glass slides and stained with 1% toluidine blue. Thin sections (50–80 nm) were made at selected intervals, collected on bare grids or on Padget-film-supported-1-hole grids, stained with lead-citrate, and examined with a Tecnai G2 12 Bio Twin (FEI, Hillsboro, OR) equipped with AMT CCD Camera (Advanced Microscopy Techniques, Danvers, MA). Two older images were obtained using a Philips 400 transmission electron microscopy.

Actin Staining

Samples were fixed in 4% paraformaldehyde in HBSS for 20 min. Fixative was rinsed out with multiple changes of Hanks' Balanced Salts Solution (HBSS) pH 7.6. Cultures were permeabilized for 5 min with 0.1% Triton-X-100 in HBSS. Wholemount samples were permeabilized for 10 min. Triton-X-100 was removed with three 5 min distilled water rinses. Rhodamine-Phalloidin (Invitrogen) stock was prepared in methanol as directed, diluted 1:200 into the sample buffer and used at a concentration of 1.5 units/ml. Cultures were incubated for 10 min and wholemount samples were incubated for 20 min, then rinsed in HBSS twice, 10 min each. HBSS was removed and DAPI/antifade (Invitrogen) added to cover the samples in small culture dishes, which were coverslipped and viewed.

Lipid Labels and Inhibitor

DiI Staining

Cell cultures were fixed with 4% paraformaldehyde at room temperature for 20 min, rinsed in HBSS, then incubated with DiI (1 mg/ml in 100% ethanol) for 15 min. Dishes were rinsed briefly in ethanol to remove unbound DiI. Cultures were incubated in HBSS for 1 h to allow DiI to partition from membranes to lipid droplets. Antifade with DAPI (Invitrogen) was added, cultures coverslipped and viewed with a Nikon Eclipse TE 2000-U inverted phase contrast and fluorescence microscope.

Oil Red O Staining

For neutral lipid staining, a stock solution of Oil Red O (Sigma Aldrich) was prepared by dissolving 0.25 g/40 ml of 2-propanol. Solution was warmed at 37°C to dissolve the dye. Before use, a 3:2 dilution of the dye/propanol was made with water and 0.22 micron filtered. Working solution was prepared immediately before use. Cultures were fixed in paraformaldehyde, rinsed in HBSS, then water. After a brief rinse with 60% 2-propanol the working dye solution was added for 1–2 min. Staining was observed on an inverted microscope. Dye was removed, dishes briefly rinsed once with 60% 2-propanol then distilled water (10 min) and digital images captured.

Polar Lipid Live Stain

To visualize neutral and polar lipids together, the DyRect Live-Cell Neutral Lipid Imaging Kit (Marker Gene Technologies, Inc.) was used. In this live foam cell stain, neutral lipids fluoresce green and polar lipids fluoresce red. The green fluorescence overlaps with green autofluorescence in our cells, so only the polar lipid staining properties were useful. DyRect reagent was reconstituted in ethanol at 1 mg/ml and diluted to 1 μg/ml in culture medium immediately before use. The dye-medium containing cultures were incubated at room temperature for 1 h, rinsed in HBSS and imaged live.

Ox-LDL Uptake

DiI-labeled Ox-LDLs (Invitrogen L3482) were diluted to 25 ug/ml in E3 medium (see Axolotl Tissue Culture section for composition) and applied to cultures for 24 h. The cultures were rinsed with HBSS and fresh medium was applied before observation via fluorescence microscopy.

CD36 Inhibition

CD36 inhibition medium was created by adding sulfo-N-succinimidyl oleate to E3 medium at a final concentration of 100 uM. Culture dishes were incubated with the CD36 inhibition media for 24 h, then DiI labeled Ox-LDLs (25 ug/ml) were added to the dish for 24 h incubation. Culture dishes were rinsed with HBSS, and fresh E3 media was added before observation under fluorescence microscopy.

Glucosamine Uptake, Autoradiography

For glucosamine uptake experiments, explant cultures were established and grown for 6 days. Five μCi (185 μBq) of D-[6-^{3}H(N)]-glucosamine (Perkin-Elmer) was added per ml of E3 medium and the cultures were incubated for 24 h. Labeled medium was removed and cultures rinsed three times in HEPES buffered saline, fixed in ice-cold 5% acetic acid in ethanol for 10 min at 4°C, rinsed three times with 100% ethanol, and air dried. The dry plates were coated with 0.5 ml Kodak-NB2 nuclear tracking emulsion (Eastman Kodak Co) and allowed to expose for 2 weeks at 4°C in a light-tight box containing desiccant. After 2 weeks the plates were brought to room temperature, developed with Kodak D-19 developer for 10 min at room temperature, rinsed, fixed with Kodafix (diluted 1: 3) for 10 min, rinsed again, and allowed to air dry. Coverslips were applied to the dishes with Histomount permanent mounting medium (Ted Pella).

Immunohistochemistry

Paraffin Sections

Dissected tissues were fixed in 4% paraformaldehyde in HBSS, pH 7.6, at 4°C for at least 1 h, rinsed in HBSS and dehydrated in a graded ethanol series, followed by two xylene rinses, paraffin penetration and paraffin embedding. The sections were cut to 10 μm thickness by microtome and "baked" at 60°C overnight onto Superfrost/Plus Microscope glass slides (Fisher). After deparaffinizing and rinsing with PBT (phosphate-buffered saline, PBS, plus 0.1% Tween-20), the sections were placed in 90°C 0.01 M citrate buffer (pH 6.0) for 10 min, for post-fixation antigen recovery, unless otherwise noted. Sections were then treated with blocking buffer as follows: PBT with 10% normal goat serum (NGS), diluted 1:1 with Superblock (Pierce Chemical). Primary antibody was added in HBSS and incubated overnight at 4°C. After rinsing three times with HBSS, sections were incubated with Alexa Fluor 594 secondary antibody (1:2,000, Invitrogen) for 2 h at room temperature. CD36 antibody (R&D Systems MAB25191) was diluted to 2.5 ug/ml. After washing with HBSS twice, sections were mounted in SlowFade Gold antifade reagent with DAPI as the nuclear counterstain (Invitrogen) and

coverslipped. Specimens were observed with a Nikon Eclipse E800 fluorescence/DIC microscope.

Cell Cultures

Culture dishes were fixed with 4% paraformaldehyde for 30 min at room temperature and rinsed three times with HBSS before incubation in SuperBlock blocking buffer in PBS (Thermo). Dishes were rinsed three times with HBSS, and the appropriately diluted primary antibody applied and incubated overnight. Then dishes were rinsed three times with HBSS, and Alexa Flour 595 secondary antibody was applied and incubated for 2.5 h, rinsed three times with HBSS, mounted in SlowFade Gold antifade reagent with DAPI and coverslipped. Specimens were observed with a Nikon Eclipse TE 2000-U inverted phase contrast and fluorescence microscope or a Keyence BZ-X Fluorescence, phase, DIC Microscope. TLR4 polyclonal Ab (Novus Bio NB100-56580SS) and TLR4 polyclonal Ab (Novus Bio NB100-56581SS) were diluted to 5 ug/mL in HBSS. CD36 Ab (R&D Systems MAB25191), and CD36 Ab (Novus Bio NB400-145SS) were diluted to 2.5 ug/mL in HBSS. Cathepsin K Ab (Abcam ab19027) was applied at 1:75 dilution in HBSS (antibody information shown in table form in **Supplemental Figure 1**).

Myelin Experiments

Extraction and Labeling

Twelve axolotl brains were isolated and homogenized in a 0.32 M sucrose solution with a sterile plastic pestle in 1.5 ml microcentrifuge tubes. The homogenate was layered over a 0.8 M sucrose solution and centrifuged at a G-force of 16,000 (Sorvall Biofuge Pico, radius = 8.5 cm, 13,000 rpm) for 15 min. The myelin was collected at the interface of the two sucrose solutions. 1,1′-dioctadecyl-3,3,3′3′-tetramethylindocarbocyanine perchlorate (DiI) in ethanol (1 mg/mL) was applied to the myelin extract and incubated for 30 min at RT. The labeled myelin extract was rinsed three times with HBSS to remove any unbound DiI.

Endogeneous Myelin Staining

Fluoromyelin Red (Fisher F34652) was added at 1/300 dilution in HBSS to fixed cultures and incubated for 40 min then rinsed in HBSS. DAPI and antifade (Invitrogen) was added to the dishes and coverslipped. Cultures were imaged with fluorescence microscopy.

Myelin Uptake

DiI-labeled myelin extract (100 μL/2 ml culture medium) was added to the 35 mm dish cultures and incubated for 48 h. Dishes were rinsed with HBSS and new E3 media added before cultures were observed by fluorescence microscopy.

Statistical Analysis

Ninety-two unique photographic fields from >16 cultured explants in untreated controls from seven separate untreated regeneration control experiments were compiled and sorted into categories of outgrowth: condensed ependymal outgrowth with no foam cells, condensed ependymal outgrowth with foam cells, dispersed ependymal cells with foam cells, dispersed ependymal cells without foam cells and mixed forms. Each form was tabulated for each of the seven experiments. Using Graphpad Prism, A one-way analysis of variance (ANOVA) with Tukey's *post-hoc* Multiple Comparisons Test was performed. In this type of analysis significance is first determined by ANOVA, then an stricter adjusted *p*-value is determined for each comparison (58).

RESULTS

Overview of Meninges, Meningeal Matrix, and Foamy Macrophages

The results provide a structural overview of the organization of reactive Axolotl meninges, fibrotic ECM and associated foamy macrophages and MNGCs. Control cords were compared with the regeneration stage when invasive meninges have produced interstitial ECM and reactive ependymal cells grow out from the central.

Figure 1A shows a trichrome stained histological cross-section of intact adult lumbar region Axolotl spinal cord. The normal meningeal layers were very thin and stain with aniline blue, indicating the presence of collagen. A stereoscopic image of a wholemount preparation of control cord was stained with metanil yellow for collagen and alcian blue for acidic proteoglycans (**Figure 1B**). The entire cord and the nerve roots are ensheathed with the collagen-containing meninges (**Figure 1B**). Small areas of alcian blue represent mainly basal lamina associated with capillaries (**Figure 1B**). Following transection, meningeal fibrosis produced a mass of interstitial ECM seen here in an unstained stereoscopic wholemount preparation (**Figure 1C**). The tapered regenerating outgrowth of the cord was embedded in the meningeal matrix. In a parasagittal paraffin section, the trichrome stain showed a large amount of aniline blue-stained fibrillar collagen with cells interspersed (purple) across the lesion site (**Figure 1D**). The violet material on the right was associated with a fibrin clot.

One bulbous end of a 2-weeks regenerating cord showed several features (**Figure 1E**). An extensive amount of alcian blue-stained sulfated proteoglycan-containing ECM overlayed metanil yellow-stained fibrillar collagen-containing ECM. This meningeal investment of the regenerating cord stump showed numerous dark orange cells on the ECM (arrows). This appearance reflected the large amount of yellowish lipid seen against the stained ECM. In regenerating spinal cord labeled solely with alcian blue and dissected in a parasagittal plane, the lipid-laden cells were found throughout the fibrotic ECM at the tip of the regenerative outgrowth (**Figure 1F**).

Organic solvents used to embed material for sectioning extracted most of lipid present in the lipid-laden cells like those shown in **Figures 1E,F**, precluding lipid staining in paraffin sections. However, DAPI nuclear label in a cross-section of stump near the lesion site showed the presence of numerous multinucleated cells in fibrotic meninges surrounding the spinal cord in the regenerating tissue (**Figures 1G,H**).

To characterize the lipid-laden cells described in **Figure 1**, regenerating cord was labeled with the lipophilic membrane stain DiI and the fluorescent F-actin probe rhodamine-phalloidin. **Figure 2A** shows a wholemount view of unstained spinal cord

with outgrowth from one side of a transected, regenerating cord. Dark melanocytes were present on stump meninges, as they are on control cords. The dashed line shows the margin of injury-reactive material accumulated near the cut end (**Figure 2A**). A region of this regenerating outgrowth is shown in the DiI wholemount stain that follows (**Figure 2B**). DiI/DAPI labeling showed a region of lipid-containing cells concentrated in the meninges, on the regenerative outgrowth (**Figure 2B**). These lipid-laden cells were not present on the surface of the stump distant from the transection (∼2 cm from the regenerating end; **Figure 2C**). DiI staining of the distal stump showed only the white matter axonal myelin just beneath the cord surface (**Figure 2C**).

Rhodamine-phalloidin labeling for F-actin showed a small group of MNGCs on the reactive meninges of another lesioned cord (**Figure 2D**). The distinctive podosome actin dots of the sealing ring were seen around the margin of the MNGCs, along with regions of the more interior ruffled border (**Figure 2D**). These structures were localized to the margins of spread MNGCs, like that shown in lesion site outgrowth *in vitro* (**Figure 2E**). The outgrowth shown in **Figure 2E** was from a distal end region of the regenerating cord like that shown in **Figure 2A**.

Fine-structural detail of ECM, ependymal cells, foam cells and MNGCs in regenerating Axolotl cord was obtained by transmission electron microscopy (TEM). A toluidine blue-stained plastic thick section of a 2-weeks lesion site showed an overview of a lesion site examined by TEM (**Figure 3A**). A MNGC, in which nuclei were visualized through several sections, is circled with a dashed yellow line. TEM examination of this area showed juxtaposition of the MNGC, ependymal cells and foam cells (**Figure 3B**, enlarged area **Supplemental Figure 2**). At increased magnification, masses of vimentin intermediate filaments were seen around one of the MNGC nuclei [**Figure 3C**; (59)]. An enlargement of the zone of intermediate filaments is shown in **Supplemental Figure 2B**. The dark structure next to the MNGC appeared to be a telopode [**Figure 3C**; (60)].

Figure 3D shows a higher magnification view of an area between foam cells and ependymal cells. A large amount of fibrillar collagen was present and appeared to be in the process of engulfment (**Figure 3D**). **Figures 3E,F** shows a foam cell among meningeal cells, deeper in the lesion site. Fibrillar collagen was absent from this zone. Other white blood cells are found within the 2 weeks regenerate lesion site: **Supplemental Figures 3A,B** show a macrophage engulfing red blood cells and a lymphocyte among ependymal and meningeal cells (61, 62).

Later in the regeneration process ependymal outgrowth re-epithelializes to reform the central canal, re-extend radial processes, re-form endfeet and form channels through which regenerating axons extend (2, 5, 10). **Figure 4** shows the 4–5 weeks period of regeneration at which the regenerating ends of the cord had met and axonal regrowth is underway to restore the full thickness spinal cord. In **Figure 4A**, a trichrome-stained paraffin cross-section of a 5 weeks regenerate lesion site shows an asymmetrical regenerate with enlarged central canal. The meninges were excluded to the periphery and were still highly reactive, filling the entire space between the regenerating cord and neural arch and vertebral body. **Figure 4B** shows a higher magnification view of a section like **Figure 4A**. The enlarged central canal contained extruded cellular material. The collagenous denticulate ligament (arrow) was adjacent to the regenerating cord. This is significant because the denticulate ligament is an extension of the *pia mater*, and indicated pial restoration around the regenerating cord. A toluidine-stained plastic section showing a cross-section of a proximal stump from a 4 weeks regenerating cord showed the reactive meninges adjacent to the white matter (**Figure 4C**). This region contained a denticulate ligament profile, comparable to **Figures 4A,B**. The reactive meninges contained foamy cells and a variety of white blood cells and meningeal cells (**Figure 4C**).

Ependymal and Foamy Macrophage Lipid Content and Uptake

The presence of neutral and polar lipid in both ependymal cells and foamy macrophages was shown by using Oil Red O stain for neutral lipid, and DiI staining and DyRect, a proprietary stain, for polar lipids. CD36 was identified as a significant lipid transporter in these cells, in association with TLR4, through antibody localization *in vivo* and *in vitro* and treatment with a CD36 inhibitor *in vitro*. Exposure to DiI-labeled Ox-LDL showed the capacity for additional uptake of Ox-LDL *in vitro* in foamy macrophages.

Neutral and Polar Lipids

When 14D regenerating spinal cord outgrowth was placed in culture, accumulation of small lipid droplets in phase contrast images of live ependymal outgrowth, and a larger mass of lipid in foamy macrophages can be clearly seen (**Figure 5A**). The fluorescent lipophilic cationic indocarbocyanine dye, DiI, is used here as a direct lipid probe. The amount of DiI stained foamy macrophage lipid was greater, and lipid droplets generally larger, than that in ependymal cells, but both cell types were labeled (**Figure 5B**). To examine the presence of neutral lipids, Oil Red O staining was performed. Oil Red O stains both ependymal cells and foamy macrophages showing that some of the lipid in both cell types was neutral lipid (**Figures 5C,D**). At higher magnification both labeled and unlabeled lipid droplets can be seen in foamy macrophages and ependymal cells (**Figures 5C,D** insets).

Identification of the types of lipid labeled by DiI has never been clear, beyond its known intercalation behavior into cell membrane phospholipid layers (63). While this implies an affinity for polar lipids, the targets are not certain. To further explore polar lipid content, a proprietary polar lipid label was applied to live cultures. Ependymal and foam cells both showed polar lipid content (DyRect Kit; **Figures 5E,F**). The polar lipid label showed strong overlap with the DiI staining, suggesting polar lipid components were detected by DiI in our cells. In addition to mononucleated foamy macrophages, small MNGCs with lipid also stained strongly for polar lipids (**Figure 5F**). The **Figure 5F** inset indicates the location of 4 nuclei. Nuclear counterstaining was not possible because this was a live cell labeling process and cells could not be permeabilized. The neutral lipid staining properties of the DyRect reagent were not useable in the Axolotl cells. The neutral lipid probe fluorescence overlapped too

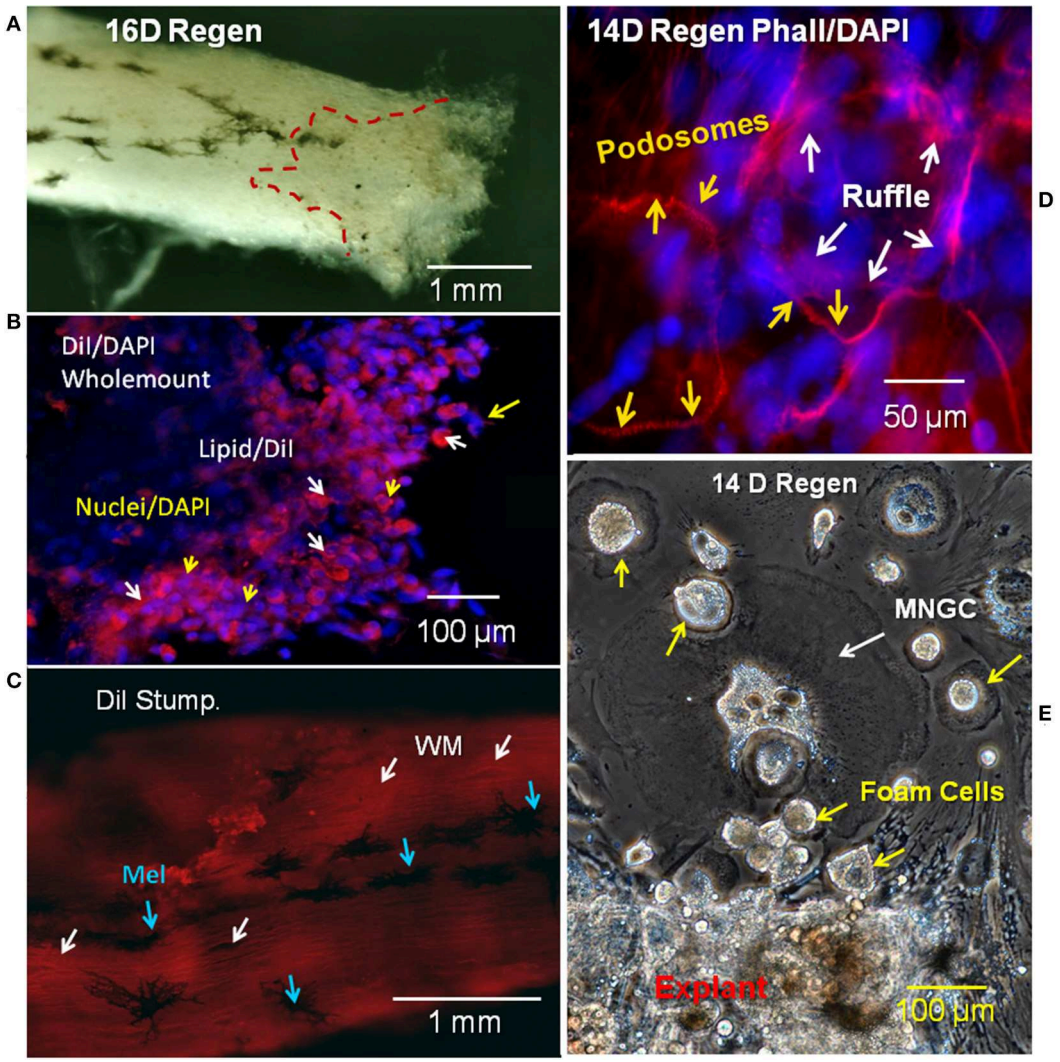

FIGURE 2 | Regenerating cord meninges MNGCs and foam cells. **(A)** Red dashed lines shows the region of regenerating outgrowth with lipid-laden cells in one side of a 16D spinal cord regenerate. **(B)** Lesioned wholemount cord from 16D regenerating cord dual-labeled with DiI (red/lipid) and DAPI (blue/nuclei). Lipid-laden cells are clustered near the regenerating end. White arrows show cells labeled with DiI and yellow arrows show labeled nuclei. **(C)** Image near the surface of 16D wholemount distal stump of a regenerating cord labeled with DiI. White arrows show white matter in axonal tracts, while blue arrows indicate surface melanocytes. **(D)** Regenerating 14D spinal cord wholemount labeled with rhodamine phalloidin (red/actin) and DAPI (blue/nuclei). Podosomes labeled with rhodamine phalloidin (yellow arrows) can be seen surrounding the nuclei of MNGCs. The ruffled border is indicated by white arrows. **(E)** Phase contrast image of unlabeled outgrowth from a 14D regenerate in culture 11 days. MNGCs were detected in the outgrowth (white arrows), in addition to foam cells (yellow arrows). Regen, regenerating; wm, white matter; mel, melanocyte; MNGC, multinucleated giant cells; DIV, days *in vitro*. Magnification bar is shown in the lower portion of each image.

strongly with green autofluorescence and was of no utility (see **Supplemental Figure 4**).

Lipid Transporters

The fatty acid translocase/lipid scavenger receptor CD36 is the best candidate for lipid transport in the injured Axolotl spinal cord based on foamy macrophage behavior in other tissues (25). An antibody was identified that reacted with CD36 in paraffin-embedded Axolotl tissue and *in vitro*. In other sources of foam cells, TLR4 co-localizes with CD36 and assists in the lipid transport process, so TLR4 localization was also examined (40). A combination of two TLR4 antibodies to different TLR4 sites was identified that reacts with strongly Axolotl cells *in vitro*, and was effective in paraffin sections.

In intact adult Axolotl spinal cord sections, the lipid scavenger receptor CD36 was seen in the ependymal endfeet and in small zones of the ependymal cell bodies (**Figures 6A,B**). In the proximal stump region of the lesioned spinal cord, CD36 was expressed in the reactive meninges, as well as the ependymal cells (**Figures 6C,D**). *In vitro*, CD36 was strongly expressed by foamy macrophages and small MNGCs (**Figures 6E** inset). Reactive ependymal cells retained CD36 expression *in vitro*, as well (**Figure 6F**).

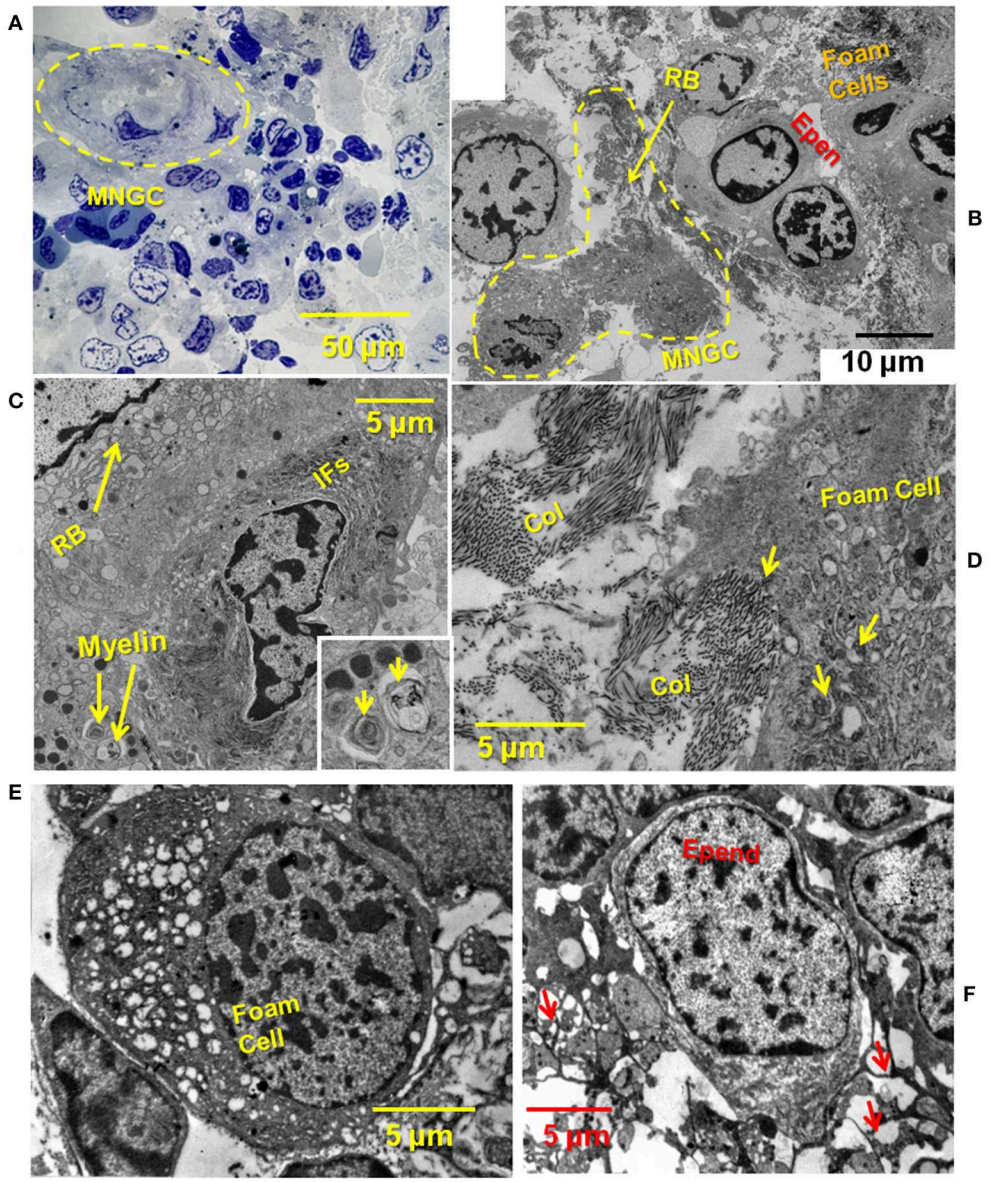

FIGURE 3 | TEM showing close relationship between MNGC, ECM, ependymal cells, and foam cells. **(A)** Thick section of plastic embedded 2-weeks spinal cord regenerate outgrowth stained with toluidine blue. Yellow dashed circle surrounds MNGC. **(B)** Thin section TEM of lesion site shown in **(A)**. A portion of the MNGC is circled in yellow (dashed line). Arrow indicates portion of the ruffled border. Foamy macrophages and ependymal cells are present. **(C)** A portion of the ruffled border, and perinuclear intermediate filaments are shown. Engulfed myelin fragments are present within the cytoplasm. Engulfed myelin enlarged in inset (arrows) **(D)** Foamy macrophage engulfing fibrillar collagen within the lesion site. Arrows show intracytoplasmic collagen. **(E)** Deeper within the lesion site a foamy macrophage is present among ependymal and meningeal cells. **(F)** Deeper within the lesion site an ependymal cells show a network of processes (arrows). MNGC, multinucleated giant cells; RB, ruffled border; RBC, red blood cell; Epen, ependymal cells; Ifs, intermediate filaments; Col, collagen; Mening, meningeal cell; macr, macrophage; Nucl, nucleus. Magnification bar is shown in the lower portion of each image.

Localization of CD36 in foamy macrophages was, generally, central/perinuclear and overlapped the zone of lipid droplets (**Figure 6E**). CD36 was also present in ependymal cells (**Figure 6F**).

TLR4 was expressed in both the foamy macrophages and ependymal cells (**Figures 6G,H**). The region of TLR4 localization in ependymal cells was comparable that seen for CD36 expression, but smaller that that seen in the foamy macrophages (**Figures 6F,H**). TLR4 was not detected in large, lipid droplet-free MNGCs (**Figure 6G**).

Ox-LDL Uptake *in vitro*

At the time of isolation, all lesion site foamy macrophages and ependymal cells contained lipid acquired *in situ* and both cell types expressed lipid transporters (**Figures 5**, **6**). Results shown in **Figure 7** address the ability of foamy macrophages

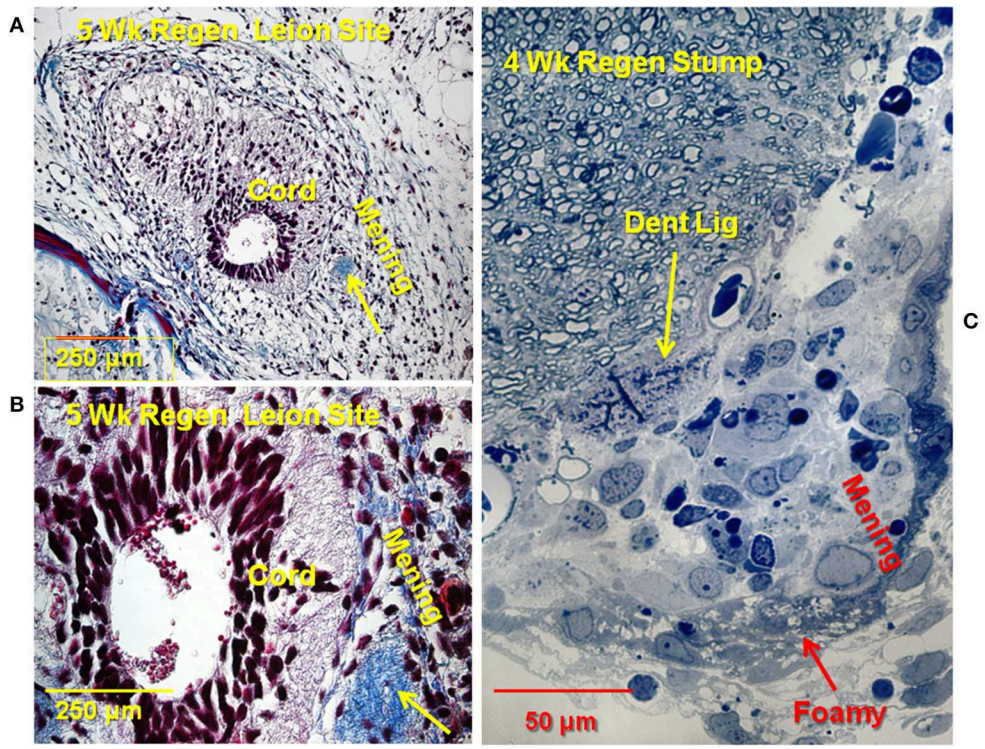

FIGURE 4 | Later stage of the lesion site: rejoined cord. **(A)** Trichrome stained section through 5 weeks regenerate lesion site. Cord is asymmetrical, with enlarged central canal, white matter not fully reconstructed. Extensive reactive meninges around the cord. Arrow: denticulate ligament. Collagen is blue. **(B)** Higher magnification view of a trichrome stained section through the 5 weeks regenerate. Extruded material visible in central canal Arrow: denticulate ligament. **(C)** Toluidine blue stained plastic thick section 4 weeks regenerate. Stump near lesion site. Reactive meninges with white blood cells and some foamy cells (red arrow), area of denticulate ligament (yellow arrow). Magnification bar shown in the lower portion of each image. Dent Lig, denticulate ligament; Mening, meninges; Wk, week.

and reactive ependymal cells to take up additional lipid *in vitro*. Explant cultures were established and exposed to DiI-Ox-LDL. A subset of foamy macrophages took up significant amounts of DiI-Ox-LDL (**Figures 7A–E**). High uptake foam cells were found migrating on the plastic dish, as well as on and under the explants (**Figures 7A,B,D,E**). The limited number of MNGCs seen in these cultures did not take up DiI-Ox-LDL (e.g., **Figure 7A**). Ependymal cells also did not take up DiI-Ox-LDL *in vitro* (**Figure 7B**). All of the foamy macrophages and ependymal cells contained extensive lipid stores (**Figures 7A–C**), so it is not clear whether those not actively transporting did so because they had reached maximum LDL content, or whether the culture conditions were not fully optimal for lipid uptake.

Functional involvement of CD36 in the *in vitro* Ox-LDL uptake was shown by combining DiI-Ox-LDL uptake with treatment using the CD36 inhibitor sulfo-N-succinimidyl oleate, a modified fatty acid (64). Typical dense DiI-Ox-LDL uptake label was seen in actively transporting control cultures (**Figure 8A**). Co-treatment with the Ox-LDL label and the oleate inhibitor reduced the area of uptake to small patches and streaks (**Figure 9B**). This inhibition of Ox-LDL uptake shows a functional role for CD36 in lipid uptake in the Axolotl spinal meninges foam cells.

Myelin Uptake

Myelin fragments produced from damaged white matter in urodele SCI are seen within lesion site cells in TEM studies [**Figure 2C**; (5, 12)]. To determine whether the foamy macrophages and/or ependymal cells were serving this function in our experimental system, the presence of myelin engulfed *in situ* (lesion site myelin uptake) was examined along with the ability of lesion site cells to take up additional myelin *in vitro*.

To avoid the enormous amount of autofluorescence found in Axolotl lesion site white matter, endogenous myelin content was assayed by staining primary cultures with fluoromyelin red. Fluoromyelin-labeling of myelin fragments taken up while *in situ*, were seen in cells within the lesion site explants (**Figure 9A**), in ependymal cells (**Figures 9A,B**) and foamy macrophages migrating on the culture dishes (**Figures 9B–D**). In areas of outgrowth showing large numbers of foam cells mixed with ependymal cells, more myelin label appeared in the foam cells (**Figure 9B**). Within a given culture there were areas of foam cells with different amounts of myelin stain (**Figures 9C,D**).

The continuing ability of lesion site cells to take up myelin fragments was also assayed *in vitro*. The probe was DiI-labeled Axolotl brain myelin. New myelin uptake was seen by cells within the explants (**Figures 10A,E,F**). In the cellular outgrowth, some zones of ependymal cells showed extensive myelin uptake

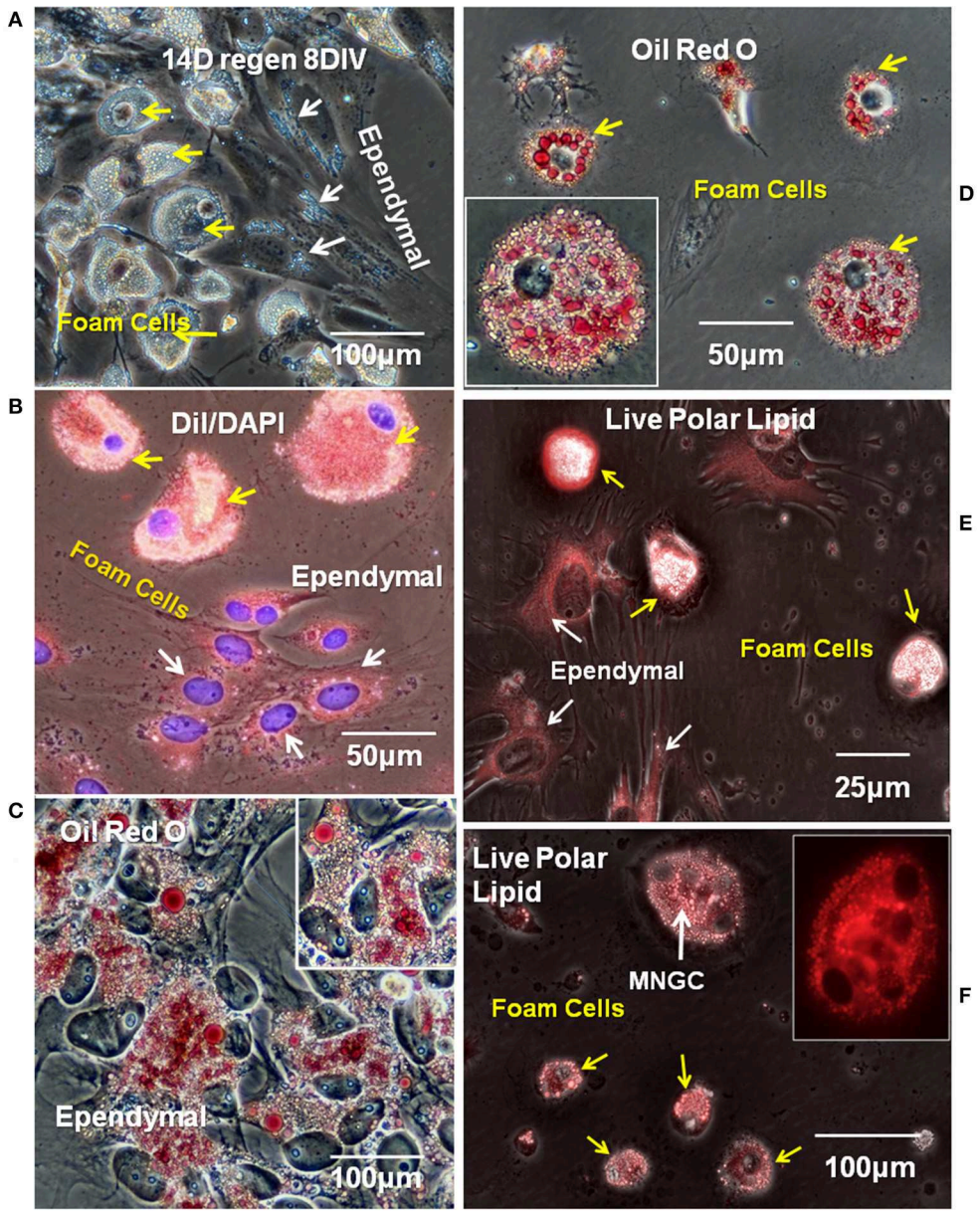

FIGURE 5 | Ependymal cells and foamy macrophages take up neutral and polarized lipids in regenerating spinal cord explants. **(A)** Lipid droplets were apparent ependymal (white arrows) and foamy macrophages (yellow arrow) in unstained explant cultures of 14 days regenerating spinal cord. Phase contrast image **(B)** Ependymal (white arrows) and foamy macrophages (yellow arrows) in regenerating explant cultures are labeled with polar lipid marker DiI. Fluorescence/Phase contrast image. **(C)** Ependymal cell lipid droplets label with neutral lipid marker Oil Red O. Phase contrast image. **(D)** Foamy macrophages lipid droplets also label with neutral lipid marker Oil Red O. Phase contrast image Insets in **(C,D)** show higher magnification images of ependymal cells and foamy cells, respectively. **(E,F)** Ependymal cells (white arrows in **E**), foamy macrophages (yellow arrows in **E,F**), and MNGCs (white arrow in **F**) all labeled with a commercial polar lipid marker. Fluorescence/Phase image, Inset in **(F)** shows a higher magnification of an MNGC with 4 nuclei, fluorescence only. Regen, regenerating; DIV, days *in vitro*. Magnification bar is shown in the lower portion of each image.

(**Figure 10A**), while in others there was little (**Figures 10C,D**). The regions with extensive ependymal myelin uptake appeared to be free of foam cells, as in **Figure 10A**. Foamy macrophages showed robust DiI-myelin uptake *in vitro* (**Figures 10B–D**). A 2-days period of exposure was used for the labeled myelin uptake. Cells were cultured without DiI-myelin for an additional 12 days, during which the ependymal cells appeared to turn over most of the labeled myelin (**Figure 10A** compared with **Figure 10E**). During the 12 days chase period foamy macrophages seemed to retain more of the labeled myelin, or turnover had released free DiI in these cells which partitioned into lipids stored within the cells (**Figure 10F**).

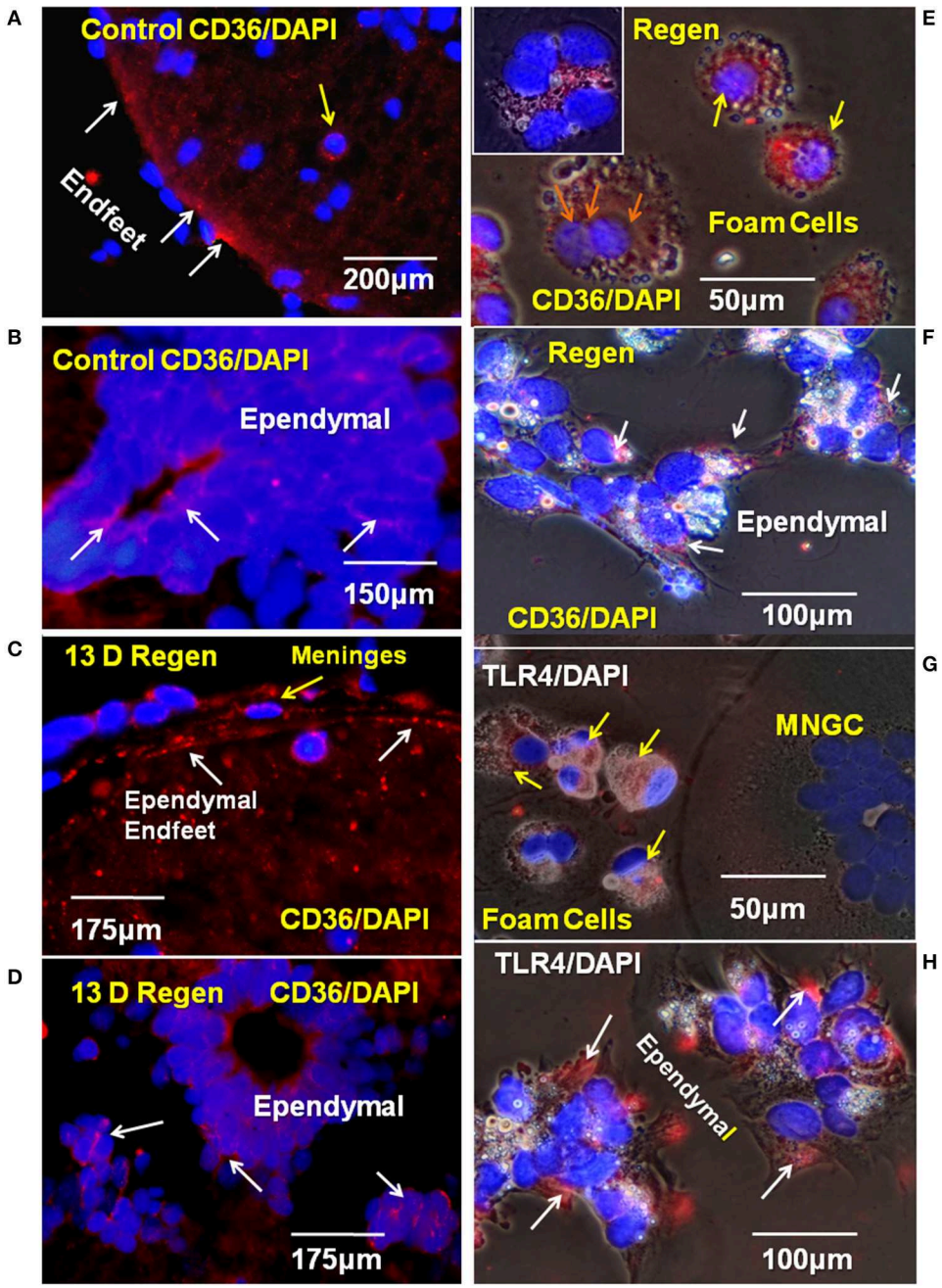

FIGURE 6 | CD36 and TLR4 in regenerating cord *in vivo* and *in vitro*. **(A)** The scavenger receptor CD36 was detected on the endfeet of ependymal cells in control cord paraffin cross-sections. Fluorescence image. **(B)** CD 36 is also present on ependymal cell bodies in intact adult Axolotl spinal cord. Fluorescence image. **(C)** In paraffin sections from regenerating cord stump CD36 was detected in ependymal endfeet in the reactive meninges. Fluorescence image. **(D)** CD36 also present on ependymal cell bodies in regenerating cord, proximal stump. Fluorescence image. **(E)** *In vitro*, CD36 is found on foamy macrophages from 10D regenerate spinal cords 6 days *in vitro* (yellow arrows). Orange arrows show three nuclei in $CD36^+$ MNGC. Inset in **(E)** shows a $CD36^+$ MNGC with six nuclei. **(F)** $CD36^+$ Ependymal cells (white arrows) in explant cultures from a 10D regenerate spinal cord 6 days *in vitro*. **(G)** TLR4 was detected in foamy macrophages (yellow arrows) in culture on cells from 14 days regenenerates, 17 days *in vitro*. **(H)** Ependymal cells from 14 days regenenerates, 17 days *in vitro* are also $TLR4^+$ (white arrows). D, day; Regen, regenerating; MNGC, multinucleated giant cells; TLR4, toll like receptor 4. Magnification bar is shown in the lower portion of each image.

Cathepsin K

The cysteine protease cathepsin K catabolizes several ECM molecules, including collagen, elastin, and gelatin. We hypothesized that cathepsin K present in Axolotl cells within the regenerating cord might be involved in catabolizing the fibrous collagen in the lesion site, allowing the regenerating cells to form

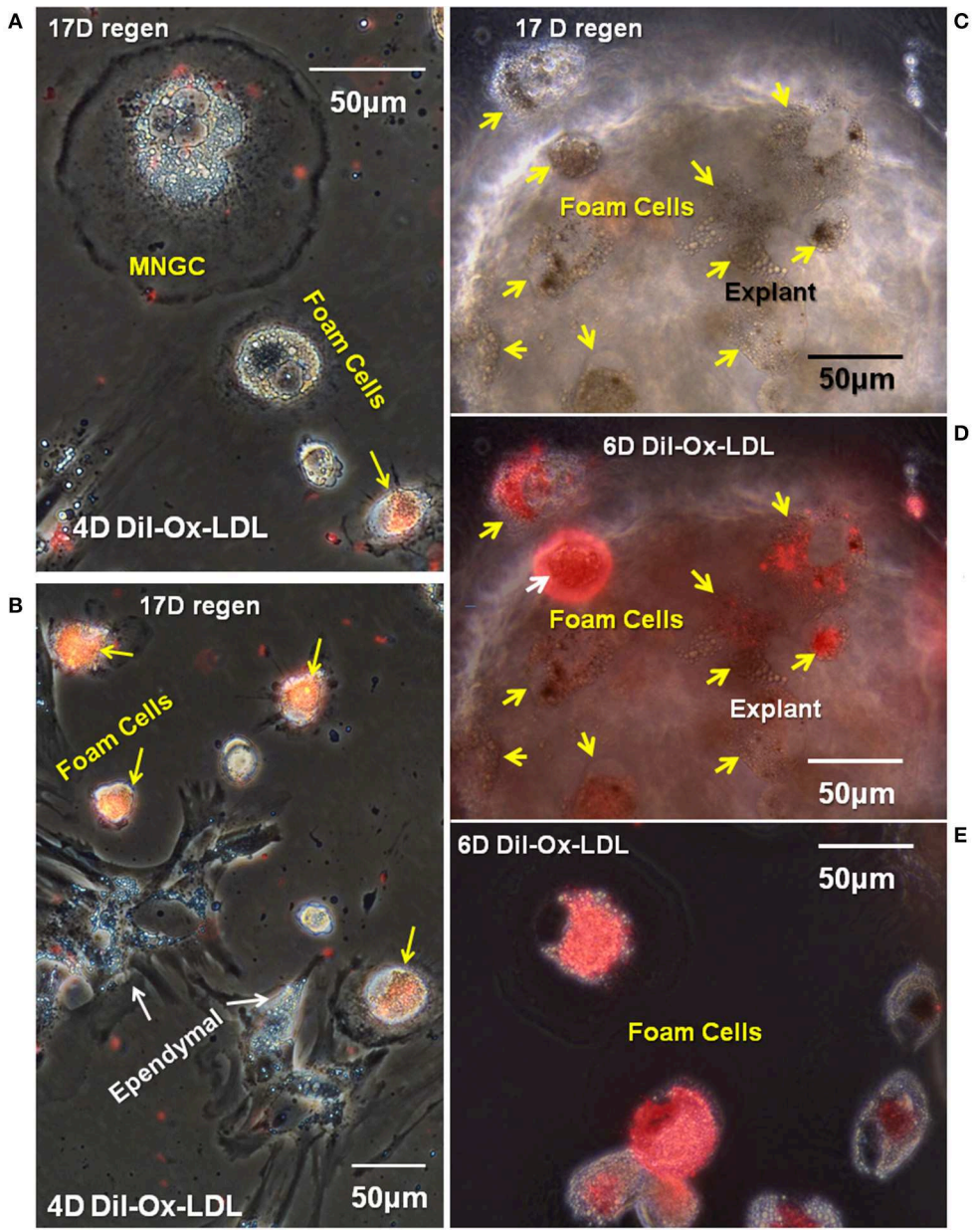

FIGURE 7 | A subpopulation of foamy macrophages takes up DiI-labeled oxidized low-density lipoprotein receptor. Seventeen days cord regenerates were cultured for 11 days *in vitro* **(A,B)** or 17 days *in vitro* **(C–E)** and were treated with DiI-Ox-LDL for 4 days **(A,B)** or 6 days *in vitro* **(C–E)**. MNGCs and ependymal cells (white arrows) were not labeled; however, a subpopulation of foamy macrophages (yellow arrows) were labeled. **(C,D)** Are the same field, with the explant shown in phase contrast in **(C)** and overlaid with fluorescence to highlight the foamy macrophages that have taken up DiI-Ox-LDL (yellow arrows). **(E)** Shows foamy macrophages that have migrated out of the explants and taken up DiI-Ox-LDL in culture. D, day; Regen, regeneration. Magnification bar is shown in the upper portion of images A and E, and the lower portion of images **(B–D)**.

a more regeneration-friendly region in which new ECM might be secreted. To determine if cathepsin K was expressed in the lesion site, cells *in vivo* and *in vitro* were labeled with cathepsin K antibody. **Figure 11A** shows a reactive meningeal flatmount from the lesion site where cells were labeled with cathepsin K antibody. In culture, there was expression of the enzyme in cells within the explants and in foamy macrophages and ependymal cells growing out of the explants (**Figures 11B–E**). In favorably oriented foamy macrophages, the cathepsin K was seen concentrated between the foam cell and the plastic substratum within the sealing ring (**Figures 11B,C**). In migrating ependymal cells, substantial portions of the cytoplasm were cathepsin K-positive (**Figures 11D,E**). Small MNGCs also expressed cathepsin K (**Figure 11E**).

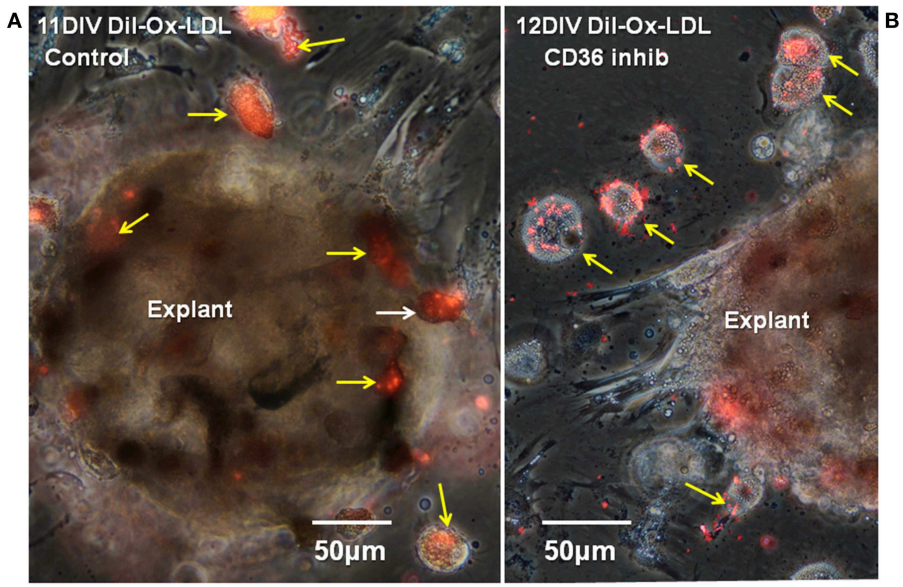

FIGURE 8 | CD36 inhibition reduces DiI-Ox-LDL uptake by foamy macrophages. Seventeen days regenerate spinal cord regenerate explants, were treated with DiI-Ox-LDL at 10DIV for 24 h as the control **(A)** or with the CD36 inhibitor sulfo-N-succinimidyl oleate added at 10DIV plus DiI-Ox-LDL added at 11DIV for 24 h. **(B)** Inhibitor-treated explants showed less uptake of DiI-Ox-LDL in comparison to control. D, day; DIV, days *in vitro*; Ox-LDL, oxidized low-density receptor; inhib, inhibitor; Regen, regeneration. Magnification bar is shown in the lower portion of each image.

Glycosaminoglycan Synthesis

Both foam cells and ependymal cell produce ECM-degrading enzymes [**Figure 11**; (20)], but ependymal cells also rebuild the regenerating spinal cord, including reforming the basal lamina of the *glia limitans* (10). Comparison of the ECM synthetic capacity of foamy macrophages and ependymal cells was performed using ^{3}H-glucosamine incorporation and autoradiography as an assessment of glycosaminoglycan and proteoglycan synthetic capacity (65).

Extensive ^{3}H-glucosamine uptake by mesenchymal ependymal cells occurred over a 24-h incubation in established cultures (**Figures 12A,C**). Label occurs in the cytoplasm and nucleus, and there is deposition of material onto the substrate near the explants where ependymal cells were most densely distributed. The nuclear label is associated with nuclear pore complex incorporation of O-linked N-acetyl glucosamine synthesized from the ^{3}H-glucosamine (66). No incorporation of ^{3}H-glucosamine was seen in or around any of the foamy macrophages, identified on the basis of their lipid droplet content comparable to those cells labeled with Oil Red O and DiI (**Figures 5**, **12B,C**). This indicates a major difference in lesion-site remodeling roles between ependymal cells and foamy macrophages.

Foam Cell/Ependymal Interaction

To observe foam cell interaction with the ependymal cells, regenerating tissue was placed in culture conditions that maintain mesenchymal ependymal outgrowth and proliferation of reactive Axolotl spinal cord ependymal cells (56). Pieces of tissue with reactive meninges and ependymal cells grown in culture typically showed three stages of growth: (1) at 3 h after the start of culture, the attachment period, the explant was firmly adherent and cells at the margins started to extend processes (**Figure 13A**), (2) after 1 day of culture (**Figure 6B**), injury-reactive ependymal cells were migrating out of the explants and meningeal tissue was spreading, and (3) at 4 days in culture, the explants had extensive, dispersed ependymal outgrowth with foamy macrophages on and among the ependymal cells (**Figure 13C**). The extensive outgrowth period persists though at least 22 days *in vitro*.

Labeling of cultured 2-weeks regenerating spinal cord with fluorescent-phalloidin showed localization of F-actin in sealing rings of foamy macrophages on the ependymal outgrowth (**Figure 13D**). At 4 weeks of regeneration, the ependymal outgrowth was reconnected between the cranial and caudal stumps (10). When 4-weeks lesion site regenerate tissue was excised and cultured, the foam cells were no longer localized with the ependymal cells (**Figure 13E**).

In analysis of cellular arrangement in culture, outgrowth could be divided into 5 forms of foamy macrophage/ependymal interaction: (1) condensed outgrowth with no foamy macrophages (**Figure 14A**), (2) condensed outgrowth with foamy macrophages (**Figure 14B**), (3) dispersed outgrowth with foamy macrophages (**Figure 14C**), (4) dispersed outgrowth without foamy macrophages (**Figure 14D**), and (5) mixed (**Figure 14E**). Ninety-two photographic fields from >16 explants in 7 experiments were sorted into the categories listed above. A one-way analysis of variance (ANOVA) with a *post-hoc* Tukey analysis showed a highly statistically significant difference

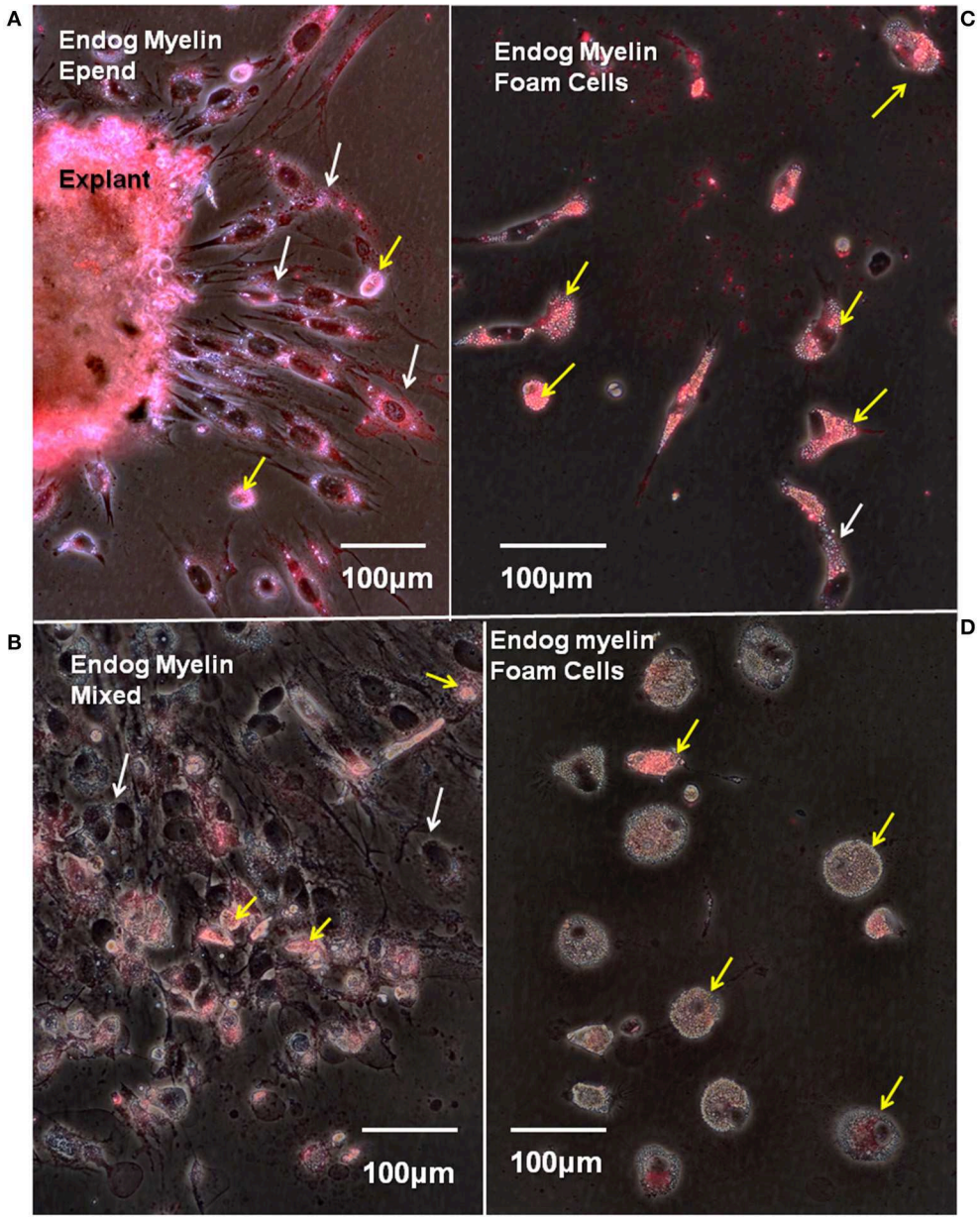

FIGURE 9 | Endogenous myelin uptake is robust in ependymal cells and foamy macrophages. Fourteen days regenerate spinal cord explants were cultured for 8 days *in vitro* and stained with fluoromyelin label to reveal endogenous myelin uptake from the lesion site. Fluorescence/phase images. **(A)** The explant periphery is heavily labeled as is a zone of ependymal outgrowth (white arrows). There are a few, scattered myelin-containing foam cells (yellow arrows). **(B)** In a mixed zone of outgrowth foam cells are labeled (yellow arrows), but ependymal cells show little label (white arrows). **(C)** A zone with heavily myelin-laden foam cells (yellow arrows). White arrow shows one myelin-laden ependymal cell. **(D)** A zone of foam cells with little endogenous myelin uptake (yellow arrows). Endog, endogenous; Epend, ependymal. Magnification bar is shown in the lower portion of each image. Magnification bars are in the lower portion of images.

between the presence of foamy cells with dispersed vs. condensed ependymal cells (**Figure 14F**). The occurrence of dispersed ependymal growth with foamy macrophages was far more prevalent when compared to the dispersed ependymal cells without foamy macrophages. This difference is highly significant with a p-value < 0.0001. Conversely, a condensed form of reactive ependymal cell outgrowth occurs in the absence of foam cells, compared to the occurrence of condensed outgrowth in the presence of foam cells (p-value < 0.0001). Further test details are included in **Supplemental Figure 5**.

DISCUSSION

Diagrammatic Summary

The cell and ECM associations shown in **Figures 1–3** are interpreted diagrammatically in **Figure 15A**. Fibrillar collagen

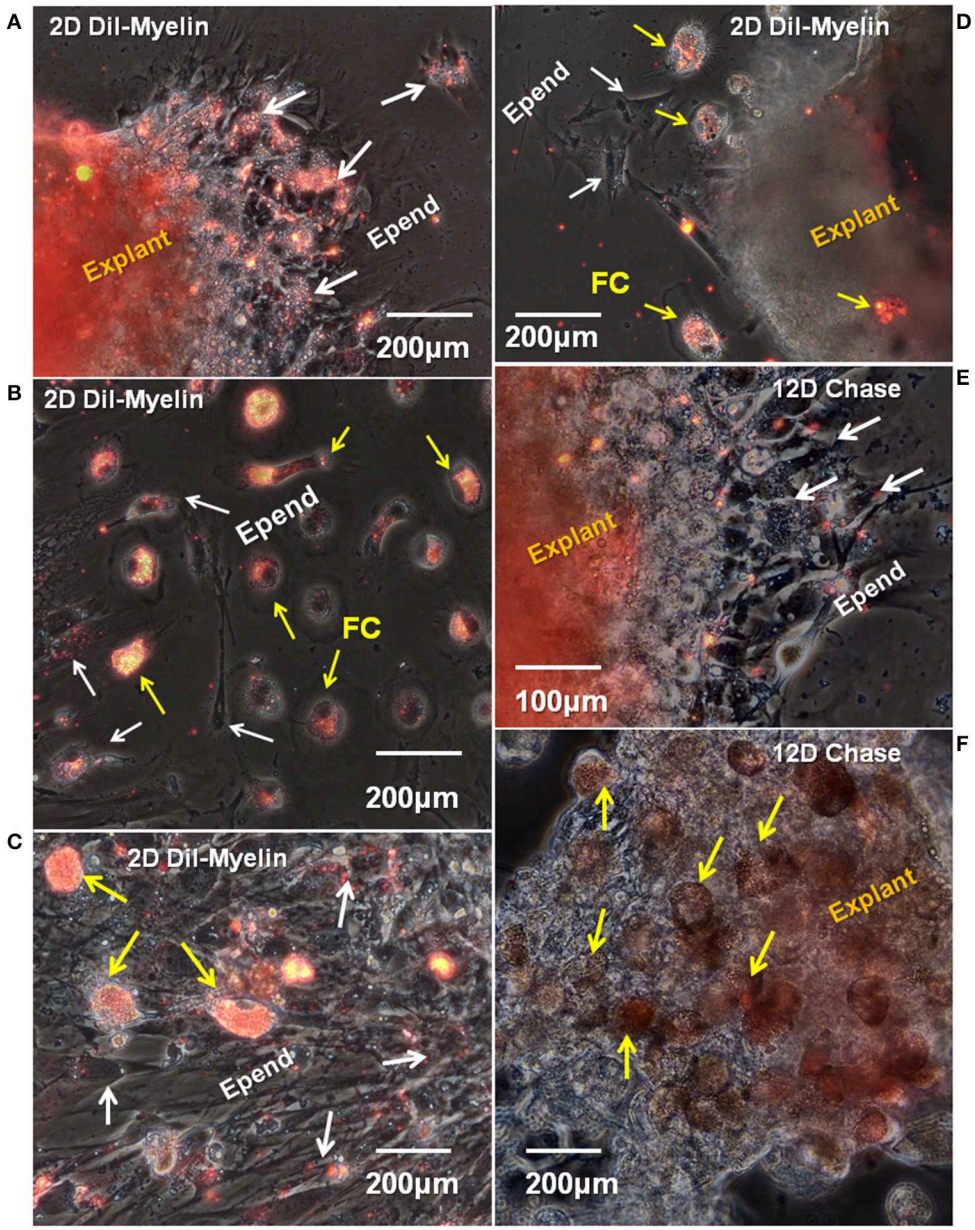

FIGURE 10 | *In vitro* uptake and turnover of myelin in ependymal cells and foamy macrophages. Fourteen days regenerating cord explants were cultured for 8 days, then incubated with DiI-labeled Axolotl brain myelin for an additional 2 days. A representative combination of outgrowth and explants labeling images are shown. **(A)** In a region with ependymal cell outgrowth only, the explants and ependymal outgrowth took up significal levels of labeled myelin fragments (white arrows). **(B)** In an area of mixed, dispersed foam cell and ependymal cell outgrowth, only the foam cells are heavily labeled. **(C)** An denser area of dispersing ependymal cells (white arrows) plus foam cells (yellow arrows) shows heavy myelin uptake *in vitro* only in the foam cells. **(D)** A sparsely labeled explants has strongly labeled foam cell outgrowth (yellow arrows) and unlabeled ependymal cells (white arrows). **(E,F)** Show a 12 days myelin-free chase period following 2 days of DiI-Axolotl-myelin uptake. **(E)** Shows part of the same region shown in **(A)**. Labeled myelin in the ependymal outgrowth is greatly reduced (white arrows). The explants is still labeled. **(F)** Even after the 12 days chase period, foam cells. D, day; Epend, ependymal; FC, foam cell. Magnification bar is shown in the lower portion of each image.

from the meninges was found throughout the lesion site between the retracted spinal cord stumps after transection. Sulfated proteoglycan was found throughout the outgrowth, but concentrated closer to periphery. Meningeal cells invaded from the periphery while reactive ependymal cells withdrew their radial processes, became mesenchymal and migrated out into the lesion site (16). Macrophages and foamy macrophages were present.

Figure 15B shows a composite model of markers to be used throughout the experimental results, illustrating foam cell specializations that were characteristic to this cell type and are indicators of function within the Axolotl cord lesion site. On

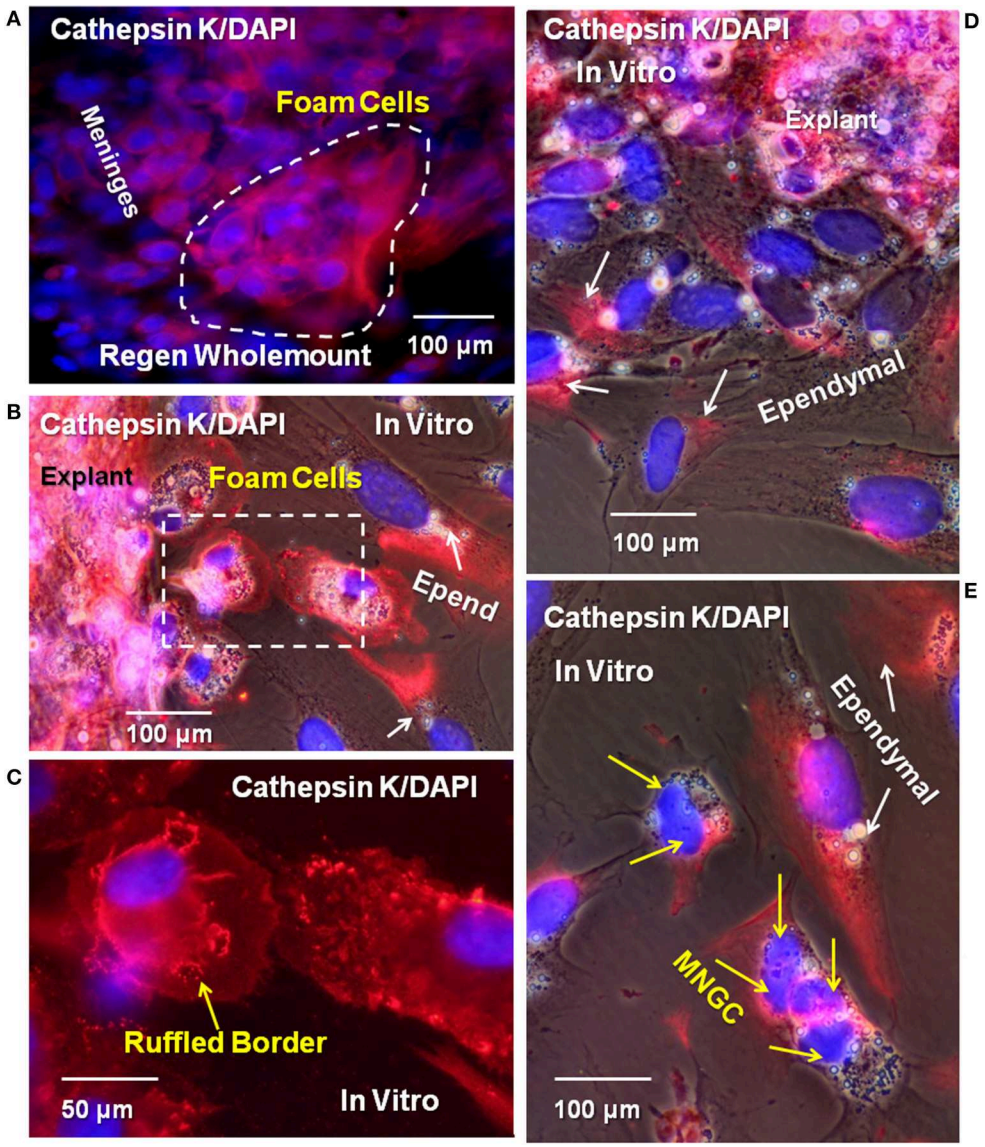

FIGURE 11 | Cysteine protease cathepsin K was detected in meninges, ependymal cells, foamy macrophages, and MNGCs *in vitro* and *in vivo*. **(A)** Wholemount cord tissue from 16D regenerating cord were co-labeled for cathepsin K (red) and DAPI (blue). Cells on the surface of the meninges are positive for cathepsin K (dashed white line). Explants from 16D regenerate cord, cultured for 10DIV, showed labeled ependymal cells **(B,D,E)**, foamy macrophages (**B**, dashed square), and an MNGC **(E)**. Yellow arrows indicate foam cells, white arrows indicate ependymal cells. Ruffled borders sequestering cathepsin K between foam cells and the culture substratum were also detected (yellow arrow, **C**). Yellow arrows indicate nuclei in MNGCs positive for cathepsin K in **(E)**. Regen, regenerating; D, day; DIV, days *in vitro*; MNGC, multinucleated giant cells. Magnification bar is shown in the lower portion of the images.

the unattached cell surface, is the lipid transporter CD36 which would mediate uptake of lipids, to be sequestered within the cytoplasm. TLR4/TLR6 acts in concert with CD36 in transport and are also known to be involved in fusion into MNGCs (23). The sealing ring structures and cathepsin K are show on and associated with the ECM-attached surface.

Organization of the Lesion Site

There are species differences in urodele SCI responses, just as there are in rodents (10, 67). The ependymal outgrowth process during gap regeneration in newts is more in the form of an epithelioid bulb than mesenchymal outgrowth, but newt transection lesion sites share features with those seen here in the Axolotl (5, 12, 16, 68). In early stages of spinal cord regeneration in both *Notophthalmus viridescens* (Eastern Red-Spotted Newt) and *Ambystoma mexicanum* (Axolotl) a fibrillar collagen-rich ECM wraps the regenerating tissue (Zukor et al., Figure 7; our **Figure 1E**). In the Axolotl, fibrillar collagen-containing matrix encases and bridges the cut ends of the cord, and cells grow out into that material (**Figures 1C,D**). Zukor et al.

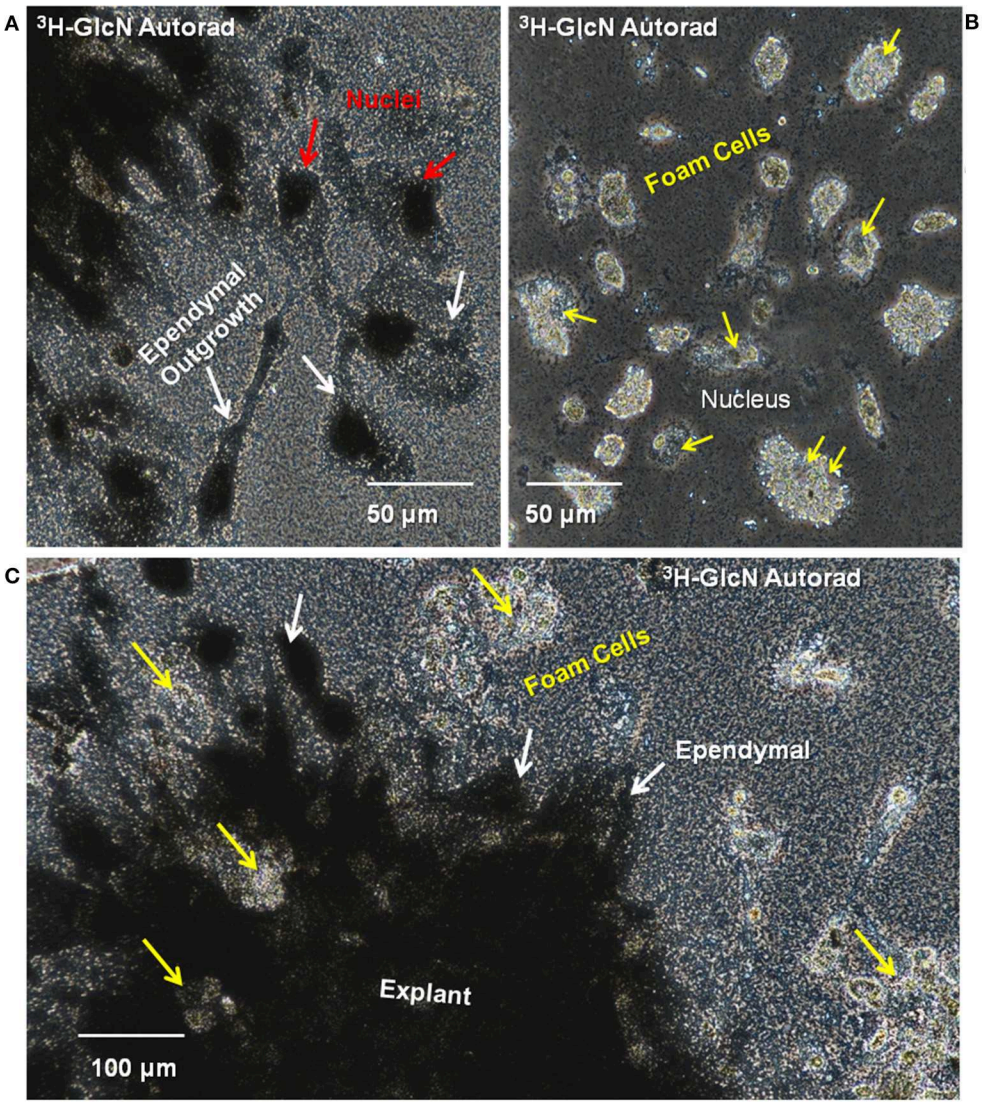

FIGURE 12 | Ependymal cells in cord explant cultures synthesize ECM components. Synthesis of glycosaminoglycan and proteoglycan was investigated by incubating explants with ^{3}H-glucosamine and performing culture dish autoradiography. **(A)** Silver grains were detected in the ependymal cell nuclei (red arrows) and cytoplasm (yellow arrows). **(B)** No silver grains were deposited on or around the foamy macrophages. Yellow arrows indicate foamy macrophage nuclei. **(C)** Lesion site explants is heavily labeled with silver grains. Patches of unlabeled foamy macrophages are found within the explants (yellow arrows) and beyond the ependymal cells (white arrows). 3H, tritiated; GlcN, glucosamine; Autorad, autoradiography. Magnification bars are shown in the lower portion of the images.

(12) showed the accumulation of CSPG in the meninges after transection in the newt. The Axolotl ECM that supported foam cell, MNGC and ependymal cell invasion also contained sulfated proteoglycans (**Figures 1E,F**). In both the newt and Axolotl there is little sulfated proteoglycan present before injury (**Figure 1B**). Compared to mammalian SCI ECM, it still not entirely clear whether the interstitial matrix that forms with meningeal fibrosis in urodeles is intrinsically non-inhibitory in composition or organization, or whether regeneration proceeds because of successful removal of this material (69–71). Production of cathepsin K by the foamy macrophages, MMP and cathepsin production by ependymal cells, plus known MMP production by foamy macrophages in other tissues suggests that removal of the ECM material is likely a strong component of the process [**Figure 11**; (20, 72)].

Axolotl lesion site ECM appeared to have two zones: one closely wrapped around the regenerating cranial and caudal ends of the cord plus the material between the cut ends. Following fixation, they were separable, the wrapped material remained firmly attached to the regenerating cord (**Figures 1C,E,F**). Inflammatory response cells accumulate in this material in both the newt and Axolotl [(12); **Figures 1–4**; **Supplemental Figure 2**]. Though not explicitly identified, the newt TEM images shows lipid-laden

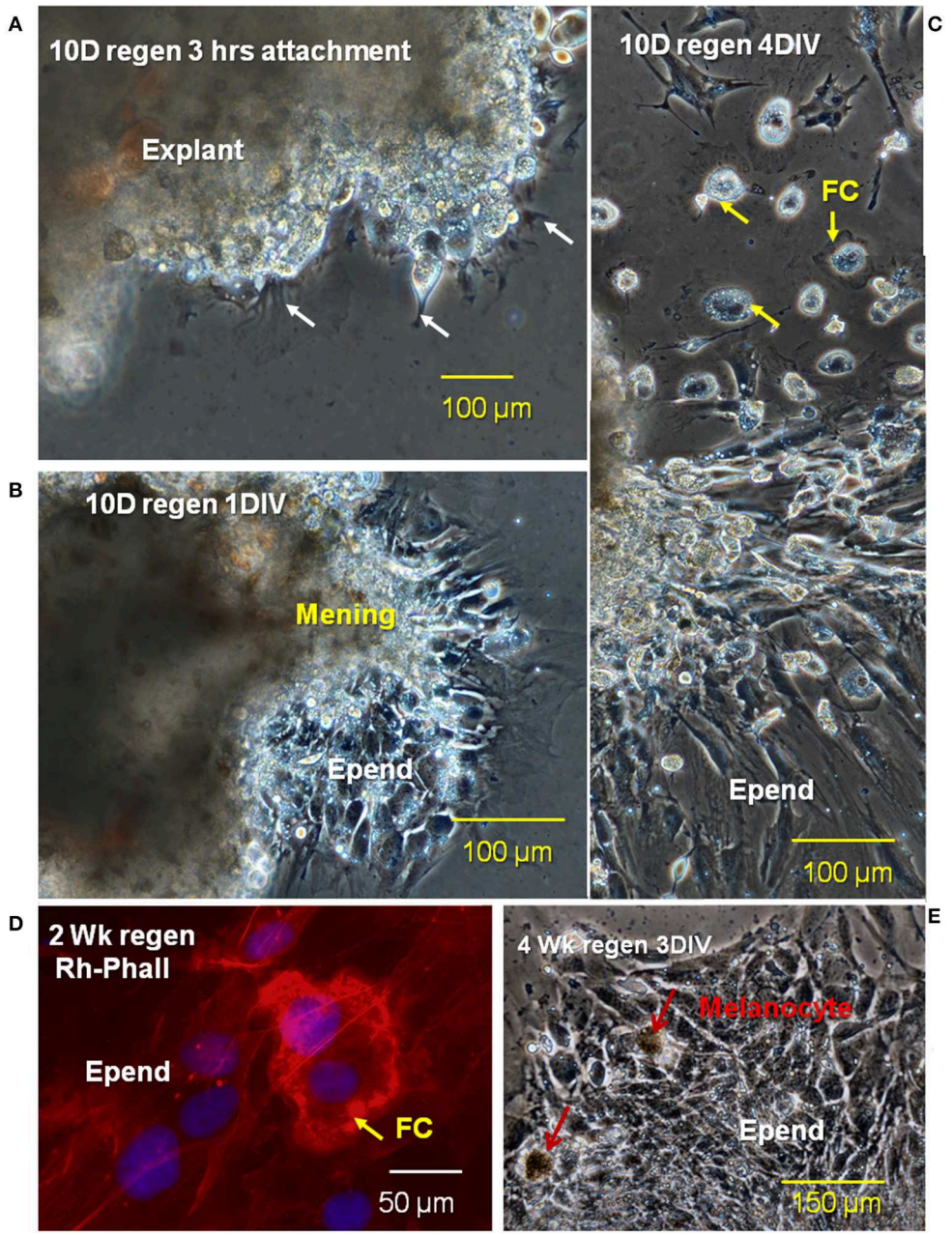

FIGURE 13 | Stages of migration of ependymal and foam cells from lesion site explants *in vitro*. Phase images of a 10D regenerating cord explant showing three different stages of cellular outgrowth; **(A)** at 3 h after the beginning of culture, the explant was firmly attached to the fibronectin-coated dishes and cellular processes begin to extend away from the edges of the explant **(B)**, after 1D *in vitro* (1DIV), ependymal cells are migrating out of explants, while meningeal tissue is spreading, **(C)** after 4DIV, there is extensive dispersed ependymal outgrowth as well as foamy macrophages on and among the ependymal cells **(D)**. Rhodamine-phalloidin label of a cultured 2 weeks regenerating cord (red) showed the sealing ring of a foamy macrophage (FC arrow). **(E)** Cultured 4 weeks regenerates showed no foamy cells attached to ependymal cells. Regen, regenerating; hrs, hours; D, day; DIV, days *in vitro*; mening, meningeal cells; Epend, ependymal cells; Rh-Phall, rhodamine-phalloidin. Magnification bar is shown in the lower portion of each image.

cells among the immune response cells accumulated in the reactive meninges (12). In the Axolotl lesion site, the foamy macrophages were concentrated in and on the meninges of the regenerating cranial and caudal stumps (**Figures 1**, **2**).

In situ, MNGCs are found in clusters on and in the fibrotic meninges (**Figures 1G,H**, **2D**, **3A–C**). It is not known if representative numbers of these cells are growing out of the lesion site explants *in vitro*, or whether they are so strongly attached to lesion site ECM that they are under-represented on the

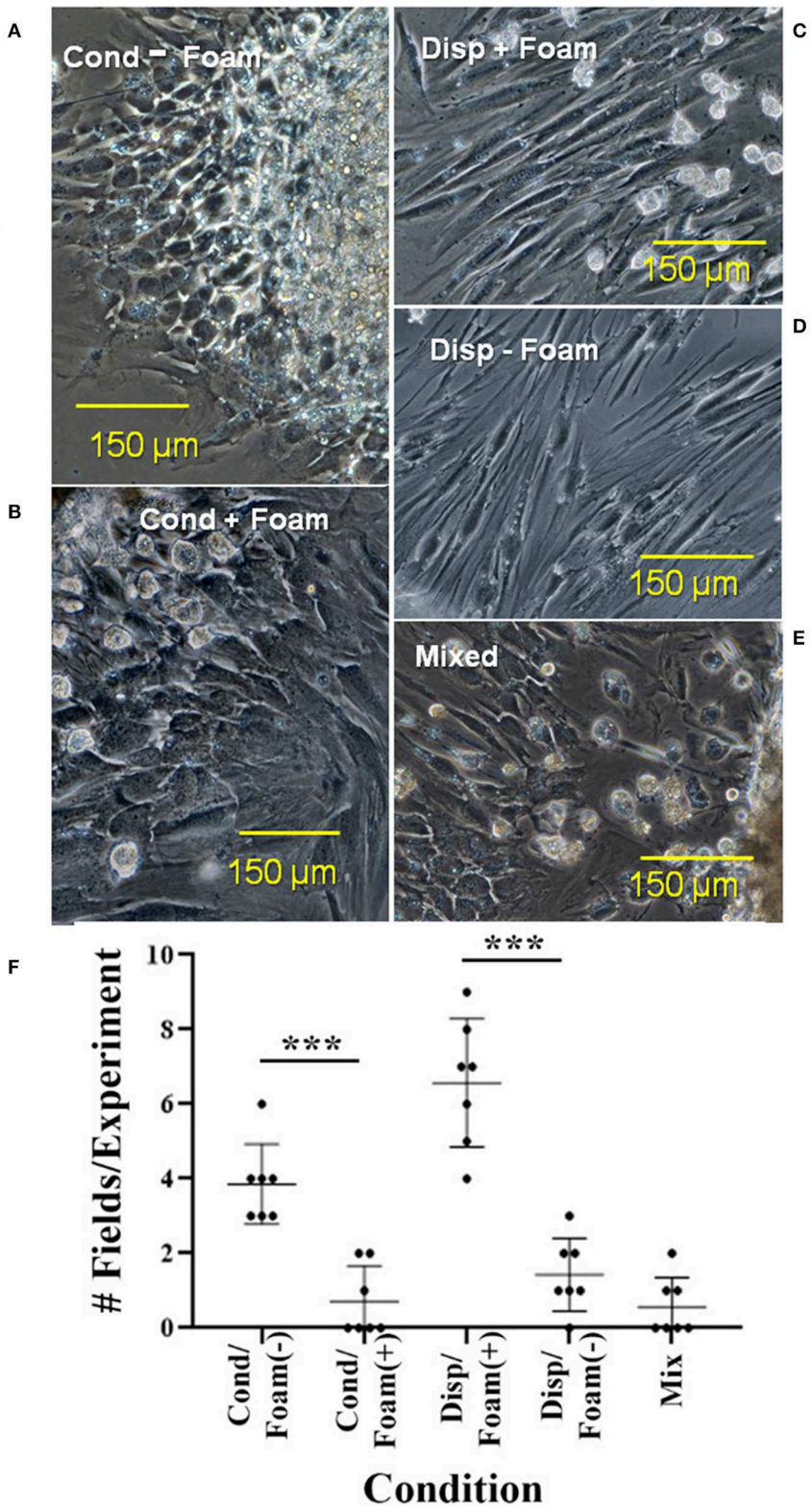

FIGURE 14 | Five types of cellular interactions between ependymal cells and foam cells in cultured regenerative outgrowth. Cultures in which foam cells were associated with condensed or dispersed ependymal cells from 14 to 17D spinal cord outgrowths were quantitated. Dispersed ependymal cells show a preference for associating with foam cells: **(C)** As opposed to condensed ependymal cells **(A,B)** or mixed condensed and dispersed ependymal cells **(E)**. **(D)** Shows a limited region of dispersed ependymal cells without foam cells. **(F)** Shows a graph depicting the quantitation of cultures. Cond, condensed; disp, dispersed. ***$p \leq 0.0001$. Magnification bar is shown in the lower portion of each image.

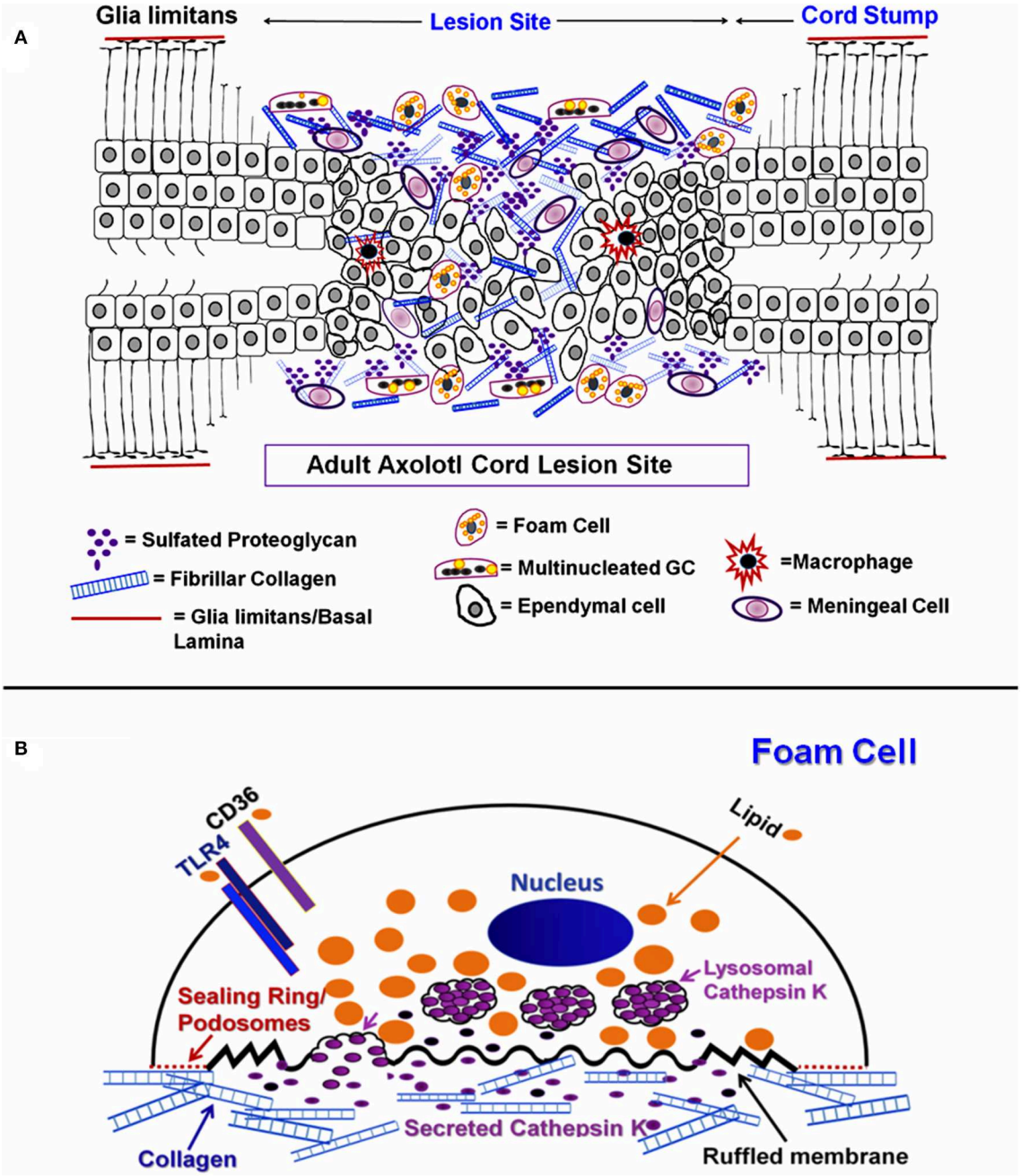

FIGURE 15 | Diagram of ECM and cellular associations in regenerating cord. **(A)** Diagrammatic representation of mesenchymal ependymal cell outgrowth and meningeal invasion gap regeneration of the Axolotl cord lesion site. Ependymal cells, foam cells, MNGCs, macrophages and meningeal cells are shown within extracellular matrix. Neurons and oligodendrocytes are not represented. **(B)** Diagrammatic representation of a foamy macrophage producing cathepsin K.

culture dish. Cluster of MNGCs are not seen in the culture dish outgrowth (**Supplemental Figure 6**). Further studies of axolotl meningeal MNGC formation and behavior are required.

Identification of Ependymal Cells

In these culture conditions (+EGF, fibronectin coating), the cells that grow out of the lesion site explants are ependymal cells, foamy macrophages, MNGCs and, rarely, melanocytes [**Figures 2E**, **5–11**, **13**; **Supplemental Figure 7**; (6, 16, 56, 73)]. Other cord or meningeal cells fail to exit the explants. The Axolotl ependymal cells have been thoroughly characterized in prior marker studies. Intact Axolotl cord ependymal cells are cytokeratin and glial fibrillary acidic protein (GFAP)-positive and the cytokeratins and GFAP are

lost during epithelial-mesenchymal transition (6, 16, 73). All of the injury-reactive Axolotl ependymal cells express the stem/progenitor cell marker mRNA-binding protein Musashi1 (16). A Musashi1 expression image is shown, again, at reviewer request along with GFAP intermediate filaments in the process of turnover. The appearance of the large ependymal nuclei is also quite distinctive (56). Examples of control culture Musashi1 localization and perinuclear GFAP *in vitro* are shown in **Supplemental Figure 8**.

Identification of Axolotl Foamy Macrophages

The identification of the lipid-laden mononucleated cells in the Axolotl lesion site *in situ* and *in vitro* as foamy macrophages was based on systematic examination of markers used in mammalian foamy macrophages. The labeling of lipid droplets with Oil Red O was primarily perinuclear (**Figure 5**), as it was in mammalian foamy macrophages (29). The cells also took up DiI-Ox-LDL like mammalian foam cells [**Figure 7**; (28, 74)]. The lipid transporters localized in the Axolotl foamy macrophages were CD36 and TLR4, the primary transporter and co-transporter used by mammalian foamy macrophages [**Figure 6**; (75)]. An active role for CD36 in lipid transport was supported by the specific inhibition of Ox-LDL uptake by the modified fatty acid Sulfo-*N*-succinimidyl Oleate [**Figure 8**; (64)]. Axolotl spinal cord foamy macrophages took up myelin fragments *in vivo* and *in vitro*, like foam cells in diseases including multiple sclerosis, and within mammalian spinal cord after SCI [**Figures 2C**, **9**, **10**; (27, 34)]. Myelin uptake by macrophages in mammalian SCI and multiple sclerosis models is a phagocytic process, and membrane-bound myelin inclusions are seen in our foamy macrophages and smaller MNGCs by TEM [(41, 76); **Figure 3C** inset]. Axolotl foamy macrophages produced cysteine proteinase cathepsin K characteristic of mammalian foam cells, and cathepsin K was seen localized within sealing rings [**Figure 11**; (54)]. Finally, TEM examination shows ultrastructural features like a ruffled border and perinuclear intermediate filaments seen in mammalian foamy macrophages [**Figures 3B,C**; **Supplemental Figure 2**; (59)].

Misidentification of Axolotl Foamy Macrophages

Macrophages have been described in injured salamander spinal cord, but not foamy macrophages (36). Results presented here (**Figures 1B**, **2C**) showed that foamy macrophages were absent from distal stump and control Axolotl cord but accumulated in the fibrotic meninges within 1–1.5 mm on each side of the transection site. There is a history of noting, but not accurately identifying, these cells in the urodele regeneration literature. Our early studies show the presence of lipid-laden mono- and multinucleated cells in reactive axolotl cord ependymal cultures that were considered to be osteoclasts and their precursors that had migrated from neural arch following laminectomy performed to expose the cord for transection (56). Maier and Miller (77) noted the presence of what appear to be foamy macrophages among newt limb blastema cells in culture, but called them signet cells because they had eccentrically positioned nuclei. Washabaugh and Tsonis (78) identified these cells as signet cells following Maier and Miller [(78), **Figure 1B**] in regenerating newt limb blastema cultures, noting the presence of granules that appear to be lipid droplets. In a newt spinal cord regeneration study, Zukor et al. (12) showed macrophages and other white blood cells in and around the newt spinal cord lesion site by TEM, and some of these appear to have foamy cytoplasm [(12), **Figures 7C,D**]. The present studies are the first to show that these lipid-laden cells concentrate in and on the meninges at the lesion site in urodele spinal cord regeneration and to characterize them as foamy macrophages based on functional markers, lipid labeling and uptake studies.

Possible Source of Foamy Macrophages

Two waves of macrophage recruitment have been described in mammalian SCI: first M1 (pro-inflammatory) macrophages of splenic origin, then M2 (anti-inflammatory) macrophages from either bone marrow or resident tissue immune cells (79). In a mouse spinal cord contusion system, M1 macrophages precursor cells were carried in the vasculature of the leptomeninges (mainly the arachnoid layer), which exit through the subarachnoid space to become M1 macrophages within the cord (80). Precursors to the M2 macrophages enter the brain ventricular-choroid plexus, travel through the cerebrospinal fluid, then invade the injured spinal cord and became M2 macrophages (80). It appears that conversion to mammalian cord foamy macrophages occurs within the spinal cord tissue (34, 35). Control Axolotl cord and stump tissue meninges have no foam cells (**Figures 1B**, **2C**), but they are abundant in the lesion site. The source of these foamy macrophages and MNGCs is not yet known. Future studies will be required to determine whether the entire population is recruited from circulating monocytes and macrophages or if resident macrophages proliferate locally and invade the lesion site.

Multinucleated Giant Cells

Activity differs between large and smaller MNGCs in our tissue culture system: smaller MNGCs and mononucleated foamy macrophages were more like each other than were large and small MNGCs. Cathepsin K activity, expression of the lipid transporter CD36 and co-transporter TLR4 were found in mononucleated foam cells and small MNGCs ($\leq$6 nuclei, **Figures 6E,G**, **11E**). TLR4 was absent from very large MNGCs (**Figure 6G**), consistent with the absence of lipid droplets. Very large MNGCs were generally lipid droplet free: one with 36 nuclei is shown in **Figure 6G** and **Supplemental Figure 6D** along with other non-lipid-containing MNGCs (**Supplemental Figure 6**), so their origin or metabolic state may be very different from the smaller lipid-laden MNGCs. Small MNGCs displayed cathepsin K activity (**Figure 11E**), but large MNGCs were not seen in any of the cathepsin K antibody labeled cultures, so the relationship of large numbers of nuclei and ECM proteolysis is not yet known in our system.

Cytoskeleton Identity and Function

F-actin localization showed that the foamy macrophages (**Figure 13D**) and MNGCs (**Figure 2D**) attach to the reactive meninges with characteristic podosome-studded sealing rings. These integrin and actin-containing structures are present in other types of macrophages and osteoclasts, where they are associated with a polarized (substratum-attached vs. free surface) morphology needed for normal secretory and transport functions (24, 32).

TEM studies show Axolotl meningeal foamy macrophages and MNGCs with masses of perinuclear intermediate filaments (**Figure 3C**; **Supplemental Figure 2B**). Vimentin intermediate filament accumulation is characteristic of mononucleated osteoclast precursors, osteoclasts and osteoclast-like MNGCs in mammals and clustering of nuclei in MNGCs occurs within a netlike "nest" of vimentin intermediate filaments (59).

Cathepsin K *in vivo* and *in vitro*

The cysteine protease cathepsin K is probably best known for its role in osteoclast pit production on bone (24, 32). Cathepsin K also performs a role in foamy macrophage and macrophage-derived MNGC ECM degradation (32, 52–55). Foamy macrophages in the Axolotl spinal cord lesion site showed cathepsin K localization (**Figure 11A**) and, *in vitro,* foamy macrophages and small MNGCs were all cathepsin K positive (**Figures 11B,C,E**). *In vitro*, cathepsin K was localized within the sealing ring between the cell and culture substrate and also within the cytoplasm of foamy macrophages (**Figures 11B,C,E**).

In the normal CNS, cathepsin K is expressed in mouse choroid plexus ependymal cells, but it is not a universal feature of intact ependymal cells throughout the mouse CNS (81). It is not known how widely distributed cathepsin K might be in the urodele CNS.

The activation of cathepsins is a complex process. Association of cathepsins with negatively charged glycosaminoglycan chains of proteoglycans allows autocatalytic activation (82). In regenerating urodele spinal cord there is abundant sulfated proteoglycan, including CSPG [**Figure 1**; (12)]. CSPG, specifically, has been shown to be involved in extracellular autoprocessing of pro-cathepsin K in osteoclasts (83), and is a good candidate for the same role in reactive Axolotl ependymal cells, foamy macrophages and MNGCs. This response to the fibrotic meningeal sulfated proteoglycan would mediate matrix degrading activity locally, contributing to prevention of permanent scar formation.

Intracellular Distribution of Cathepsin K

Ependymal cell cathepsin K localization was markedly asymmetrical (**Figures 11B,D,E**) and could be related to leading edge/trailing edge polarity. In studies of tumor cells, related to understanding metastatic migration, attempts have been made to assign cathepsin localization to the leading edge or trailing edge of migrating cells. In stationary breast carcinoma cells, the localization of cathepsin B is perinuclear, but it is concentrated on one side of the nucleus in a moving cell (84). It is reported that this is the trailing edge of the cell (84). In a study of cathepsin H localization in a prostate cancer cell line, the cathepsin co-localizes with talin, a leading-edge protein associated with focal adhesions in cell migration (85). The cathepsin H was also abundant around the nuclei. The Jevnikar et al. (85) paper is the only one showing a leading edge or trailing edge marker (talin) co-localized with a cathepsin.

In our cultured foamy macrophages and MNGCs, the cathepsin K was localized either within the sealing ring (**Figures 11B,C**) or in a polarized fashion in elongated cells (**Figures 11B,E**). In primary T-lymphocytes and T-lymphocyte lines, cathepsin X is found strongly localized in the both the leading edge and in the uropod, the trailing, deadhesive structure of lymphocytes (86).

While associated with leading edge/trailing edge polarity morphologically, correlation of cathepsin localization with a mechanism of directional cell migration is not possible at this time in either the ependymal cells or foamy macrophages.

Lipid in Ependymal Cells and Foamy Macrophages

TEM examination has shown that normal urodele ependymal cells contain some small lipid droplets. During regeneration, newt tail cord TEM examination shows the accumulation of lipid droplets in ependymal cells (2). The cytoplasm of intact mammalian ependymal cells label with DiI, but the magnification and resolution of the published images in that study do not permit identification of lipid droplets (87). In other mammalian studies, normal, young, non-pathological CNS ependymal cells do not contain stores of lipid. In the ventral portion of the brain, lateral ventricles of young mice stained with Oil Red O shows little lipid in the ependymal cells (88). There is more lipid in middle-aged mice and a high level of lipid in aged mouse ependymal cells (88). Similarly, there is a large increase of lipid in Alzheimer's Disease choroid plexus ependymal cells connected to expression of receptors for the transcytosis of LDL, lipoprotein receptor-related proteins-1 and 2 (megalin) (89, 90). So lipid accumulation in ependymal cells is associated with a disturbed or pathological state in ependymal cells.

The combined Oil Red O, DiI and DyRect labeling showed both neutral lipid and polar lipid content in both ependymal cells and foamy macrophages (**Figure 5**). The Axolotl ependymal cells and foamy macrophages also expressed the lipid scavenger receptor CD36 *in vivo* and *in vitro* indicating a common mechanism of lipid uptake (**Figure 6**). Therefore, both ependymal cells and foamy macrophages could be participating in removal of toxic lipids released or formed after neural injury. The source of neutral and polar lipids in both populations of cells could involve uptake of native and oxidized lipoproteins as well as myelin breakdown products from the Axolotl spinal cord lesion site.

Autofluorescence

Autofluorescence in Axolotl foamy macrophages confounds the use of green fluorochromes, including the Dyrect neutral lipid fluorochrome (**Supplemental Figure 4**). The source is not necessarily unique, but foamy macrophages can take up lipofuscin (ceroids) in pathological conditions (Dvorak and Monahan-Early, 1992). Foam cells exposed to Ox-LDL accumulate lipofuscin, and lipofuscin autofluorescence has even

been used as a marker for phagocytic CNS macrophages (74, 91). Lipofuscin can also be liberated by neuronal death. Autofluorescence of lipofuscin has an emission spectrum in the region of 430–490 nm, with a maximum in the yellow range (92). This would bleed through typical green fluorescence filters. The degree of autofluorescence of foamy macrophages and ependymal cells varies, suggesting differential uptake of autofluorescent compounds or differential exposure to them within the lesion site. Maier and Miller (77) noted the autofluorescence of what they termed "signet cells" from regenerating newt limb blastemas.

Myelin Uptake

The myelin uptake behavior seen in the present study could be beneficial in regeneration. The axolotl form of the myelin-associated inhibitory molecules Nogo-A (axNogo), the Nogo receptor and myelin associated glycoprotein (MAG) are expressed in the Axolotl CNS, including during regeneration, suggesting that they are not inhibitory. Localization of axNogo and MAG in urodeles is primarily in gray matter neurons and ependymal cells, unlike the myelin/oligodendrocyte localization in mammals (93, 94). Despite these differences in the effects of myelin-associated molecules between mammals and urodeles, lesion site myelin was removed by ependymal cells and foamy macrophages during activity *in vivo* and *in vitro* (**Figures 9**, **10**). One additional consideration regarding removal of myelin is the role this process plays in modulating M1 pro-inflammatory to M2 anti-infammatory phenotype of foamy macrophages in multiple sclerosis models (22, 27, 34, 95–97). Pro- or anti-inflammatory properties of Axolotl spinal cord foamy macrophages remain to be studied.

There were distinct differences in initial myelin content in ependymal cells placed in culture: some regions of explants outgrowth labeled heavily and some not at all. This could be dependent on their initial location within the lesion site. The foamy macrophages are concentrated around the regenerating ends of the cord, while the ependymal cells are growing out into this zone from the spinal cord stumps. In regions close to the transection site, the foamy macrophages may be the initial cell population to engulf myelin fragments, outcompeting the later-arriving ependymal cells. Deeper within the lesion site, where there are fewer foamy macrophages (**Figures 2A,B**), ependymal cells may be the primary cells to take up myelin.

Are Some Cells "Full" of Ox-LDLIn Culture?

Lipid droplets are the most visible form of cellular lipid storage. A mature lipid droplet is described as a mass of neutral lipid within a single phospholipid leaflet membrane (98). Lipid droplets have a complex genesis and breakdown process within cells. Neutral lipids are generated enzymatically in the ER and can be trafficked to many parts of the cell including and the nucleus, lysosomes and vacuoles. Intracellular storage of lipids reflects a balance between uptake, consumption, interconversion of lipid forms and release (98, 99). Cellular stress and immune factors play significant roles in lipid balance (99).

The mechanisms underlying lipid balance in macrophages have been studied most extensively in non-neural diseases, such as atherosclerosis, non-alcoholic fatty liver disease (NAFLD) and pulmonary alveolar proteinosis (PAP), including the conversion of high levels of LDL to Ox-LDL related to foamy macrophage formation and function (29, 100). Ox-LDLs are not recognized by a macrophage's native LDL receptor, but they are recognized by the CD36 scavenger receptor (29, 75). Lipid uptake *via* scavenger receptors is not subject to feedback regulation and can lead to excessive accumulation of lipids in affected cells (75, 90, 101). Cholesterol esters are hydrolyzed enzymatically into free cholesterol, which can be utilized by cellular processes, exported from the cell, or converted back to cholesterol esters to prevent toxic effects from excess free cholesterol. Export of high-density lipoprotein is the primary means of lipid efflux from cells under normal conditions, though there is some passive free cholesterol efflux (29, 100).

Cholesterol ester hydrolysis may be actively inhibited by Ox-LDLs after prolonged exposure (102, 103). Exposure to Ox-LDLs can lead to lysosomal accumulation of lipids, rather than cytosolic accumulation of lipid droplets (102–104). However, there are species-specific differences in Ox-LDL response: free cholesterol and cholesterol esters were present in pigeon macrophage lysosomes after Ox-LDL exposure, while lipid accumulation was cytosolic in mouse macrophages (103). Lysosomal dysfunction caused by Ox-LDLs may not be easily reversed, which could explain why some of our foam cells don't take up much additional Ox-LDL *in vitro* (**Figure 7**). Other modified LDLs can be metabolized without adversely affecting essential lysosomal acidity and our foam cells are likely taking up many types of modified LDLs, but those with a high existing Ox-LDL burden would be inactive in the DiI-Ox-LDL uptake experiments (105, 106). Prolonged lysosomal dysfunction could be why our foam cells remain so full of lipid long after removal from the injury site. The absence of DiI-Ox-LDL uptake in ependymal cells *in vitro* (**Figures 7A,B**, **8A**) could reflect natural uptake of less oxidized forms of LDL *in vivo,* or a greater tendency toward lysosomal dysfunction.

ECM Degradation vs. Synthesis

ECM Degradation

Cells migrate into the Axolotl cord lesion site through a collagen- and proteoglycan-rich ECM (**Figures 1D–F**). The regenerating cord shows a massive increase in the amount of ECM investing the cord, compared with the normal cord meningeal ECM, with a disproportional increase in sulfated proteoglycan content (**Figures 1B,E**).

ECM is known to be phagocytosed and degraded intracellularly by a variety of amphibian cell types, including anuran (frog and toad) macrophages during the ECM turnover associated with metamorphosis (107). TEM studies, here, show foam cells are attached to, and embedded in, fibrillar collagen (**Figures 3B,D**). TEM examination shows phagocytosed fibrillar collagen in a foamy MNGC (**Figure 3D**; **Supplemental Figure 2A**). In an enlargement of **Figure 3B** (**Supplemental Figure 2A**) interstitial fibrillar collagen can be seen among a group of ependymal cells, but none of them showed phagocytosed collagen. Either phagocytosis of the fibrillar collagen is accomplished only by the foamy

macrophages, or reactive ependymal cell collagen uptake is in the form of smaller peptides resulting from extracellular degradation. In **Figure 3F** an image from a site in a zone farther from the transection site where the interstitial collagen has already been removed: no intracellular collagen was seen.

The ependymal cathepsin K production described here, and ependymal MMP production characterized previously in Axolotl cord regeneration, show that ependymal cells can participate actively in ECM degradation mediated by secreted proteases [**Figure 11**; (20)]. Foamy macrophages are known to produce MMP9 and cathepsin K in diseases including atherosclerosis, and MMP9 in multiple sclerosis (53, 108, 109).

Axolotl foamy macrophages and smaller MNGCs participate in ECM removal by secretion of cathepsin K as well as phagocytosis (**Figures 3D**, **11A–C,E**; **Supplemental Figure 2A**). MNGCs are seen in or on the reactive meninges (**Figures 1G,H**, **2D**, **3A,B**) and are known to participate in ECM degradation in other system including MNGC tumors (32, 52). In our primary tissue culture system, smaller MNGC actively produce cathepsin K, while all of the foam cells do so (**Figure 11**). A full understanding of the ECM proteolytic repertoire of cord lesion site MNGCs will require much larger numbers in future studies involving stimulated fusion *in vitro*.

ECM Synthesis

The participation of ependymal cell endfeet in reforming the *glia limitans* has long suggested that they are producing ECM in later stages of the regeneration process (2). The expectation regarding ECM production by meningeal foam cells is not at all clear. In a few experimental disease-related models, a fibrotic role has been indicated for macrophages. This includes exposure of human macrophages to native LDL which stimulates proteoglycan secretion, a phenomenon with implications for vascular wall trapping of apolipoprotein B-containing lipoproteins in atherosclerotic plaques (110). This phenomenon may be related to the production of a proteoglycan form of macrophage colony stimulating factor in atherosclerotic plaque macrophages (111). In mice with surgical sponge-induced granulomas, and in atherosclerotic plaques, a variety of genes associated with fibrosis are expressed in transcriptome analysis: several collagen peptides and the small proteoglycans decorin and biglycan (112). This expression is higher in foamy macrophages vs. non-foamy macrophages (112).

The *in vitro* ^{3}H-glucosamine uptake results presented here suggest that ependymal cells are producing glycosaminoglycans and proteoglycans during the ependymal outgrowth process, depositing new ECM even as they are engaging in lesion site matrix turnover (**Figures 14A,C**). The foamy macrophages, however, show no evidence of ECM production from the ^{3}H-glucosamine uptake studies (**Figures 14B,C**).

Foamy Macrophage/Ependymal Interactions: Beneficial to Regeneration or Not?

In mammalian SCI, macrophages support scar formation and inhibit axonal regrowth (55, 113, 114). Macrophages are required in Axolotl limb and heart regeneration, so there is evidence that innate immune system cells can have a positive role in urodele regeneration (115, 116). In mouse heart, this positive role for macrophages does not extend beyond the neonatal stage (117).

Less is known about macrophages and macrophage/target cell interactions in urodele spinal cord regeneration. A study using lectin probes shows macrophages within the injured Axolotl spinal cord (36). In the newt studies by Zukor et al. (12), TEM examination shows macrophages in contact with neurons in an early stage of axonal regrowth called "wisping," as well as being present in the reactive meninges (12). In the Zukor et al., **Figure 7D**, a lipid-laden macrophage that could be a foam cells is shown in contact with an axon, and foam cell-like white blood cells are shown in the reactive meninges (12), **Figure 7C**. Though not identified as such, foamy macrophages may be present in the regenerating newt cord.

The present study examined the interaction between foamy macrophages and ependymal cells (**Figures 13**, **14**). Mononucleated foamy macrophages were abundant in Axolotl cord lesion site tissue *in situ* and *in vitro* (**Figures 2B,E**, **6C**, **13C**). Statistical analysis showed a highly significant association of the presence of foamy macrophages with an increased degree of dispersal of ependymal cells *in vitro* (**Figures 2E**, **5A,C**, **13**, **14**). It is not known whether the interaction involves cell-cell contact or secreted factors.

The co-migration of foamy macrophages and ependymal cells was strong during the period of adult Axolotl cord gap regeneration corresponding to mesenchymal ependymal outgrowth (2 weeks, **Figures 13A–D**), while at 4 weeks of regeneration, when the ependymal cells from cranial and caudal stumps have reconnected, the foam cells were no longer present (**Figure 13E**). It is not yet known whether the foamy macrophages and MNGCs are excluded to the periphery with the meninges, undergo cell death or both.

The position of these cells on and within the reactive meninges investing the regenerating stumps suggests a model in which the foam cells and smaller MNGCs act on the invasive meninges from the "outside-in," while the ependymal cells act from within the cord into the lesion site to remove fibrotic meningeal ECM [**Figures 1E–H**, **2A,B**, **15A**; (16, 20)]. Because they are attached to and within the invasive meninges, the foamy macrophages are concentrated in the lesion site distal to the zone of ependymal outgrowth. The ependymal cells grow out to meet and mix with the foamy macrophages.

Foamy macrophages can release growth factors, such as FGF2 and TGFβ, that are bound by ECM (118). Decellularized human meninges retains FGF2 and VEGF, suggesting that the release of ECM-bound growth factors by the foamy macrophages proteases could be of importance in the Axolotl cord lesion site (119). Urodele ependymal cells respond to TGFβ and FGF2 (6, 120).

The relationship of foamy macrophages to ependymal outgrowth, and their known activity, places the macrophages in a position to open the way for ependymal cells through ECM *in vitro* during ependymal outgrowth. In combination with the ECM degrading and synthetic capacity of the reactive ependymal cells, this juxtaposition of the foamy macrophages and ependymal cells could help maintain directional outgrowth across the lesion site.

DATA AVAILABILITY STATEMENT

The datasets generated for this study are available on request to the corresponding author.

ETHICS STATEMENT

The animal study was reviewed and approved by IUPUI School of Science Institutional Animal Care and Use Committee (SARC).

AUTHOR CONTRIBUTIONS

NE, HT, HS, ME, TB-A, and EC contributed the conception and design of the study. SS developed the wholemount staining procedures and their application to this study. TB-A performed the statistical analysis. ME and DS performed the TEM analysis and interpretation. DS planned and performed the examination of the time course of meningeal regeneration. DS-B provided the immunological interpretation essential for experimental design. MK developed and applied the wholemount actin organization studies. TB-A, EC, and DS-B developed the diagrammatic interpretation of the lesion site, foamy macrophages, and MNGCs. EC, TB-A, and NE wrote, and EC and TB-A coordinated the revisions to the manuscript. HT and HS initiated this project as students in the laboratory of EC.

FUNDING

This work was funded by the Indiana University Foundation Regenerative Biology Fund I380010385.

SUPPLEMENTARY MATERIAL

The Supplementary Material for this article can be found online at: https://www.frontiersin.org/articles/10.3389/fimmu.2019.02558/full#supplementary-material

REFERENCES

1. Butler EG, Ward MB. Reconstitution of the spinal cord following ablation in adult *Triturus*. *Dev Biol.* (1967) 15:464–86. doi: 10.1016/0012-1606(67)90038-3
2. Egar M, Singer M. The role of ependyma in spinal cord regeneration in the urodele, *Triturus*. *Exp Neurol*. (1972) 37:422–30. doi: 10.1016/0014-4886(72)90085-4
3. Hunter K, Maden M, Summerbell D, Eriksson U, Holder N. Retinoic acid stimulates neurite outgrowth in the amphibian spinal cord. *Proc Nat Acad Sci USA*. (1991) 88:3666–70. doi: 10.1073/pnas.88.9.3666
4. Caubit X, Riou JF, Coulon J, Arsanto JP, Benraiss A, Boucaut JC, et al. Tenascin expression in developing, adult and regenerating caudal spinal cord in the urodele amphibians. *Int J Dev Biol*. (1994) 38:661–72.
5. Stensaas LJ. Regeneration in the spinal cord of the newt *Notopthalamus (Triturus) pyrrhogaster*. In: Kao CC, Bunge RP, Reier PJ, editors. *Spinal Cord Reconstruction*. New York, NY: Raven Press (1983). p. 121–49.
6. O'Hara CM, Chernoff EAG. Growth factor modulation of injury-reactive ependymal cell proliferation and migration. *Tissue Cell.* (1994) 26:599–611. doi: 10.1016/0040-8166(94)90012-4
7. Chernoff EAG. Spinal cord regeneration: a phenomenon unique to urodeles? *Int J Dev Biol.* (1996) 40:823–31.
8. Ferretti P, Zhang F, Santos-Ruiz L, Clarke JDW. FGF signalling and blastema 1064 growth during amphibian tail regeneration. *Int J Dev Biol.* (2001) 45:127–8. doi: 10.1387/ijdb.01450127
9. Ferretti P, Zhang F, O'Neill P. Changes in spinal cord regenerative ability through phylogenesis and development: lessons to be learnt. *Dev Dyn*. (2003) 226:245–56. doi: 10.1002/dvdy.10226
10. Chernoff EAG, Stocum DL, Nye HLD, Cameron JA. Urodele spinal cord regeneration and related processes. *Dev Dyn*. (2003) 226:295–307. doi: 10.1002/dvdy.10240
11. McHedlishvili L, Epperlein HH, Telzerow A, Tanaka EM. A clonal analysis of neural progenitors during axolotl spinal cord regeneration reveals evidence for both spatially restricted and multipotent progenitors. *Development*. (2007) 134:2083–93. doi: 10.1242/dev.02852
12. Zukor KA, Kent DT, Odelberg SJ. Meningeal cells and glia establish a permissive environment for axon regeneration after spinal cord injury in newts. *Neural Dev.* (2011) 6:1–22. doi: 10.1186/1749-8104-6-1
13. Carter C, Clark A, Spencer G, Carlone R. Cloning and expression of a retinoic acid receptor β2 subtype from the adult newt: evidence for an early role in tail and caudal spinal cord regeneration. *Dev Dyn*. (2011) 240:2613–25. doi: 10.1002/dvdy.22769
14. Becker CG, Becker T. Neuronal regeneration from Ependymo-radial glial cells: cook, little pot, cook. *Dev Cell.* (2015) 32:516–27. doi: 10.1016/j.devcel.2015.01.001
15. Tazaki A, Tanaka EM, Fei J-F. Salamander spinal cord regeneration: the ultimate positive control in vertebrate spinal cord regeneration. *Dev Biol*. (2017) 432:63–71. doi: 10.1016/j.ydbio.2017.09.034
16. Chernoff EAG, Sato K, Salfity HVN, Sarria DA, Belecky-Adams T. Musashi and plasticity of Xenopus and Axolotl spinal cord ependymal cells. *Front Cell Neurosci.* (2018) 12:45. doi: 10.3389/fncel.2018.00045
17. Freitas PD, Yandulskaya AS, Monaghan JR. Spinal cord regeneration in amphibians: a historical perspective. *Dev Neurobiol*. (2019) 79:437–52. doi: 10.1002/dneu.22669
18. Fernández-Klett F, Priller J. The fibrotic scar in neurological disorders. *Brain Pathol*. (2014) 24:404–13. doi: 10.1111/bpa.12162
19. Oliveira Dias D, Göritz C. Fibrotic scarring following lesions to the central nervous system. *Matrix Biol.* (2018) 68–69:561–70. doi: 10.1016/j.matbio.2018.02.009
20. Chernoff EAG, O'Hara CM, Bauerle D. Bowling, M. Matrix metalloproteinase production in regenerating axolotl spinal cord. *Wound Rep Reg.* (2000) 8:282–91. doi: 10.1046/j.1524-475x.2000.00282.x
21. Vignery A. Macrophage fusion: the making of osteoclasts and giant cells. *J Exp Med*. (2005) 202:337–40. doi: 10.1084/jem.20051123
22. Grajchen E, Hendriks JJA, Bogie JFJ. The physiology of foamy phagocytes in multiple sclerosis. *Acta Neuropathol Commun.* (2018) 6:124. doi: 10.1186/s40478-018-0628-8
23. Helming L, Winter J, Gordon S. The scavenger receptor CD36 plays a role in cytokine-induced macrophage fusion. *J Cell Sci*. (2009) 122:453–9. doi: 10.1242/jcs.037200
24. Pereira M, Petretto E, Gordon S, Bassett JHD, Williams GR, Behmoaras J. Common signalling pathways in macrophage and osteoclast multinucleation. *J Cell Sci.* (2018) 131:jcs216267. doi: 10.1242/jcs.216267
25. Febbraio M, Hajjar DP, Silverstein RL. CD36: a class B scavenger receptor involved in angiogenesis, atherosclerosis, inflammation, and lipid metabolism. *J Clin Invest*. (2001) 108:785–91. doi: 10.1172/JCI14006
26. Christiakov DA, Bobryshev YV, Orekhov AN. Macrophage-mediated cholesterol handling in atherosclerosis. *J Cell Molec Med*. (2015) 20:1–12. doi: 10.1111/jcmm.12689
27. Boven LA, Van Meurs M, Van Zwam M, Wierenga-Wolf A, Hintzen RQ, Boot RG, et al. Myelin-laden macrophages are anti-inflammatory, consistent with foam cells in multiple sclerosis. *Brain.* (2006) 129:517–26. doi: 10.1093/brain/awh707
28. Xu S, Huang Y, Xie Y, Lan T, Le K, Chen J, et al. Evaluation of foam cell formation in cultured macrophages: an improved method with Oil

Red O staining and DiI-oxLDL uptake. *Cytotechnology*. (2010) 62:473–81. doi: 10.1007/s10616-010-9290-0
29. Dubland JA, Francis GA. Lysosomal acid lipase: at the crossroads of normal and atherogenic cholesterol metabolism. *Front Cell Dev Biol*. (2015) 3:3. doi: 10.3389/fcell.2015.00003
30. Xu P, Li J, Liu J, Wang J, Wu Z, Zhang X, et al. Mature adipocytes observed to undergo reproliferation and polyploidy. *FEBS Open Bio*. (2017) 7:652–8. doi: 10.1002/2211-5463.12207
31. Brodbeck WG, Anderson JM. Giant cell formation and function. *Curr Opin Hematol*. (2009) 16:53–7. doi: 10.1097/MOH.0b013e32831ac52e
32. Väänänen HK, Zhao H, Mulari M, Halleen JM. The cell biology of osteoclast function. *J Cell Sci*. (2000) 113:377–81.
33. Borrell-Pagès M, Romero JC, Juan-Babot O, Badimon L. Wnt pathway activation, cell migration, and lipid uptake is regulated by low-density lipoprotein receptor-related protein 5 in human macrophages. *Eur Heart J*. (2011) 32:2841–50. doi: 10.1093/eurheartj/ehr062
34. Wang X, Cao K, Sun X, Chen Y, Duan Z, Sun L, et al. Macrophages in spinal cord injury: phenotypic and functional change from exposure to myelin debris. *Glia*. (2015) 63:635–51. doi: 10.1002/glia.22774
35. Guo L, Rolfe AJ, Wang X, Tai W, Cheng Z, Cao K, et al. Rescuing macrophage normal function in spinal cord injury with embryonic stem cell conditioned media. *Mol Brain*. (2016) 9:48–62. doi: 10.1186/s13041-016-0233-3
36. Zammit PS, Clarke JD, Golding JP, Goodbrand IA, Tonge DA. Macrophage response during axonal regeneration in the axolotl central and peripheral nervous system. *Neuroscience*. (1993) 54:781–9. doi: 10.1016/0306-4522(93)90247-D
37. Monaghan JR, Walker JA, Page RB, Putta S, Beachy CK, Voss SR. Early gene expression during natural spinal cord regeneration in the salamander *Ambystoma mexicanum*. *J Neurochem*. (2007) 101:27–40. doi: 10.1111/j.1471-4159.2006.04344.x
38. Yamada Y, Doi T, Hamakubo T, Kodama T. Scavenger receptor family proteins: roles for atherosclerosis, host defense and disorders of the central nervous system. *Cell Mol Life Sci*. (1998) 54:628–40. doi: 10.1007/s000180050191
39. Zani IA, Stephen SL, Mughal NA, Russell D, Homer-Vanniasinkam S, Wheatcroft SB, et al. Scavenger receptor structure and function in health and disease. *Cells*. (2015) 4:178–201. doi: 10.3390/cells4020178
40. Oury C. CD36: linking lipids to the NLRP3 inflammasome, atherogenesis and atherothrombosis. *Cell Mol Immunol*. (2014) 11:8–10. doi: 10.1038/cmi.2013.48
41. Imai M, Watanabe M, Suyama K, Okada T, Sakai D, Kawada H, et al. Delayed accumulation of activated macrophages and inhibition of remyelination after spinal cord injury in an adult rodent model. *J Neurosurg Spine*. (2008) 8:58–66. doi: 10.3171/SPI-08/01/058
42. Vargas ME, Barres BA. Why is Wallerian degeneration in the CNS so slow? *Annu Rev Neurosci*. (2007) 30:153–79. doi: 10.1146/annurev.neuro.30.051606.094354
43. Love S. Demyelinating diseases. *J Clin Pathol*. (2006) 59:1151–9. doi: 10.1136/jcp.2005.031195
44. Chumasov EI, Svetikova KM. Structure and nature of macrophages participating in the Wallerian degeneration of nerve fibers. *Neurosci Behav Physiol*. (1992) 22:408–14. doi: 10.1007/BF01186634
45. Shen Z-L, Lassner F, Bader A, Becker M, Walter GF, Berger A. Cellular activity of resident macrophages during Wallerian degeneration. *Microsurgery*. (2000) 20:255–61. doi: 10.1002/1098-2752(2000)20:5<255::AID-MICR6>3.0.CO;2-A
46. Dibaj P, Steffens H, Zschüntzsch J, Nadrigny F, Schomburg ED, Kirchhoff F, et al. *In vivo* imaging reveals distinct inflammatory activity of CNS microglia versus PNS macrophages in a mouse model for ALS. *PLoS ONE*. (2011) 6:e17910. doi: 10.1371/journal.pone.0017910
47. Groh J, Weis J, Zieger H, Stanley ER, Heuer H, Martini R. Colony-stimulating factor-1 mediates macrophage-related neural damage in a model for Charcot-Marie-Tooth disease type 1X. *Brain*. (2012) 135:88–104. doi: 10.1093/brain/awr283
48. Yuan X, Klein D, Kerscher S, West BL, Weis J, Katona I, Martin R. Macrophage depletion ameliorates peripheral neuropathy in aging mice. *J Neurosci*. (2018) 38:4610–20. doi: 10.1523/JNEUROSCI.3030-17.2018
49. Chiu IM, Phatnani H, Kuligowski M, Tapia JC, Carrasco MA, Zhang M, et al. Activation of innate and humoral immunity in the peripheral nervous system of ALS transgenic mice. *Proc Natl Acad Sci USA*. (2009) 106:20960–5. doi: 10.1073/pnas.0911405106
50. Hooten KG, Beers DR, Zhao W, Appel SH. Protective and toxic neuroinflammation in amyotrophic lateral sclerosis. *Neurotherapeutics*. (2015) 12:364–75. doi: 10.1007/s13311-014-0329-3
51. Mammana S, Fagone P, Cavalli E, Basile MS, Petralia MC, Nicoletti F, et al. The role of macrophages in neuroinflammatory and neurodegenerative pathways of alzheimer's disease, amyotrophic lateral sclerosis, and multiple sclerosis: pathogenetic cellular effectors and potential therapeutic targets. *Int J Mol. Sci.* (2018) 19:831. doi: 10.3390/ijms19030831
52. Ueda Y, Imai K, Tsuchiya H, Fujimoto N, Nakanishi I, Katsuda S, et al. Matrix metalloproteinase 9 (gelatinase B) is expressed in multinucleated giant cells of human giant cell tumor of bone and is associated with vascular invasion. *Am J Pathol*. (1996) 148:611–22.
53. Newby AC, George SJ, Ismail Y, Johnson JL, Sala-Newby GB, Thomas AC. Vulnerable atherosclerotic plaque metalloproteinases and foam cell phenotypes. *Thromb Haemost*. (2009) 101:1006–11. doi: 10.1160/TH08-07-0469
54. Turk V, Stoka V, Vasiljeva O, Renko M, Sun T, Turk B, et al. Cysteine cathepsins: from structure, function and regulation to new frontiers. *Biochimica et Biophysica Acta*. (2012) 1824:68–88. doi: 10.1016/j.bbapap.2011.10.002
55. Zhu Y, Lyapichev K, Lee DH, Motti D, Ferraro NM, Zhang Y, et al. Macrophage transcriptional profile identifies lipid catabolic pathways that can be therapeutically targeted after spinal cord injury. *J Neurosci*. (2017) 37:2362–76. doi: 10.1523/JNEUROSCI.2751-16.2017
56. Chernoff EAG, Munck CM, Mendelsohn LG, Egar MW. Primary culture of axolotl spinal cord ependymal cells. *Tissue Cell*. (1990) 22:601–13. doi: 10.1016/0040-8166(90)90058-H
57. Kalt MR, Tandler B. A study of fixation of early amphibian embryos for electron microscopy. *J Ultrastruct Res*. (1971) 36:633–45. doi: 10.1016/S0022-5320(71)90020-7
58. Hsu J. *Multiple Comparisons Theory and Methods*. Boca Raton, FL: Chapman and Hall/CRC (1996).
59. Cain H, Kraus B, Krauspe R, Osborn M, Weber K. Vimentin filaments in peritoneal macrophages at various stages of differentiation and with altered function. *Virchows Archiv B Cell Pathol*. (1983) 42:65–81. doi: 10.1007/BF02890371
60. Popescu BO, Gherghiceanu M, Kostin S, Ceafalan L, Popescu LM. Telocytes in meninges and choroid plexus. *Neurosci Lett*. (2012) 516:265–9. doi: 10.1016/j.neulet.2012.04.006
61. Tooze J, Davies HG. Light and electron microscopic observations on the spleen and the splenic leukocytes of the newt *Triturus cristatus*. *Am J Anat*. (1968) 123:521–55. doi: 10.1002/aja.1001230308
62. Lopez D, Lin L, Monaghan JR, Cogle CR, Bova FJ, Maden M, et al. Mapping hematopoiesis in a fully regenerative vertebrate: the axolotl. *Blood*. (2014) 124:1232–41. doi: 10.1182/blood-2013-09-526970
63. Loura LMS, Prates Ramalho JP. Fluorescent membrane probes' behavior in lipid bilayers: insights from molecular dynamics simulations. *Biophys Rev*. (2009) 1:141–8. doi: 10.1007/s12551-009-0016-5
64. Kuda O, Pietka TA, Demianova Z, Kudova E, Cvacka J, Kopecky J, et al. Sulfo-N-succinimidyl oleate (SSO) inhibits fatty acid uptake and signaling for intracellular calcium via binding CD36 lysine 164: SSO also inhibits oxidized low density lipoprotein uptake by macrophages. *J Biol Chem*. (2013) 288:15547–55. doi: 10.1074/jbc.M113.473298
65. King IA, Tabiowo A, Williams RH. Incorporation of L-[^{3}H]fucose and D-^{3}[H]glucosamine into cell-surface-associated glycoconjugates in epidermis of cultured pig skin slices. *Biochem J*. (1980) 190:65–77. doi: 10.1042/bj1900065
66. Hanover JA, Cohen CK, Willingham MC, Park MK. O-linked N-acetylglucosamine is attached to proteins of the nuclear pore. Evidence for cytoplasmic and nucleoplasmic glycoproteins. *J Biol Chem*. (1987) 262:9887–94.
67. Sroga JM, Jones TB, Kigerl KA, McGaughy VM, Popovich PG. Rats and mice exhibit distinct inflammatory reactions after spinal cord injury. *J Comp Neurol*. (2003) 462:223–40. doi: 10.1002/cne.10736

68. Zhang F, Ferretti P, Clarke JDW. Recruitment of postmitotic neurons into the regenerating spinal cord of urodeles. *Dev Dyn.* (2003) 226:341–8. doi: 10.1002/dvdy.10230
69. Seitz A, Aglow E, Heber-Katz E. Recovery from spinal cord injury: a new transection model in the C57Bl/6 mouse. *J Neurosci Res.* (2002) 67:337–45. doi: 10.1002/jnr.10098
70. Grimpe B, Silver J. The extracellular matrix in axon regeneration. *Prog Brain Res.* (2002) 137:333–48. doi: 10.1016/S0079-6123(02)37025-0
71. Diaz Quiroz JF, Echeverri K. Spinal cord regeneration: where fish, frogs and salamanders lead the way, can we follow? *Biochem J.* (2013) 451:353–64. doi: 10.1042/BJ20121807
72. Silver J, Miller JH. Regeneration beyond the glial scar. *Nat Rev Neurosci.* (2004) 5:146–56. doi: 10.1038/nrn1326
73. O'Hara CM, Egar M, Chernoff EAG. Reorganization of the ependyma during axolotl spinal cord regeneration: Changes in intermediate filament and fibronectin expression. *Dev Dyn.* (1992) 193:103–15. doi: 10.1002/aja.1001930202
74. Shimasaki H, Maeba R, Tachibana R, Ueda N. Lipid peroxidation and ceroid accumulation in macrophages cultured with low density lipoprotein. *Gerontology.* (1995) 41:39–51. doi: 10.1159/000213724
75. Moore KJ, Freeman MW. Scavenger receptors in atherosclerosis: beyond lipid uptake. *Arterioscler Thromb Vasc Biol.* (2006) 26:1702–11. doi: 10.1161/01.ATV.0000229218.97976.43
76. Bogie JF, Stinissen P, Hellings N, Hendriks JJ. Myelin phagocytosing macrophages modulate autoreactive T cell proliferation. *J Neuroinflamm.* (2011) 8:85. doi: 10.1186/1742-2094-8-85
77. Maier CE, Miller RH. *In vitro* and *in vivo* characterization of blastemal cells from regenerating newt limbs. *J Exp Zool.* (1992) 262:180–92. doi: 10.1002/jez.1402620208
78. Washabaugh CH, Tsonis PA. Mononuclear leukocytes in the newt limb blastema: *in vitro* behavior. *Int J Dev Biol.* (1994) 38:745–9.
79. Milich L, Ryan C, Lee J. The origin, fate, and contribution of macrophages to spinal cord injury pathology. *Acta Neuropathol.* (2019) 137:785–97. doi: 10.1007/s00401-019-01992-3
80. Shechter R, Miller O, Yovel G, Rosenzweig N, London A, Ruckh J, et al. Recruitment of beneficial M2 macrophages to injured spinal cord is orchestrated by remote brain choroid plexus. *Immunity.* (2013) 38:555–69. doi: 10.1016/j.immuni.2013.02.012
81. Dauth S, Sîrbulescu RF, Jordans S, Rehders M, Avena L, Oswald J, et al. Cathepsin K deficiency in mice induces structural and metabolic changes in the central nervous system that are associated with learning and memory deficits. *BMC Neurosci.* (2011) 12:74–96. doi: 10.1186/1471-2202-12-74
82. Vidak E, Javoršek U, Vizovišek M, Turk B. Cysteine cathepsins and their extracellular roles: shaping the microenvironment. *Cells.* (2019) 8:264–88. doi: 10.3390/cells8030264
83. Lemaire PA, Huang L, Zhuo Y, Lu J, Bahnck C, Stachel SJ, et al. Chondroitin sulfate promotes activation of cathepsin K. *J Biol Chem.* (2014) 289:21562–72. doi: 10.1074/jbc.M114.559898
84. Mohamed MM, Sloane BF. Cysteine cathepsins: multifunctional enzymes in cancer. *Nature Rev Cancer.* (2006) 6:764–75. doi: 10.1038/nrc1949
85. Jevnikar Z, Rojnik M, Jamnik P, Doljak B, Fonovic UP, Kos J. Cathepsin H mediates the processing of talin and regulates migration of prostate cancer cells. *J Biol Chem.* (2013) 288:2201–9. doi: 10.1074/jbc.M112.436394
86. Jevnikar Z, Obermajer N, Kos J. LFA-1 fine-tuning by cathepsin X. *IUBMB Life.* (2011) 63:686–93. doi: 10.1002/iub.505
87. Johansson CB, Momma S, Clarke DL, Risling M, Lendahl U, Frisén J. Identification of a neural stem cell in the adult mammalian central nervous system. *Cell.* (1999) 96:25–34. doi: 10.1016/S0092-8674(00)80956-3
88. Shimabukuro MK, Langhi LGP, Cordeiro I, Brito JM, Claudia Batista CMC, Mattson MP, et al. Lipid-laden cells differentially distributed in the aging brain are functionally active and correspond to distinct phenotypes. *Sci Rep.* (2016) 6:23795. doi: 10.1038/srep23795
89. Erickson MA, Banks WA. Neuroimmune axes of the blood–brain barriers and blood–brain interfaces: bases for physiological regulation, disease states, and pharmacological interventions. *Pharmacol Rev.* (2018) 70:278–314. doi: 10.1124/pr.117.014647
90. Zlokovic BV, Martel CL, Matsubara E, McComb JG, Zheng G, McCluskey RT, et al. Glycoprotein 330/megalin: probable role in receptor-mediated transport of apolipoprotein J alone and in a complex with Alzheimer disease amyloid beta at the blood-brain and blood-cerebrospinal fluid barriers. *Proc Natl Acad Sci USA.* (1996) 93:4229–34. doi: 10.1073/pnas.93.9.4229
91. Greenhalgh AD, David S. Differences in the phagocytic response of microglia and peripheral macrophages after spinal cord injury and its effects on cell death. *J Neurosci.* (2014) 34:6316–22. doi: 10.1523/JNEUROSCI.4912-13.2014
92. Shimasaki H. Assay of fluorescent lipid peroxidation products. *Methods Enzymol.* (1994) 233:338–46. doi: 10.1016/S0076-6879(94)33039-5
93. Hui SP, Monaghan JR, Voss SR, Ghosh S. Expression pattern of Nogo-A, MAG, and NgR in regenerating urodele spinal cord. *Dev Dyn.* (2013) 242:847–60. doi: 10.1002/dvdy.23976
94. Chen MS, Huber AB, Van Der Haar ME, Frank M, Schnell L, Spillmann AA, et al. Nogo-A is a myelin-associated neurite outgrowth inhibitor and an antigen for monoclonal antibody IN-1. *Nature.* (2000) 403:434–9. doi: 10.1038/35000219
95. Liu C, Li Y, Yu J, Feng L, Hou S, Liu Y, et al. Targeting the shift from M1 to M2 macrophages in experimental autoimmune encephalomyelitis mice treated with fasudil. *PLoS ONE.* (2013) 8:e54841. doi: 10.1371/journal.pone.0054841
96. Bogie JF, Stinissen P, Hendriks J J. Macrophage subsets and microglia in multiple sclerosis. *Acta Neuropathol.* (2014) 128:191–213. doi: 10.1007/s00401-014-1310-2
97. Wang J, Wang J, Wang J, Yang B, Weng Q, He Q. Targeting microglia and macrophages: a potential treatment strategy for multiple sclerosis. *Front Pharmacol.* (2019) 10:286. doi: 10.3389/fphar.2019.00286
98. Gao Q, Goodman JM. The lipid droplet-a well-connected organelle. *Front Cell Dev Biol.* (2015) 3:49. doi: 10.3389/fcell.2015.00049
99. Pol A, Gross SP, Parton RG. Biogenesis of the multifunctional lipid droplet: lipids, proteins, and sites. *J Cell Biol.* (2014) 204:635–46. doi: 10.1083/jcb.201311051
100. Remmerie A, Scott CL. Macrophages and lipid metabolism. *Cell Immunol.* (2018) 330:27–42. doi: 10.1016/j.cellimm.2018.01.020
101. Brown MS, Goldstein JL. Lipoprotein metabolism in the macrophage: implications for cholesterol deposition in atherosclerosis. *Annu Rev Biochem.* (1983) 52:223–61. doi: 10.1146/annurev.bi.52.070183.001255
102. Yancey PG, Jerome WG. Lysosomal cholesterol derived from mildly oxidized low density lipoprotein is resistant to efflux. *J Lipid Res.* (2001) 42:317–27.
103. Griffin EE, Ullery JC, Cox BE, Jerome WG. Aggregated LDL and lipid dispersions induce lysosomal cholesteryl ester accumulation in macrophage foam cells. *J Lipid Res.* (2005) 46:2052–60. doi: 10.1194/jlr.M500059-JLR200
104. Orso E, Grand M, Schmitz G. Oxidized LDL-induced endolysosomal phospholipidosis and enzymatically modified LDL-induced foam cell formation determine specific lipid species modulation in human macrophages. *Chem Phys Lipids.* (2011) 164:479–87. doi: 10.1016/j.chemphyslip.2011.06.001
105. Cox BE, Griffin EE, Ullery JC, Jerome WG. Effects of cellular cholesterol loading on macrophage foam cell lysosome acidification. *J Lipid Res.* (2007) 48:1012–21. doi: 10.1194/jlr.M600390-JLR200
106. Jerome WG, Cox BE, Griffin EE, Ullery JC. Lysosomal cholesterol accumulation inhibits subsequent hydrolysis of lipoprotein cholesteryl ester. *Microsc Microanal.* (2008) 14:138–49. doi: 10.1017/S1431927608080069
107. Usuku G, Gross J. Morphologic studies of connective tissue resorption in the tail fin of metamorphosing bullfrog tadpole. *Dev Biol.* (1965) 11:352–70. doi: 10.1016/0012-1606(65)90044-8
108. Galis ZS, Sukhova GK, Franzhofer R, Clark S, Libby P. Macrophage foam cells from experimental atheroma constitutively produce matrix-degrading proteinases. *Proc Natl Acad Sci USA.* (1965) 92:402–6. doi: 10.1073/pnas.92.2.402
109. Cossins JA, Clements JM, Ford J, Miller KM, Pigott R, Vos W, et al. Enhanced expression of MMP-7 and MMP-9 in demyelinating multiple sclerosis lesions. *Acta Neuropathol.* (1997) 94:590–8. doi: 10.1007/s004010050754
110. Lindholm MW, Nilsson J, Moses J. Low density lipoprotein stimulation of human macrophage proteoglycan secretion. *Biochem Biophys Res Comm.* (2005) 328:455–60. doi: 10.1016/j.bbrc.2005.01.003

111. Chang MY, Olin KL, Tsoi C, Wight TN, Chait A. Human monocyte-derived macrophages secrete two forms of proteoglycan-macrophage colony-stimulating factor that differ in their ability to bind low density lipoproteins. *J Biol Chem*. (1998) 273:15985–92. doi: 10.1074/jbc.273.26.15985
112. Thomas AC, Eijgelaar WJ, Daemen MJAP, Newby AC. Foam cell formation *in vivo* converts macrophages to a pro-fibrotic phenotype. *PLoS ONE.* (2015) 10:e0128163. doi: 10.1371/journal.pone.0128163
113. Horn KP, Busch SA, Hawthorne AL, Rooijen N, Silver J. Another barrier to regeneration in the CNS: activated macrophages induce extensive retraction of dystrophic axons through direct physical interactions. *J Neurosci*. (2008) 28:9330–41. doi: 10.1523/JNEUROSCI.2488-08.2008
114. Zhu Y, Soderblom C, Krishnan V, Ashbaugh J, Bethea JR, Lee JK. Hematogenous macrophage depletion reduces the fibrotic scar and increases axonal growth after spinal cord injury. *Neurobiol Dis*. (2015) 74:114–25. doi: 10.1016/j.nbd.2014.10.024
115. Godwin JW, Pinto AR, Rosenthal NA. Macrophages are required for adult salamander limb regeneration. *Proc Natl Acad Sci USA*. (2013) 110:9415–20. doi: 10.1073/pnas.1300290110
116. Godwin JW, Debuque R, Salimova E, Rosenthal NA. Heart regeneration in the salamander relies on macrophage-mediated control of fibroblast activation and the extracellular landscape. *NPJ Regen Med*. (2017) 2:22. doi: 10.1038/s41536-017-0027-y
117. Aurora AB, Porrello ER, Tan W, Mahmoud AI, Hill JA, Bassel-Duby R, et al. Macrophages are required for neonatal heart regeneration. *J Clin Invest*. (2014) 124:1382–92. doi: 10.1172/JCI 72181
118. Falcone DJ, McCaffrey TA, Haimovitz-Friedman A, Vergilio J-A, Nicholson AC. Macrophage and foam cell release of matrix-bound growth factors. *J Biol Chem*. (1993) 268:11951–8.
119. Vishwakarma SK, Bardia A, Lakkireddy C, Paspala SAB, Khan AA. Bioengineering human neurological constructs using decellularized meningeal scaffolds for application in spinal cord injury. *Front Bioeng Biotechnol.* (2018) 6:150. doi: 10.3389/fbioe.2018.00150
120. Zhang F, Clarke JDW, Ferretti P. FGF-2 Up-regulation and proliferation of neural progenitors in the regenerating amphibian spinal cord *in vivo*. *Dev Biol*. (2000) 225:381–91. doi: 10.1006/dbio.2000.9843

Conflict of Interest: The authors declare that the research was conducted in the absence of any commercial or financial relationships that could be construed as a potential conflict of interest.

frontiers in Immunology

REVIEW
published: 17 December 2019
doi: 10.3389/fimmu.2019.02958

The CD40-ATP-P2X$_7$ Receptor Pathway: Cell to Cell Cross-Talk to Promote Inflammation and Programmed Cell Death of Endothelial Cells

Carlos S. Subauste [1,2*]

[1] Division of Infectious Diseases and HIV Medicine, Department of Medicine, Case Western Reserve University, Cleveland, OH, United States, [2] Department of Pathology, Case Western Reserve University, Cleveland, OH, United States

Extracellular adenosine 5′-triphosphate (ATP) functions not only as a neurotransmitter but is also released by non-excitable cells and mediates cell–cell communication involving glia. In pathological conditions, extracellular ATP released by astrocytes may act as a "danger" signal that activates microglia and promotes neuroinflammation. This review summarizes *in vitro* and *in vivo* studies that identified CD40 as a novel trigger of ATP release and purinergic-induced inflammation. The use of transgenic mice with expression of CD40 restricted to retinal Müller glia and a model of diabetic retinopathy (a disease where the CD40 pathway is activated) established that CD40 induces release of ATP in Müller glia and triggers in microglia/macrophages purinergic receptor-dependent inflammatory responses that drive the development of retinopathy. The CD40-ATP-P2X$_7$ pathway not only amplifies inflammation but also induces death of retinal endothelial cells, an event key to the development of capillary degeneration and retinal ischemia. Taken together, CD40 expressed in non-hematopoietic cells is sufficient to mediate inflammation and tissue pathology as well as cause death of retinal endothelial cells. This process likely contributes to development of degenerate capillaries, a hallmark of diabetic and ischemic retinopathies. Blockade of signaling pathways downstream of CD40 operative in non-hematopoietic cells may offer a novel means of treating diabetic and ischemic retinopathies.

Keywords: CD40, glia, retina, endothelial cell, ATP, cytokine, diabetes

OPEN ACCESS

Edited by:
Antje Kroner, Medical College of Wisconsin, United States

Reviewed by:
Rishein Gupta, University of Texas at San Antonio, United States
Bruce Hostager, The University of Iowa, United States
Steven F. Abcouwer, Michigan Medicine, United States

***Correspondence:**
Carlos S. Subauste
carlos.subauste@case.edu

Specialty section:
This article was submitted to Multiple Sclerosis and Neuroimmunology, a section of the journal Frontiers in Immunology

Received: *28 May 2019*
Accepted: *02 December 2019*
Published: *17 December 2019*

Citation:
Subauste CS (2019) The CD40-ATP-P2X$_7$ Receptor Pathway: Cell to Cell Cross-Talk to Promote Inflammation and Programmed Cell Death of Endothelial Cells. Front. Immunol. 10:2958. doi: 10.3389/fimmu.2019.02958

INTRODUCTION

Glia orchestrate homeostasis in neural tissue through cell-to-cell interactions. Communication among glial subsets and communication between glia and other cells of the nervous system are also important during the development of disorders with an inflammatory component. ATP released by astrocytes appears to cause neuroinflammation by activating pro-inflammatory responses in microglia (1). Retinopathies caused by diabetes and ischemia are driven to a significant extent by chronic inflammation (2–4). The CD40 pathway is activated in these retinopathies and CD40 has emerged as a central mediator of inflammatory responses and pathology in these disorders (5–7). Herein I will review our work that identified CD40 expressed in retinal Müller glia as a trigger

for secretion of ATP that in turn engages the $P2X_7$ receptor leading to pro-inflammatory cytokine production by monocyte/macrophages/microglia and programmed cell death of retinal endothelial cells (7, 8). Through this process, CD40 present in a non-hematopoietic cell amplifies inflammation and causes tissue pathology.

CD40

CD40 is a member of the TNF receptor superfamily that is expressed in various hematopoietic and non-hematopoietic cells including antigen-presenting cells (B cells, dendritic cells, and monocyte/macrophages), endothelial cells, epithelial cells, vascular smooth muscle cells, retinal Müller glia, fibroblasts, and neurons (6, 9–13). CD154 (CD40 ligand) is expressed primarily on activated $CD4^+$ T cells, platelets, and is also present as a biologically active soluble protein present in plasma (14, 15).

Studies in patients with congenital absence of functional CD154 (Hyper IgM syndrome, X-HIM) provide clinical evidence for the central role of this pathway in adaptive immunity (16). CD40-CD154 interaction promotes dendritic cell maturation inducing licensing of these cells for efficient T cell priming (14, 17, 18). This pathway stimulates IL-12 secretion by dendritic cells that in turn promotes $CD4^+$ T cell differentiation into Th1 cells (14, 17, 18). It also supports $CD8^+$ cytotoxic T lymphocytes (CTL) development and prevents CTL exhaustion (19). CD40-CD154 interaction promotes pro-inflammatory cytokine production by macrophages and activates effector functions that are central to control of intracellular pathogens (14, 18). Indeed, the most important clinical feature of patients with X-HIM is the increased susceptibility to opportunistic infections normally controlled by cell-mediated immunity (16). The CD40-CD154 pathway is also central for humoral immune responses including B cell proliferation, germinal center formation, antibody production, immunoglobulin class switch, and the generation of B cell memory (14, 17, 18).

In contrast to hematopoietic cells, little is known about the physiologic role of CD40 in non-hematopoietic cells. It has been proposed that CD40 promotes survival of neurons in the brain since old $CD40^{-/-}$ mice (16 months of age) have reduced expression of neurofilament isoforms and exhibit evidence compatible with increased neuronal programmed cell death ($TUNEL^+$ neurons) (12). In addition, in developing neural tissue, CD40 promotes axon growth in sympathetic neurons and has effects on dendrite growth that vary depending on the class of neurons: CD40 promotes dendrite growth in hippocampal excitatory neurons while it suppresses dendrite growth in striatal inhibitory neurons (20, 21). It is not known whether CD40 regulates the development and survival of retinal neurons. Moreover, the physiologic function of CD40 expressed in non-hematopoietic compartments in other organs is unclear. This may be explained by the low levels of CD40 expression in these compartments under basal conditions. In contrast, CD40 is upregulated in various inflammatory disorders and, through ligand engagement, CD40 triggers pro-inflammatory responses in endothelial cells, vascular smooth muscle cells and epithelial cells that play a key role in the pathogenesis of various disorders such as inflammatory bowel disease, systemic lupus erythematosus, rheumatoid arthritis, multiple sclerosis, graft rejection, and atherosclerosis (22, 23). These responses include increased protein expression of adhesion molecules, chemokines, metalloproteinases, and tissue factor (22, 23). The effects of CD40 ligation on retinal non-hematopoietic cells are discussed below.

DIABETIC AND OTHER ISCHEMIC RETINOPATHIES

Diabetes mellitus has become one of the most important health problems in the world. It is estimated that there are 422 million patients with diabetes worldwide (World Health Organization; www.who.int/diabetes/global-report). Diabetic retinopathy (DR) is a major complication of diabetes and eventually occurs in ∼35% of patients with diabetes (24). In addition, DR is the most common cause of vision loss among working-age adults in developed countries (25). The development of DR appears to be multifactorial and mechanisms such as oxidative stress, increased polyol and hexosamine pathway flux, protein kinase C activation, increased formation of advanced glycation-end products and alterations in systemic and local lipid metabolism have been linked to the development of the disease (26, 27). Ample experimental data indicate that low-grade chronic inflammation also plays an important role in the development of DR (2–4).

The vitreous of patients with DR (28) and retinal endothelial cells from diabetic humans and rodents exhibit increased expression of ICAM-1, an event that promotes adherence of leukocytes to the retinal vasculature (leukostasis) (29, 30). This phenomenon is important since blockade of ICAM-1–CD18 interaction diminishes the development of degenerate capillaries in diabetic mice (31). These structures are a hallmark of early diabetic retinopathy and are formed as a consequence of the death of endothelial cells and pericytes, leading to the transformation of capillaries into collapsed sheaths of collagen/extracellular matrix structures that lack blood flow (32). The ensuing ischemia can promote transition to proliferative DR (PDR) that is characterized by retinal neovascularization. DR is also accompanied by increased expression of TNF-α and IL-1β (33–36). Microglia/macrophages express TNF-α in the diabetic retina (34). TNF-α and IL-1β play a pathogenic role in DR since they contribute to diabetes-induced degeneration of retinal capillaries (37, 38). Inducible nitric oxide synthase (NOS2) is expressed in the retinas of patients with DR and of diabetic rodents (39, 40). Furthermore, diabetic $NOS2^{-/-}$ mice have reduced retinal leukostasis and capillary degeneration (41, 42). CCL2 levels are increased in the vitreous fluid in patients with PDR (43) and in retinas of diabetic rodents (44). This chemokine appears to play a pathogenic role in DR since there is a correlation between CCL2 protein levels in the vitreous with the severity of DR (43).

Ischemic retinopathies including those caused by central retinal artery occlusion, retinal vein occlusion, and retarded retinal vascular development in premature infants are important causes of permanent visual impairment and blindness in

adults and children (45–47). Like DR, inflammatory responses including TNF-α, IL-1β, nitro-oxidative stress, and chemokines likely play an important role in the pathogenesis of these diseases (48). Retinal injury induced by ischemia/reperfusion (I/R) is a commonly used animal model of ischemic retinopathy (49). I/R-induced retinopathy is characterized by retinal inflammation, loss of ganglion cells, and development of capillary degeneration (49). I/R of the retina causes upregulation of ICAM-1, TNF-α, IL-1, NOS2, and COX-2 (5, 49–53). These responses are pathogenic since approaches to inhibit them are protective against retinal pathology (50–54).

CD40 IN THE DEVELOPMENT OF DIABETIC AND I/R-INDUCED RETINOPATHIES

CD40 is expressed in the retina at the level of endothelial cells, Müller glia (important macroglia in the retina), microglia, ganglion cells, and retinal pigment epithelial cells (5, 6, 55, 56). The levels of CD40 expression are low under basal conditions. However, induction or upregulation of CD40 expression is a feature of inflammatory disorders driven by CD40 (57). Indeed, CD40 mRNA is upregulated in the retina of mice with diabetes and mice subjected to retinal I/R (5, 6). Immunohistochemistry and flow cytometry studies to assess protein expression revealed that CD40 is upregulated in retinal endothelial cells, Müller glia and microglia of diabetic mice (6). Importantly, $CD40^{-/-}$ mice are protected from I/R-induced retinopathy and early diabetic retinopathy (5, 6).

Ligation of CD40 in retinal Müller glia upregulates ICAM-1, CCL2, NOS2 at the protein level and stimulates PGE_2 production (5, 6, 58). CD40 ligation in retinal endothelial cells upregulates ICAM-1 and CCL2 protein levels (5, 6, 58). Retinal endothelial cells also produce CXCL1 following CD40 stimulation, a response that is markedly potentiated by a low concentration of IL-1β (5).

CD40 is central for the development of retinal inflammation and retinopathy induced by I/R. In contrast to wild-type mice, $CD40^{-/-}$ mice subjected to I/R are protected from upregulation of ICAM-1, CXCL1, NOS2, and COX-2 mRNA levels (5). The reduced expression of NOS2 and COX-2 is explained at least in part by diminished recruitment of $NOS2^{+}$ $COX\text{-}2^{+}$ leukocytes into the retina of $CD40^{-/-}$ mice (5). Importantly, the loss of ganglion cells and the development of capillary degeneration are markedly attenuated in ischemic retinas of $CD40^{-/-}$ mice (5). The protection from development of ischemic retinopathy observed in $CD40^{-/-}$ mice is likely explained by diminished leukocyte infiltration and reduced expression of pro-inflammatory molecules since blockade of ICAM-1, NOS2, or COX-2 protect from retinal pathology after ischemia (51, 52, 54). Altogether, CD40 is a central mediator of inflammation and neuro-vascular degeneration after I/R-induced injury of the retina. The model that likely explains these findings is as follows: ischemia-induced activation of CD40 in retinal endothelial cells triggers ICAM-1 and KC/CXCL1 upregulation leading to recruitment of NOS2 and COX-2-expressing leukocytes that would in turn promote neurovascular degeneration in the retina (5). However, it is also possible that Müller glia from ischemic retinas could be a source of increased NOS2 and/or COX-2 expression after activation via CD40.

The upregulation of CD40 and CD154 indicate that this pathway is activated in diabetes. CD40 protein expression in increased in the retina of diabetic mice and in the kidneys of patients with diabetic nephropathy (6, 59). CD40 mRNA levels are upregulated in the retinas of diabetic mice (6). Peripheral blood mononuclear cells from poorly controlled patients with type I diabetes exhibit increased mRNA levels of the functional type I isoform of CD40 (60). It is not known whether changes in micro RNA that control CD40 transcription [i.e., miR-155, miR-424, miR-503 (61, 62)] explain the upregulation of CD40 mRNA. In addition, CD154 protein levels are elevated in the blood from patients with diabetic microangiopathy and mice with diabetes (7, 63, 64). CD154 upregulation is biologically relevant since serum CD154 from diabetics triggers pro-inflammatory responses in endothelial cells and monocytes (63). It is likely that CD154 levels are also increased in the retina because microthrombosis occurs in diabetic retinopathy and activated platelets express CD154 (65).

CD40 is relevant to DR since diabetic $CD40^{-/-}$ mice are protected from upregulation of ICAM-1 in retinal endothelial cells, leukostasis, upregulation of TNF-α, IL-1β, and NOS2 mRNA levels, retinal protein nitration and elevated CCL2 mRNA levels in the retina (6, 7, 58). Importantly, diabetic $CD40^{-/-}$ mice do not develop capillary degeneration (6, 7). Taken together, CD40 is critical for development of various inflammatory responses in the diabetic retina and the development early DR (6, 7).

CD40 IN MÜLLER GLIA RECRUITS INFLAMMATORY RESPONSES IN BYSTANDER MICROGLIA/MACROPHAGES

Leukocytes are recognized key players in the development of inflammatory disorders. Indeed, expression of NOS2 or poly(ADP-ribosyl) polymerase 1 (PARP1) in bone marrow cells is necessary for the development of early DR (66). Similarly, CD40 in hematopoietic cells has been deemed a central driver of inflammation. However, studies in mice using bone marrow chimeras revealed that CD40 expressed in non-hematopoietic cells is also required for inflammation (5). Absence of CD40 in the retina inhibits ICAM-1 mRNA upregulation, leukocyte recruitment to the retina and neurovascular degeneration after I/R of the retina (5). Importantly, studies using transgenic mice have established that CD40 expression in a non-hematopoietic cell—Müller glia—is sufficient for development of an inflammatory disorder (7).

Müller glia link with neurons and capillaries, and are central to retina homeostasis (67, 68). Müller glia become dysfunctional and acquire expression of proinflammatory genes in diabetic and other ischemic retinopathies (69–71). The fact that Müller glia

express CD40 raised the possibility that CD40 present in these cells may be an important activator of inflammation and retinal injury. Studies in transgenic mice that expressed CD40 restricted to Müller glia demonstrated that, after induction of diabetes, the presence of CD40 in these cells was sufficient for upregulation of ICAM-1, NOS2, TNF-α, IL-1β, CCL2 mRNA levels as well as for development of leukostasis and capillary degeneration (7). This work identified CD40 in Müller glia as a central regulator of inflammation and development of early diabetic retinopathy.

Despite the fact that CD40 in Müller glia from diabetic mice drives TNF-α and IL-1β *in vivo*, work done *in vitro* revealed that human and rodent Müller glia are unable to secrete these pro-inflammatory cytokines in response to CD40 ligation even though these cells react to CD40 stimulation (CCL2 secretion and ICAM-1 protein upregulation) (7). This apparent discrepancy raised the possibility that CD40 in Müller glia acts on bystander microglia/macrophages to promote expression of TNF-α and IL-1β.

Testing whether Müller glia activated by CD40 induce IL-1β and TNF-α production in bystander monocytes/macrophages was done by adding human CD154 to human $CD40^+$ Müller glia incubated with $CD40^-$ human monocytic cells (to avoid the effects of direct CD40 ligation on these cells), or by adding human CD154 to human CD40-expressing mouse Müller glia incubated with mouse macrophages (human CD154 does not stimulate mouse CD40 expressed in macrophages) (7). While Müller glia and monocyte/macrophages failed to secrete TNF-α and IL-1β in response to CD154, addition of CD154 to the co-culture of these cells triggered TNF-α and IL-1β production (7). The *in vitro* studies have an *in vivo* correlate since diabetic mice that express CD40 restricted to Müller glia upregulate TNF-α protein levels in microglia/macrophages but not in Müller glia while the latter cells upregulate CCL2 protein levels (7). Taken together, these studies revealed that Müller glia activated by CD40 induce pro-inflammatory responses in bystander microglia/macrophages.

THE CD40-ATP-P2X7 PATHWAY AND INFLAMMATORY RESPONSES IN BYSTANDER MICROGLIA/MACROPHAGES

ATP functions not only as a neurotransmitter for neurons but can also be secreted by non-excitable cells (72, 73). Moreover, various cell types express P2 purinergic receptors. These receptors are divided into ATP-gated ionotropic P2X receptors and metabotropic, G protein-coupled P2Y receptors (72, 73). The seven subtypes of P2X receptors are ligand-gated channels permeable to Ca^{2+}, Na^+, and K^+. $P2X_7$ receptor is characterized by the ability to form large trans-membrane pores in response to repetitive or prolonged exposure to ATP (72, 73). $P2X_7$ receptor is key for IL-1β and TNF-α secretion by microglia/macrophages stimulated with ATP (74, 75). Indeed, secretion of ATP by astrocytes may cause $P2X_7$-dependent microglial activation that would drive neuroinflammatory and degenerative disorders (76).

In vitro and *in vivo* studies were conducted to determine whether CD40 acts through ATP-$P2X_7$ signaling to induce cytokine production in bystander myeloid cells. These studies showed that CD40 is an inducer of ATP release in Müller glia (7). Moreover, purinergic signaling explains TNF-α and IL-1β secretion in bystander monocytes/macrophages incubated with Müller glia activated by CD40. Blockade of the $P2X_7$ receptor either by pharmacologic approaches, knockdown of $P2X_7$ or the use of macrophages from $P2X_7^{-/-}$ mice results in marked inhibition of TNF-α and IL-1β secretion (7). In addition, a purinergic receptor ligand (Bz-ATP) enhances cytokine production by monocytic cells (7).

As described above, studies in diabetic transgenic mice that express CD40 only in Müller glia revealed that TNF-α is expressed in a distinct compartment—microglia/macrophages (7). Moreover, $P2X_7$ receptor mRNA levels are enhanced in the retinas of diabetic mice and $P2X_7$ receptor protein expression is increased in microglia/macrophages from these animals (7). This is relevant since increased levels of $P2X_7$ receptor facilitate the effects of the receptor (77). Mice treated with the $P2X_7$ receptor inhibitor BBG as well as $P2X_7^{-/-}$ mice are protected from diabetes-induced upregulation of IL-1β and TNF-α mRNA levels (7). The mice are also protected from increased expression of ICAM-1 and NOS2, molecules that are upregulated by IL-1β and TNF-α (78, 79). Taken together, Müller glia activated by CD40 secrete extracellular ATP and drive $P2X_7$ receptor-dependent pro-inflammatory cytokine expression in bystander microglia/macrophages *in vitro* and *in vivo* (**Figure 1** and **Table 1**). These findings support a model whereby CD40 engagement in non-hematopoietic cells triggers inflammatory

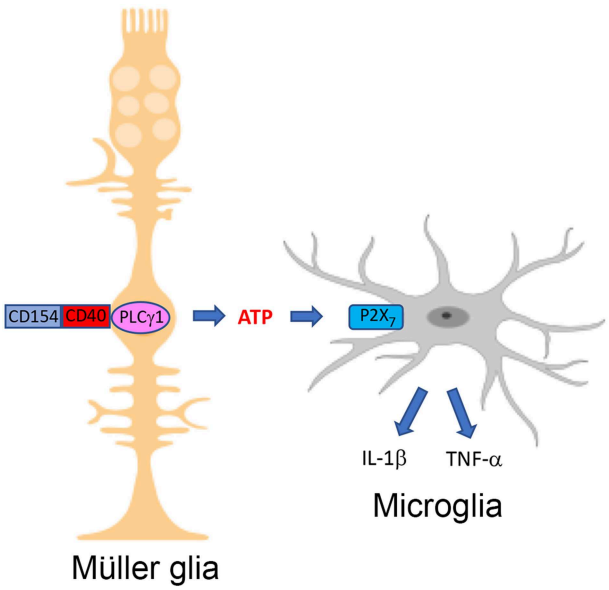

FIGURE 1 | The CD40-ATP-$P2X_7$ pathway links cellular responses in Müller glia with the induction of inflammatory responses in bystander microglia/macrophages in DR. Blood levels of CD154 and expression of CD40 in Müller glia are increased in diabetes. CD40 ligation in Müller glia causes PLCγ1 (PLC) activation and secretion of extracellular ATP. $P2X_7$ receptor is upregulated in microglia/macrophages in the diabetic retina. ATP binds $P2X_7$ receptor leading to secretion of TNF-α and IL-1β. Created in part with BioRender.com.

TABLE 1 | Components of the CD40-ATP-P2X$_7$ pathway in retinopathies.

Müller glia	Important macroglia in the retina that closely communicates with various retinal cells (67, 68)
CD40	Expressed in Müller glia, retinal endothelial cells, microglia/macrophages, and is upregulated in diabetic and I/R-induced retinopathies (5, 6, 55, 56)
CD154	Major ligand of CD40 that is upregulated in plasma and likely in retinal microthrombi in diabetes (7, 63–65)
PLCγ1	Activated by CD40 ligation in Müller glia and triggers release of extracellular ATP (7)
ATP	Secreted by CD40-activated Müller glia and mediates Müller glia—microglia/macrophages and Müller glia—endothelial cell communication (7, 8)
P2X$_7$ receptor	ATP receptor upregulated in microglia and retinal endothelial cells in a CD40-dependent manner. Induces pro-inflammatory cytokine secretion by macrophages/microglia and programmed cell death in endothelial cells (7, 8)
TNF-α/IL-1β	Upregulated in diabetic and I/R-induced retinopathies, and linked to development of these retinopathies (33–38, 48–50, 53). CD40 promotes TNF-α/IL-1β upregulation (11)
ICAM-1	Upregulated in endothelial cells in diabetic and I/R-induced retinopathies and linked to development of these retinopathies (3, 29, 30, 49, 54). CD40 promotes ICAM-1 upregulation in retinal endothelial cells (5, 6, 58)
CCL2	Upregulated in diabetic retinopathy and levels of CCL2 are associated with severity of the disease (43, 44). CD40 promotes CCL2 production in endothelial cells and Müller glia (6, 58)
CXCL1	Upregulated in I/R-induced retinopathy (5). CD40 promotes CXCL1 production by endothelial cells (5)
NOS2/COX-2	Upregulated in diabetic and/or I/R-induced retinopathies and linked to development of retinopathies (39–42, 49, 51, 52). CD40 drives NOS2/COX-2 upregulation (5, 6)

responses not only in these cells (i.e., chemokine and adhesion molecule upregulation) but also amplifies inflammation by enabling bystander myeloid cells to secrete pro-inflammatory cytokines in a manner dependent on ATP-P2X$_7$ receptor.

Increased intracytoplasmic Ca^{2+} triggers ATP release (80) and CD40 elevates intracytoplasmic Ca^{2+} levels (81, 82). Indeed, BAPTA-AM, a chelator of intracellular Ca^{2+}, impairs CD40-mediated ATP release in Müller cells (7). In addition, CD40 ligation in Müller glia causes rapid Tyr783 phosphorylation of phospholipase Cγ1 (PLCγ1) (7), a signaling molecule that increases intracytoplasmic Ca^{2+} (83), and pharmacologic inhibition of PLC impairs ATP release by Müller glia activated by CD40 (7). Thus, CD40 ligation phosphorylates PLCγ1 and CD40 likely functions via PLCγ1 to trigger ATP release in Müller glia.

CD40 IN MÜLLER GLIA AND PROGRAMMED CELL DEATH OF BYSTANDER RETINAL ENDOTHELIAL CELLS

Retinal endothelial cells undergo programmed cell death (PCD) in the diabetic retina (32, 84–86). This process would contribute to the development of capillary degeneration, a central feature of early diabetic retinopathy (32). CD40 is necessary for the development of capillary degeneration (6, 7) and yet, ligation of CD40 in endothelial cells does not induce PCD likely because CD40 typically triggers pro-survival signals (87). This raised the possibility of CD40 promoting death of retinal endothelial cells by acting through other cells of the retina. Müller cells were a likely culprit since they encircle retinal endothelial cells.

Whereas direct CD40 ligation in retinal endothelial cells does not cause PCD, CD40 stimulation enhances PCD of endothelial cells when they are incubated with CD40$^+$ Müller cells (8). This effect is not driven by NOS2, oxidative stress, TNF-α, IL-1β, or Fas ligand (8). As described above, CD40 ligation in Müller glia increases release of ATP. CD40 ligation in retinal endothelial cells upregulates P2X$_7$ receptor expression making these cells susceptible to ATP-induced PCD (8). Indeed, pharmacologic inhibition of P2X$_7$ receptor prevents PCD of the endothelial cells (8). These results are consistent with the ability of the P2X$_7$ to form trans-membrane pores that are permeable to hydrophilic molecules of up to 900 Da (88) and mediate cell death (89, 90). The *in vitro* studies described above have an *in vivo* correlate since retinal P2X$_7$ mRNA levels and P2X$_7$ receptor expression in retinal endothelial cells are increased in diabetic mice in a CD40-dependent manner (8), CD40 appears to be necessary for PCD of retinal endothelial cells from diabetic mice (8), and CD40 is known to be required for retinal capillary degeneration (6, 7). Taken together, CD40 has a dual role in promoting PCD of retinal endothelial cells: it causes release of extracellular ATP by Müller glia and makes retinal endothelial cells susceptible to P2X$_7$-driven PCD (**Figure 2** and **Table 1**). The latter effect may be explained by CD40-driven upregulation of the P2X$_7$ receptor in endothelial cells that would overcome the pro-survival signals activated by CD40 ligation. This mechanism may contribute to increased susceptibility to ATP-mediated PCD that appears to occur in diabetes (91). Other potential mechanisms by which CD40 increases susceptibility to P2X$_7$ receptor-mediated PCD may include modulation of ATP-gated channel expression, ectoATPase activity, and/or coupling to downstream cell signaling pathways that promote cell death. Finally, while CD40-induced activation of ATP-P2X$_7$ receptor signaling mediates PCD of retinal endothelial cells, CD40 may also promote death of these cells and capillary degeneration through mechanisms that include: enhancement of retinal leukostasis, upregulation of NOS2, TNF-α, and IL-1β in the retinas of diabetic mice (6, 7), events linked to PCD of retinal endothelial cells and capillary degeneration (31, 37, 38, 40, 42, 86).

In summary, the studies discussed here discovered the CD40-ATP-P2X$_7$ receptor pathway and revealed that this pathway links

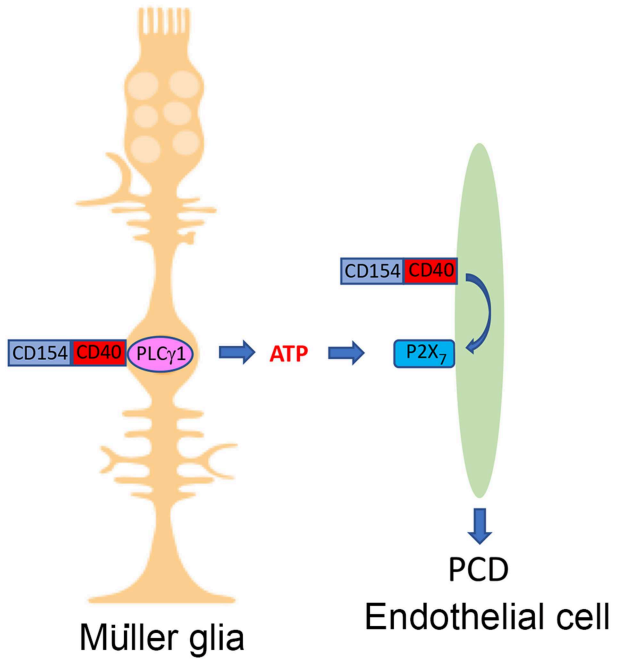

FIGURE 2 | The CD40-ATP-P2X$_7$ pathway links cellular responses in Müller glia with programmed cell death of bystander retinal endothelial cells in DR. Blood levels of CD154 and expression of CD40 on Müller glia are increased in diabetes. CD40 ligation in Müller glia causes PLCγ1 (PLC)-dependent secretion of extracellular ATP. CD40 ligation in retinal endothelial cells upregulates P2X$_7$ receptor, making these cells susceptible to P2X$_7$-induced programmed cell death. Created in part with BioRender.com.

a macroglia to microglia/macrophages and endothelial cells for the induction of inflammatory responses and endothelial cell death, respectively. By enabling myeloid cells to secrete TNF-α and IL-1β, this process would circumvent the poor capacity of CD40 to directly trigger secretion of these cytokines in non-hematopoietic cells, thus causing amplification of inflammation. These findings may be operative in I/R-induced retinopathy given its similarity to DR. The CD40-ATP-P2X$_7$ receptor pathway may also be relevant to neuro-inflammatory and neuro-degenerative brain disorders. For example, astrocytes acquire CD40 expression after incubation with IFN-γ (92), neural tissue injury or in a transgenic mouse model of amyotrophic lateral sclerosis (93), a disease driven by CD40. Thus, the CD40-ATP-P2X$_7$ receptor pathway may potentiate pro-inflammatory cytokine production by microglia further driving neuro-inflammation. Finally, this pathway may be functional in other diseases driven by CD40 such as inflammatory bowel disease, atherosclerosis and lupus nephritis. CD40 present in non-hematopoietic cells of the intestine, blood vessels and kidney may induce release of ATP that would bind purinergic receptors present in infiltrating myeloid cells.

The existence of the CD40-ATP-P2X$_7$ receptor pathway may have therapeutic implications. Pre-clinical data revealed that administration of anti-CD154 mAb to inhibit CD40-CD154 signaling effectively controlled various inflammatory and neurodegenerative disorders (22, 23). Unfortunately, anti-CD154 mAbs caused thromboembolic complications in humans that are unrelated to inhibition of CD40 (94). Targeting signaling pathways downstream of CD40 may represent an alternative approach to treat CD40-driven diseases. CD40 functions by recruiting TNF Receptor Associated Factors (TRAF) to its TRAF2,3 or TRAF6 binding sites (95). Blockade of CD40-TRAF2,3 signaling markedly impairs pro-inflammatory responses in non-hematopoietic cells (58, 96). Blocking this signaling pathway may also inhibit pro-inflammatory responses in neighboring myeloid cells. Pharmacologic approaches to inhibit CD40-TRAF2,3 signaling (cell penetrating CD40-TRAF2,3 blocking peptide or small molecule CD40-TRAF2,3 inhibitor) may prove an effective approach to treat diabetic and ischemic retinopathies, and potentially other CD40-driven inflammatory disorders. Given that TRAF6 is critical for dendritic cell maturation and development (96, 97), CD40-mediated IL-12 production by dendritic cells (98) and induction of antimicrobial effector mechanisms in macrophages (99, 100), pharmacologic inhibition of CD40-TRAF2,3 signaling would minimize the risk of opportunistic infections by leaving CD40-TRAF6 signaling intact.

AUTHOR CONTRIBUTIONS

The author confirms being the sole contributor of this work and has approved it for publication.

FUNDING

CS was funded by NIH-R01 EY018341 and NIH-R01 EY019250.

ACKNOWLEDGMENTS

The author thanks all the members of the Subauste lab for their feedback on this manuscript.

REFERENCES

1. Franke H, Verkhratsky A, Burnstock G, Illes P. Pathophysiology of astroglial purinergic signalling. *Purinergic Signal.* (2012) 8:629–57. doi: 10.1007/s11302-012-9300-0
2. Tang J, Kern TS. Inflammation in diabetic retinopathy. *Prog Retin Eye Res.* (2011) 30:343–58. doi: 10.1016/j.preteyeres.2011.05.002
3. Antonetti DA, Klein R, Gardner TW. Diabetic retinopathy. *N Engl J Med.* (2012) 366:1227–39. doi: 10.1056/NEJMra1005073
4. Rubsam A, Parikh S, Fort PE. Role of inflammation in diabetic retinopathy. *Int J Mol Sci.* (2018) 19:E942. doi: 10.3390/ijms19040942
5. Portillo J-AC, Van Grol J, Zheng L, Okenka G, Gentil K, Garland A, et al. CD40 mediates retinal inflammation and neuro-vascular degeneration. *J Immunol.* (2008) 181:8719–26. doi: 10.4049/jimmunol.181.12.8719
6. Portillo J-AC, Greene JA, Okenka G, Miao Y, Sheibani N, Kern TS, et al. CD40 promotes the development of early diabetic retinopathy. *Diabetologia.* (2014) 57:2222–31. doi: 10.1007/s00125-014-3321-x

7. Portillo J-AC, Lopez Corcino Y, Miao Y, Tang J, Sheibani N, Kern TS, et al. CD40 in retinal Muller cells induces P2X7-dependent cytokine expression in macrophages/microglia in diabetic mice and development of early experimental diabetic retinopathy in mice. *Diabetes.* (2017) 66:483–93. doi: 10.2337/db16-0051
8. Portillo J-A, Lopez Corcino Y, Dubyak GR, Kern TS, Matsuyama S, Subauste CS. Ligation of CD40 in human retinal Muller cells induces P2X7 receptor-dependent death of retinal endothelial cells. *Invest Ophthalmol Vis Sci.* (2016) 57:6278–86. doi: 10.1167/iovs.16-20301
9. Clark EA, Ledbetter J. Activation of human B cells mediated through two distinct cell surface differentiation antigens, Bp35 and Bp50. *Proc Natl Acad Sci USA.* (1986) 83:4494–8. doi: 10.1073/pnas.83.12.4494
10. Karmann K, Hughes CCW, Schechner J, Fanslow WC, Pober JS. CD40 on human endothelial cells: inducibility by cytokines and functional regulation of adhesion molecule expression. *Proc Natl Acad Sci USA.* (1995) 92:4342–6. doi: 10.1073/pnas.92.10.4342
11. Kiener PA, Moran-Davis P, Rankin BM, Wahl AF, Aruffo A, Hollenbaugh D. Stimulation of CD40 with purified soluble gp39 induces proinflammatory responses in human monocytes. *J Immunol.* (1995) 155:4917–25.
12. Tan J, Town T, Mori T, Obregon D, Wu Y, Delledonne A, et al. CD40 is expressed and functional on neuronal cells. *EMBO J.* (2002) 21:643–52. doi: 10.1093/emboj/21.4.643
13. Borcherding F, Nitschke M, Von Smolinski D, Bieber K, Van Kooten C, Lehnert H, et al. The CD40-CD40L pathway contributes to the proinflammatory function of intestinal epithelial cells in inflammatory bowel disease. *Am J Pathol.* (2010) 176:1816–27. doi: 10.2353/ajpath.2010.090461
14. Van Kooten C, Banchereau J. CD40-CD40 ligand. *J Leuk Biol.* (2000) 67:2–17. doi: 10.1002/jlb.67.1.2
15. Xu H, Zhang X, Mannon RB, Kirk AD. Platelet-derived or soluble CD154 induces vascularized allograft rejection independent of cell-bound CD154. *J Clin Invest.* (2006) 116:769–74. doi: 10.1172/JCI27155
16. Levy J, Espanol-Boren T, Thomas C, Fischer A, Tovo P, Bordigoni P, et al. Clinical spectrum of X-linked hyper-IgM syndrome. *J Pediatr.* (1997) 131:47–54. doi: 10.1016/S0022-3476(97)70123-9
17. Elgueta R, Benson MJ, De Vries VC, Wasiuk A, Guo Y, Noelle RJ. Molecular mechanism and function of CD40/CD40L engagement in the immune system. *Immunol Rev.* (2009) 229:152–72. doi: 10.1111/j.1600-065X.2009.00782.x
18. Laman JD, Claassen E, Noelle RJ. Functions of CD40 and Its Ligand, gp39 (CD40L). *Crit Rev Immunol.* (2017) 37:371–420. doi: 10.1615/CritRevImmunol.v37.i2-6.100
19. Ara A, Ahmed KA, Xiang J. Multiple effects of CD40-CD40L axis in immunity against infection and cancer. *Immunotargets Ther.* (2018) 7:55–61. doi: 10.2147/ITT.S163614
20. Mcwilliams TG, Howard L, Wyatt S, Davies AM. Regulation of autocrine signaling in subsets of sympathetic neurons has regional effects on tissue innervation. *Cell Rep.* (2015) 10:1443–9. doi: 10.1016/j.celrep.2015.02.016
21. Carriba P, Davies AM. CD40 is a major regulator of dendrite growth from developing excitatory and inhibitory neurons. *Elife.* (2017) 6:e30442. doi: 10.7554/eLife.30442
22. Mach F, Schonbeck U, Sukhova GK, Atkinson E, Libby P. Reduction of atherosclerosis in mice by inhibition of CD40 signaling. *Nature.* (1998) 394:200–3. doi: 10.1038/28204
23. Peters AL, Stunz LL, Bishop GA. CD40 and autoimmunity: the dark side of a great activator. *Semin Immunol.* (2009) 21:293–300. doi: 10.1016/j.smim.2009.05.012
24. Yau JW, Rogers SL, Kawasaki R, Lamoureux EL, Kowalski JW, Bek T, et al. Global prevalence and major risk factors of diabetic retinopathy. *Diabetes Care.* (2012) 35:556–64. doi: 10.2337/dc11-1909
25. Bourne RR, Stevens GA, White RA, Smith JL, Flaxman SR, Price H, et al. Causes of vision loss worldwide, 1990-2010: a systematic analysis. *Lancet Glob Health.* (2013) 1:e339–49. doi: 10.1016/S2214-109X(13)70113-X
26. Giacco F, Brownlee M. Oxidative stress and diabetic complications. *Circ Res.* (2010) 107:1058–70. doi: 10.1161/CIRCRESAHA.110.223545
27. Eid S, Sas KM, Abcouwer SF, Feldman EL, Gardner TW, Pennathur S, et al. New insights into the mechanisms of diabetic complications: role of lipids and lipid metabolism. *Diabetologia.* (2019) 62:1539–49. doi: 10.1007/s00125-019-4959-1
28. Adamiec-Mroczek J, Oficjalska-Mlynczak J, Misiuk-Hojlo M. Proliferative diabetic retinopathy - the influence of diabetes control on the activation of the intraocular molecule system. *Diabetes Res Clin Pract.* (2009) 84:46–50. doi: 10.1016/j.diabres.2009.01.012
29. Mcleod DS, Lefer DJ, Merges C, Lutty GA. Enhanced expression of intracellular adhesion molecule-1 and P-selectin in the diabetic human retina and choroid. *Am J Pathol.* (1995) 147:642–53.
30. Miyamoto K, Khorsrof S, Bursell SE, Rohan R, Murata T, Clermont AC, et al. Prevention of leukostasis and vascular leakage in streptozotocin-induced diabetic retinopathy via intercellular adhesion molecule-1 inhibition. *Proc Natl Acad Sci USA.* (1999) 96:10836–41. doi: 10.1073/pnas.96.19.10836
31. Joussen AM, Poulaki V, Le ML, Koizumi K, Esser C, Janicki H, et al. A central role for inflammation in the pathogenesis of diabetic retinopathy. *FASEB J.* (2004) 18:1450–2. doi: 10.1096/fj.03-1476fje
32. Mizutani M, Kern TS, Lorenzi M. Accelerated death of retinal microvascular cells in human and experimental diabetic retinopathy. *J Clin Invest.* (1996) 97:2883–90. doi: 10.1172/JCI118746
33. Krady JK, Basu A, Allen CM, Xu Y, Lanoue KF, Gardner TW, et al. Minocycline reduces proinflammatory cytokine expression, microglial activation, and caspase-3 activation in a rodent model of diabetic retinopathy. *Diabetes.* (2005) 54:1559–65. doi: 10.2337/diabetes.54.5.1559
34. Yang L-P, Sun H-L, Wu L-M, Guo X-J, Dou H-L, Tso MOM, et al. Baicalein reduces inflammatory process in a rodent model of diabetic retinopathy. *Invest Ophthalmol Vis Sci.* (2009) 50:2319–27. doi: 10.1167/iovs.08-2642
35. Vujosevic S, Micera A, Bini S, Berton M, Esposito G, Midena E. Proteome analysis of retinal glia cells-related inflammatory cytokines in the aqueous humour of diabetic patients. *Acta Ophthalmol.* (2016) 94:56–64. doi: 10.1111/aos.12812
36. Boss JD, Singh PK, Pandya HK, Tosi J, Kim C, Tewari A, et al. Assessment of neurotrophins and inflammatory mediators in vitreous of patients with diabetic retinopathy. *Invest Ophthalmol Vis Sci.* (2017) 58:5594–603. doi: 10.1167/iovs.17-21973
37. Vincent JA, Mohr S. Inhibition of caspase-1/interleukin-1β signaling prevents degeneration of retinal capillaries in diabetes and galactosemia. *Diabetes.* (2007) 56:224–30. doi: 10.2337/db06-0427
38. Joussen AM, Doehmen S, Le ML, Koizumi K, Radetzky S, Krohne TU, et al. TNF-α mediated apoptosis plays an important role in the development of early diabetic retinopathy and long-term histopathological alterations. *Mol Vision.* (2009) 15:1418–28.
39. Abu El-Asrar AM, Desmet S, Meersschaert A, Dralands L, Missotten L, Geboes K. Expression of the inducible isoform of nitric oxide synthase in the retinas of human subjects with diabetes mellitus. *Am J Ophthalmol.* (2001) 132:551–6. doi: 10.1016/S0002-9394(01)01127-8
40. Du Y, Smith MA, Miller CM, Kern TS. Diabetes-induced nitrative stress in the retina, and correction by aminoguanidine. *J Neurochem.* (2002) 80:771–9. doi: 10.1046/j.0022-3042.2001.00737.x
41. Leal EC, Manivannan A, Hosoya K-I, Terasaki T, Cunha-Vaz J, Ambrosio AF, et al. Inducible nitric oxide synthase isoform is a key mediator of leukostasis and blood-retinal barrier breakdown in diabetic retinopathy. *Invest Ophthalmol Vis Sci.* (2007) 48:5257–65. doi: 10.1167/iovs.07-0112
42. Zheng L, Du Y, Miller C, Gubitosi-Klug RA, Kern TS, Ball S, et al. Critical role of inducible nitric oxide synthase in degeneration of retinal capillaries in mice with streptozotocin-induced diabetes. *Diabetologia.* (2007) 50:1987–96. doi: 10.1007/s00125-007-0734-9
43. Taghavi Y, Hassanshahi G, Kounis NG, Koniari I, Khorramdelazad H. Monocyte chemoattractant protein-1 (MCP-1/CCL2) in diabetic retinopathy: latest evidence and clinical considerations. *J Cell Commun Signal.* (2019) 1–12. doi: 10.1007/s12079-018-00500-8
44. Zhang SX, Wang JJ, Gao G, Shao C, Mott R, Ma J-X. Pigmented epithelium-derived factor (PEDF) is na endogenous antiinflammatory factor. *FASEB J.* (2006) 20:323–5. doi: 10.1096/fj.05-4313fje
45. Gilbert C, Rahi J, Eckstein M, O'sullivan J, Foster A. Retinopathy of prematurity in middle-income countries. *Lancet.* (1997) 350:12–4. doi: 10.1016/S0140-6736(97)01107-0
46. Varma DD, Cugati S, Lee AW, Chen CS. A review of central retinal artery occlusion: clinical presentation and management. *Eye.* (2013) 27:688–97. doi: 10.1038/eye.2013.25

47. Ashraf M, Souka AA, Singh RP. Central retinal vein occlusion: modifying current treatment protocols. *Eye.* (2016) 30:505–14. doi: 10.1038/eye.2016.10
48. Rivera JC, Dabouz R, Noueihed B, Omri S, Tahiri H, Chemtob S. Ischemic retinopathies: oxidative stress and inflammation. *Oxid Med Cell Longev.* (2017) 2017:3940241. doi: 10.1155/2017/3940241
49. Zheng L, Gong B, Hatala DA, Kern TS. Retinal ischemia and reperfusion causes capillary degeneration: similarities to diabetes. *Invest Ophthalmol Vis Sci.* (2007) 48:361–7. doi: 10.1167/iovs.06-0510
50. Yoneda S, Tanihara H, Kido N, Honda Y, Goto W, Hara H, et al. Interleukin-1 beta mediates ischemic injury in the rat retina. *Exp Eye Res.* (2001) 73:661–7. doi: 10.1006/exer.2001.1072
51. Neufeld AH, Kawai S, Das S, Vora S, Gachie E, Connor JR, et al. Loss of retinal ganglion cells following retinal ischemia: the role of inducible nitric oxide synthase. *Exp Eye Res.* (2002) 75:521–8. doi: 10.1006/exer.2002.2042
52. Choi JS, Kim D, Hong YM, Mizuno S, Joo CK. Inhibition of nNOS and COX-2 expression by lutein in acute retinal ischemia. *Nutrition.* (2006) 22:668–71. doi: 10.1016/j.nut.2005.08.011
53. Vinores SA, Xiao WH, Shen J, Campochiaro PA. TNF-α is critical for ischemia-induced leukostasis, but not retinal neovascularization nor VEGF-induced leakage. *J. Neuroimmunol.* (2007) 182:73–9. doi: 10.1016/j.jneuroim.2006.09.015
54. Tsujikawa A, Ogura Y, Hiroshiba N, Miyamoto K, Kiryu J, Tojo SJ, et al. Retinal ischemia-reperfusion injury attenuated by blocking of adhesion molecules of vascular endothelium. *Invest Ophthalmol Vis Sci.* (1999) 40:1183–90.
55. Portillo J-AC, Okenka G, Kern TS, Subauste CS. Identification of primary retinal cells and *ex vivo* identification of pro-inflammatory molecules in retinal cells using flow cytometry. *Mol Vis.* (2009) 15:1383–9.
56. Van Grol J, Muniz-Feliciano L, Portillo J-AC, Bonilha VL, Subauste CS. CD40 induces anti-*Toxoplasma gondii* activity in non-hematopoietic cells dependent on autophagy proteins. *Infect Immun.* (2013) 81:2002–11. doi: 10.1128/IAI.01145-12
57. Yellin MJ, D'agati V, Parkinson G, Han AS, Szema A, Baum D, et al. Immunohistologic analysis of renal CD40 and CD40L expression in lupus nephritis and other glomerulonephritis. *Arthritis Rheum.* (1997) 40:124–34. doi: 10.1002/art.1780400117
58. Portillo J-A, Schwartz I, Zarini S, Bapputy R, Kern TS, Gubitosi-Klug RA, et al. Pro-inflammatory responses induced by CD40 in retinal endothelial and Muller cells are inhibited by blocking CD40-TRAF2,3 or CD40-TRAF6 signaling. *Invest Ophthalmol Vis Sci.* (2014) 55:8590–7. doi: 10.1167/iovs.14-15340
59. Kuo HL, Huang CC, Lin TY, Lin CY. IL-17 and CD40 ligand synergistically stimulate the chronicity of diabetic nephropathy. *Nephrol Dial Transplant.* (2018) 33:248–56. doi: 10.1093/ndt/gfw397
60. Chatzigeorgiou AE, Lembessis PE, Mylona-Karagianni CF, Tsouvalas EA, Diamanti-Kandarakis E, Kamper EF. CD40 expression and its association with low-grade inflammation in a Greek population of type 1 diabetic juveniles: evidence for differences in CD40 mRNA isoforms expressed by peripheral blood mononuclear cells. *Exp Clin Endocrinol Diabetes.* (2010) 118:38–46. doi: 10.1055/s-0029-1224151
61. Yan S, Yim LY, Tam RC, Chan A, Lu L, Lau CS, et al. MicroRNA-155 mediates augmented CD40 expression in bone marrow derived plasmacytoid dendritic cells in symptomatic lupus-prone NZB/W F1 mice. *Int J Mol Sci.* (2016) 17:E1282. doi: 10.3390/ijms17081282
62. Lee A, Papangeli I, Park Y, Jeong HN, Choi J, Kang H, et al. A PPARγ-dependent miR-424/503-CD40 axis regulates inflammation mediated angiogenesis. *Sci Rep.* (2017) 7:2528. doi: 10.1038/s41598-017-02852-4
63. Cipollone F, Chiarelli F, Davi G, Ferri C, Desideri G, Fazia M, et al. Enhanced soluble CD40 ligand contributes to endothelial cell dysfunction *in vitro* and monocyte activation in patients with diabetes mellitus: effect of improved metabolic control. *Diabetologia.* (2005) 48:1216–24. doi: 10.1007/s00125-005-1750-2
64. Lamine LB, Turki A, Al-Khateeb G, Sellami N, Amor HB, Sarray S, et al. Elevation in circulating soluble CD40 ligand concentrations in type 2 diabetic retinopathy and association with its severity. *Exp Clin Endocrinol Diabetes.* (2018). doi: 10.1055/a-0647-6860
65. Boeri D, Maiello M, Lorenzi M. Increased prevalence of microthromboses in retinal capillaries of diabetic individuals. *Diabetes.* (2001) 50:1432–9. doi: 10.2337/diabetes.50.6.1432
66. Li G, Veenstra AA, Talahalli RR, Wang X, Gubitosi-Klug RA, Sheibani N, et al. Marrow-derived cells regulate the devlopment of early diabetic retinopathy and tactile allodynia in mice. *Diabetes.* (2012) 61:3294–303. doi: 10.2337/db11-1249
67. Bringmann A, Pannicke T, Grosche J, Francke M, Widemann P, Skatchkov SN, et al. Muller cells in the healthy and diseases retina. *Prog Retin Eye Res.* (2006) 25:397–424. doi: 10.1016/j.preteyeres.2006.05.003
68. Devoldere J, Peynshaert K, De Smedt SC, Remaut K. Muller cells as a target for retinal therapy. *Drug Discov Today.* (2019) 24:1483–98. doi: 10.1016/j.drudis.2019.01.023
69. Gerbardinger C, Biarnes Costa M, Coulombe MC, Toth I, Hoehn T, Grosu P. Expression of acute-phase response proteins in retinal Muller cells in diabetes. *Invest Ophthalmol Vis Sci.* (2005) 46:349–57. doi: 10.1167/iovs.04-0860
70. Powers MR, Davies MH, Eubanks JP. Increased expression of chemokine KC, an interleukin-8 homologue, in a model of oxygen-induced retinopathy. *Curr Eye Res.* (2005) 30:299–307. doi: 10.1080/02713680590923276
71. Wang J, Xu X, Elliot MH, Zhu M, Le Y-Z. Muller cell-derived VEGF is essential for diabetes-induced retinal inflammation and vascular leakage. *Diabetes.* (2010) 59:2297–305. doi: 10.2337/db09-1420
72. James G, Butt AM. P2Y and P2X purinoceptor mediated Ca2+ signalling in glial cell pathology in the central nervous system. *Eur J Pharmacol.* (2002) 447:247–60. doi: 10.1016/S0014-2999(02)01756-9
73. Fields RD, Burnstock G. Purinergic signalling in neuron-glia interactions. *Nat Rev Neurosci.* (2006) 7:423–36. doi: 10.1038/nrn1928
74. Ferrari D, Chiozzi P, Falzoni S, Dal Susino M, Melchiorri L, Baricordi OR, et al. Extracellular ATP triggers IL-1 beta release by activating the purinergic P2Z receptor of human macrophages. *J Immunol.* (1997) 159:1451–8.
75. Hide I, Tanaka M, Inoue A, Nakajima K, Kohsaka S, Inoue K, et al. Extracellular ATP triggers tumor necrosis factor-alpha release from rat microglia. *J Neurochem.* (2000) 75:965–72. doi: 10.1046/j.1471-4159.2000.0750965.x
76. Monif M, Burnstock G, Williams DA. Microglia: proliferation and activation driven by the P2X7 receptor. *Int J Biochem Cell Biol.* (2010) 42:1753–6. doi: 10.1016/j.biocel.2010.06.021
77. Monif M, Reid CA, Powell KL, Smart ML, Williams DA. The P2X7 receptor drives microglial activation and proliferation: a trophic role for P2X7R pore. *J Neurosci.* (2009) 29:3781–91. doi: 10.1523/JNEUROSCI.5512-08.2009
78. Liu J, Zhao ML, Brosnan CF, Lee SC. Expression of type II nitric oxide synthase in primary human astrocytes and microglia: role of IL-1beta and IL-1 receptor antagonist. *J Immunol.* (1996) 157:3569–76.
79. Joussen AM, Poulaki V, Mitsiades N, Kirchhoff B, Koizumi K, Dohmen S, et al. Nonsteroidal anti-inflammatory drugs prevent early diabetic retinopathy via TNF-α suppression. *FASEB J.* (2002) 16:438–40. doi: 10.1096/fj.01-0707fje
80. Bal-Price A, Moneer Z, Brown GC. Nitric oxide induces rapid, calcium-dependent release of vesicular glutamate and ATP from cultured rat astrocytes. *Glia.* (2002) 40:312–23. doi: 10.1002/glia.10124
81. Klaus GG, Choi MS, Holman M. Properties of mouse CD40. Ligation of CD40 activates B cells via a Ca(++)-dependent, FK506-sensitive pathway. *Eur J Immunol.* (1994) 24:3229–32. doi: 10.1002/eji.1830241248
82. Lazaar AL, Amrani Y, Hsu J, Panettieri RA Jr, Fanslow WC, Albelda SM, et al. CD40-mediated signal transduction in human airway smooth muscle. *J Immunol.* (1998) 161:3120–7.
83. Yang YR, Follo MY, Cocco L, Suh PG. The physiological roles of primary phospholipase C. *Adv Biol Regul.* (2013) 53:232–41. doi: 10.1016/j.jbior.2013.08.003
84. Kern TS, Tang J, Mizutani M, Kowluru RA, Nagaraj RH, Romeo G, et al. Response of capillary cell death to aminoguanidine predicts the development of retinopathy: comparison of diabetes and galactosemia. *Invest Ophthalmol Vis Sci.* (2000) 41:3972–8.
85. Joussen AM, Poulaki V, Mitsiades N, Cai W-Y, Suzuma I, Pak J, et al. Suppression of Fas-FasL-induced endothelial cell apoptosis prevents diabetic blood-retinal barrier breakdown in a model of streptozotocin-induced diabetes. *FASEB J.* (2002) 17:76–8. doi: 10.1096/fj.02-0157fje

86. Behl Y, Krothapalli P, Desta T, Dipiazza A, Roy S, Graves DT. Diabetes-enhanced tumor necrosis factor-alpha production promotes apoptosis and the loss of retinal microvascular cells in type 1 and type 2 models of diabetic retinopathy. *Am J Pathol.* (2008) 172:1411–8. doi: 10.2353/ajpath.2008.071070
87. Deregibus MC, Buttiglieri S, Russo S, Bussolati B, Camussi G. CD40-dependent activation of phosphatidylinositol 3-kinase/Akt pathway mediates endothelial cell survival and *in vitro* angiogenesis. *J Biol Chem.* (2003) 278:18008–14. doi: 10.1074/jbc.M300711200
88. Surprenant A, Rassendren F, Kawashima E, North RA, Buell G. The cytolytic P2Z receptor for extracellular ATP identified as a P2X receptor (P2X7). *Science.* (1996) 272:735–8. doi: 10.1126/science.272.5262.735
89. Di Virgilio F, Chiozzi P, Falzoni S, Ferrari D, Sanz JM, Venketaraman V, et al. Cytolytic P2X purinoceptors. *Cell Death Differ.* (1998) 5:191–9. doi: 10.1038/sj.cdd.4400341
90. Jun DJ, Kim J, Jung SY, Song R, Noh JH, Park YS, et al. Extracellular ATP mediates necrotic cell swelling in SN4741 dopaminergic neurons through P2X7 receptors. *J Biol Chem.* (2007) 282:37350–8. doi: 10.1074/jbc.M707915200
91. Sugiyama T. Enhancement of of P2X7-induced pore formation and apoptosis: an early effect of diabetes on the retinal microvasculature. *Invest Ophthalmol Vis Sci.* (2004) 45:1026–32. doi: 10.1167/iovs.03-1062
92. Tan L, Gordon KB, Mueller JP, Matis LA, Miller SD. Presentation of proteolipid protein epitopes and B7-1-dependent activation of encephalitogenic T cells by IFN-γ-activated SJL/J astrocytes. *J Immunol.* (1998) 160:4271–9.
93. Okuno T, Nakatsuji Y, Kumanogoh A, Koguchi K, Moriya M, Fujimura H, et al. Induction of cyclooxygenase-2 in reactive glial cells by the CD40 pathway: relevance to amyotrophic lateral sclerosis. *J Neurochem.* (2004) 91:404–12. doi: 10.1111/j.1471-4159.2004.02727.x
94. Boumpas DT, Furie R, Manzi S, Ilei GG, Wallace DJ, Balow JE, et al. A short course of BG9588 (anti-CD40 ligand antibody) improves serologic activity and decreases hematuria in patients with proliferative lupus glomerulonephritis. *Arthritis Rheum.* (2003) 48:719–27. doi: 10.1002/art.10856
95. Bishop GA, Hostager BS, Brown KD. Mechanisms of TNF receptor-associated factor (TRAF) regulation in B lymphocytes. *J Leuk Biol.* (2002) 72:19–23. doi: 10.1189/jlb.72.1.19
96. Portillo J-AC, Greene JA, Schwartz I, Subauste MC, Subauste CS. Blockade of CD40-TRAF2,3 or CD40-TRAF6 interactions is sufficient to impair pro-inflammatory responses in human aortic endothelial cells and human aortic smooth muscle cells. *Immunology.* (2015) 144:21–33. doi: 10.1111/imm.12361
97. Kobayashi T, Walsh PT, Walsh MC, Speirs KM, Chiffoleau E, King CG, et al. TRAF6 is a critical factor for dendritic cell maturation and development. *Immunity.* (2003) 19:353–63. doi: 10.1016/S1074-7613(03)00230-9
98. Mackey MF, Wang Z, Eichelberg K, Germain RN. Distinct contributions of different CD40 TRAF binding sites to CD154-induced dendritic cell maturation and IL-12 secretion. *Eur J Immunol.* (2003) 33:779–89. doi: 10.1002/eji.200323729
99. Andrade RM, Wessendarp M, Portillo J-AC, Yang J-Q, Gomez FJ, Durbin JE, et al. TRAF6 signaling downstream of CD40 primes macrophages to acquire anti-microbial activity in response to TNF-α. *J. Immunol.* (2005) 175:6014–21. doi: 10.4049/jimmunol.175.9.6014
100. Portillo J-AC, Muniz-Feliciano L, Subauste MC, Heinzel FP, Subauste CS. CD40 and TNF-α synergize to induce nitric oxide synthase in macrophages. *Immunology.* (2012) 135:140–50. doi: 10.1111/j.1365-2567.2011.03519.x

Conflict of Interest: The author declares that the research was conducted in the absence of any commercial or financial relationships that could be construed as a potential conflict of interest.

frontiers in Neurology

MINI REVIEW
published: 27 May 2020
doi: 10.3389/fneur.2020.00377

The Chitinases as Biomarkers for Amyotrophic Lateral Sclerosis: Signals From the CNS and Beyond

Nayana Gaur[1]*, *Caroline Perner*[1,2], *Otto W. Witte*[1,3] and *Julian Grosskreutz*[1,3]

[1] Hans Berger Department of Neurology, Jena University Hospital, Jena, Germany, [2] Center for Immunology and Inflammatory Diseases, Massachusetts General Hospital, Charlestown, MA, United States, [3] Jena Center for Healthy Ageing, Jena University Hospital, Jena, Germany

Amyotrophic lateral sclerosis (ALS) is a late-onset neurodegenerative condition, most widely characterized by the selective vulnerability of motor neurons and the poor life expectancy of afflicted patients. Limited disease-modifying therapies currently exist, which only further attests to the substantial heterogeneity associated with this disease. In addition to established prognostic factors like genetic background, site of onset, and age at onset, wide consensus on the role of neuroinflammation as a disease exacerbator and driver has been established. In lieu of this, the emerging literature on chitinases in ALS is particularly intriguing. Individual groups have reported substantially elevated chitotriosidase (CHIT1), chitinase-3-like-1 (CHI3L1), and chitinase-3-like-2 (CHI3L2) levels in the cerebrospinal, motor cortex, and spinal cord of ALS patients with multiple—and often conflicting—lines of evidence hinting at possible links to disease severity and progression. This mini-review, while not exhaustive, will aim to discuss current evidence on the involvement of key chitinases in ALS within the wider framework of other neurodegenerative conditions. Implications for understanding disease etiology, developing immunomodulatory therapies and biomarkers, and other translational opportunities will be considered.

Keywords: neurodegeneration, biomarker (BM), neuroinflammation, chitinases, amyotrophic lateral sclerosis (ALS)

OPEN ACCESS

Edited by:
Sven G. Meuth, University Hospital Münster, Germany

Reviewed by:
Stefanie Schreiber, University Hospital Magdeburg, Germany
Marc Pawlitzki, University Hospital Münster, Germany

***Correspondence:**
Nayana Gaur
nayana.gaur@med.uni-jena.de

Specialty section:
This article was submitted to Multiple Sclerosis and Neuroimmunology, a section of the journal Frontiers in Neurology

Received: *28 November 2019*
Accepted: *14 April 2020*
Published: *27 May 2020*

Citation:
Gaur N, Perner C, Witte OW and Grosskreutz J (2020) The Chitinases as Biomarkers for Amyotrophic Lateral Sclerosis: Signals From the CNS and Beyond. Front. Neurol. 11:377. doi: 10.3389/fneur.2020.00377

INTRODUCTION

ALS and Neuroinflammation

Amyotrophic lateral sclerosis (ALS) is the most prevalent form of adult-onset motor neuron disease and clinically presents with the relentless destruction of primarily (but not exclusively) upper and lower motor neurons (UMN, LMN). Riluzole, the sole treatment available, confers only modest effects via a median increase of 2–3 months in survival; most patients eventually succumb to respiratory failure. Although there is a pressing need for treatment modalities that tackle disease aggressiveness, therapeutic development has been severely constrained by the disease's characteristic heterogeneity; this stems from age-at-onset and site-of-onset, presence of disease-associated mutations, and comorbidities, including frontotemporal dementia (FTD) (1). Progression and survival rates are also highly variable; while the median survival is 2–3 years from symptom onset, some patients present with a disease duration of over 10 years (2). Cellular and animal studies have provided elegant evidence that neuroinflammation contributes to ALS pathology and that concomitant glial dysregulation is necessary for motor neuronal

degeneration (3–5). Numerous immunological changes, including the functional alteration and pro-inflammatory phenotype of circulating myeloid cells (6), dysregulated leukocytic chemokine receptor expression (7), the reduction of regulatory T cells (8), and cytotoxic T cell infiltration, have also been reported in patients (9).

Despite this, there remains a paucity of biological tools that adequately capture the neuroinflammatory response across the disease; this may partially explain the failure of immunomodulatory therapies to date. Biomarkers that reflect target engagement and assess the efficacy of novel treatments are therefore crucial. Although molecular imaging studies of microglial activation are underway, fluid-based biomarkers are more accessible and can provide important insights into disease pathomechanisms. For instance, cerebrospinal fluid (CSF) and humoral levels of the neurofilament proteins have been validated as robust diagnostic and prognostic markers for ALS. Several inflammatory cytokines have also been reported as dysregulated in ALS, including TNF-α, MCP-1, and IL-6 (10–12). In lieu of this, recent reports of elevated chitinase levels in ALS are particularly interesting, as these have already been reported as surrogate markers of a chronic inflammatory response in non-neuronal conditions.

Mammalian Chitinases: Novel Players in Neurodegeneration?

The chitinases belong to the family 18 glycosyl hydrolases (GH18) and are characterized by their ability to cleave chitin, a natural polysaccharide found in the coating of various pathogens. The GH18 family is ubiquitously expressed across a wide range of organisms, from bacteria to humans; evolutionary conservation in the latter is particularly interesting, given the lack of endogenous chitin synthesis. This has led to the view that chitin is a defense target for the mammalian immune system or an "immune stimulator." Indeed, it is recognized by several pattern recognition receptors and can trigger associated immune responses in a fragment-size and tissue-dependent manner (13). Mammalian chitinases include the enzymatically active chitinases chitotriosidase (CHIT1) and acidic mammalian chitinase (AMCase) that can degrade chitin, and the chi-lectins (CLs) chitinase 3-like 1 and -like 2 (CHI3L1, CHI3L2). Despite being able to bind chitin with high affinity, the CLs possess no chitinolytic activity, owing to the absence of the catalytic motif. CHIT1 is primarily expressed by cells of myeloid lineage, particularly mature macrophages (14, 15). Like CHIT1, CHI3L1 is absent in monocytes and strongly upregulated during later stages of macrophage differentiation (16). CHI3L1 is also produced by reactive astrocytes and associated with chronic neuroinflammation, as will be further discussed in the Section Chitinases Across the ALS-FTD Spectrum (17–19). While CHI3L2 hasn't been as extensively studied, expression has been noted in chondrocytes, synoviocytes, and alternatively activated "M2" macrophages (20).

Although the exact roles of these moieties remain to be fully elucidated, it is clear that they extend beyond innate immunity against chitin-containing pathogens. Chitinases have been reported in the context of adaptive Th2 response mediation (21, 22), tissue remodeling and repair, and, most recently, oligodendrogenesis (23). Dysregulated chitinase levels have been reported in several chronic neurodegenerative conditions, including Alzheimer's disease (AD) and FTD. *In vitro* evidence suggests that, at least in ALS, they may act in a "feed-forward" loop that sustains neuroinflammation and exacerbates disease, as illustrated in **Figure 1**. For instance, in a transgenic rat model, TDP-43 induced astrocytic *CHI3L1* up-regulation; in turn, synthetic CHI3L1 caused neuronal death in a dose-dependent manner (19). Similarly, Raju et al. reported that CSF from ALS patients impacted cell viability and upregulated CHIT1 expression in murine microglial cultures (24). Subsequent exposure to CHIT1 itself caused microglial activation, indicating again a "self-propagating" inflammatory mechanism (25).

This review, while not exhaustive, will summarize current evidence for chitinase dysregulation in ALS and its implications for understanding disease etiology and progression, and therapeutic and biomarker development. CHIT1, CHI3L1, and CHI3L2 will be focused on, since these have been most extensively studied in a neurodegenerative context.

THE CHITINASES IN ALS

Evidence Concerning Diagnostic Potential

Varghese et al. (26) were the first to report chitinases in the context of ALS; using quantitative mass spectrometry (MS) and ELISA-based validation in an independent cohort, they showed that CSF levels of CHIT1, CHI3L1, and CHI3L2 were significantly elevated in ALS patients relative to healthy controls (HCs). This elevation has since been confirmed by several studies using a range of proteomic and transcriptomic methods (27–33). Recent studies have predominantly focused on assessing discriminatory power with regard to mimic conditions, and other neurodegenerative diseases. However, studies have differed with respect to (a) the chitinases and secondary targets investigated; (b) cohort demographics; (c) bio-fluids assessed, and (d) experimental and analytical methods used (**Table 1**). Thompson et al. subsequently investigated all three chitinases and reported that they were significantly higher in the CSF of ALS patients relative to HCs, mimics, and asymptomatic mutation carriers (MCs) and that increased CHIT1 levels corresponded to active forms of the enzyme. While all three could reliably distinguish ALS from HCs and mimics, they were outperformed by pNfH. Furthermore, all three chitinases performed poorly in distinguishing ALS from primary lateral sclerosis (PLS) (28). A

Abbreviations: AD, Alzheimer's Disease; ALS, Amyotrophic Lateral Sclerosis; ALSFRS-R, Amyotrophic Lateral Sclerosis Functional Rating Scale Revised; CHIT1, Chitotriosidase; CHI3L1, Chitinase 3-Like 1; CHI3L2, Chitinase 3-Like 2; CLs, Chi-lectins; fALS, Familial ALS; FTD, Frontotemporal Dementia; gALS, genetic ALS; GH18, family 18 Glycosyl Hydrolases; HCs, Healthy Controls; IFN-γ, Interferon gamma; IL-6, Interleukin 6; LMN, Lower Motor Neuron; LPS, Lipopolysaccharide; MCs, Mutation Carriers; MCP-1, Monocyte Chemoattractant Protein 1; MS, Mass Spectrometry; NDCs, Neurological Disease Controls; NfL, Neurofilament Light Chain; PLS, Primary Lateral Sclerosis; pNfH, Phosphorylated Neurofilament Heavy Chain; PR, Progression Rate; sALS, sporadic ALS; sAPPβ, soluble Amyloid Precursor Protein Beta; Th2, T Helper Type 2; TNF-α, Tumor Necrosis Factor alpha; TREM2, Triggering Receptor expressed on Myeloid Cells 2; UMN, Upper Motor Neuron.

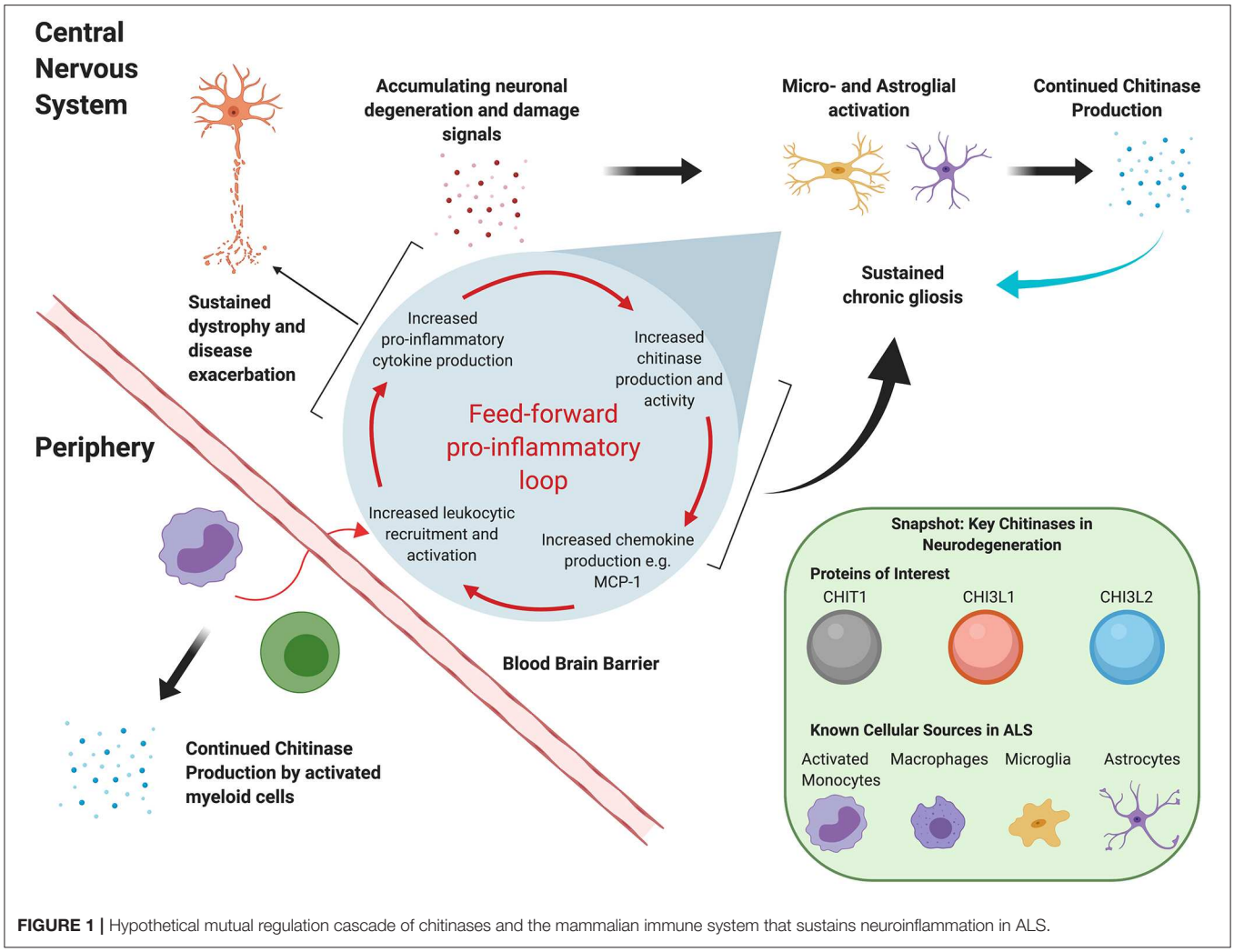

FIGURE 1 | Hypothetical mutual regulation cascade of chitinases and the mammalian immune system that sustains neuroinflammation in ALS.

prior MS-based study by the same group also noted a modest fold change for only CSF CHIT1 and CHI3L2 between ALS and PLS (31). Similarly, while Steinacker et al. (33) recommended CHIT1 as a potential differential diagnostic marker for ALS, they also noted that levels were increased in other neurodegenerative conditions and that pNfH and NfL had superior discriminatory power. In the same vein, Gille et al. (10) reported that elevated CSF CHIT1 and CHI3L1 levels were only weakly specific to ALS patients relative to neurological disease controls (NDCs). Observations of significant ALS-associated chitinase elevations in blood have been limited, barring one study that reported significantly elevated CHIT1 activity in dried blood spots (30) and another that noted higher CHIT1 levels in a genetic ALS (gALS) cohort (27) (both relative to HCs). This, coupled with reports of poor correlations between peripheral and CSF chitinase levels, makes a blood-based marker unlikely.

Applicability as stand-alone diagnostic markers is also likely to be constrained by the effect of functional variants. For instance, polymorphisms in the *CHI3L1* locus contribute to almost 15% of the variance in CSF CHI3L1 levels (34). Likewise, duplication in exon 10 of the *CHIT1* gene reduces both expression and activity; although this polymorphism is highly prevalent in European populations, no significant differences in genotype frequency have been observed between ALS patients and healthy individuals (27, 30). Additionally, presence of the *CHIT1* polymorphism has no influence on neurofilament levels or age of onset in patients, making a causative role in ALS pathogenesis unlikely. Importantly however, both CHIT1 expression and activity are significantly elevated in ALS patients (relative to HCs) independent of genotype and other factors like gender and age, indicating that disease status—rather than the presence of the polymorphism—determines the extent of dysregulation (12, 27, 30).

Evidence Concerning Prognostic Potential

The prognostic potential of the chitinases has been examined in relation to several clinical outcomes, including disease severity (overall ALSFRS-R score), the ALSFRS-R-derived progression rate (PR), survival, and disease duration, with several conflicting results as discussed below. The majority of the results discussed here focus on CSF, as almost no robust and consistent links between blood chitinase levels and prognostic factors have been

TABLE 1 | An overview of recent studies investigating chitinases in the context of ALS.

Study PMID	Study targets	Participants				Sample type	Methods used	Relative expression in ALS*	Correlation with neurofilament levels*	Other targets	Proposed bio mechanism	Proposed utility
		ALS	HCs	Mimics NDegs, NDCs	Other groups							
31175169	CHIT1 and CHI3L1	105		16 mimics, 102 NDCs		CSF and serum	ELISA and chemiluminescent assays	CSF CHIT and CHI3L1 ↑NDCs,Mimics	All with pNfH and NfL (in CSF)	MCP-1	Surrogate markers of Gliosis	Monitoring therapy response and stratification
31123140	CHIT1, CHI3L1, CHI3L2	82	25	12 mimics, 10 PLS	5 asym gALS MCs	CSF and serum	ELISA, enzymatic activity assay	CSF All ↑HCs,Mimics,MCs, CSF CHIT, CHI3L2↑PLS	All with pNfH (in CSF)	C-RP	Glial activity	Adjunctive predictor of progression, monitoring glial response to therapy
30224549	CHIT1 CHI3L1	70 sALS, 65 gALS	36 HCs	26 sFTD, 23 gFTD	26 asym. gALS MCs	CSF and blood	ELISA	CSF CHIT↑HCs,MCs,gFTD, Blood CHIT↑HCs, CSF CHI3L1 for gALS, and gFTD↑HCs,MCs	All with pNfH and NfL (in CSF)	GFAP	Microglial activity and astrogliosis. Neuroinflammation is common to gALS and sALS	
30215603	CHI3L1	IHC 11, ELISA 86, RT-qPCR 12 all sALS	IHC 23, ELISA 21, RT-qPCR 10			CSF, blood, spinal cord and frontal cortex PMT	RT-qPCR, IHC, ELISA, IB	PMT *CHI3L1*, CHI3L1 ↑HCs, CSF CHI3L1↑HCs	NfL	*AIF1*, *CD68*, IBA1, GFAP	Increased astroglial activity	Potential prognostic marker when used with NfL
29142138	CHIT1	ELISA 60, IHC 3	ELISA 25, IHC 2	ELISA 46 NDCs and 135 Ndegs, IHC NDegs 4		CSF, blood, spinal cord PMT	ELISA, IHC	CSF CHIT↑HCs, NDCs,NDegs, Spinal cord PMT CHIT↑ NDegs,HCs	pNfH and NfL (in CSF)	IBA1, CD68	Microglial/ macrophage activation	Biomarker for immune activation; can be used to monitor efficacy of immunomodulatory therapies
29331073	CHIT1, CHI3L1, CHI3L2	43	25	6 PLS, 12 mimics, 20 NDeg		CSF	High throughput MS, ELISA (for pNfH)	CHIT1, CHI3L2 ↑HCs,Mimics,NDeg,PLS, CHI3L1↑HCs,Mimics,NDeg	All with pNfH		Microglial activity	Distinguishing between ALS and ALS mimic conditions
30134252	CHIT1	29	36			CSF and blood	ELISA, chemiluminescence, enzymatic activity assay	CSF CHIT1 activity↑HCs		CCL18, TNF-α, IL6, *CHIT1*	Microglial activation	Neuroinflammation biomarker
30291183	CHI3L1	38	49	86 FTD		CSF	ELISA	CHI3L1↑HCs	NfL	sAPPβ		Staging and prognosis along ALS-FTD spectrum
25563799	CHIT1	75	106			Blood	Enzymatic activity assay	CHIT1 activity↑HCs		Lysosomal enzyme activity	Microglial activity and possible chronic triggering of the innate immune system	
27634542	CHIT1	40 sALS		40 NDCs		CSF	ELISA	CHIT1↑ NDCs	pNfH	S100-β, Cystatin C		Improves diagnostic potential when used with pNfH

(Continued)

TABLE 1 | Continued

Study PMID	Study targets	Participants				Sample type	Methods used	Relative expression in ALS*	Correlation with neurofilament levels*	Other targets	Proposed bio mechanism	Proposed utility
		ALS	HCs	Mimics NDegs, NDCs	Other groups							
24295388	CHIT1, CHI3L1, CHI3L2	26 sALS	23			CSF	LC-MS/MS, ELISA, enzymatic activity assay	CHIT1, CHI3L2 $\uparrow^{HCs}$, CHIT activity $\uparrow^{HCs}$		Osteopontin	Microglial activity and potential response to deposition of chitin-like substances in CNS aggregates	

**Reported results were statistically significant.*

AIF-1, Allograft inflammatory factor 1; asym, asymptomatic; CCL-18, Chemokine ligand 18; C-RP, C Reactive Protein; CSF, cerebrospinal fluid; ELISA, Enzyme-linked Immunosorbent assay; FTD, frontotemporal dementia; gALS, genetic Amyotrophic Lateral Sclerosis; GFAP, glial fibrillary acidic protein; gFTD, genetic Frontotemporal Dementia; HCs, Healthy Controls; IB, Immunoblotting; IHC, Immunohistochemistry; IL-6, interleukin 6; LC-MS, Liquid Chromatography Mass Spectrometry; MCs, Mutation Carriers; MCP-1, Monocyte chemoattractant protein 1; MS, Mass Spectrometry; NDCs, Neurological Disease Controls; NDegs, Neurodegenerative Disease Controls; NfL, neurofilament light chain; PLS, Primary Lateral Sclerosis; PMT, Post-mortem Tissue; pNfH, phosphorylated neurofilament heavy chain; RT-qPCR, Real-time Quantitative Polymerase Chain Reaction; sALS, sporadic ALS; sAPPβ, soluble amyloid precursor protein beta; sFTD, sporadic Frontotemporal Dementia; TNF-α, tumor necrosis factor alpha.

reported. It is worth noting, however, that studies have only now begun to examine CHIT1 enzymatic activity in addition to protein levels and that links between the periphery and prognostic factors, as reported by Pagliardini et al. (30), may yet emerge.

Links With Disease Severity and Progression

Evidence for a link with disease severity and progression has been tenuous at best. Martinez-Merino et al. (12) controlled for *CHIT1* genotype and reported that while ALS patients had significantly elevated CHIT1 activity, it correlated with neither disease severity nor progression. Thompson et al. (28) reported a significant albeit modest correlation between CHIT and CHI3L2 levels—but not CHI3L1—and PR after controlling for gender, age at onset, and site of onset; however, a stronger correlation was noted for pNfH. Conversely, Illán-Gala et al. (32) and Andres-Benito et al. (35) reported that CSF CHI3L1 levels correlated with PR to almost the same degree as CSF NfL levels.

Gille et al. (10) noted that both CSF CHIT1 and CHI3L1 only weakly correlated with PR at time of sampling; however, "fast" progressors had significantly higher levels of CHIT1 and CHI3L1 than "slow" progressors. One study reported that CSF CHIT1 also significantly correlated with both disease severity and PR (inversely) and to almost the same magnitude as NfL and pNfH. However, these correlations did not persist when patients were stratified based on PR, despite "fast" progressors having significantly higher levels of CHIT1 (33). Chen et al. (29) too reported no significant differences in CHIT1 levels between PR-stratified patients.

It is worth noting that establishing any association between the chitinases and PR is likely confounded by the lack of any external consensus on the thresholds for "high" or "low" PR. These are often arbitrarily set based on individual cohorts, thus constraining inter-study comparability and potentially occluding genuine biological signals.

Links With Disease Duration

Evidence for an association with disease duration has also been inconsistent, even by the few studies that have included longitudinal sampling. CSF CHIT1 activity did not significantly differ between patients stratified based on time since onset to sampling (12). A MS-based study reported a small increase in CSF CHI3L1 levels over time in patients who had low levels at onset (31). However, a subsequent ELISA-based verification noted that CSF chitinase levels in ALS and PLS patients did not significantly increase over a follow-up period of ∼2 years, even when patients were stratified by PR (28). Similarly, no significant associations between CSF CHIT1 and CHI3L1 and disease duration were observed in a cohort of 105 ALS patients (10). Indeed, evidence from asymptomatic ALS and FTD MCs suggests that chitinase elevation is a feature of the early symptomatic phase of the disease and is unlikely by itself to trigger disease onset, given that no significant differences were observed between patients with either genetic or sporadic disease (27).

Links With Survival and Mortality

Studies examining survival have also reported discrepant results. Di Rosa et al. analyzed microarray datasets and reported that patients with a shorter survival had significantly higher *CHI3L1* and *CHI3L2* in their motor cortex than those that survived longer; levels also inversely correlated with survival in the entire patient cohort (36). Cox proportional hazards analyses have also revealed a significant association between CSF CHIT1 levels and mortality, while one study reported that the association was independent of pNfH levels, another by the same group reported the opposite (28, 31). However, neither study had data on other prognostic factors, e.g., respiratory and *C9orf72* status, thus precluding a definitive conclusion on the influence of CHIT1. In contradiction, Gille et al. (10) reported that CSF CHI3L1, but not CHIT1, significantly affected mortality; this is compelling because they included data for eight established prognostic markers. The authors did not however compare how the chitinases performed relative to neurofilaments. Building on this, Illán-Gala et al. (32) also reported that increased CSF CHI3L1 levels were associated with shortened survival, even after adjustment for sex, age at onset and site of onset, NfL levels, and ALSFRS-R score at time of sampling. Taken together however, the currently available evidence doesn't unequivocally establish the degree to which the chitinases influence survival and whether they outperform established prognostic factors.

Links With Additional Indices

Although data are limited, some studies have also begun to examine a wider range of clinical outcomes; for instance, peripheral CHIT1 activity was significantly inversely correlated with forced vital capacity (30). Additionally, CSF CHIT1 and CHI3L1 levels correlated with the number of regions clinically affected by both UMN and LMN and only UMN degeneration, respectively (10, 28). Frontotemporal cortical thickness, as assessed by structural MRI, directly correlated with the CSF sAPPβ:CHI3L1 ratio in both ALS and FTD patients (32). Finally, whether chitinase levels also reflect the poorer outcomes associated with factors like bulbar onset or genetic status (e.g., C9orf72) needs further investigation.

CHITINASES ACROSS THE ALS-FTD SPECTRUM

Studies focusing on the broader ALS-FTD spectrum have noted that the two conditions present with specific chitinase dysregulation patterns. When examined alongside glial activation markers, these suggest different underlying inflammatory processes: increased microglial (as evidenced by CHIT1) and astroglial (as evidenced by CHI3L1) activation in ALS and FTD, respectively.

For instance, although CSF CHIT1 is elevated in FTD patients relative to both HCs and asymptomatic MCs, it is significantly higher in ALS patients (27, 33). Furthermore, CHIT1 immunostaining in post-mortem spinal cord tissue was observed only in ALS cases, where it co-localized with IBA1-positive microglia and CD68-positive macrophages, and not in other neurodegenerative disorders, including FTD and AD (27, 33). Conversely, despite considerable overlap, CSF CHI3L1 levels were higher in patients with sporadic FTD relative to those with sporadic ALS, albeit only slightly. CHI3L1 elevation also correlated with cognitive dysfunction, as assessed by the Edinburgh Cognitive and Behavioral ALS Screen (ECAS), suggesting that it skews more closely to the FTD phenotype (28). Illán-Gala et al. (32) reported that although neither absolute CSF CHI3L1 levels nor the sAPPβ:CHI3L1 ratio significantly differed between FTD and ALS patients, CHI3L1 and global cognitive performance only correlated in the FTD subgroup. Furthermore, a robust inverse correlation was noted between the sAPPβ:CHI3L1 ratio and the FTD-Clinical Dementia Rating score in FTD patients. CHI3L1 immunoreactivity has been observed in astrocytes, but not microglia and neurons; its expression correlates with GFAP, particularly in acute inflammatory conditions like multiple sclerosis, suggesting that CHI3L1 is indicative of reactive astrocytosis (18, 19, 37). Crucially, negligible CHI3L1-positive astrocytes were observed in post-mortem ALS cortical tissue and no significant differences in *GFAP* mRNA in the spinal cord were noted between ALS patients and HCs (18, 35). CSF GFAP levels were also significantly increased in FTD patients while they were unaffected in ALS patients (27).

In summary, while the chitinases may not be specific markers for either condition, they allude to distinct neuroinflammatory profiles. If corroborated by other modalities, e.g., PET imaging (38), these profiles could help delineate the underlying pathology and provide specific targets for immunomodulatory therapy.

CHITINASES IN THE BROADER NEUROINFLAMMATORY AND NEURODEGENERATIVE MILIEU

While much remains unknown about their cellular origin, it is evident that chitinase expression is not exclusive to ALS. It has been noted in multiple neurodegenerative conditions, where it predicts both clinical severity and long-term risk (39–41). The chitinases also robustly correlate with established neurodegenerative markers, including, e.g., the neurofilaments (10, 27, 31) and both total and phosphorylated tau (40, 42). Studies investigating multivariate panels have additionally reported close links to other inflammatory mediators. For instance, CSF chitinase levels correlated with MCP-1, and C-reactive protein in ALS patients and soluble TREM2 in cognitively unimpaired individuals (10, 28, 43). Transcriptomic studies have shown that *CHIT1* correlates with *IL-16, IL-18*, and *CHI3L1* and *CHI3L2* with complement *C1s* subcomponent (36, 41). Therefore, it is probable that the chitinases reflect the inflammation that is characteristic of the wider neurodegenerative process. Given the evidence from post-mortem co-localization studies and that significant dysregulations have been primarily observed in CSF rather than blood, we further speculate that the chitinases are proxies for reactive gliosis. It is worth noting, however, that systemic conditions may also influence chitinase levels, potentially "masking" alterations in blood.

While there is considerable overlap between neurodegenerative conditions, expression patterns differ, underscoring the different pathomechanisms at play; for instance, while CSF CHI3L1 increases as cognitive deficits worsen along the AD continuum, no similar associations have been noted with the ALSFRS-R, the primary indicator of disease severity in ALS (40). However, limitations with using the ALSFRS-R and derived parameters have been previously described (44). Instead, disease progression models could be particularly informative, as they allow interpretation of biomarker profiles within the disease course.

It is also imperative to expand beyond studying the chitinases as just fold changes within a case–control paradigm, given the evidence that they act as active immune modulators rather than just passive indicators of pathology. For instance, TNF-α, LPS, and IFN-γ stimulation increased both *CHIT1* expression and activity in human macrophages (45). Conversely, CHIT1, CHI3L1, and AMCase stimulation increased the transmigratory capacity of leukocytes from patients with multiple sclerosis (46).

In conclusion, studies should address how immune activation—vis-à-vis chitinase elevation—presents across the ALS disease course, whether it differs between glial cell types and what the functional consequences are. Studies also need to account for physiological aging, given multiple reports that it influences chitinase levels (27, 31, 47).

CONCLUSIONS AND FUTURE DIRECTIONS

What can be concluded of the chitinases holds true for all biomarkers; no single molecule can capture all the pathogenic processes at play in a disease as heterogeneous as ALS. This is particularly relevant in the case of inflammatory markers: these cannot be viewed in isolation because of their functional abundance and intricate signaling networks. It is the interaction with the disease microenvironment and the interplay between different cell types that drives pathology, rather than the singular action of a specific target. Multivariate biomarker panels are more likely to capture the dynamic immune signatures associated with different functional disease phases and identify optimal treatment windows and patients who would most benefit from immunomodulatory therapies. Therefore, the chitinases represent valuable additions to the current immuno-biomarker repertoire; while their diagnostic and prognostic efficacy is unlikely to supersede that of the neurofilaments, they can assist with subtle distinctions between different neurodegenerative conditions and delineate the mechanisms underlying glial dysregulation. Additional mechanistic studies could focus on how the chitinases reflect the dynamicity of glial cell responses across the disease. For instance, current evidence already indicates that the chitinases reflect a neuroinflammatory component that is common to both genetic and sporadic forms of ALS (27). Future prospective studies could focus on recruiting MCs and following them as they transition to clinical disease to better understand how chitinase elevation manifests, what triggers it, and how it relates to other modalities.

AUTHOR CONTRIBUTIONS

All authors listed have made a substantial, direct and intellectual contribution to the work, and approved it for publication.

FUNDING

NG was supported by a doctoral scholarship (Landesgraduiertenstipendien) from the Graduate Academy of Friedrich Schiller University, Jena, Germany. This work was also supported by the German Bundesministerium für Bildung und Forschung (BMBF) grant ONWebDUALS to JG under the aegis of the EU Joint Programme-Neurodegenerative Disease Research (JPND) and a BMBF grant PYRAMID to JG in the framework of the ERANET E-RARE program.

ACKNOWLEDGMENTS

We extend our sincere thanks to Klara Metzner for bibliography curation and management. **Figure 1** was created with www.BioRender.com.

REFERENCES

1. Talbot K, Feneberg E, Scaber J, Thompson AG, Turner MR. Amyotrophic lateral sclerosis: the complex path to precision medicine. *J Neurol.* (2018) 265:2454–62. doi: 10.1007/s00415-018-8983-8
2. Pupillo E, Messina P, Logroscino G, Beghi E, Group S. Long-term survival in amyotrophic lateral sclerosis: a population-based study. *Ann Neurol.* (2014) 75:287–97. doi: 10.1002/ana.24096
3. Zhao W, Beers DR, Henkel JS, Zhang W, Urushitani M, Julien JP, et al. Extracellular mutant SOD1 induces microglial-mediated motoneuron injury. *Glia.* (2010) 58:231–43. doi: 10.1002/glia.20919
4. Liao B, Zhao W, Beers DR, Henkel JS, Appel SH. Transformation from a neuroprotective to a neurotoxic microglial phenotype in a mouse model of ALS. *Exp Neurol.* (2012) 237:147–52. doi: 10.1016/j.expneurol.2012.06.011
5. Beers DR, Zhao W, Liao B, Kano O, Wang J, Huang A, et al. Neuroinflammation modulates distinct regional and temporal clinical responses in ALS mice. *Brain Behav Immun.* (2011) 25:1025–35. doi: 10.1016/j.bbi.2010.12.008
6. Zondler L, Muller K, Khalaji S, Bliederhäuser C, Ruf WP, Grozdanov V, et al. Peripheral monocytes are functionally altered and invade the CNS in ALS patients. *Acta Neuropathol.* (2016) 132:391–411. doi: 10.1007/s00401-016-1548-y
7. Perner C, Perner F, Stubendorff B, Förster M, Witte OW, Heidel FH, et al. Dysregulation of chemokine receptor expression and function in leukocytes from ALS patients. *J Neuroinflammation.* (2018) 15:99. doi: 10.1186/s12974-018-1135-3
8. Beers DR, Zhao W, Wang J, Zhang X, Wen S, Neal D, et al. ALS patients' regulatory T lymphocytes are dysfunctional, and correlate with disease progression rate and severity. *JCI Insight.* (2017) 2:e89530. doi: 10.1172/jci.insight.89530
9. Coque E, Salsac C, Espinosa-Carrasco G, Varga B, Degauque N, Cadoux M, et al. Cytotoxic $CD8^+$ T lymphocytes expressing ALS-causing SOD1 mutant

selectively trigger death of spinal motoneurons. *Proc Natl Acad Sci USA.* (2019) 116:2312–7. doi: 10.1073/pnas.1815961116
10. Gille B, De Schaepdryver M, Dedeene L, Goossens J, Claeys KG, Van Den Bosch L, et al. Inflammatory markers in cerebrospinal fluid: independent prognostic biomarkers in amyotrophic lateral sclerosis? *J Neurol Neurosurg Psychiatry.* (2019) 90:1338–46. doi: 10.1136/jnnp-2018-319586
11. Ehrhart J, Smith AJ, Kuzmin-Nichols N, Zesiewicz TA, Jahan I, Shytle RD, et al. Humoral factors in ALS patients during disease progression. *J Neuroinflammation.* (2015) 12:127. doi: 10.1186/s12974-015-0350-4
12. Martinez-Merino L, Iridoy M, Galbete A, Roldán M, Rivero A, Acha B, et al. Evaluation of chitotriosidase and CC-chemokine ligand 18 as biomarkers of microglia activation in amyotrophic lateral sclerosis. *Neurodegener Dis.* (2018) 18:208–15. doi: 10.1159/000490920
13. Fuchs K, Cardona Gloria Y, Wolz OO, Herster F, Sharma L, Dillen CA, et al. The fungal ligand chitin directly binds TLR2 and triggers inflammation dependent on oligomer size. *EMBO Rep.* (2018) 19:e46065. doi: 10.15252/embr.201846065
14. Di Rosa M, De Gregorio C, Malaguarnera G, Tuttobene M, Biazzo F, Malaguarnera L. Evaluation of AMCase and CHIT-1 expression in monocyte macrophages lineage. *Mol Cell Biochem.* (2013) 374:73–80. doi: 10.1007/s11010-012-1506-5
15. Di Rosa M, Malaguarnera G, De Gregorio C, D'Amico F, Mazzarino MC, Malaguarnera L. Modulation of chitotriosidase during macrophage differentiation. *Cell Biochem Biophys.* (2013) 66:239–47. doi: 10.1007/s12013-012-9471-x
16. Di Rosa M, Malaguarnera G, De Gregorio C, Drago F, Malaguarnera L. Evaluation of CHI3L-1 and CHIT-1 expression in differentiated and polarized macrophages. *Inflammation.* (2013) 36:482–92. doi: 10.1007/s10753-012-9569-8
17. Bonneh-Barkay D, Bissel SJ, Kofler J, Starkey A, Wang G, Wiley CA. Astrocyte and macrophage regulation of YKL-40 expression and cellular response in neuroinflammation. *Brain Pathol.* (2012) 22:530–46. doi: 10.1111/j.1750-3639.2011.00550.x
18. Bonneh-Barkay D, Wang G, Starkey A, Hamilton RL, Wiley CA. *In vivo* CHI3L1 (YKL-40) expression in astrocytes in acute and chronic neurological diseases. *J Neuroinflammation.* (2010) 7:34. doi: 10.1186/1742-2094-7-34
19. Huang C, Huang B, Bi F, Yan LH, Tong J, Huang J, et al. Profiling the genes affected by pathogenic TDP-43 in astrocytes. *J Neurochem.* (2014) 129:932–9. doi: 10.1111/jnc.12660
20. Litviakov N, Tsyganov M, Larionova I, Ibragimova M, Deryusheva I, Kazantseva P, et al. Expression of M2 macrophage markers YKL-39 and CCL18 in breast cancer is associated with the effect of neoadjuvant chemotherapy. *Cancer Chemother Pharmacol.* (2018) 82:99–109. doi: 10.1007/s00280-018-3594-8
21. Hong JY, Kim M, Sol IS, Kim KW, Lee CM, Elias JA, et al. Chitotriosidase inhibits allergic asthmatic airways via regulation of TGF-β expression and Foxp3^{+} Treg cells. *Allergy.* (2018) 73:1686–99. doi: 10.1111/all.13426
22. Elias JA, Homer RJ, Hamid Q, Lee CG. Chitinases and chitinase-like proteins in T_H^2 inflammation and asthma. *J Allergy Clin Immunol.* (2005) 116:497–500. doi: 10.1016/j.jaci.2005.06.028
23. Starossom SC, Campo Garcia J, Woelfle T, Romero-Suarez S, Olah M, Watanabe F, et al. Chi3l3 induces oligodendrogenesis in an experimental model of autoimmune neuroinflammation. *Nat Commun.* (2019) 10:217. doi: 10.1038/s41467-018-08140-7
24. Mishra PS, Dhull DK, Nalini A, Vijayalakshmi K, Sathyaprabha TN, Alladi PA, et al. Astroglia acquires a toxic neuroinflammatory role in response to the cerebrospinal fluid from amyotrophic lateral sclerosis patients. *J Neuroinflammation.* (2016) 13:212. doi: 10.1186/s12974-016-0698-0
25. Mishra PS, Vijayalakshmi K, Nalini A, Sathyaprabha TN, Kramer BW, Alladi PA, et al. Etiogenic factors present in the cerebrospinal fluid from amyotrophic lateral sclerosis patients induce predominantly pro-inflammatory responses in microglia. *J Neuroinflammation.* (2017) 14:251. doi: 10.1186/s12974-017-1028-x
26. Varghese AM, Sharma A, Mishra P, Vijayalakshmi K, Harsha HC, Sathyaprabha TN, et al. Chitotriosidase - a putative biomarker for sporadic amyotrophic lateral sclerosis. *Clin Proteomics.* (2013) 10:19. doi: 10.1186/1559-0275-10-19
27. Oeckl P, Weydt P, Steinacker P, Anderl-Straub S, Nordin F, Volk AE, et al. Different neuroinflammatory profile in amyotrophic lateral sclerosis and frontotemporal dementia is linked to the clinical phase. *J Neurol Neurosurg Psychiatry.* (2019) 90:4–10. doi: 10.1136/jnnp-2018-318868
28. Thompson AG, Gray E, Bampton A, Raciborska D, Talbot K, Turner MR. CSF chitinase proteins in amyotrophic lateral sclerosis. *J Neurol Neurosurg Psychiatry.* (2019) 90:1215–20. doi: 10.1136/jnnp-2019-320442
29. Chen X, Chen Y, Wei Q, Ou R, Cao B, Zhao B, et al. Assessment of a multiple biomarker panel for diagnosis of amyotrophic lateral sclerosis. *BMC Neurol.* (2016) 16:173. doi: 10.1186/s12883-016-0689-x
30. Pagliardini V, Pagliardini S, Corrado L, Lucenti A, Panigati L, Bersano E, et al. Chitotriosidase and lysosomal enzymes as potential biomarkers of disease progression in amyotrophic lateral sclerosis: a survey clinic-based study. *J Neurol Sci.* (2015) 348:245–50. doi: 10.1016/j.jns.2014.12.016
31. Thompson AG, Gray E, Thezenas ML, Charles PD, Evetts S, Hu MT, et al. Cerebrospinal fluid macrophage biomarkers in amyotrophic lateral sclerosis. *Ann Neurol.* (2018) 83:258–68. doi: 10.1002/ana.25143
32. Illán-Gala I, Alcolea D, Montal V, Dols-Icardo O, Muñoz L, de Luna N, et al. CSF sAPPβ, YKL-40, and NfL along the ALS-FTD spectrum. *Neurology.* (2018) 91:e1619–e28. doi: 10.1212/WNL.0000000000006383
33. Steinacker P, Verde F, Fang L, Feneberg E, Oeckl P, Roeber S, et al. Chitotriosidase (CHIT1) is increased in microglia and macrophages in spinal cord of amyotrophic lateral sclerosis and cerebrospinal fluid levels correlate with disease severity and progression. *J Neurol Neurosurg Psychiatry.* (2018) 89:239–47. doi: 10.1136/jnnp-2017-317138
34. Deming Y, Black K, Carrell D, Cai Y, Del-Aguila JL, Fernandez MV, et al. Chitinase-3-like 1 protein (CHI3L1) locus influences cerebrospinal fluid levels of YKL-40. *BMC Neurol.* (2016) 16:217. doi: 10.1186/s12883-016-0742-9
35. Andres-Benito P, Dominguez R, Colomina MJ, Llorens F, Povedano M, Ferrer I. YKL40 in sporadic amyotrophic lateral sclerosis: cerebrospinal fluid levels as a prognosis marker of disease progression. *Aging (Albany NY).* (2018) 10:2367–82. doi: 10.18632/aging.101551
36. Sanfilippo C, Longo A, Lazzara F, Cambria D, Distefano G, Palumbo M, et al. CHI3L1 and CHI3L2 overexpression in motor cortex and spinal cord of sALS patients. *Mol Cell Neurosci.* (2017) 85:162–9. doi: 10.1016/j.mcn.2017.10.001
37. Querol-Vilaseca M, Colom-Cadena M, Pegueroles J, San Martín-Paniello C, Clarimon J, Belbin O, et al. YKL-40 (Chitinase 3-like I) is expressed in a subset of astrocytes in Alzheimer's disease and other tauopathies. *J Neuroinflammation.* (2017) 14:118. doi: 10.1186/s12974-017-0893-7
38. Corcia P, Tauber C, Vercoullie J, Arlicot N, Prunier C, Praline J, et al. Molecular imaging of microglial activation in amyotrophic lateral sclerosis. *PLoS One.* (2012) 7:e52941. doi: 10.1371/journal.pone.0052941
39. Mollgaard M, Degn M, Sellebjerg F, Frederiksen JL, Modvig S. Cerebrospinal fluid chitinase-3-like 2 and chitotriosidase are potential prognostic biomarkers in early multiple sclerosis. *Eur J Neurol.* (2016) 23:898–905. doi: 10.1111/ene.12960
40. Nordengen K, Kirsebom BE, Henjum K, Selnes P, Gísladóttir B, Wettergreen M, et al. Glial activation and inflammation along the Alzheimer's disease continuum. *J Neuroinflammation.* (2019) 16:46. doi: 10.1186/s12974-019-1399-2
41. Di Rosa M, Dell'Ombra N, Zambito AM, Malaguarnera M, Nicoletti F, Malaguarnera L. Chitotriosidase and inflammatory mediator levels in Alzheimer's disease and cerebrovascular dementia. *Eur J Neurosci.* (2006) 23:2648–56. doi: 10.1111/j.1460-9568.2006.04780.x
42. Rodrigues FB, Byrne LM, McColgan P, Robertson N, Tabrizi SJ, Zetterberg H, et al. Cerebrospinal fluid inflammatory biomarkers reflect clinical severity in huntington's disease. *PLoS One.* (2016) 11:e0163479. doi: 10.1371/journal.pone.0163479
43. Falcon C, Monte-Rubio GC, Grau-Rivera O, Suárez-Calvet M, Sánchez-Valle R, Rami L, et al. CSF glial biomarkers YKL40 and sTREM2 are associated with longitudinal volume and diffusivity changes in cognitively unimpaired individuals. *Neuroimage Clin.* (2019) 23:101801. doi: 10.1016/j.nicl.2019.101801
44. Rutkove SB. Clinical measures of disease progression in amyotrophic lateral sclerosis. *Neurotherapeutics.* (2015) 12:384–93. doi: 10.1007/s13311-014-0331-9

45. Malaguarnera L, Musumeci M, Di Rosa M, Scuto A, Musumeci S. Interferon-γ, tumor necrosis factor-α, and lipopolysaccharide promote chitotriosidase gene expression in human macrophages. *J Clin Lab Anal.* (2005) 19:128–32. doi: 10.1002/jcla.20063
46. Correale J, Fiol M. Chitinase effects on immune cell response in neuromyelitis optica and multiple sclerosis. *Mult Scler.* (2011) 17:521–31. doi: 10.1177/1352458510392619
47. Del Campo M, Galimberti D, Elias N, Boonkamp L, Pijnenburg YA, van Swieten JC, et al. Novel CSF biomarkers to discriminate FTLD and its pathological subtypes. *Ann Clin Transl Neurol.* (2018) 5:1163–75. doi: 10.1002/acn3.629

Conflict of Interest: The authors declare that the research was conducted in the absence of any commercial or financial relationships that could be construed as a potential conflict of interest.

Advantages of publishing in Frontiers

OPEN ACCESS
Articles are free to read for greatest visibility and readership

FAST PUBLICATION
Around 90 days from submission to decision

HIGH QUALITY PEER-REVIEW
Rigorous, collaborative, and constructive peer-review

TRANSPARENT PEER-REVIEW
Editors and reviewers acknowledged by name on published articles

Frontiers
Avenue du Tribunal-Fédéral 34
1005 Lausanne | Switzerland

Visit us: www.frontiersin.org
Contact us: info@frontiersin.org | +41 21 510 17 00

REPRODUCIBILITY OF RESEARCH
Support open data and methods to enhance research reproducibility

DIGITAL PUBLISHING
Articles designed for optimal readership across devices

FOLLOW US
@frontiersin

IMPACT METRICS
Advanced article metrics track visibility across digital media

EXTENSIVE PROMOTION
Marketing and promotion of impactful research

LOOP RESEARCH NETWORK
Our network increases your article's readership